

**DESIGN, SYNTHESIS AND
CHARACTERIZATION OF ORGANIC
RECEPTORS FOR THE SELECTIVE
DETECTION OF BIOLOGICALLY AND
ENVIRONMENTALLY IMPORTANT ANIONS**

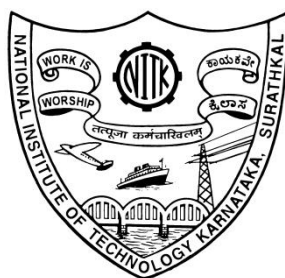
Thesis

Submitted in partial fulfilment of the requirements for the degree of

DOCTOR OF PHILOSOPHY

by

SRIKALA P.



DEPARTMENT OF CHEMISTRY

NATIONAL INSTITUTE OF TECHNOLOGY KARNATAKA,

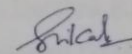
SURATHKAL, MANGALORE-575025

June, 2018

DECLARATION

By the Ph.D. Research Scholar

I hereby *declare* that the Research Thesis entitled "Design, Synthesis, and Characterization of Organic Receptors for the Selective Detection of Biologically and Environmentally Important Anions" which is being submitted to the **National Institute of Technology Karnataka, Surathkal** in partial fulfilment of the requirements for the award of the Degree of **Doctor of Philosophy** in Chemistry is a *bonafide report of the research work carried out by me*. The material contained in this Research Thesis has not been submitted to any University or Institution for the award of any degree.


SRIKALA P.

Reg. No. 145074CY14F02

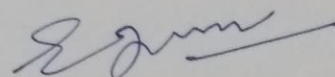
Department of Chemistry

Place: NITK - Surathkal

Date: 30-05-2018

CERTIFICATE

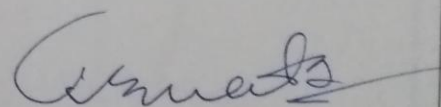
This is to *certify* that the Research Thesis "Design, Synthesis, and Characterization of Organic Receptors for the Selective Detection of Biologically and Environmentally Important Anions" submitted by Ms. Srikala P. (Register Number: 145074CY14F02) as the record of the research work carried out by her, is *accepted as the Research Thesis submission* in partial fulfilment of the requirements for the award of degree of Doctor of Philosophy.



Dr. Darshak R. Trivedi

Research Guide

Date: 30/5/2018



Chairman - DRPC

Date: 1/6/18

***DEDICATED
TO MY
SPIRITUAL
TEACHER***



ACKNOWLEDGEMENT

“Experience is the best teacher”

It has been a great experience pursuing research career at National Institute of Technology Karnataka (NITK) Surathkal with proficient and unique individuals who have helped me to achieve what I have up to this point. I would like to express my deepest appreciation for the help and support of the kind people around me, to only some of whom it is possible to give a particular mention here.

I wholeheartedly express my deep sense of gratitude to my research supervisor Dr. Darshak R. Trivedi for his benevolent guidance, his patience and above all his belief in me. Being very optimistic and sincere by nature that few could hope to match, from him, I have learnt to work with perfection and dedication. Throughout my doctoral work he has been a constant source of encouragement and sound advice. I thank him for having instilled in me the work ethic and determination to achieve this goal. Be it failure and success, trial and error, ennui and exuberance, he was there for all of it. His unstained support throughout the course of my research work has made my thesis appear in the present form. I feel privileged and fortunate for being his student.

I am grateful to NITK for the research infrastructure and fellowship that allowed me to work at a smoother pace.

I owe a very important debt to Prof. A. Chitharanjan Hegde, Former Head, Department of Chemistry for his profound encouragement and showing me the right direction at the most crucial moment which seems to be difficult to forget throughout my life.

I am grateful to Prof. D. Krishna Bhat, Head, Department of Chemistry and Chairman – DRPC and Prof. B. Ramachandra Bhat, Former Head, Department of Chemistry for the kind support.

I am thankful to the RPAC members, Prof. A. Nityananda Shetty, Department of Chemistry for the continuous guidance whenever I approached him which led to fruitful

discussions on research problems and also Prof. H. D. Shashikala, Department of Physics for her appreciative comments.

I thank Prof. A. Vasudeva Adhikari, Prof. Arun M. Isloor, Dr. Udaya Kumar D., Dr. Sib Sankar Mal, Dr. Beneesh P.B., Dr. Saikat Datta and Dr. Debashree Chakraborty for their support during the research work.

I wish to convey my sincere thanks to Dr. Kartick Tarafder, Department of Physics, NITK Surathkal for the kind help and productive discussions on DFT, Dr. Prafulla K. Jha, Department of Physics, Faculty of Science, The M.S. University of Baroda, Vadodara, Dr. Venu Mankad and Ms. Swetha Dabhi, Department of Physics, Maharaja Krishnakumarsinhji Bhavnagar University, Bhavnagar, Dr. Satyam Shinde, School of Technology, Pandit Deendayal Petroleum University, Gandhinagar for their prompt help in DFT calculations. I am thankful to Dr. Ajith K. M., Assistant Professor, Department of Physics, NITK Surathkal for his support in providing access to Gaussian 09 package.

I would like to express my deepest appreciation to our research collaborator Dr. Norifumi Fujita, Department of Applied Chemistry, Meijo University, Nagoya, Japan for the timely help and support.

I sincerely thank Dr. Keyur Raval, Department of Chemical Engineering, NITK Surathkal and Dr. Ritu Raval, Department of Biotechnology, MIT Manipal for their selfless help in the biological studies.

I extend my gratitude to Department of Science and Technology, Govt. of India for providing SCXRD facility to Department of Chemistry, NITK Surathkal, under FIST program.

I am thankful to MIT Manipal, Molecular Biophysics Unit, IISc Bangalore, CDRI Lucknow for the timely analytical support.

I would like to thank Alumni Association, NITK for the financial support during international visit for research interaction.

I would like to express my special thanks to my friends and colleagues, Mr. Momidi Bharath Kumar, Mr. Sunil Kumar N., Mr. Venkatadri Tekuri and Ms. Archana Singh

who have helped and supported me in many ways. I also thank the postgraduate project students of our group, Ms. Bhagyashree, Ms. Neethu P. P., Mr. Vikram T., NITK Surathkal and Ms. Arshiya Kaur, IITM, Chennai, for giving me a chance to understand and discuss the most interesting topics in host-guest chemistry in the due course of their learning process.

I extend my thanks to the nonteaching staff of the department, Mrs. Shamila, Mrs. Kasturi, Mrs. Sharmila, Mrs. Deepa, Mr. Prashanth, Mr. Harish, Mr. Pradeep and Mr. Santhosh for their timely assistance in the departmental work.

I earnestly yearn to thank my parents, Mr. P. Venkatramana Pangannaya and Mrs. Varada P. and my in-laws Mr. Mohan R. and Mrs. Brinda M. for their love and sacrifice that motivated me to achieve this goal. They have given up many things for me to be at NITK; they have cherished with me every great moment and supported me whenever I needed it. I am extremely thankful to my sister-in-law Mrs. Rekha M, my brother Mr. Krishna Kripa Das, my niece Sriya for their love, prayers and support. I am ceaselessly grateful to all of you and pray for your continued mercy upon me.

I owe my deepest gratitude to my husband, Mr. Makesh M., for being very supportive and encouraging me for higher studies. He has been a sure and steady source of inspiration for me and there have been countless moments while pursuing my research that, without him, I feel I would have succumbed to defeat. I thank him from the bottom of my heart for the undivided support and being a witness for every step of the way. I thank him for all the sacrifices he has gone through to give me the best of the best things in life.

Srikala P.

ABSTRACT

Nature in its fullest form is a reservoir of biochemical processes, regulated by various ionic species, which are primarily known to sustain the ecological balance in the living system. Among them, anions such as fluoride (F^-), dihydrogen phosphate ($H_2PO_4^-$), acetate (AcO^-) and cyanide (CN^-) have profound impact on human health, both beneficial and detrimental, depending on the amount present in the living system. In this direction, design and synthesis of artificial organic receptors have garnered great attention to mimic molecular recognition at physiological level.

Owing to the profound utility of the artificial receptors, the present work has been focused towards rational design of organic receptors which can aid the colorimetric detection of anions. Seven different series of receptors based on various backbones following binding site-signaling unit approach have been designed, synthesized and characterized by standard spectroscopic techniques. The anion binding ability of the receptors have been evaluated in appropriate solvent system and confirmed by UV-Vis titration, 1H -NMR titration, cyclic voltammetric and DFT studies. The binding constant and binding ratio have been evaluated using Benesi-Hildebrand (B-H) equation and B-H plot respectively. The lower detection limit values of the receptors achieved towards active anions signifies their efficacy in real life applications. Biological applications of the selected active receptors such as DNA binding studies; detection of F^- in sea water and commercially available mouthwash; detection of $H_2PO_4^-$ in detergents; detection of AcO^- ions in vinegar and bacterial culture and detection of CN^- ions in sprouting potatoes prove their utility as chemosensors. The sol-gel transition of the organic receptors in the presence of anions highlights the utility of soft materials in the sensor applications. Based on the experimental findings, it could be concluded that artificial organic receptors are potent candidates to mimic molecular recognition at physiological level.

Keywords: Organic Receptors; Colorimetric; Anions; Ratiometric; Tautomerism; Solvatochromism; bacterial studies; DNA binding; Gelation

CONTENTS

DECLARATION

CERTIFICATE

ACKNOWLEDGEMENT

ABSTRACT

CONTENTS

i

LIST OF FIGURES

vii

LIST OF SCHEMES

xxiii

LIST OF TABLES

xxv

NOMENCLATURE

xxvi

CHAPTER 1

INTRODUCTION

1.1	SUPRAMOLECULAR CHEMISTRY	1
1.2	HOST-GUEST CHEMISTRY	1
1.3	ANIONS	2
1.3.1	Environmentally and biologically important anions	3
1.3.1.1	Fluoride	3
1.3.1.2	Cyanide	3
1.3.1.3	Acetate	3
1.3.1.4	Phosphate	4
1.3.1.5	Arsenite	4
1.4	ANION RECEPTOR CHEMISTRY	4
1.4.1	Challenges in anion receptor chemistry	5
1.4.2	History of anion receptor chemistry	7
1.5	COLORIMETRIC CHEMOSENSORS	12
1.5.1	Types of colorimetric chemosensors	13
1.6	SUPRAMOLECULAR GELS	16
1.7	LITERATURE REVIEW	18
1.8	SCOPE OF THE PRESENT WORK	28
1.9	OBJECTIVES OF THE WORK	29

CHAPTER 2

SYNTHESES AND EVALUATION OF COLORIMETRIC ANION SENSING PROPERTIES OF ORGANIC RECEPTORS: TIME DEPENDENCY AND DFT STUDIES

2.1	INTRODUCTION	31
2.2	EXPERIMENTAL SECTION	32
2.2.1	Materials and methods	32
2.2.2	Synthesis of receptors R and L	33
2.2.3	Characterization data of receptors	35
2.3	RESULTS AND DISCUSSION	39
2.3.1	Colorimetric studies	39
2.3.2	UV-Vis titration studies	41
2.3.3	Time dependency studies	53
2.3.4	Reversibility studies	57
2.3.5	¹ H-NMR titration studies	58
2.3.6	Theoretical results	60
2.3.7	Calculation of binding constant from UV-Vis studies	65
2.3.8	Binding ratio and detection limit	65
2.3.9	Binding mechanism	66
2.4	CONCLUSIONS	68

CHAPTER 3

DESIGN, SYNTHESIS AND SPECTRAL INVESTIGATION OF ORGANIC RECEPTORS AS COLORIMETRIC AND ABSORPTION RATIO-METRIC ANION CHEMOSENSOR

3.1	INTRODUCTION	69
3.2	EXPERIMENTAL SECTION	70
3.2.1	Materials and methods	70
3.2.2	Synthesis of receptor S1R1	71
3.2.3	Synthesis of receptor S1R2	72
3.2.4	Characterization data of receptors	72

3.3	RESULTS AND DISCUSSION	75
3.3.1	Colorimetric detection of anions	75
3.3.2	UV-Vis titration studies	77
3.3.3	Competitive studies	93
3.3.4	Fluorescence studies	94
3.3.5	Cyclic voltammetric studies	95
3.3.6	¹ H-NMR titration studies	98
3.3.7	Calculation of binding constant from UV-Vis studies	99
3.3.8	Binding mechanism	99
3.4	CONCLUSIONS	101

CHAPTER 4

SYNTHESIS OF ORGANIC RECEPTORS FOR ANIONS: SOLVENT DEPENDENT CHROMOGENIC RESPONSE AND DFT STUDIES

4.1	INTRODUCTION	103
4.2	EXPERIMENTAL SECTION	104
4.2.1	Materials and methods	104
4.2.2	Synthesis of receptor S2R1	105
4.2.3	Synthesis of receptor S2R2	106
4.2.4	Synthesis of receptor S2R3	107
4.2.5	Synthesis of receptor S2R4	107
4.2.6	Synthesis of receptor S2R5	108
4.2.7	Characterization data of receptors	109
4.3	RESULTS AND DISCUSSION	115
4.3.1	Colorimetric detection of anions	115
4.3.2	UV-Vis titration studies	120
4.3.3	Solvatochromism studies	137
4.3.4	Electrochemical studies	143
4.3.5	¹ H-NMR studies	146
4.3.6	pH dependency studies	148

4.3.7	DFT studies	149
4.3.8	Calculation of binding constant from UV-Vis studies	153
4.3.9	Binding mechanism	154
4.4	Conclusions	156

CHAPTER 5

DESIGN, SYNTHESIS AND EVALUATION OF FURYL FUNCTIONALIZED HYDRAZINE DERIVATIVES AS COLORIMETRIC CHEMOSENSORS FOR ANION RECOGNITION

5.1	INTRODUCTION	157
5.2	EXPERIMENTAL SECTION	158
5.2.1	Materials and methods	158
5.2.2	Preparation of agar plates containing receptor S3R1	159
5.2.3	Preparation of <i>E.coli</i> BL21 cultures	159
5.2.4	Synthesis of receptors S3R1 , S3R2 and S3R3	159
5.2.5	Characterization data of receptors	161
5.3	RESULTS AND DISCUSSION	164
5.3.1	Colorimetric detection of anions	164
5.3.2	UV-Vis titration studies	167
5.3.3	pH dependency studies	184
5.3.4	Calculation of binding constant from UV-Vis studies	189
5.3.5	¹ H-NMR titration studies	190
5.3.6	DFT studies	192
5.3.7	Binding mechanism	196
5.3.8	Biological applications	196
5.4	Conclusions	197

CHAPTER 6

RATIONALLY DESIGNED MULTI-ANION RESPONSIVE COLORIMETRIC RECEPTOR: AN INSIGHT ON THE EFFECTIVE INTERPLAY OF CHEMISTRY AND BIOLOGY IN REAL LIFE APPLICATIONS

6.1	INTRODUCTION	199
6.2	EXPERIMENTAL SECTION	201
6.2.1	Materials and methods	201
6.2.2	Synthesis of receptor S4R1	201
6.2.3	Synthesis of receptor S4R2	202
6.2.4	Synthesis of receptor S4R3	203
6.2.5	Characterization data of receptors	204
6.3	RESULTS AND DISCUSSION	208
6.3.1	Colorimetric detection of anions	208
6.3.2	UV-Vis titration studies	211
6.3.3	Fluorescence studies	214
6.3.4	pH dependency studies	217
6.3.5	Binding studies in organo-aqueous medium	218
6.3.6	¹ H-NMR titration studies	222
6.3.7	Electrochemical studies	223
6.3.8	DNA binding studies	224
6.3.9	Detection of CN ⁻ ions in sprouting potatoes	226
6.3.10	Detection of H ₂ PO ₄ ⁻ ions in detergent sample	227
6.3.11	Calculation of binding constant from UV-Vis studies	228
6.3.12	Binding mechanism	228
6.4	Conclusions	229

CHAPTER 7

COLORIMETRIC AND FLUOROMETRIC TURN ON SENSOR FOR SELECTIVE DETECTION OF FLUORIDE ION: SOL-GEL TRANSITION STUDIES

7.1	INTRODUCTION	231
7.2	EXPERIMENTAL SECTION	232
7.2.1	Materials and methods	232
7.2.2	Synthesis of receptor S5R1	232
7.2.3	Characterization data of receptor	233
7.3	RESULTS AND DISCUSSION	235
7.3.1	Complexation studies	235
	7.3.1.1 UV-Vis and fluorescence studies	235
	7.3.1.2 ¹ H-NMR titration studies	240
7.3.2	Gelation studies	241
7.3.3	Calculation of binding constant from UV-Vis studies	244
7.3.4	Binding mechanism	245
7.4	Conclusions	245

CHAPTER 8

SUMMARY AND CONCLUSIONS

8.1	SUMMARY	247
8.2	CONCLUSIONS	248
8.3	SCOPE FOR FUTURE WORK	250
	<i>REFERENCES</i>	251
	<i>PUBLICATIONS</i>	275
	<i>CURRICULUM VITAE</i>	277

LIST OF FIGURES

CHAPTER 1

1.1	Representation of the structural aspects of supramolecular Chemistry	1
1.2	Different shapes and sizes of anions	5
1.3	Basic components of a chemosensor	13
1.4	General representation of binding site-signaling unit approach	14
1.5	General representation of the displacement assay approach	15
1.6	General representation of the chemodosimeter approach	16
1.7	Schematic representation of the formation of a supramolecular gel	17

CHAPTER 2

2.1	FT-IR spectrum of the receptor R	35
2.2 (a)	¹ H-NMR spectrum of receptor R	35
2.2 (b)	¹³ C NMR spectrum of receptor R	36
2.3	Mass spectrum of the receptor R	36
2.4	FT-IR spectrum of receptor L	37
2.5 (a)	¹ H-NMR spectrum of receptor L	37
2.5 (b)	¹³ C NMR spectrum of receptor L	38
2.6	Mass spectrum of receptor L	38
2.7	Color changes of receptor R upon addition of 2 equiv. of various anions in dry DMSO	39
2.8	UV-Vis absorption spectra of receptor R (1×10^{-4} M in DMSO) after the addition of 2 equiv. of different anions at 519 nm	40
2.9	Color change observed for L (4.5×10^{-5} M in DMSO) with the addition of 1 equiv. of different anions (1×10^{-2} M in DMSO)	40
2.10	UV-visible absorption spectra of L (4.5×10^{-5} M in DMSO) upon addition of 1 equiv. of various anions as TBA salts	41
2.11	UV-Vis titration spectra of receptor R (1×10^{-4} M in DMSO) with incremental addition of TBAF (0-2 equiv.). Inset showing the binding isotherm at selected wavelength (519 nm)	42
2.12	UV-Vis titration spectra of receptor R (1×10^{-4} M in DMSO) with incremental addition of TBAAcO (0-2 equiv.). Inset showing the binding isotherm at selected wavelength (528 nm)	43
2.13	UV-Vis titration spectra of receptor R (1×10^{-4} M in DMSO) with incremental addition of NaF (0-2 equiv.). Inset showing the binding isotherm at selected wavelength (513 nm)	44
2.14	B-H plot of R –F [–] (TBAF) complex at a selected wavelength of 519 nm	45
2.15	B-H plot of R –AcO [–] (TBAAcO) complex at a selected wavelength of 528 nm	45

2.16	B-H plot of R -F ⁻ (NaF) complex at a selected wavelength of 513 nm	46
2.17	Colour changes of receptor R upon addition of 2 equiv. of NaF and mouthwash	47
2.18	UV-Vis titration spectra of receptor R (1x10 ⁻⁴ M in DMSO) with incremental addition of mouthwash (0-3 equiv.). Inset showing the binding isotherm at selected wavelength (513 nm)	47
2.19	Calibration curve for the determination of F ⁻ ion in mouthwash	48
2.20	UV-Vis titration spectra of receptor L (4.5x10 ⁻⁵ M in DMSO) with the incremental addition of 0.1 equiv of TBAF (1x10 ⁻² M in DMSO). Inset plot representing the binding isotherm at 560 nm	49
2.21	UV-Vis titration spectra of receptor L (4.5x10 ⁻⁵ M in DMSO) with the incremental addition of 0.1 equiv of TBAClO (1x10 ⁻² M in DMSO). Inset plot representing the binding isotherm at 560 nm	49
2.22	B-H plot of receptor L - F ⁻ (TBAF) complex at a selected wavelength of 560 nm	50
2.23	B-H plot of receptor L - AcO ⁻ complex at a selected wavelength of 560 nm	50
2.24	UV-Vis titration spectra of receptor L (4.5x10 ⁻⁵ M in 9:1, v/v, DMSO:H ₂ O) with the addition of 0.1 equiv. of NaF (1x10 ⁻² M in distilled water). Inset plot representing the variation of absorbance with concentration of NaF at 556 nm	51
2.25	UV-Vis titration spectra of receptor L (4.5x10 ⁻⁵ M in 9:1, v/v, DMSO:H ₂ O) with the addition of 0.1 equiv. of NaAcO (1x10 ⁻² M in distilled water). Inset plot representing the variation of absorbance with concentration of NaAcO at 559 nm	51
2.26	B-H plot of receptor L - F ⁻ (Na ⁺) complex at a selected wavelength of 556 nm	52
2.27	B-H plot of receptor L - AcO ⁻ (Na ⁺) complex at a selected wavelength of 559 nm	52
2.28	Color change of receptor L upon addition of NaF and mouthwash	53
2.29	Time evolution study of receptor R (10 ⁻⁴ M in DMSO) in the presence of TBA salt of F ⁻ ion	54
2.30	Time evolution study of receptor R (10 ⁻⁴ M in DMSO) in the presence of TBA salt of AcO ⁻ ion	54
2.31	Time dependent plot of first order rate equation to determine rate constant from UV-Vis spectral change of L in the presence of AcO ⁻ ion at 560 nm	56
2.32	Time dependent plot of first order rate equation to determine rate constant from UV-Vis spectral change of L in the presence of F ⁻ ion at 560 nm	56
2.33	UV-Vis spectra representing reversibility of receptor R -F ⁻ complex	57

	in the presence of $\text{Ca}(\text{NO}_3)_2$	
2.34	UV-Vis spectra representing reversibility of receptor R - AcO^- complex in the presence of $\text{Ca}(\text{NO}_3)_2$	58
2.35	^1H NMR titration spectra of receptor R upon addition of 0.5, 1.0, 1.5 and 2.0 equiv. of a) F^- and b) AcO^- ion	59
2.36	^1H -NMR titration spectra of L on incremental addition of AcO^- ion	60
2.37	Optimized geometry of receptor (A), receptor with NaF (B) and receptor with TBAAcO^- (C)	61
2.38	Optimized structure of receptor L ; (a) HOMO, (b) LUMO	64
2.39	Optimized structure of receptor L - F^- complex; (a) HOMO, (b) LUMO	64
2.40	Optimized structure of receptor L - AcO^- complex; (a) HOMO, (b) LUMO	65

CHAPTER 3

3.1(a)	FT-IR spectrum of receptor S1R1	72
3.1(b)	FT-IR spectrum of receptor S1R2	72
3.2	^1H NMR spectrum of receptor S1R1	73
3.3	^1H NMR spectrum of receptor S1R2	73
3.4(a)	Mass spectrum of receptor S1R1	74
3.4(b)	Mass spectrum of receptor S1R2	74
3.5	Color change of the receptors S1R1 (10^{-4} M in DMSO) with the addition of 1equiv. of TBA salts of anions (10^{-2} M in DMSO)	75
3.6	Color change of the receptors S1R2 (10^{-4} M in DMSO) with the addition of 1equiv. of TBA salts of anions (10^{-2} M in DMSO)	75
3.7	UV-Vis spectra of receptor S1R1 (10^{-4} M in DMSO) with the addition of 1eq.of tertabutylammonium salts of various anions (10^{-2} M in DMSO)	76
3.8	UV-Vis spectra of receptor S2R2 (10^{-4} M in DMSO) with the addition of 1 eq. of tertabutylammonium salts of various anions (10^{-2} M in DMSO)	76
3.9	UV-Vis titration spectra of receptor S1R1 (10^{-4} M in DMSO) with the incremental addition of TBAF (10^{-2} M in DMSO). Inset plot representing the absorption isotherm at 531 nm	78
3.10	B-H plot of receptor S1R1 - TBAF complex at a selected wavelength of 531 nm	78
3.11	UV-Vis titration spectra of receptor S1R1 (10^{-4} M in DMSO) with the incremental addition of TBAH_2PO_4 (10^{-2} M in DMSO). Inset plot representing the absorption isotherm at 531 nm	79
3.12	B-H plot of receptor S1R1 - TBAH_2PO_4 complex at a selected wavelength of 531 nm	79

3.13	UV-Vis titration spectra of receptor S1R1 (10^{-4} M in DMSO) with the incremental addition of TBAOAc (10^{-2} M in DMSO). Inset plot representing the absorption isotherm at 534 nm	80
3.14	B-H plot of receptor S1R1 - TBA ⁺ AcO ⁻ complex at a selected wavelength of 534 nm	80
3.15	Color change of the receptor S1R1 (DMSO: HEPES buffer, 9:1, v/v) with the addition of 1eq. of TBA salts of anions	81
3.16	UV-Vis spectra of receptor S1R1 (10^{-4} M in DMSO: HEPES buffer, 9:1, v/v) with the addition of 1eq.of tertabutylammonium salts of various anions (10^{-2} M in DMSO)	81
3.17	UV-Vis titration spectra of receptor S1R1 (10^{-4} M in DMSO: HEPES buffer, 9:1, v/v) with the incremental addition of TBAOAc (10^{-2} M in DMSO)	82
3.18	UV-Vis titration spectra of receptor S1R2 (10^{-4} M in DMSO) with the incremental addition of TBAF (10^{-2} M in DMSO). Inset plot representing the absorption isotherm at 533 nm	83
3.19	B-H plot of receptor S1R2 - TBAF complex at a selected wavelength of 533 nm	84
3.20	UV-Vis titration spectra of receptor S1R2 (10^{-4} M in DMSO) with the incremental addition of TBAOAc (10^{-2} M in DMSO). Inset plot representing the absorption isotherm at 537 nm	84
3.21	B-H plot of receptor S1R2 - TBA ⁺ AcO ⁻ complex at a selected wavelength of 537 nm	85
3.22	UV-Vis titration spectra of receptor S1R2 (10^{-4} M in DMSO) with the incremental addition of TBAOH (10^{-2} M in DMSO)	85
3.23	Ratiometric response of receptor S1R2 with the increasing concentration of AcO ⁻ ion	86
3.24	Ratiometric response of receptor S1R2 with the increasing concentration of OH ⁻ ion	86
3.25	Ratiometric plot of A_{537}/A_{389} (receptor S1R2) with the increasing equiv. of AcO ⁻ ion	87
3.26	UV-Vis titration spectra of S1R1 (1×10^{-4} M, 9:1, v/v DMSO/H ₂ O) with the incremental addition of standard solution of NaF (1×10^{-2} M in distilled water). Inset showing binding isotherm at 530 nm	88
3.27	B-H plot of receptor S1R1 - NaF complex at a selected wavelength of 530 nm	88
3.28	UV-Vis titration spectra of S1R1 (1×10^{-4} M, 9:1, v/v DMSO/H ₂ O) with the incremental addition of standard solution of NaAcO (1×10^{-2} M in distilled water). Inset showing binding isotherm at 532 nm	89
3.29	B-H plot of receptor S1R1 - NaAcO complex at a selected wavelength of 532 nm	89

3.30	UV-Vis titration spectra of S1R2 (1×10^{-4} M, 9:1, v/v DMSO/H ₂ O) with the incremental addition of standard solution of NaF (1×10^{-2} M in distilled water). Inset showing binding isotherm at 535 nm	90
3.31	B-H plot of receptor S1R2 - NaF complex at a selected wavelength of 535 nm	90
3.32	UV-Vis titration spectra of S1R2 (1×10^{-4} M, 9:1, v/v DMSO/H ₂ O) with the incremental addition of standard solution of NaAcO (1×10^{-2} M in distilled water). Inset showing binding isotherm at 534 nm	91
3.33	B-H plot of receptor S1R2 - NaAcO complex at a selected wavelength of 534 nm	91
3.34	Color change of receptor S1R1 in the presence of 1 equiv. of NaF and NaOAc, mouthwash and seawater	92
3.35	Color change of receptor S1R2 in the presence of 1 equiv. of NaF, NaAcO, mouthwash and seawater	92
3.36	UV-Vis spectra of S1R1 with the addition of seawater and mouthwash	93
3.37	UV-Vis spectra of S1R2 with the addition of seawater and mouthwash	93
3.38	UV-Vis spectra of S1R1 with the addition of 1 equiv. of AcO ⁻ ion to the receptor solution containing 1 equiv. of other test anions	94
3.39	Colorimetric response of receptor S1R1 towards AcO ⁻ ion in the presence of other interfering ions	94
3.40	Fluorescence spectra of S1R1 (10^{-4} M in DMSO) with the addition of 1 eq. of tertabutylammonium salts of various anions (10^{-2} M in DMSO)	95
3.41	Fluorescence spectra of S1R1 (10^{-4} M in DMSO) with the incremental addition of 1 eq. of tertabutylammonium salts of AcO ⁻ ions (10^{-2} M in DMSO)	95
3.42	Cyclic voltammogram of receptor S1R1 with the incremental addition of AcO ⁻ ion	96
3.43	Cyclic voltammogram of receptor S1R2 with the incremental addition of AcO ⁻ ion	97
3.44	¹ H NMR titration of receptor S1R1 with incremental addition of TBAAcO (0-1 equiv.)	98
3.45	¹ H NMR titration of receptor S1R2 with incremental addition of TBAAcO ion (0-1 equiv.)	99
CHAPTER 4		
4.1	FT-IR spectrum of receptor S2R1	109
4.2	FT-IR spectrum of receptor S2R2	110
4.3	FT-IR spectrum of receptor S2R3	110
4.4	FT-IR spectrum of receptor S2R4	111

4.5	FT-IR spectrum of receptor S2R5	111
4.6	¹ H-NMR spectrum of receptor S2R1	112
4.7	¹ H-NMR spectrum of receptor S2R2	112
4.8	¹ H-NMR spectrum of receptor S2R2	113
4.9	¹ H-NMR spectrum of receptor S2R4	113
4.10	¹ H-NMR spectrum of receptor S2R5	114
4.11	ORTEP diagram of receptor S2R5	114
4.12	Colour change of the receptors S2R1 to S2R5 with the addition of 1eq. of TBA salts of anions	117
4.13	UV-Vis spectra of receptor S2R1 (10^{-4} M in DMSO) with the addition of tertabutylammonium salts of various anions (10^{-2} M in DMSO)	118
4.14	UV-Vis spectra of receptor S2R2 (10^{-4} M in DMSO) with the addition of tertabutylammonium salts of various anions (10^{-2} M in DMSO)	118
4.15	UV-Vis spectra of receptor S2R3 (10^{-4} M in DMSO) with the addition of tertabutylammonium salts of various anions (10^{-2} M in DMSO)	119
4.16	UV-Vis spectra of receptor S2R4 (10^{-4} M in DMSO) with the addition of tertabutylammonium salts of various anions (10^{-2} M in DMSO)	119
4.17	UV-Vis spectra of receptor S2R5 (10^{-4} M in DMSO) with the addition of tertabutylammonium salts of various anions (10^{-2} M in DMSO)	120
4.18	UV-Vis titration spectra of receptor S2R1 (10^{-4} M in DMSO) with the incremental addition of TBAAcO (10^{-2} M in DMSO). Inset plot representing the absorption isotherm at 545 nm	121
4.19	B-H plot representing 1:1 binding ratio of S2R1 -TBAAcO complex	122
4.20	UV-Vis titration spectra of receptor S2R2 (10^{-4} M in DMSO) with the incremental addition of TBAAcO (10^{-2} M in DMSO). Inset plot representing the absorption isotherm at 497 nm	122
4.21	B-H plot representing 1:1 binding ratio of S2R2 -TBAAcO complex	123
4.22	UV-Vis titration spectra of receptor S2R3 (10^{-4} M in DMSO) with the incremental addition of TBAAcO (10^{-2} M in DMSO). Inset plot representing the absorption isotherm at 570 nm	124
4.23	B-H plot representing 1:1 binding ratio of S2R3 -TBAAcO complex	124
4.24	UV-Vis titration spectra of S2R4 (1×10^{-4} M in dry DMSO) with the incremental addition of standard solution of TBAAcO (1×10^{-2} M in dry DMSO). Inset showing the binding isotherm at 572 nm	125
4.25	B-H plot of receptor S2R4 - TBAAcO complex at a selected wavelength of 572 nm	126

4.26	UV-Vis titration spectra of S2R4 (1×10^{-4} M, DMSO) with the incremental addition of standard solution of TBAOH (1×10^{-2} M in DMSO)	126
4.27	UV-Vis titration spectra of S2R4 (1×10^{-4} M in dry DMSO) with the incremental addition of standard solution of TBAH ₂ PO ₄ (1×10^{-2} M in dry DMSO). Inset showing the binding isotherm at 572 nm	127
4.28	B-H plot of receptor S2R4 - TBAH ₂ PO ₄ complex at a selected wavelength of 572 nm	127
4.29	UV-Vis titration spectra of S2R4 (1×10^{-4} M in dry DMSO) with the incremental addition of standard solution of TBAF (1×10^{-2} M in dry DMSO). Inset showing the binding isotherm at 578 nm	128
4.30	B-H plot of receptor S2R4 - TBAF complex at a selected wavelength of 578 nm	128
4.31	UV-Vis titration spectra of receptor S2R5 (10^{-4} M in DMSO) with the incremental addition of TBAAcO (10^{-2} M in DMSO). Inset plot representing the absorption isotherm at 495 nm	129
4.32	B-H plot representing 1:1 binding ratio of S2R5 -TBAAcO complex	130
4.33	UV-Vis titration spectra of receptor S2R1 (10^{-4} M in 9:1, v/v DMSO:H ₂ O) with the incremental addition of NaF (10^{-2} M in distilled H ₂ O). Inset plot representing the absorption isotherm at 544 nm	131
4.34	B-H plot of receptor S2R1 - NaF complex at a selected wavelength of 544 nm	131
4.35	UV-Vis titration spectra of receptor S2R2 (10^{-4} M in DMSO) with the incremental addition of NaF (10^{-2} M in distilled H ₂ O). Inset plot representing the absorption isotherm at 500 nm	132
4.36	B-H plot of receptor S2R2 -NaF complex at a selected wavelength of 500 nm	132
4.37	UV-Vis titration spectra of receptor S2R3 (10^{-4} M in DMSO) with the incremental addition of NaAcO (10^{-2} M in distilled H ₂ O). Inset plot representing the absorption isotherm at 576 nm	133
4.38	B-H plot of receptor S2R3 - NaAcO complex at a selected wavelength of 576 nm	133
4.39	UV-Vis titration spectra of S2R4 (1×10^{-4} M, 9:1, v/v DMSO/H ₂ O) with the incremental addition of standard solution of NaAcO (1×10^{-2} M in distilled water). Inset showing binding isotherm at 574 nm	134
4.40	B-H plot of receptor S2R4 - NaAcO complex at a selected wavelength of 574 nm	134
4.41	UV-Vis titration spectra of receptor S2R5 (10^{-4} M in DMSO) with the incremental addition of NaAcO (10^{-2} M in distilled H ₂ O). Inset plot representing the absorption isotherm at 489 nm	135

4.42	B-H plot of receptor S2R5 - NaAcO complex at a selected wavelength of 489 nm	135
4.43	UV-Vis titration spectra of S2R4 (1×10^{-4} M, 9:1, v/v DMSO/H ₂ O) with the incremental addition of standard solution of NaF (1×10^{-2} M in distilled water). Inset showing binding isotherm at 575 nm	136
4.44	B-H plot of receptor S2R4 - NaF complex at a selected wavelength of 575 nm	136
4.45	Solvatochromic effect observed with the addition of 1 eq. of TBAAcO to receptor solution (10^{-4} M) in various polar aprotic solvents. Top row: 10^{-4} M in different solvents; Bottom row: S2R4 + AcO ⁻ ion	138
4.46	UV-Vis absorption spectra of receptor S2R4 (1×10^{-4} M) in various polar aprotic solvents with the addition of 1 eq. of TBAAcO (10^{-2} M in dry DMSO)	138
4.47	UV-Vis spectra of S2R4 (1×10^{-4} M in THF) upon addition of 1 equiv. of TBA salts of F ⁻ , AcO ⁻ and H ₂ PO ₄ ⁻ ions (1×10^{-2} M in dry DMSO)	139
4.48	Colour change of S2R4 (1×10^{-4} M in THF) upon addition of 1 equiv. of F ⁻ , AcO ⁻ and H ₂ PO ₄ ⁻ (1×10^{-2} M as TBA salts in dry DMSO)	139
4.49	Solvatochromic effect observed with the addition of 1 equiv. of TBAH ₂ PO ₄ to receptor solution S2R4 (1×10^{-4} M) in various polar aprotic solvents	140
4.50	Solvatochromic effect observed with the addition of 1 equiv. of TBAF to receptor solution S2R4 (1×10^{-4} M) in various polar aprotic solvents	140
4.51	UV-Vis spectra of S2R4 (1×10^{-4} M in DMSO) upon addition of a drop of mouthwash, seawater and vinegar Color change of S2R1 , S2R2 , S2R3 and S2R4 (1×10^{-4} M in DMSO)	141
4.52	upon addition of a drop of mouthwash, seawater and vinegar	142
4.53	Color change of receptor S2R4 upon dry grinding of receptor S2R4 with 1 equiv. of TBAAcO; S2R4 alone (left), S2R4 + TBAAcO (right)	142
4.54(a)	Cyclic voltammogram of receptor S2R1 (5×10^{-5} M) with incremental addition of TBAAcO ion (0-1 equiv.)	144
4.54(b)	Cyclic voltammogram of receptor S2R2 (5×10^{-5} M) with incremental addition of TBAAcO ion (0-1 equiv.)	144
4.54(c)	Cyclic voltammogram of receptor S2R3 (5×10^{-5} M) with incremental addition of TBAAcO ion (0-1 equiv.)	145
4.54(d)	Cyclic voltammogram of receptor S2R4 (5×10^{-5} M) with incremental addition of TBAAcO ion (0-1 equiv.)	145

	Cyclic voltammogram of receptor S2R5 ($5 \times 10^{-5} \text{M}$) with incremental addition of TBAAcO ion (0-1 equiv.)	146
4.54(e)	$^1\text{H-NMR}$ titration of receptor S2R4 with incremental addition of TBAOAc ion (0-1 eq.)	147
4.55	$^1\text{H NMR}$ titration of receptor S2R3 with incremental addition of TBAAcO ion (0-2 equiv.)	148
4.56	UV-Vis titration spectra of receptor S2R4 (DMSO/Tris HCl (9:1, v/v, 10^{-4}M) with incremental addition of standard solution of TBAAcO ($1 \times 10^{-2} \text{M}$ in dry DMSO). Inset showing the absorption isotherm at 569 nm	149
4.57	B-H plot of receptor S2R4 - TBAAcO complex (buffer media) at a selected wavelength of 569 nm	149
4.58	Optimized geometry of the receptor S2R4 in gas phase	150
4.59(a)	HOMO of the receptor S2R4 in gas phase	151
4.59(b)	LUMO of the receptor S2R4 in gas phase	151
4.59(c)	Optimized structure of the deprotonated receptor S2R4 in acetone	151
4.60(a)	HOMO of the deprotonated receptor S2R4 in acetone	151
4.61(b)	LUMO of the deprotonated receptor S2R4 in acetone	152
4.60(c)	Schematic representation of (a) chemical structure of deprotonated receptor S2R4 (b) DFT derived optimized structure of the deprotonated receptor S2R4 in DCM. Isosurface in (c) representing distribution of HOMO and (d) LUMO in deprotonated receptor S2R4	152
4.61	UV-Vis spectra of the receptor S2R4 in gas phase, in solvents such as DCM and acetone with addition of AcO^- ion	153
4.62	CHAPTER 5	
5.1	FT-IR spectrum of S3R1	161
5.2	FT-IR spectrum of S3R2	162
5.3	FT-IR spectrum of S3R3	162
5.4	$^1\text{H NMR}$ spectrum of S3R1	163
5.5	$^1\text{H NMR}$ spectrum of S3R2	163
5.6	$^1\text{H NMR}$ spectrum of S3R3	164
5.7	Color change of the receptors S3R1 , S3R2 and S3R3 ($1 \times 10^{-5} \text{M}$ in DMSO) with the addition of 1 eq. of TBA salts of anions ($1 \times 10^{-2} \text{M}$ in DMSO)	165
5.8	UV-visible absorption spectra of S3R1 ($1 \times 10^{-5} \text{M}$ in DMSO) upon addition of 1 equiv. of various anions as TBA salts	166
5.9	UV-visible absorption spectra of S3R2 ($1 \times 10^{-5} \text{M}$ in DMSO) upon addition of 1 equiv. of various anions as TBA salts	166
	UV-visible absorption spectra of S3R3 ($1 \times 10^{-5} \text{M}$ in DMSO) upon	

5.10	addition of 1 equiv. of various anions as TBA salts	167
5.11	UV-Vis titration spectra of receptor S3R1 (10^{-5} M in DMSO) with the incremental addition of TBAF (10^{-2} M in DMSO); Inset plot representing the variation of absorbance with increasing concentration of TBAF	168
5.12	UV-Vis titration spectra of receptor S3R1 (10^{-5} M in DMSO) with the incremental addition of TBAH ₂ PO ₄ (10^{-2} M in DMSO); Inset plot representing the variation of absorbance with increasing concentration of TBAH ₂ PO ₄	168
5.13	UV-Vis titration spectra of receptor S3R1 (10^{-5} M in DMSO) with the incremental addition of TBAAcO (10^{-2} M in DMSO); Inset plot representing the variation of absorbance with increasing concentration of TBAAcO	169
5.14	B-H plot for S3R1 -TBAF complex	169
5.15	B-H plot for S3R1 -TBAH ₂ PO ₄ complex	170
5.16	B-H plot for S3R1 -TBAAcO complex	170
5.17	UV-Vis titration spectra of receptor S3R2 (10^{-5} M in DMSO) with the incremental addition of TBAF (10^{-2} M in DMSO); Inset plot representing the variation of absorbance with increasing concentration of TBAF	171
5.18	UV-Vis titration spectra of receptor S3R2 (10^{-5} M in DMSO) with the incremental addition of TBAH ₂ PO ₄ (10^{-2} M in DMSO); Inset plot representing the variation of absorbance with increasing concentration of TBAH ₂ PO ₄	172
5.19	UV-Vis titration spectra of receptor S3R2 (10^{-5} M in DMSO) with the incremental addition of TBAAcO (10^{-2} M in DMSO); Inset plot representing the variation of absorbance with increasing concentration of TBAAcO	172
5.20	B-H plot for S3R2 -TBAF complex	173
5.21	B-H plot for S3R2 -TBAH ₂ PO ₄ complex	173
5.22	B-H plot for S3R2 -TBAAcO complex	174
5.23	UV-Vis titration spectra of receptor S3R3 (10^{-5} M in DMSO) with the incremental addition of TBAF (10^{-2} M in DMSO); Inset plot representing the variation of absorbance with increasing concentration of TBAF	175
5.24	UV-Vis titration spectra of receptor S3R3 (10^{-5} M in DMSO) with the incremental addition of TBAH ₂ PO ₄ (10^{-2} M in DMSO); Inset plot representing the variation of absorbance with increasing concentration of TBAH ₂ PO ₄	175
5.25	UV-Vis titration spectra of receptor S3R3 (10^{-5} M in DMSO) with the incremental addition of TBAAcO (10^{-2} M in DMSO); Inset plot	176

	representing the variation of absorbance with increasing concentration of TBAAcO	
5.26	B-H plot for S3R3 -TBAF complex	176
5.27	B-H plot for S3R3 -TBAH ₂ PO ₄ complex	177
5.28	B-H plot for S3R3 -TBAAcO complex	177
5.29	UV-Vis titration spectra of receptor S3R1 (10 ⁻⁵ M in DMSO) with the incremental addition of NaF (10 ⁻² M in H ₂ O); Inset plot representing the variation of absorbance with increasing concentration of NaF	178
5.30	UV-Vis titration spectra of receptor S3R1 (10 ⁻⁵ M in DMSO) with the incremental addition of NaAcO (10 ⁻² M in H ₂ O); Inset plot representing the variation of absorbance with increasing concentration of NaAcO	179
5.31	UV-Vis titration spectra of receptor S3R2 (10 ⁻⁵ M in DMSO) with the incremental addition of NaF (10 ⁻² M in H ₂ O); Inset plot representing the variation of absorbance with increasing concentration of NaF	179
5.32	UV-Vis titration spectra of receptor S3R2 (10 ⁻⁵ M in DMSO) with the incremental addition of NaAcO (10 ⁻² M in H ₂ O); Inset plot representing the variation of absorbance with increasing concentration of NaAcO	180
5.33	UV-Vis titration spectra of receptor S3R3 (10 ⁻⁵ M in DMSO) with the incremental addition of NaF (10 ⁻² M in H ₂ O); Inset plot representing the variation of absorbance with increasing concentration of NaF	180
5.34	UV-Vis titration spectra of receptor S3R3 (10 ⁻⁵ M in DMSO) with the incremental addition of NaAcO (10 ⁻² M in H ₂ O); Inset plot representing the variation of absorbance with increasing concentration of NaAcO	181
5.35	B-H plot for S3R1 -NaF complex	181
5.36	B-H plot for S3R1 -NaAcO complex	182
5.37	B-H plot for S3R2 -NaF complex	182
5.38	B-H plot for S3R2 -NaAcO complex	183
5.39	B-H plot for S3R3 -NaF complex	183
5.40	B-H plot for S3R3 -NaAcO complex	184
5.41	Color change of receptors S3R1 , S3R2 and S3R3 (1x10 ⁻⁵ M in HEPES: DMSO, 1:9, v/v) with the addition of TBA salt of anions (1x10 ⁻² M in DMSO)	185
5.42	UV-visible absorption spectra of S3R1 (1x10 ⁻⁵ M in HEPES: DMSO, 1:9 v/v) upon addition of 1 equiv. of various anions as TBA salts (1x10 ⁻² M in DMSO)	186

5.43	UV-visible absorption spectra of S3R2 (1×10^{-5} M in HEPES: DMSO, 1:9 v/v) upon addition of 1 equiv. of various anions as TBA salts (1×10^{-2} M in DMSO)	186
5.44	UV-visible absorption spectra of S3R3 (1×10^{-5} M in HEPES: DMSO, 1:9 v/v) upon addition of 1 equiv. of various anions as TBA salts (1×10^{-2} M in DMSO)	187
5.45	UV-Vis titration spectra of receptor S3R1 (1×10^{-5} M in HEPES: DMSO, 1:9 v/v) with the incremental addition of TBAAcO (10^{-2} M in DMSO); Inset plot representing the variation of absorbance with increasing concentration of TBAAcO	187
5.46	UV-Vis titration spectra of receptor S3R2 (1×10^{-5} M in HEPES: DMSO, 1:9 v/v) with the incremental addition of TBAAcO (10^{-2} M in DMSO); Inset plot representing the variation of absorbance with increasing concentration of TBAAcO	188
5.47	UV-Vis titration spectra of receptor S3R3 (1×10^{-5} M in HEPES: DMSO, 1:9 v/v) with the incremental addition of TBAAcO (10^{-2} M in DMSO)	188
5.48	^1H NMR titration studies of receptor S3R1 with the addition of TBAAcO	190
5.49	^1H NMR titration studies of receptor S3R2 with the addition of TBAAcO	191
5.50	^1H NMR titration studies of receptor S3R3 with the addition of TBAAcO	191
5.51	Molecular orbitals of receptors S3R1 , S3R2 and S3R3 and receptor-anion complex with their energy levels at 6-31+G (d,p)	193
5.52	DFT derived UV-Vis spectra of the S3R1 and S3R1 + F^- complex	194
5.53	DFT derived UV-Vis spectra of the S3R2 and S3R2 + F^- complex	195
5.54	DFT derived UV-Vis spectra of the S3R3 and S3R3 + F^- complex	195
5.55	(A) Fluorescence observed using <i>E.coli</i> BL21 at different time intervals of the growth in LB Agar plate, (B) fluorescence observed by acetic acid, water and LB agar, respectively, on a glass plate	197
CHAPTER 6		
6.1	FT-IR spectrum of receptor S4R1	204
6.2	FT-IR spectrum of receptor S4R2	204
6.3	FT-IR spectrum of receptor S4R3	205
6.4	^1H -NMR spectrum of receptor S4R1	205
6.5	^1H -NMR spectrum of receptor S4R2	206
6.6	^1H -NMR spectrum of receptor S4R3	206
6.7	ESI-MS spectrum of receptor S4R1	207
6.8	ESI-MS spectrum of receptor S4R2	207
6.9	ESI-MS spectrum of receptor S4R3	208

6.10	Color change of the receptors S4R1 , S4R2 and S4R3 (10^{-5} M in ACN) with the addition of 1 eq. of TBA salts of anions (10^{-3} M in ACN)	209
6.11	UV-visible absorption spectra of S4R1 (10^{-5} M in ACN) upon addition of 1 equiv. of various anions as TBA salts (10^{-3} M in ACN)	209
6.12	UV-visible absorption spectra of S4R2 (10^{-5} M in ACN)) upon addition of 10 equiv. of various anions as TBA salts (10^{-3} M in ACN)	210
6.13	UV-visible absorption spectra of S4R3 (10^{-5} M in ACN) upon addition of 10 equiv. of various anions as TBA salts (10^{-3} M in ACN)	210
6.14	UV-Vis titration spectra of receptor S4R1 (10^{-5} M in ACN) with the incremental addition of TBA salts of anions (10^{-3} M in ACN); Inset plot representing the variation of absorbance with concentration of: (a) Receptor S4R1 + TBAF, (b) Receptor S4R1 + TBAOAc; (c) Receptor S4R1 + TBAH ₂ PO ₄ ; (d) Receptor S4R1 + TBACN	212
6.15	B-H plot for 1:1 complex (a) Receptor S4R1 : TBAF, (b) Receptor S4R1 : TBAOAc; (c) Receptor S4R1 : TBAH ₂ PO ₄ ; (d) Receptor S4R1 : TBACN	213
6.16	UV-Vis titration spectra of receptor S4R2 (10^{-5} M in ACN) with the incremental addition of TBAOAc (10^{-3} M in ACN)	213
6.17	Fluorescence spectra of receptor S4R1 (10^{-5} M in ACN) with the incremental addition of TBAF(10^{-3} M in ACN)	214
6.18	Fluorescence spectra of receptor S4R1 (10^{-5} M in ACN) with the incremental addition of TBAAcO(10^{-3} M in ACN)	214
6.19	Fluorescence spectra of receptor S4R1 (10^{-5} M in ACN) with the incremental addition of TBACN(10^{-3} M in ACN)	215
6.20	Fluorescence spectra of receptor S4R1 (10^{-5} M in ACN) with the incremental addition of TBAH ₂ PO ₄ (10^{-3} M in ACN)	215
6.21	Fluorescence spectra of receptor S4R2 (10^{-5} M in ACN) with the incremental addition of TBAF (10^{-3} M in ACN)	216
6.22	Fluorescence spectra of receptor S4R2 (10^{-5} M in ACN) with the incremental addition of TBAAcO (10^{-3} M in ACN)	216
6.23	Fluorescence spectra of receptor S4R3 (10^{-5} M in ACN) with the incremental addition of TBAF (10^{-3} M in ACN)	217
6.24	Fluorescence spectra of receptor S4R3 (10^{-5} M in ACN) with the incremental addition of TBAAcO (10^{-3} M in ACN)	217
6.25	Color change of receptor S4R1 (ACN: Tris HCl, 8:2, v/v) with the addition of TBAF, TBAOAc, TBAH ₂ PO ₄ and TBACN	218
6.26	UV-Vis titration spectra of receptor S4R1 (10^{-5} M in ACN) with the incremental addition of NaF (10^{-3} M in distilled water); Inset plot representing the absorption isotherm at 455 nm	218
6.27	UV-Vis titration spectra of receptor S4R1 (10^{-5} M in ACN) with the	219

	incremental addition of NaAcO (10^{-3} M in distilled water); Inset plot representing the absorption isotherm at 457 nm	
6.28	B-H plot for 1:1 complex of S4R1 -NaF	219
6.29	B-H plot for 1:1 complex of S4R1 -NaAcO	220
6.30	(a) Color change of receptor S4R1 with the addition of 1 eq. of NaAsO ₂ ; (b) UV-Vis titration spectra of receptor S4R1 (10^{-5} M in ACN) with the incremental addition of NaAsO ₂ (10^{-3} M in distilled water); Inset plot representing the variation of absorbance with concentration of NaAsO ₂ at 500 nm	221
6.31	B-H plot for 1:1 complex of S4R1 -NaAsO ₂	221
6.32	Linear calibration curve between concentration of AsO ₂ ⁻ (from 0.0 M to 7.0×10^{-6} M) and absorbance of receptor S4R1 + AsO ₂ ⁻ complex, monitored wavelength at 500 nm	222
6.33	¹ H-NMR spectra of receptor S4R1 with the addition of 1 equiv. of TBAF, TBAAcO and TBAH ₂ PO ₄	223
6.34	Cyclic voltammogram of receptor S4R1 with the incremental addition of TBAH ₂ PO ₄	224
6.35	UV-Vis spectra with the addition of increasing amounts of DNA at room temperature in Tris-HCl/NaCl buffer (pH 7.2) to receptor S4R1	225
6.36	UV-Vis spectra with the addition of sprouted potato extract to receptor S4R1 (10^{-5} M in ACN)	226
6.37	Calibration plot for the quantitative estimation of phosphate in detergent sample	228

CHAPTER 7

7.1	FT-IR spectrum of receptor S5R1	234
7.2 (a)	¹ H-NMR spectrum of receptor S5R1	234
7.2 (b)	¹³ C-NMR spectrum of receptor S5R1	235
7.3	ESI-MS spectrum of receptor S5R1	235
7.4	Colour change of the receptors S5R1 (10^{-4} M in DMSO) with the addition of 2 equiv. of TBA salts of anions (10^{-2} M in DMSO)	236
7.5	UV-Vis absorption spectra of S5R1 (1×10^{-5} M in ACN) upon addition of 2 equiv. of various anions as TBA salts (10^{-2} M in DMSO)	237
7.6	Fluorometric response of the receptors S5R1 (1×10^{-5} M in ACN) with the addition of 2 eq. of TBA salts of anions (10^{-2} M in DMSO)	238
7.7	Fluorescence spectra of S5R1 (1×10^{-5} M in ACN) upon addition of 2 equiv. of various anions as TBA salts (10^{-2} M in DMSO)	238
7.8	UV-Vis titration spectra of receptor S5R1 (10^{-5} M in DMSO) with the incremental addition of TBA salts of anions (10^{-2} M in DMSO); Inset plot representing the plot of absorbance vs concentration of TBAF	240
7.9 (a)	B-H plot for S5R1 -TBAF complex	240

7.9 (b)	Job's plot for S5R1 -TBAF complex	241
7.10	Fluorescence spectra of receptor S5R1 (10^{-5} M in DMSO) with the incremental addition of TBA salt of F^{-} ion (10^{-2} M in DMSO)	242
7.11	Color change of S5R1 with the addition of 2 equiv. of TBAOH	243
7.12	Fluorometric response of S5R1 with the addition of 2 equiv. of TBAOH	243
7.13	UV-Vis spectra of S5R1 with the addition of 2 equiv. of TBAOH	243
7.14	PL spectra of S5R1 with the addition of 2 equiv. of TBAOH	244
7.15	1H -NMR spectra of S5R1 with the addition of 2 equiv. of TBAF	245
7.16	Photographs showing the gelation behavior of S5R1 in selected solvents (1) DMSO, (2) DMF, (3) Cyclohexane, (4) Chloroform, (5) Methanol, (6) ACN, (7) n-Hexane, (8) Diethyether, (9) DCM, (10) THF, (11) DMF: H_2O (1:2, v/v), (12) DMSO: H_2O (1:2, v/v), (13) Propyl alcohol, (14) Ethanol and (15) Dioxane	246
7.17	Comparison of UV-Vis spectra of S5R1 in the solution and gel state	247
7.18	Comparison of fluorescence spectra of S5R1 in the solution and gel state	247
7.19	Photographs showing the phase changes of gel (26 mg/mL) of S5R1 (obtained from DMSO upon addition of 2equiv. of TBA salts of anions	248
7.16	Gel-sol transition and fluorescent response of S5R1 with the addition of F^{-} ion	248

LIST OF SCHEMES

CHAPTER 1

1.1	Representation of Hofmeister series	7
1.2	Macrocyclic receptors with ammonium bridgehead centres and alkyl linkers	9
1.3	Macrobicyclic and macrotricyclic ammonium based receptors(cryptands)	9
1.4	Receptors bearing quaternary ammonium groups and alkyl linkers	10
1.5	Neutral zwitter ionic receptors	10
1.6	Neutral cyclophane based receptors	10
1.7	A series of acyclic tripodal receptors bearing amide groups	11
1.8	Bicyclic fused ring system with guanidinium motif	11
1.9	Porphyrin based receptor	11

CHAPTER 2

2.1	Synthesis of receptor R	34
2.2	General scheme of synthesis of receptor L	34
2.3	Proposed binding mechanism of F^- ion by receptor R	66
2.4	Proposed binding mechanism of AcO^- ion by receptor R	67
2.5	Proposed binding mechanism of L with AcO^- ion	67
2.6	Proposed binding mechanism of L with F^- ion	68

CHAPTER 3

3.1	Synthesis of S1R1	71
3.2	Synthesis of S1R2	72
3.3	Proposed binding mechanism of receptor S1R1 with F^- ion	100
3.4	Proposed binding mechanism of receptor S1R1 with AcO^- ion	100
3.5	Proposed binding mechanism of receptor S1R2 with AcO^- ion	101

CHAPTER 4

4.1	Synthesis of receptor S2R1	106
4.2	Synthesis of receptor S2R2	106
4.3	Synthesis of receptor S2R3	107
4.4	Synthesis of receptor S2R4	108
4.5	Synthesis of receptor S2R5	109

4.6	Proposed binding mechanism of receptor S2R4 with AcO^- ion	155
------------	--	-----

CHAPTER 5

5.1	General scheme for the synthesis of receptors S3R1 , S3R2 and S3R3	160
------------	---	-----

5.2	Proposed binding mechanism of receptors S3R1 , S3R2 and S3R3 with anions	196
------------	---	-----

CHAPTER 6

6.1	Synthesis of receptor S4R1	202
------------	-----------------------------------	-----

6.2	Synthesis of receptor S4R2	202
------------	-----------------------------------	-----

6.3	Synthesis of receptor S4R3	203
------------	-----------------------------------	-----

6.4	Proposed binding mechanism of receptor S4R1 with active anions	229
------------	---	-----

CHAPTER 7

7.1	Synthesis of receptor S5R1	233
------------	-----------------------------------	-----

7.2	Proposed binding mechanism of S5R1 with F^- ion	249
------------	---	-----

LIST OF TABLES

CHAPTER 2

- 2.1 Observed rate constant for the reaction of receptor **L** with AcO^- and F^- ion 56
- 2.2 Distribution of HOMO, LUMO orbital and corresponding energy gap of receptor **R** with F^- ion and AcO^- ions, obtained from TD-DFT calculations 62
- 2.3 Mulliken charges on O-H9, O-H14 in the receptor molecule upon binding of anions calculated at the (B3LYP) along with 6-311++G (d) basis set with the structural representation of receptor **R** 62
- 2.4 Binding constant, binding ratio and detection limit of receptors **R** and **L** 66

CHAPTER 3

- 3.1 Binding constant, binding ratio and detection limit of receptors **S1R1** and **S1R2** with various anions 97

CHAPTER 4

- 4.1 Crystallographic data of receptor **S2R5** 115
- 4.2 Changes in absorption maxima of receptor **S2R4** in various solvents upon addition of 1 eq. of TBAAcO in dry DMSO 138
- 4.3 Binding constant and detection limit of receptors in the presence of various anions 154

CHAPTER 5

- 5.1 Binding constant and detection limit of receptors **S3R1**, **S3R2** and **S3R3** with active anions 189
- 5.2 Energy distribution of receptor and receptor-anion complex 194

CHAPTER 6

- 6.1 Binding constant, binding ratio and detection limit values of receptor **S4R1** 211

CHAPTER 7

- 7.1 Gelation properties of **S5R1** 246

NOMENCLATURE

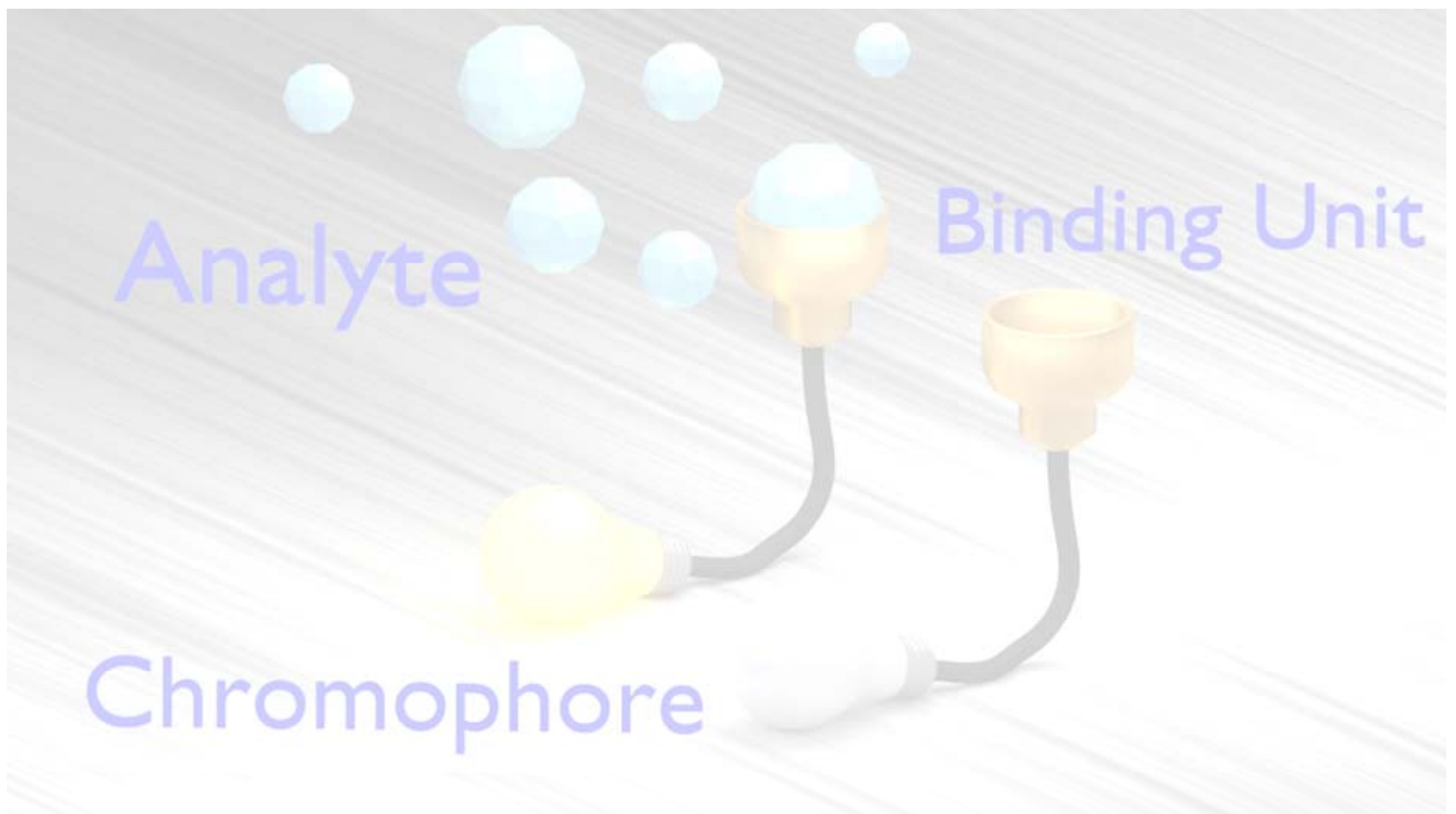
Abbreviation

ACN	Acetonitrile
AcOH	Acetic acid
AcO ⁻	Acetate ion
AsO ₂ ⁻	Arsenite
B-H	Benesi-Hildebrand
Br ⁻	Bromide
Cl ⁻	Chloride
CN ⁻	Cyanide
DCM	Dichloromethane
DFT	Density Functional Theory
DMF	Dimethylformamide
DMSO	Dimethylsulfoxide
DMSO- <i>d</i> ₆	Dimethylsulfoxide-deuterated
ESI	Electron Spray Ionized
EtOH	Ethyl alcohol
Equiv.	Equivalence
F ⁻	Fluoride
FT-IR	Fourier Transform Infra-Red
¹ H-NMR	Proton Nuclear Magnetic Resonance
H ₂ PO ₄ ⁻	Dihydrogen phosphate
HSO ₄ ⁻	Hydrogen sulfate
I ⁻	Iodide
ICT	Internal Charge Transfer
MeOH	Methanol
mp	Melting point
MS	Mass Spectra
NO ₃ ⁻	Nitrate
NaF	Sodium Fluoride
NaAcO	Sodium Acetate
ORTEP	Oak Ridge Thermal Ellipsoid Plot
RT	Room Temperature
SCXRD	Single Crystal X-Ray Diffraction
TBA	Tetra Butyl Ammonium
THF	Tetrahydrofuran
TMS	Tetramethylsilane
TLC	Thin Layer Chromatography
UV-Vis	Ultraviolet-Visible
WHO	World Health Organization

SYMBOLS AND UNITS

α	Alpha
β	Beta
cm	Centimetre
$^{\circ}$	Degree
$^{\circ}\text{C}$	Degree Celsius
δ	Delta
γ	Gamma
g	Gram
>	Greater than
h	Hour
Hz	Hertz
$^{-1}$	Inverse
λ	Lambda
<	Lesser than
L	Litre
MHz	Megahertz
mL	Millilitre
mmol	Millimole
min	Minute
M	Molar
μ	Mu
nm	Nanometre
ppm	Per parts million
θ	theta

CHAPTER 1
INTRODUCTION



1.1 SUPRAMOLECULAR CHEMISTRY

Supramolecular chemistry is a highly multidisciplinary field of science which impinges on various other disciplines, such as the traditional areas of organic and inorganic chemistry, needed to synthesize the precursors for a supermolecule; physical chemistry, to understand the properties of supramolecular systems and computational modelling to understand complex supramolecular behavior. Prof. Jean-Marie Lehn, has defined supramolecular chemistry as ‘the chemistry of molecular assemblies and of the intermolecular bond’. More commonly, it is described as ‘the chemistry of the non-covalent bond’ and ‘non-molecular chemistry’ (Steed et al. 2009). In the year 1987, Cram, Lehn and Pedersen were jointly honored with Nobel Prize for their important findings in the field. The general structural aspects of supramolecular chemistry are shown in Fig. 1.1.

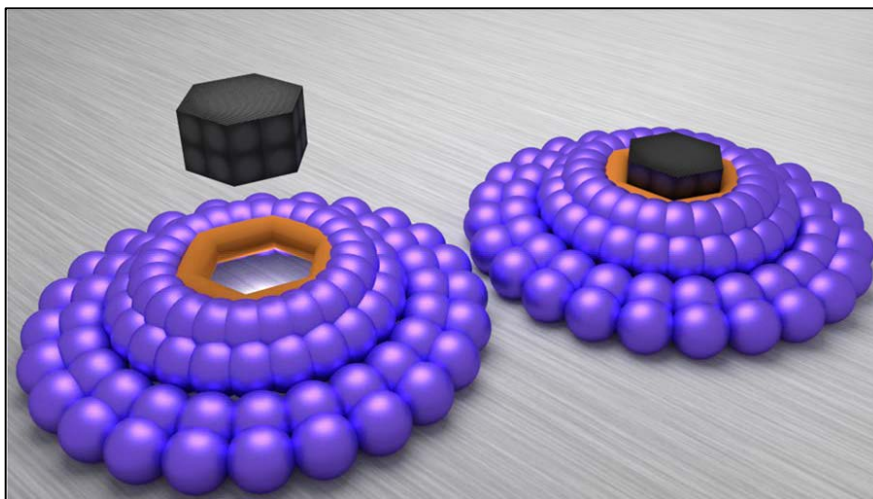


Fig. 1.1 Representation of the structural aspects of supramolecular Chemistry

1.2 Host-Guest Chemistry

Supramolecular chemistry involves the interactions of two or more components. The term “host-guest chemistry” could be correlated to complexation phenomenon. It involves the binding of the host molecule with the guest molecule forming a host-guest complex. Donald James Cram has defined host and guest components as follows. An ion

or an organic molecule whose binding sites converge in the complex is called as the host component. An ion or molecule whose binding sites diverge in a complex is called as the guest component. A region of the host or guest that is of correct size, geometry and chemical nature which can interact through non-covalent interactions is referred to as the binding site. In supramolecular chemistry, a molecular complex is said to be highly structured if it is composed of at least one host and one guest component. For an efficient host-guest relationship, there should be complementary stereo-electronic arrangement of binding sites in host and guest. Simple guests are quite abundant because the location of divergent binding sites does not involve more organization. Hosts with appropriate binding sites are rare to find, which necessitates them to be designed and synthesized. It all means to say that the binding and supporting parts of hosts which when compared to the guests have to be quite larger.

1.3 ANIONS

By definition, anions are the species that have gained an electron and are negatively charged. They possess more number of electrons than protons. Though many elements form stable atomic cations or positively charged ions, only a hand few form stable atomic anions. Elements belonging to Group 17 or the halides F, Cl, Br and I readily form anions bearing -1 charge (F^- , Cl^- , Br^- and I^-). And, group 16 elements O and S form atomic anions with -2 charge (O^{2-} and S^{2-}). Molecular ions or the polyatomic ions are abundant in nature. They are stable chemical species which retain their structure in crystals as well as in solution. Mostly, polyatomic ions are classified into three categories. (i) Diatomic anions E.g. OH^- and CN^- (ii) Anions with carbon E.g. CO_3^- , CH_3COO^- and $C_2O_4^{2-}$ (iii) oxoanions: They possess a central atom surrounded by one to four oxygen atoms. Eg. SO_4^{2-} , SO_3^{2-} , NO_3^- , NO_2^- , ClO_4^- etc

1.3.1 Environmentally and biologically important anions:

1.3.1.1 Fluoride (F^-)

Fluoride is known to have multiple implications on human health. Fluoride gains entry into the human body through the gastrointestinal tract and is readily absorbed in the stomach (Whitford 1996). Fluoride is known to decrease the incidence of dental caries and enhance the rate of enamel remineralization (Bratthall et al. 1996; Margolis and Moreno 1990; Murray 1993). However, excessive fluoride ingestion during tooth formation would lead to hypomineralization of dental enamel leading to dental fluorosis (Fejerskov et al. 1987, 1994; Richards et al. 1986). Long term exposure of smaller amounts of fluoride in drinking water can lead to skeletal fluorosis (Evans and Darvell 1995).

1.3.1.2 Cyanide (CN^-)

Cyanide is occasionally found in drinking water as a result of industrial contamination and has even encroached the dietary sources. The toxicity of cyanide is well known for its propensity to bind to the iron in cytochrome c oxidase affecting the electron transport chain and resulting in hypoxia. Cyanide induced occasional fire related deaths have been reported by several researchers (Anderson and Harland 1982; Becker 1985; Levin et al. 1990; Lou et al. 2009; Matsubara et al. 1990; Mayes 1991; Way 1984). Nevertheless, cyanide is extensively used as raw materials for synthetic fibers, resins, herbicides (Tsui et al. 2012).

1.3.1.3 Acetate (AcO^-)

Acetate, being a planar oxy-anion plays important role in chemical, environmental and biochemical metabolic process. Acetate are a common building block for biosynthesis. The fatty acids are produced by connecting C2 units derived from acetate (March 1992). They play an important role in nylon industry and also in the manufacture of paper, paints, dyes, plastics. Acetate, for example, is used as an indicator of organic decomposition in marine sediments based on the rate of acetate production and oxidation

(Christensen 1984; Sørensen et al. 1981). Also, it exhibits specific biochemical behavior in enzymes and antibodies (Vella 1990).

1.3.1.4 Phosphate (PO_4^{2-})

Phosphate is ubiquitous in biochemistry. Phosphate is usually the leaving group in metabolic reactions (Preiss and Handler 1958). Inorganic phosphates commonly used as fertilizer in agriculture are a potent cause for eutrophication of aquatic system when they runoff into rivers (Greenhalgh and Selman 2012). Maintenance of phosphate level at physiological conditions is crucial as it is one of the prime factors influencing bone health (Marks et al. 2010). Detergents are also a reservoir of polyphosphates which when let out from laundry or industries into the water sources could be a potent threat to aquatic system.

1.3.1.5 Arsenite (AsO_2^-)

Arsenic is a potent source of toxicity to the living system as it presents severe health issues at physiological level. Researchers have extensively studied the biogeochemistry of arsenic (Ferguson and Gavis 1972; M.S and Ph.D 1991) and found that arsenate is predominant in well oxidized water and arsenite is predominant in reduced environments. Owing to the relatively slow redox transformations (Masscheleyn et al. 1991), both arsenite and arsenate are found in either redox environment. Research indicates arsenite to be almost 25-60 times more toxic than arsenate and more mobile in the environment (M.S and Ph.D 1991).

1.4 ANION RECEPTOR CHEMISTRY:

The prominent feature of anions is their negative electrostatic charge which distinguishes themselves from other guest species. Also, the pre-organized placement of complementary binding sites on the receptors constitutes the basic design criteria. Combining above two features, it could be said that anion receptor chemistry involves in designing new synthetic receptors for quantifying and sensing anions (Sessler et al. 2006).

1.4.1 Challenges of Anion Receptor Chemistry:

The design of anion receptors involves the criteria of specificity arising from the pre-organized placement of complementary binding sites. Even if the above necessity is fulfilled, certain properties of anions make the task a little more challenging. They could be summarized as follows:

- i) Anions being larger than cations require larger receptors which can accommodate them. F^- , being the smallest anion has a radius comparable to that of K^+ (Shannon 1976) Cations are generally found as spherical species, with the exception of organic cations while anions exist in many shapes and sizes. Examples include: Halides – Spherical, SCN^- -linear, NO_3^- - planar, HPO_4^- -tetrahedral and PF_6^- octahedral. On the other hand, biologically important anions like nucleotides and proteins have complex shapes.(Fig 1.2)

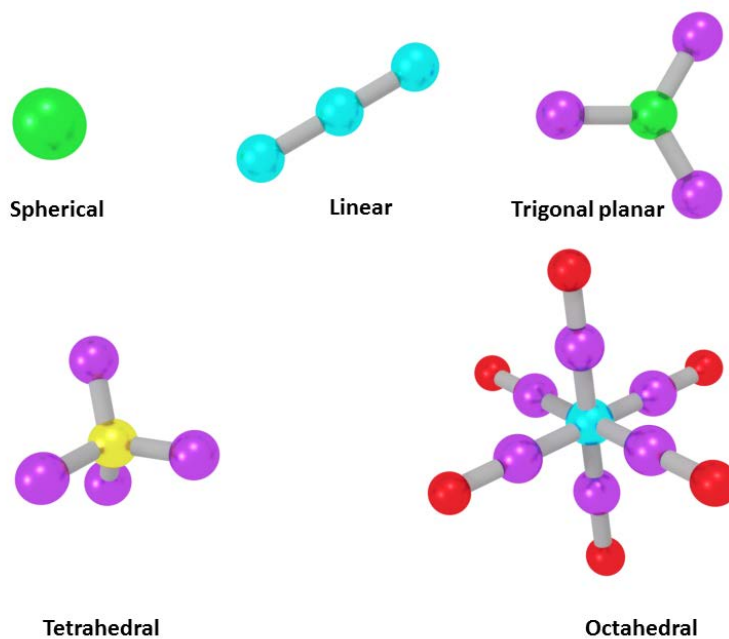


Fig 1.2 Different shapes and sizes of anions

- ii) Anions have high free energy of solvation and thus the nature of the solvent interferes in the anion binding event through the factors such as binding strength and selectivity.

Electrostatic interactions stabilize the anions in solution dwarfing other recognition forces. Hydroxylic solvents are potent enough to form strong hydrogen bond with anions. Therefore, a potential anion receptor has to face a tough competition with the solvent environment in an anion recognition event. Considering the example of a neutral receptor where the interaction with the anion is primly hydrogen bonding, it is less likely to be capable of competing with the polar protic solvation shell present around the target anion in a hydroxylic solvent. Thus, it can only function as an anion receptor in aprotic organic solvents. While a charged receptor incurs benefit from electrostatic effects and as a result it competes more effectively with polar protic solvents. Lastly it is the anion receptor that must not just compete with the solvent, but also with the counter anion paired with the target anion.

- iii) Anions may become protonated at low pH, tending to lose their negative charge. So, by virtue of the pH sensitive nature, receptors must function within the pH window of the target anions. This problem arises with the protonated receptors whose protonation window must be carefully looked upon. On the other part, neutral receptors and those containing permanent built-in charges designed to work in aprotic media overrule the above problem.
- iv) Anions being co-ordinatively saturated, bind to the receptor through weak interactions, such as hydrogen bonding and van der Waals interactions. Positively charged receptor is generally used in anion binding studies. Cation- anion binding event leads to either a solvent separated or contact-ion pair. Due to the difference in electrostatic charge, anion binds to neutral receptors despite there being large difference between cations and anions. Neutral receptors, devoid of the burden of competing with counter anion offer the possibility of enhanced selectivity. In order to overcome the non-directional nature of electrostatic interactions, introduction of a Lewis-acidic site would be more suitable as most anions are Lewis basic. This basically signifies the hydrogen bond acceptor and hydrogen bond donor property of the anions. The Lewis acid base interaction is strong and directional too. As the anions are polarizable, van der Waals interactions play a vital role in binding. This

case is encountered when anion has been encapsulated within the cavity of a host system and exhibit a high degree of surface area contact.

- v) Hydrophobicity is one of the factors influencing the selectivity of the receptor. It could be well explained with the Hofmeister series (HOFMEISTER 1888) which is the result of studies on the effect of salts on the solubility of the proteins (Scheme 1.9). This series orders anions by their decreasing hydrophobicity and consequent increase in the degree of aqueous solvation. Hydrophobicity could be used in the design of anion receptors to bias selectivity towards larger anions with low charge. Both hydrophobicity and Hofmeister series could be used in solvent extraction of anions from aqueous solution. Those anion receptors which perturb the Hofmeister series from its normal order help in the selective extraction of a particular anion.

Organic anions > ClO_4^- > SCN^- > I^- > salicylate > NO_3^- > Br^- > Cl^- > HCO_3^- > H_2PO_4^- > F^- > SO_4^{2-} > H_2PO_4^-

Scheme 1.1 Representation of Hofmeister series

1.4.2 History of Anion Receptor Chemistry:

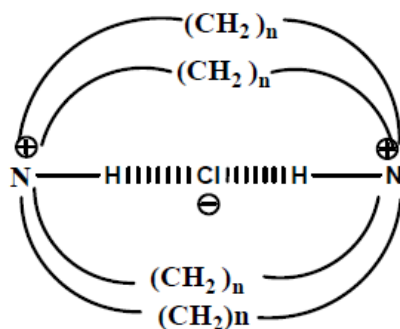
The design and synthesis of anion receptors commenced in 1968 by Simmons and Park, (Park and Simmons 1968) with a report on halide binding properties of macrobicyclic receptors with two ammonium bridgehead centers spanned by three alkyl linkers (Scheme 1.2). It showed high affinity for chloride when a linker having 7 to 10 methylene groups in length was introduced.

Following this, Lehn and coworkers (Graf and Lehn 1976) designed variety of macrobicyclic and macrotricyclic ammonium based receptors (cryptands) which demonstrated the optimization of the anion fit for a given charged cavity for stronger binding (Scheme 1.3). Further they extended their work to the synthesis of protonated cryptands to bind linear species like azide (Scheme 1.4). The crystal structure of the azide bound receptor showed the presence of hydrogen-bonding interactions. It was

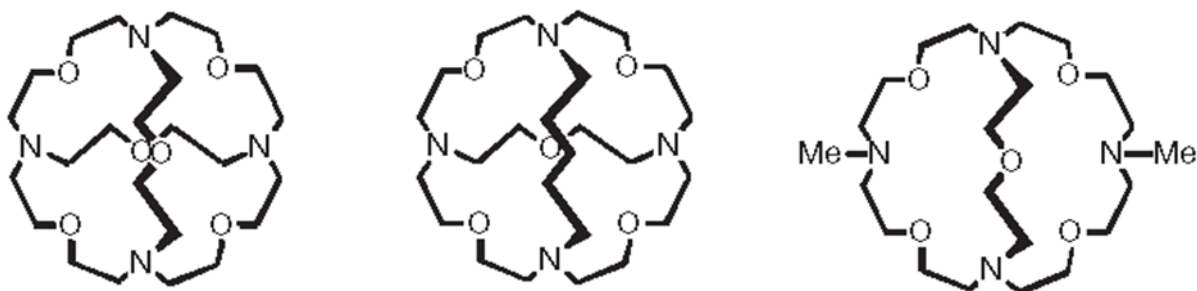
Schmidtchen (Schmidtchen 1977; Schmidtchen and Müller 1984) who designed and synthesized a series of receptors having quaternary ammonium groups arranged in a tetrahedral fashion that bind anions in their cage like structure through electrostatic interactions. The selectivity towards anions was increased by altering the alkyl chain length between ammonium centers (Scheme 1.5). Since ammonium based receptors were positively charged, they were accompanied with counter ions which made them compete with the anions in the binding process. To overcome this issue, neutral zwitter ionic receptors were synthesized by the same group for the binding of fluoride ion (Scheme 1.6). On the contrary, Pascal and coworkers (Pascal Jr. et al. 1986) reported the hydrogen bonding between neutral receptors and anions, wherein the receptors included groups like amide, urea or pyrroles within the cyclophane host (Scheme 1.7). In 1993, a series of acyclic tripodal receptors containing amide groups were synthesized by Reinhoudt and coworkers (Valiyaveetil et al. 1993) as shown in Scheme 1.8 measured by conductivity measurements in acetonitrile.

Apart from these pioneering works, nature has also contributed in the validation of some naturally available compounds as receptors. Positively charged guanidinium group present in the biological system as a side chain of arginine, helps in the binding of anions. These receptors by virtue of the strong electrostatic interactions allow binding of anions in aqueous as well as partially aqueous environment. Using guanidinium unit as a binding motif, Lehn and coworkers (Dietrich et al. 1978) designed a synthetic anion receptor which showed relatively poor anion affinities. Schmidtchen further incorporated bicyclic fused ring system into the guanidinium motif, and hydrogen bonding array as in urea was observed which showed activity towards carboxylates and phosphates (Scheme 1.9). In 1980's studies on the role of porphyrin based receptors like sapphyrin, a pentapyrrolic macrocycle was reported (Bauer et al. 1983; Shionoya et al. 1992) (Scheme 1.10). As it was susceptible to protonation readily, generation of monocationic and dicationic macrocycle was much easier. In an attempt to crystallize bis(hexa)fluorophosphate salt of porphyrin, rather a mixed fluoride/bis(hexa)fluorophosphate salt were obtained. This proved the binding of fluoride ion

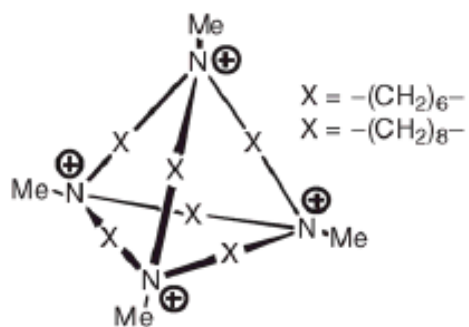
within the macrocyclic core doubly protonated sapphyrin. Pyrrole based cyclic and acyclic receptors, having relatively good anion binding properties have been extensively studied. With this a rich anion complexation chemistry, pyrrole based receptors have been extensively worked upon by Gale, Sessler and others (Brooks et al. 2006; Gale et al. 1996; Sessler and Seidel 2003).



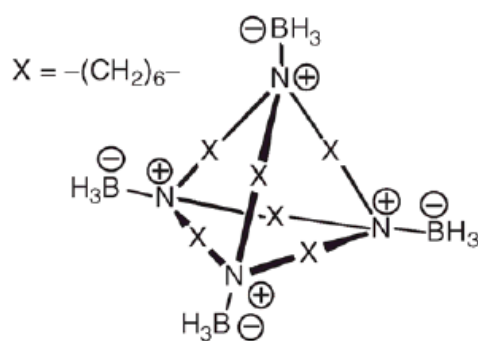
Scheme 1.2 Macrobicyclic receptors with ammonium bridgehead centres and alkyl linkers



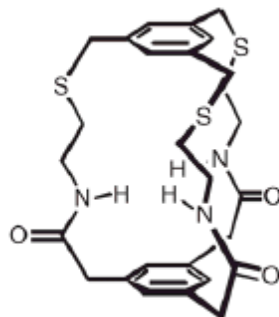
Scheme 1.3 Macrobicyclic and macrotricyclic ammonium based receptors (cryptands)



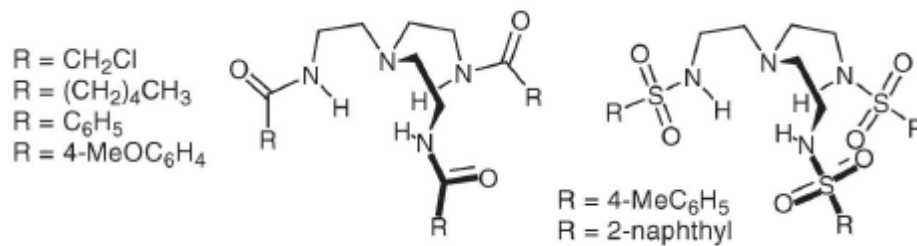
Scheme 1.4 Receptors bearing quaternary ammonium groups and alkyl linkers



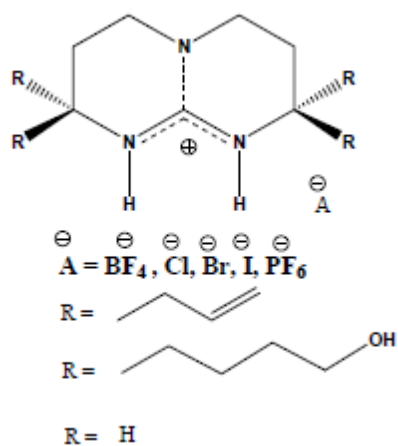
Scheme 1.5 Neutral zwitter ionic receptors



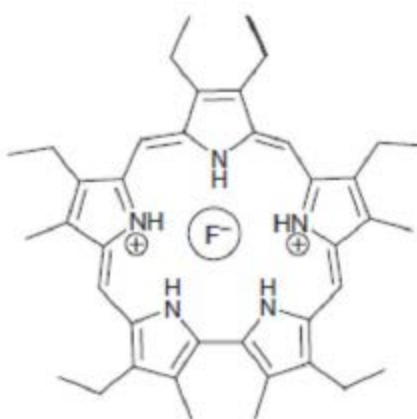
Scheme 1.6 Neutral cyclophane based receptors



Scheme 1.7 A series of acyclic tripodal receptors bearing amide groups



Scheme 1.8 Bicyclic fused ring system with guanidinium motif



Scheme 1.9 Porphyrin based receptor

1.5 COLORIMETRIC CHEMOSENSORS:

The design and synthesis of new receptors since its inception has focused on practical applications. Molecular sensing is one such field which has received more attention in the last decade. According to analytical chemistry, sensor is a device that can detect and quantify the concentration of the analyte. In the field of supramolecular chemistry, molecular biology and biochemistry, the term “sensor” is closely associated with a molecular event. Receptor could be called as a sensor when a chemical receptor gives a measurable signal in response to the binding of an analyte. It was Antony Czarnick, who coined the term ‘chemosensor’ to differentiate between the designed chemical receptors and biosensors (Czarnick 1994). Design of new synthetic receptors for sensing applications could be referred to as a fertile ground for the creativity of the supramolecular chemists. As receptor design is vital for the sensing process, binding strategy is much more important.

Depending on the type of signal produced on the binding event, chemosensors can be classified into two categories as, electronic sensors and optical sensors. Electronic sensors exhibit change in the electrochemical properties and optical sensors exhibit change in the optical signals on the binding event. In general, three components get together in the construction of optical anion sensors; anion binding site, the chromophore or signaling unit and the method of measuring the change and converting it into useful information (Suksai and Tuntulani 2003). A general representation of colorimetric chemosensor is shown in Fig. 1.3.

Optical sensors could be further classified as follows;

- i) **Chromogenic / Colorimetric chemosensors:** Here, the signaling unit results in colour change on the binding of guest moiety by the receptor.
- ii) **Fluorogenic/ Fluorimetric chemosensors:** In this type, the interaction between the guest moiety and the receptor results in changes in the fluorescence behavior of the signaling unit.

Optical approaches like colorimetry and fluorometry are the commonly used techniques to quantify and sense anions. Simple instrumentation involved with the colorimetric techniques and possibility of achieving lower detection limits through fluorimetry have made them much more appealing.

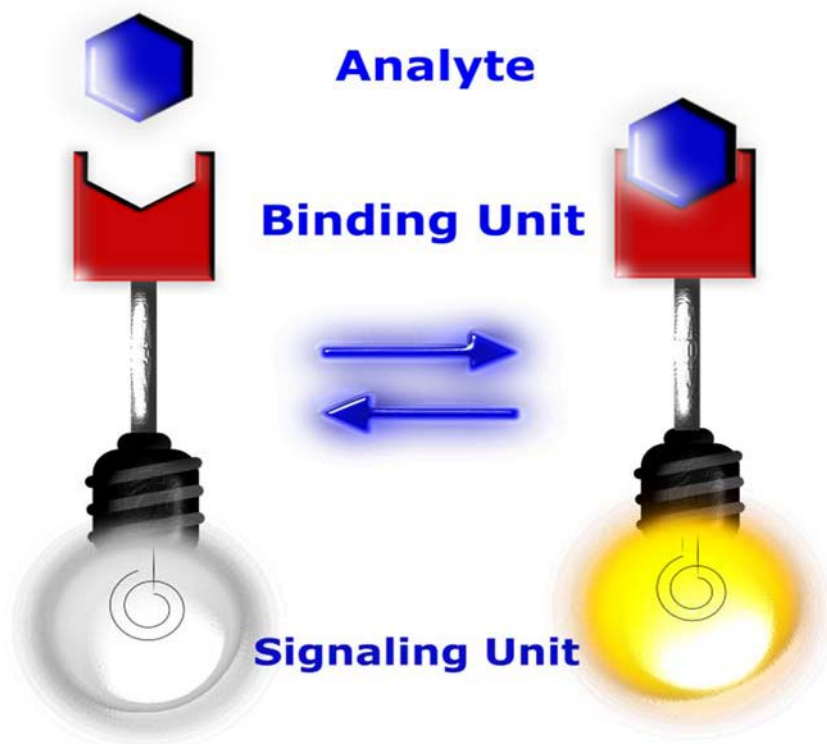


Fig. 1.3: Basic components of a chemosensor

1.5.1. Types of colorimetric chemosensors

Depending on the nature of interaction of binding site with the signaling unit, three different approaches have been used by various groups in pursuing the synthetic receptors.

i. Binding site-signaling unit approach

This involves the attachment of binding site to the signaling unit through covalent bonds. Interaction of the anion with the binding site changes the electronic property of the

signaling unit. This leads to the sensing of target anion through color or emission modulation. And, in this approach sensing feature could be observed only in organic solvents. The color change could be related to the basicity of the anions that either form hydrogen bond interaction or/and induce deprotonation of the receptor (Amendola et al. 2006; Gunnlaugsson et al. 2005, 2006). A schematic representation of binding site-signalling unit approach is shown in Fig 1.4.

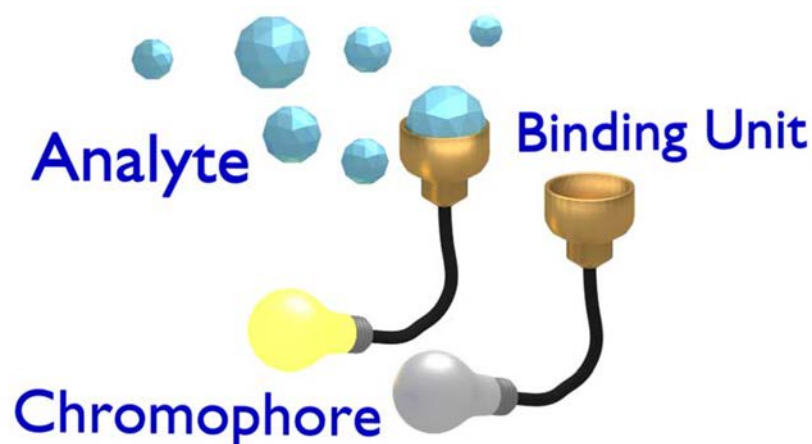


Fig 1.4: General representation of binding site-signaling unit approach

ii. The Displacement assay approach

This approach is commonly used due to its wide application in immunoassay protocols. Here, the receptor forms an inclusion complex with the dye and upon introduction of anion results in displacement of the dye which goes into the solution. It involves non-covalent interactions between the binding site and indicator group that in turn allows testing of large number of combinations in order to obtain a tuned sensing system. It allows the design of realistic sensing protocol because it could be applied to both aqueous as well as organic-aqueous system (Nguyen and Anslyn 2006; Wiskur et al. 2001). A general representation of displacement assay approach is shown in Fig. 1.5.

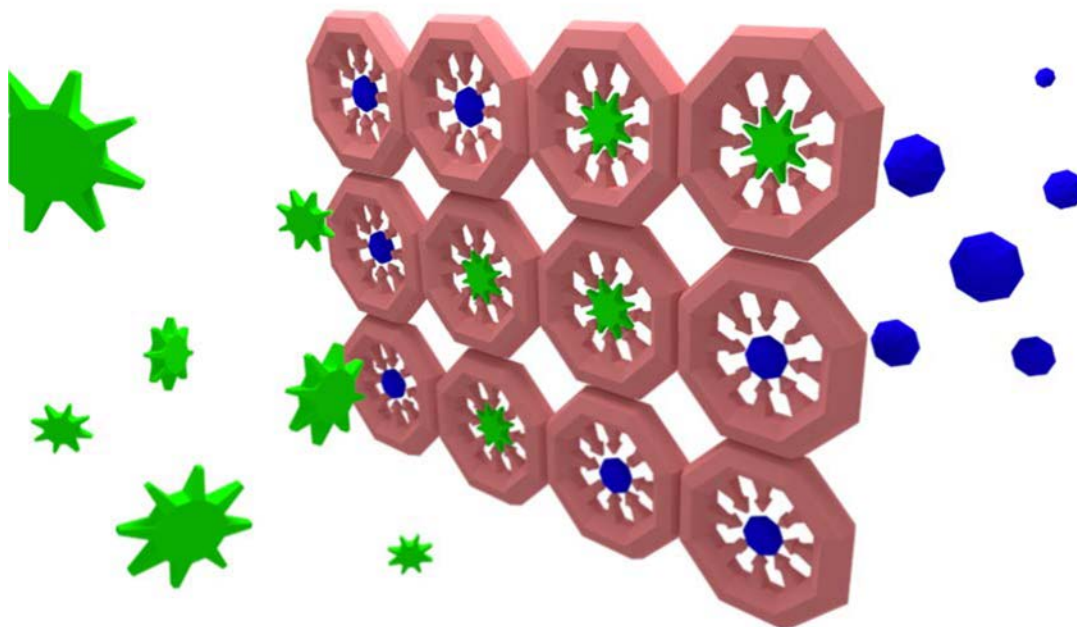


Fig. 1.5: General representation of the displacement assay approach

iii. The Chemodosimeter approach

This represents a well-established procedure for the design of anion receptors. It involves specific anion-induced reactions involving the rupture and formation of covalent bonds. It results in major chemical changes in the receptor along with remarkable spectroscopic changes. This approach involves nucleophilic attack of target species to electron deficient functional groups which leads to a re-organization of electron density in the entire molecule and results in color change (Xu et al. 2009). The general representation of chemodosimeter approach is shown in Fig 1.6.

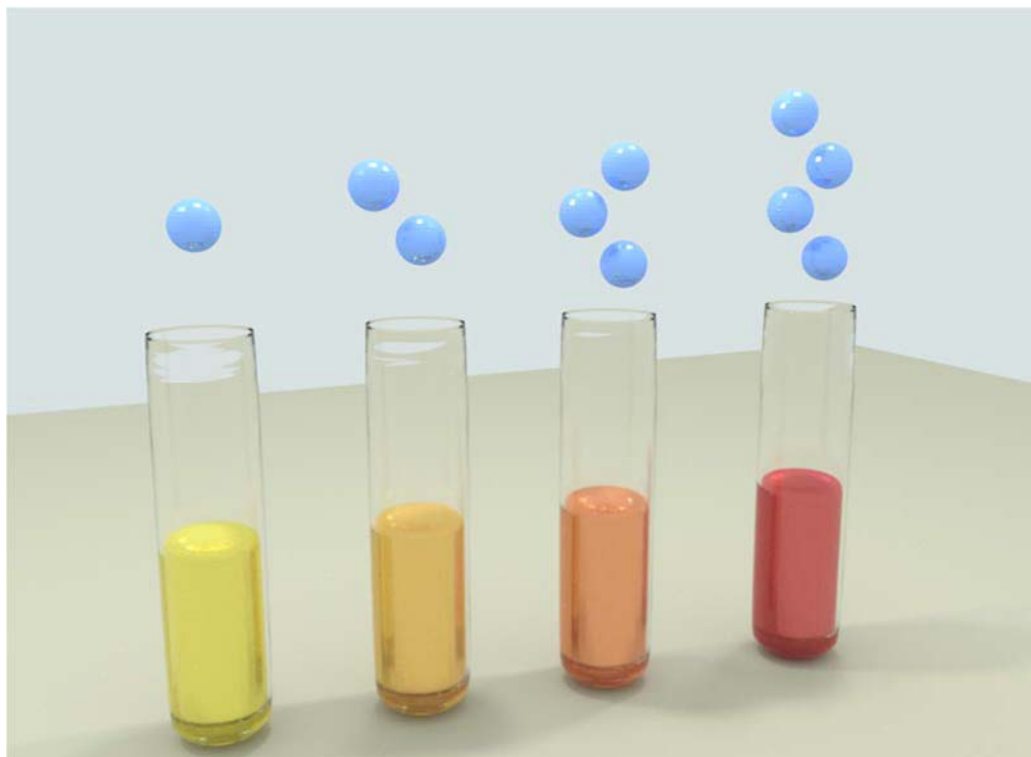


Fig. 1.6 General representation of the chemodosimeter approach

1.6 SUPRAMOLECULAR GELS

Supramolecular gels are a fascinating class of soft materials. Their gelators can self-assemble into nano or micro-scale superstructures, such as fibers, ribbons, sheets and spheres in an appropriate solvent, thereby resulting in the formation of 3D networks which are interconnected by multiple non-covalent interactions, such as hydrogen bonding, metal coordination, van der Waals interactions, p-p stacking interactions, solvophobic forces (hydrophobic forces for hydrogels) etc. (Banerjee et al. 2009; Lloyd and Steed 2009; Maeda 2008; W. Steed 2010). The dynamic and reversible nature of the noncovalent interactions that contribute to the formation of these network structures together gives these supramolecular gels the inherent ability to respond to external stimuli. The process of formation of supramolecular gel is represented in Fig.1.7.

Soft materials have been attracting increasing attention as a “transformable” functional class of materials, owing to their moderate mobility and flexibility, which readily enables them to change their bulk shape and properties depending on the conditions. (Estroff and Hamilton 2004; Terech and Weiss 1997). Gels are soft materials that are reasonably less mobile agglomerates with mechanical properties ranging from soft and weak to hard and tough. Gels are defined as substantially dilute cross-linked systems, which exhibit no flow in the steady-state. This internal network structure may result from physical bonds (physical gels) or chemical bonds (chemical gels), as well as crystallites or other junctions that remain intact within the extending fluid.

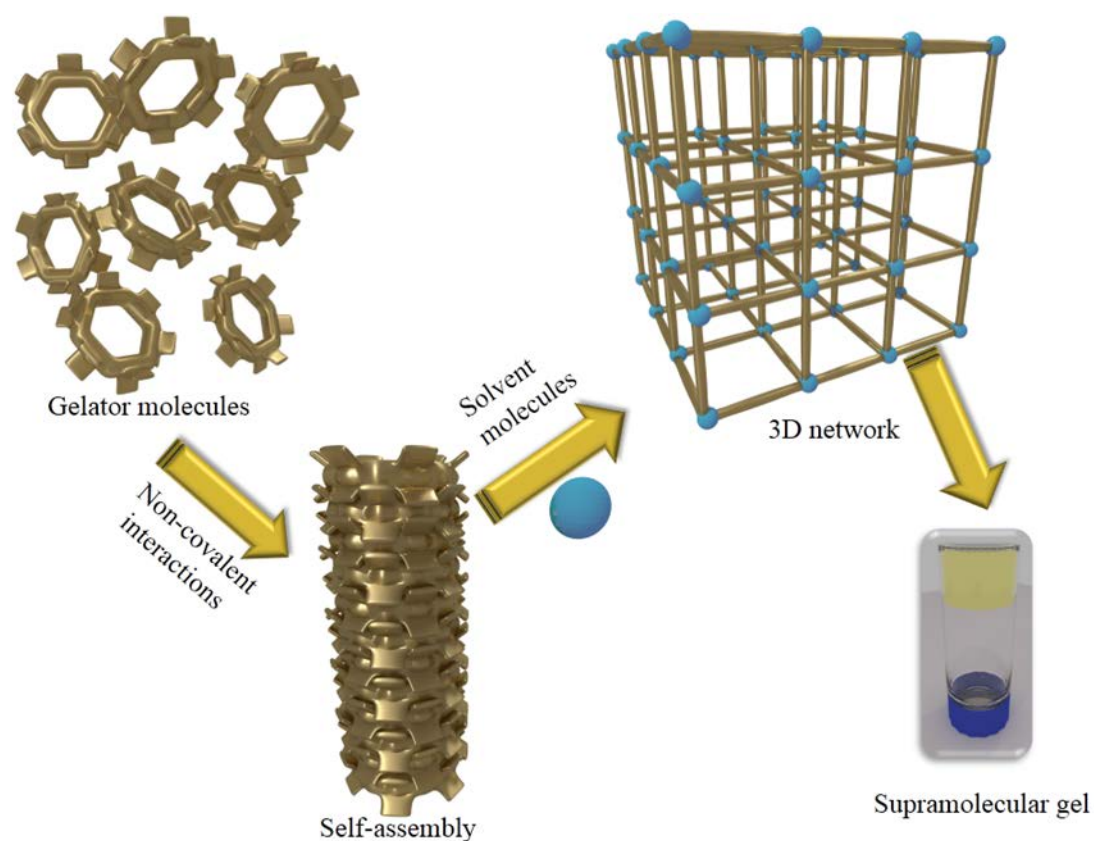
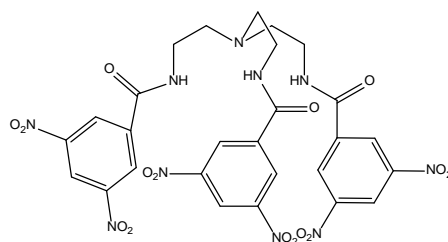


Fig. 1.7 Schematic representation of the formation of a supramolecular gel

1.7 LITERATURE REVIEW

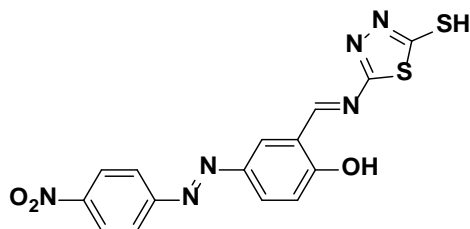
Despite there being challenges towards the anion detection process, researchers have extensively worked upon designing artificial receptors which can bind anions through various non-covalent interactions such as hydrogen bonding, anion- π and reactions like hydrogen abstraction and electron transfer (Beer et al. 2003).

Dey et al. (2011) have synthesized dinitrophenyl functionalized tris-(amide) receptor **S 1.1** for the selective detection of fluoride by encapsulation within the tripodal pseudocavity in polar aprotic solvents exhibiting solvatochromism and solvatomorphism. UV-Vis studies confirmed the nature of the chromophoric change to be a result of $F^- \cdots \pi$ CT interactions wherein F^- is hydrogen bonded to the NH groups which was evident in the crystal structure of solvatomorph.



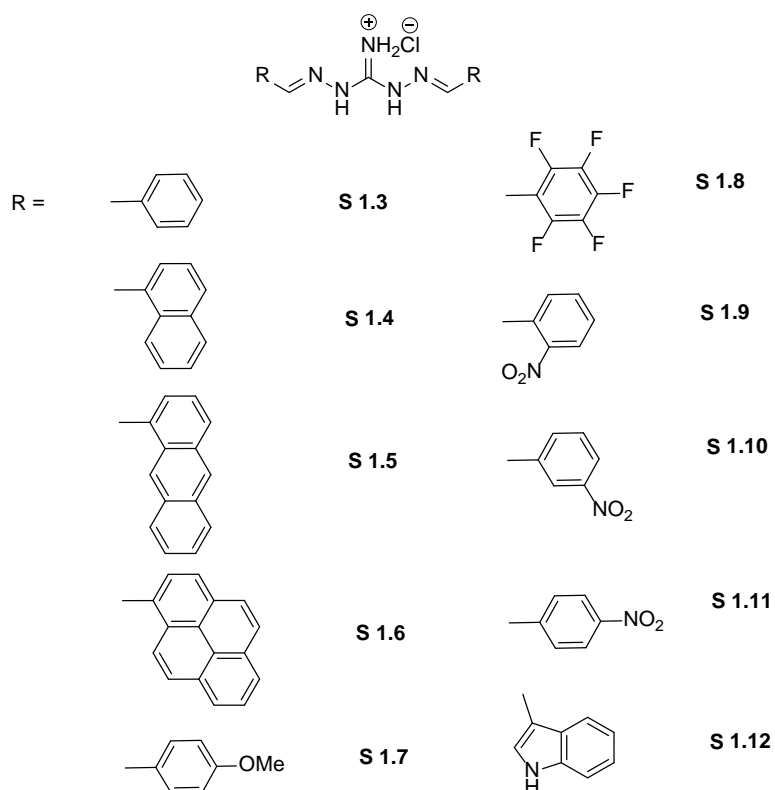
S 1.1

Li et al. (2011) have designed and synthesized a novel acetate selective anion sensor **S 1.2** based on azophenol and mercapto thiadiazole. Sensor exhibits selectivity and sensitivity for AcO^- anion over other anions such as F^- , Cl^- , Br^- , I^- , $H_2PO_4^-$, HSO_4^- and ClO_4^- by naked-eye and UV-Vis spectra changes in aqueous solution ($H_2O/DMSO$, 5:5, v/v). The color of the solution containing sensor had an obvious change from colorless to orange after the addition of AcO^- in aqueous solution while other anions did not cause obvious color change. The binding constant was found to be $7.35 \times 10^3 M^{-1}$. The detection limit of the sensor for AcO^- was $1.0 \times 10^{-6} mol L^{-1}$.

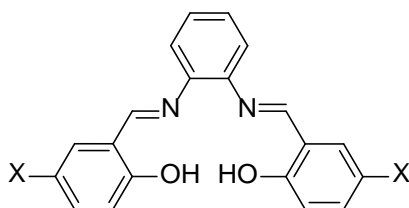


S 1.2

Bose et al. (2011) have designed and synthesized a series of new symmetrically functionalized guanidinium chlorides (S 1.3, S 1.4, S 1.5, S 1.6, S 1.7, S 1.8, S 1.9, S 1.10, S 1.11, S 1.12) wherein the reactivity towards anions have been tuned by varying the functional groups attached to the guanidinium moiety. Addition of fluoride ion induces vivid color changes from yellow to red to reddish orange and finally to blue color. One of the receptors exhibited NIR signature at 930 nm. Single crystal X-ray analyses supports –NH deprotonation in the presence of highly basic F^- and 1:1 binding in the presence of less basic anion benzoate.



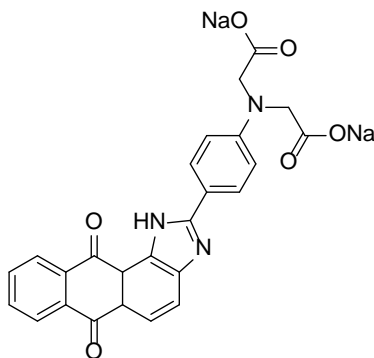
Dalapati et al. (2011) have reported two organic receptors S 1.13 and S 1.14 possessing –OH functionality as binding site for anions. Receptor S 1.13 exhibited colorimetric response towards F^- and AcO^- ions with a color change from colorless to pale yellow. UV –Vis titration studies performed in 95:5, v/v, CH_3CN : DMSO with the gradual addition of anions. The binding of anions by the receptor has been confirmed from the density functionality studies (DFT). Binding constant was found to be $1.36 \times 10^4 M^{-1}$ with F^- ion (1 : 1 complex) and $7.05 \times 10^9 M^{-2}$ with AcO^- ion (1:2 complex).



S 1.13: X=H

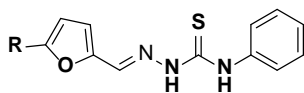
S 1.14: X=NO₂

Kumari et al. (2011) have designed and synthesized colorimetric probes based on anthraimidazolediones of which one of the probes, S 1.15 exhibited selective detection of both fluoride and cyanide ions in organic medium whereas in aqueous organic medium, it exhibited selective detection of cyanide ions with a ratiometric response. Job's plot revealed 1:1 binding ratio of the probe with fluoride and cyanide ions.

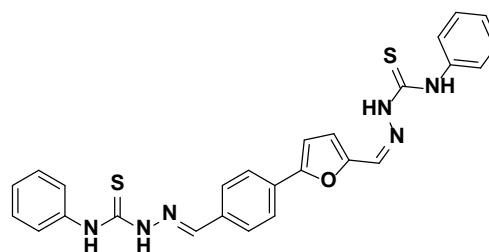


S 1.15

Santos-Figueroa et al. (2012) have synthesized a family of heterocyclic thiosemicarbazone dyes, S 1.16 – S 1.22 containing furyl groups, and their response in acetonitrile in the presence of selected anions was studied. Acetonitrile solutions of receptors showed absorption bands in the 335–396 nm range which are modulated by the electron donor or acceptor strength of the heterocyclic systems appended to the thiosemicarbazone moiety. Fluoride, chloride, bromide, iodide, dihydrogen phosphate, hydrogen sulphate, nitrate, acetate and cyanide anions were used in recognition studies. From these anions, only sensing features were seen for fluoride, cyanide, acetate and dihydrogen phosphate.

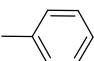
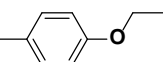

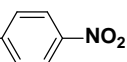
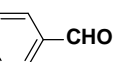


S 1.16 - 1.22



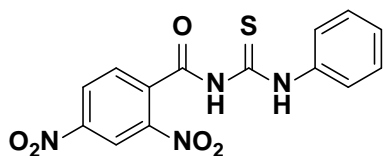
S 1.23

S 1.16: R = Br

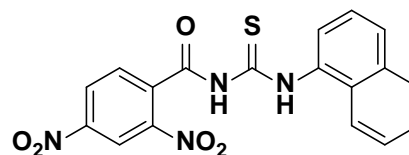
S 1.17: R = NO₂S 1.18: R = S 1.19: R = S 1.20: R = S 1.21: R = S 1.22: R = 

Basu et al. (2013) have synthesized two amidothiurea based receptors (S 1.24 and S 1.25) containing π -acidic 3, 5-dinitrophenyl chromophore in good yields and their anion recognition properties were evaluated both in organic and aqueous organic environment by spectroscopic techniques. Anions such as F⁻, AcO⁻ and H₂PO₄⁻ were examined to be suitable analytes for the receptor molecules, displaying optical signaling from colorless to orange/red, whereas anions of lesser basicity such as Cl⁻, Br⁻, I⁻, NO₃⁻ and HSO₄⁻ did not cause any discernable spectral changes. Highly basic OH⁻ ions

induced stepwise color change with increasing equivalence from red to green and anion-- π interactions has been confirmed.

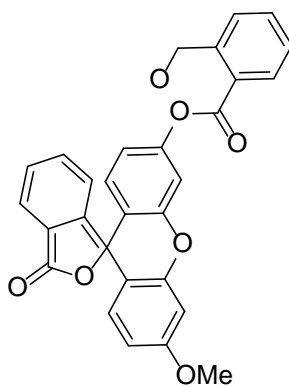


S 1.24



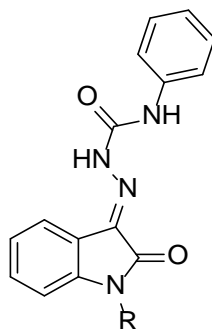
S 1.25

Roy et al. (2014) have synthesized a cascade reaction based colorimetric and fluorescent probe, S 1.26 for the selective detection of fluoride ions. The fast response time, considerably low detection limit and biological applications prove the efficacy of the receptor in sensor applications.



S 1.26

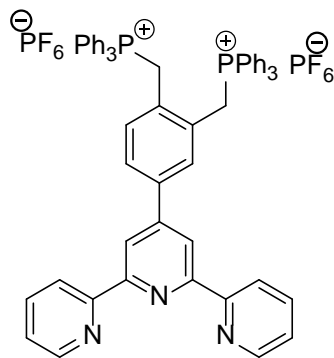
Jakusova et al. (2014) have designed receptors based on isatinphenylcarbazone S 1.27 and S 1.28 which is capable of detecting F^- and AcO^- ions in organic and semiaqueous media. The ability of receptor to exhibit tautomerism in the presence of anions has been supported by UV-Vis and 1H -NMR titration studies. The acid base properties of anions are known to influence the equilibrium ration of tautomeric forms.



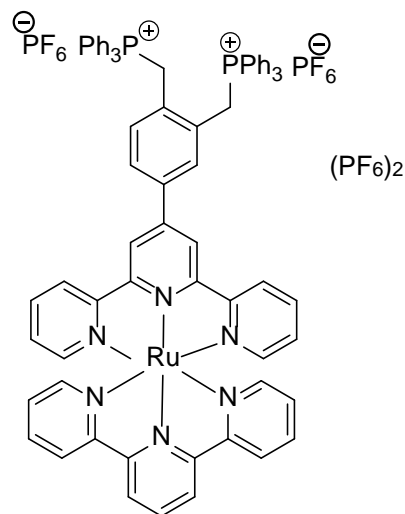
S 1.27: R=H

S 1.28: R=CH₃

Agarwalla et al. (2014) have reported the synthesis of two new receptors S 1.29 and S 1.30 bearing positively charged phosphonium ion aiding the binding of fluoride and acetate to the methylene functionality. The role of hydrogen bonding interaction between hydrogen atoms of the active methylene group and anionic analyte has been explored and the experimental results were rationalized with the detailed computational studies.

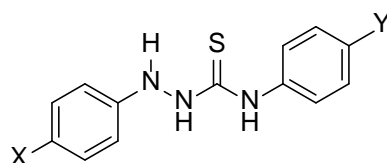


S 1.29



S 1.30

Farrugia et al. (2014) have reported a series of four new receptors S 1.31 – 1.34 based on thiosemicarbazide substituted with phenyl/nitrophenyl units which exhibited colorimetric response towards OH^- , Cl^- , F^- , AcO^- and H_2PO_4^- ions. UV-Vis titration studies of receptors in 9:1, v/v, DMSO: H_2O revealed red shift of original absorption band of receptor accompanied by dramatic color changes visible to the naked eye. The deprotonation of NH functionality has been confirmed by the NMR titration studies.



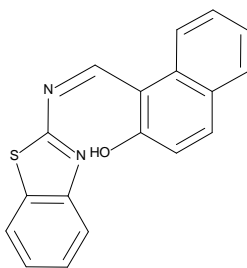
S 1.31: X=H, Y=H

S 1.32: X=H, Y= NO_2

S 1.33: X= NO_2 , Y=H

S 1.34: X= NO_2 , Y= NO_2

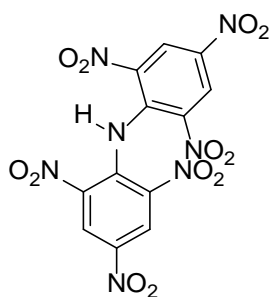
You et al. (2014) (You et al. 2014) have synthesized a colorimetric and fluorometric chemosensor, S 1.35 bearing aminobenzothiazole moiety for the selective detection of acetate and cyanide ions without inference between the two analytes.



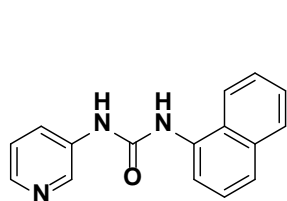
S 1.35

Gunupuru et al. (2014) have studied the anion binding properties of dipicrylamine (DPA), S 1.36, wherein $-\text{NH}$ group solely acts as binding site and $-\text{NO}_2$ functionality acts as signaling unit. This suggests that the acidic nature of $-\text{NH}$ group is sufficient enough to

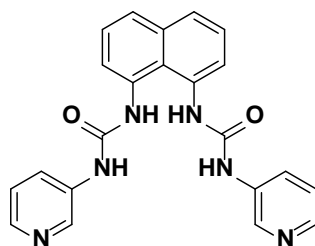
bind anion through single strong hydrogen bond interaction. The interaction of DPA in acetonitrile with wide range of anions revealed strong interactions with F^- , AcO^- and $H_2PO_4^-$ with sharp color changes from yellow to red. UV-Vis titration studies performed with the addition of anions revealed the significant red shift of the original absorption band of receptor with clear isobestic point. 1H -NMR titration and computational studies of DPA in the presence of anions reveal the binding of anion by the $-NH$ functionality followed by deprotonation process.

**S 1.36**

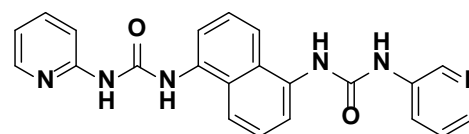
Ghosh et al. (2015) have examined the gelation and anion responsive behavior of some 3-aminopyridine-based urea molecules (S 1.37, S 1.38, S 1.39, S 1.40 and S 1.41). Of the different pyridyl ureas, two compounds formed instant gel from DMSO/H₂O and DMF/H₂O solvents. Here, the influence of hydrogen bonding of the urea groups, π -stacking of the naphthyl units and role of water in linking the pyridine ring nitrogen make a possible cross-linked arrangement in solution to undergo gelation. Among them, only the gel state of one of the compounds has been noted, for the first time, to detect iodide ion over a series of other anions through a color change involving no phase transformation.



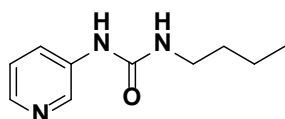
S 1.37



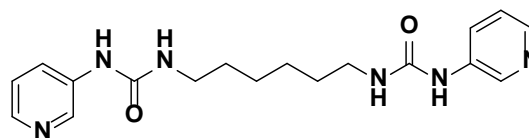
S 1.38



S 1.39

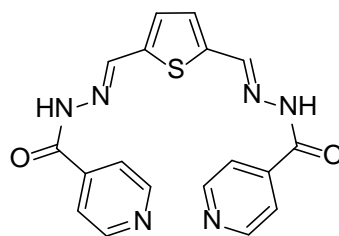


S 1.40



S 1.41

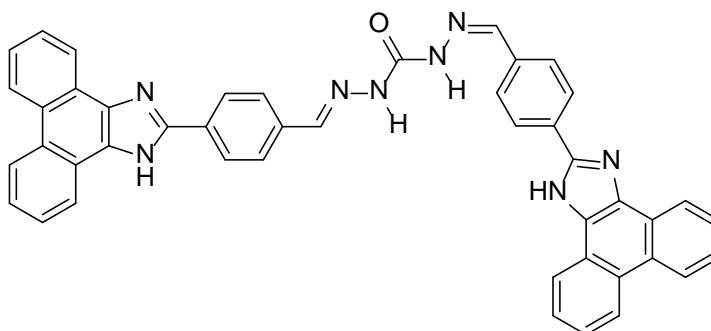
Suganya et al. (2015) have designed and synthesized the receptor S 1.42, for the detection of both cations and anions. Receptor- Zn^{2+} complex formed has been utilized for the reversible recognition of $H_2PO_4^-$ ions selectively.



S 1.42

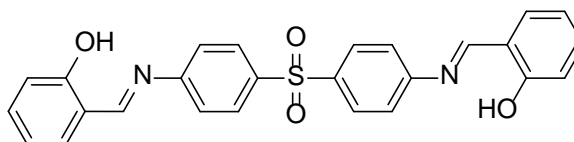
Mahapatra et al. (2015) have reported an anion chemosensor based on phenanthroimidazole conjugate of bis-carbonohydrazone, S 1.43 which could selectively detect F^- ion with remarkable spectroscopic changes. The ratiometric response of the receptor towards F^- ion is revealed from the gradual color change from colorless to yellow and orange with the incremental addition of F^- ion. UV-Vis, NMR titration and

DFT studies clearly indicates the binding of F^- ion by the imidazole $-NH$ and urea $-NH$ proton and a subsequent deprotonation process leading to the visible color changes.



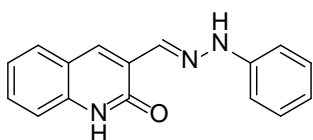
S 1.43

Wan et al. (2016) have designed and synthesized Schiff base chemosensor, S 1.44 for the selective detection of fluoride and cyanide ions. The anion binding mechanism has been proved by DFT and 1H -NMR titration experiments.

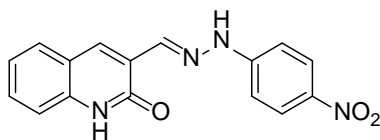


S 1.44

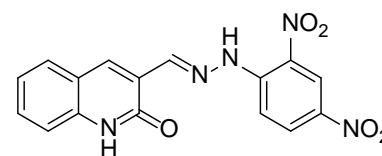
Nie et al. (2017) have reported three hydrazone derivatives, S 1.45, S 1.46 and S 1.47 possessing electron withdrawing groups which could selectively detect fluoride ions with a ratiometric colorimetric response.



S 1.45



S 1.46



S 1.47

1.8 SCOPE OF THE WORK

Anions, though ubiquitous in the biological system have to be present in optimum amount because too much or too less of anions both have an equal impact on the human health. Right from the pioneering work on anion receptor chemistry, researchers have employed fluorometry and colorimetry methods in the detection of anions. Though being a thrust area of research, fluorometry is accompanied with complications in the detection process owing to its sensitivity towards environmental changes. Light used for excitation can even lead to photochemical changes. In this scenario, there is lot of opportunity to look into colorimetric sensing method where quantitative detection of anions is relatively easier by virtue of the simple instrumentation used.

Water is unique in its own way with its property to form highly structured infinite dynamic network of hydrogen bonds among themselves. In general, the formation of hydrogen bond between anions and water molecules is possible due to the hydrogen bond donor or acceptor nature of water. In biological system, natural receptors such as enzymes and antibodies interact with guest molecules through non-covalent interactions which are specific and mediated through functional groups present on them. Mimicking this naturally occurring system, model compounds have been designed by researchers which can recognize the host-guest complexation event in organic, non-polar solvents. For practical applications like the detection of anions in sea water or commercially available mouthwash, there is a need for organic receptors that are active in water. Water being a competitive solvent, it mediates interactions between the receptor and anions. Detection of anions in water is highly challenging in the field of research by virtue of the high solvation energy, large size of anions and its tendency to involve in protonation equilibrium in aqueous solution. Researchers have so far reported positively charged receptors and neutral anion receptors capable of detecting anions mostly in non-competitive organic solvents such as DMSO, CH₃CN etc. and in solvent mixtures such as DMSO:H₂O(v/v) and very few reports are available on anion recognition in purely

aqueous media. For practical applications, there is a need to design and synthesize organic receptors that can detect anions in competitive media.

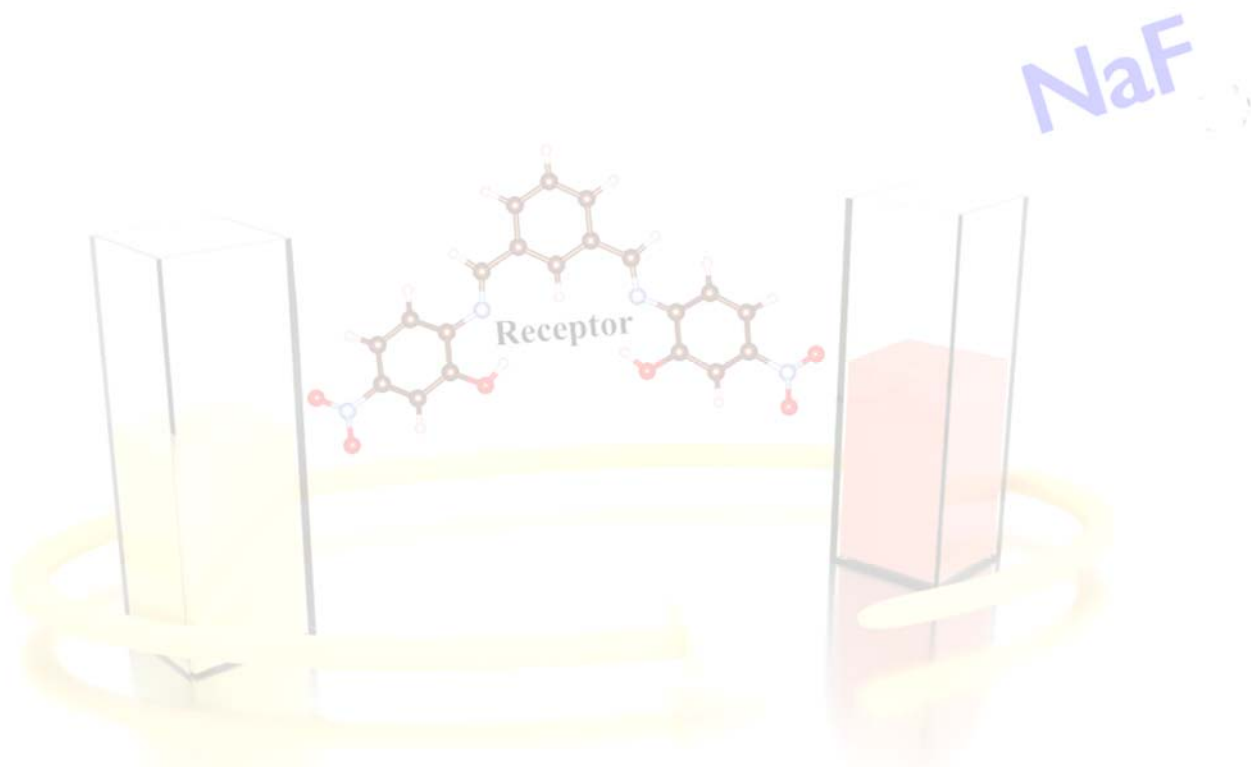
OBJECTIVES

- To design and synthesize organic receptors with suitable binding sites.
- To characterize and analyze the receptors through FT-IR, $^1\text{H-NMR}$, elemental analysis and ESI-MS.
- To monitor the color change through naked eye on addition of appropriate equivalent of anions to the receptor and quantify the color change by UV-Vis spectrophotometric titration by monitoring the shift in the λ_{max} .
- To analyze the binding event through NMR titration experiments.
- To determine the binding constant through Benesi-Hildebrand (B-H) method and the binding ratio either by method of continuous variation (Job's plot) or B-H plot.
- To apply the designed sensor system to realize real life applications like detection of fluoride in sea water and commercially available mouthwash.
- To arrive at the binding mechanism for selective receptors.
- To calculate the detection limit of the receptors towards particular anion.

Overall, the present research is focused on synthesis of organic receptors aiming towards biological and environmental applications. In this regard, six different series of receptors have been synthesized and analysed for the detection of anions. **Chapter 2** deals with the syntheses of a receptors based on nitrophenol derivative and pyridine derivative for the detection of anions. Fluoride ion in commercially available mouthwash have been quantitatively analyzed and presented. UV-Vis spectral and DFT studies have been performed to confirm the anion binding process and discussed in detail. **Chapter 3** deals syntheses of dinitrophenylhydrazine based receptors for the colorimetric detection of fluoride, acetate and dihydrogen phosphate ions in organic media. Further, the absorption ratiometric response of receptor in the presence of anion has been studied. The anion

induced azo-hydrazone tautomerism has been observed and confirmed by $^1\text{H-NMR}$ titration studies. **Chapter 4** describes syntheses and characterization of five organic receptors based on positional substitution of $-\text{NO}_2$ and $-\text{OH}$ functionalities on dinitrophenylhydrazine derivatives. Solvatochromism property of one of the receptors has been studied in the presence of acetate ion. UV-Vis titration, $^1\text{H NMR}$ titration, cyclic voltammetry and DFT studies has been discussed in detail. **Chapter 5** describes syntheses of furan based colorimetric receptors for selective detection of acetate ion have been discussed. The colorimetric anion sensing properties, electrochemical properties have been studied in detail. Biological studies have been performed with one of the receptors for the detection of acetate in physiological conditions. **Chapter 6** comprises syntheses of thiadiazole Schiff's base derivatives for multianion colorimetric detection. In addition, the selected active receptor was used to study the DNA binding ability, detection of cyanide in sprouting potatoes and detection of dihydrogen phosphate in detergent sample. **Chapter 7** encompasses synthesis of naphthaldehyde based receptor which has been employed in the selective colorimetric and fluorometric detection of fluoride ion. The gelation property of the receptor and sol-gel transition in the presence of anion have been discussed in detail. Towards the end, **Chapter 8** summarizes the conclusion of the present research work and highlights the scope for future work.

CHAPTER 2
SYNTHESES AND EVALUATION OF
COLORIMETRIC ANION SENSING
PROPERTIES OF ORGANIC
RECEPTORS: TIME DEPENDENCY AND
DFT STUDIES



Abstract: In this chapter, the design, syntheses of organic receptors have been described. The anion binding properties of the receptors have been studied and confirmed by UV-Vis spectrophotometric, ¹H-NMR and DFT studies.

2.1 INTRODUCTION

The development of new organic receptors for the detection of anions is of key interest to supramolecular chemists owing to the biological and environmental importance of anions (A. Gale et al. 2008, 2014; Caltagirone and Gale 2009; Gale 2006, 2010; Sessler et al. 2006; Wenzel et al. 2012). The leading role of anions such as fluoride, acetate and phosphate at physiological level in promoting tooth and bone health, metabolism and genetic transduction has been well established (Tetilla et al. 2011; Amendola et al. 2010; A. Gale et al. 2008; Boiocchi et al. 2005; Duke and Gunnlaugsson 2011; Ali et al. 2008). Increasing research interest on selective and sensitive detection of anions has enriched the field of anion receptor chemistry with a wide array of design strategies (Gunnlaugsson et al. 2004; Misra et al. 2009; He et al. 2014; Camiolo et al. 2003). Among these various analytical techniques, colorimetry has drawn significant attention among chemists for its rapid response rate, low cost, easy method and high selectivity (Yang et al. 2013; He et al. 2014; Hsieh et al. 2009; Wang et al. 2014; Ye et al. 2013; Huang et al. 2013; Yin et al. 2010). The choice of appropriate detection technique is highly essential as it directly dictates the efficacy of the sensor. Anion binding with colorimetric probes comprising of a binding site and a signaling unit work in a coordinative way yielding an optical output visible to the naked eye. The detection of anions is commonly encountered with challenges in the receptor- anion interactions such as size and shape effects, pH, and solvation effects. In this regard, considerable efforts have been devoted towards the design of a receptor in the past few decades. Numerous receptors for anions have been developed based on various modes of interactions such as hydrogen bond and electrostatic interactions which are reliant on directionality and distance-dependent nature respectively. Hydrogen bond is further tuned by the acidity of protons by virtue of the presence of electron withdrawing substituents (Sessler et al. 2006). Pyridine based derivatives have been designed by researchers in the context of detection of anions involving hydrogen bonding and a deprotonation mechanism. Gunnlaugsson and coworkers

have reported pyridine- based thiosemicarbazide derivative for the detection of OH^- , F^- and AcO^- ions through hydrogen bond interaction followed by a deprotonation process (Gunnlaugsson et al. 2005; Pandurangan et al. 2013).

In this direction, we report the design and synthesis of new organic receptors **R** and **L** with suitable substitution of electron withdrawing substituent nitro functionality as signaling unit on the aromatic ring. With a vision towards enhancement of the chromogenic signaling output, signaling unit has been linked to a conjugated system possessing $-\text{OH}$ functionality which acts as binding site for anions. UV-Vis, ^1H NMR titration studies along with the DFT studies of **R** and **L** would help to arrive at the binding mechanism.

2.2 EXPERIMENTAL SECTION

2.2.1 Materials and methods

All the chemicals used in the present study were procured from Sigma-Aldrich and Alfa Aesar and were used as received without further purification. All the solvents were purchased from SD Fine, India, were of HPLC grade and used without further distillation.

Melting point was measured on Stuart SMP3 melting-point apparatus in open capillaries. Infrared spectrum was recorded on Bruker Apex FTIR spectrometer. UV-Vis spectroscopy was performed with analytik jena Specord S600 spectrometer in standard 3.0 mL quartz cell with 1cm path length. The ^1H NMR spectra were recorded on Bruker Ascend (400 MHz) instrument using TMS as internal reference and DMSO-d_6 as solvent. ^{13}C NMR spectra were recorded on Bruker Ascend (100 MHz) instrument using TMS as internal reference and DMSO-d_6 as solvent. Resonance multiplicities are described as s (singlet), d (doublet), t (triplet) and m (multiplet). Mass spectrum was recorded on Bruker Daltonics *ESI Q TOF*.

Density functional theory simulation have been performed on the receptor molecules using GAUSSIAN 09 package. A closed shell Becke–Lee–Yang–Parr hybrid exchange-correlation three-parameter functional (B3LYP) (Becke 1993; Lee et al. 1988; Perdew and Wang 1992) along with 6-311++G (d,p) basis set were used in the simulation to derive a complete geometry optimization for isolated receptor as

well as the receptor binding with AcO^- and F^- ions. The basis set 6-311 ++G (d,p) augmented by 'd' polarization functions on heavy atoms and 'p' polarization functions on hydrogen atoms were used (Petersson et al. 1988; Petersson and Al-Laham 1991). Molecular geometry was fully optimized by using Berny's optimization algorithm, which uses redundant internal coordinates. Molecular Orbitals (HOMO-LUMO) were plotted using Gauss View software. In a second step, the time dependent DFT (TD-DFT) method were used considering the same B3LYP exchange-correlation functional with 6-311++G (d,p) basis set to obtain the UV-Visible absorption spectra of free and ion bonded receptor in DMSO solvent.

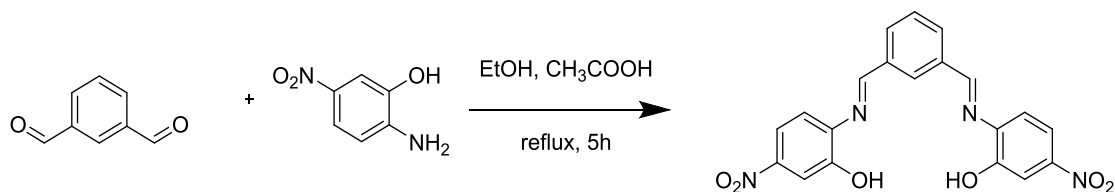
2.2.2 Synthesis of receptors **R** and **L**

Receptors **R** and **L** have been synthesized by simple Schiff base condensation reaction of aromatic aldehyde and amine (Scheme 2.1 and Scheme 2.2).

R: (2-((E)-((E)-3-((E)-(2-hydroxy-4-nitrophenylimino)methyl)benzylidene)amino)-5-nitrophenol)

Isophthalaldehyde (0.15 g, 1.14 mmol) and 2-amino,5-nitrophenol (0.4 g, 2.29 mmol) were mixed in 5 ml ethanol. A drop of acetic acid was added and the reaction mixture was refluxed for 5 h. The formation of the product was confirmed through TLC by the generation of single spot indicative of the disappearance of starting materials.

Yield: 80%., m. p. 210 °C. ^1H NMR (DMSO- d_6 , 400 MHz, ppm): δ 10.31 (br. s, 1H), 10.07 (br. S., 1H), 8.81 (m, 1H), 8.55(br. S., 1H), 8.34 (br. s, 1H), 8.12 (br. s, 1H), 7.61-7.48 (7.66 (ddd, $J = 7.9, 1.7, 1.3$ Hz, 4H)), 7.33 (m, 1H), 6.60 (d, $J = 7.8$, 2H) 6.20 (br. s, 2H). FT-IR (cm^{-1}): (C-O) 1155, (C-O) 1228, (NO_2) 1342, (C=C) 1513, (C=N) 1625, (C-H) 2902, (C-H) 2984, (OH) 3426. ^{13}C NMR (DMSO- d_6 , 100 MHz, ppm): δ 108.61, 110.96, 111.12, 115.03, 118.22, 120.58, 129.70, 133.82, 134.71, 136.59, 145.48, 150.56. Mass (ESI): m/z Calculated: 406.09 Obtained: 428.9 (M + Na^+).

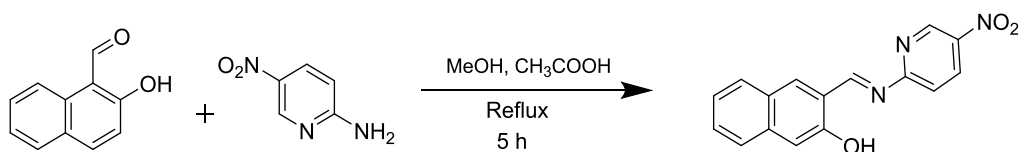


Scheme 2.1 Synthesis of receptor **R**

L: (E)-3-(((5-nitropyridine-2-yl)imino)methyl)naphthalene-2-ol)

2-amino-5 nitropyridine (0.1g, 0.71 mmol) and 2-hydroxynaphthaldehyde (0.12 g, 0.71 mmol) were appropriately weighed and transferred to a round bottom flask. 5 ml of methanol and a drop of acetic acid was added and the mixture was refluxed for about 5h. The progress of reaction was confirmed by TLC. After cooling to room temperature, the reaction mixture was filtered through filter paper, washed with methanol to obtain pure product.

Yield: 78 %, Melting point: 227 °C, FT-IR (cm⁻¹):(ring stretch) 1545, (C=N stretch) 1630, (C=N),(=C-H) 2978, 3364 (Ar CH), (-OH stretch) 3494,¹H NMR (DMSO-d₆, 400 MHz, ppm): δ 14.78 (s, OH), 9.71 (s, 1H), 9.29 (dd, *J* = 1.5, 0.5 Hz, 1H), 8.66 (ddt, *J* = 8.8, 1.9, 0.4 Hz, 1H), 8.30(ddt, *J* = 8.1, 1.7, 0.4 Hz, 1H), 7.92 (ddt, *J* = 8.1, 1.7, 0.4 Hz, 2H), 7.71 (dddd, *J* = 7.6, 7.4, 1.7s, 1H), 7.37-7.56 (dd, *J*=8.8, 0.5 Hz, 2H), 6.78 (dd, *J*=8.8, 0.5 Hz, 1H), Mass: Calculated: 293.08, Obtained:(M+ H⁺)294.15, Anal. calcd for C₁₆H₁₁N₃O₃: C, 65.53; H, 3.78; N, 14.33; O, 16.36; found: C, 65.48; H, 3.72; N, 14.19; O, 16.29.



Scheme 2.2 Synthesis of receptor **L**

2.2.3 CHARACTERIZATION DATA

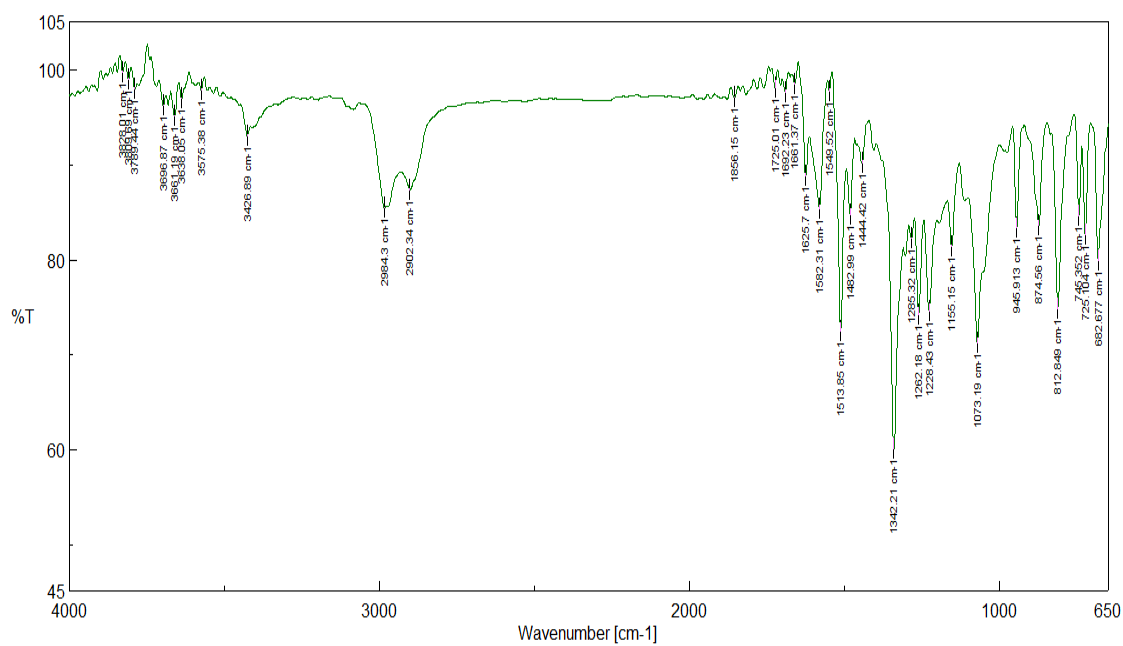
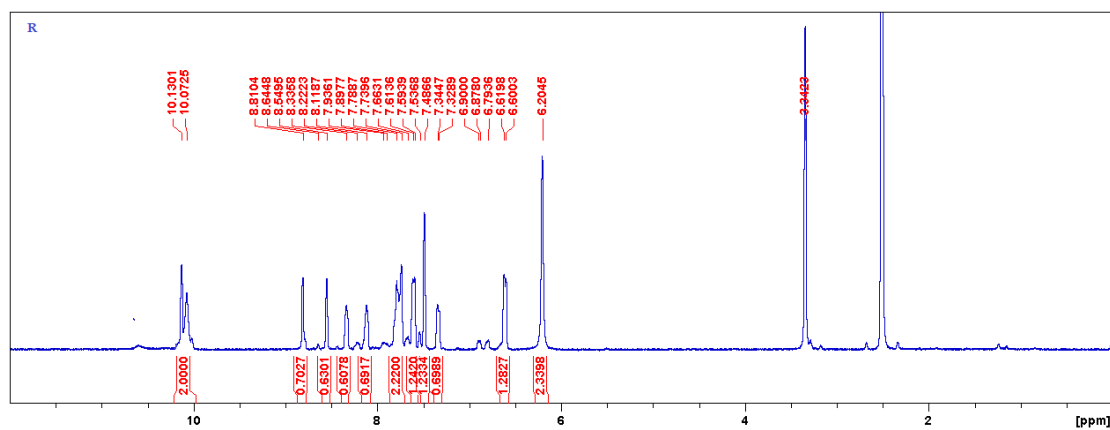


Fig. 2.1 FT-IR spectrum of the receptor R

Fig. 2.2 (a) ¹H-NMR spectrum of receptor L

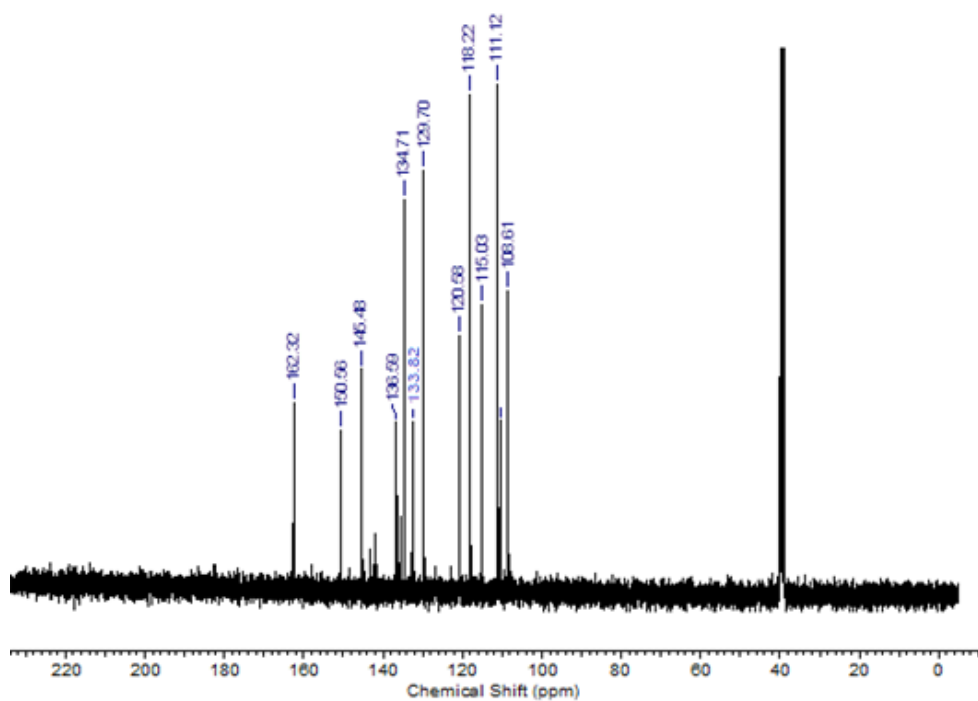


Fig. 2.2 (b) ^{13}C NMR spectrum of receptor R

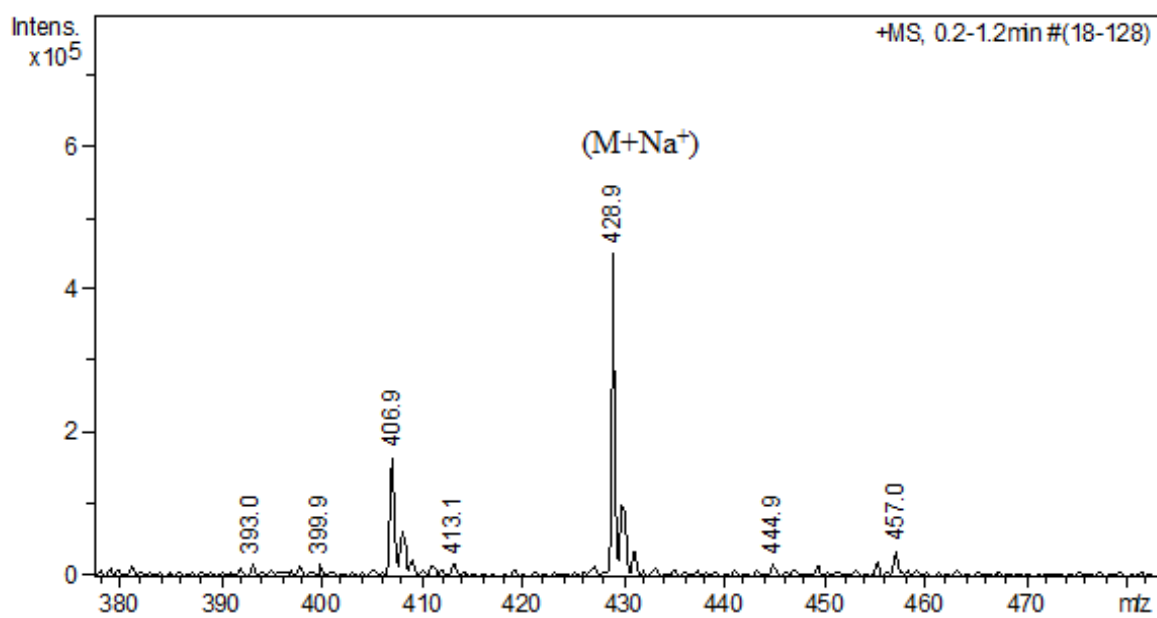


Fig. 2.3 Mass spectrum of the receptor R

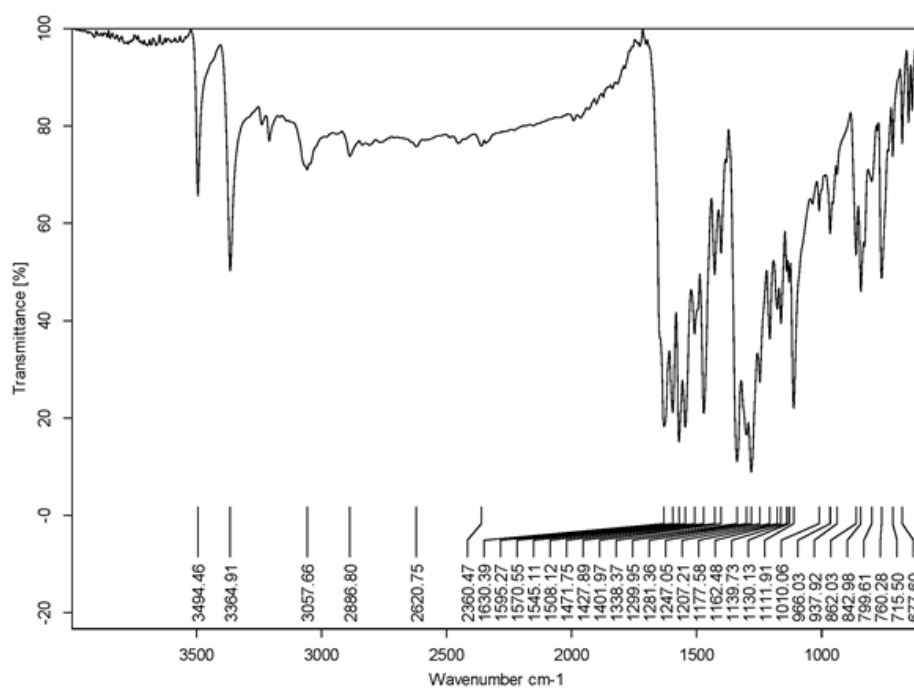
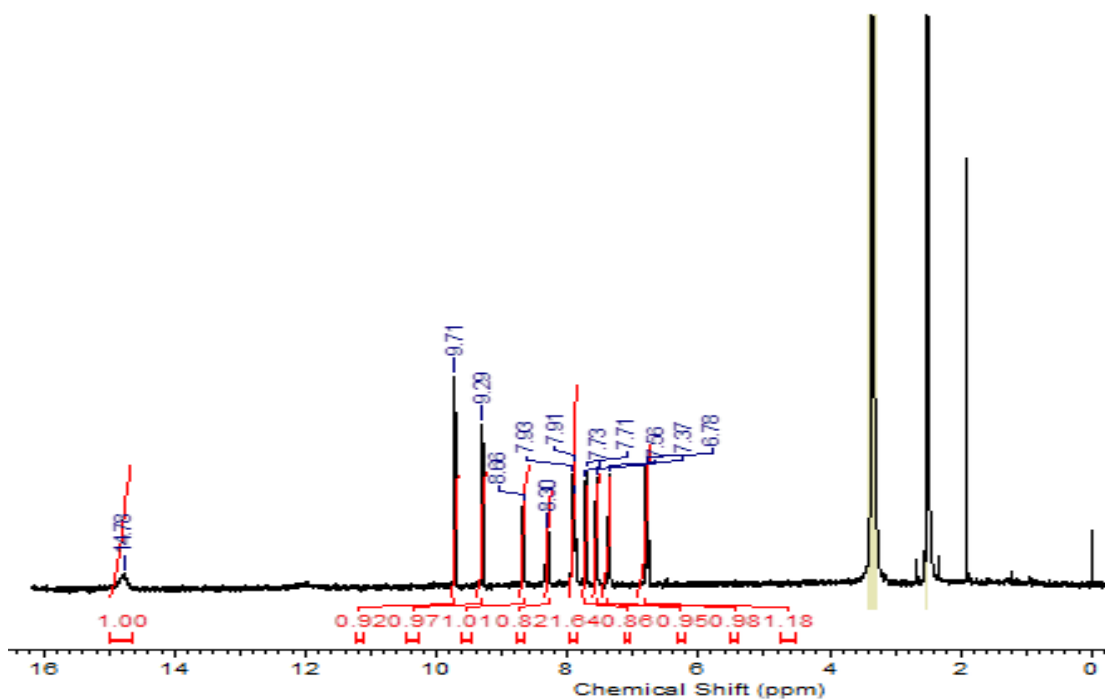


Fig. 2.4 FT-IR spectrum of receptor L

Fig. 2.5 (a) $^1\text{H-NMR}$ spectrum of receptor L

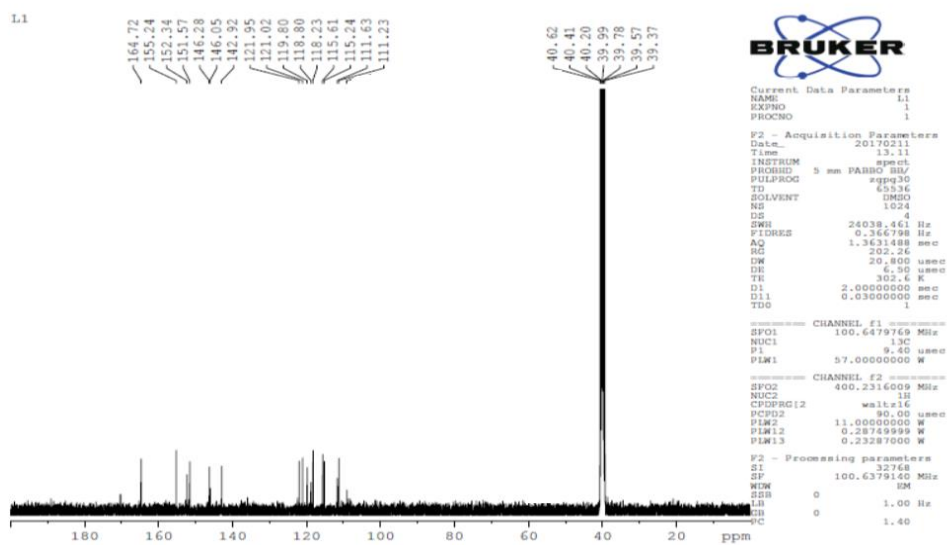
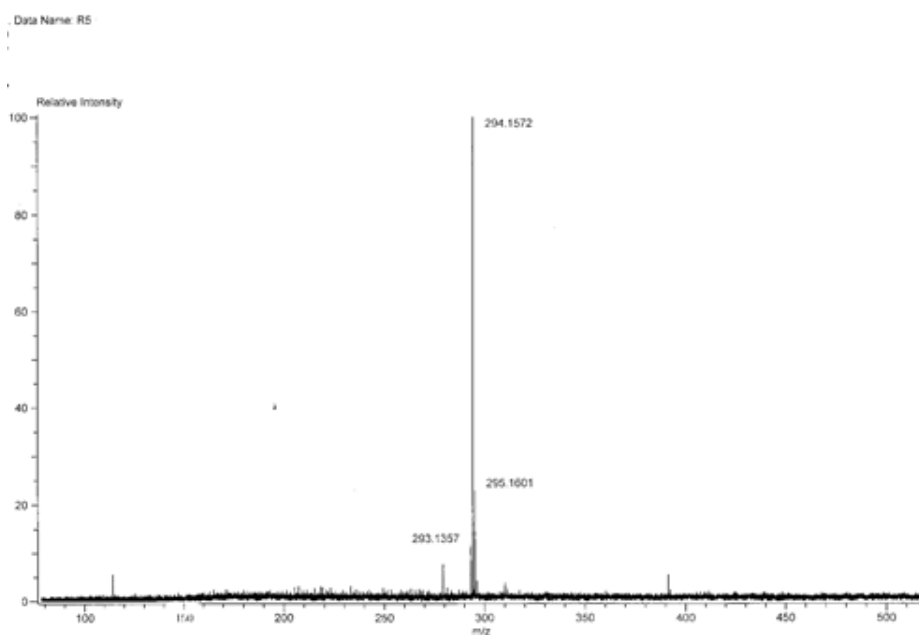
Fig. 2.5 (b) ^{13}C -NMR spectrum of receptor L

Fig. 2.6 Mass spectrum of receptor L

2.3 RESULTS AND DISCUSSION

2.3.1 Colorimetric studies

The receptor **R** and **L**, comprising of chromogenic signaling unit and hydrogen bond donor functionality viz, $-\text{NO}_2$ and $-\text{OH}$ respectively are likely to exhibit appreciable color change in the presence of anions. Preliminarily, qualitative analysis has been performed to figure out the interaction of various anions with the receptor. Receptor solution of 1×10^{-4} M has been prepared in dry DMSO. Standard solution of anions (TBA salts of F^- , Cl^- , Br^- , I^- , HSO_4^- , H_2PO_4^- and AcO^-) as 1×10^{-2} M has been prepared in dry DMSO. With the addition of 2 equiv. of test anions to the receptor solution, visible color change was observed for F^- and AcO^- ions from pale yellow to pale red and pale pink respectively. There was no appreciable color response upon addition of other anions. In this regard, the receptor could serve the purpose of detecting F^- and AcO^- ions amongst all as depicted in Fig. 2.7. UV-Vis absorption spectra were recorded to confirm the color change, with the addition of test anions to receptor solution. Initial absorption peak of the receptor at 325 nm corresponds to the transitions between the π orbitals localized on the azomethine group ($\text{C}=\text{N}$) and second absorption peak at 383 nm could be assigned to the intramolecular charge transfer occurring within the schiff's base moiety. The azomethine and the nitro functionality lead to pale yellow coloration of the receptor. The shift in the λ_{max} was observed for F^- and AcO^- differing by a unit of 135 nm and 145 nm respectively in comparison with the free receptor and a subsequent decrease in the absorption band centered at 383 nm. The shift in the λ_{max} was not observed with the addition of other anions involved in the present study as shown in Fig. 2.8.

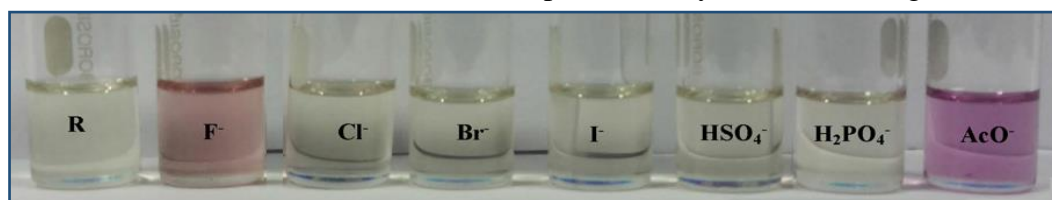


Fig. 2.7 Color changes of receptor **R** upon addition of 2 equiv. of various anions in dry DMSO

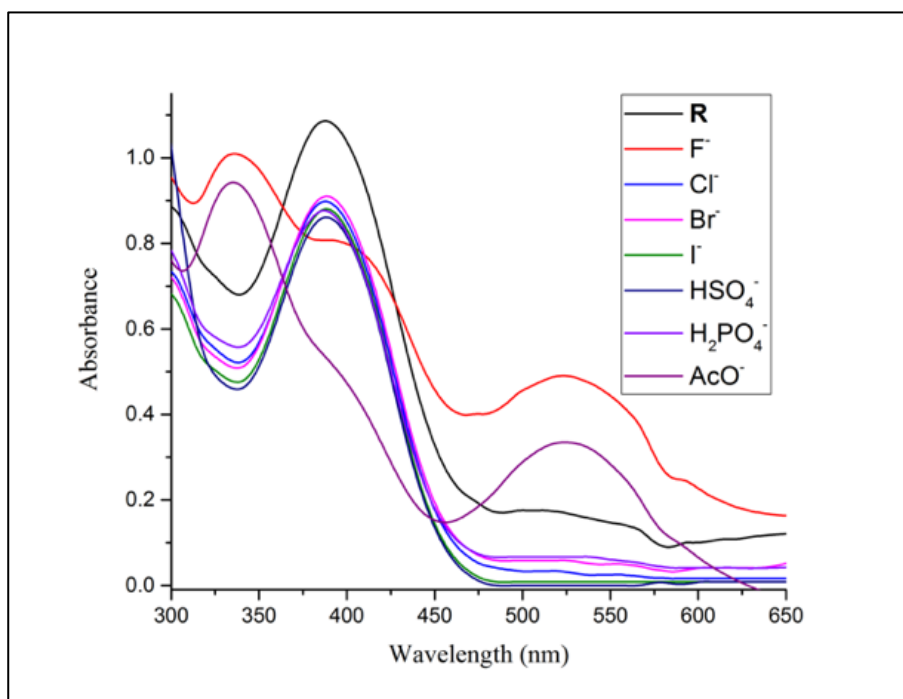


Fig. 2.8 UV-Vis absorption spectra of receptor **R** (1×10^{-4} M in DMSO) after the addition of 2 equiv. of different anions at 519 nm

Anion binding properties of receptor **L** (4.5×10^{-5} M in DMSO) has been studied with the addition of 2 equiv. of a series of anions as tetrabutylammonium salts (F⁻, Cl⁻, Br⁻, I⁻, NO₃⁻, HSO₄⁻, H₂PO₄⁻ and AcO⁻ of concentration 1×10^{-2} M in DMSO). Receptor **L** exhibited significant color change from pale yellow to orange and blue respectively in the presence of F⁻ and AcO⁻ ions. The color change is shown in Fig. 2.9. The observed color changes reflect the corresponding redshift in the absorption spectra as seen in Fig. 2.10.

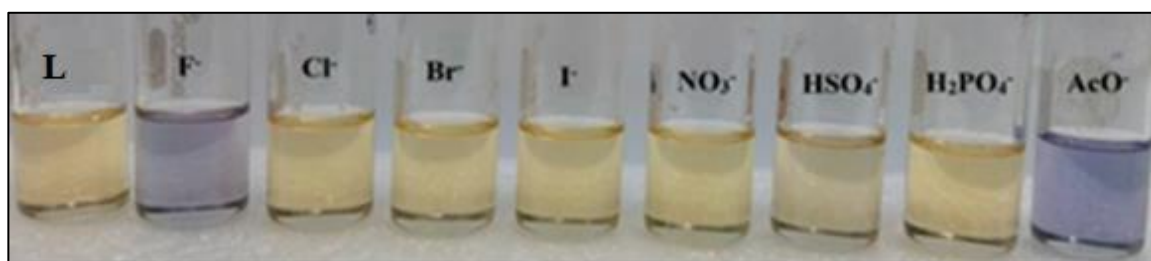


Fig. 2.9 Color change observed for **L** (4.5×10^{-5} M in DMSO) with the addition of 1 equiv. of different anions (1×10^{-2} M in DMSO)

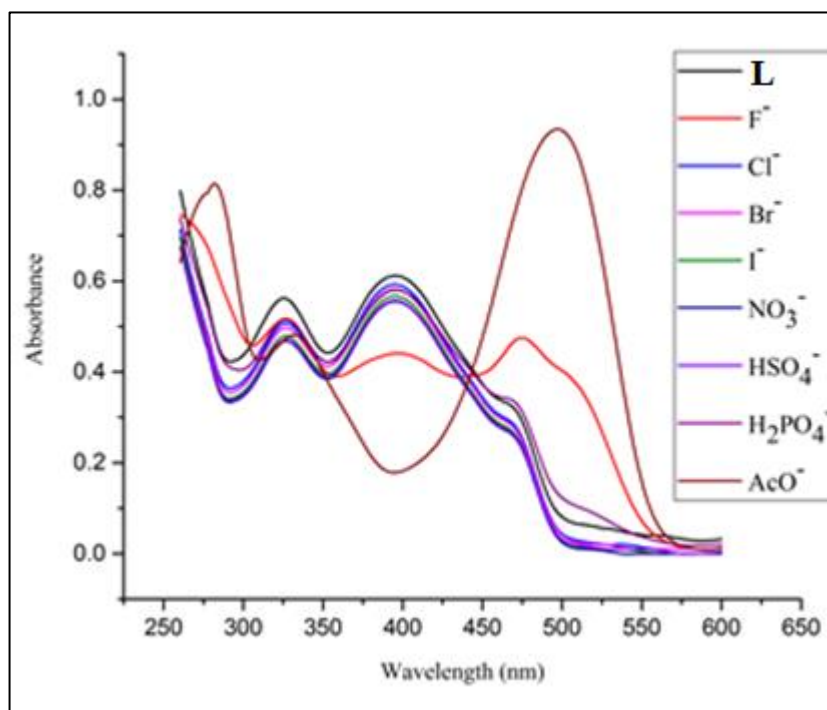


Fig. 2.10 UV-Vis absorption spectra of **L** (4.5×10^{-5} M in DMSO) upon addition of 1 equiv. of various anions as TBA salts

2.3.2 UV-Vis titration studies

UV-Vis spectrophotometric titration was performed as a means to quantify the observed shift in absorption maxima. The receptor solution was prepared in organic media, 1×10^{-4} M in DMSO and TBAF as 1×10^{-2} M in DMSO. To a measured quantity of receptor, incremental amount of F^- (0.1 equiv.) was added each time until absorbance attained saturation. Bathochromic shift was observed with the emergence of new peak at 519 nm, reason being the charge transfer interactions between the proton donor $-OH$ functionality and the acceptor viz., F^- ion. The concomitant decrease in the absorption maxima at 383 nm depicts subsiding O-H---N intramolecular charge transfer within the receptor moiety upon binding of F^- ion. The binding is further strengthened due to the presence of ancillary substituent in the receptor viz., $-NO_2$ functionality which increases acidity of hydroxyl moiety. The presence of isobestic points at 360 nm and 426 nm indicate the complex formation process and the presence of equilibrium between the free receptor and the anion-

receptor complex. Upon addition of 2 equiv. of F^- , the absorption spectra reached a plateau indicating the saturation point of the receptor as shown in Fig. 2.11.

Similar results were obtained with the incremental addition of standard solution of AcO^- ion (0.1 equiv.) to a measured quantity of receptor. A new peak was observed at 528 nm with a concomitant decrease in the peak centered at 383 nm. The red shift by a unit of 145 nm could be due to the bifurcated hydrogen bonding interaction of AcO^- ion with hydroxyl moiety. The geometry of the receptor suits well with the trigonal planar structure of AcO^- ion with a bond angle of 120° . The bond distance between two oxygen atoms of AcO^- ion is appropriate to bind to the hydroxyl protons present on complementary positions in the receptor. Presence of conformational complementarity between the receptor **R** and AcO^- ion assists the binding process. The presence of isobestic points at 362 nm and 434 nm represent the formation of a new complex in the system. The titration reached saturation value with the addition of 1 equiv. of AcO^- ion as represented in Fig. 2.12.

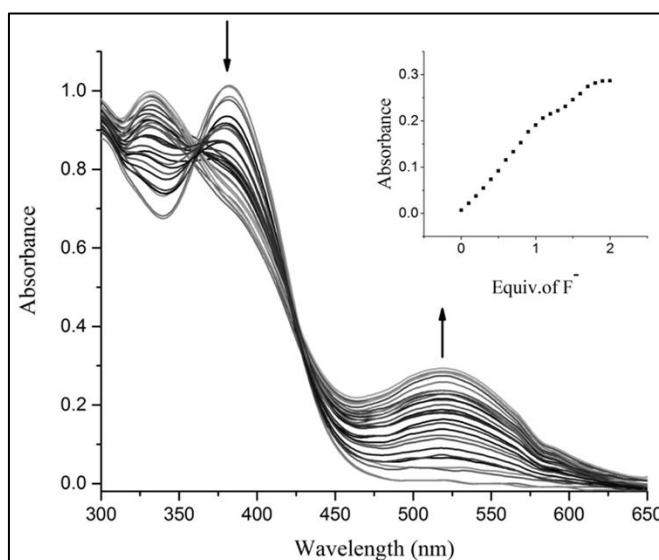


Fig. 2.11 UV-Vis titration spectra of receptor **R** (1×10^{-4} M in DMSO) with incremental addition of TBAF (0-2 equiv.). Inset showing the binding isotherm at selected wavelength (519 nm)

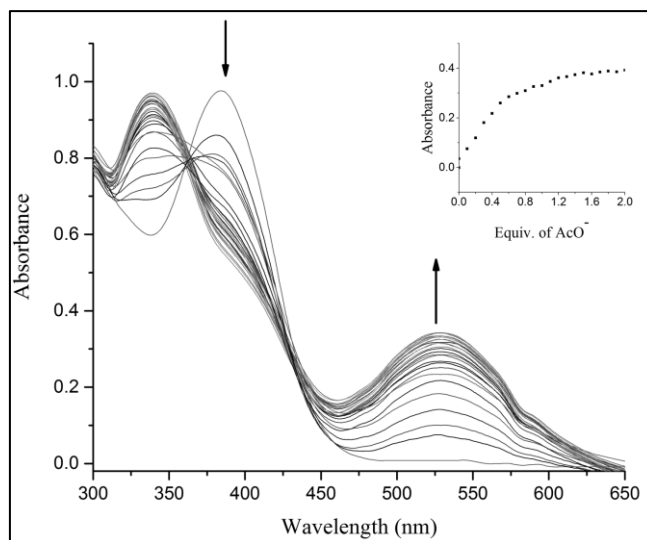


Fig. 2.12 UV-Vis titration spectra of receptor **R** (1×10^{-4} M in DMSO) with incremental addition of TBAAcO (0-2 equiv.). Inset showing the binding isotherm at selected wavelength (528 nm)

Inorganic fluoride, NaF is an essential part of the biological system which must be present in optimum amount to maintain the physiological process. Deficiency or excess of it leads to disorders in the ecosystem. In this regard, the detection of F⁻ ion is essential. The study has been extended to detect NaF (1×10^{-2} M in distilled water). With the incremental addition of F⁻ (0.1 equiv.) to the measured quantity of the receptor solution (1×10^{-4} M in DMSO), a new peak emerged at 513 nm due to the hydrogen bonding interactions. The saturation point was reached with the addition of 2 equiv. of F⁻ as represented in Fig. 2.13. This reflects the property of the receptor to detect F⁻ ions present in aqueous medium.

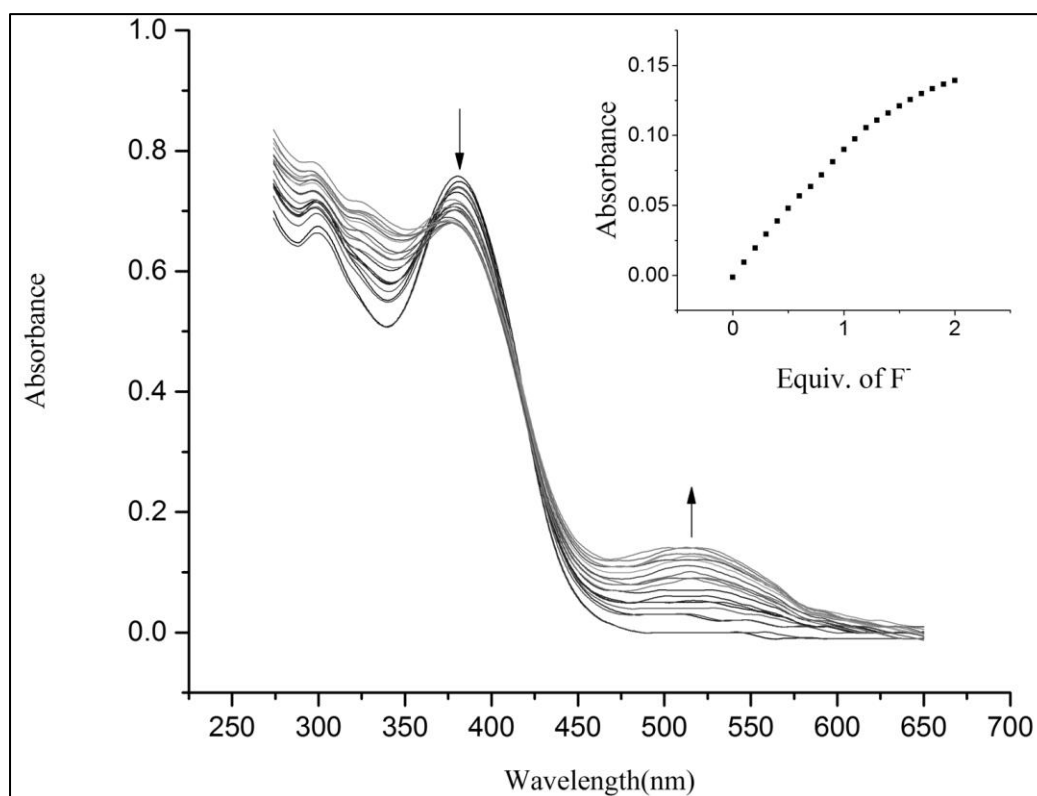


Fig. 2.13 UV-Vis titration spectra of receptor **R** (1×10^{-4} M in DMSO) with incremental addition of NaF (0-2 equiv.). Inset showing the binding isotherm at selected wavelength (513 nm)

With the UV-Vis titration studies as the basis, the stoichiometric ratio of binding of receptor to anion has been analyzed by Benesi-Hildebrand (B-H) plot (Benesi and Hildebrand 1948). The plot of $1/[A-A_0]$ vs $1/[F^-]$ gave a straight line confirming the 1:2 binding process between receptor and F^- . Due to the geometrical considerations, one AcO^- ion could effectively bind to a receptor yielding 1:1 binding ratio with B-H plot. This is represented in Fig. 2.14, Fig. 2.15 and Fig. 2.16.

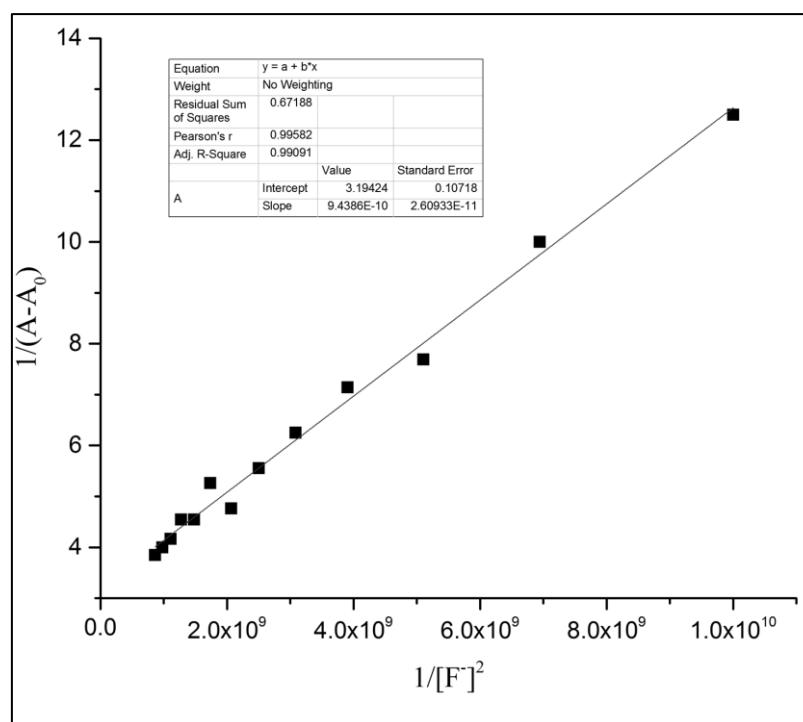


Fig. 2.14 B-H plot of $R-F^-(TBAF)$ complex at a selected wavelength of 519 nm

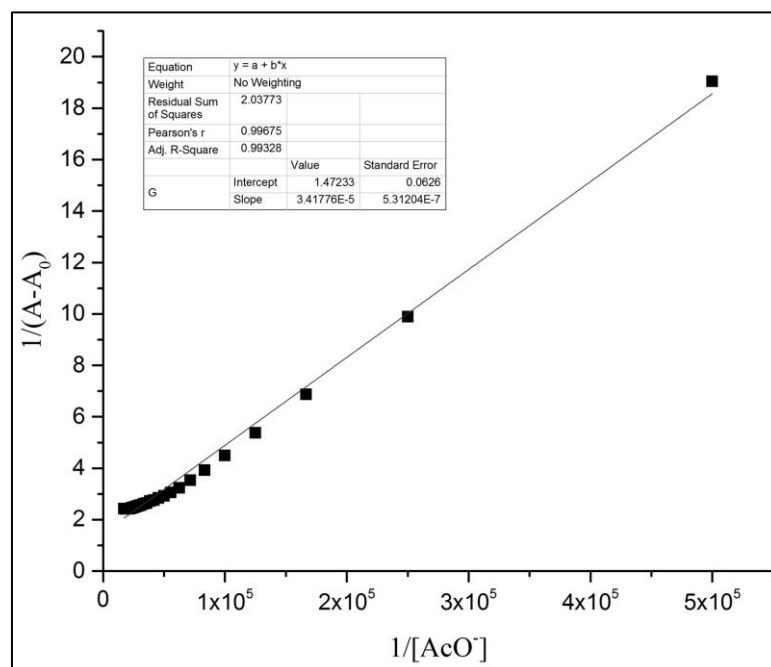


Fig. 2.15 B-H plot of $R-AcO^-(TBAAcO)$ complex at a selected wavelength of 528 nm

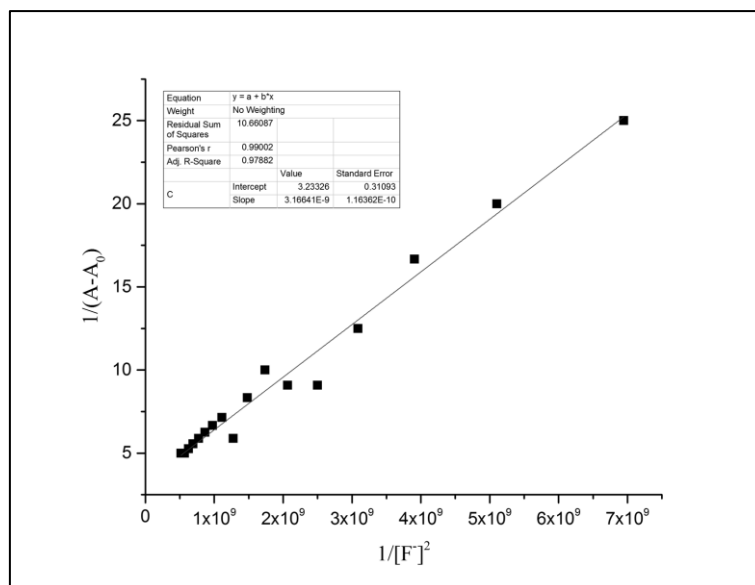


Fig. 2.16 B-H plot of $\mathbf{R-F}^-(\text{NaF})$ complex at a selected wavelength of 513 nm

With the above results, the receptor \mathbf{R} was further utilized for the detection of F^- in commercially available mouthwash. The receptor \mathbf{R} exhibited a color change from pale yellow to red by the addition of a drop of mouthwash into a measured quantity of receptor as shown in Fig. 2.17. As a quantification procedure, the UV-Vis titration analysis was performed with incremental addition of mouthwash (0.1 equiv.) to the measured volume of receptor. The titration profile exhibited a significant shift in λ_{max} by 120 units in comparison with the free receptor with the emergence of new peak at 513 nm and a subsequent decrease in the peak at 382 nm as displayed in Fig. 2.18. Calibration curve of absorbance vs concentration of F^- ion has been plotted to determine the amount of F^- in mouthwash. Prior to the analysis, mouthwash was diluted 50 times and the value obtained from the standard plot has been multiplied by an appropriate dilution factor to arrive at the actual concentration of F^- in mouthwash. It is represented in Fig. 2.19. The value obtained from the standard plot for mouthwash is 225 ppm which is comparable with standard values (WHO report, 1994).

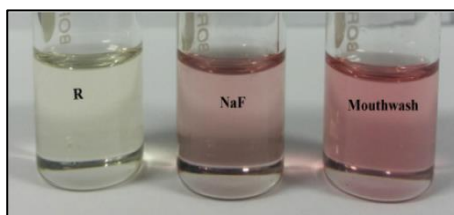


Fig. 2.17 Colour changes of receptor **R** upon addition of 2 equiv. of NaF and mouthwash

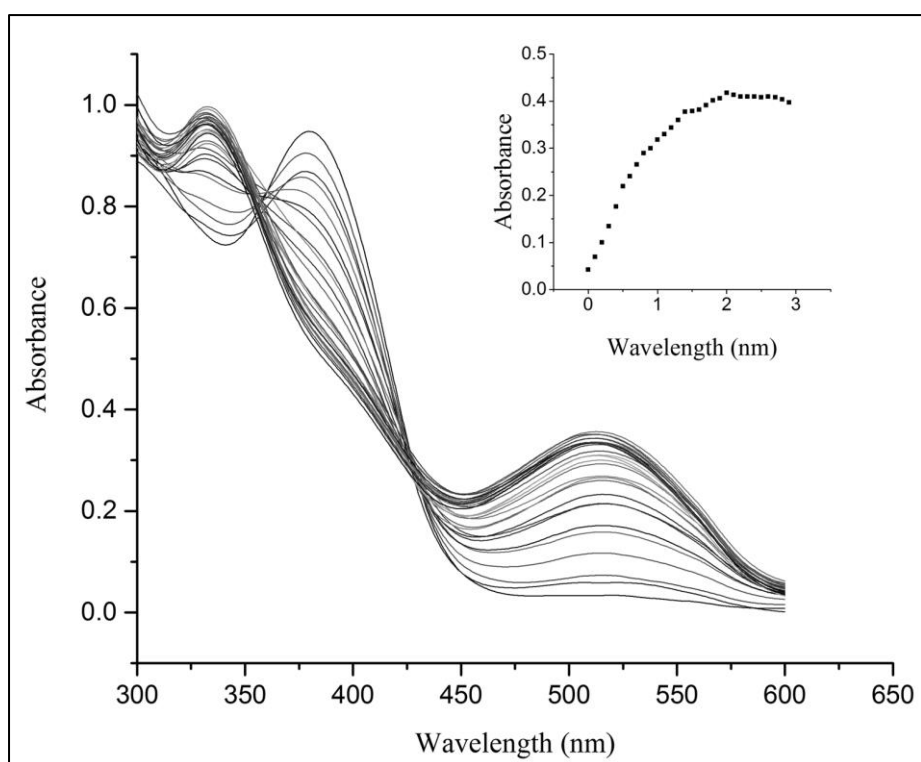


Fig. 2.18 UV-Vis titration spectra of receptor **R** (1×10^{-4} M in DMSO) with incremental addition of mouthwash (0-3 equiv.). Inset showing the binding isotherm at selected wavelength (513 nm)

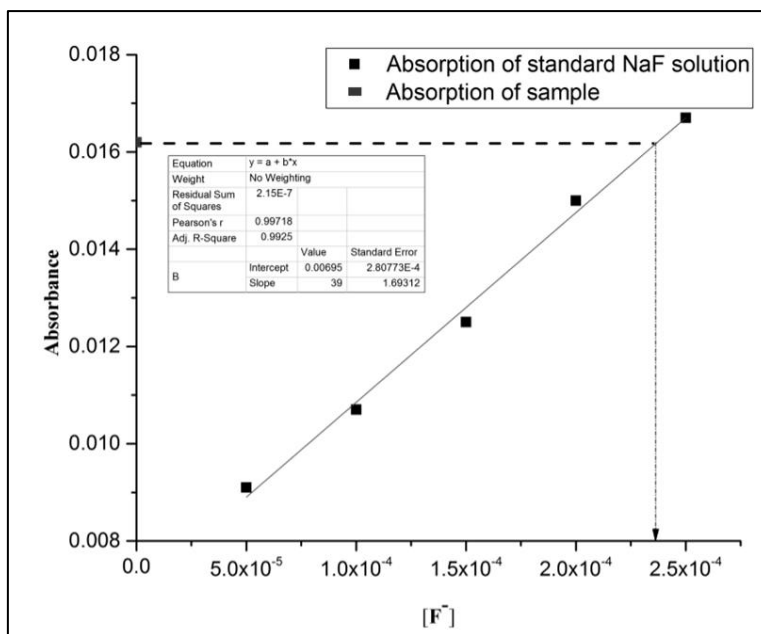


Fig. 2.19 Calibration curve for the determination of F^- ion in mouthwash

Similarly, UV–Vis spectral analysis has been performed as part of quantitative analysis to support the observed color changes. Receptor **L** exhibits absorption band at 363 nm corresponding to transitions of azomethine group along with low energy band at 459 nm relating to the ICT transition from naphthyl –OH moiety(donor) to the –NO₂ substituent (acceptor) of the pyridine group. Upon incremental addition of 0.1 equiv. of F^- and AcO^- ions to receptor **L**, absorption band at 459 nm red shifted to 560 nm indicative of the strong influence of –R and –I effect of –NO₂ substituent on the intermolecular proton transfer process. Substantial enhancement of ICT in **L** indicates an efficient push pull tendency existing in the host-guest interaction mechanism. Appearance of clear isobestic point at 500 nm clearly indicates the formation of new complex. The complete disappearance of the peak at 459 nm at higher equivalence of F^- and AcO^- ions is suggestive of the deprotonation mechanism. The saturation point was achieved with the addition of 2 equiv. of F^- and AcO^- ions indicating the completion of reaction. Titration profile of **L** with F^- and AcO^- ions is represented in Fig. 2.20 and Fig 2.21. B-H plot for **L**- F^- and **L**- AcO^- complex yielded a linear plot with second power of concentration of anions indicating the strong hydrogen bond formation followed by deprotonation of receptor. B-H plot of **L** with F^- and AcO^- ions is shown in Fig. 2.22 and Fig 2.23.

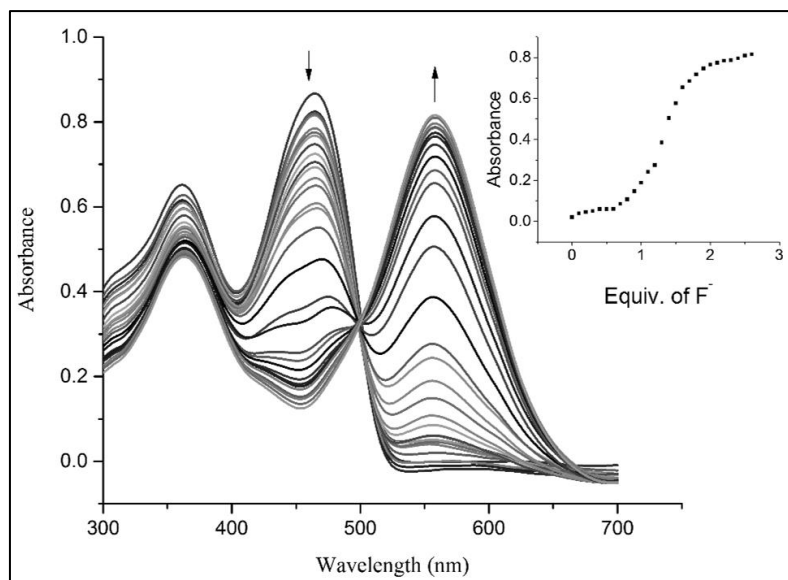


Fig. 2.20 UV-Vis titration spectra of receptor **L** (4.5×10^{-5} M in DMSO) with the incremental addition of 0.1 equiv. of TBAF (1×10^{-2} M in DMSO). Inset plot representing the binding isotherm at 560 nm

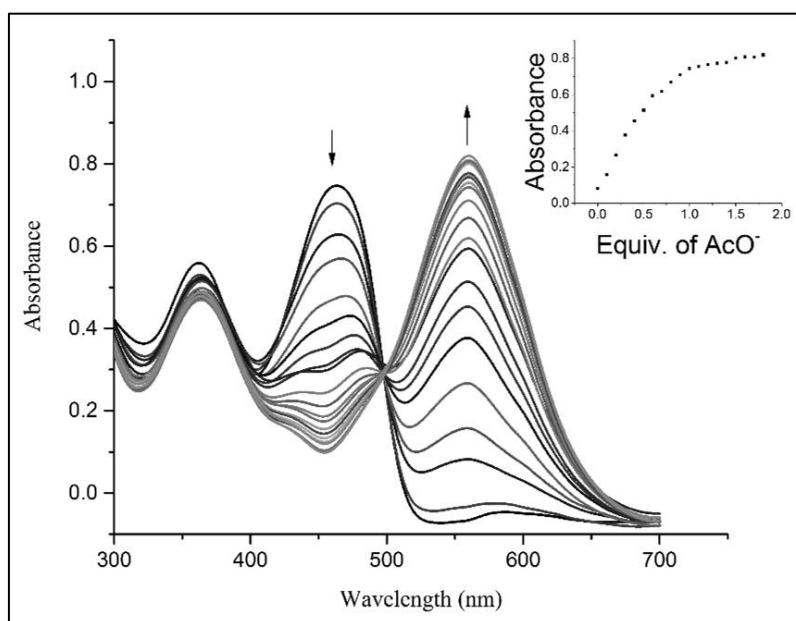


Fig. 2.21 UV-Vis titration spectra of receptor **L** (4.5×10^{-5} M in DMSO) with the incremental addition of 0.1 equiv. of TBAAcO (1×10^{-2} M in DMSO). Inset plot representing the binding isotherm at 560 nm

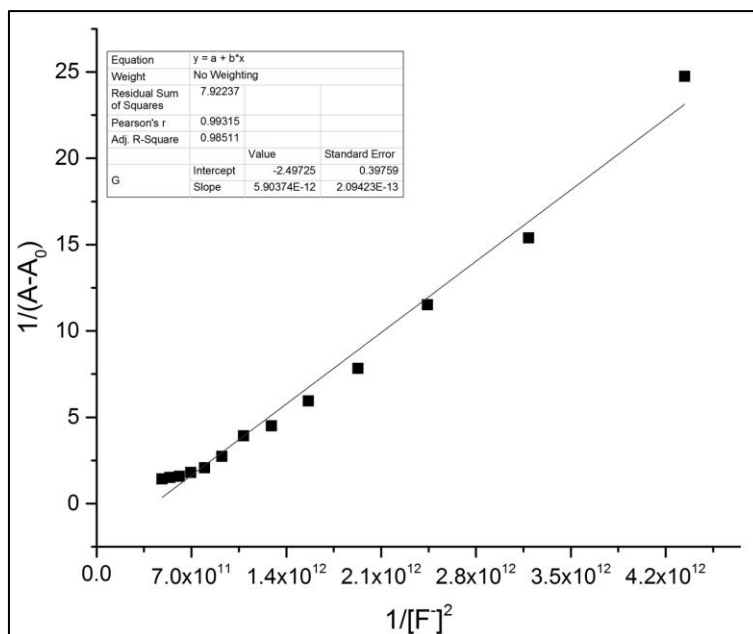


Fig. 2.22 B –H plot of receptor **L**- F⁻ (TBAF) complex at a selected wavelength of 560 nm

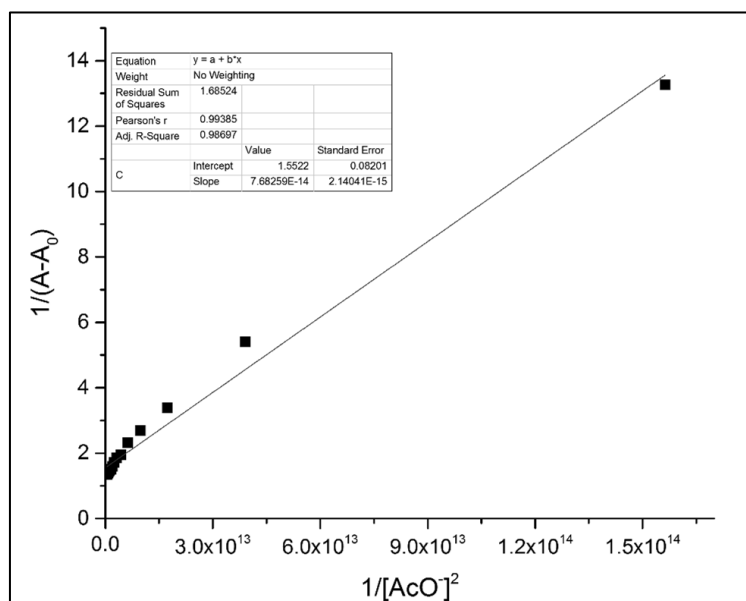


Fig. 2.23 B –H plot of receptor **L**- AcO⁻ complex at a selected wavelength of 560 nm

Titration experiments of **L** with sodium salts of F⁻ and AcO⁻ ions revealed redshift of band to 556 nm and 559 nm correspondingly with clear isobestic points indicative of the complex formation. Titration profile of **L** with the addition of sodium salt of F⁻ and AcO⁻ ions is shown in Fig. 2.24 and Fig. 2.25. Stoichiometric ratio of

1:2 between $L-F^-$ and $L-AcO^-$ complex is represented in Fig. 2.26 and Fig. 2.27. The resultant binding constant calculated using B-H equation and detection limit for L has been tabulated in Table 2.1.

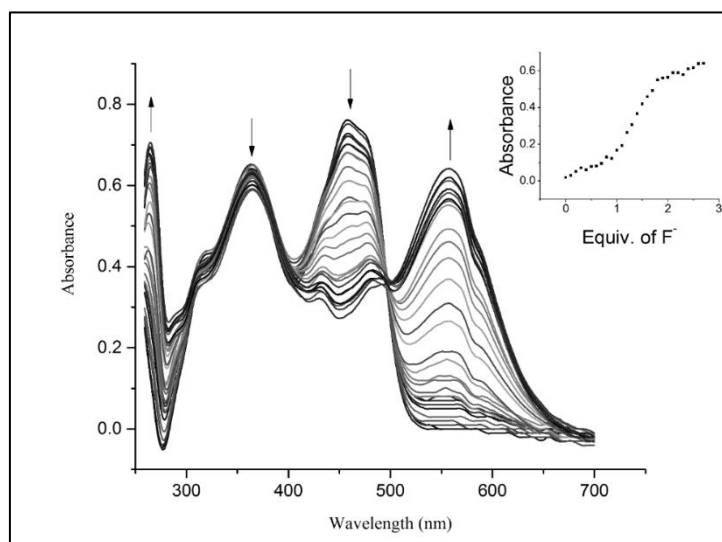


Fig. 2.24 UV-Vis titration spectra of receptor L (4.5×10^{-5} M in 9:1, v/v, DMSO:H₂O) with the addition of 0.1 equiv. of NaF (1×10^{-2} M in distilled water). Inset plot representing the variation of absorbance with concentration of NaF at 556 nm

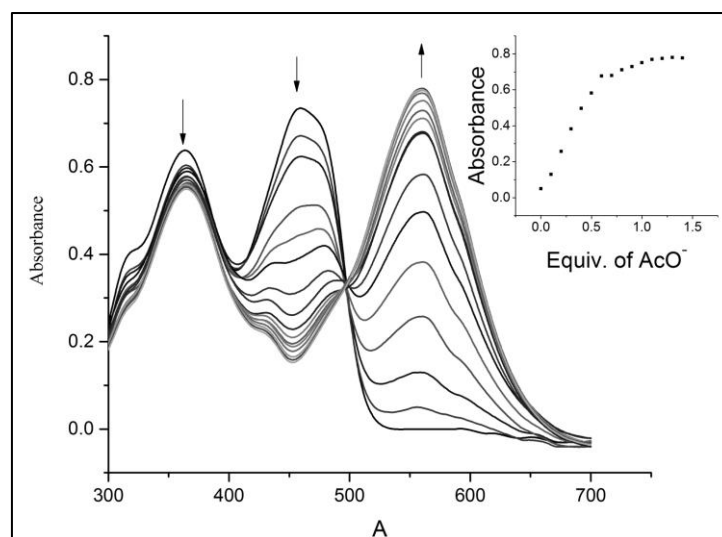


Fig. 2.25 UV-Vis titration spectra of receptor L (4.5×10^{-5} M in 9:1, v/v, DMSO:H₂O) with the addition of 0.1 equiv. of NaAcO (1×10^{-2} M in distilled water). Inset plot representing the variation of absorbance with concentration of NaAcO at 559 nm

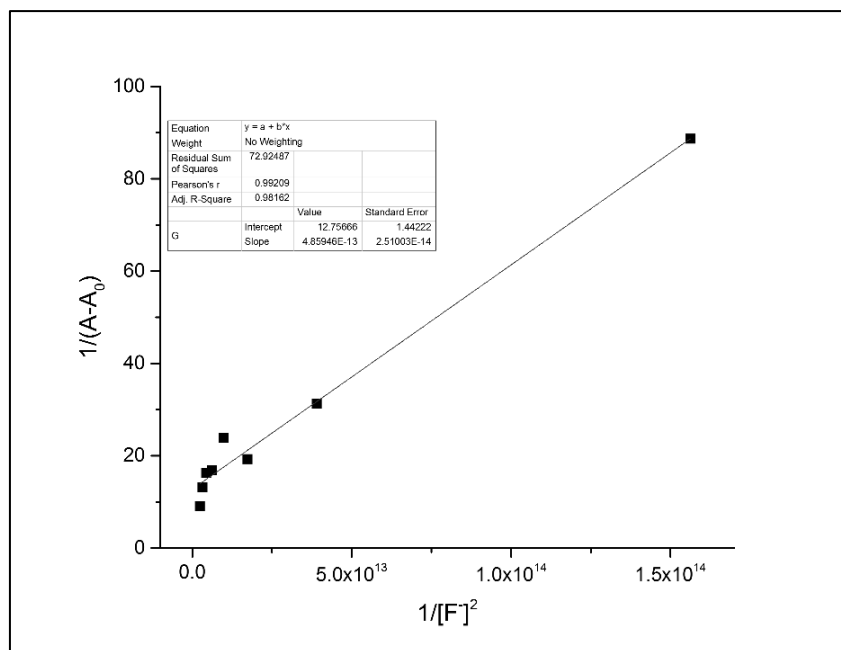


Fig. 2.26 B –H plot of receptor L- F (Na⁺) complex at a selected wavelength of 556 nm

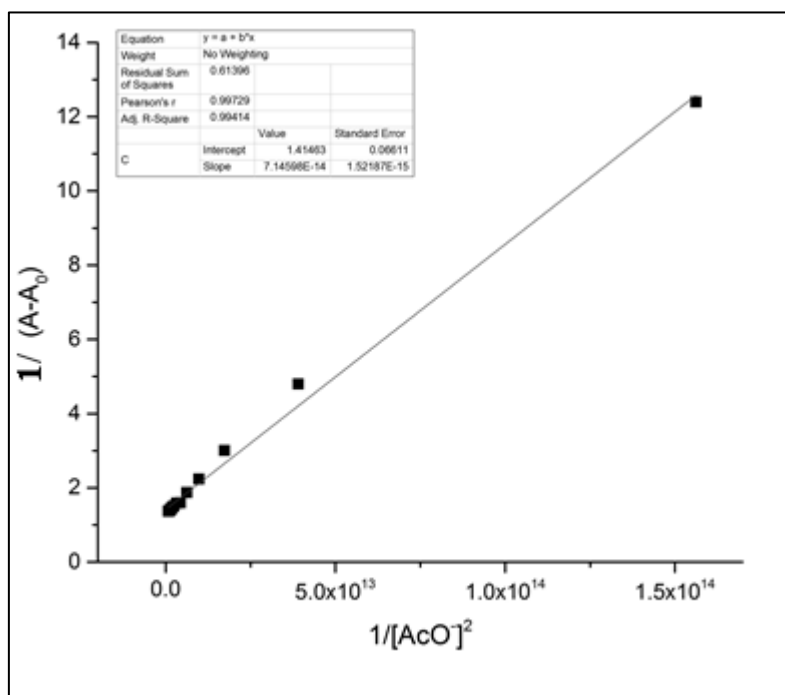


Fig. 2.27 B –H plot of receptor L- AcO⁻ (Na⁺) complex at a selected wavelength of 559 nm

The ability to detect anions in aqueous media reflects the suppression of solvent interferences in the detection process. Anion binding studies of **L** has been extended to detect F^- ion in commercially available mouthwash sample. **L** exhibited remarkable color change from pale yellow to blue with the addition of 2 equiv. of mouthwash. The color change observed is shown in Fig. 2.28.

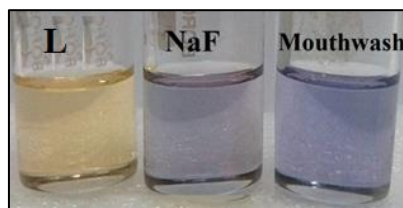


Fig. 2.28 Color change of receptor **L** upon addition of NaF and mouthwash

2.3.3 Time dependency studies

With a view to validate the real time detection of anions, time evolution of receptor **R** in the presence of 2 equiv. of F^- and AcO^- ion was investigated. Binding interaction between **R** and F^- ion continued till the 10th minute while the binding of **R** with AcO^- was almost completed at the 5th minute beyond which the receptor attained saturation (Fig. 2.29 and Fig. 2.30). Owing to the geometrical complementarity combined with the bifurcated hydrogen bond interaction, the binding of **R**--- AcO^- ion involved a short response time. The requirement of two F^- ions to bind the receptor **R** in 2:1 binding ratio would have been the probable reason for the longer response time required for the detection process.

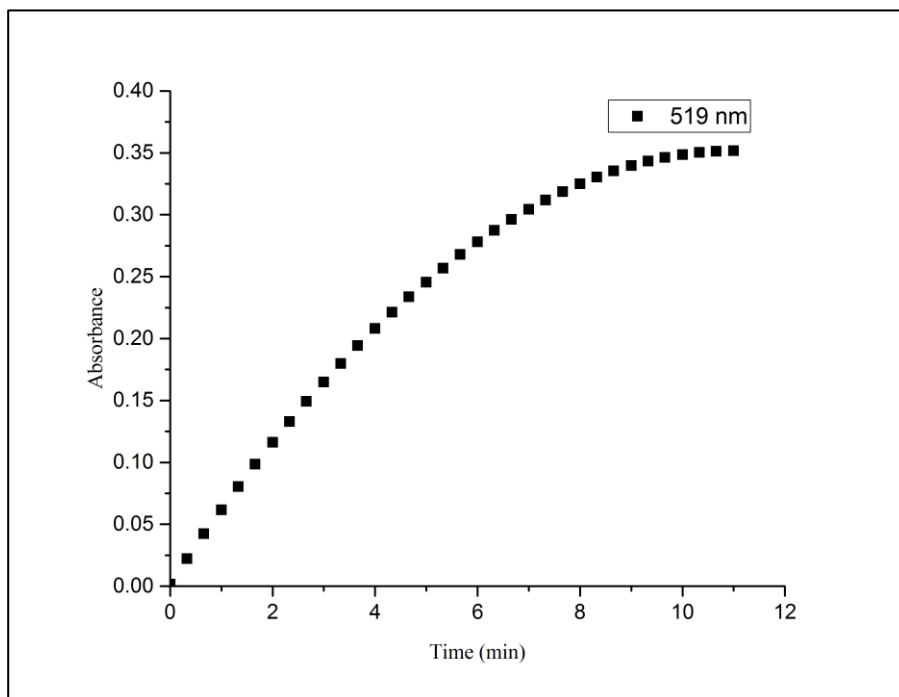


Fig. 2.29 Time evolution study of receptor **R** (10^{-4} M in DMSO) in the presence of TBA salt of F^{-} ion

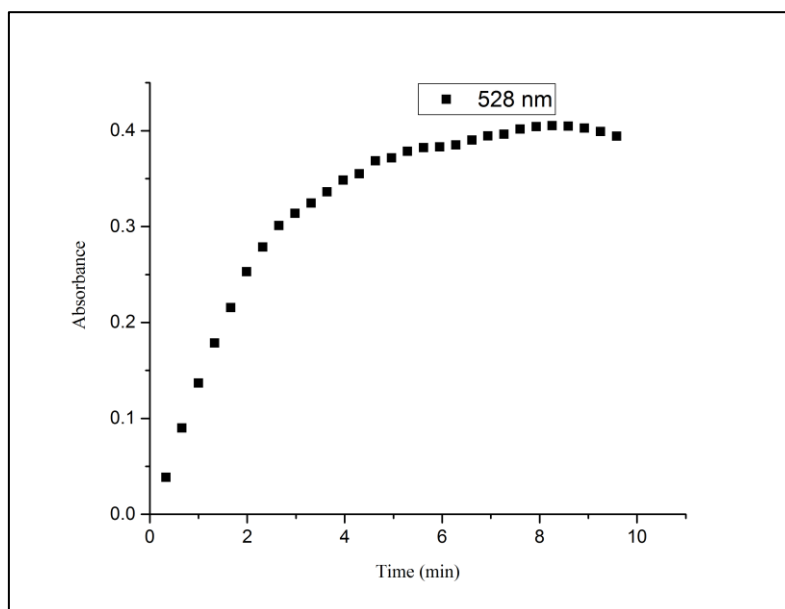
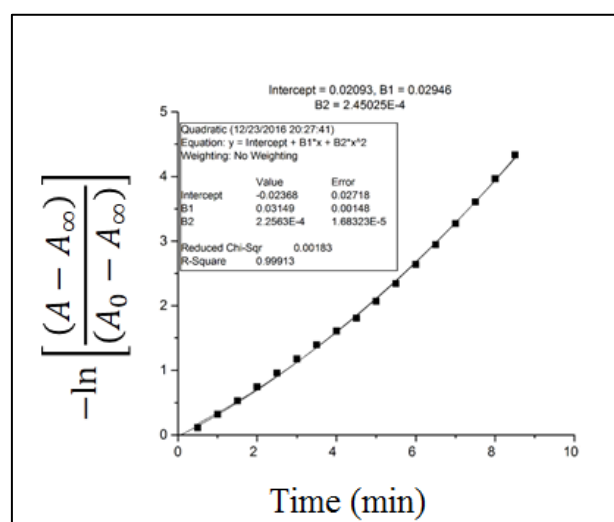
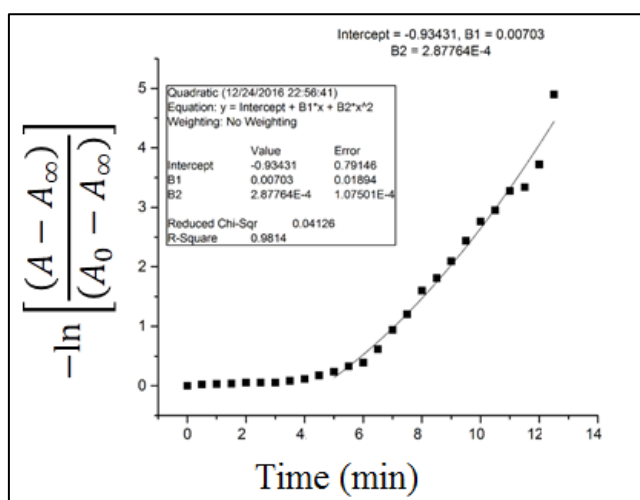


Fig. 2.30 Time evolution study of receptor **R** (10^{-4} M in DMSO) in the presence of TBA salt of AcO^{-} ion

The colorimetric response of receptor **L** towards AcO^- ion was found to be instantaneous. During the titration process, it was found that with the increase in equiv. of AcO^- ion, the spectral changes exhibited a substantial increase in the absorption value corresponding to the linear dependence on concentration. The decrease in the intensity of the original absorption band of receptors **L** centered at 459 nm, and the gradual increase of the band centered at 560 nm with clear isobestic points indicates the complexation process. It gives an indication that AcO^- ion interacted with the receptors forming an intermediate compound which further transformed into a stable complex. It was observed that the binding of anions attained saturation at 2 eq. of anions at 10th minute beyond which there was no significant alteration of the intensity of the absorption band. With this in view, spectral changes have been recorded as a function of time with the incremental addition of AcO^- ion to receptors **L**. Owing to the sharp changes in UV-Vis titration spectra with clear isobestic points, it could be assumed that there were no significant side reactions. Consequently, we tried fit the data of change in absorbance as a function of time to the first order rate equation $\ln |A - A_\infty| = -kt + \ln |A_0 - A_\infty|$ where A_0 is the initial absorbance (0th min), A is the absorbance at an intermediate (5th min) and A_∞ is the absorbance at saturation (10th min)(Gunupuru et al. 2014). The rate constant was calculated for **L** as a comparison over the reactivity of receptors towards AcO^- ion. The rate constant was calculated at two different wavelengths corresponding to the original absorption band of free receptor and red shift band observed in presence of AcO^- ion for **L**. The time response for AcO^- ion monitoring the band at 560 nm for **L** is shown in Fig. 2.31. The rate constant calculated for the band at 459 nm and 560 nm are too close indicating the relative dependence of anion concentration on the reacting species. Similarly, the rate constant has been calculated for receptors **L** in the presence of F^- ion. The lower order of magnitude of the rate constant in the presence of F^- ion could be correlated to the pK_a value of 3.2 (F^- ion) in comparison with AcO^- ion whose pK_a value is 4.8. The time response of receptors **L** in the presence of F^- ion is represented in Fig. 2.32. The observed rate constant at different wavelength for **L** is summarized in Table 2.1.

Table 2.1 Observed rate constant for the reaction of receptor **L** with AcO^- and F^- ion

Anion	Rate constant k (min^{-1})	
	459 nm	560nm
L + AcO^-	0.00216	0.0027
L + F^-	0.00005	0.00014

**Fig. 2.31** Time dependent plot of first order rate equation to determine rate constant from UV-Vis spectral change of **L** in the presence of AcO^- ion at 560 nm**Fig. 2.32** Time dependent plot of first order rate equation to determine rate constant from UV-Vis spectral change of **L** in the presence of F^- ion at 560 nm

2.3.4 Reversibility studies

In order to analyse the reversibility of the anion detection process, UV-Vis study has been performed with the addition of $\text{Ca}(\text{NO}_3)_2$ as an anion binding agent. Upon addition of $\text{Ca}(\text{NO}_3)_2$ (2 equiv.) to a mixture of receptor **R** and F^- ion (2 equiv.), the UV-Vis spectra displayed the original absorption band of the free receptor **R** as shown in Fig. 2.33. The disappearance of the absorption band corresponding to the receptor **R**- F^- complex reflects the effective displacement of F^- ion from the receptor unit by Ca^{2+} ions. Correspondingly, with the addition of $\text{Ca}(\text{NO}_3)_2$ (2 equiv.) to a mixture of receptor **R** and AcO^- ion (2 equiv.), there was no complete restoration of original absorption band of the free receptor **R** as shown in Fig. 2.34. The bifurcated hydrogen bonding interaction between AcO^- ion and the receptor being more stronger, hindered the complete reversibility of the anion detection process. The study clearly indicate the successful reversal of F^- ion binding process.

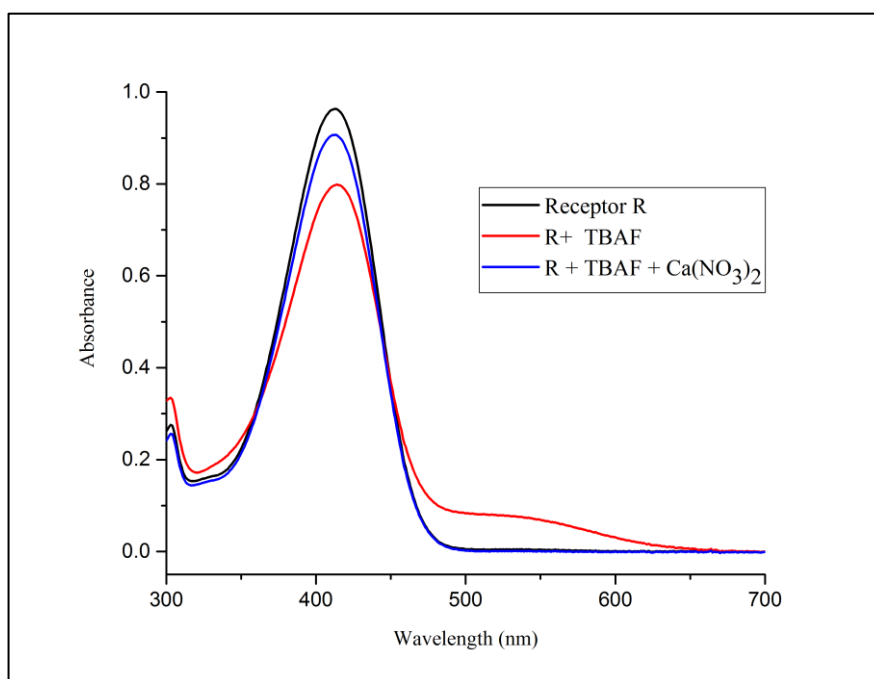


Fig. 2.33 UV-Vis spectra representing reversibility of receptor **R**– F^- complex in the presence of $\text{Ca}(\text{NO}_3)_2$

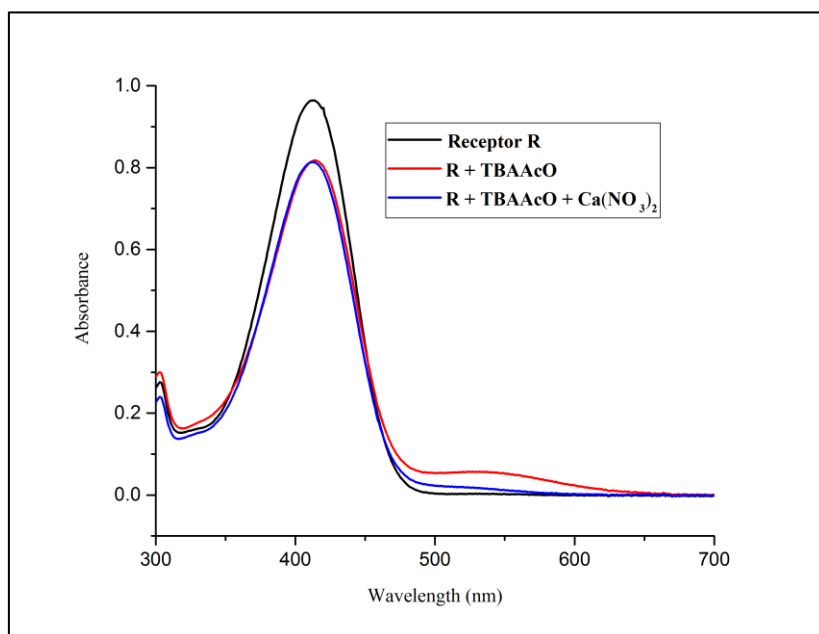
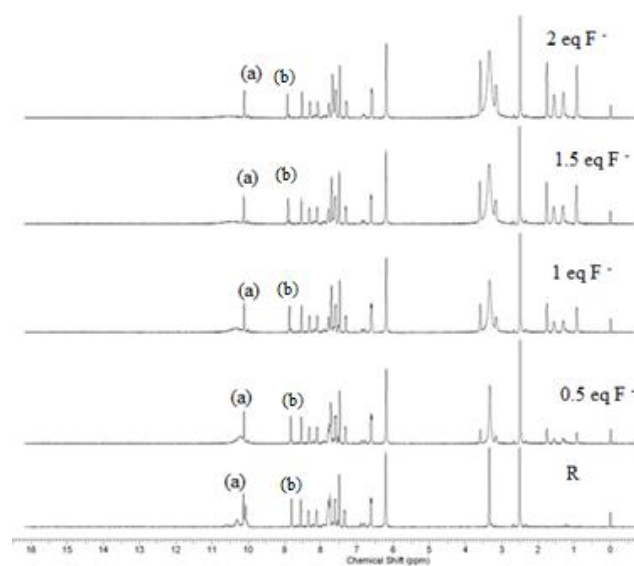


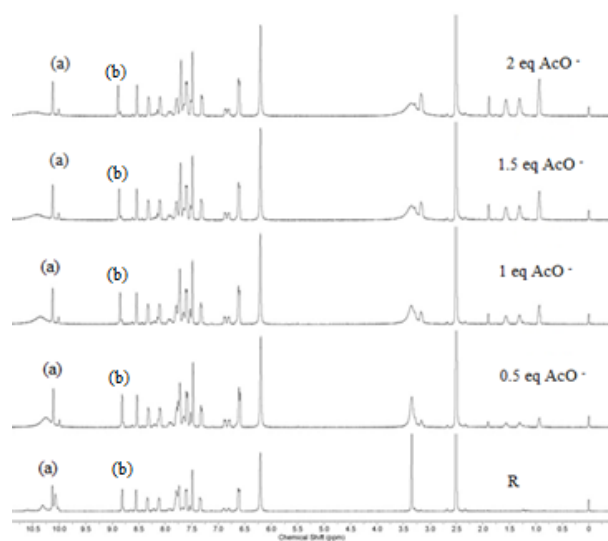
Fig. 2.34 UV-Vis spectra representing reversibility of receptor **R** –AcO[−] complex in the presence of Ca(NO₃)₂

2.3.5 ¹H-NMR titration studies

The study has been further extended to monitor the binding of anions by the receptors **R** and **L** through ¹H NMR titration in DMSO- *d*₆ solvent. The ¹H-NMR spectrum of **R** is characterized by the peaks for (a) –OH proton around δ 10.31 ppm, (b) imine proton at 8.8 ppm and aromatic protons at 6.2–8.5 ppm. It was observed that with the successive addition of F[−] ion, the OH proton experienced an upfield shift with slight broadening depicting the strong hydrogen bonding interaction with F[−] ion. This was accompanied with a downfield shift of the imine proton. There was no formation of triplet at 16 ppm which suggests the absence of the deprotonation process. Similar observation was obtained with the successive addition of AcO[−] ion to the receptor. In both of the above cases, there was no shift in the peaks corresponding to the aromatic region, reflecting that there was no delocalization of the charges as shown in Fig. 2.35 a and b. The formation of receptor **R**-anion complex was thus confirmed and the binding mechanism has been proposed.



(a)



(b)

Fig. 2.35 ^1H NMR titration spectra of receptor **R** upon addition of 0.5, 1.0, 1.5 and 2.0 equiv. of a) F^- and b) AcO^- ion

Similarly, to obtain an insight into the binding mechanism, ^1H -NMR titration studies have been performed with the incremental addition of TBAACO to DMSO- d_6 solution of receptor **L**. The unbound receptor exhibited OH proton signal at ~ 14 ppm owing to the presence of intramolecular hydrogen bond interaction with the imine

nitrogen (Farinha et al. 2010; Thiampanya et al. 2012; Yadav et al. 2014). The proton corresponding to the $-OH$ functionality centered at 14.9 ppm exhibited strong hydrogen bond with AcO^- ion indicated by the broadening of the signal upon successive addition of 0.5 and 1 eq. of anion. With the addition of 2 eq. of AcO^- ion, the proton signal diminished indicating the deprotonation mechanism. The imine proton did not exhibit upfield or downfield shift, yet the signal decreased in intensity upon successive addition indicative of its involvement in the bifurcated hydrogen bond interaction with AcO^- ion. The aromatic protons in **L** exhibited a gradual decrease in intensity indicating the charge transfer interactions occurring in the presence of AcO^- ion. 1H -NMR titration spectra of **L** in the presence of AcO^- ion is given in Fig. 2.36.

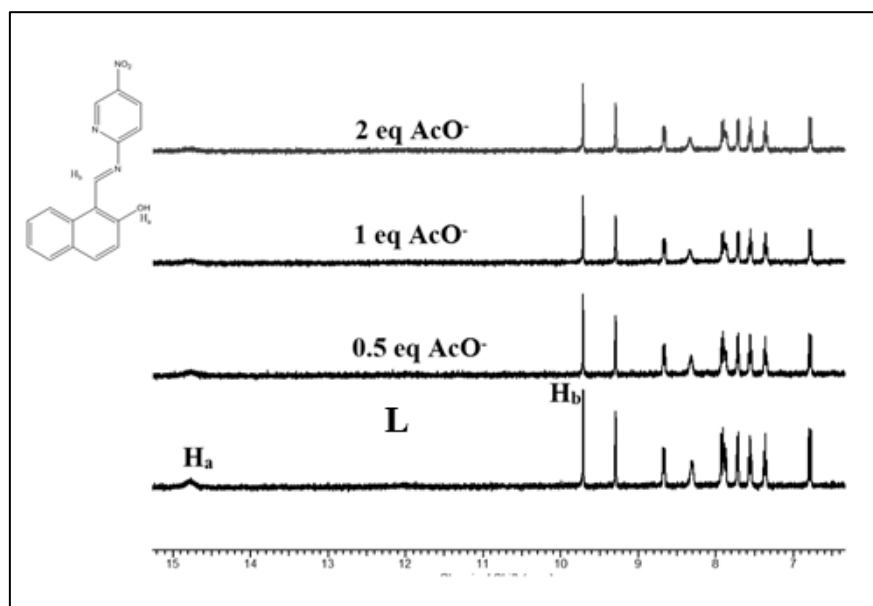


Fig. 2.36 1H -NMR titration spectra of **L** on incremental addition of AcO^- ion

2.3.6 Theoretical results

To support the experimental study and to understand the stability and the intermolecular charge transfer of the receptor **R** upon ion reception, we performed density functional theory calculation. Simulation does not show significant conformational change in the receptor upon binding of F^- and AcO^- ions, however binding with an additional ion leads to more stable structure of the receptor. The calculated value of interaction energies ($E_{int} = E_{R+ion} - E_R - E_{ion}$) are -28 kcal/mol and -

12 kcal/mol respectively for F^- and AcO^- ion reception. The DFT result shows that the HOMO and LUMO of the receptor spread over whole π -unit viz. over both aryl rings. The presence of nitro group is responsible for the spatial distribution of charges. Since both of the nitrophenyl ring bears $-OH$ functionality, in the case of $R+F^-$, one of the nitrophenyl units linked to isophthalaldehyde through imine linkage acts as HOMO and another nitrophenyl unit alone acts as LUMO. The HOMO-LUMO gap is reduced by 0.056 units from 0.3506 eV (band gap of **R**) to 0.345 eV in the presence of F^- ion. The reduction of band gap is due to the intramolecular charge transfer. Mulliken population analysis confirms the intramolecular charge transfer occurring within the receptor moiety upon reception of F^- ion.

Similar observation is found in the case of binding of receptor **R** with AcO^- ion where one of the nitrophenyl units linked to isophthalaldehyde through imine linkage acts as HOMO and another nitrophenyl unit alone acts as LUMO. There is stabilization of the HOMO and LUMO upon binding of AcO^- ion, which is represented by the reduced band gap by 0.046 eV in comparison with the free receptor **R**. This in turn reflects the intramolecular charge transfer occurring in the system. The optimized structure of free and anion bonded receptors are shown in Fig. 2.37. The distribution of HOMO, LUMO states and their energy differences are shown in Table 2.2.

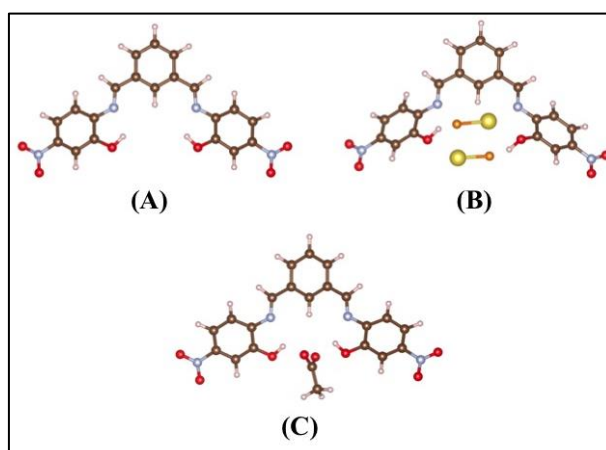


Fig. 2.37 Optimized geometry of receptor (A), receptor with NaF (B) and receptor with TBAAcO⁻ (C)

Charge distribution calculations confirms the acidity of the –OH functionality with a very high positive charge of the O-H1 and O-H14 protons. The corresponding Mulliken's atomic charge at O atoms varies from negative to a more negative value confirming the intramolecular charge transfer process existing between the anion and receptor. Mulliken charge distribution is represented in Table 2.3.

Table 2.2 Distribution of HOMO, LUMO orbital and corresponding energy gap of receptor **R** with F^- ion and AcO^- ions, obtained from TD-DFT calculations

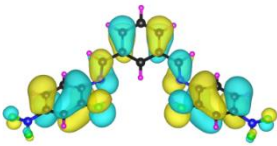
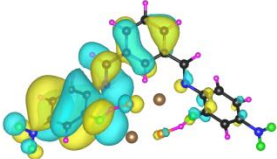
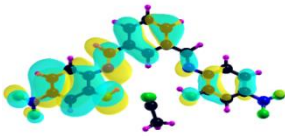
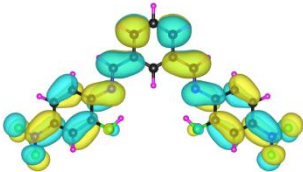
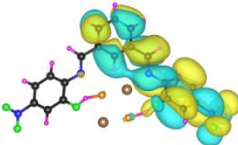
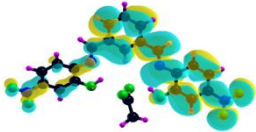
Molecular Orbitals	Receptor (R)	Receptor R + F^- ion	Receptor R + AcO^- ion
HOMO			
LUMO			
Band gap	3.506 eV	3.45 eV	3.46 eV

Table 2.3 Mulliken charges on O-H9, O-H14 in the receptor molecule upon binding of anions calculated at the (B3LYP) along with 6-311++G (d) basis set with the structural representation of receptor **R**

Molecule	O-H9	O-H14	O1-H	O4-H
Receptor R	0.330604	0.330603	-0.551569	-0.551567
R + $2F^-$	0.478032	0.470679	-0.723528	-0.712401
R + AcO^-	0.447474	0.446262	-0.665529	-0.656278

The optimized structure of the receptors **L** with the distribution of its HOMO and LUMO levels has been represented in Fig. 2.38. It was found that there were no any conformational changes observed in receptors **L** with the addition of anions indicating the structural stability of the receptor – anion complex. The results show that HOMO and LUMO are spread over both the aromatic rings due to the presence of electron withdrawing -NO₂ functionalities. ΔE which corresponds to energy difference between HOMO and LUMO ($E_{\text{HOMO}} - E_{\text{LUMO}}$) of **L** has been calculated and found to be 0.1252 E_h. In order to confirm the stability of receptor anion complex, the HOMO and LUMO in the presence of F⁻ and AcO⁻ ion has been studied. Significant reduction in the value of ΔE to 0.08 Ha (**L**+ F⁻ and **L** + AcO⁻) confirms the presence intramolecular charge transfer transitions during the anion detection process. The reduction in the band gap values is supported with red shift of the original absorption band of receptors **L**. The emergence of new band at higher wavelength confirms the complex formation process. HOMO and LUMO of **L**-F⁻ and **L**-AcO⁻ is represented in Fig. 2.39 and Fig. 2.40. The decrease in the bond length value corresponding to the -OH group from 0.96 Å to 1.47 Å and 1.55 Å reflects the host-guest supramolecular interaction. The Mulliken charge distribution calculations exhibits the alteration of magnitude of atomic charge on oxygen atom of receptor **L** from less negative to more negative value indicative of the intramolecular charge transfer transitions upon anion binding. Theoretical calculations yield the absorption maxima at 361 and 487 nm for **L**. The shift in absorption maxima to 572 and 571 nm for **L**-F⁻ and **L**-AcO⁻ ion complex provides full proof of the anion binding process.

The substantial increase in the dipole moment of receptor-F⁻ complex indicates efficient charge separation aiding the formation of hydrogen bond interaction between OH and F⁻. While the receptor **L** – AcO⁻ complex exhibited one-fold increase in the dipole moment implying the bifurcated nature of hydrogen bonding interact which involves equal sharing of one OH proton with two electronegative oxygen atoms of acetate ion.

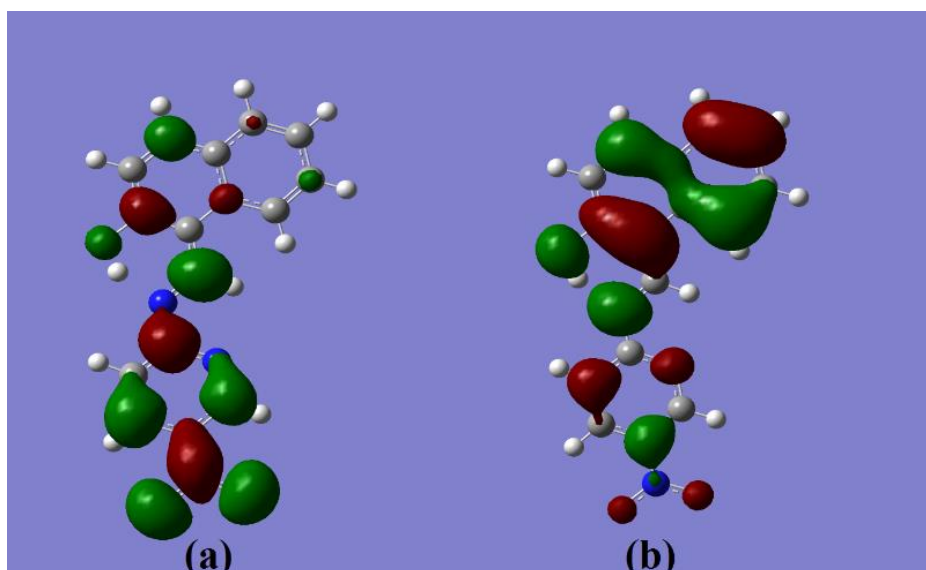


Fig. 2.38 Optimized structure of receptor **L**; (a) HOMO, (b) LUMO

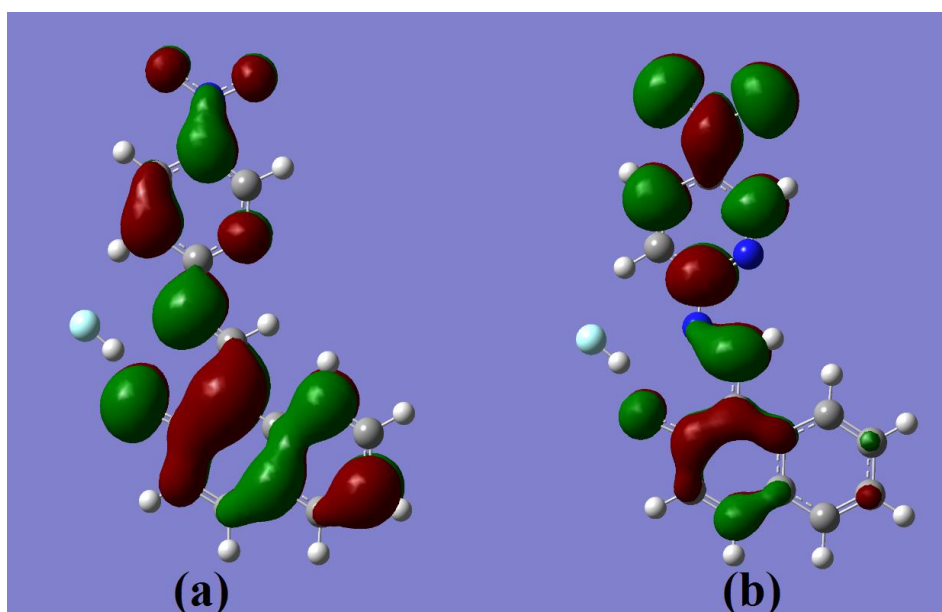


Fig. 2.39 Optimized structure of receptor **L**-F⁻ complex; (a) HOMO, (b) LUMO

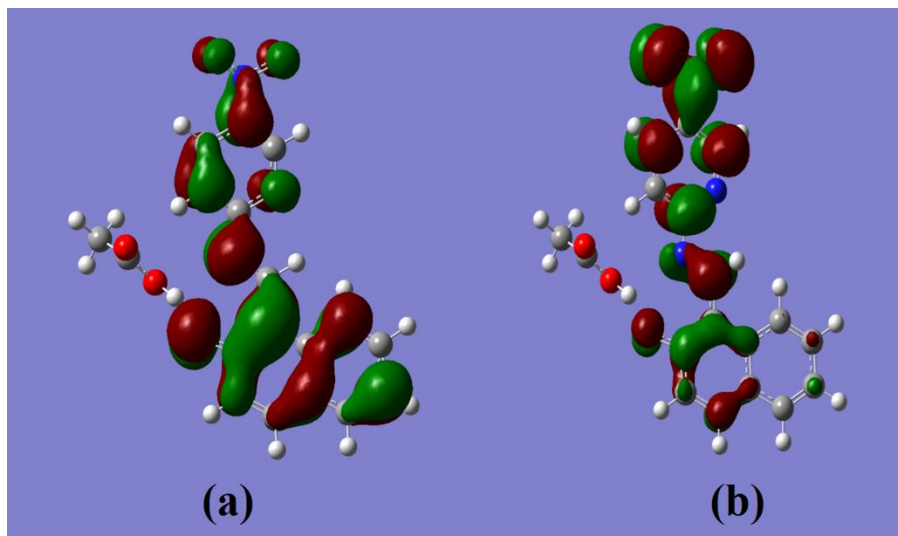


Fig. 2.40 Optimized structure of receptor **L**- AcO⁻ complex; (a) HOMO, (b) LUMO

2.3.7 Calculation of binding constant from UV-Vis studies

Binding constant has been calculated using Benesi-Hildebrand equation (Benesi and Hildebrand 1948) as given below;

$$1/(A - A_0) = 1/(A_{\max} - A_0) + 1/K [X^-]^n (A_{\max} - A_0)$$

where, A_0 , A , A_{\max} are the absorption considered in the absence of anion, at an intermediate, and at a concentration of saturation. K is binding constant, $[X^-]$ is concentration of anion and n is the stoichiometric ratio.

2.3.8 Binding ratio and detection limit

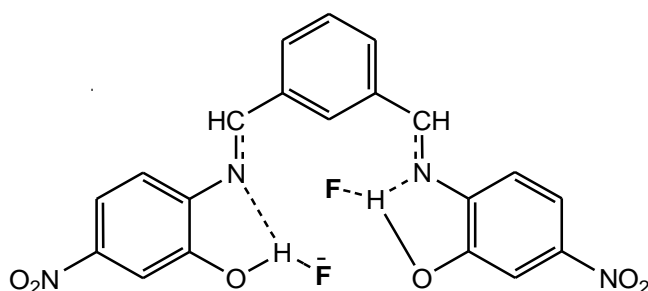
The binding ratio has been obtained from B-H plot. The detection limit was calculated and in particular, the detection limit was for F⁻ ion was found to be 1.12 ppm organic media and 2 ppm in aqueous media. The reason for relatively higher detection limit could be ascribed to the solvent-anion interactions prevailing during the anion binding event. The binding ratio, binding constant and detection limit are given in Table 2.4.

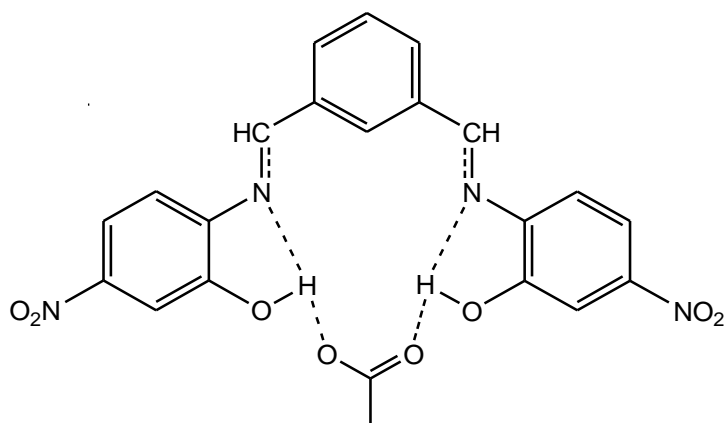
Table 2.4 Binding constant, binding ratio and detection limit of receptors **R** and **L**

Receptor	Anions	Binding ratio	Binding constant (K)	LOD (ppm)
R	F ⁻ (TBAF)	1:2	1.52x10 ⁴ M ⁻²	1.12
	AcO ⁻ (TBAAcO)	1:1	5.54x10 ⁴ M ⁻¹	3.01
	F ⁻ (NaF)	1:2	7.01x10 ³ M ⁻²	2.00
L	F ⁻ (TBAF)	1:2	0.30 x10 ⁴ M ⁻²	5.2
	AcO ⁻ (TBAAcO)	1:2	5.6 x10 ⁴ M ⁻²	3.39
	F ⁻ (NaF)	1:2	0.85 x10 ⁴ M ⁻²	0.94
	AcO ⁻ (NaAcO)	1:2	6.3 x 10 ⁴ M ⁻²	0.92

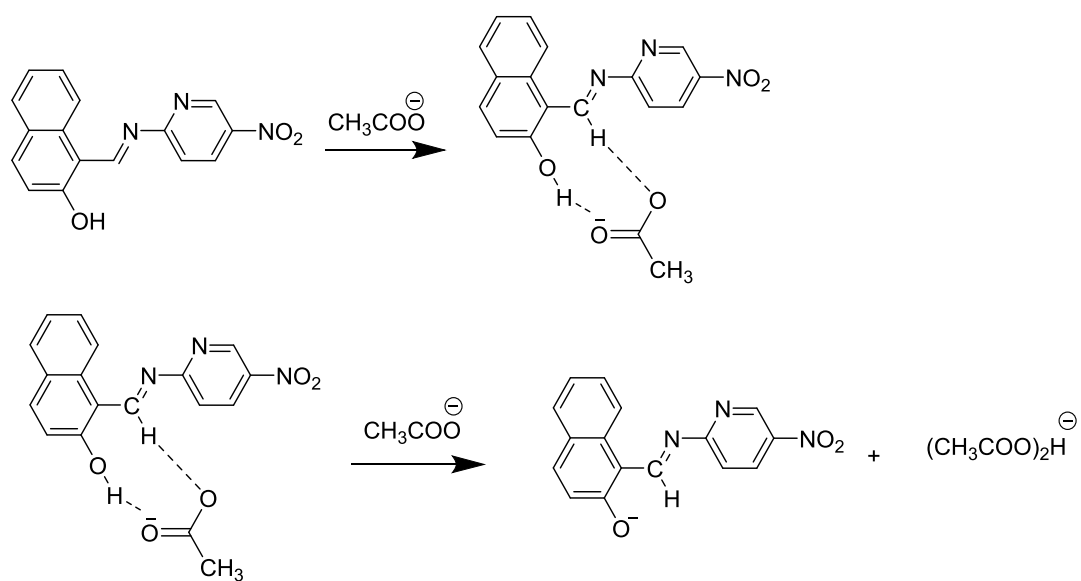
2.3.9 Binding mechanism

Based on UV-Vis titration studies, ¹H-NMR studies and DFT studies, the probable binding mechanism has been proposed. Receptor **R** is involved in strong hydrogen bond interactions with of F⁻ and AcO⁻ ions. Receptor **L** exhibited anion induced deprotonation of the -OH moiety with incremental addition of F⁻ and AcO⁻ ions. Binding of **R** and **L** with F⁻ and AcO⁻ ions are represented in Scheme 2.3, 2.4, 2.5 and 2.6 correspondingly.

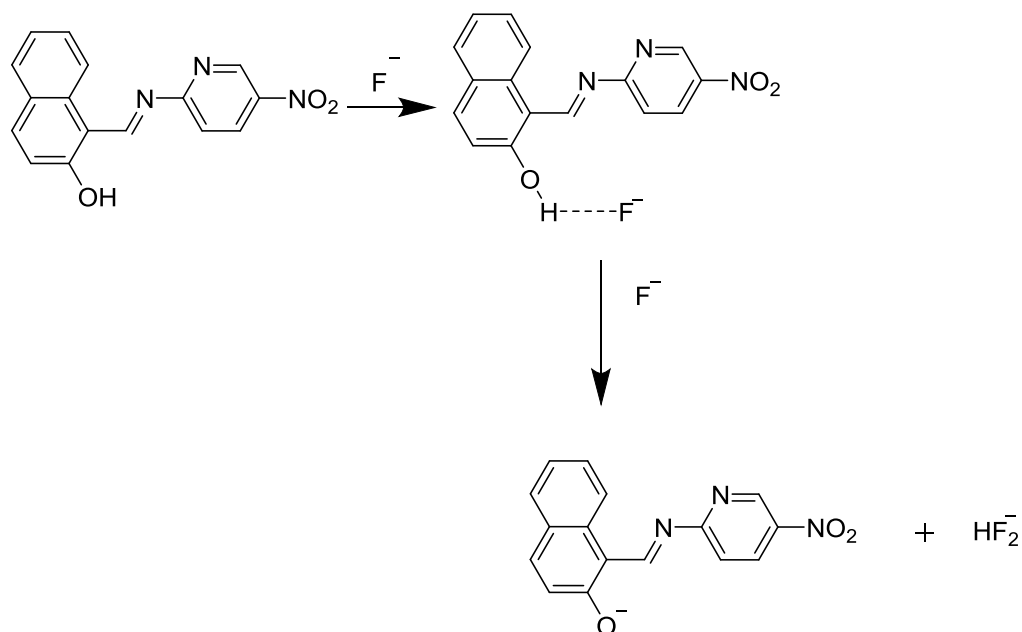
**Scheme 2.3** Proposed binding mechanism of F⁻ ion by receptor **R**



Scheme 2.4 Proposed binding mechanism of AcO^- ion by receptor **R**



Scheme 2.5 Proposed binding mechanism of **L** with AcO^- ion



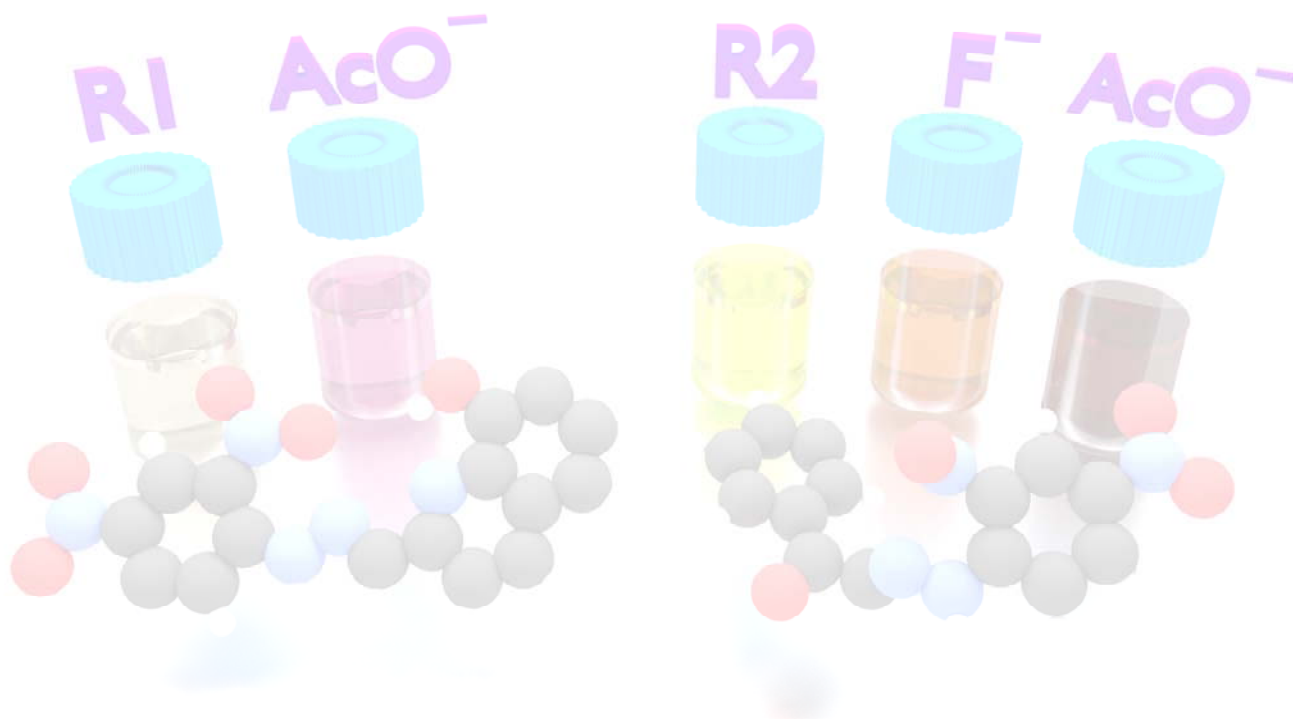
Scheme 2.6 Proposed binding mechanism of **L** with F^- ion

2.4 CONCLUSIONS

Organic receptors **R** and **L** could detect F^- and AcO^- ions with distinct color changes. The UV-Vis titration studies confirmed the binding of anions with a significant shift in absorption maxima and clear isobestic points. The lower detection limit of 1.12 ppm achieved in the organic media gives way for its practical utility. The applicability of detecting F^- ion in mouthwash makes it appropriate to be regarded as a real time colorimetric sensor. Lower detection limit of 0.92 ppm for sodium salt of AcO^- ion reflect the sensitivity of receptor **L** in the anion detection surpassing the constraints of the aqueous media. Time dependent studies confirm the first order rate equation for the anion binding process. 1H -NMR and TD-DFT calculations further confirm the anion binding process of receptor **R** and **L** with F^- and AcO^- ions.

CHAPTER 3

DESIGN, SYNTHESIS AND SPECTRAL INVESTIGATION OF ORGANIC RECEPTORS AS COLORIMETRIC AND ABSORPTION RATIO-METRIC ANION CHEMOSENSOR



Abstract

In this chapter, design, syntheses and characterization of two organic receptors have been described. Anion induced color change of the receptor has been monitored through UV-Vis, ¹H-NMR, electrochemical techniques. The plausible binding mechanism of the receptor towards active anion has been proposed.

3.1 INTRODUCTION

Colorimetric technique for the detection of anions have been in the limelight for their capability of providing qualitative and quantitative insight of the anion binding mechanism (Cho et al. 2005; Duke et al. 2010; Sakai et al. 2012). To date, numerous organic receptors featuring binding site-signaling unit approach have been reported, most of which are restricted to work in organic solvents (Cho et al. 2005; Kubik 2010). Higher solvation energy of anions in aqueous media result in restricted interaction between the host and guest (Bencini et al. 2012; Huang et al. 2012; Wang et al. 2011). Therefore, there is a need to strategically design organic receptors capable of detecting anions by surpassing the constraints of the aqueous media. In addition, compared with the usual detection method utilising an absorbance value at a single wavelength, the absorption ratiometric method provides more reliable quantitative information since it employs the ratio of absorption intensity at two different wavelengths as a function of analyte concentration, thereby a built-in correction for adverse environmental effects is obtained (Bao et al. 2013). Researchers have developed myriads of receptors having sound knowledge of how the receptor-anion binding operates (Santos-Figueroa et al. 2012). Most of the anion binding receptors are based on hydrogen bonding and electrostatic interactions (Blondeau et al. 2007; Gale 2006; Yoon et al. 2006). In comparison with the purely electrostatic interactions, which are distant dependent, hydrogen bonds have garnered great attention as it offers the advantage of being directional and discriminate anions of different geometries (Li et al. 2010; Lin et al. 2009). In this regard, presence of potential hydrogen bond donors like –OH and –NH functionalities in the receptor which can increase the binding affinity of anion via highly dissociable protons are desirable. The presence of –NO₂ group as a chromophore generally tends to exert –I

and -R effects which increases the acidity of the –OH and –NH proton (Ghosh et al. 2015).

Furthermore, azo-hydrazone tautomerism is an age-old mechanism wherein the tautomers are known to show different optical and physical properties (Adegoke 2011). Azo-hydrazone tautomerism is a phenomenon commonly encountered with azo dyes having substituent conjugated to azo linkage possessing a labile proton that can be intramolecularly exchanged (Ball and Nicholls 1982). It could be correlated to the fact that a receptor exhibiting such structural features would exhibit anion sensing behavior. Further, with the addition of anion, depending on the acidity of proton, abstraction could be possible which would lead to conversion of one tautomeric form to another exhibiting a color change visible to naked eye (Satheskumar et al. 2014). Electroanalytical techniques such as cyclic voltammetry is found to be of great use in this regard as it provides clear cut idea of the redox process and stability of the complex formed.

With these concepts in view, we demonstrate two organic receptors: (E)-2-((2-(2,4-dinitrophenyl)hydrazono)methyl)quinolin-8-ol namely **S1R1** and (E)-2-(2-(2,4-dinitrophenyl)hydrazono)-1-phenylethan-1-one as **S1R2**. Among them, **S1R1** exhibits a selective response towards AcO^- ion in the presence of HEPES buffer and **S1R2** exhibits an absorption ratiometric response towards AcO^- ion and azo-hydrazone tautomerism. UV-Vis titration studies, cyclic voltammetric studies and $^1\text{H-NMR}$ titration studies are known to provide full proof of the binding mechanism.

3.2 EXPERIMENTAL SECTION

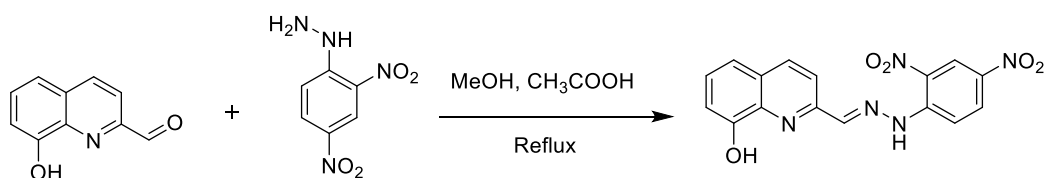
3.2.1 Materials and methods

All the chemicals used in the present study were procured from Sigma-Aldrich and Alfa Aesar and were used as received without further purification. All the solvents were purchased from SD Fine, India, were of HPLC grade and used without further distillation. Melting point was measured on Stuart SMP3 melting-point apparatus in open capillaries. Infrared spectrum was recorded on Bruker Apex FTIR spectrometer. UV-Vis spectroscopy was performed with Thermo Scientific Genysys

10S spectrometer in standard 3.0 mL quartz cell with 1 cm path length. The ^1H NMR spectra were recorded on Bruker Ascend (400 MHz) instrument using TMS as internal reference and $\text{DMSO-}d_6$ as solvent. Resonance multiplicities are described as s (singlet), d (doublet), t (triplet) and m (multiplet). Mass spectra was recorded on JMS- T100LC, Accu TOF Mass Spectrometer. Cyclic voltammogram was recorded on Ivium electrochemical workstation (Vertex) at a scan rate of 20 mV/s with the potential range 1.0 mV to -1.0 mV. Fluorescence spectra were recorded on Horiba spectrofluorometer.

3.2.2 Synthesis of receptor S1R1: (E)-2-((2-(2,4-dinitrophenyl) hydrazono) methyl) quinolin-8-ol

8-hydroxy,quinoline-2carboxaldehyde (0.2 g, 1.15 mmol) and 2,4-dinitrophenylhydrazine (0.22 g, 1.15 mmol) were refluxed in 6 ml methanol at 60 $^{\circ}\text{C}$ for 5 h in the presence of acetic acid as catalyst. (Scheme 2.1) The formation of the product was confirmed through TLC by the generation of single spot indicative of the disappearance of starting materials. After cooling to room temperature, the reaction mixture was filtered through filter paper, washed with methanol to obtain pure product.

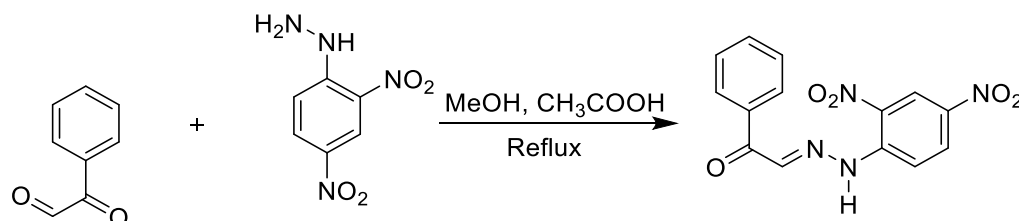


Scheme 3.1 Synthesis of S1R1

Yield: 75%, m. p. 252 $^{\circ}\text{C}$., ^1H NMR ($\text{DMSO-}d_6$, 400 MHz, ppm): δ 7.15 (dd, $J = 8.7$, 0.5 Hz, 1H), 7.42-7.50 (2H, 7.50 (dd, $J = 8.7$, 1.7 Hz), 7.46 (td, $J = 7.9$, 0.5 Hz)), 8.24-8.43 (3H, 8.25 (dd, $J = 7.9$, 1.3 Hz), 8.42 (dd, $J = 1.7$, 0.5 Hz)), 8.88 (td, $J = 1.7$, 0.5 Hz), 9.9 (s, 1H), 11.99 (s, 1H). FTIR (KBr)(cm^{-1}): 3302 (NH), 3222 (OH), 3038 (Ar-CH), 1612 (CH=N), 1505 (C=C), 1487 (C=C), 1374 (NO_2), 1099 (C-H). Mass (ESI): m/z Calculated: 353.08 Obtained: 354.00 ($\text{M}+\text{H}^+$).

3.2.3 Synthesis of S1R2: (E)-2-(2-(2,4-dinitrophenyl)hydrazono)-1-phenylethan-1-one

Phenylglyoxal (0.1 g, 0.74 mmol) and 2,4-dinitrophenylhydrazine (0.14 g, 0.74 mmol) were refluxed in 6 ml methanol at 60 °C for 5 h in the presence of acetic acid as catalyst. (Scheme 2.2) The formation of the product was confirmed through TLC by the generation of single spot indicative of the disappearance of starting materials. After cooling to room temperature, the reaction mixture was filtered through filter paper, washed with methanol to obtain pure product.



Scheme 3.2 Synthesis of S1R2

Yield: 75%, m. p. 252 °C., ¹H NMR (DMSO- d₆, 400 MHz, ppm): δ 7.85 (tt, *J* = 7.4, 1.5 Hz, 2H), 8.56 (s, 2H), 8.67 (s, H), 8.79 (dd, *J* = 7.8, 0.5 Hz, 1H), 9.02 (dd, *J* = 7.8, 1.9 Hz, 1H), 9.76 (dd, *J* = 1.9, 0.5 Hz, 1H), 11.34 (s, 1H). FTIR (KBr)(cm⁻¹): 3386 (NH), 3102 (Ar-CH), 1694 (C=O), 1615 (CH=N), 1505 (C=C), 1337 (NO₂), 1099 (C-H). Mass (ESI): *m/z* Calculated: 314.07 Obtained: 315.15 (M+H⁺).

3.2.4 Characterization data

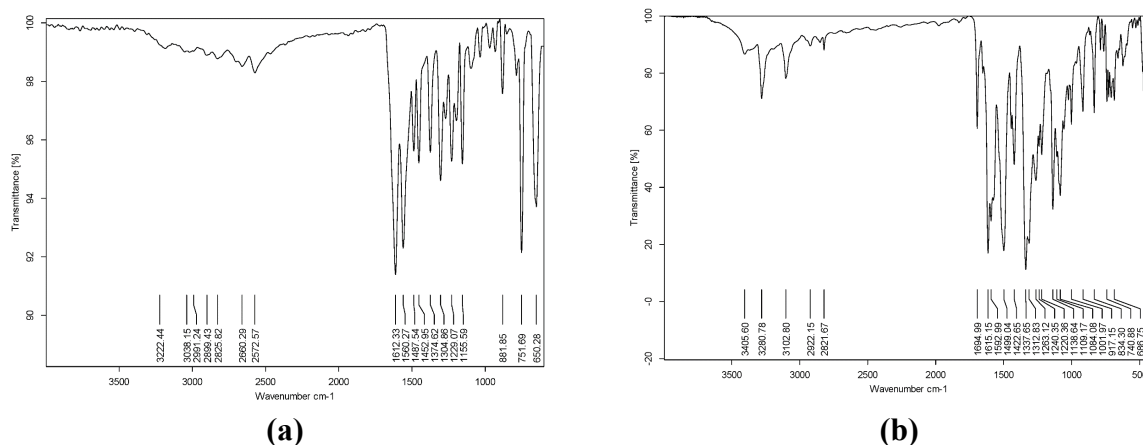
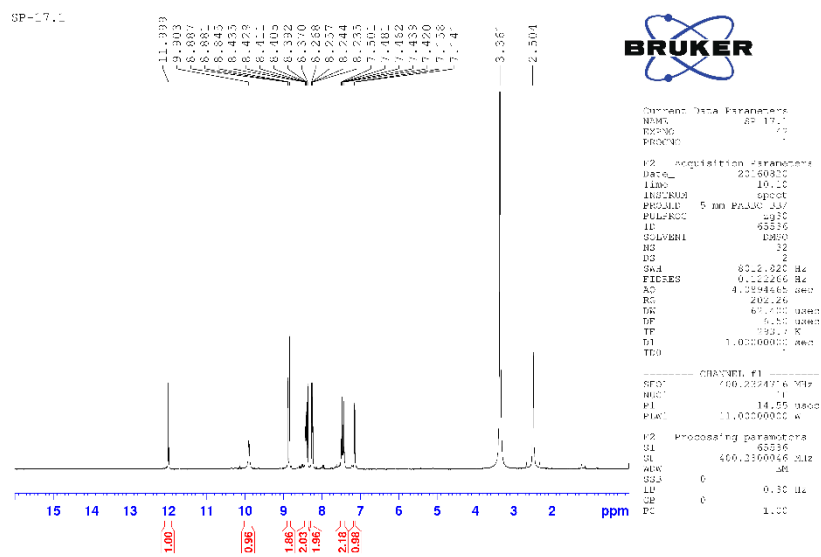
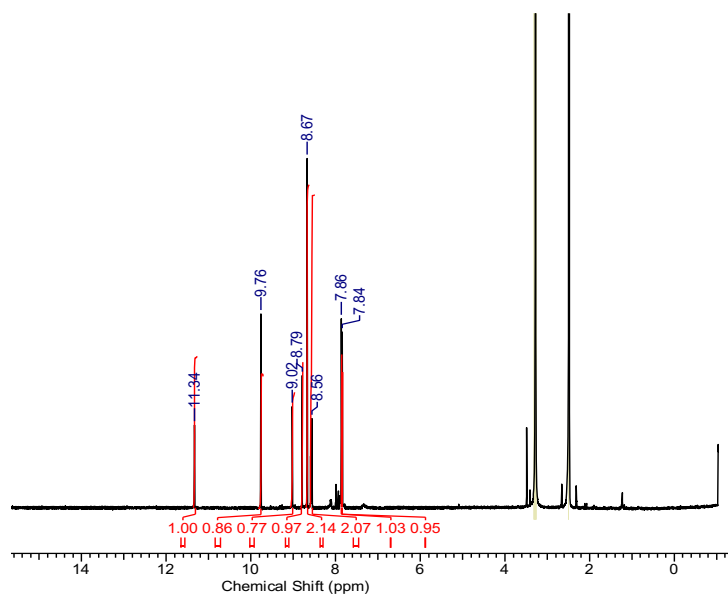


Fig. 3.1(a) FT-IR spectrum of receptor S1R1; (b) FT-IR spectrum of receptor S1R2

Fig. 3.2 ^1H NMR spectrum of receptor S1R1Fig. 3.3 ^1H NMR spectrum of receptor S1R2

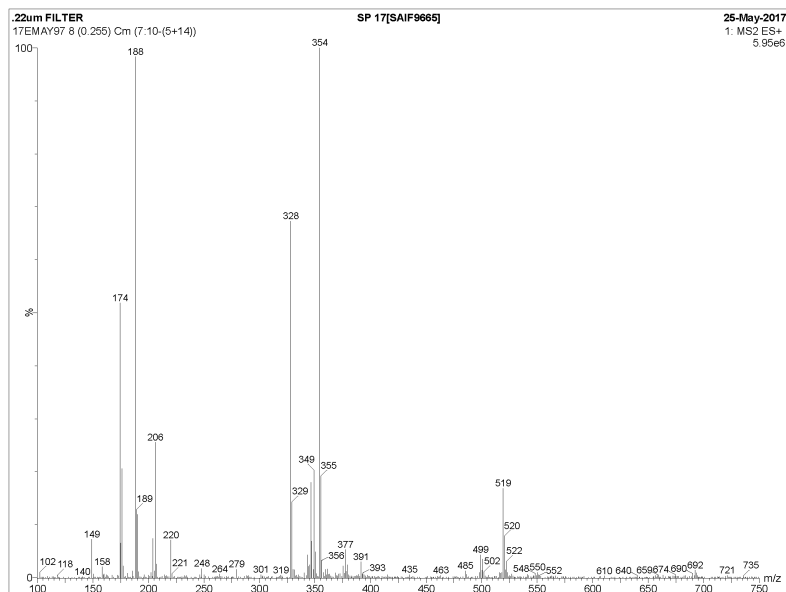


Fig. 3.4 (a) Mass spectrum of receptor S1R1

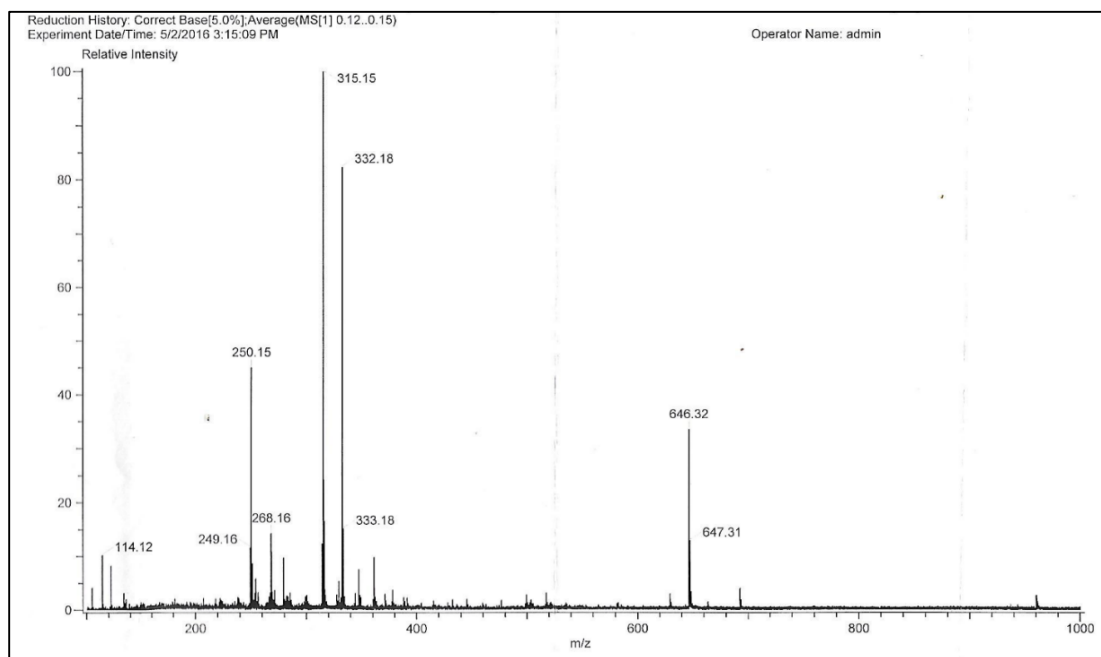


Fig. 3.4 (b) Mass spectrum of receptor S1R2

3.3 RESULTS AND DISCUSSION

3.3.1 Colorimetric detection of anions

Receptor **S1R1** displayed significant colorimetric response towards F^- , $H_2PO_4^-$ and AcO^- ions with a color change from pale yellow to bright pink, red and purple respectively (Fig. 3.5). Receptor **S1R2** exhibited color change from pale yellow to orange and purple with the addition of F^- and AcO^- ions correspondingly (Fig. 3.6). UV-Vis spectra of **S1R1** and **S1R2** has been recorded with the addition of 1 equiv. of tetrabutylammonium salts of anions (1×10^{-2} M in DMSO) such as F^- , Cl^- , Br^- , I^- , NO_3^- , HSO_4^- , $H_2PO_4^-$ and AcO^- as shown in Fig. 3.7 and Fig. 3.8 respectively.

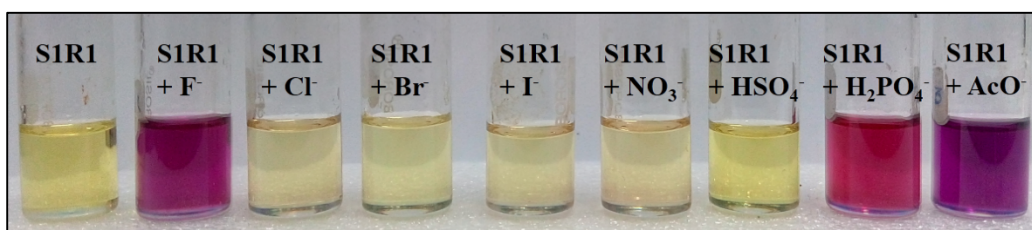


Fig. 3.5 Color change of the receptors **S1R1** (10^{-4} M in DMSO) with the addition of 1 equiv. of TBA salts of anions (10^{-2} M in DMSO)

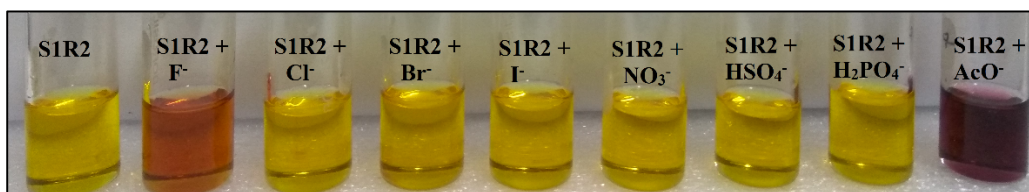


Fig. 3.6 Color change of the receptors **S1R2** (10^{-4} M in DMSO) with the addition of 1 equiv. of TBA salts of anions (10^{-2} M in DMSO)

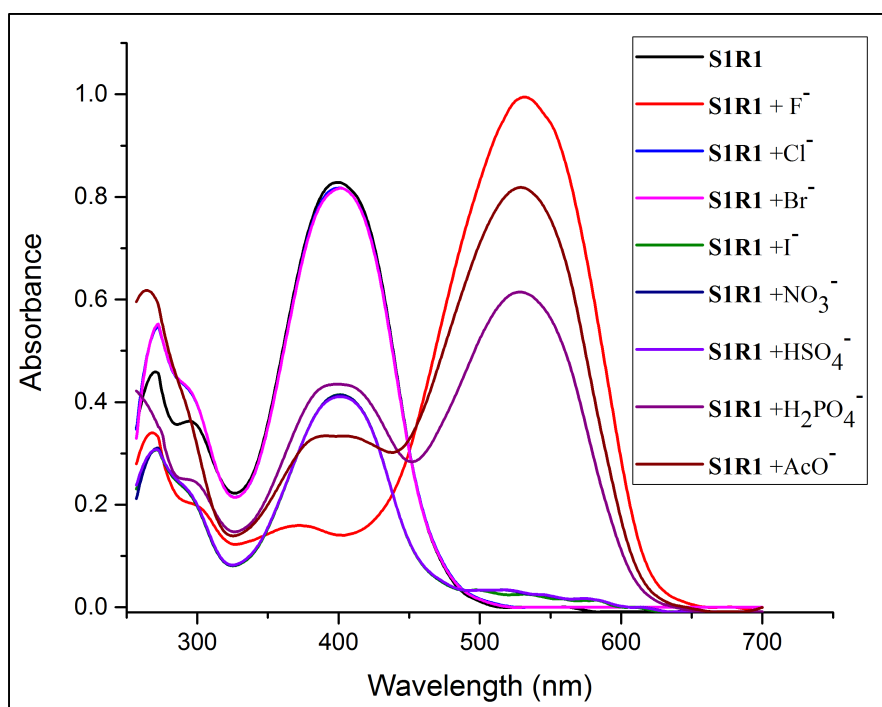


Fig. 3.7 UV-Vis spectra of receptor **S1R1** (10^{-4} M in DMSO) with the addition of 1 equiv. of tertabutylammonium salts of various anions (10^{-2} M in DMSO)

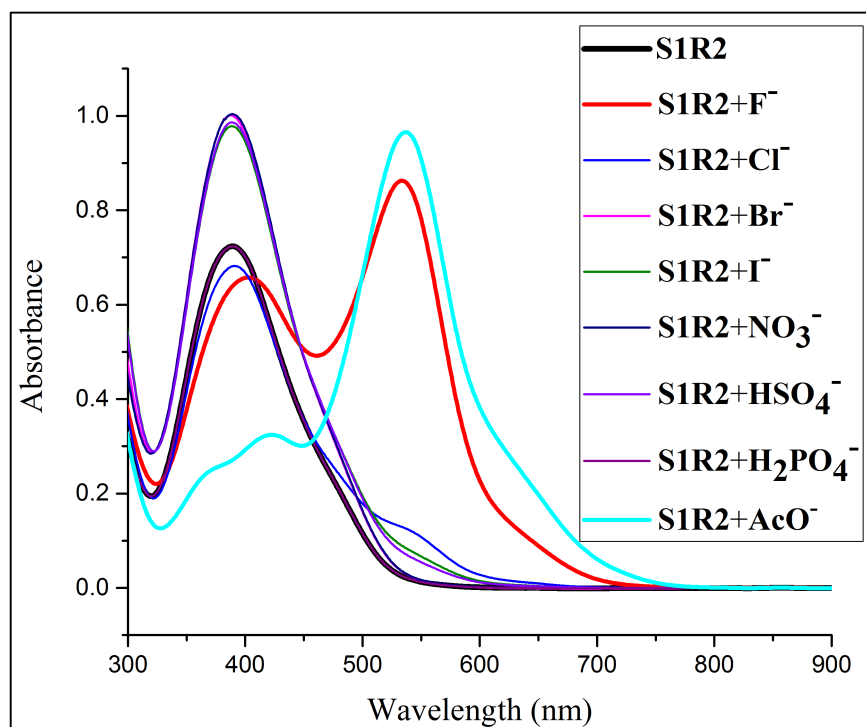


Fig. 3.8 UV-Vis spectra of receptor **S1R2** (10^{-4} M in DMSO) with the addition of 1 equiv. of tertabutylammonium salts of various anions (10^{-2} M in DMSO)

3.3.2 UV-Vis titration studies

UV-Vis spectrophotometric titration has been performed with the incremental addition of TBA salt of F^- , $H_2PO_4^-$ and AcO^- ion in order to investigate the interaction of **S1R1** and **S1R2** with different anions. In case of free receptor **S1R1** and **S1R2** (1×10^{-4} M in DMSO), a strong absorption band was observed at 402 nm and 389 nm correspondingly indicating the intramolecular charge transfer interaction within the receptor.

Interaction of **S1R1** with F^- , $H_2PO_4^-$ and AcO^- ion resulted in redshift of original absorption band to 531 nm and 534 nm respectively. The appearance of clear isobestic point at 450 nm indicate the formation of anion-receptor complex. Titration profile of **S1R1** with F^- , $H_2PO_4^-$ and AcO^- ion is represented in Fig. 3.9, Fig. 3.11 and Fig. 3.13 correspondingly. The B-H plot indicated the binding ratio of 1:2 and 1:1 for **S1R1**- F^- and **S1R1**- $H_2PO_4^-$ / **S1R1**- AcO^- complex (Fig. 3.10, Fig. 3.12 and Fig. 3.14).

The color change of **S1R1** on interaction with F^- and AcO^- can be explained by the fact that the intramolecular charge transfer (ICT) process occurred between the oxygen of hydroxyl functionality of quinolone ring and the electron withdrawing phenyl ring with the formation of a hydrogen bonded complex between the hydroxyl groups of **S1R1** and the anion added (Gunnlaugsson et al. 2005). A slight color change was also depicted in the case of $H_2PO_4^-$ but it was not prominent as for F^- and AcO^- . Moreover, the requirement of two F^- ions to bind with the receptor **S1R1** implies the strong hydrogen bond tendency of $-OH$ and NH proton individually with the anion. It could be clearly visualized that a single AcO^- / $H_2PO_4^-$ anion is sufficient to form a stable complex involving $-OH$ and NH functionality through bifurcated hydrogen bond interactions resulting in a 1:1 receptor-anion complex.

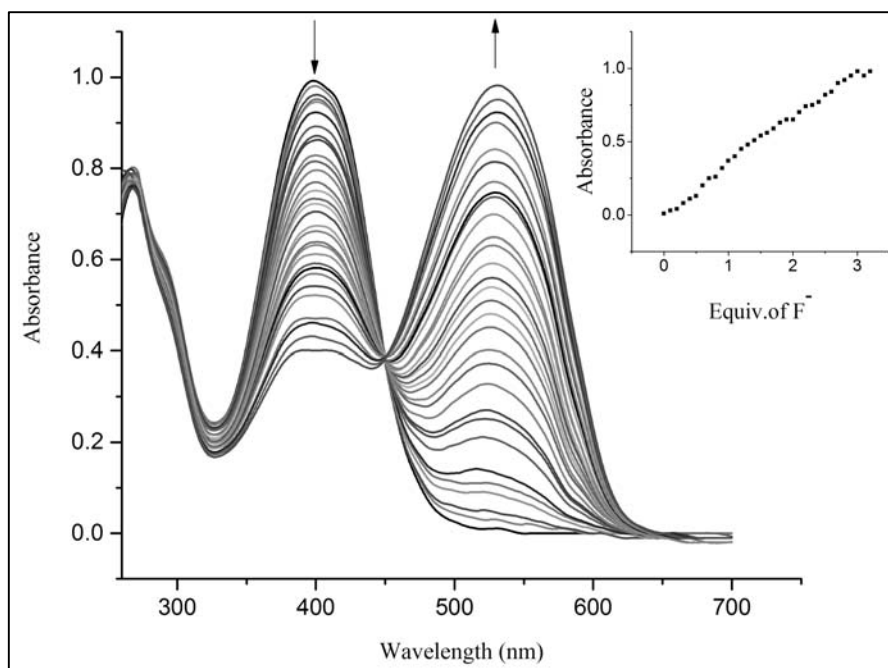


Fig. 3.9 UV-Vis titration spectra of receptor **S1R1** (10^{-4} M in DMSO) with the incremental addition of TBAF (10^{-2} M in DMSO). Inset plot representing the absorption isotherm at 531 nm

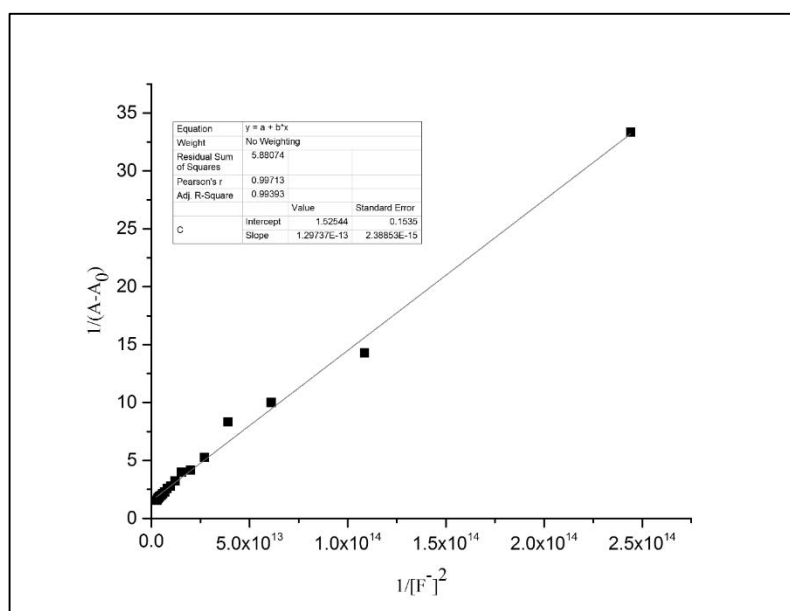


Fig. 3.10 B-H plot of receptor **S1R1**- TBAF complex at a selected wavelength of 531 nm

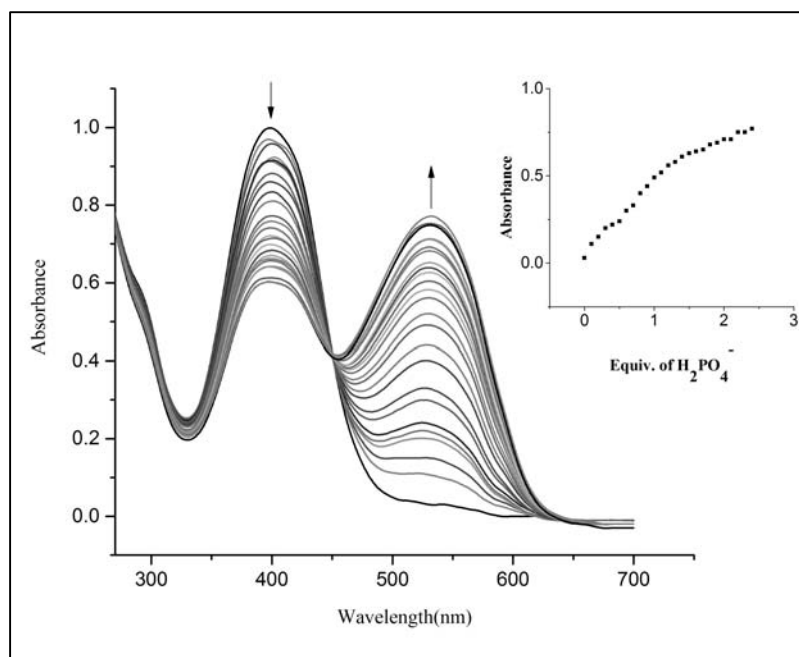


Fig. 3.11 UV-Vis titration spectra of receptor **S1R1** (10^{-4} M in DMSO) with the incremental addition of TBAH_2PO_4 (10^{-2} M in DMSO). Inset plot representing the absorption isotherm at 531 nm

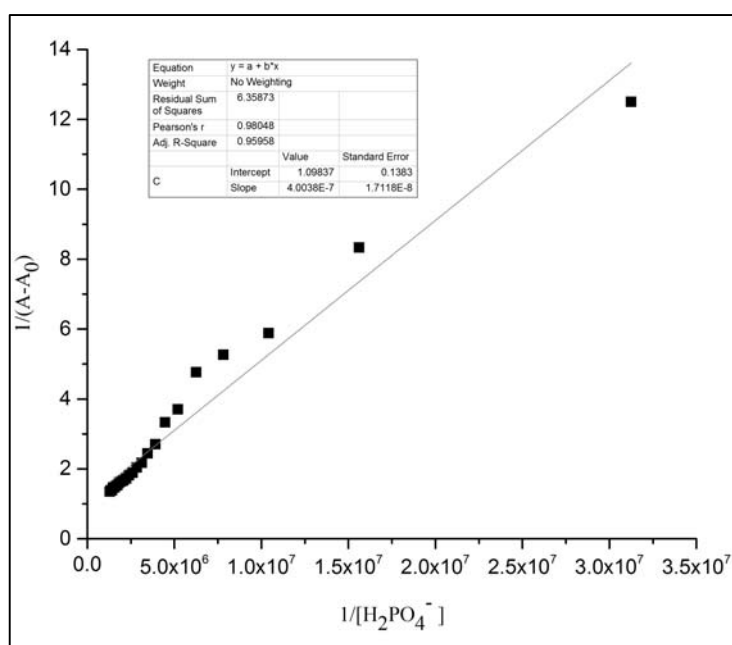


Fig. 3.12 B-H plot of receptor **S1R1**- TBAH_2PO_4 complex at a selected wavelength of 531 nm

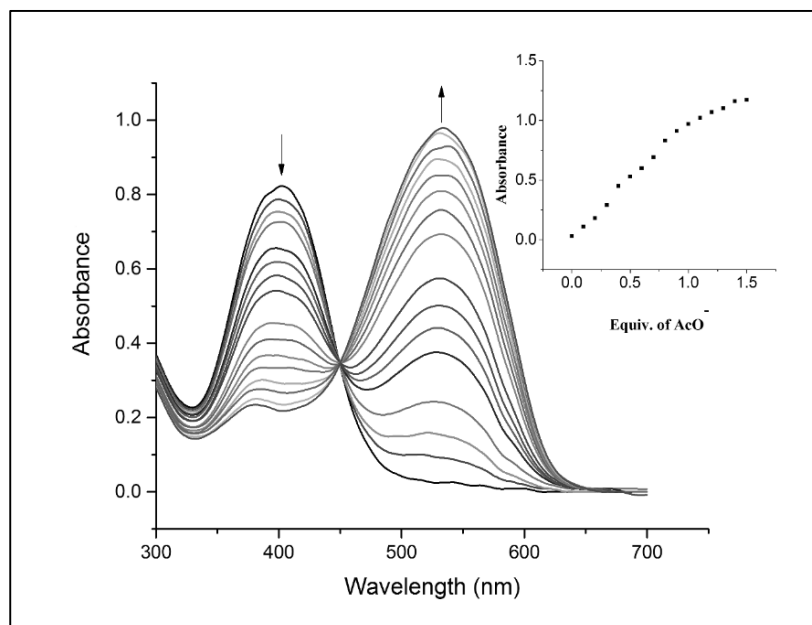


Fig. 3.13 UV-Vis titration spectra of receptor **S1R1** (10^{-4} M in DMSO) with the incremental addition of TBAOAc (10^{-2} M in DMSO). Inset plot representing the absorption isotherm at 534 nm

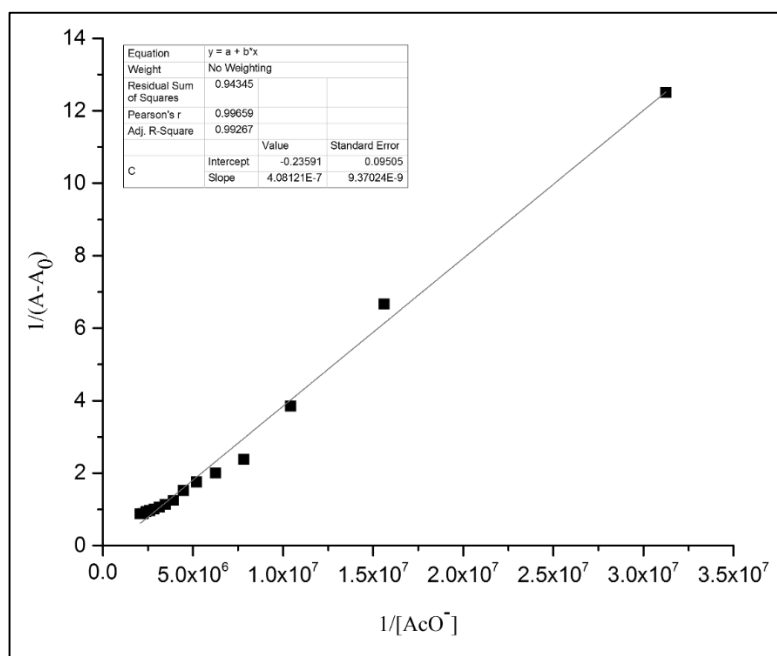


Fig. 3.14 B-H plot of receptor **S1R1**- TBAAcO complex at a selected wavelength of 534 nm

UV-Vis studies of receptor **S1R1** in DMSO/HEPES buffer solution (9:1, v/v, pH 7.4) revealed excellent selectivity of the receptor towards AcO^- ion with pale pink coloration (Fig. 3.15 and Fig. 3.16). The titration spectra revealed the shift of original absorption band to 520 nm with an isobestic point at 450 nm indicating complex formation process (Fig. 3.17). Yet, unlike receptor **S1R1**, **S2R2** did not exhibit selective response towards a particular anion in the presence of HEPES buffer.

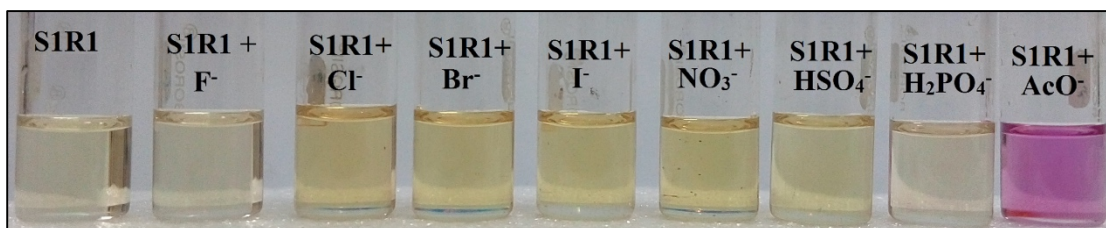


Fig. 3.15 Color change of the receptor **S1R1**(DMSO: HEPES buffer, 9:1, v/v) with the addition of 1 equiv. of TBA salts of anions

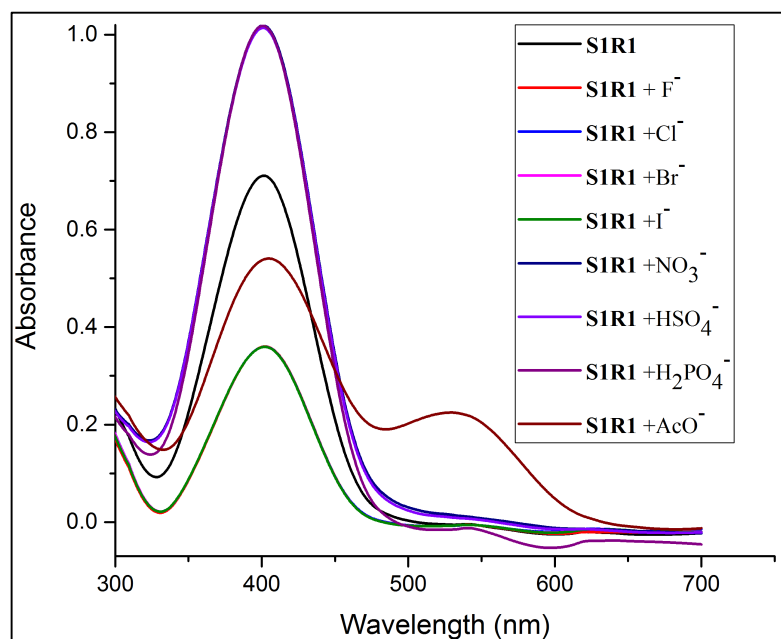


Fig. 3.16 UV-Vis spectra of receptor **S1R1** (10^{-4} M in DMSO: HEPES buffer, 9:1, v/v) with the addition of 1 equiv. of tertabutylammonium salts of various anions (10^{-2} M in DMSO)

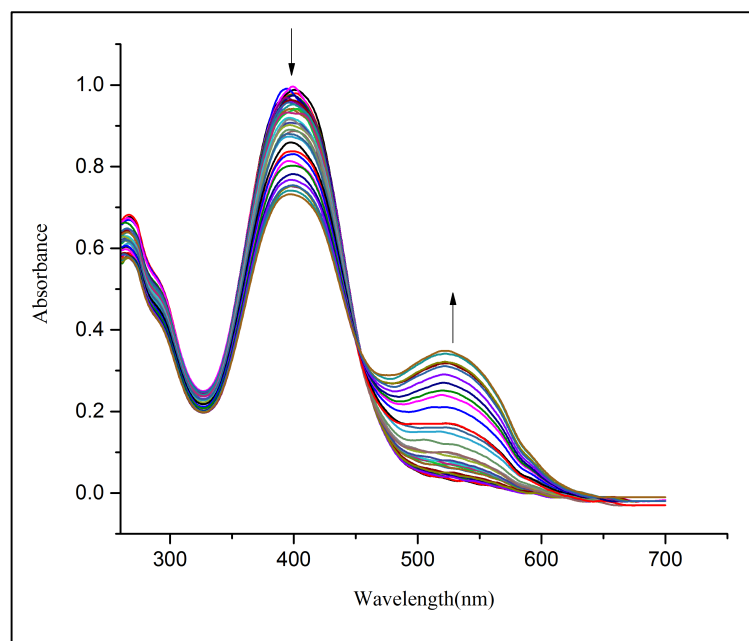


Fig. 3.17 UV-Vis titration spectra of receptor **S1R1** (10^{-4} M in DMSO: HEPES buffer, 9:1, v/v) with the incremental addition of TBAAcO (10^{-2} M in DMSO)

UV-Vis titration spectra of **S1R2** with the incremental addition of F^- and AcO^- ion resulted in distinct changes with respect to colorimetric response and red shift of original absorption band (Fig. 3.18 and Fig. 3.20). Further, more significant colorimetric response has been observed with TBA salt of AcO^- ion owing to the geometrical complementarity of the receptor. Until the addition of 0.5 equiv. of AcO^- ion to the solution of **S1R2**, original absorption band of **S1R2** shifted from 403 nm to 537 nm and spectra showed clear isobestic point at 439 nm. This is indicative of the typical hydrogen bond formation between **S1R2** and AcO^- ion. However, when an excess equiv. of anion were added, a broad shoulder band appeared at 628 nm which could be attributed to the deprotonated receptor resulting in improved ICT process (Chowdhury et al. 2015). In addition, spectra revealed a new isobestic point centered at 468 nm confirming the deprotonation process. B-H plot indicated 1:1 binding ratio of **S1R2** with F^- and AcO^- ions as shown in Fig. 3.19 and Fig. 3.21 respectively. The corresponding color change of **S1R2** from pale yellow to orange with 0.25 equiv. of AcO^- ion indicates that solution exists as a mixture of hydrogen bond complex of receptor and its deprotonated form. Deprotonation of receptor has been verified with the titration of **S1R2** with TBAOH (Fig. 3.22). With the addition of 1 equiv. of AcO^-

ion, the color changes from orange to purple which could be ascribed to the deprotonation of $-NH$ fragment (Fig. 3.23). The gradual color change from yellow to purple with significant redshift of original absorption band and simultaneous appearance of broad shoulder clearly suggest the deprotonation mechanism (Fig. 3.24). The gradual increment in the color with the addition of anions confirms the ratiometric colorimetric response of the receptor **S1R2**. Gratifyingly, a good linear relationship was obtained between the A_{537}/A_{389} ratio and the concentration of AcO^- ion to receptor **S1R2** thus enabling the receptor to work as an absorption ratiometric chemosensor for the quantitative detection of AcO^- ion (Fig. 3.25).

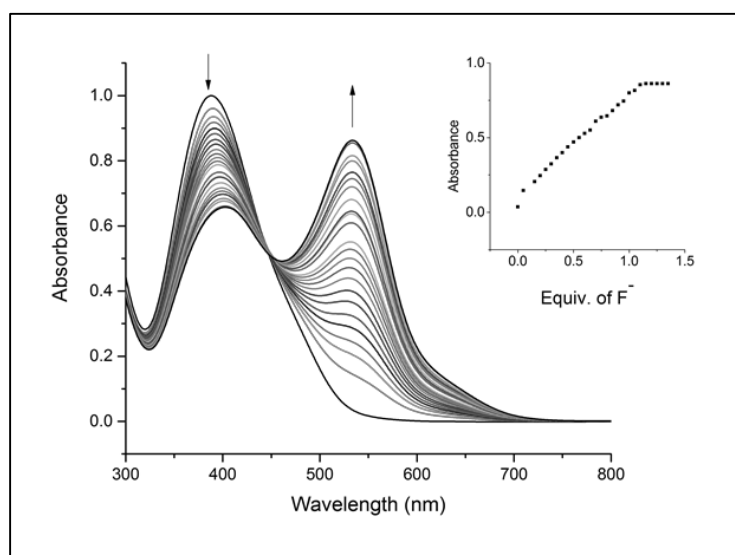


Fig. 3.18 UV-Vis titration spectra of receptor **S1R2** (10^{-4} M in DMSO) with the incremental addition of TBAF (10^{-2} M in DMSO). Inset plot representing the absorption isotherm at 533 nm

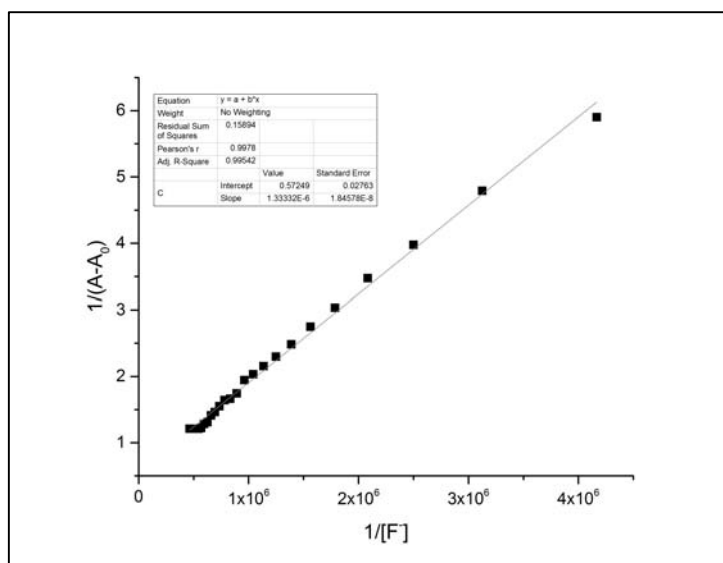


Fig. 3.19 B-H plot of receptor **S1R2** - TBAF complex at a selected wavelength of 533 nm

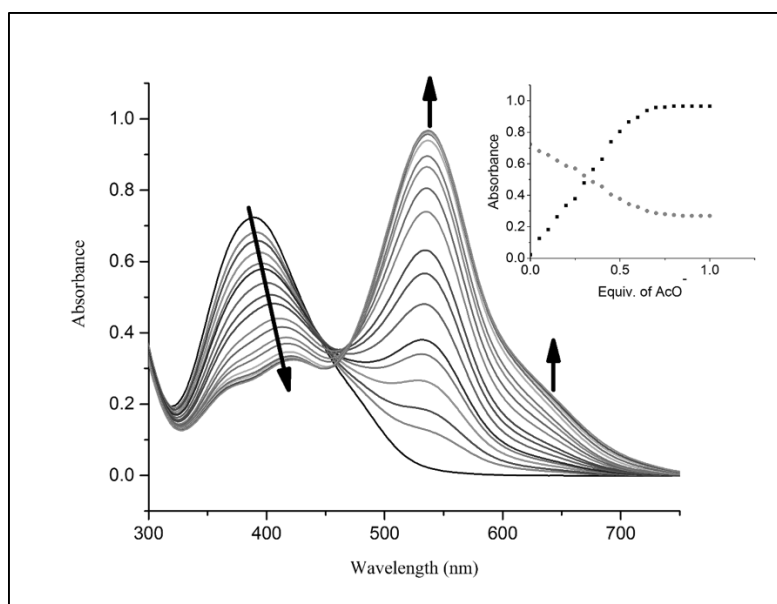


Fig. 3.20 UV-Vis titration spectra of receptor **S1R2** (10^{-4} M in DMSO) with the incremental addition of TBAAcO (10^{-2} M in DMSO). Inset plot representing the absorption isotherm at 537 nm

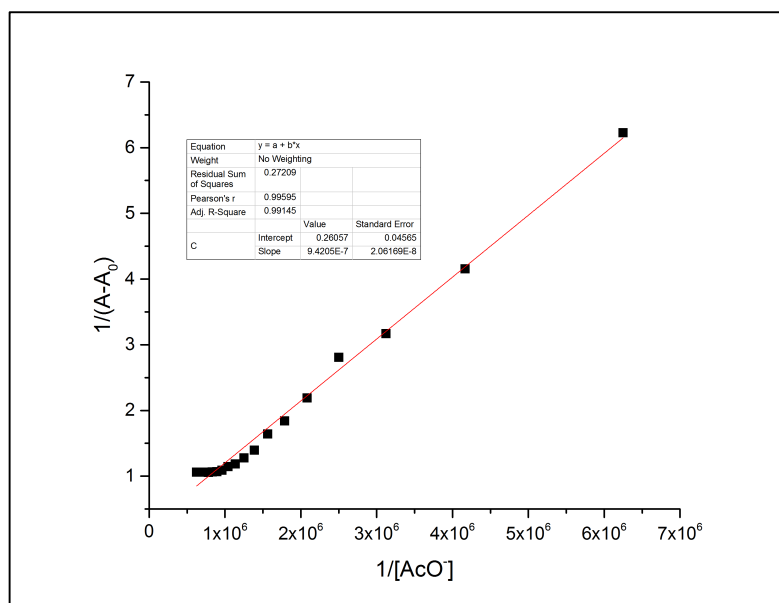


Fig. 3.21 B-H plot of receptor **S1R2**- TBAAcO complex at a selected wavelength of 537 nm

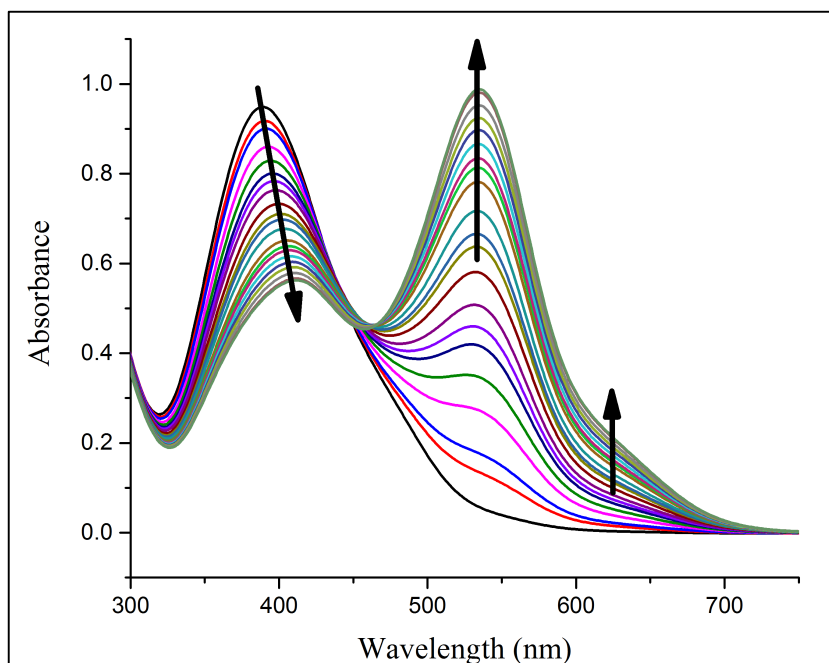


Fig. 3.22 UV-Vis titration spectra of receptor **S2R2** (10^{-4} M in DMSO) with the incremental addition of TBAOH (10^{-2} M in DMSO)

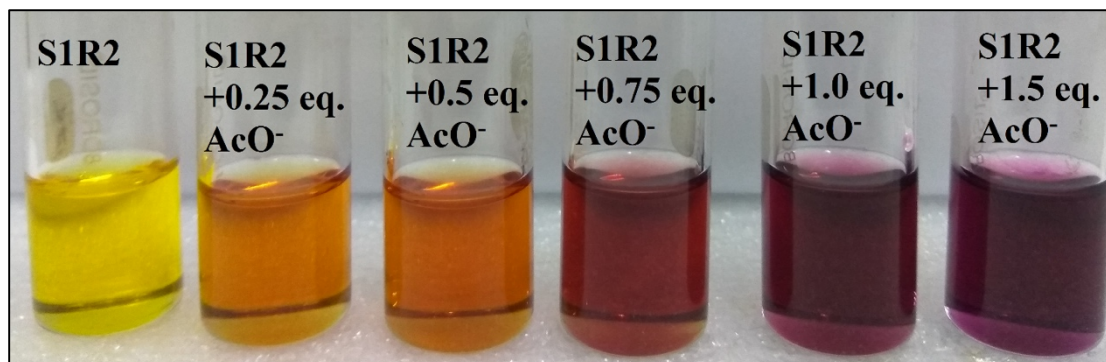


Fig. 3.23 Ratiometric response of receptor **S1R2** with the increasing concentration of AcO⁻ ion

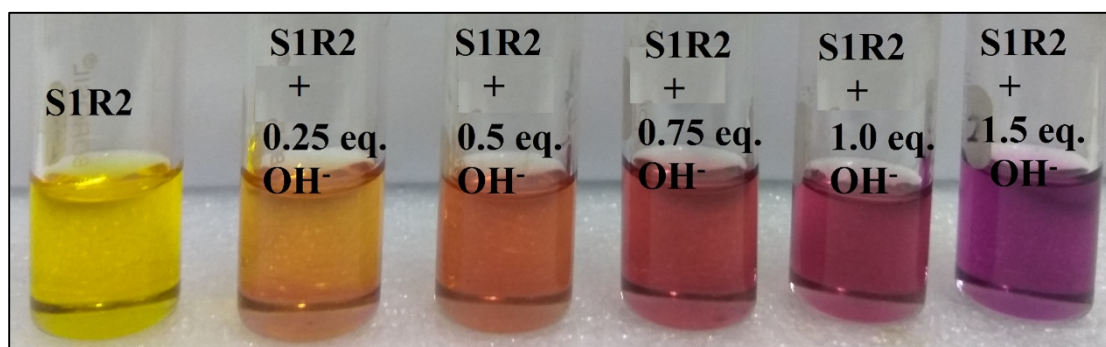


Fig. 3.24 Ratiometric response of receptor **S1R2** with the increasing concentration of OH⁻ ion

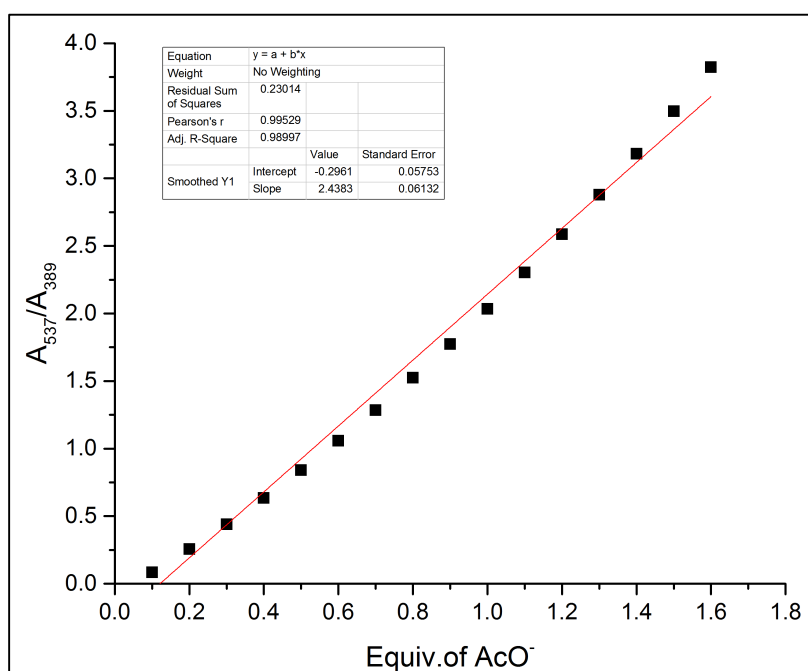


Fig. 3.25 Ratiometric plot of A_{537}/A_{389} (receptor **S1R2**) with the increasing equiv. of AcO^- ion

Fluoride and acetate ion are present in the form of sodium salt at physiological level. With this in view, it gains more interest to develop sensors which can detect anions in aqueous media. Titration studies performed with the incremental addition of F^- and AcO^- ions as sodium salt to receptor **S1R1** revealed comparable red shift of original absorption band as seen in the presence of TBA salts (Fig. 3.26 and 3.28). The corresponding B-H plot for **S1R1**- F^- and **S1R1**- AcO^- complex is shown in Fig. 3.27 and Fig. 3.29. Similarly, titration studies performed with the incremental addition of F^- and AcO^- ions as sodium salt to receptor **S1R2** revealed comparable red shift of original absorption band as seen in the presence of TBA salts (Fig. 3.30 and 3.32). B-H plot are represented in Fig. 3.31 and 3.33 for **S1R1**- F^- and **S1R1**- AcO^- complex respectively. The corresponding binding constant, binding ratio and detection limit is presented in Table 3.1.

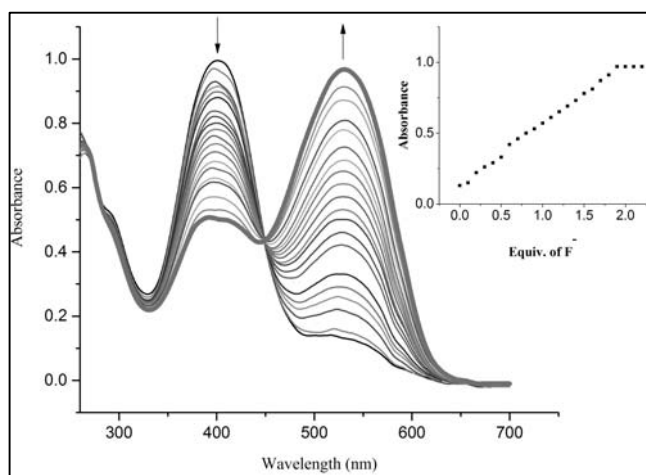


Fig. 3.26 UV-Vis titration spectra of **S1R1** (1×10^{-4} M, 9:1, v/v DMSO/ H_2O) with the incremental addition of standard solution of NaF (1×10^{-2} M in distilled water). Inset showing binding isotherm at 530 nm

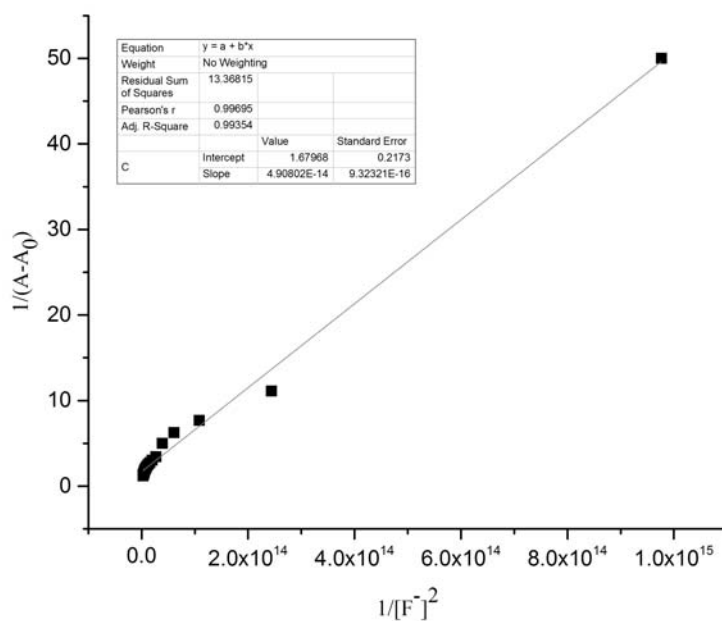


Fig. 3.27 B-H plot of receptor **S1R1**- NaF complex at a selected wavelength of 530 nm

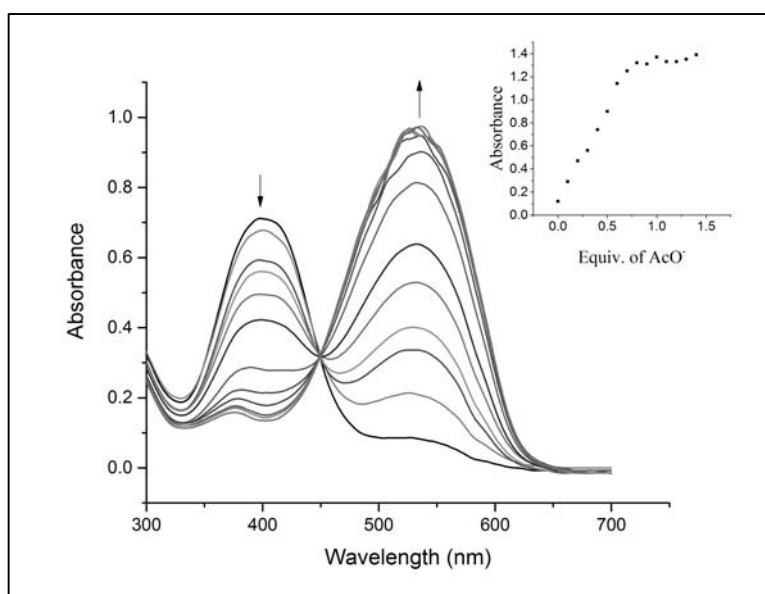


Fig. 3.28 UV-Vis titration spectra of **S1R1** (1×10^{-4} M, 9:1, v/v DMSO/H₂O) with the incremental addition of standard solution of NaAcO (1×10^{-2} M in distilled water). Inset showing binding isotherm at 532 nm

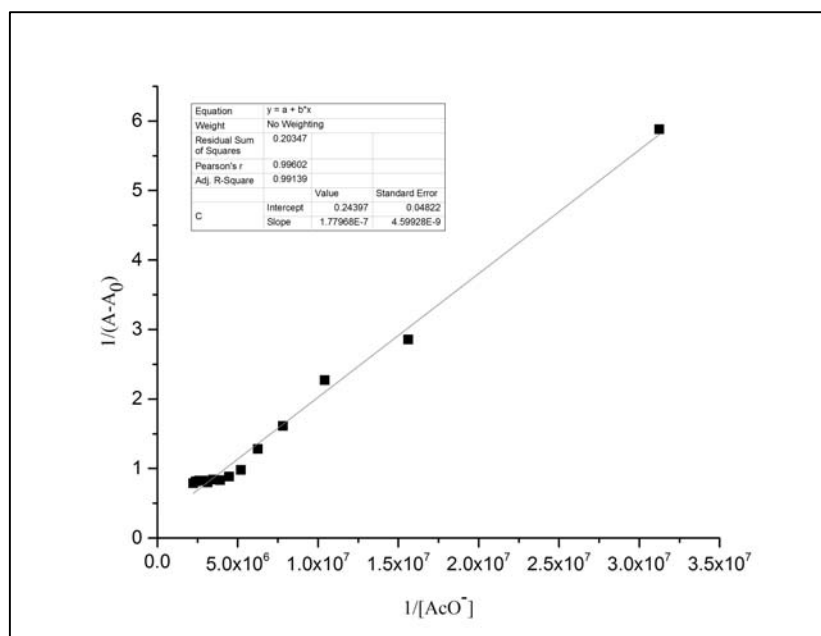


Fig. 3.29 B-H plot of receptor **S1R1**- NaAcO complex at a selected wavelength of 532 nm

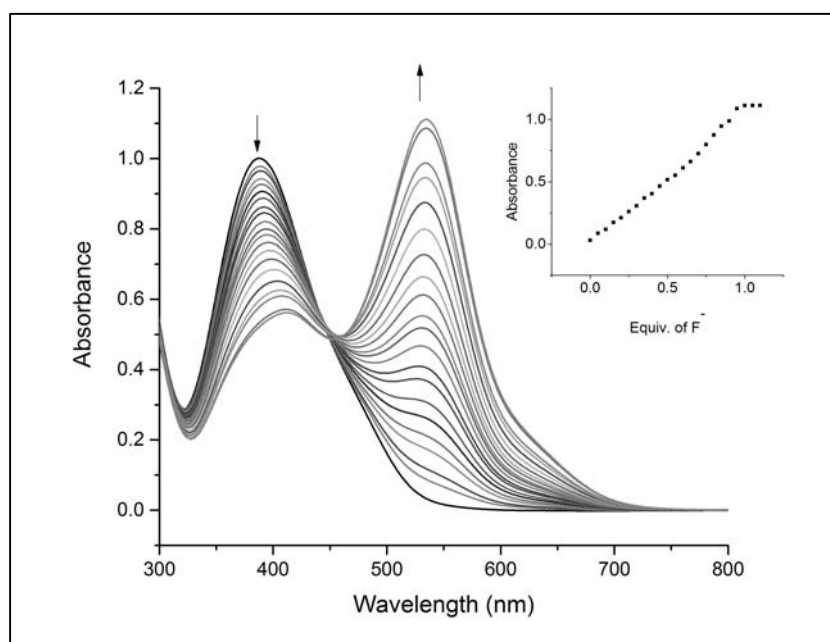


Fig. 3.30 UV-Vis titration spectra of **S1R2** (1×10^{-4} M, 9:1, v/v DMSO/H₂O) with the incremental addition of standard solution of NaF (1×10^{-2} M in distilled water). Inset showing binding isotherm at 535 nm

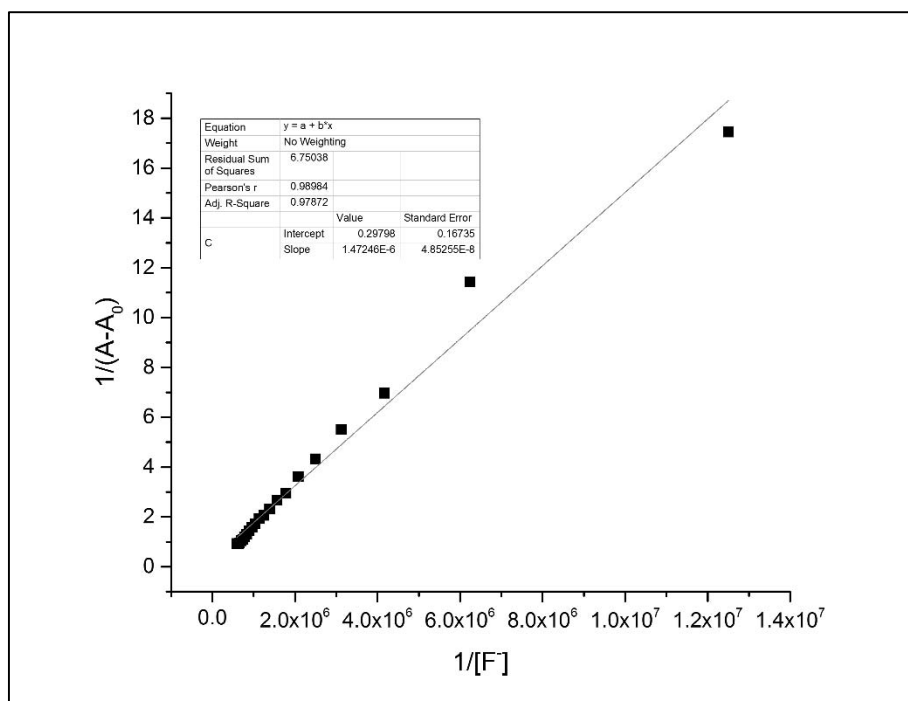


Fig. 3.31 B-H plot of receptor **S1R2**- NaF complex at a selected wavelength of 535 nm

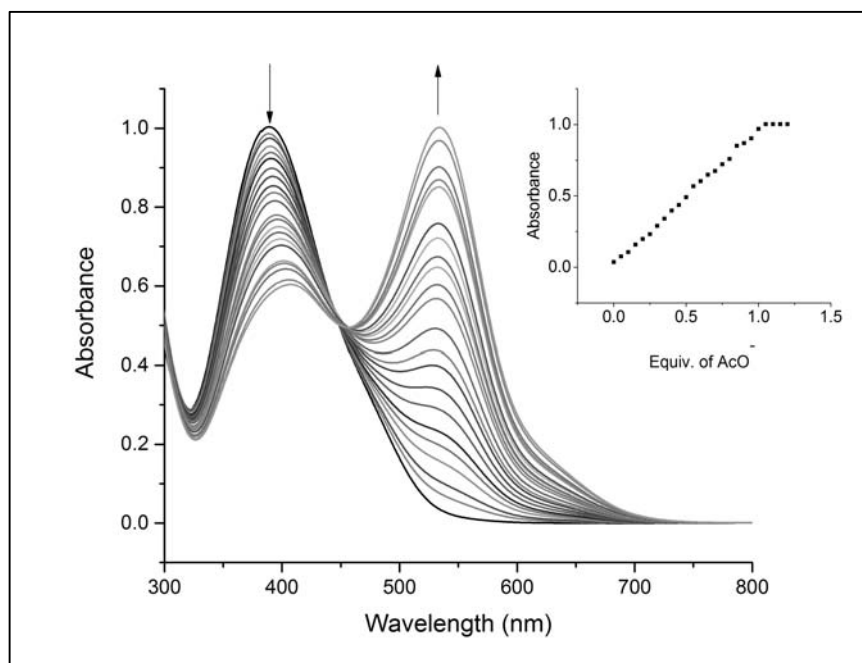


Fig. 3.32 UV-Vis titration spectra of **S1R2** (1×10^{-4} M, 9:1, v/v DMSO/H₂O) with the incremental addition of standard solution of NaAcO (1×10^{-2} M in distilled water). Inset showing binding isotherm at 534 nm

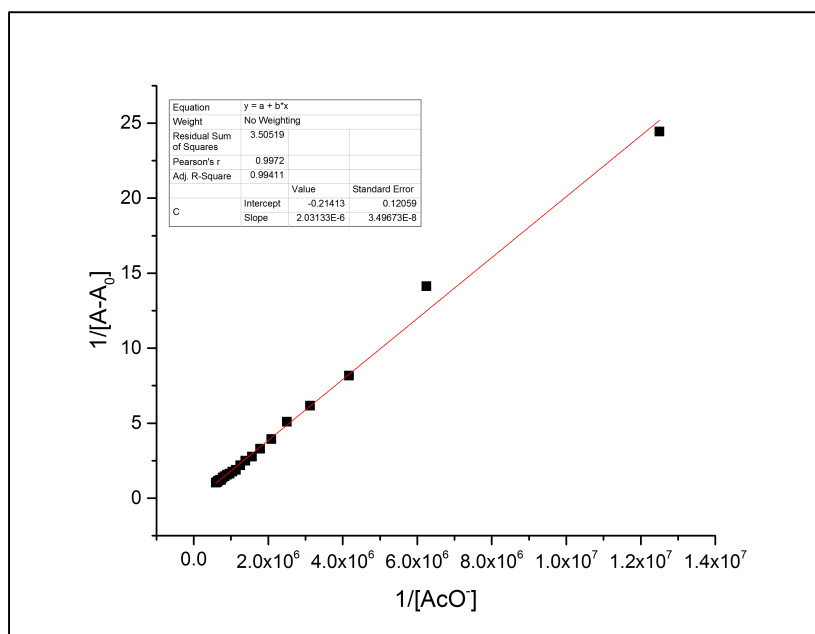


Fig. 3.33 B-H plot of receptor **S1R2**- NaAcO complex at a selected wavelength of 534 nm

The color change of the receptor **S1R1** in the presence of NaF and NaOAc is shown in Fig. 3.34. Receptor **S1R1** and **S1R2** showed color change in the presence of mouthwash and seawater (Fig. 3.35). UV-Vis spectra recorded with the addition of seawater and mouthwash exhibits redshift band and were comparable to the spectra obtained with the addition of standard solution of fluoride to **S1R1** and **S1R2** (Fig. 3.36 and Fig. 3.37).

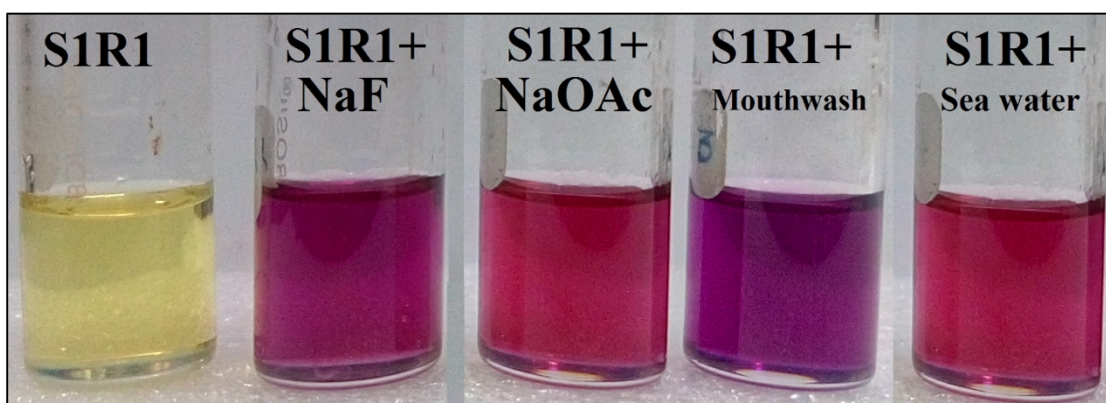


Fig. 3.34 Color change of receptor **S1R1** in the presence of 1 equiv. of NaF and NaAcO, mouthwash and seawater

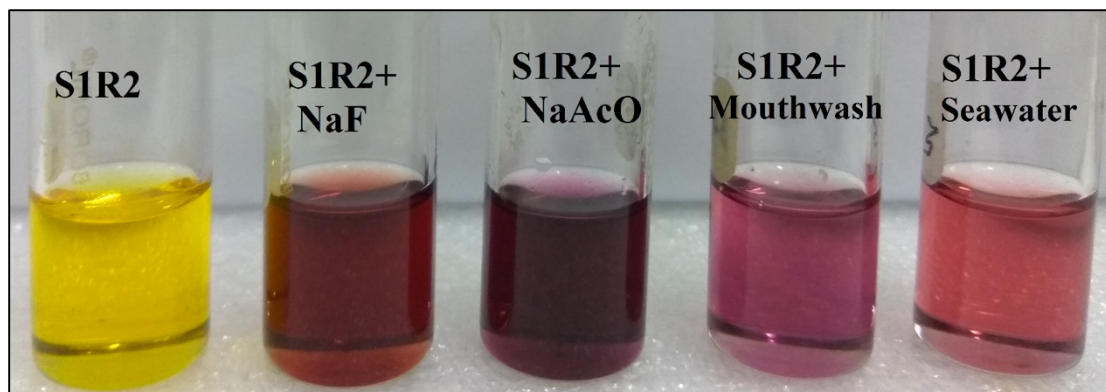


Fig. 3.35 Color change of receptor **S1R2** in the presence of 1 equiv. of NaF, NaAcO, mouthwash and seawater

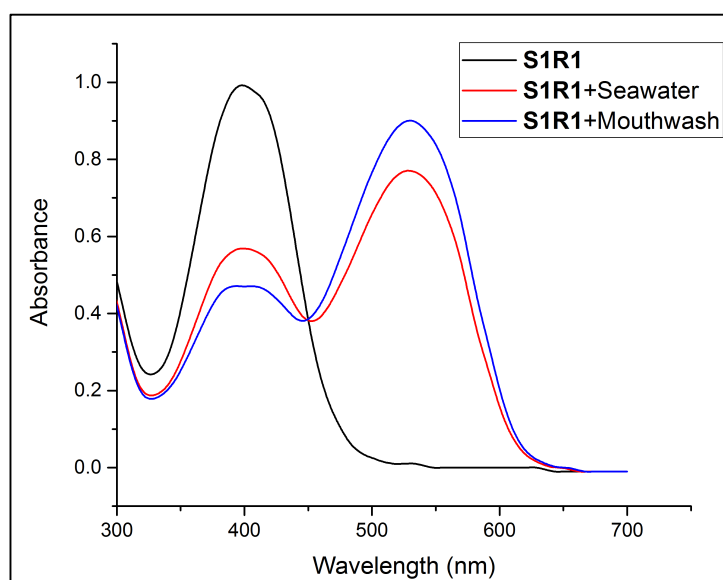


Fig. 3.36 UV-Vis spectra of **S1R1** with the addition of seawater and mouthwash

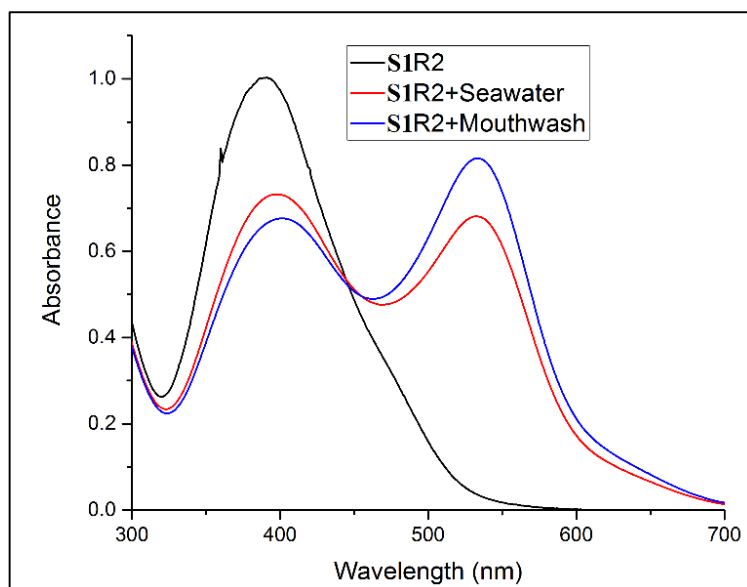


Fig. 3.37 UV-Vis spectra of **S1R2** with the addition of seawater and mouthwash

3.3.3 Competitive studies

In order to investigate the interference of other anions in the detection process, UV-Vis absorption study has been performed with the addition of 1 equiv. of AcO^- ion to the receptor solution containing 1 equiv. of other anions. UV-Vis spectra displayed a significant red shift with a new peak centered at 520 nm as shown in Fig. 3.38. The color change has been represented in Fig. 3.39. The spectral pattern was similar to that obtained on the addition of F^- ion or AcO^- ion alone to the free receptor. Thus, the receptor **S1R1** is found to be selective in the detection of AcO^- ions in mixed media. Whereas **S1R2**, devoid of selective nature showed equal colorimetric response in the presence of other interfering ions such as F^- , H_2PO_4^- and AcO^- ions.

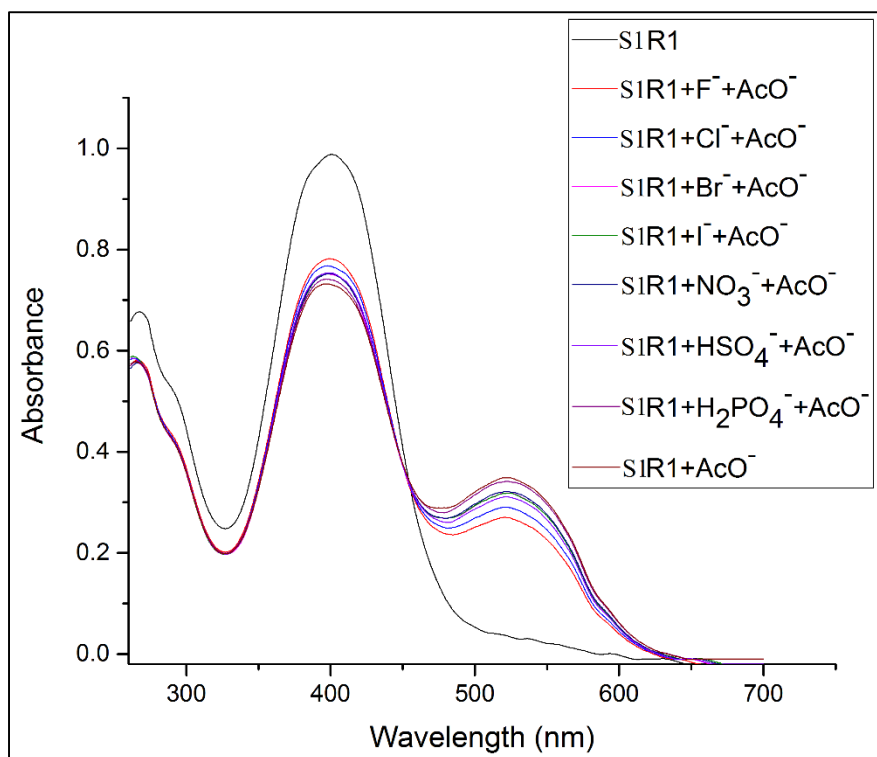


Fig. 3.38 UV-Vis spectra of **S1R1** with the addition of 1 equiv. of AcO⁻ ion to the receptor solution containing 1 equiv. of other test anions

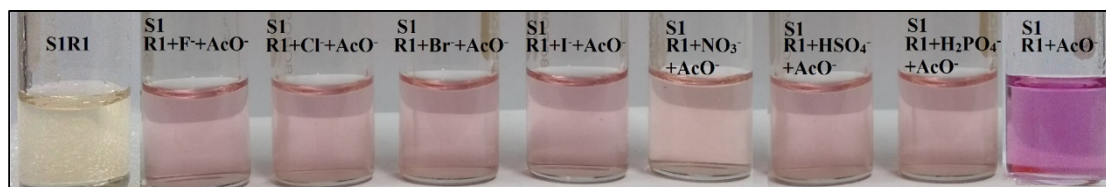


Fig. 3.39 Colorimetric response of receptor **S1R1** towards AcO⁻ ion in the presence of other interfering ions

3.3.4 Fluorescence studies

Fluorescence spectra has been recorded with the addition of TBA salt of anions in order to investigate the interaction of **S1R1** with different anions. The Fluorescence spectra is shown in Fig. 3.40. In case of free receptor, **S1R1** (1×10^{-4} M in DMSO), with an excitation wavelength of 395 nm, an emission band was observed at 486 nm. Incremental addition of AcO⁻ ions to **S1R1** yielded successive increase of band at 436 nm and 633 nm with isoemissive points centered at 578 nm and 475 nm (Fig. 3.41).

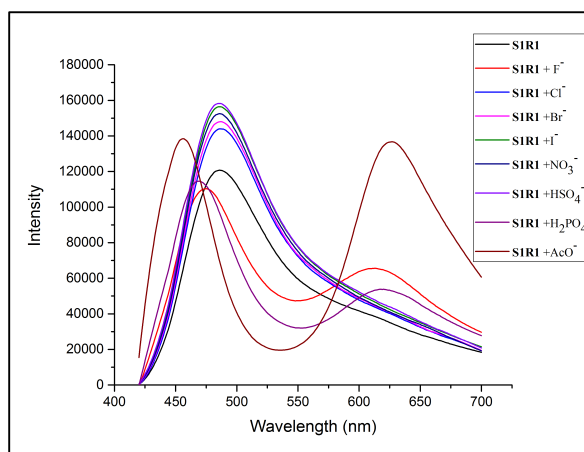


Fig. 3.40 Fluorescence spectra of **SIR1** (10^{-4} M in DMSO) with the addition of 1 equiv. of tertabutylammonium salts of various anions (10^{-2} M in DMSO)

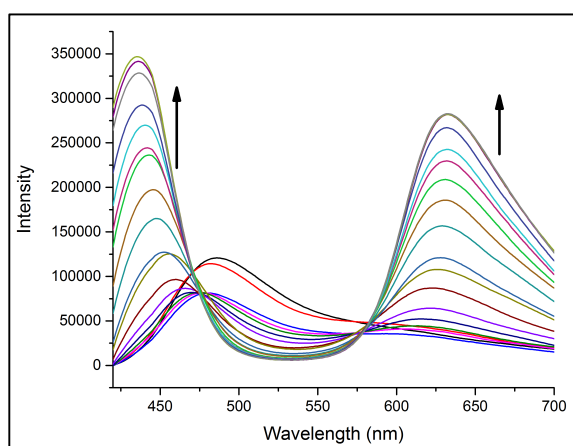


Fig. 3.41 Fluorescence spectra of **SIR1** (10^{-4} M in DMSO) with the incremental addition of 1 equiv. of tertabutylammonium salts of AcO⁻ ions (10^{-2} M in DMSO)

3.3.5 Cyclic voltammometric studies

Receptor **SIR1** exhibits oxidation peak at 0.5 V clearly indicating the role of –NH functionality in the oxidation process. The reduction peak appears at -0.84 V with the incremental addition of acetate ion signifying the role of –NO₂ functionality undergoing reduction process (Fig. 3.42). As the receptor **SIR2** possesses keto functionality, the investigation of electrochemical properties would pave way to arrive at the binding mechanism. Cyclic voltammogram reveals the presence of oxidation peak at 0.37 V corresponding to the –NH functionality and the reduction peak at 0.29 V and -0.5 V corresponding to the reduction of keto and nitro functionalities. With the

incremental addition of AcO^- ion, there was subsequent increase in the intensity of oxidation peak to 0.53 V and reduction peak to 0.25 V and -0.62 V respectively (Fig. 3.43).

The concomitant shift of the peak to more negative potential represents the difficulty in electroreduction of the keto functionality. The probable reason could be the deprotonation of $-\text{NH}$ proton by AcO^- ion which render the oxygen atom relatively electron rich by delocalization of electrons through the conjugated system. Further, the conversion of $\text{C}=\text{O}$ to $\text{C}-\text{O}^-$ renders the electroreduction of keto group gradually more difficult (Anzenbacher et al. 2005).

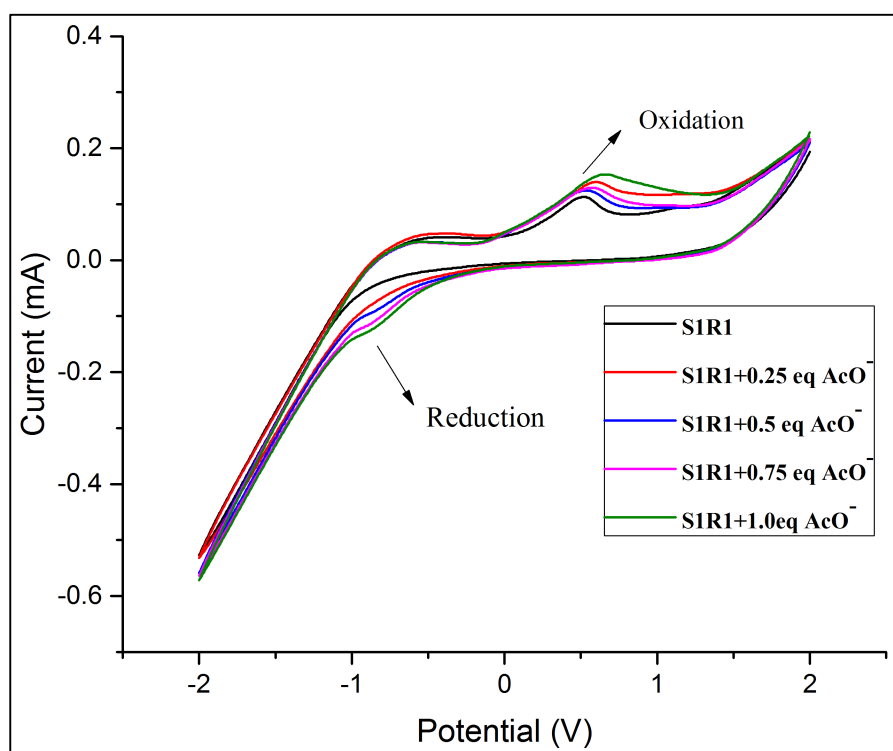


Fig. 3.42 Cyclic voltammogram of receptor **S1R1** with the incremental addition of AcO^- ion

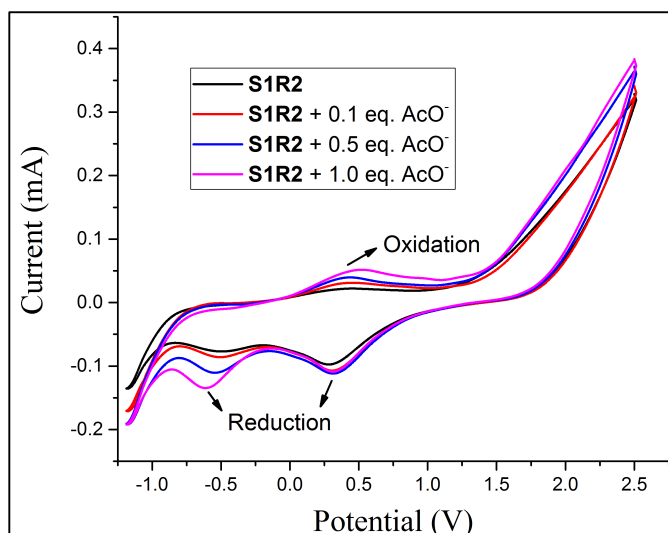


Fig. 3.43 Cyclic voltammogram of receptor **S1R2** with the incremental addition of AcO^- ion

Table 3.1 Binding constant, binding ratio and detection limit of receptors **S1R1** and **S1R2** with various anions

Receptor	Anion	Solvent system	Binding constant	Binding ratio	Detection limit (ppm)
S1R1	F^- (TBAF)	DMSO	$2.33 \times 10^4 \text{ M}^{-2}$	1:2	0.78
	AcO^- (TBAAcO)	DMSO	$1.37 \times 10^2 \text{ M}^{-1}$	1:1	1.5
	H_2PO_4 (TBAH ₂ PO ₄)	DMSO	$1.07 \times 10^2 \text{ M}^{-1}$	1:1	1.7
	F^- (NaF)	DMSO:H ₂ O (9:1, v/v)	$0.9 \times 10^4 \text{ M}^{-2}$	1:2	1.2
	AcO^- (NaAcO)	DMSO:H ₂ O (9:1, v/v)	$1.08 \times 10^2 \text{ M}^{-1}$	1:1	2.1
	AcO^- (TBAAcO)	DMSO:HEPES (9:1, v/v)	$1 \times 10^2 \text{ M}^{-1}$	1:1	1.9
S1R2	F^- (TBAF)	DMSO	$1.46 \times 10^2 \text{ M}^{-1}$	1:1	1.35
	AcO^- (TBAAcO)	DMSO	$3.14 \times 10^2 \text{ M}^{-1}$	1:1	1.5
	F^- (NaF)	DMSO:H ₂ O (9:1 v/v)	$0.98 \times 10^2 \text{ M}^{-1}$	1:1	0.25
	AcO^- (NaAcO)	DMSO:H ₂ O (9:1 v/v)	$0.95 \times 10^2 \text{ M}^{-1}$	1:1	0.41

3.3.6 ^1H -NMR titration studies

With a view to unveil the nature of reaction between receptor **S1R1** and **S1R2** with AcO^- ion, ^1H -NMR titration studies have been performed. With the incremental addition of 0.5, 1.0 equiv. of TBAAcO to **S1R1** and **S1R2**, the disappearance of NH proton was observed indicating the formation of strong hydrogen bond interaction between AcO^- and receptor. The aromatic proton signals in **S1R2** underwent an upfield shift indicating the presence of through-bond effect which tends to increase the electron density on the aromatic ring (Fig. 3.44 and Fig. 3.45). The disappearance of the splitting pattern in the aromatic region indicates the formation of $\text{NH}\cdots\text{AcO}^-$ hydrogen bond followed by a deprotonation process. The appearance of vinylic proton represents the successful conversion of hydrazone form (with $\text{C}=\text{N}$ chromophore) of the receptors to the azo form (with $\text{N}=\text{N}$ chromophore).

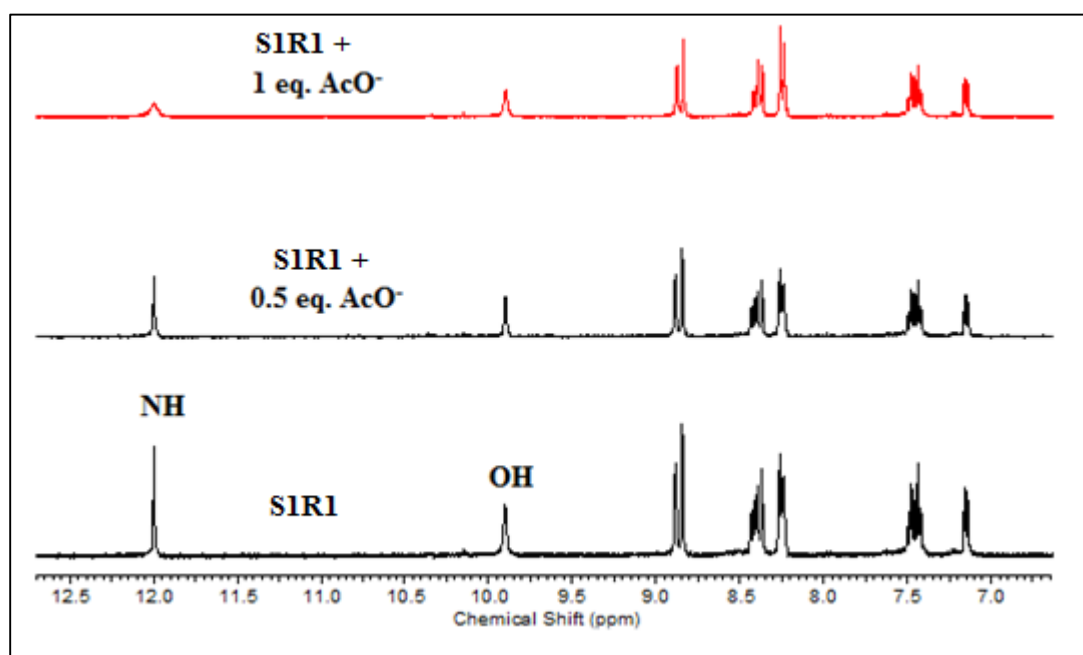


Fig. 3.44 ^1H NMR titration of receptor **S1R1** with incremental addition of TBAAcO (0-1 equiv.)

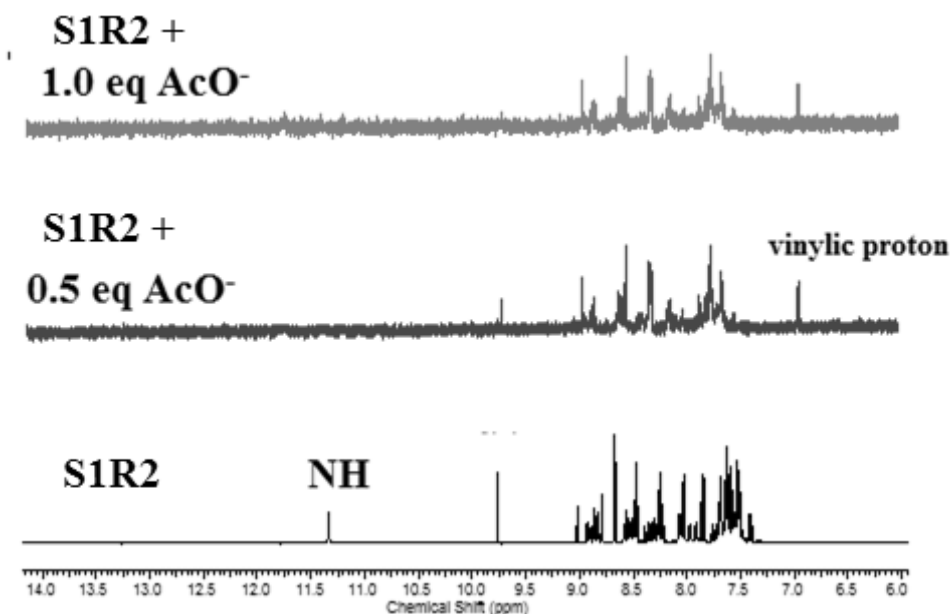


Fig. 3.45 ^1H NMR titration of receptor **S1R2** with incremental addition of TBAcO⁻ ion (0-1 equiv.)

3.3.7 Calculation of binding constant from UV-Vis studies

Binding constant has been calculated using Benesi-Hildebrand equation (Benesi and Hildebrand 1948) as given below;

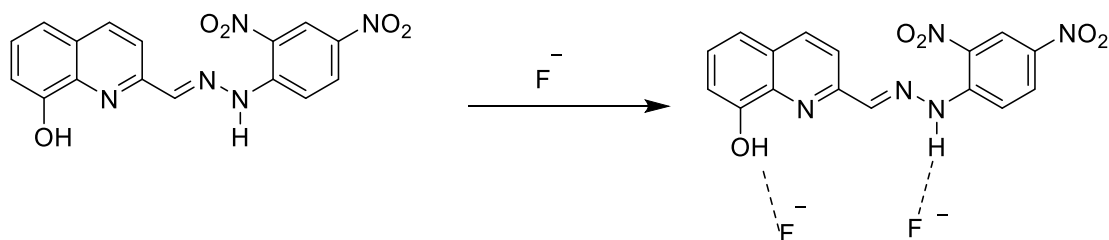
$$1/(A - A_0) = 1/(A_{\max} - A_0) + 1/K [X^-]^n (A_{\max} - A_0)$$

where, A_0 , A , A_{\max} are the absorption considered in the absence of anion, at an intermediate, and at a concentration of saturation. K is binding constant, $[X^-]$ is concentration of anion and n is the stoichiometric ratio.

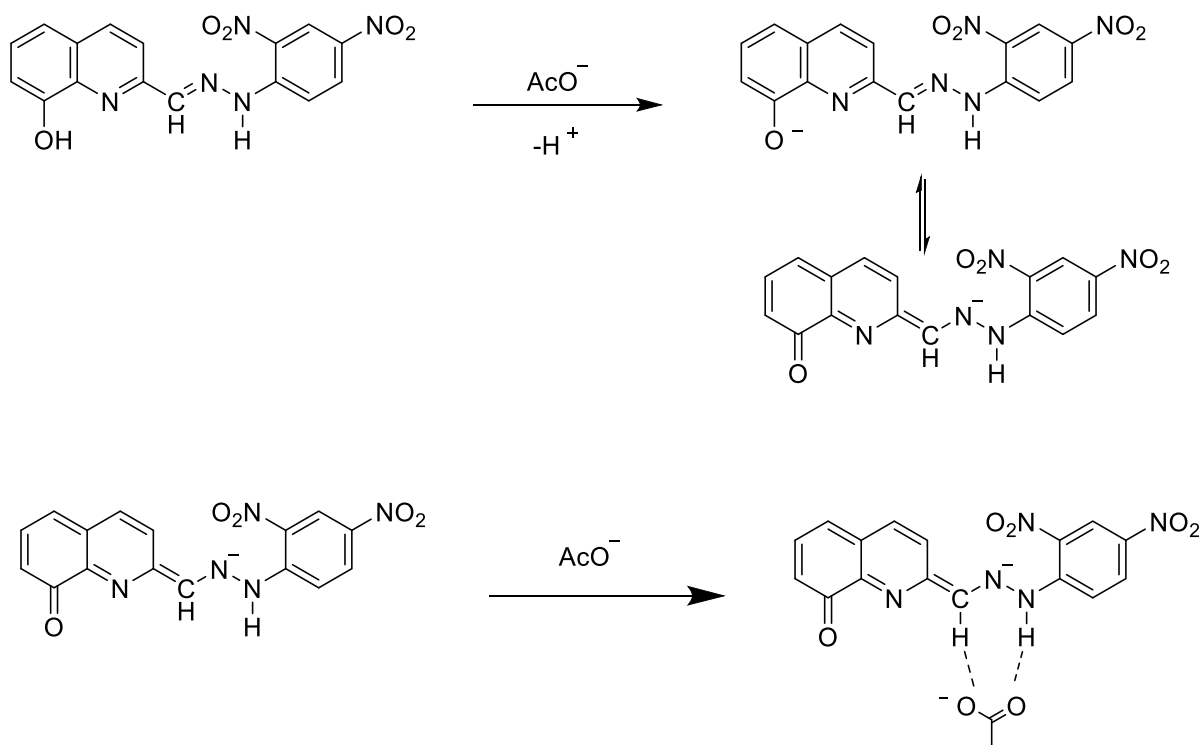
3.3.8 Binding mechanism

The selectivity for specific anions can be rationalized on the basis of the guest basicity and the shape complementarity. In this regard, multiple hydrogen-bond interaction is a necessary factor in anion binding process. In terms of basicity of anions, H_2PO_4^- , F^- , and AcO^- can offer much stronger interactions with receptor than other halogen anions. Furthermore, **S1R1** is an appropriate receptor for oxoanions because of the formation of N—H...O bonds and O—H...O bond with the two consecutive oxygen atoms of the anion. Consequently, the triangular acetate anion

with an O–C–O angle of ca. 120° may be the best fitting for the curvature shape of the binding sites of receptor among the anions tested (Boiocchi et al. 2004). Consequently, AcO^- might be selectively recognized from other anions. The plausible binding mechanism of **S1R1** with F^- and AcO^- ion is shown in Scheme 3.3 and Scheme 3.4 respectively.



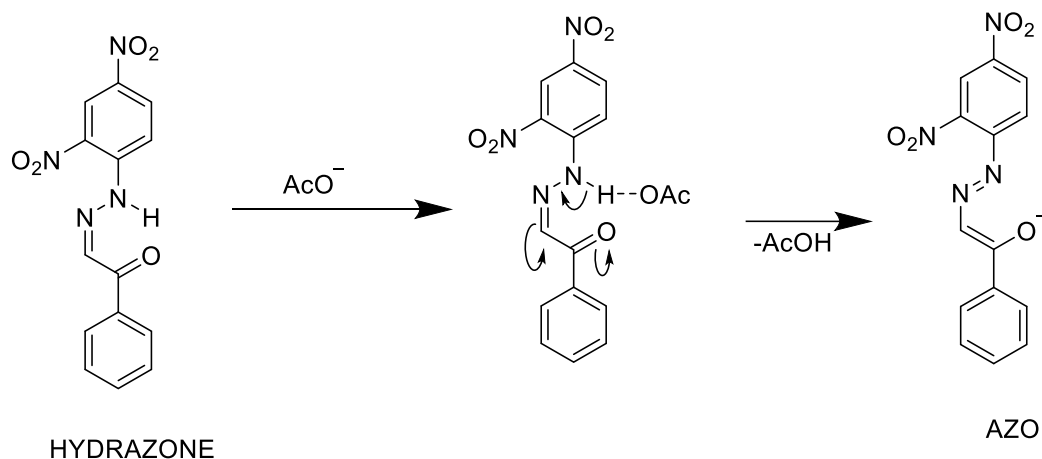
Scheme 3.3 Proposed binding mechanism of receptor **S1R1** with F^- ion



Scheme 3.4 Proposed binding mechanism of receptor **S1R1** with AcO^- ion

With the addition of incremental amounts of acetate ions to the solution of **S1R2**, the absorbance of the higher energy peak (due to C=N chromophore)

diminished gradually and that of the lower energy peak (due to N=N chromophore) increased gradually. This observation suggested that addition of acetate ion might have converted the hydrazone form (with C=N chromophore) of the receptors to the azo form (with N=N chromophore). The plausible binding mechanism of **S1R1** with AcO^- ion is shown in Scheme 2.5.



Scheme 3.5 Proposed binding mechanism of receptor **S1R2** with AcO^- ion

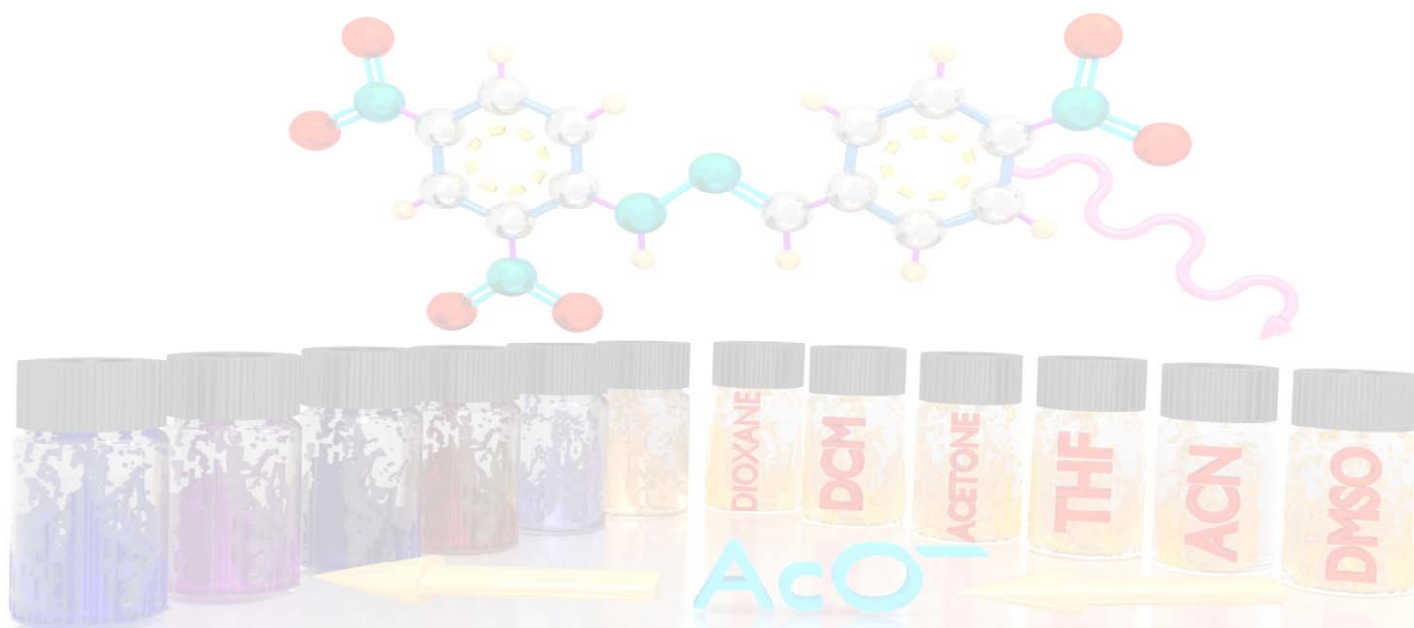
3.4 CONCLUSIONS

Colorimetric studies performed on **S1R1** and **S1R2** with the addition of anions revealed color change visible to naked eye. UV-Vis studies in DMSO/HEPES buffer solution (9:1 v/v, pH 7.4) revealed excellent selectivity of the receptor towards AcO^- ion with pale pink coloration. Receptor **S1R1** exhibited excellent colorimetric sensing behavior towards F^- , H_2PO_4^- and AcO^- ions in DMSO and specificity towards AcO^- ion in DMSO/HEPES buffer solution. Lower detection limit of 0.7 ppm, 1.7 ppm and 1.5 ppm achieved for F^- , H_2PO_4^- and AcO^- ions with receptor **S1R1** proves its utility as a chemosensor. F^- and AcO^- ion sensing property of receptor **S1R2** via anion induced tautomerism of C=N to N=N has been investigated and supported by UV-Vis spectroscopic studies. **S1R1** exhibits an emission spectra with fluorescence enhancement with the addition of AcO^- ions. Electrochemical studies performed on receptor **S1R2** in the presence of AcO^- ion revealed the deprotonation of -NH functionality in the anion binding process. Lower detection limit of **S1R2** of the order

0.25 ppm and 0.41 ppm towards F^- and AcO^- ions suggests its utility in the detection of anions in commercially available samples. To sum up, based on UV-Vis spectroscopic studies, 1H NMR titration studies and electrochemical studies receptors **S1R1** and **S1R2** could be regarded as efficient colorimetric chemosensors for anions.

CHAPTER 4

SYNTHESIS OF ORGANIC RECEPTORS FOR ANIONS: SOLVENT DEPENDENT CHROMOGENIC RESPONSE AND DFT STUDIES



Abstract

In this chapter, design, syntheses and characterization of five organic receptors have been described. The applicability of the receptors in the colorimetric detection of anions have been discussed in detail through UV-Vis spectrophotometric, ¹H NMR titration, electrochemical and DFT studies. The binding mechanism of the receptors towards active anion have been included.

4.1 INTRODUCTION

Anion receptor chemistry has grown into an area of great interest for supramolecular chemists opening up new arena for precise design strategy. Primarily, binding interactions with anions being hydrogen bond or electrostatic force imposes vigilant insight for a constructive design unlike the simple metal-ligand coordination interactions involved in cation-receptor chemistry (A. Gale 2008; Best et al. 2003; Choi and Hamilton 2003; Davis and Joos 2003; Hay et al. 2005; Miyaji et al. 2000; Schmuck and Schwegmann 2005; Sessler et al. 2003; Sessler and Seidel 2003).

Binding site-signalling unit approach involving covalent attachment of the chromophore and neutral receptor bearing hydrogen bond donor unit has been most commonly utilized in designing chromogenic receptors. Few receptors reported in the literature have successfully surpassed the challenges set by the anionic substrates such as similar basicity and surface charge density in the commonly encountered F⁻, AcO⁻ and H₂PO₄⁻ ions. Despite these setbacks, colorimetric receptors bearing chromophores such as indoles (Caltagirone et al. 2008a; b; O. Yu et al. 2008; Pfeffer et al. 2007), bisindole (Chang et al. 2005; Kim et al. 2008b; Naidu et al. 2008), carbazole (Chmielewski et al. 2004; Hiscock et al. 2009; J. Chmielewski et al. 2008; Piątek et al. 2004; Suk and Jeong 2008), nitrophenyl (Black et al. 1999; Boiocchi et al. 2004; Cho et al. 2005; Kwon et al. 2004), quinone (Jiménez et al. 2002; Jose et al. 2004; Miyaji et al. 2000; Miyaji and Sessler 2001), nitrobenzene (Lee et al. 2001, 2003; Nishiyabu and Anzenbacher 2005; Sancenón et al. 2002), azo groups and other electron withdrawing moieties (Chmielewski et al. 2004; Hiscock et al. 2009; J. Chmielewski et al. 2008; Piątek et al. 2004; Suk and Jeong 2008) have been developed.

In the design of anion chemosensors, various non-covalent interactions such as hydrogen bonding, anion- π and reactions like hydrogen abstraction, electron transfer have been commonly encountered (A. Gale and Caltagirone 2015; Ajayakumar et al. 2010; Beer and Hayes 2003; Dickson et al. 2008; Kim et al. 2008a; Lazarides et al. 2005; Lin et al. 2007, 2006; R. Ajayakumar et al. 2013; Sharma et al. 2013). Studies performed with molecules comprising of secondary amine groups possessing highly acidic proton are known to promote hydrogen bond interactions with anions (Gunupuru et al. 2014). Furthermore, electroanalytical technique such as cyclic voltammetry could be a valuable tool to analyse the binding of anion by the receptors through redox process. Concurrently, band gap of the receptor and receptor-anion complex could be calculated. In addition, the presence of NO_2 group as a signalling unit at position *para* to the NH functionality induced a strong colorimetric response visible to the naked eye. The anion binding studies performed reveals significant colorimetric response visible to the naked eye paving way for the quantitative study through UV-Vis, ^1H NMR spectroscopy and cyclic voltammetric studies. Besides, the nature of interaction by increasing the number of $-\text{NO}_2$ groups and introduction of $-\text{OH}$ functionality on the receptor molecule and its impact on anion binding has been studied.

4.2 EXPERIMENTAL SECTION

4.2.1 Materials and methods

All the chemicals used in the present study were procured from Sigma-Aldrich and Alfa Aesar and were used as received without further purification. All the solvents were purchased from SD Fine, India, were of HPLC grade and used without further distillation.

Melting point was measured on Stuart SMP3 melting-point apparatus in open capillaries. Infrared spectrum was recorded on Bruker Apex FTIR spectrometer. UV-Vis spectroscopy was performed with analytik jena Specord S600 spectrometer in standard 3.0 mL quartz cell with 1 cm path length. The ^1H NMR spectra were recorded on Bruker Ascend (400 MHz) instrument using TMS as internal reference and DMSO-d_6 as solvent. Resonance multiplicities are described as s (singlet), d

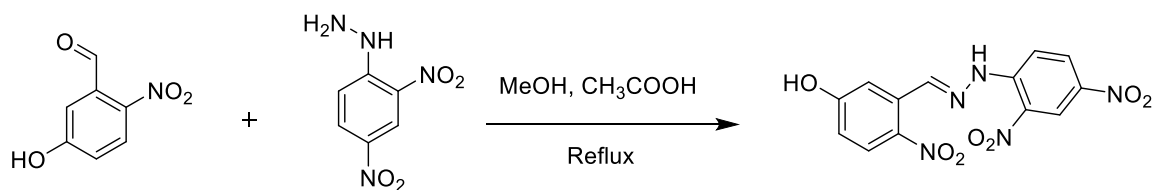
(doublet), t (triplet) and m (multiplet). Mass spectrum was recorded on Bruker Daltonics *ESI*Q TOF. Cyclic voltammogram was recorded on Ivium electrochemical workstation (Vertex) at a scan rate of 20 mV/s with the potential range 1.0 mV to -1.0 mV. The single-crystal X-ray diffraction (SCXRD) was performed on Bruker AXS APEX II system.

Density Functional Theory (DFT) simulation has been performed on the receptor molecule using GAUSSIAN 09 package. A closed shell Becke–Lee–Yang–Parr hybrid exchange-correlation three-parameter functional (B3LYP) along with 6-311++G(d) basis set were used in the simulation to derive a complete geometry optimization for isolated receptor and its deprotonated form in the binding process. Berny's optimization algorithm was used to fully optimize the molecular geometry, which involves redundant internal coordinates. To confirm the convergence to the minima on the potential energy surface, the harmonic vibrational wavenumbers were calculated using analytic second derivatives and properly scale down to control the systematic errors caused by incompleteness of the basis set. In a second step, the time dependent DFT (TD-DFT) method were used considering the same B3LYP exchange-correlation functional with 6-311++G (d,p) basis set to obtain the UV-Visible absorption spectra of free and deprotonated receptor.

4.2.2 Synthesis of receptor S2R1

(E)-3-((2-(2,4-dinitrophenyl)hydrazono)methyl)-4-nitrophenol (S2R1)

2-nitro, 5-hydroxybenzaldehyde (0.05 g, 0.29 mmol) and 2,4-dinitrophenylhydrazine (0.059 g, 0.29 mmol) were refluxed in 5 ml methanol for 5 h in the presence of acetic acid as catalyst. The formation of the product was confirmed through TLC by the generation of single spot indicative of the disappearance of starting materials. After cooling to room temperature, the reaction mixture was filtered through filter paper, washed with methanol to obtain pure product (Scheme 4.1).



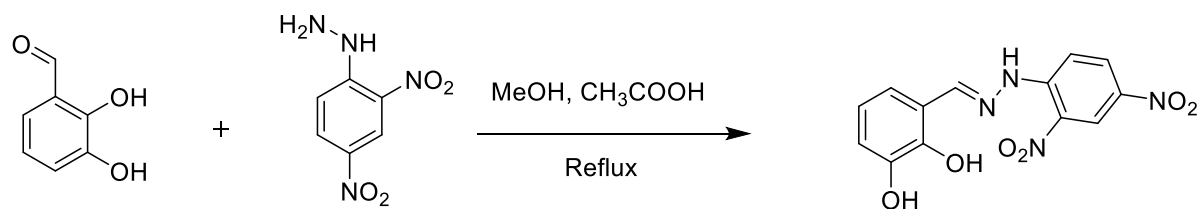
Scheme 4.1 Synthesis of receptor S2R1

Yield: 75%, m. p. 246 °C. ^1H NMR (DMSO- d_6 , 400 MHz, ppm): δ 7.45 (dd, $J = 8.2$, 1.9 Hz, 1H), 7.13-7.0 (dd, $J = 1.9$, 0.5 Hz, 1H), 8.08-8.02 (dd, $J = 8.2$, 0.5 Hz, 2H), 8.43 (s, 1H), 8.86 (dd, $J = 7.8$, 1.9 Hz, 1H), 9.19 (dd, $J = 1.9$, 0.5 Hz, 1H), 11.16 (s, 1H), 11.95 (s, 1H). FTIR (KBr)(cm^{-1}): 3386 (OH), 3286 (Ar-CH), 3103 (NH), 1609 (CH=N), 1505 (C=C), 1330 (NO_2), 1099 (C-H). Mass (ESI): m/z Calculated: 347.05 Obtained: 331.13

4.2.3 Synthesis of receptor S2R2

(E)-3-((2-(2,4-dinitrophenyl)hydrazono)methyl)benzene-1,2-diol

2,3-dihydroxybenzaldehyde (0.05 g, 0.36 mmol) and 2,4-dinitrophenylhydrazine (0.071 g, 0.36 mmol) were refluxed in 5 ml methanol for 5 h in the presence of acetic acid as catalyst. The formation of the product was confirmed through TLC by the generation of single spot indicative of the disappearance of starting materials. After cooling to room temperature, the reaction mixture was filtered through filter paper, washed with methanol to obtain pure product (Scheme 4.2).



Scheme 4.2 Synthesis of receptor S2R2

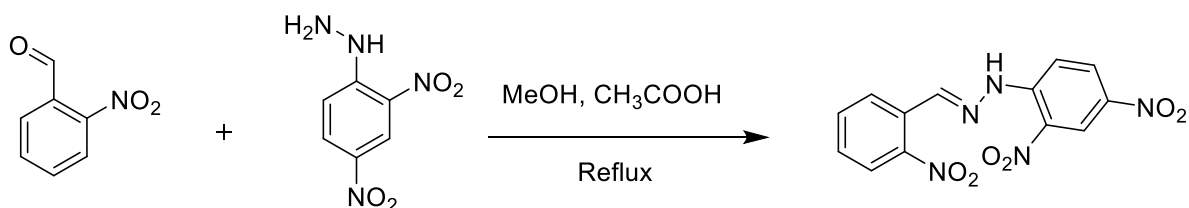
Yield: 70%, m. p. 246 °C. ^1H NMR (DMSO- d_6 , 400 MHz, ppm): δ 6.74 (dd, $J = 8.6$, 2.3 Hz, 1H), 6.87 (dd, $J = 8.2$, 2.3 Hz, 1H), 7.3 (dd, $J = 7.8$ Hz, 0.5 Hz, 1H), 8.01 (dd, $J = 8.6$, 8.2 Hz, 1H), 8.37 (dd, $J = 7.3$, 0.5 Hz, 1H), 8.87 (s, 1H), 8.97 (dd, $J = 7.8$, 1.9

Hz, 1H), 9.28 (dd, $J = 1.9, 0.5$ Hz, 1H), 9.66 (s, 1H), 11.71 (s, 1H). FTIR (KBr) (cm^{-1}): 3458 (OH), 3252 (Ar-CH), 2922 (NH), 1616 (CH=N), 1338 (NO_2), 1112 (C-H). Mass (ESI): m/z Calculated: 318.06 Obtained: 319.13 ($\text{M}+\text{H}$)⁺

4.2.4 Synthesis of receptor S2R3

(E)-1-(2,4-dinitrophenyl)-2-(2-nitrobenzylidene)hydrazine

2-nitrobenzaldehyde (0.05 g, 0.33 mmol) and 2,4-dinitrophenylhydrazine (0.065 g, 0.33 mmol) were refluxed in 5 ml methanol for 5 h in the presence of acetic acid as catalyst. The formation of the product was confirmed through TLC by the generation of single spot indicative of the disappearance of starting materials. After cooling to room temperature, the reaction mixture was filtered through filter paper, washed with methanol to obtain pure product (Scheme 4.3).



Scheme 4.3 Synthesis of receptor S2R3

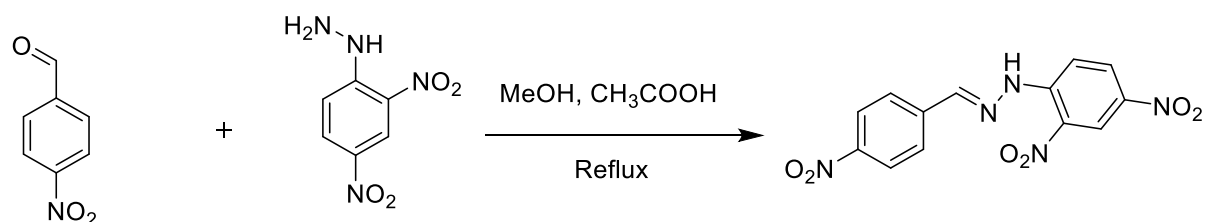
Yield: 85%, m. p. 280 °C. ¹H NMR (DMSO- d_6 , 400 MHz, ppm): δ 7.82-7.70 (2H, 7.80 (td, $J = 7.9, 1.9$ Hz), 7.67-8.03 (ddd, $J = 8.3, 7.7, 1.5$ Hz)), 7.84 (ddd, $J = 7.7, 1.5, 0.5$ Hz, 2H), 8.20 (ddd, $J = 8.3, 1.9, 0.5$ Hz, 1H), 8.40 (dd, $J = 7.8, 1.9$ Hz, 1H), 8.86 (dd, $J = 1.9, 0.5$ Hz, 1H), 9.08 (s, 1H), 11.96 (s, 1H). FTIR (KBr)(cm^{-1}): 3285(NH), 3087 (Ar-CH), 1615 (CH=N), 1502 (C=C), 1334 (NO_2), 1138 (C-H). Mass (ESI): m/z Calculated: 331.06 Obtained: 332.13($\text{M}+\text{H}$)⁺

4.2.5 Synthesis of receptor S2R4

(E)-1-(4-nitrobenzylidene)-2-(2,4-dinitrophenyl)hydrazine (S2R4)

4-nitrobenzaldehyde (0.05 g, 0.33 mmol) and 2,4-dinitrophenylhydrazine (0.065 g, 0.33 mmol) were mixed in 5 ml methanol. A drop of acetic acid was added and the reaction mixture was refluxed for 5 h. The formation of the product was confirmed

through TLC by the generation of single spot indicative of the disappearance of starting materials. After cooling to room temperature, the reaction mixture was filtered through filter paper, washed with methanol to obtain pure product (Scheme 4.4).



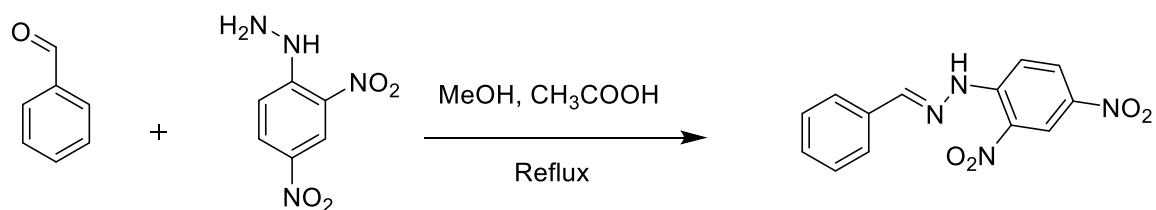
Scheme 4.4 Synthesis of receptor **S2R4**

Yield: 85%, m. p. 280 °C. ^1H NMR (DMSO- d_6 , 400 MHz, ppm): δ 8.05 (dd, $J = 7.8$, 0.5 Hz, 1H), 8.16 (s, 1H), 8.32-8.41 (ddd, $J = 8.7$, 1.8, 0.5 Hz, 4H), 8.80 (dd, $J = 7.8$, 1.9 Hz, 1H), 8.86 (dd, $J = 1.9$, 0.5 Hz, 1H), 11.85 (s, 1H). FTIR (KBr) (cm^{-1}): 3279(NH), 3089(Ar-CH), 1613(CH=N), 1510(C=C), 1331(NO_2), 1088(C-H). Mass (ESI): m/z Calculated: 331.06 Obtained: 338($\text{M}+\text{N}^+$)

4.2.6 Synthesis of receptor **S2R5**

(E)-1-benzylidene-2-(2,4-dinitrophenyl)hydrazine

Benzaldehyde (0.05 g, 0.47 mmol) and 2,4-dinitrophenylhydrazine (0.093 g, 0.47 mmol) were mixed in 5 ml ethanol. A drop of acetic acid was added and the reaction mixture was refluxed at 60 °C for 5 h. The formation of the product was confirmed through TLC by the generation of single spot indicative of the disappearance of starting materials. After cooling to room temperature, the reaction mixture was filtered through filter paper, washed with methanol to obtain pure product (Scheme 4.5). The structure of **S2R5** has been confirmed by single crystal X-ray diffraction study. Single crystals were obtained by slow evaporation of **S2R5** from a binary solvent system comprising of acetonitrile and dimethylformamide. The ORTEP diagram of **S2R5** is shown in Fig. 4.11 and the crystallographic data is presented in Table 4.1.



Scheme 4.5 Synthesis of receptor **S2R5**

Yield: 85%, m. p. 230 °C. ^1H NMR (DMSO- d_6 , 400 MHz, ppm): δ 7.4 (dddd, $J = 7.9, 1.5, 1.3, 0.5$ Hz, 3H), 7.8 (s, 2H), 8.13 (tt, $J = 7.4, 1.3$ Hz, 1H), 8.38 (dd, $J = 7.8, 0.5$ Hz, 1H), 8.72 (dd, $J = 7.8, 1.9$ Hz, 1H), 8.87 (dd, $J = 1.9, 0.5$ Hz, 1H), 11.68 (s, 1H). FTIR (KBr) (cm^{-1}): 3282(NH), 3086(Ar-CH), 1610 (CH=N), 1505 (C=C), 1324 (NO_2), 1128 (C-H). Mass (ESI): m/z Calculated: 286.07 Obtained: 287.13 ($\text{M}+\text{H}$) $^+$.

4.2.7 Characterization data of receptors

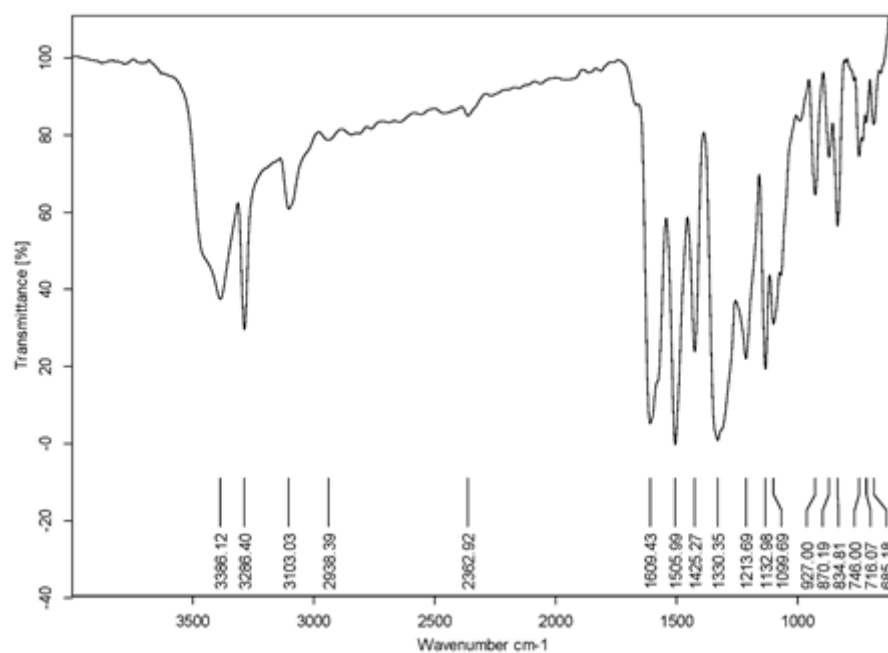


Fig. 4.1 FT-IR spectrum of receptor **S2R1**

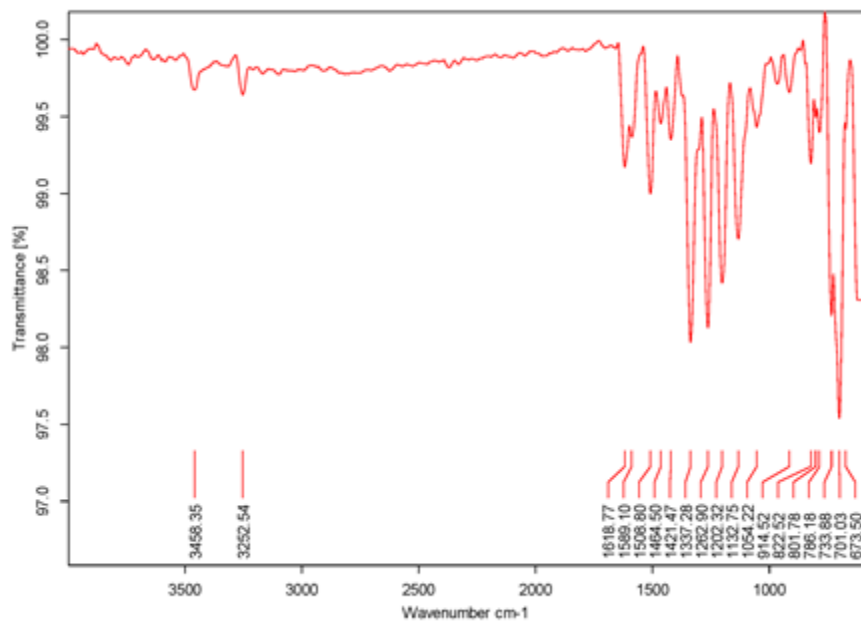


Fig. 4.2 FT-IR spectrum of receptor S2R2

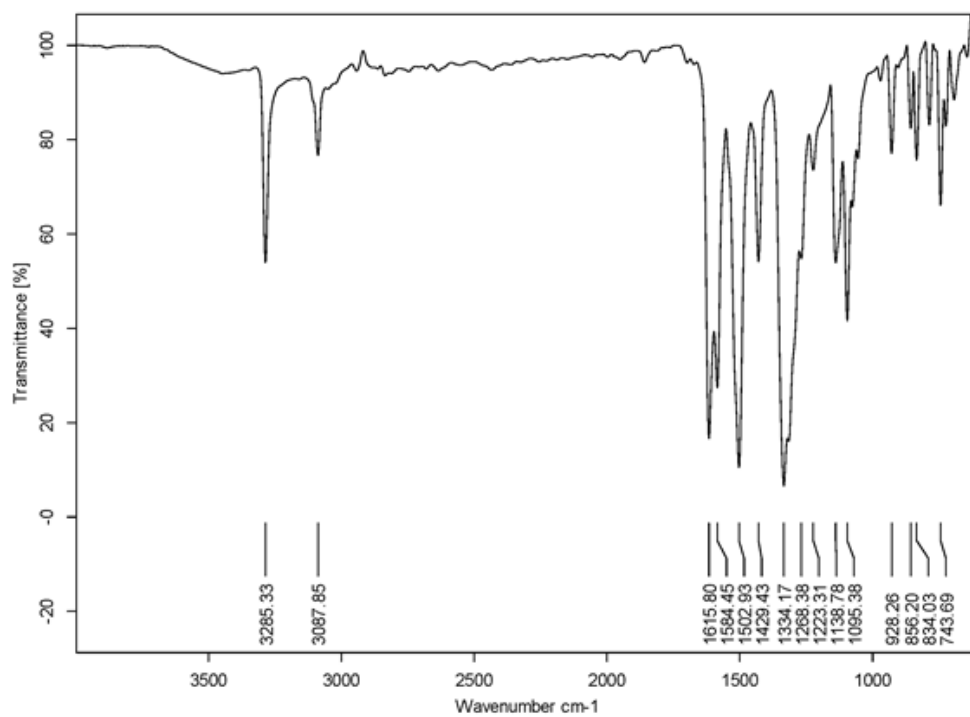


Fig. 4.3 FT-IR spectrum of receptor S2R3

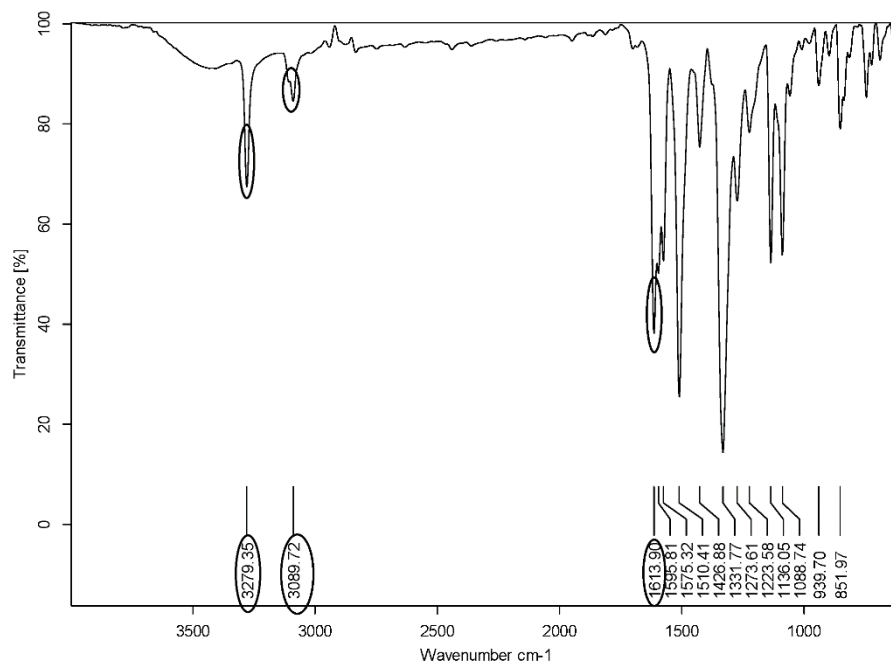


Fig. 4.4 FT-IR spectrum of receptor S2R4

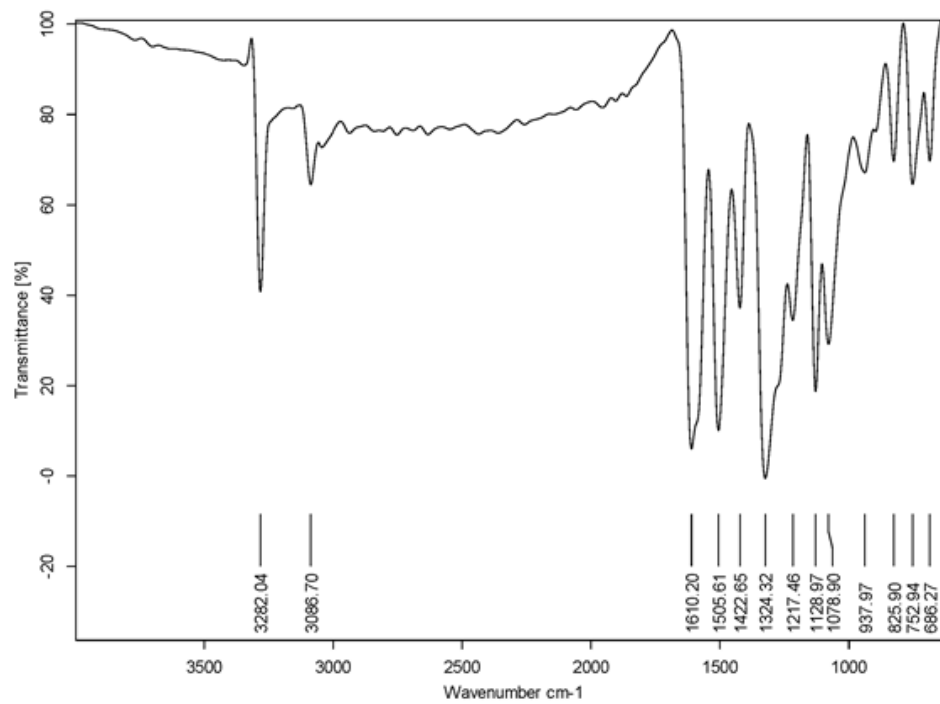
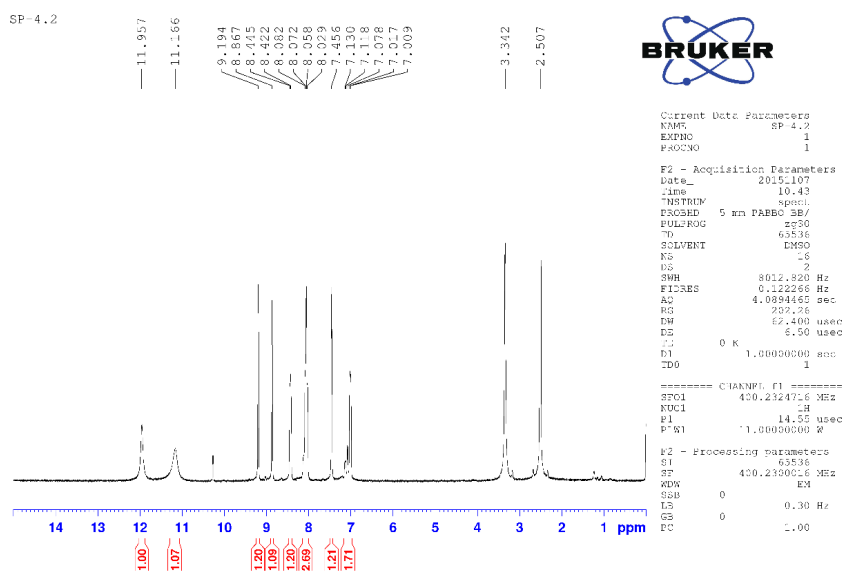
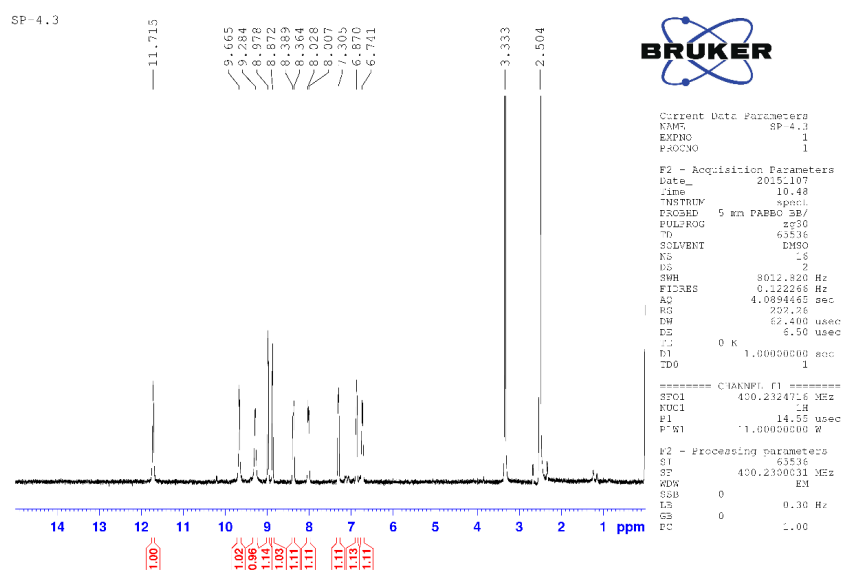
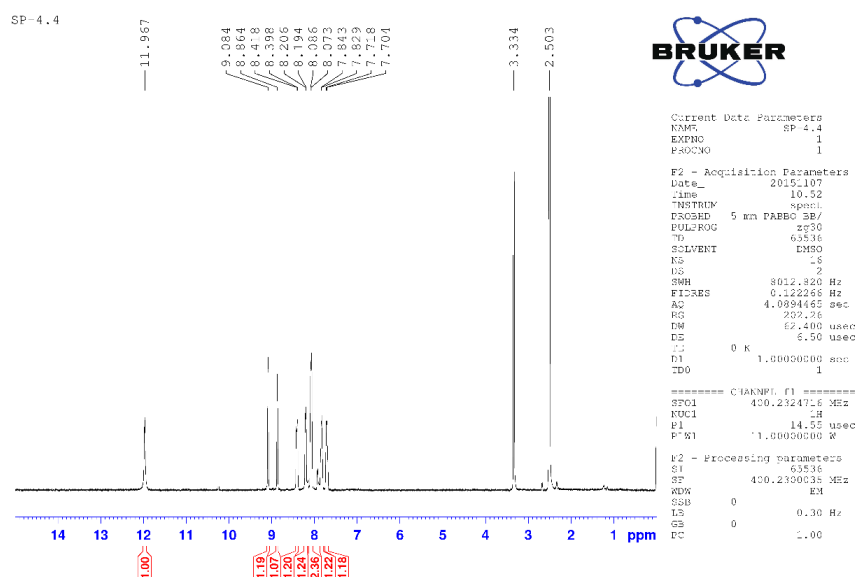
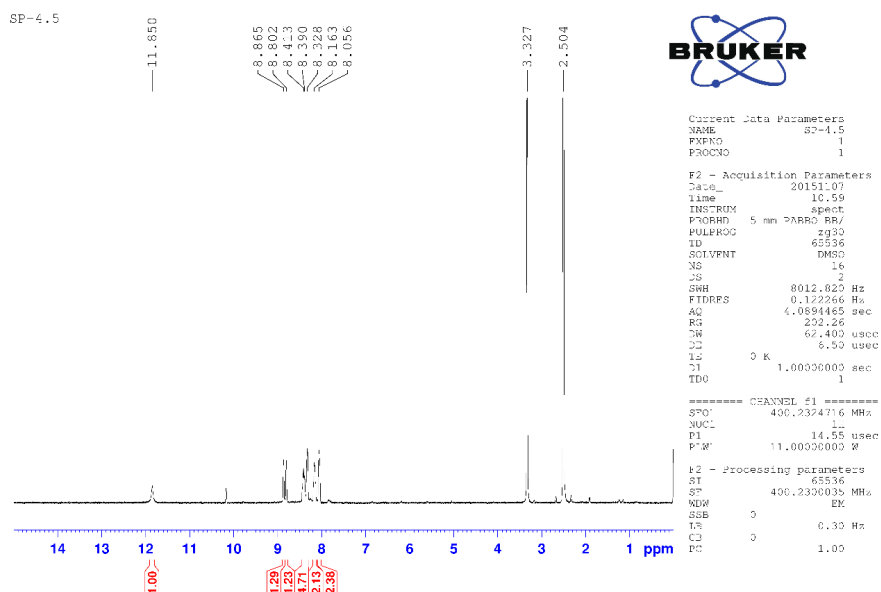


Fig. 4.5 FT-IR spectrum of receptor S2R5

Fig. 4.6 ^1H -NMR spectrum of receptor S2R1Fig. 4.7 ^1H -NMR spectrum of receptor S2R2

Fig. 4.8 ^1H -NMR spectrum of receptor S2R2Fig. 4.9 ^1H -NMR spectrum of receptor S2R4

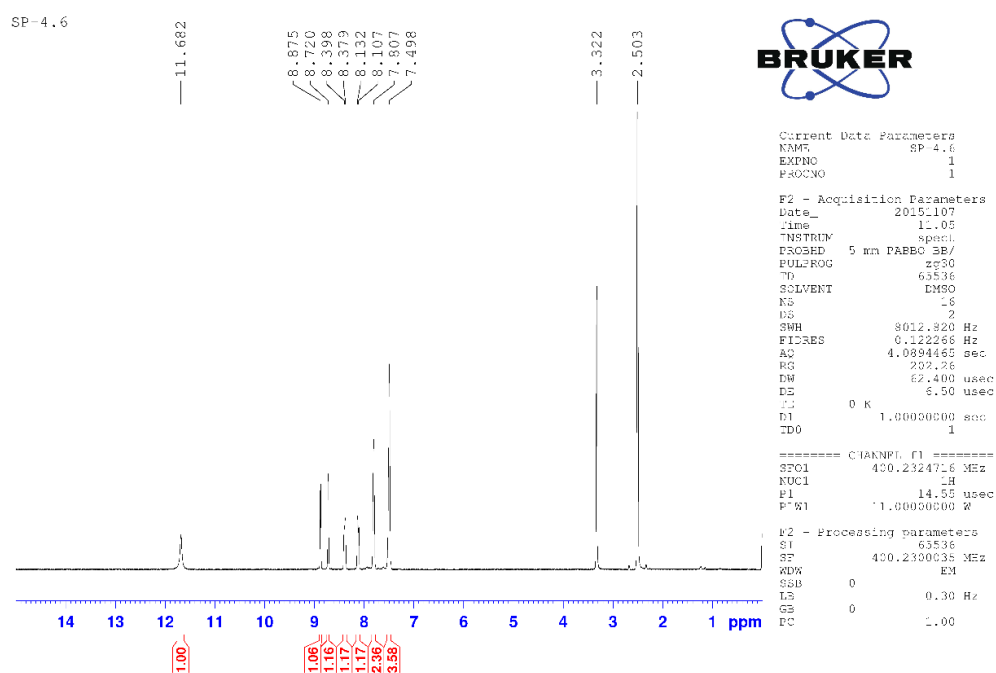


Fig. 4.10 ^1H -NMR spectrum of receptor S2R5

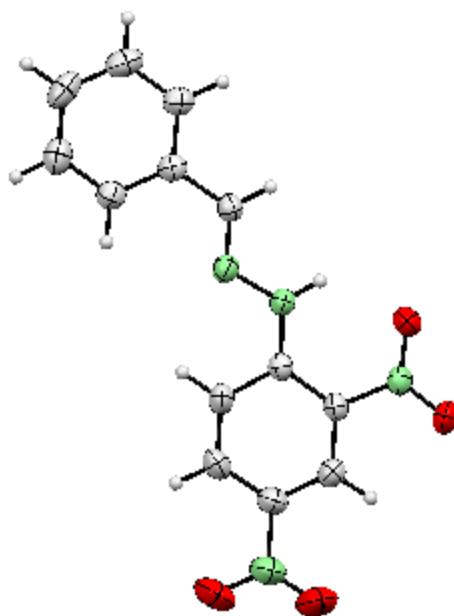


Fig. 4.11 ORTEP diagram of receptor S2R5

Table 4.1 Crystallographic data of receptor **S2R5**

Crystal parameters	S2R5
Empirical formula	C ₁₃ H ₁₀ N ₄ O ₄
Formula weight (g mol ⁻¹)	286.25
Temperature	296 (2) K
Wavelength	0.71073
Crystal system, space group	Monoclinic, 'P 21/n'
Unit cell dimension	a = 13.2961(5), $\alpha = 90^0$ b = 6.8247(3), $\beta = 92.563^0$ C(2) c = 14.3454(6), $\gamma = 90^0$
Volume	1300.43(9)Å ³
Z, calculated density	4, 1.462 gcm ⁻³
Absorption coefficient	0.112
F (000)	592
Theta range for data collection	1.533 to 25.987 ⁰
Index ranges	-16<=h<=16, -8<=k<=8, -17<=l<=17
Reflections collected	18519
Completeness to theta =25.242 ⁰	99.4 %
Absorption correction	Semi-empirical from equivalents
Refinement method	Full-matrix least-squares on F ²
Data/ restraints/ parameters	2565/0/230
Goodness-of-fit on F ²	0.839
Final R indices [I>2sigma(I)]	0.1449,0.1250
R indices (all data)	0.0484
CCDC No.	1468111

4.3 RESULTS AND DISCUSSION

4.3.1 Colorimetric detection of anions

With a view to evaluate the effect of structural modification on the optical properties of phenylhydrazones, positional substitution of -OH and -NO₂ groups on the phenyl moiety have been considered as part of the design strategy. UV-Vis spectroscopic study performed with 1x10⁻⁴ M DMSO solution of the receptors **S2R1**, **S2R2** and **S2R5** displayed strong absorption band at 395 nm, 405 nm and 394 nm respectively whereas receptors **S2R3** and **S2R4** exhibited absorption band at around 413 nm. The absorption maxima for **S2R1** to **S2R4** could be assigned to the intramolecular charge transfer interactions in the presence of Ar-CH=N-NH

conjugation. The electron donor nature of $-\text{NH}$ and acceptor nature of $-\text{NO}_2$ functionality are known to impart pale yellow coloration to the receptor in DMSO.

The interaction of anion with receptors **S2R1** to **S2R5** has been assessed by color changes visible to the naked eye and quantified by UV-Vis spectral studies. UV-Vis spectroscopic studies of receptors **S2R1** to **S2R5** (1×10^{-4} M in DMSO) has been performed with the addition of tetrabutylammonium (TBA) salts of anions (1×10^{-2} M in DMSO) such as F^- , Cl^- , Br^- , I^- , NO_3^- , HSO_4^- , H_2PO_4^- and AcO^- . Receptors displayed significant colorimetric response upon the addition of 1 equiv. of AcO^- ion as shown in Fig. 4.12. Receptors **S2R1**, **S2R2** and **S2R5** displayed red shift of original absorption band to 545 nm, 497 nm and 495 nm respectively accompanied by distinct color change from pale yellow to blood red, orange red and red color visible to the naked eye (Fig. 4.13, Fig. 4.14 and Fig. 4.17). On the contrary, receptors **S2R3** and **S2R4** exhibited a unique colorimetric response from pale yellow to purple and violet with a significant red shift and appearance of new band at 570 nm and 572 nm respectively (Fig. 4.15 and Fig. 4.16). However, receptors **S2R1** to **S2R4** exhibited relatively similar but less intense colorimetric response towards F^- and H_2PO_4^- ions owing to their properties such as similar basicity and charge to radius ratio. Receptor **S2R5** exhibited selective response towards AcO^- ion. No significant changes were observed with other anions in the present study which clearly indicates the absence of complex formation.

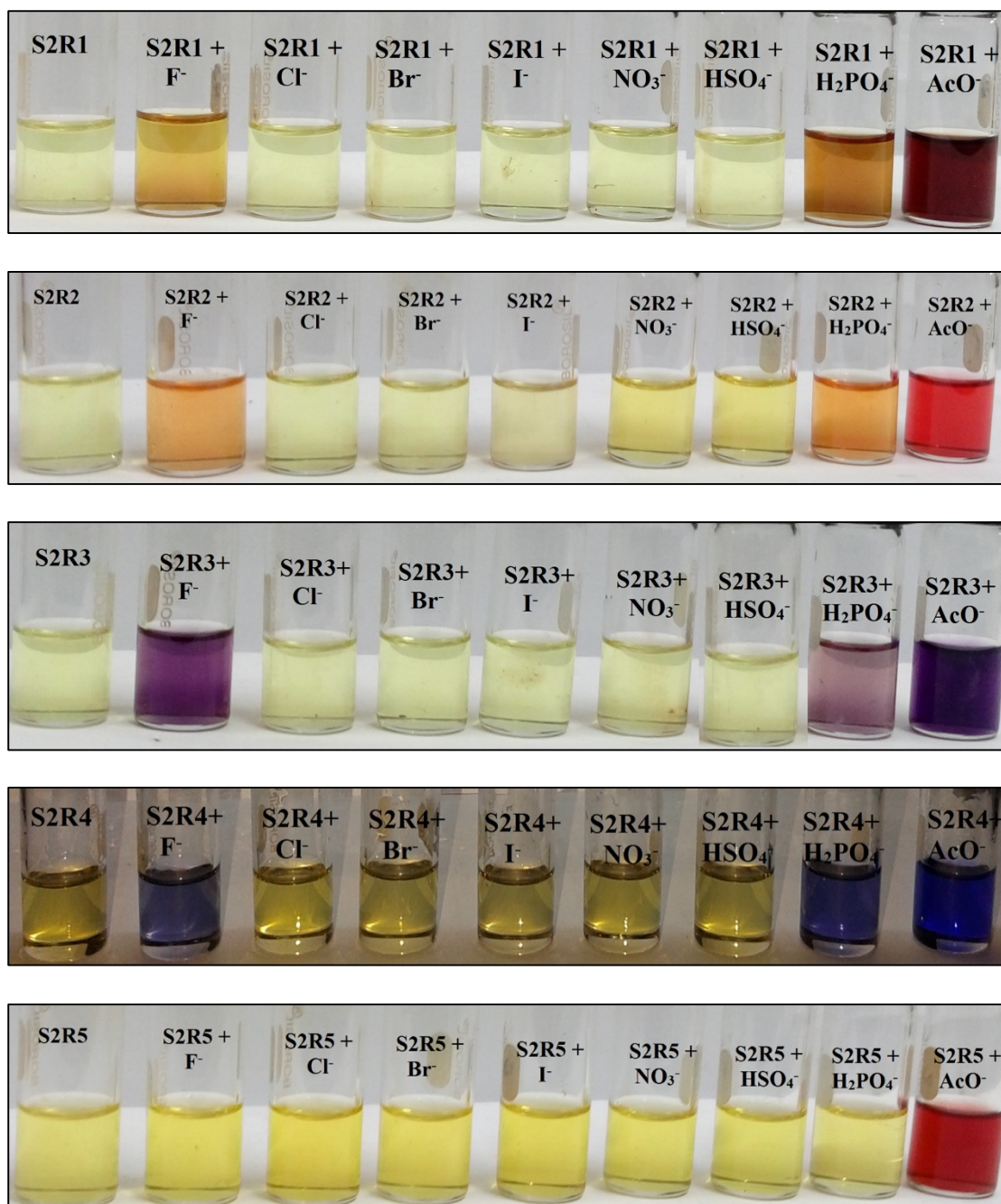


Fig. 4.12 Colour change of the receptors **S2R1** to **S2R5** with the addition of 1 equiv. of TBA salts of anions

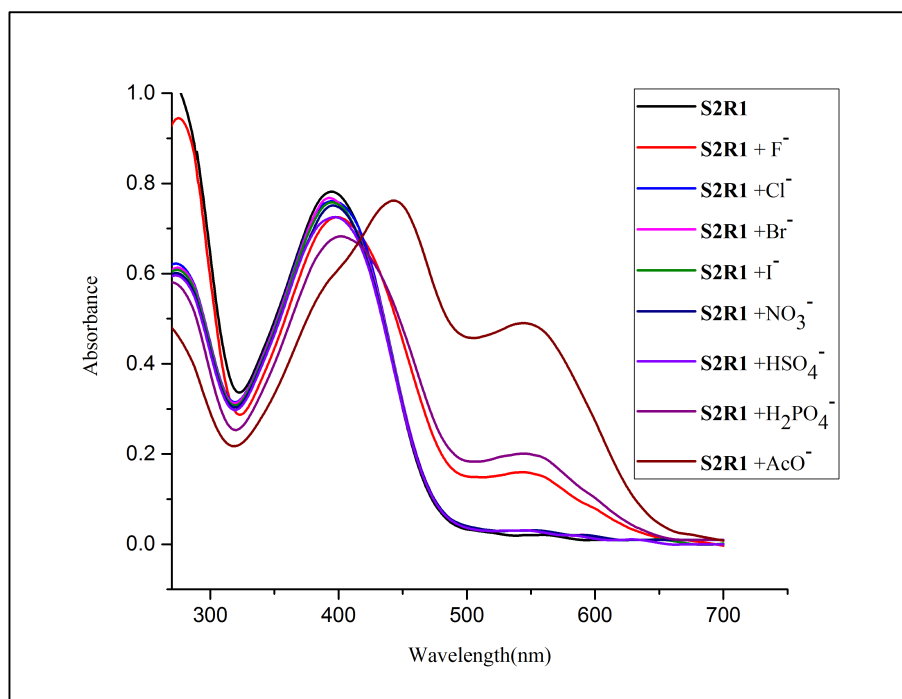


Fig. 4.13 UV-Vis spectra of receptor **S2R1** (10^{-4} M in DMSO) with the addition of tertbutylammonium salts of various anions (10^{-2} M in DMSO)

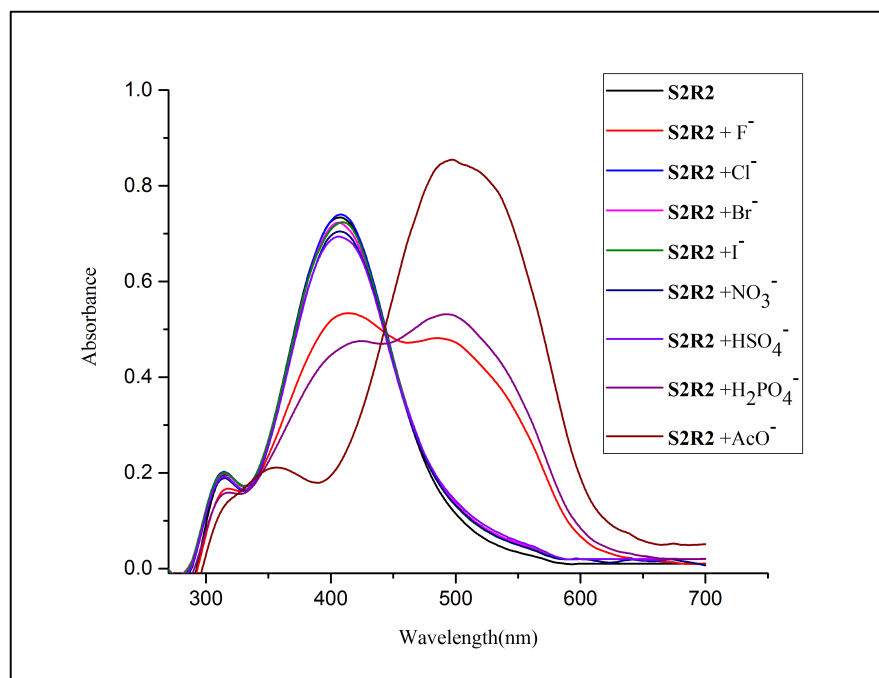


Fig. 4.14 UV-Vis spectra of receptor **S2R2** (10^{-4} M in DMSO) with the addition of tertbutylammonium salts of various anions (10^{-2} M in DMSO)

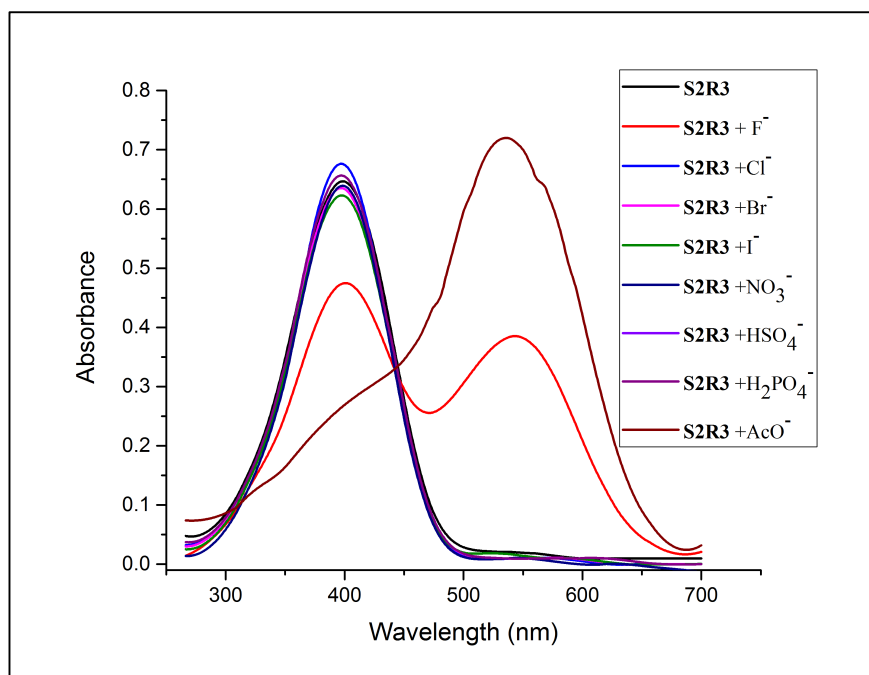


Fig. 4.15 UV-Vis spectra of receptor **S2R3** (10^{-4} M in DMSO) with the addition of tertbutylammonium salts of various anions (10^{-2} M in DMSO)

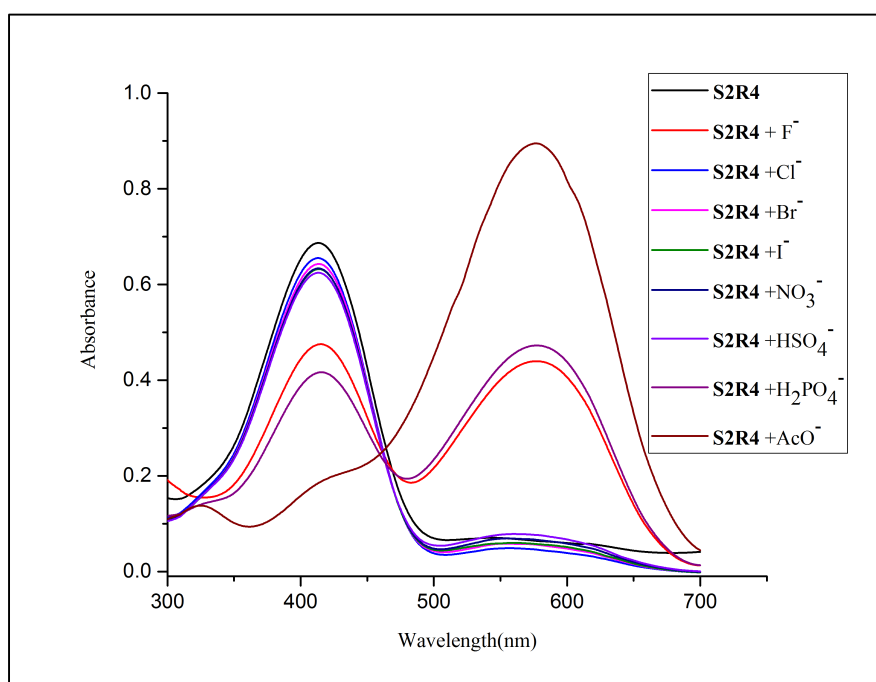


Fig. 4.16 UV-Vis spectra of receptor **S2R4** (10^{-4} M in DMSO) with the addition of tertbutylammonium salts of various anions (10^{-2} M in DMSO)

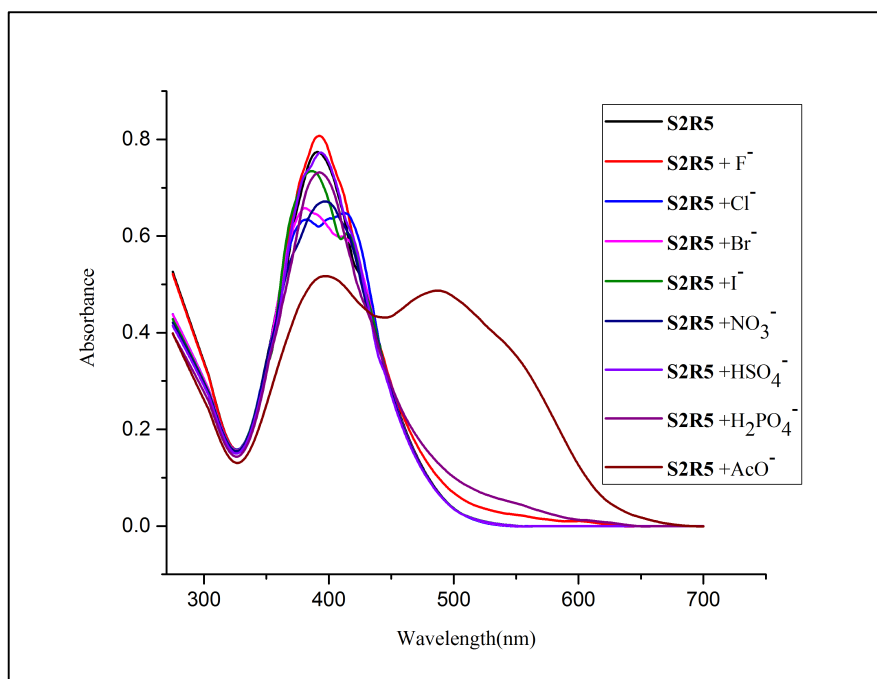


Fig. 4.17 UV-Vis spectra of receptor **S2R5** (10^{-4} M in DMSO) with the addition of tertabutylammonium salts of various anions (10^{-2} M in DMSO)

4.3.2 UV-Vis titration studies

To obtain further insight into the interaction of **S2R1** to **S2R5** with TBA salt of AcO^- ion, UV-Vis spectrophotometric titration has been performed. Fig. 4.18 shows the spectroscopic changes observed with the incremental addition of 0.1 equiv. of AcO^- ion to **S2R1**. It was interesting to note the two different processes during the progression of titration. Until the addition of 0.7 equiv. of AcO^- ion, the absorption band at 395 nm decreased in its intensity with a significant red shift differing by 150 units. With the addition of higher equiv. of AcO^- ions, there was red shift of the original absorption band from 395 nm to 454 nm with the appearance of new band at 545 nm. The saturation point was reached with the addition of 2 equiv. of AcO^- ion with complete diminution of the band at 395 nm. The first process corresponds to the strong hydrogen bond interaction between AcO^- -- H-O and H-N in the ground state. The second process provides an evidence of the deprotonation of the -OH moiety due to the interaction of hydrogen bond donor group -OH and AcO^- ion through intermolecular proton transfer process (Kaloo and Sankar 2013). Proton abstraction from the -OH moiety induces a negative charge on the oxygen atom of the hydroxyl

functionality of receptor **S2R1** which further resulted in the enhancement of the intermolecular charge transfer transition. Presence of $-\text{NO}_2$ chromophore at para position with respect to the OH group led to a colorimetric response from pale yellow to blood red visible to the naked eye. The presence of clear isobestic point at 422 nm denotes the formation of **S2R1**-- AcO^- ion complex. From the B-H plot, linearity obtained with first power of concentration of AcO^- ion confirmed the binding ratio to be 1:1 for **S2R1**-- AcO^- ion complex as depicted in Fig. 4.19 which clearly indicates the single step deprotonation process brought about by an AcO^- ion.

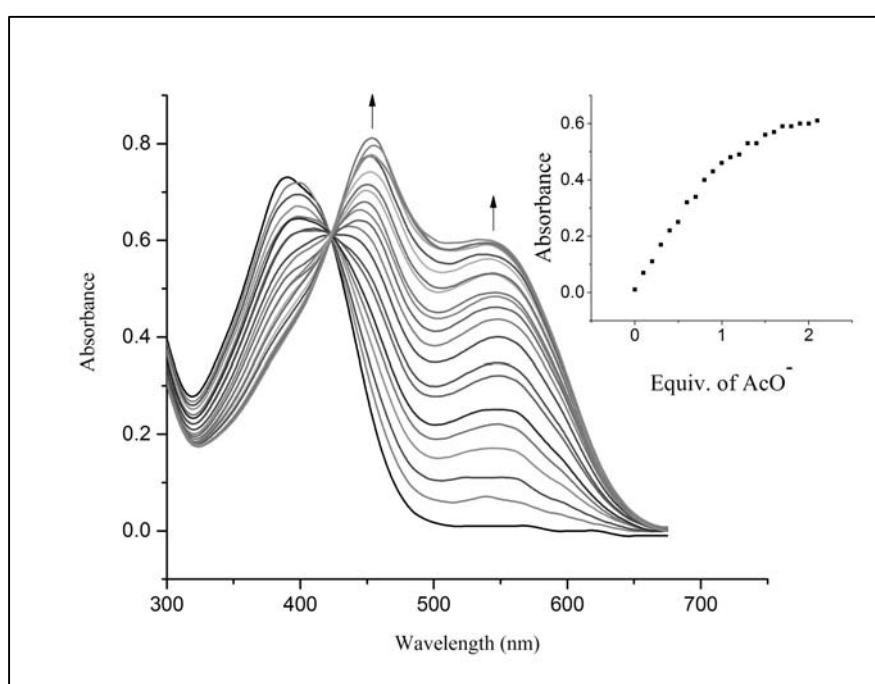


Fig. 4.18 UV-Vis titration spectra of receptor **S2R1** (10^{-4} M in DMSO) with the incremental addition of TBAAcO (10^{-2} M in DMSO). Inset plot representing the absorption isotherm at 545 nm

Titration studies performed with incremental addition of AcO^- ion to **S2R2** exhibits sharp changes in the absorption maxima accompanied by a red shift differing by 90 units and a clear isobestic point at 444 nm as displayed in Fig. 4.20. Presence of two $-\text{OH}$ and a single NH substituent are known to promote strong ground state hydrogen bond interactions with AcO^- ion. From the B-H plot, binding ratio was found to be 1:1 between **S2R2**-- AcO^- ion complex proving a single step deprotonation mechanism (Fig. 4.21).

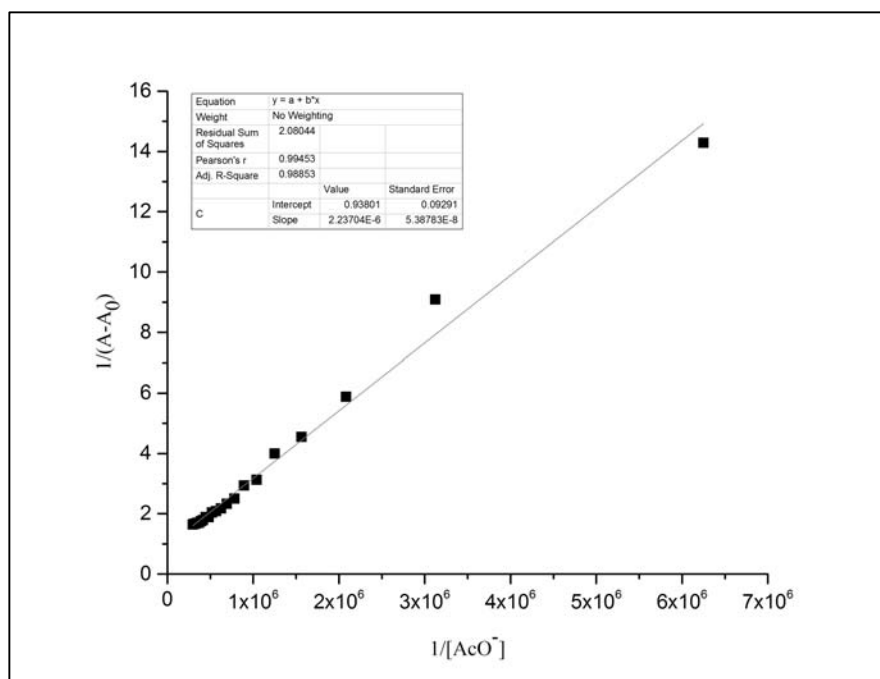


Fig. 4.19 B-H plot representing 1:1 binding ratio of **S2R1**-TBAAcO complex

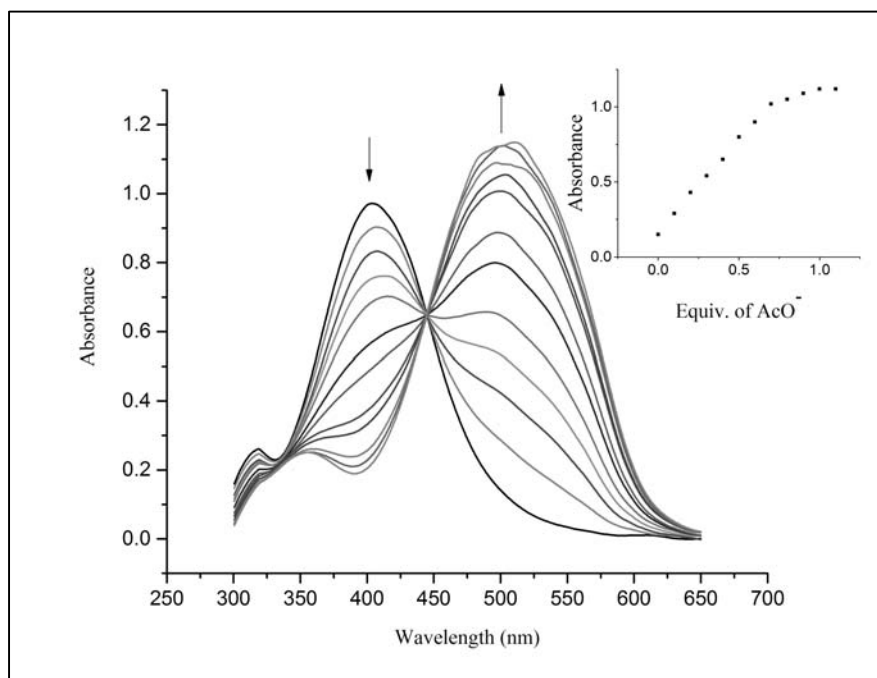


Fig. 4.20 UV-Vis titration spectra of receptor **S2R2** (10^{-4} M in DMSO) with the incremental addition of TBAAcO (10^{-2} M in DMSO). Inset plot representing the absorption isotherm at 497 nm

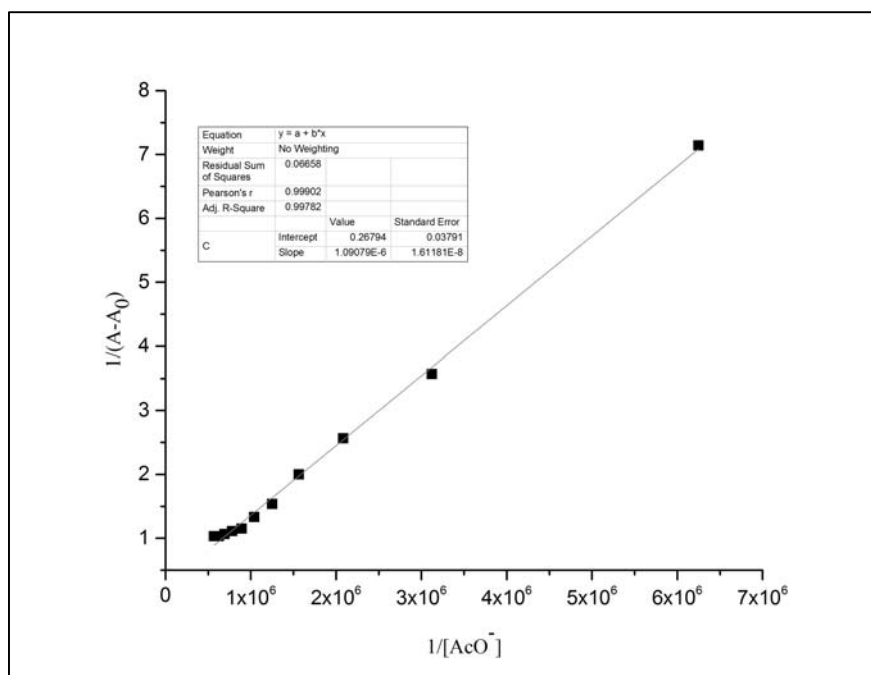


Fig. 4.21 B-H plot representing 1:1 binding ratio of **S2R2**-TBAAcO complex

S2R3 exhibited a substantial colorimetric response in the presence of AcO^- ion inducing a color change from pale yellow to purple. The presence of $-\text{NO}_2$ group at ortho position of the phenyl ring triggered strong changes in the anion detection mechanism. The position of chromophore was found to have a direct influence on the chromogenic response upon anion binding. Correspondingly, there was considerable shift in the absorption maxima differing by 157 units from the original absorption band (Fig. 4.22). The absence of $-\text{OH}$ group was balanced by introduction of $-\text{NO}_2$ substituent which enhanced the hydrogen bonding capability of the $-\text{NH}$ group by rendering it acidic in nature. This is justified by the 1:1 binding ratio between **S2R3**---
- AcO^- ion obtained from B-H plot (Fig. 4.23). Binding of AcO^- ion is a one-step process involving an initial strong hydrogen bond interaction between AcO^- --- HN group followed by deprotonation mechanism.

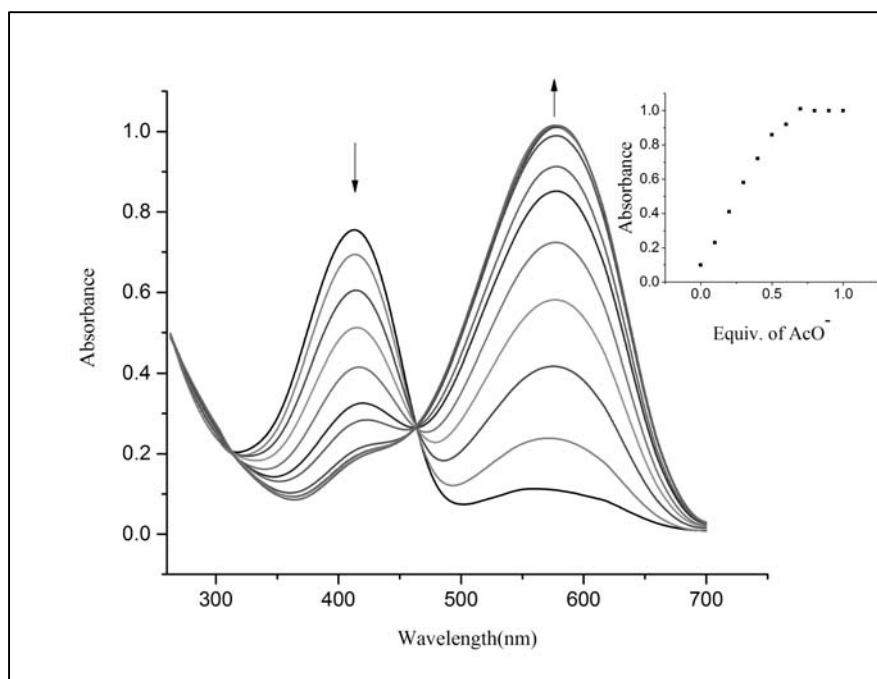


Fig. 4.22 UV-Vis titration spectra of receptor **S2R3** (10^{-4} M in DMSO) with the incremental addition of TBAAcO (10^{-2} M in DMSO). Inset plot representing the absorption isotherm at 570 nm

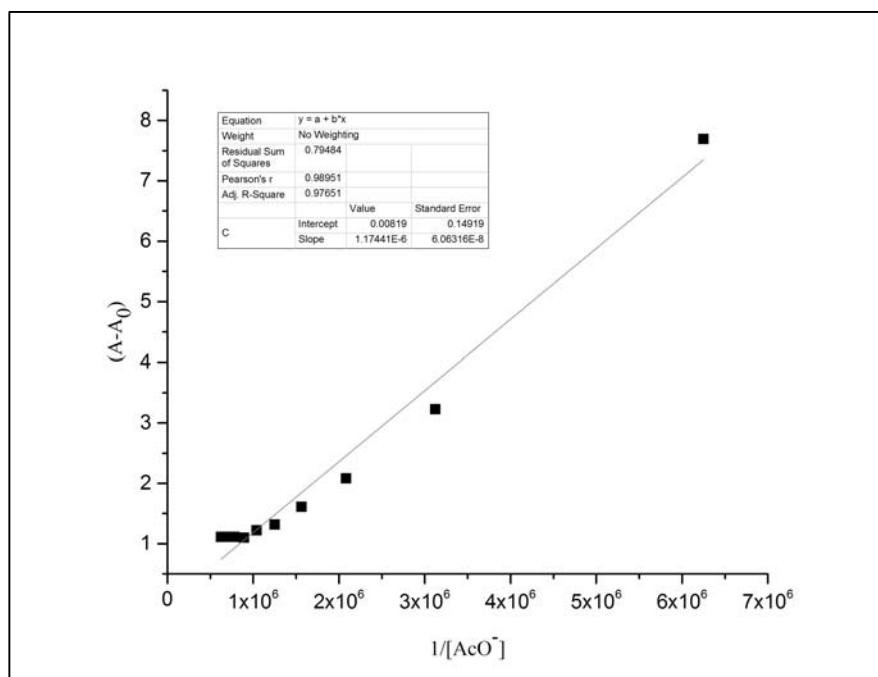


Fig. 4.23 B-H plot representing 1:1 binding ratio of **S2R3**-TBAAcO complex

Titration studies performed upon gradual addition of standard TBAAcO (1×10^{-2} M in dry DMSO) to solution of **S2R4** resulted in new absorption band centered at 572

nm with a clear isobestic point at 462 nm as shown in Fig. 4.24. The probable mechanism would be the anion- π charge transfer interactions existing between AcO^- ion and π -acidic receptor moiety. Diminution of the peak at 413 nm is a clear indication of deprotonation of the NH proton leading to a drastic color change. The 1:1 binding ratio between receptor **S2R4** and AcO^- ion has been analysed with B-H plot as represented in Fig. 4.24. Titration performed with incremental addition of TBAOH resulted in the similar titration profile confirming the deprotonation process as shown in Fig. 4.26. Similarly, incremental addition of 0.1 eq. of H_2PO_4^- and F^- ions in dry DMSO resulted in bathochromic shift differing by units of 159 nm and 165 nm in comparison with absorption band of the free receptor **S2R4**. Isobestic points centered at 462 and 464 nm each for H_2PO_4^- and F^- ions represent the complex formation as displayed in Fig. 4.27 and Fig. 4.29. Resultant 1:1 binding ratio obtained with H_2PO_4^- and F^- ions indicate the deprotonation of receptor **S2R4** in dry DMSO as represented in Fig. 4.28 and Fig. 4.30.

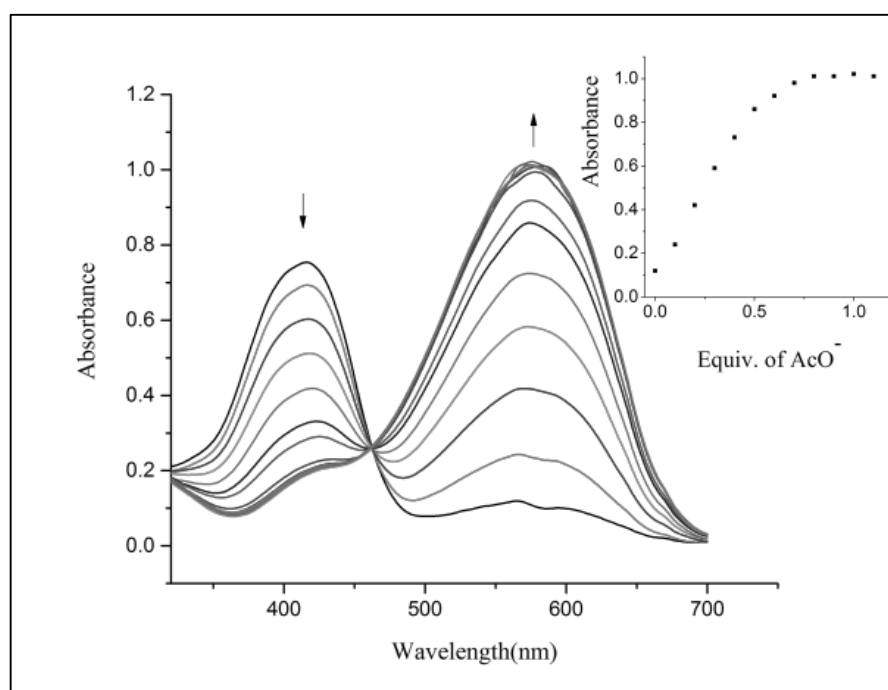


Fig. 4.24 UV-Vis titration spectra of **S2R4** (1×10^{-4} M in dry DMSO) with the incremental addition of standard solution of TBAAcO (1×10^{-2} M in dry DMSO). Inset showing the binding isotherm at 572 nm

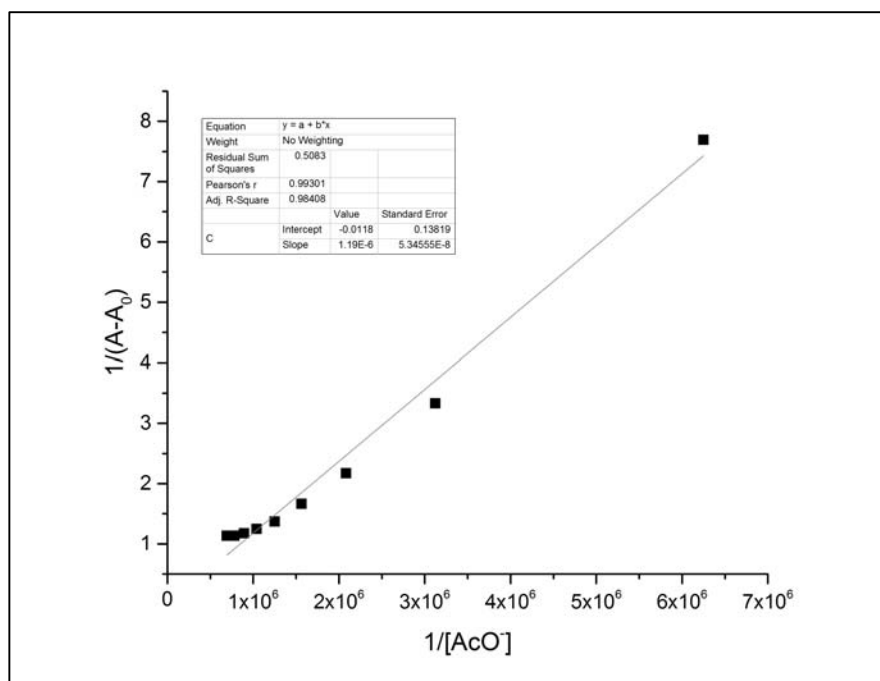


Fig. 4.25 B-H plot of receptor **S2R4**- TBAcO complex at a selected wavelength of 572 nm

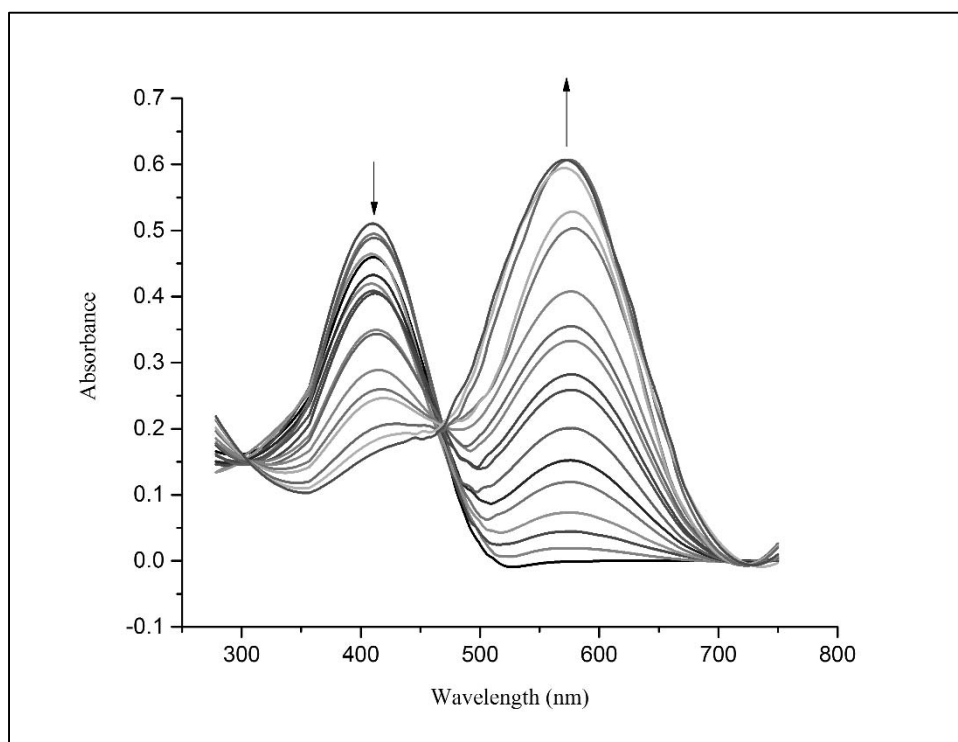


Fig. 4.26 UV-Vis titration spectra of **S2R4** (1×10^{-4} M, DMSO) with the incremental addition of standard solution of TBAOH (1×10^{-2} M in DMSO)

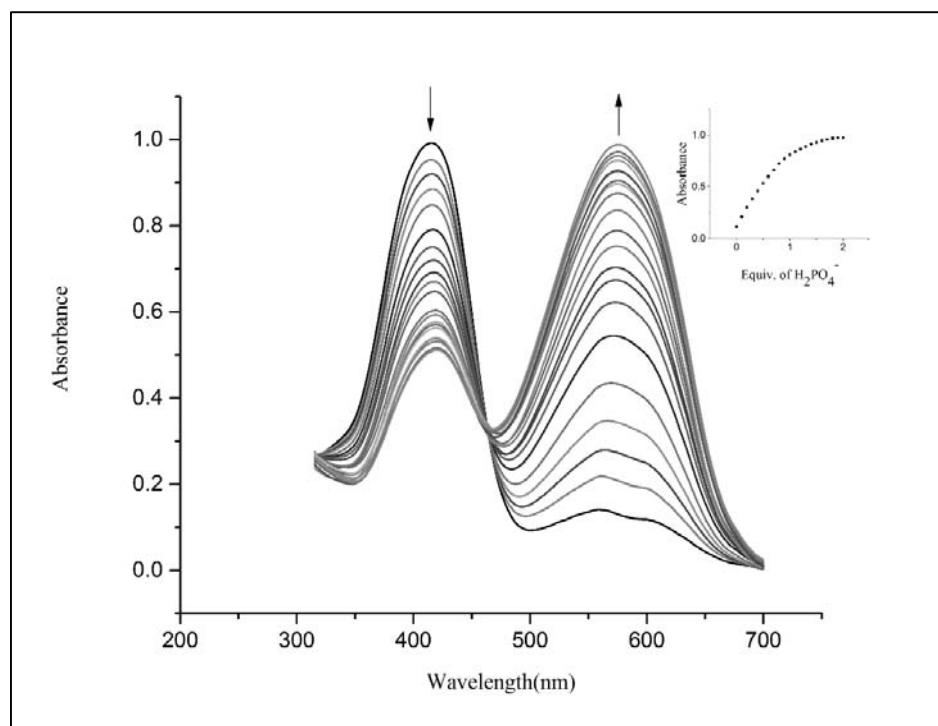


Fig. 4.27 UV-Vis titration spectra of **S2R4** (1×10^{-4} M in dry DMSO) with the incremental addition of standard solution of **TBAH₂PO₄** (1×10^{-2} M in dry DMSO). Inset showing the binding isotherm at 572 nm

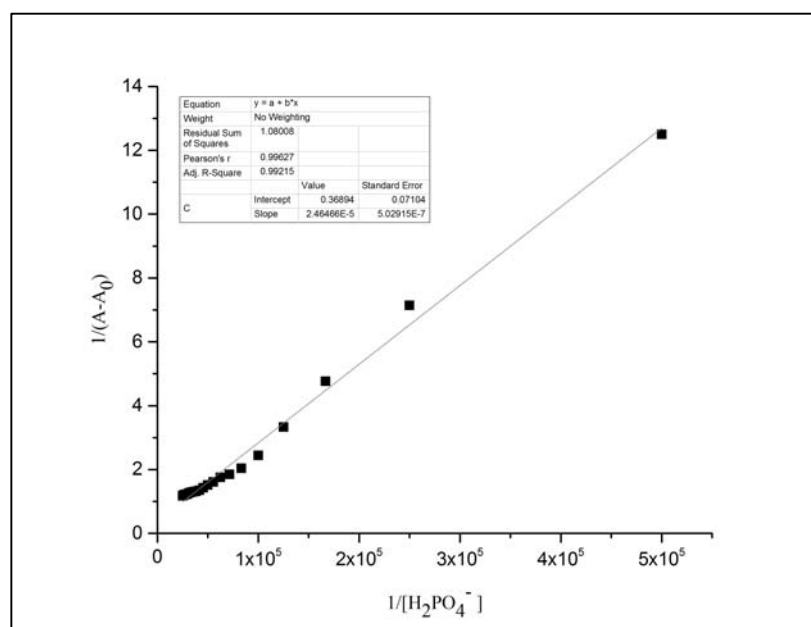


Fig. 4.28 B-H plot of receptor **S2R4**- **TBAH₂PO₄** complex at a selected wavelength of 572 nm

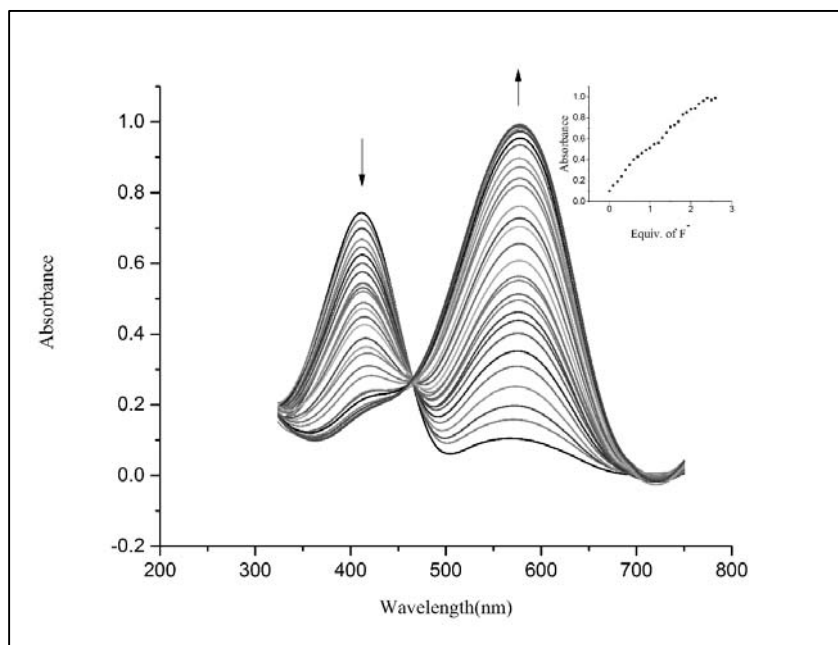


Fig. 4.29: UV-Vis titration spectra of **S2R4** (1×10^{-4} M in dry DMSO) with the incremental addition of standard solution of TBAF (1×10^{-2} M in dry DMSO). Inset showing the binding isotherm at 578 nm

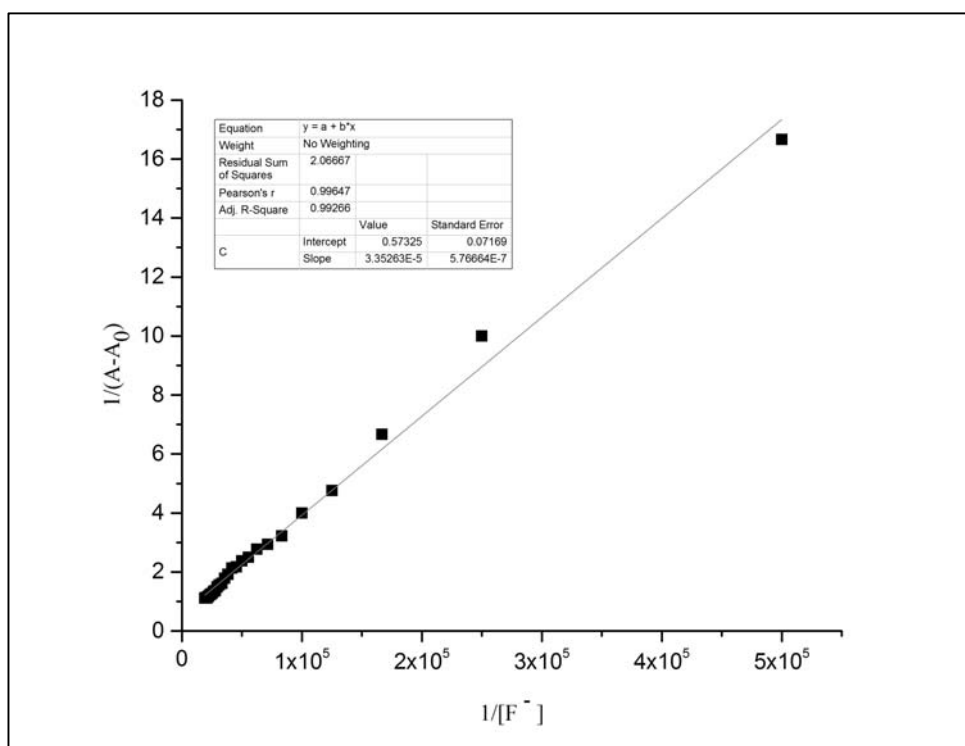


Fig. 4.30 B-H plot of receptor **S2R4**- TBAF complex at a selected wavelength of 578 nm

Receptor **S2R5**, devoid of substituent groups exhibited colorimetric response from pale yellow to orange red in the presence of AcO^- ion. The nitro substituent on the hydrazine is potent enough to introduce acidity on the NH group rendering it active for proton abstraction by AcO^- ion. Yet, the shift in absorption maxima differing by 96 units is very minute in comparison with other receptors used in the present study. The occurrence of sharp isobestic point at 435 nm indicates the complex formation process (Fig. 4.31). Binding ratio was found to be 1:1 between receptor- AcO^- ion indicating a one-step deprotonation process (Fig. 4.32).

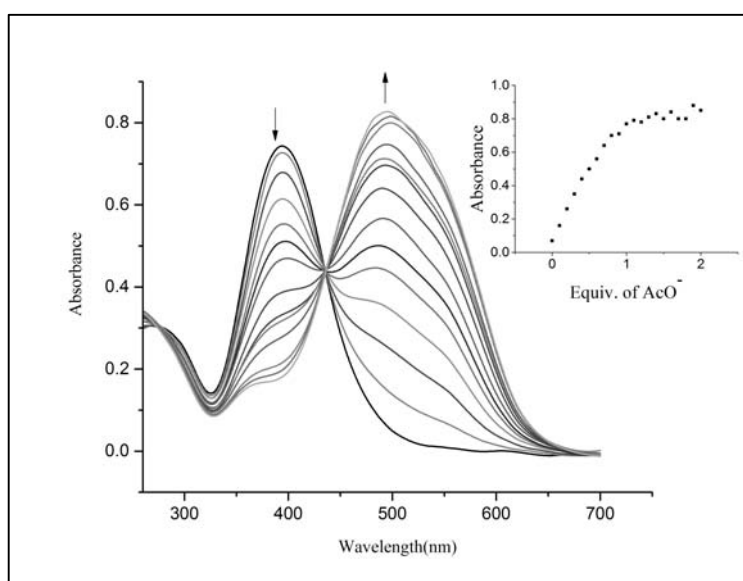


Fig. 4.31 UV-Vis titration spectra of receptor **S2R5** (10^{-4} M in DMSO) with the incremental addition of TBAcO (10^{-2} M in DMSO). Inset plot representing the absorption isotherm at 495 nm

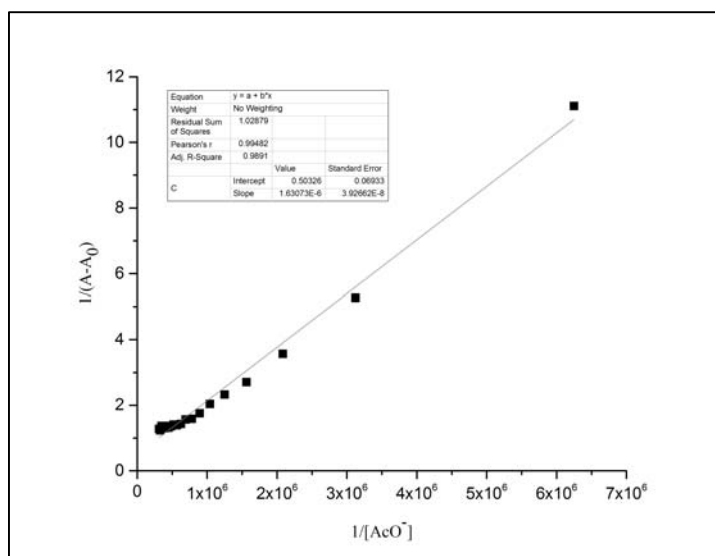


Fig. 4.32 B-H plot representing 1:1 binding ratio of **S2R5**-TBAAcO complex

Overall, the positional substitution effect of $-\text{NO}_2$ substituent is found to have a prime role in detection of anion. The presence of $-\text{OH}$ group and NO_2 substituent on the receptor cumulatively effect the anion binding probability. Sodium salts of fluoride and acetate have been a major constituent of commercially available toothpaste, mouthwash and vinegar respectively. These have encroached into the household usage in the form of food, medicine and cosmetics. Beyond an optimum amount, anions can lead to health issues. Detection of sodium salts of anions in aqueous media is gaining more interest with a view to investigate the solvent interferences in the binding process. In this regard, the anion binding studies has been performed in aqueous media, 9:1, v/v DMSO: H_2O with addition of sodium salt of AcO^- ion and F^- ion. UV-Vis titration studies have been performed with incremental addition of NaAcO and NaF to solution of receptors of concentration 1×10^{-4} M (9:1, DMSO: H_2O , v/v). **S2R1**, **S2R2**, **S2R3**, **S2R4** and **S2R5** showed a significant redshift which was comparable to the titration studies performed in 100% DMSO solvent. Titration profile of receptors **S2R1**, **S2R2**, **S2R3**, **S2R4** and **S2R5** with addition of active anions is shown in Fig. 4.33, Fig. 4.35, Fig. 4.37, Fig. 4.39 and Fig. 4.41 respectively. Appearance of clear isobestic point indicate the complex formation between receptor and anion surpassing the solvent interferences in the binding process. B-H plot represents 1:1 binding ratio between target anions and receptor complex. B-H plot of **S2R1**- F^- , **S2R2**- F^- , **S2R3**- AcO^- , **S2R4**- AcO^- and **S2R5** is

shown in Fig. 4.34, Fig. 4.36, Fig. 4.38, Fig. 4.40 and Fig. 4.42 respectively. **S2R4** showed remarkable colorimetric response with the addition of NaF as shown in Fig. 4.43. The corresponding B-H plot for **S2R4**—F⁻ complex indicated the binding ratio of 1:1 as represented in Fig. 4.44.

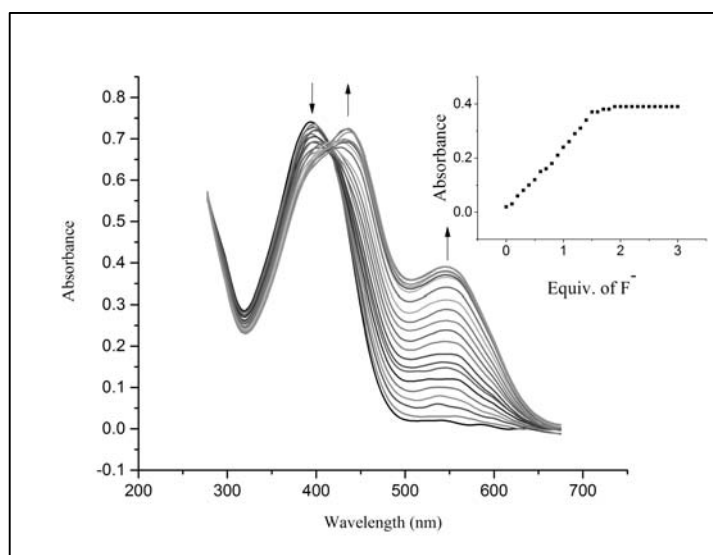


Fig. 4.33 UV-Vis titration spectra of receptor **S2R1** (10^{-4} M in 9:1, v/v DMSO: H₂O) with the incremental addition of NaF (10^{-2} M in distilled H₂O). Inset plot representing the absorption isotherm at 544 nm

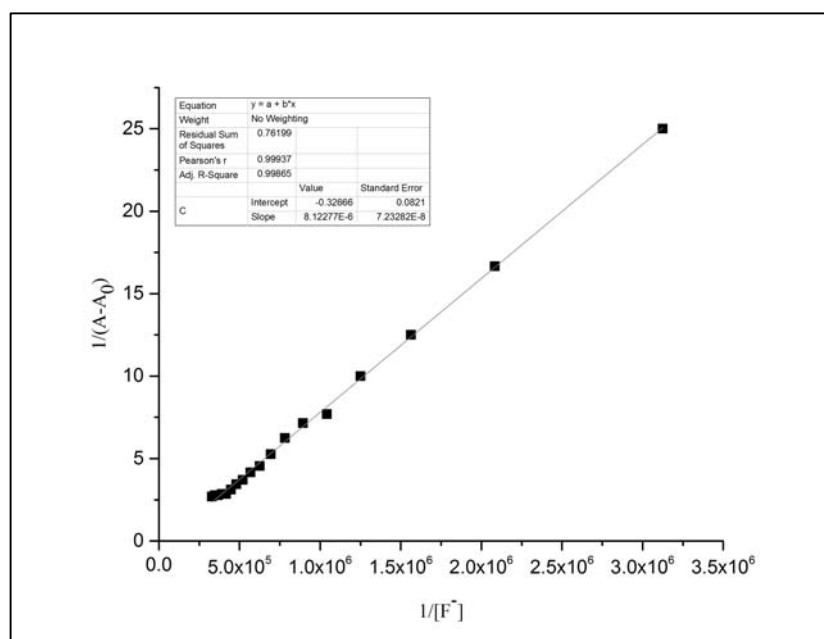


Fig. 4.34 B-H plot of receptor **S2R1**- NaF complex at a selected wavelength of 544 nm

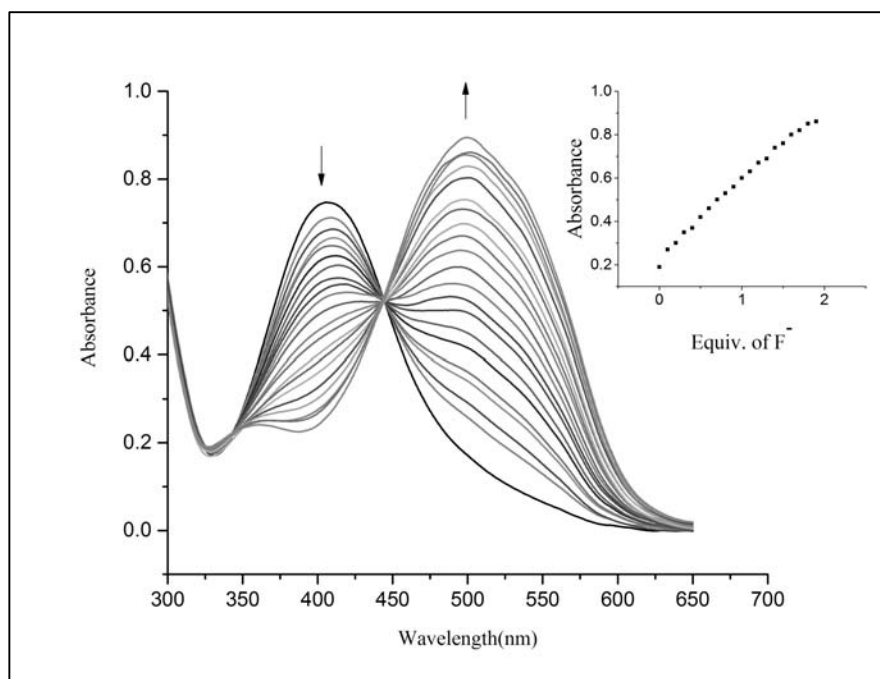


Fig. 4.35 UV-Vis titration spectra of receptor **S2R2** (10^{-4} M in DMSO) with the incremental addition of NaF (10^{-2} M in distilled H₂O). Inset plot representing the absorption isotherm at 500 nm

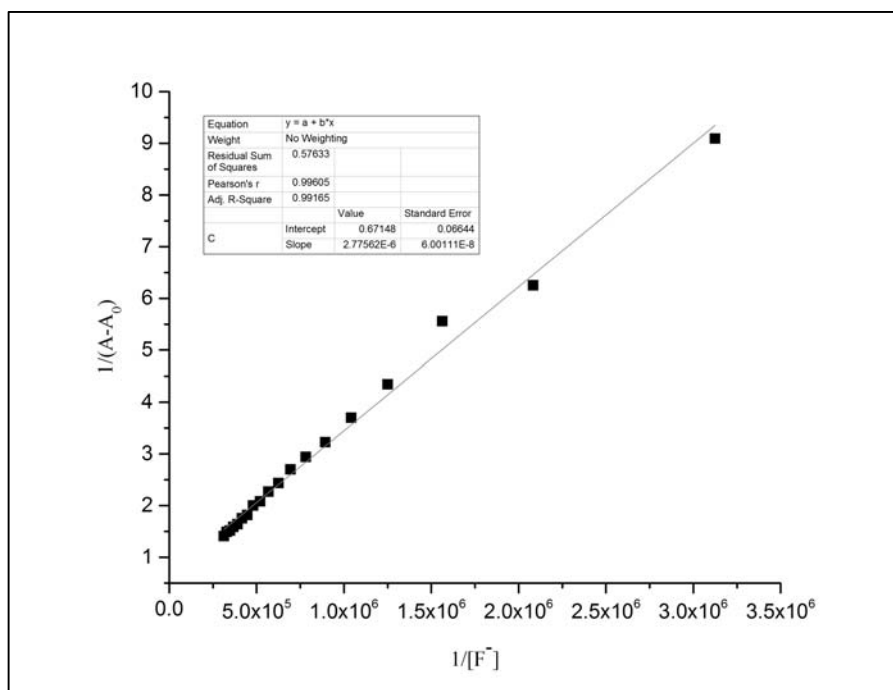


Fig. 4.36 B-H plot of receptor **S2R2**- NaF complex at a selected wavelength of 500 nm

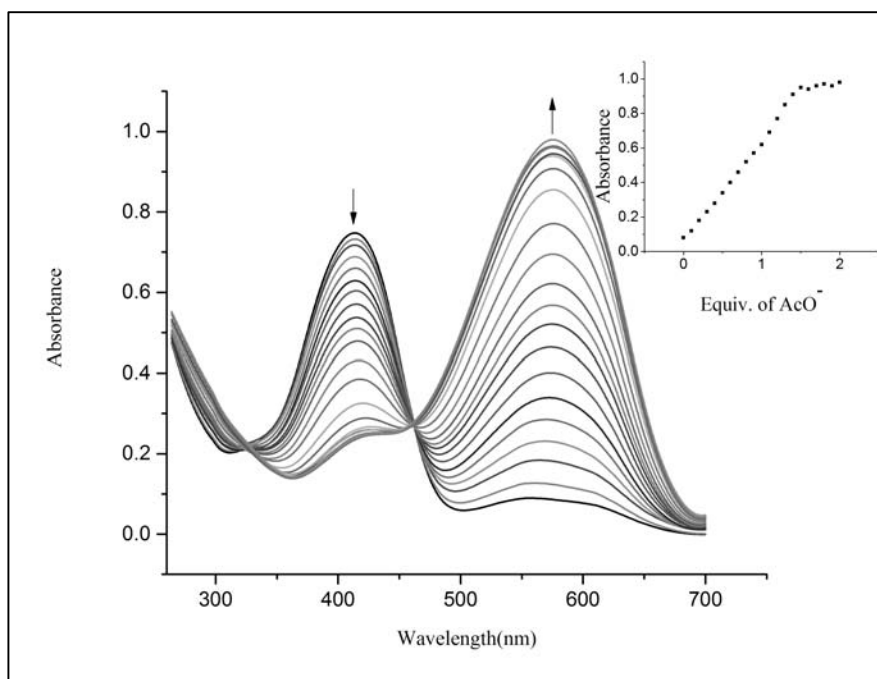


Fig. 4.37 UV-Vis titration spectra of receptor **S2R3** (10^{-4} M in DMSO) with the incremental addition of NaAcO (10^{-2} M in distilled H_2O). Inset plot representing the absorption isotherm at 576 nm

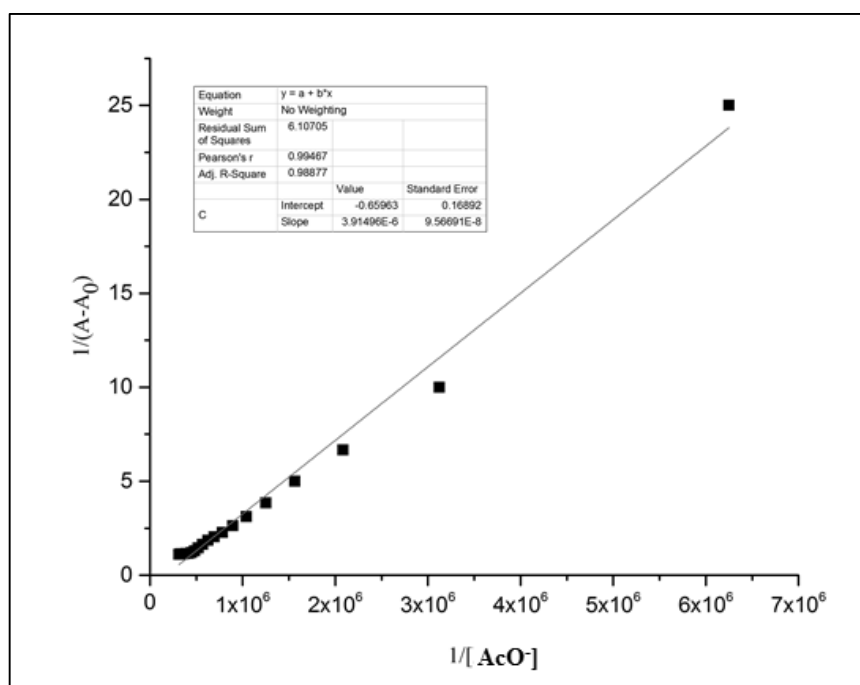


Fig. 4.38 B-H plot of receptor **S2R3**- NaAcO complex at a selected wavelength of 576 nm

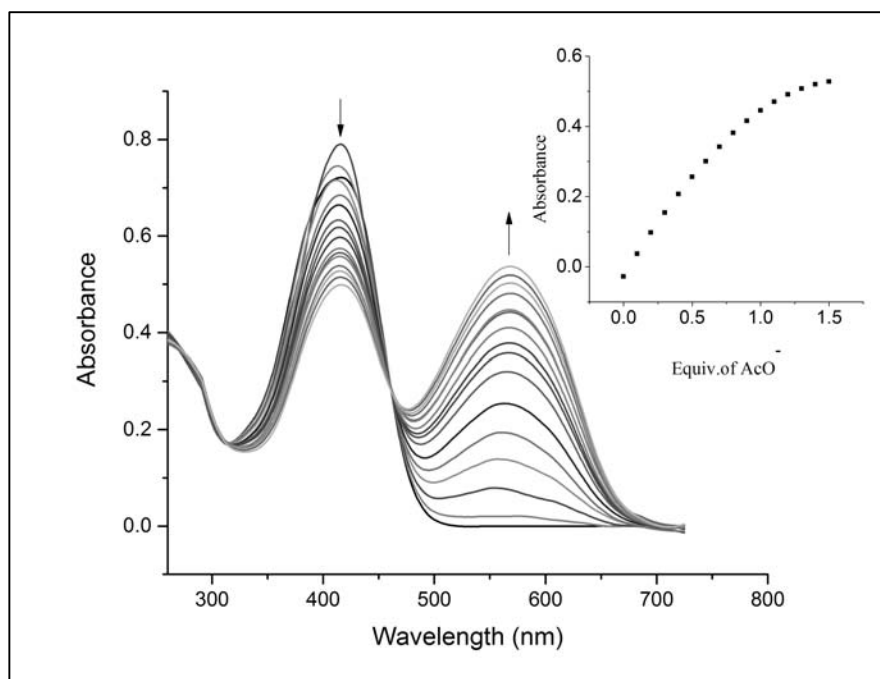


Fig. 4.39 UV-Vis titration spectra of **S2R4** (1×10^{-4} M, 9:1, v/v DMSO/H₂O) with the incremental addition of standard solution of NaAcO (1×10^{-2} M in distilled water). Inset showing binding isotherm at 574 nm

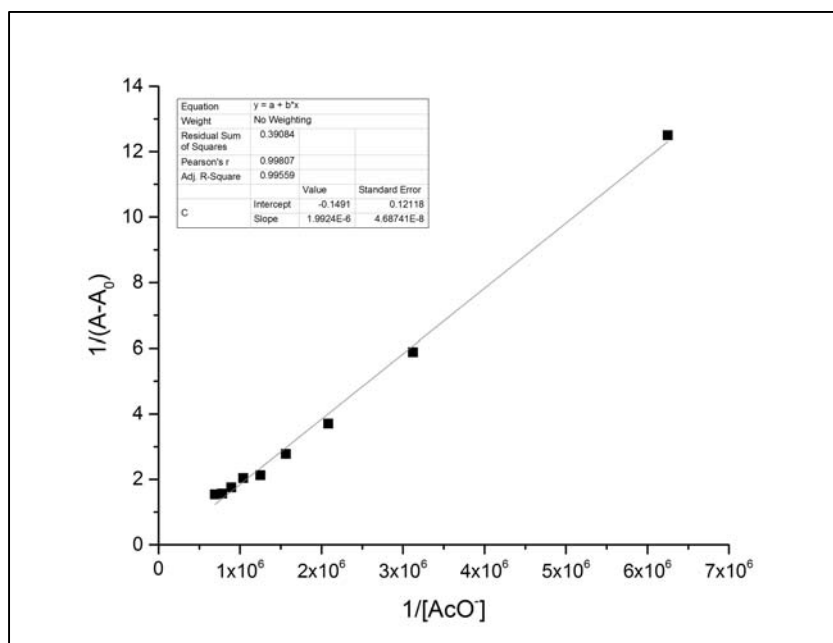


Fig. 4.40 B-H plot of receptor **S2R4**- NaAcO complex at a selected wavelength of 574 nm

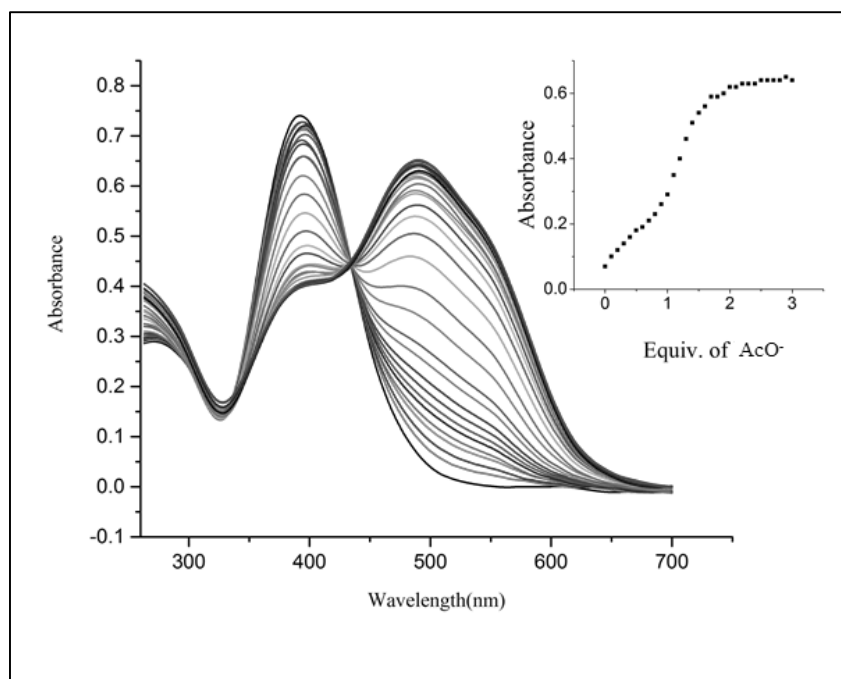


Fig. 4.41 UV-Vis titration spectra of receptor **S2R5** (10^{-4} M in DMSO) with the incremental addition of NaAcO (10^{-2} M in distilled H_2O). Inset plot representing the absorption isotherm at 489 nm

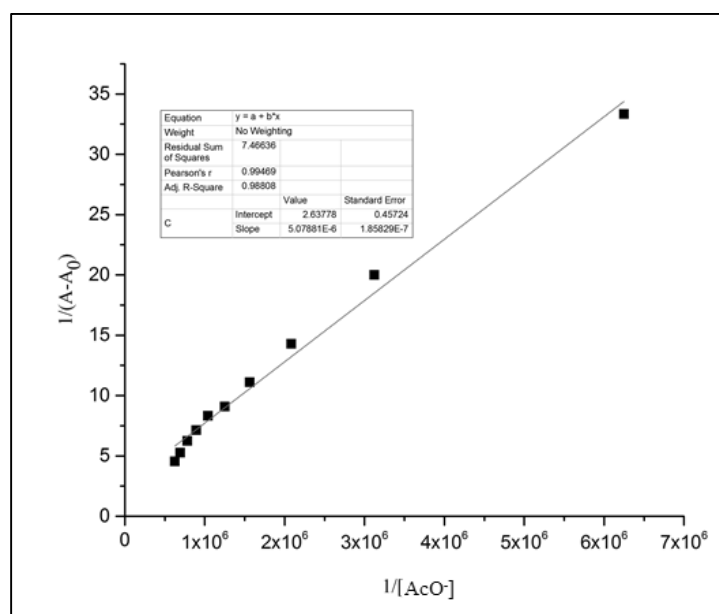


Fig. 4.42 B-H plot of receptor **S2R5**- NaAcO complex at a selected wavelength of 489 nm

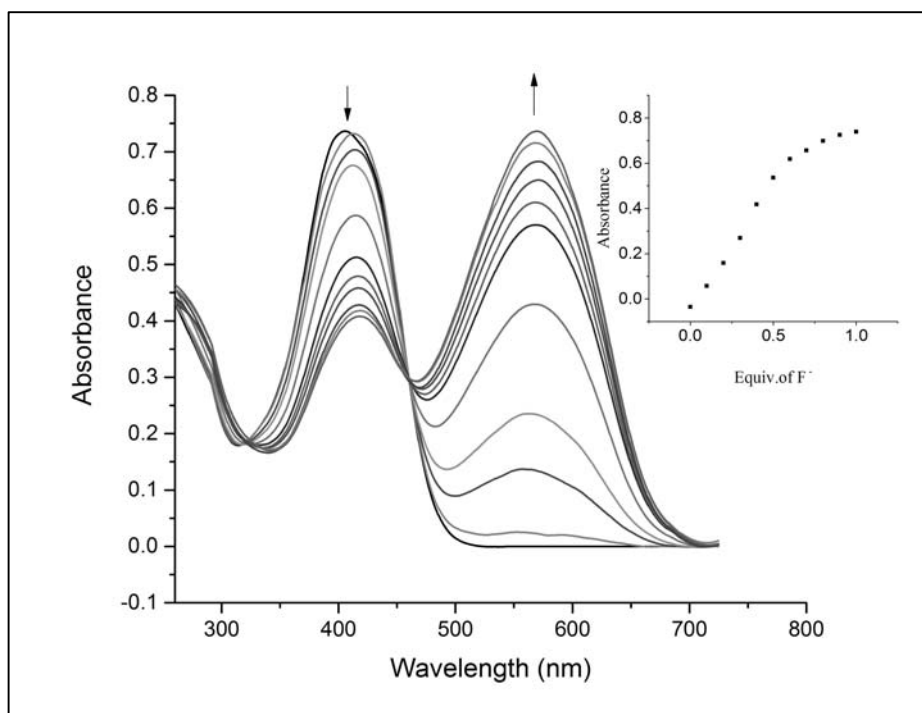


Fig. 4.43 UV-Vis titration spectra of **S2R4** (1×10^{-4} M, 9:1, v/v DMSO/H₂O) with the incremental addition of standard solution of NaF (1×10^{-2} M in distilled water). Inset showing binding isotherm at 575 nm

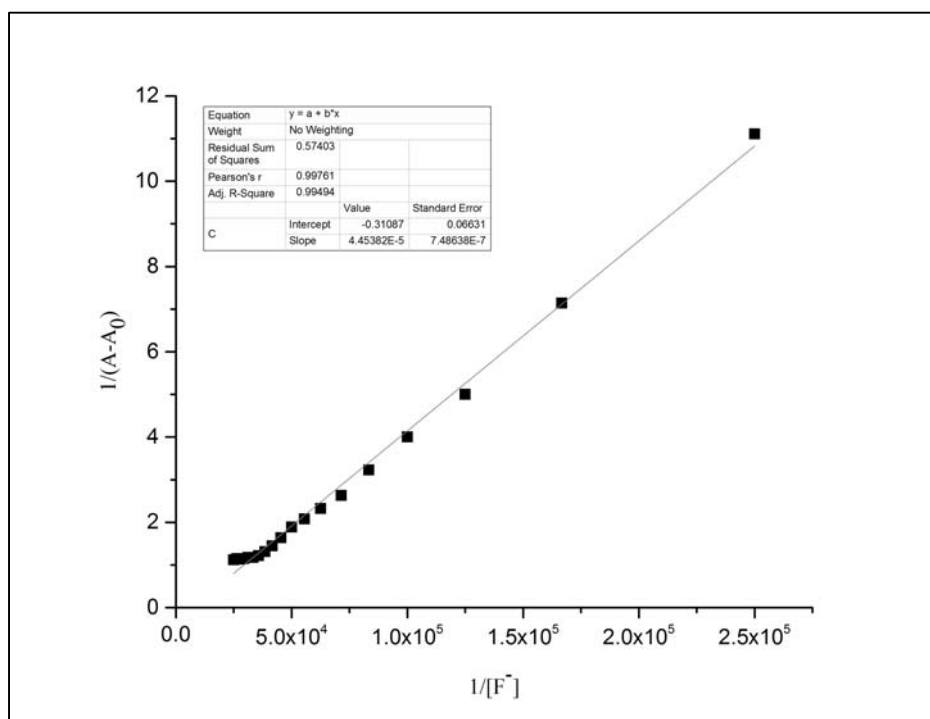


Fig. 4.44 B-H plot of receptor **S2R4** - NaF complex at a selected wavelength of 575 nm

4.3.3 Solvatochromism studies

The study was extended to investigate the solvent dependent charge transfer interactions in the presence of active anions. Addition of AcO^- ion to the receptor induced optical signalling from pale yellow to purple, deep blue, maroon, pale violet and pale brown in various aprotic polar solvents such as ACN, THF, acetone, DCM and dioxane respectively (Fig. 4.45). UV-Vis spectra recorded with addition of 1 eq. of TBAAcO to receptor in solvents of varying polarity resulted in new peak with significant bathochromic shift (Table 4.2). There was no any linear correlation observed between the solvent polarity and CT band due to the complex nature of solute solvent interactions dominated by the hydrogen bond accepting nature of the solvents. Among all the solvents, the shift in absorption maxima was greater in THF followed by DMSO, acetone and other aprotic solvents indicating the formation of a stabilized complex $[\text{S2R4} \cdots \text{AcO}^-]$. However, with 1, 4-dioxane there was minute shift in absorption maxima indicative of the minor interaction of the solvent molecules with complex $[\text{S2R4} \cdots \text{AcO}^-]$ (Dey and Das 2011)(Fig. 4.46). Mechanistically, the occurrence of $\pi\text{-}\pi^*$ transitions in the receptor unit resulted in gradual increase of the dipole moment upon excitation. Concurrently, presence of polar solvent directed the stabilization of excited state more than the ground state. This reduced the separation between the two energy states which ensued in red shift of the absorption band. Magnitude of red shift was further influenced by the extent of variation of dipole moment in the excitation process. The occurrence of smaller magnitude of dipole moment in the ground state than in the excited state, led to a substantial shift of absorption band (termed as positive solvatochromism or bathochromic shift) (B. Berryman and W. Johnson 2009; Berryman et al. 2008; Chifotides et al. 2010; Hadjmohammadi et al. 2008; Homocianu 2011; Marini et al. 2010; Saroj et al. 2011).

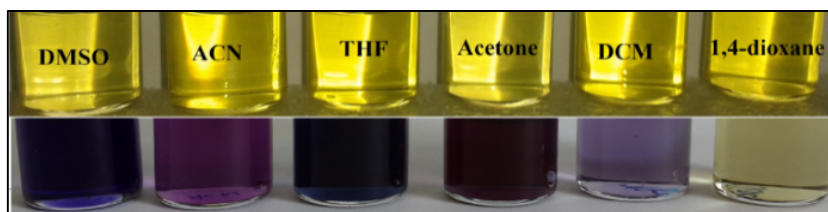


Fig. 4.45 Solvatochromic effect observed with the addition of 1 eq. of TBAAcO to receptor solution (10^{-4} M) in various polar aprotic solvents. Top row: 10^{-4} M in different solvents; Bottom row: **S2R4** + AcO^- ion

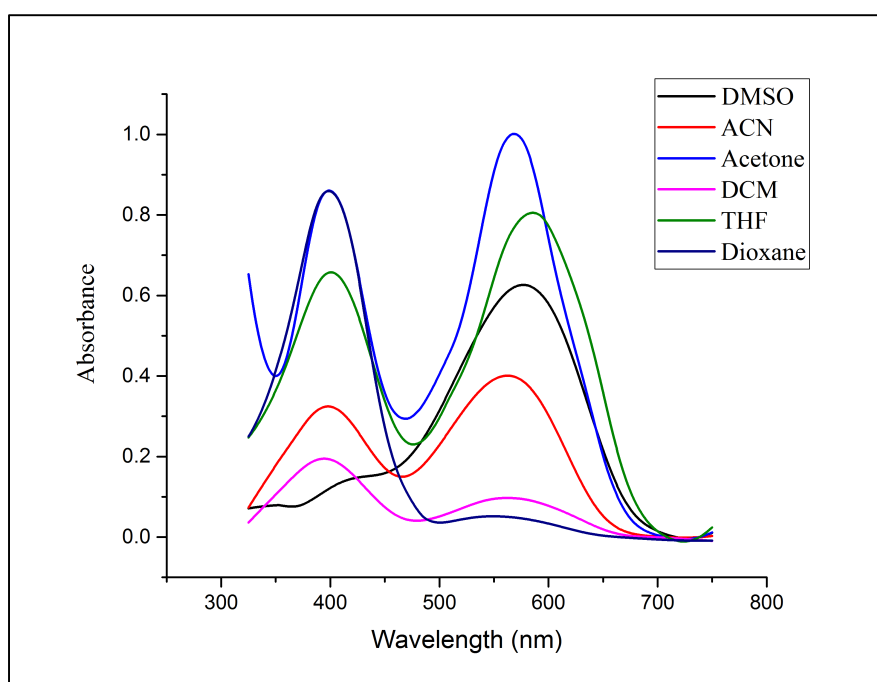


Fig. 4.46 UV-Vis absorption spectra of receptor **S2R4** (1×10^{-4} M) in various polar aprotic solvents with the addition of 1 eq. of TBAAcO (10^{-2} M in dry DMSO)

Table 4.2 Changes in absorption maxima of receptor **S2R4** in various solvents upon addition of 1 eq. of TBAAcO in dry DMSO

Solvent	Dielectric constant	λ_{max} (nm)
1,4-dioxane	2.21	553
Tetrahydrofuran	7.58	587
Dichloromethane	8.93	564
Acetone	20.70	569
Acetonitrile	37.50	563
Dimethylsulfoxide	46.80	576

It was interesting to find out the solvent dependent properties of receptor **S2R4** in the presence of H_2PO_4^- and F^- ions. THF solution of **S2R4** could colorimetrically distinguish F^- and AcO^- ion in conjunction with H_2PO_4^- and AcO^- ion. Color change from pale yellow to green with the addition of F^- and H_2PO_4^- ions and pale yellow to deep blue with addition of AcO^- ion clearly represents the selectivity of receptor **S2R4** for AcO^- ion (Fig. 4.47 and Fig. 4.48). The solvent dependent properties of the receptor **S2R4** promoted optical signalling with less vivid color change ranging from pale violet to brown with H_2PO_4^- and F^- ions. The color change was restricted to solvents such as DMSO, THF and acetone (Fig. 4.49 and Fig. 4.50).

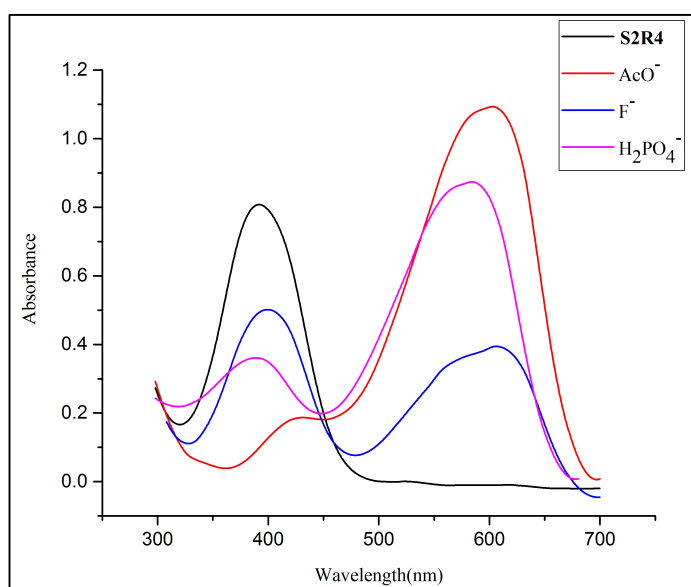


Fig. 4.47 UV-Vis spectra of **S2R4** (1×10^{-4} M in THF) upon addition of 1 eq. of TBA salts of F^- , AcO^- and H_2PO_4^- ions (1×10^{-2} M in dry DMSO)

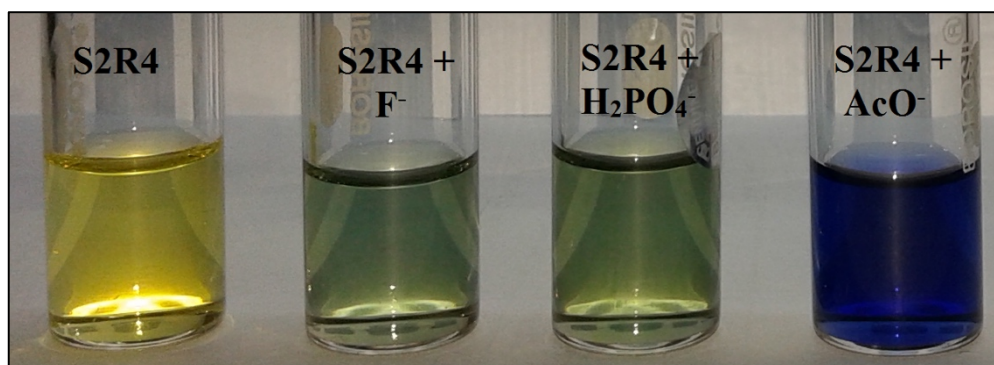


Fig. 4.48 Colour change of **S2R4** (1×10^{-4} M in THF) upon addition of 1 equiv. of F^- , AcO^- and H_2PO_4^- (1×10^{-2} M as TBA salts in dry DMSO)

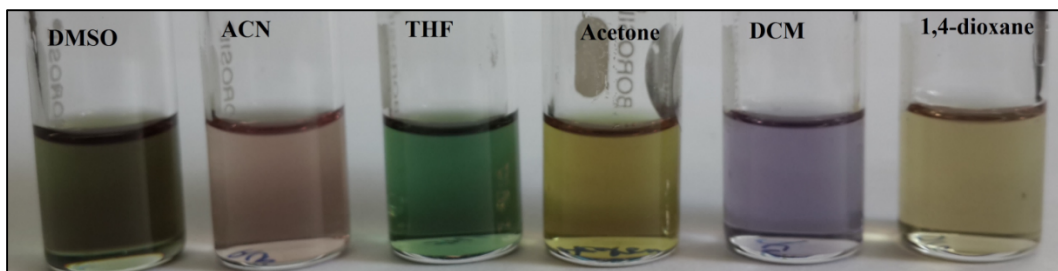


Fig. 4.49 Solvatochromic effect observed with the addition of 1 equiv. of TBAH₂PO₄ to receptor solution **S2R4** (1×10^{-4} M) in various polar aprotic solvents

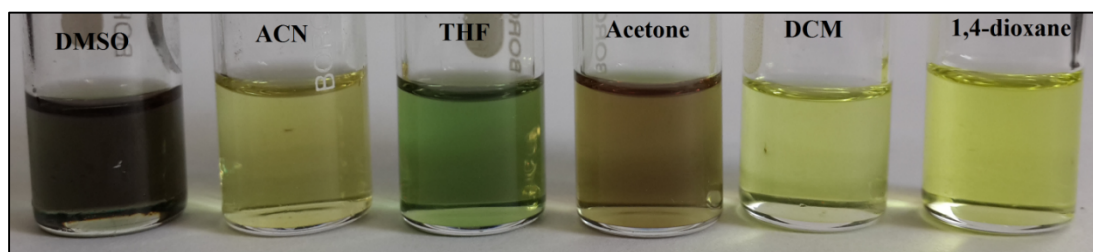


Fig. 4.50 Solvatochromic effect observed with the addition of 1 equiv. of TBAF to receptor solution **S2R4** (1×10^{-4} M) in various polar aprotic solvents

Addition of a drop of commercially available mouthwash and vinegar induced violet coloration of the receptors **S2R1**, **S2R2**, **S2R3** and **S2R4**. UV-Vis spectra of receptor **S2R4** in the presence of seawater, mouthwash and vinegar yielded similar charge transfer bands as observed in the case of standard AcO⁻ and F⁻ ions (Fig. 4.51 and Fig. 4.52). With an attempt to envisage the solidstate sensing property by grinding equimolar mixture of receptor with AcO⁻ ion, a color change from yellow to greenish black coloration has been observed (Fig. 4.53).

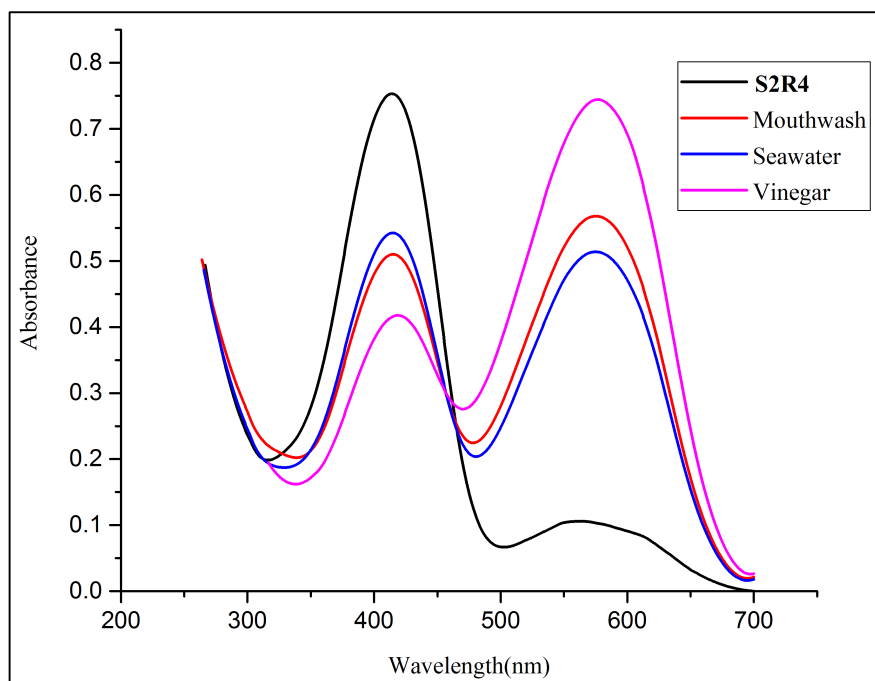


Fig. 4.51 UV-Vis spectra of **S2R4** (1×10^{-4} M in DMSO) upon addition of a drop of mouthwash, seawater and vinegar

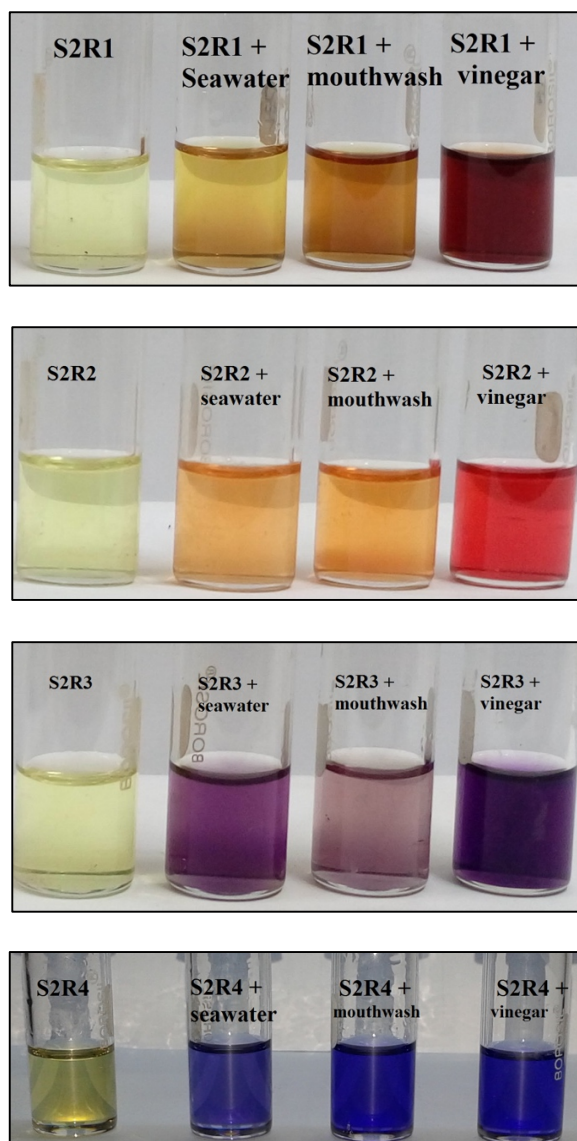


Fig. 4.52 Color change of **S2R1**, **S2R2**, **S2R3** and **S2R4** (1×10^{-4} M in DMSO) upon addition of a drop of mouthwash, seawater and vinegar



Fig. 4.53 Color change of receptor **S2R4** upon dry grinding of receptor **S2R4** with 1 equiv. of TBAAcO; **S2R4** alone (left), **S2R4**+ TBAAcO (right)

4.3.4 Electrochemical studies

The presence of $-\text{NO}_2$, $-\text{OH}$ and $-\text{NH}$ functionalities in the receptor drives in the need to investigate the impact of electrochemical reaction in the anion binding process. Considering the aforementioned fact, cyclic voltammetric studies have been performed with the incremental addition of AcO^- ion to the receptor solution. Receptor **S2R1** exhibited substantial decrease in the original oxidation peak and in the presence of AcO^- ion, there was appearance of new oxidation peak owing to the oxidation of $-\text{OH}$ and NH functionality (Fig. 4.54(a)). **S2R2** exhibited broad oxidation peak corresponding to the two OH functionalities and one NH group. There was no much shift observed in the presence of acetate ion owing to the strong hydrogen bond interaction of receptor with anion. The cyclic voltammogram is represented in Fig. 4.54(b).

In the presence of AcO^- ion, **S2R3** (Fig. 4.54(c)) and **S2R5** (Fig. 4.54(e)) exhibited substantial shift of original oxidation and reduction peak along with the appearance of new oxidation peak in the case of **S2R3** referring to the potent oxidation of the NH functionality leading to deprotonation. Cyclic voltammetric studies of receptor **S2R4** (5×10^{-5} M) performed with three electrode cell in acetonitrile medium and tetrabutylammonium perchlorate as supporting electrolyte reveal the anodic peak at 0.38 V due to the oxidation of $-\text{NH}$ group and cathodic peak at -0.41 V due to the reduction of the nitro group (Zen et al. 1999). Reduction of $-\text{NO}_2$ group is a kinetic driven process involving a slow step i.e, reduction of $-\text{NO}_2$ to $-\text{NHOH}$ and reduction of $-\text{NHOH}$ to nitroso group ($-\text{NO}$) as a fast step (Sharma et al. 2015). Addition of 1 eq. of AcO^- ion resulted in an increase in intensity of the original oxidation peak with slight shift to 0.51 V which is attributed to the abstraction of proton from $-\text{NH}$ group by AcO^- ion leaving behind N^- species. It depicts the complex electrochemical mechanism involving both electrochemical and chemical reactions. The diminution of original reduction peak and appearance of a new peak centered at -0.5 V indicates the direct involvement of redox active $-\text{NO}_2$ moiety in the detection mechanism (Fig. 4.54(d)).

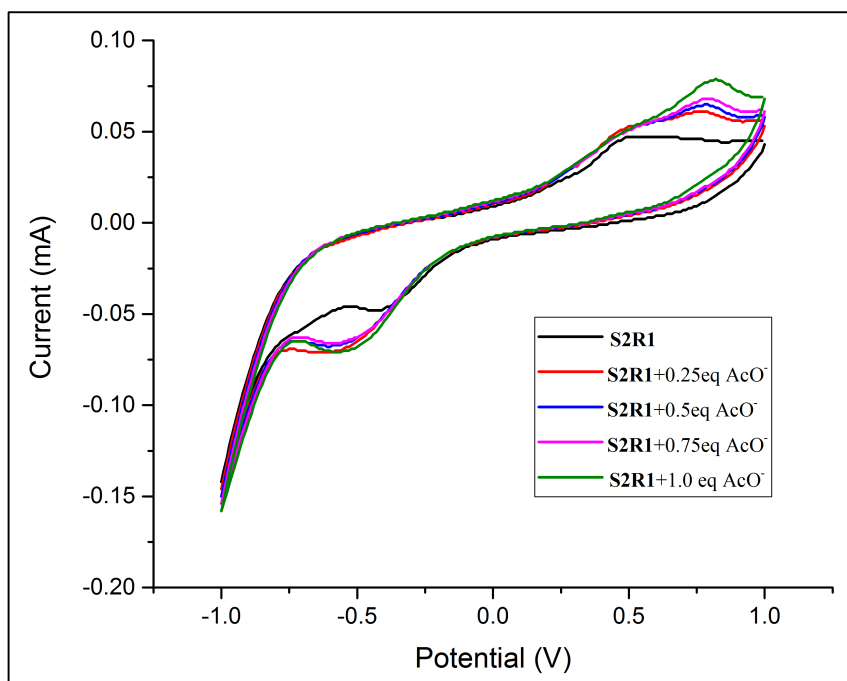


Fig. 4.54 (a) Cyclic voltammogram of receptor **S2R1** ($5 \times 10^{-5} \text{M}$) with incremental addition of TBAAcO ion (0-1 equiv.)

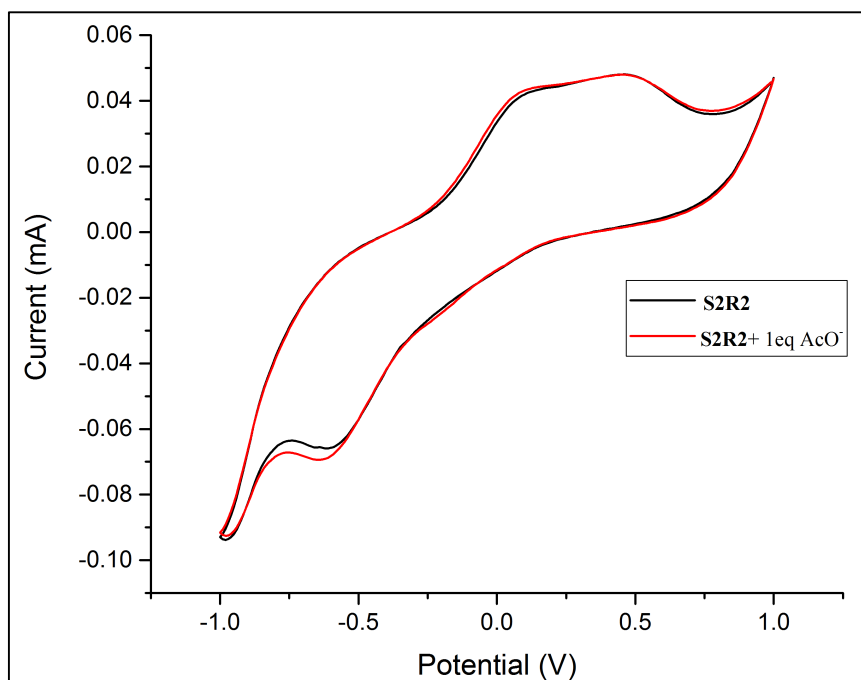


Fig. 4.54 (b) Cyclic voltammogram of receptor **S2R2** ($5 \times 10^{-5} \text{M}$) with incremental addition of TBAAcO ion (0-1 equiv.)

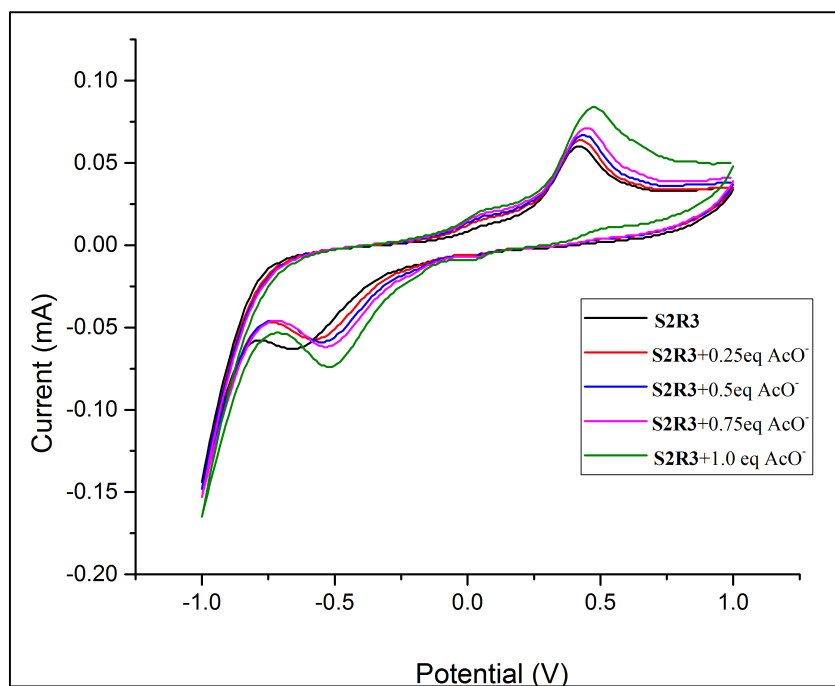


Fig. 4.54 (c) Cyclic voltammogram of receptor **S2R3** ($5 \times 10^{-5} \text{M}$) with incremental addition of TBAAcO ion (0-1 equiv.)

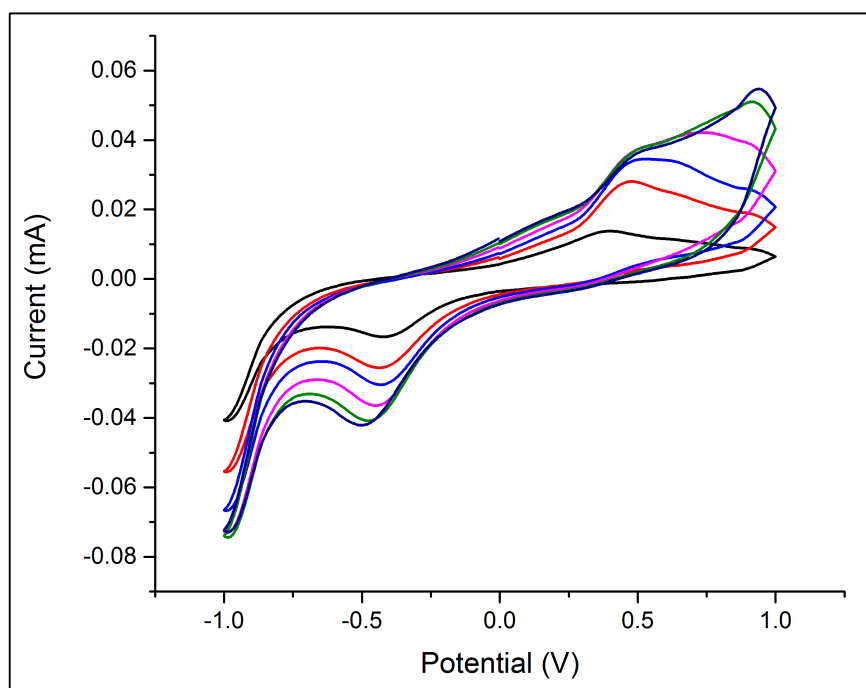


Fig. 4.54 (d) Cyclic voltammogram of receptor **S2R4** ($5 \times 10^{-5} \text{M}$) with incremental addition of TBAAcO ion (0-1 equiv.)

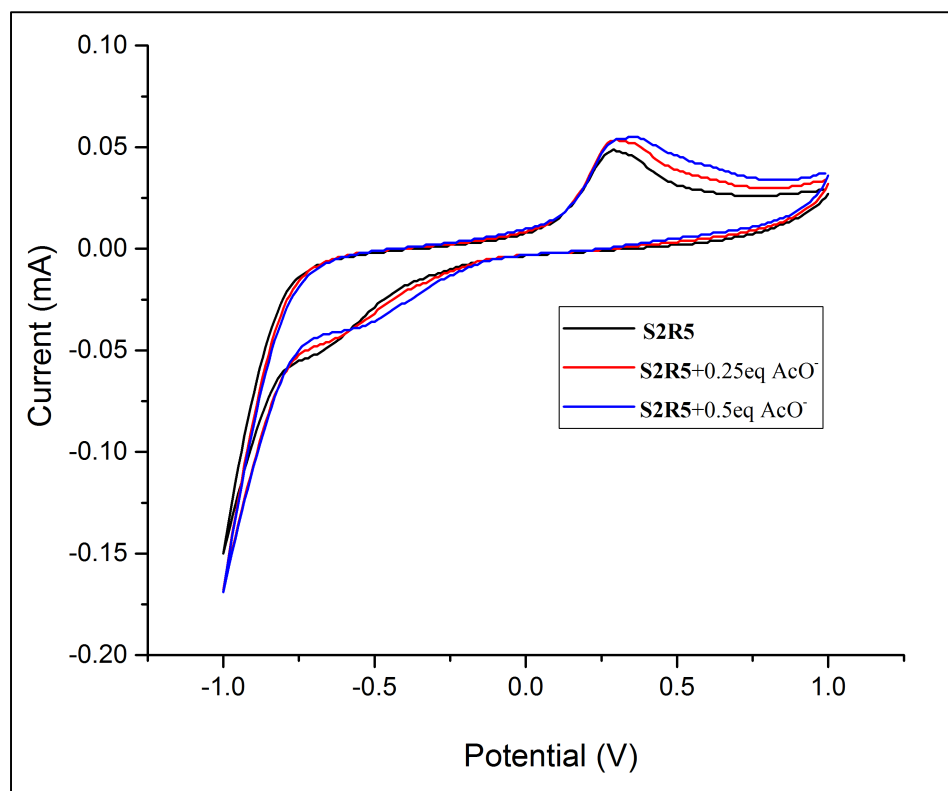


Fig. 4.54 (e) Cyclic voltammogram of receptor **S2R5** (5×10^{-5} M) with incremental addition of TBAAcO ion (0-1 equiv.)

4.3.5 ¹H-NMR titration studies

To arrive at the binding mechanism, ¹H-NMR titration studies has been performed with DMSO-*d*₆ solution of receptor **S2R3** and **S2R4** upon addition of TBA salt of acetate ion. ¹H-NMR titration was performed with 1×10^{-4} M of **S2R3** in the presence of AcO⁻ ion added as TBA salt in DMSO-*d*₆ as solvent and the corresponding anion receptor interactions has been monitored. The color change was immediate upon addition of 0.1 equiv. of AcO⁻ ion which revealed changes in the ¹H-NMR spectra. With the incremental addition of 0.5, 1.0, 1.5 and 2.0 eq. of AcO⁻ ion the -NH proton at δ 11.96 ppm of free receptor experienced simultaneous broadening with diminution of peak intensity referring to the initial hydrogen bond complex formation followed by deprotonation process. The signal corresponding to the aromatic protons and imine proton showed decrease in their intensity upon addition of higher eq. of AcO⁻ ion. The titration spectra is represented in Fig 4.55.

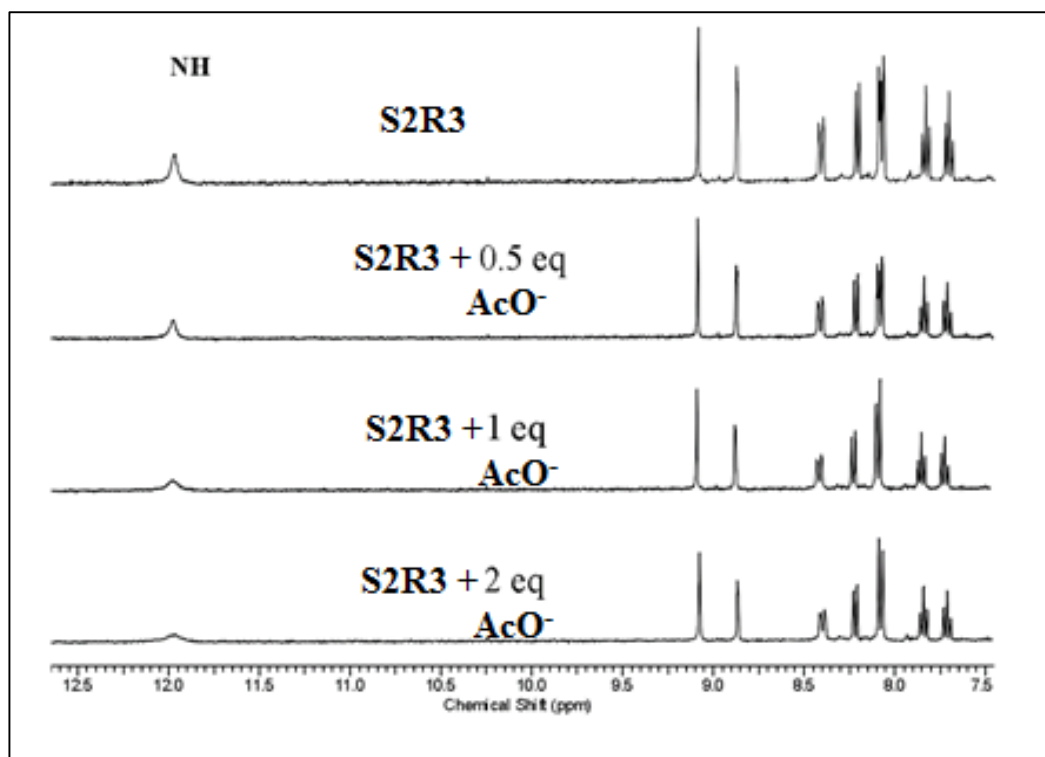


Fig. 4.55 ^1H NMR titration of receptor **S2R3** with incremental addition of TBAcO ion (0-2 equiv.)

Disappearance of resonance signal ascribable to the $-\text{NH}$ proton at 11.8 ppm upon successive addition of AcO^- ion is indicative of the deprotonation mechanism involved in the binding process (Lee et al. 2001) (Fig. 4.56). The disappearance of the splitting pattern in the aromatic region indicates the formation of $\text{NH} \cdots \text{AcO}^-$ hydrogen bond followed by a deprotonation process.

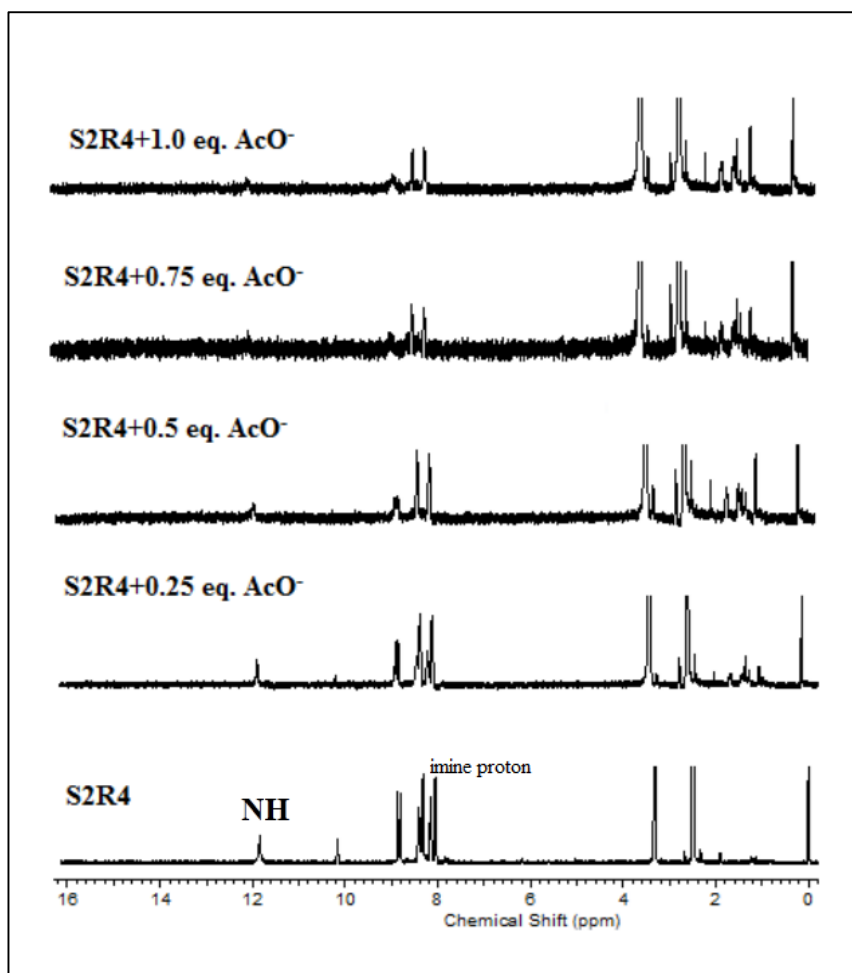


Fig. 4.56 ^1H -NMR titration of receptor **S2R4** with incremental addition of TBAOAc ion (0-1 eq.)

4.3.6 pH dependency studies

To infer the selectivity of receptors towards anions, Tris HCl buffer solution has been introduced into the receptor solution of **S2R4** in varying ratio. It was found that with 9:1, DMSO: Tris HCl buffer, pH 7.4, **S2R4** exhibited selective response towards AcO^- ion with a color change visible to naked eye. The UV-Vis titration studies performed with incremental addition of AcO^- ion added as TBA salt, represented a clear red shift of the original absorption band with growth of new isobestic point indicating the complex formation. This is represented in Fig. 4.57. The corresponding B-H plot for the **S2R4**- AcO^- complex is given in Fig. 4.58.

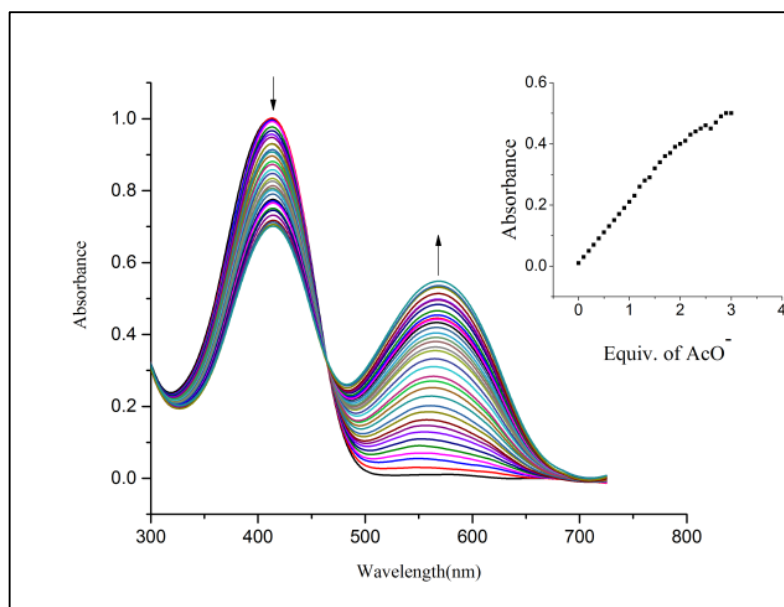


Fig. 4.57 UV-Vis titration spectra of receptor **S2R4** (DMSO/Tris HCl (9:1, v/v, 10^{-4} M) with incremental addition of standard solution of TBAAcO (1×10^{-2} M in dry DMSO). Inset showing the absorption isotherm at 569 nm

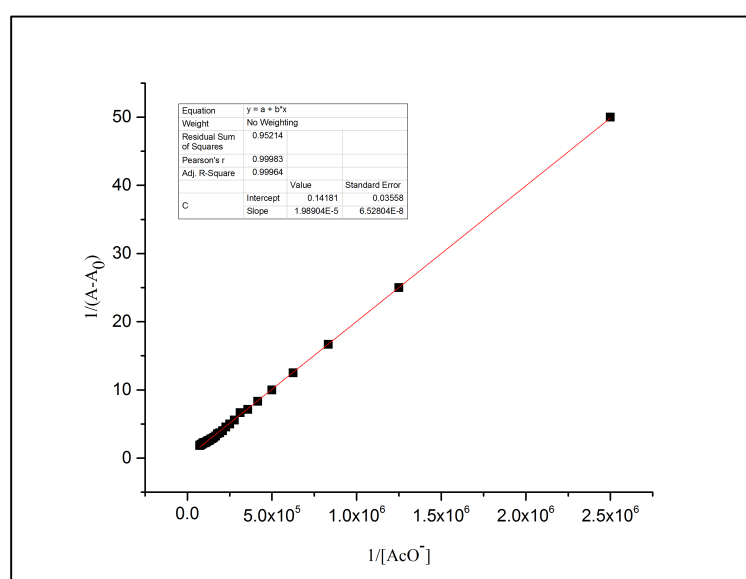


Fig. 4.58 B-H plot of receptor **S2R4**- TBAAcO complex (buffer media) at a selected wavelength of 569 nm

4.3.7 DFT studies

To support the AcO⁻ ion induced optical signalling event of the receptor S1R4 in solvents of varying polarity, DFT calculations have been performed using B3LYP/6-31G (d,p) basis set. The optimized structure of receptor **S2R4** in gas phase (Fig.

4.59(a), (b) and (c)) and the deprotonated form observed upon AcO^- ion binding in few selected solvents viz., acetone (Fig. 4.60(a), (b) and (c)) and DCM have been derived. HOMO and LUMO of the deprotonated receptor **S2R4** in DCM is represented in Fig. 4.61. The band gap for optimized structure of receptor **S2R4** in gas phase is found to be 3.36 eV. Anion induced deprotonation of receptor **S2R4** in DCM results in lowering of the band gap value from 3.36 eV to 3.02 eV which is responsible for the red shift of the band observed in UV-Vis spectra. Significant redshift of the absorption band is the resultant of deprotonation of anion binding site. Similar observations were obtained for the receptor **S2R4** in acetone with variation in band gap from 3.36 to 3.0 eV. Structure of HOMO and LUMO of deprotonated receptor **S2R4** in gas phase and acetone is given in Fig. 4.60 (a), (b) and (c) respectively. Dipole moment calculated for the receptor and its deprotonated form reveals a change from 2.59 D to 9.29 D and 9.63 D in DCM and acetone respectively. The higher dipole moment of receptor in acetone in comparison with DCM indicates efficient charge transfer from receptor to solvent in case of acetone. With these values, the role of dipole moment in stabilizing the excited state more than the ground state is justified. The receptor **S2R4** in its deprotonated form in DCM and acetone exhibited absorption band at 564 and 569 nm respectively corroborating well with the experimentally observed UV-Vis spectral results (Fig. 4.62).

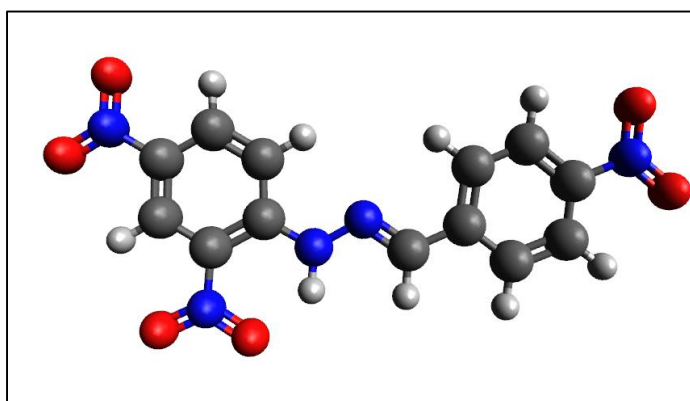


Fig. 4.59 (a) Optimized geometry of the receptor **S2R4** in gas phase

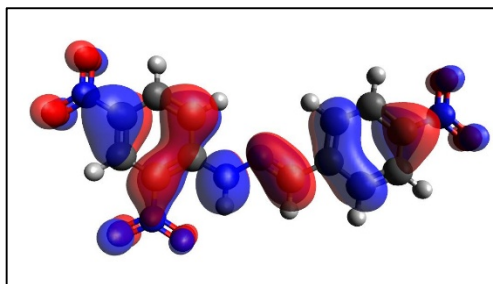


Fig. 4.59 (b) HOMO of the receptor **S2R4** in gas phase

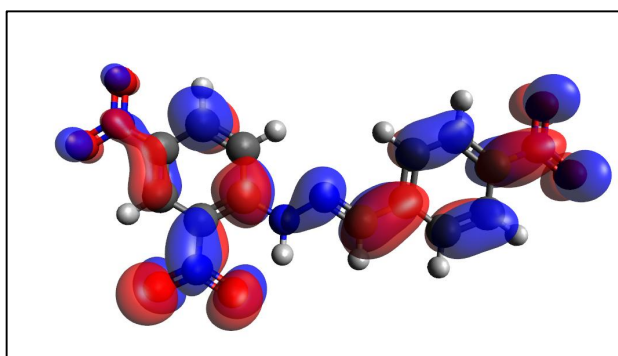


Fig. 4.59 (c) LUMO of the receptor **S2R4** in gas phase

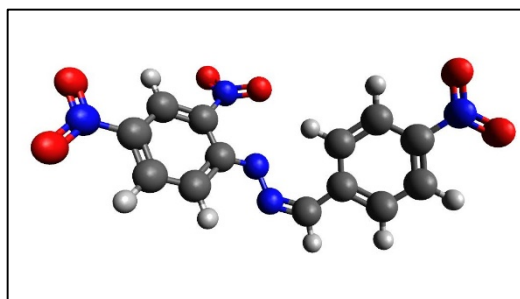


Fig. 4.60 (a) Optimized structure of the deprotonated receptor **S2R4** in acetone

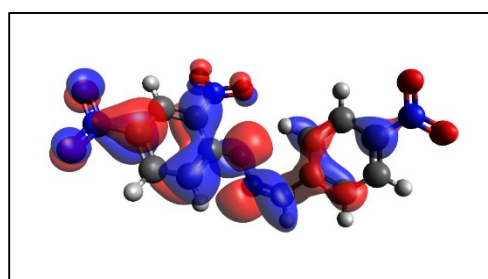


Fig. 4.60 (b) HOMO of the deprotonated receptor **S2R4** in acetone

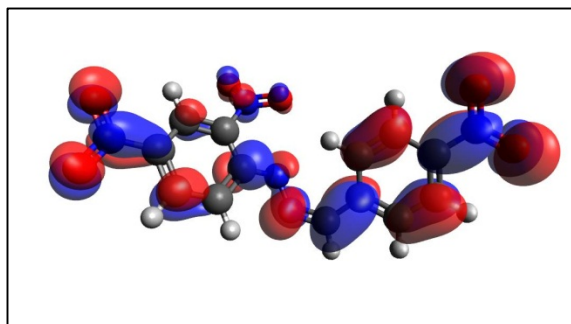


Fig. 4.60 (c) LUMO of the deprotonated receptor **S2R4** in acetone

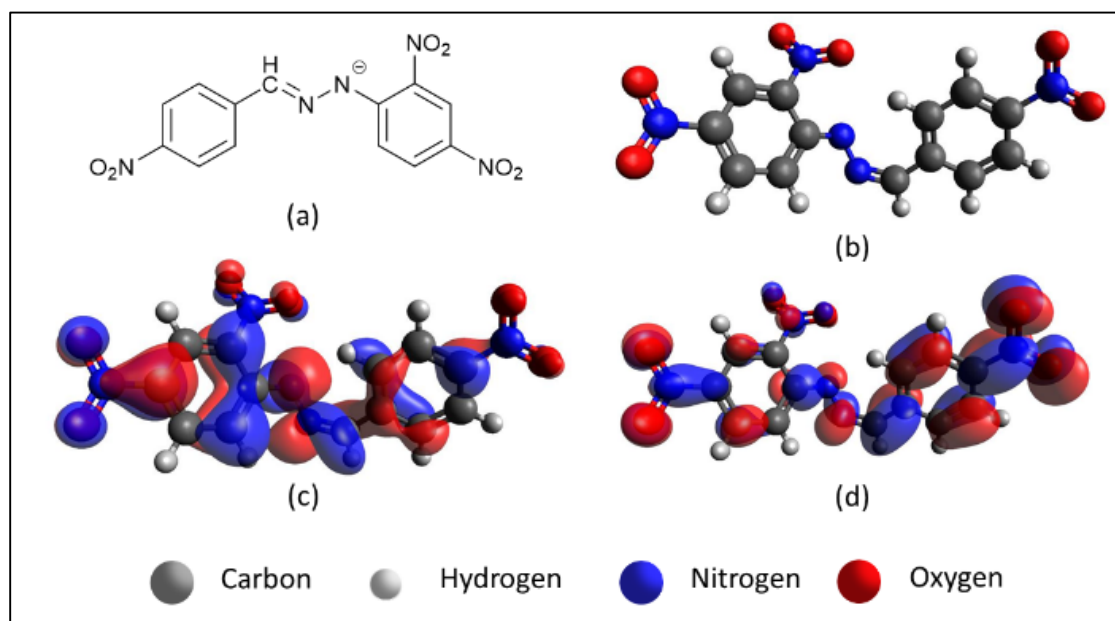


Fig. 4.61 Schematic representation of (a) chemical structure of deprotonated receptor **S2R4** (b) DFT derived optimized structure of the deprotonated receptor **S2R4** in DCM. Isosurface in (c) representing distribution of HOMO and (d) LUMO in deprotonated receptor **S2R4**

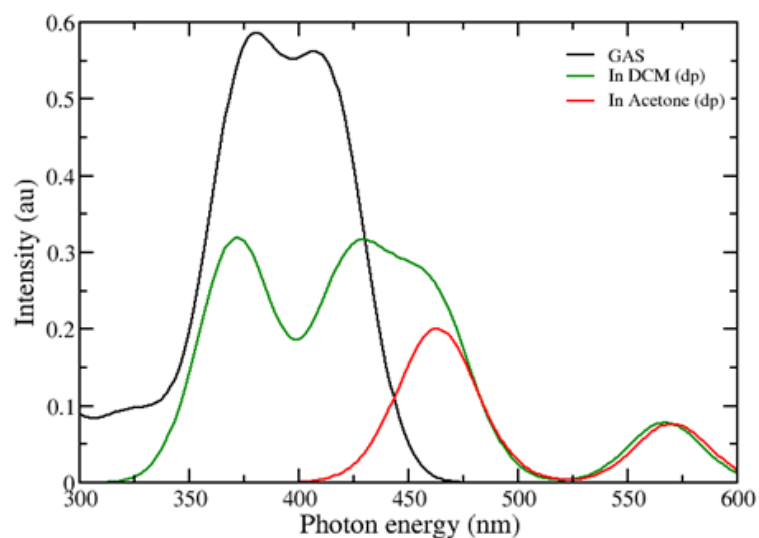


Fig. 4.62 UV-Vis spectra of the receptor **S2R4** in gas phase, in solvents such as DCM and acetone with addition of AcO^- ion

4.3.8 Calculation of binding constant from UV-Vis studies

Binding constant has been calculated using B-H equation (Benesi and Hildebrand 1948) (Eq. 1);

$$1/(A-A_0) = 1/(A_{\max} - A_0) + 1/K [X^-]^n (A_{\max} - A_0) \text{ ----- (Eq. 1)}$$

Where, A_0 , A , A_{\max} are the absorption considered in the absence of F^- , at an intermediate, and at a concentration of saturation. K is binding constant, $[X^-]$ is concentration of X^- ion and n is the stoichiometric ratio.

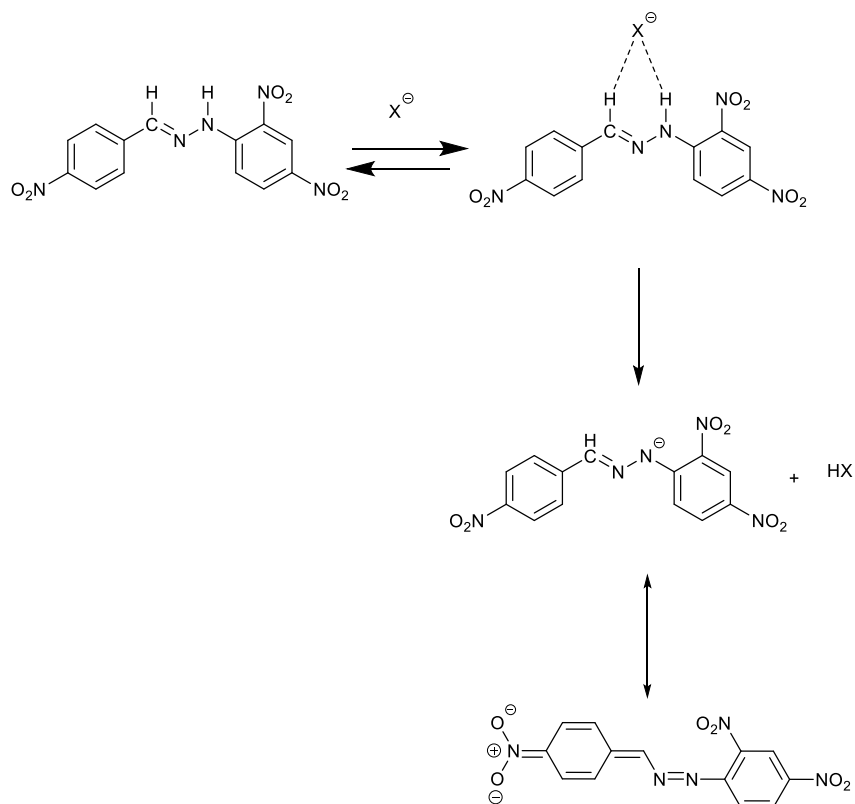
The corresponding binding constant and detection limit of receptors have been tabulated in Table 4.3.

Table 4.3 Binding constant and detection limit of receptors in the presence of various anions

Receptor	Anion	Solvent system	Binding constant (M^{-1})	Detection limit (ppm)
S2R1	AcO^- (TBAAcO)	DMSO	2.33×10^2	9
	F^- (NaF)	DMSO:H ₂ O (9:1 v/v)	1.46×10^2	1
S2R2	AcO^- (TBAAcO)	DMSO	2.18×10^2	4.5
	F^- (NaF)	DMSO:H ₂ O (9:1 v/v)	1.23×10^2	0.8
S2R3	AcO^- (TBAAcO)	DMSO	2.2×10^2	3.7
	AcO^- (NaAcO)	DMSO:H ₂ O (9:1 v/v)	1.19×10^2	1
S2R4	AcO^- (TBAAcO)	DMSO	5.28×10^2	1.5
	AcO^- (NaAcO)	DMSO:H ₂ O (9:1 v/v)	3×10^2	0.8
	F^- (TBAF)	DMSO	1.1×10^2	2.5
	F^- (NaF)	DMSO:H ₂ O (9:1 v/v)	4.2×10^2	0.4
	$H_2PO_4^-$ (TBAH ₂ PO ₄)	DMSO	3.15×10^2	3.3
S2R5	AcO^- (TBAAcO)	DMSO:Tris HCl (9:1 v/v)	1.33×10^2	15
	AcO^- (TBAAcO)	DMSO	4.5×10^2	7.7
	AcO^- (NaAcO)	DMSO:H ₂ O (9:1 v/v)	3.14×10^2	1.2

4.3.9 Binding mechanism

Based on the UV-Vis and ¹H-NMR titration studies, the following binding mechanism has been proposed. The addition of strong basic anion (AcO^-) initially leads to the bifurcated hydrogen bond interaction with the $-NH$ and imine functionality with a subsequent deprotonation of NH proton. Deprotonation process further tends to increase the electron density by introducing charge separation in the receptor **S2R4**. This facilitates ICT transition between electron deficient $-NO_2$ functionality at *para* position and electron rich N^- species resulting in the strong colorimetric response. The binding mechanism is represented in Scheme 4.6.



where X= AcO⁻

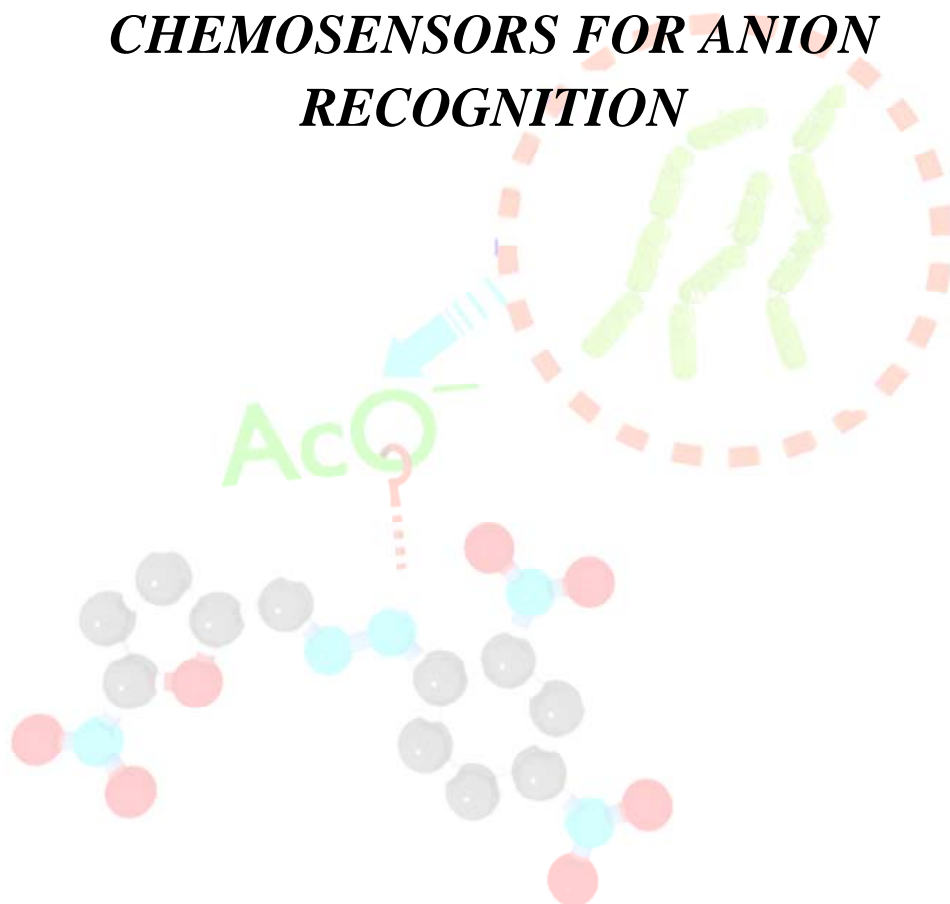
Scheme 4.6 Proposed binding mechanism of receptor **S2R4** with AcO⁻ ion

4.4 Conclusions

In conclusion, the present findings serve to illustrate the role of positional substitution of nitro functionality on the anion binding and selectivity. Receptors **S2R1**, **S2R2**, **S2R3**, **S2R4** and **S2R5** proved their ability to act as colorimetric receptor for anions. Receptor **S2R5** exhibited selective response towards AcO^- ion in organic solvent with a binding constant of the order $4.5 \times 10^2 \text{ M}^{-1}$. Receptor **S2R4**- AcO^- ion complexation induced pronounced change in the position and intensity of absorption band emphasizing the effect of solvent polarity on the anion binding process. Anion binding studies of **S2R4** performed in Tris HCl buffer medium reflects the selective detection of AcO^- ion. Lower detection limit of 0.8 ppm and 0.4 ppm observed in case of AcO^- ion and F^- ion with **S2R4** which is relatively lower than the WHO guidelines highlights the efficacy of the receptor. The binding constant value of $5.28 \times 10^4 \text{ M}^{-1}$ with TBA^+AcO^- ion and $4.2 \times 10^4 \text{ M}^{-1}$ with NaF reflect the stability of receptor **S2R4** - anion complex. Electrooptical studies, $^1\text{H-NMR}$ titrations and DFT calculations of **S2R4** in solution phase provide full proof of the deprotonation involved in the binding mechanism. Colorimetric response of receptor **S2R4** towards AcO^- ion in the organic, aqueous and solid phase signifies its practical utility as a chemosensor.

CHAPTER 5

***DESIGN, SYNTHESIS AND EVALUATION OF
FURYL FUNCTIONALIZED HYDRAZINE
DERIVATIVES AS COLORIMETRIC
CHEMOSENSORS FOR ANION
RECOGNITION***



Abstract

In this chapter, design, syntheses and characterization of three organic receptors have been described. The applicability of the receptors in the colorimetric detection of anions have been discussed in detail through UV-Vis spectrophotometric, ¹H-NMR titration studies and supported by DFT studies. The binding mechanism of the receptor towards active anions have been included. The biological application of one of the receptors in the detection of acetate in E. coli have been studied.

5.1 INTRODUCTION

Anion receptor chemistry has gained unique attention among supramolecular chemists in the light of their roles in biology and environment (Martínez-Máñez and Sancenón 2003; Sancenón et al. 2003; Gale 2003). Design-based synthetic receptors witness burgeoning interest for the selective detection of anions in aqueous media (Mizuno et al. 2002; Miyaji et al. 2000; Sessler et al. 2002; Sancenón et al. 2003). Synthetic receptors that can recognize and sense anions through visible, electrochemical and optical response are of special interest owing to the low cost and simple instrumentation required. Signaling unit-binding site approach is well known in translating receptor-anion association into an optical signal. Covalent linking of an optical signaling chromophoric fragment lead to visually observable color change assigned to the conformational changes in the receptor or charge transfer process (Atwood et al. 1996; Gale 2001; Beer and Gale 2001). Among the wide array of anions, fluoride and acetate has gained undivided attention for their significant role at physiological level. Fluoride is well known in the clinical treatments such as dental carries (Kirk 1991) and osteoporosis (Kleerekoper 1998). Physiologically, acetate ion plays a leading role in metabolic process and ecologically, it monitors the sedimentation of organic compounds in marine sediments. Diversity of function, both beneficial and otherwise urge the need for colorimetric sensors for the detection of fluoride and acetate ions relating to their size, basicity, electronegativity effects and strong hydrogen bond acceptor nature (Bhosale et al. 2009).

Receptors bearing amide, urea, thiourea units are known to promote fluoride and acetate ion binding through hydrogen-bond interaction and N-H deprotonation events. Recently, neutral-anion receptor system based on heterocyclic derivatives such as pyrrole, indole etc. which possess relatively acidic proton have been extensively studied (Jose et al. 2004; Vázquez et al. 2004; Lee et al. 2004; Esteban-Gómez et al. 2005; Cho et al. 2005; He et al. 2006; Evans et al. 2006; Quinlan et al. 2007; Lee and Gabbai 2007). In pursuit of optical sensor for anions, a new series of furan based receptors **S3R1**, **S3R2** and **S3R3** have been synthesized to gain further insight into the binding mechanism. Receptors **S3R1**, **S3R2** and **S3R3** possess an anion binding site, –NH functionality, inherent in its structure, and it is worthwhile to link it with an electron deficient group such as nitro paving way for the intramolecular charge transfer process. The choice of including –NO₂ group was based on the fact that it could act as a binding affinity control group by regulating the acidity of the hydrogen bond donor moiety. Further, the chromogenic signaling output in anion binding event could be fine-tuned by introducing substituent effect on the aromatic ring. Accordingly, depending on the basicity of the anion and increasing equivalence of the anion tendency to deprotonate acidic sites is likely to increase. **S3R1** possesses –NO₂ functionality on the furan ring *para* to phenylhydrazine group. **S3R2** comprises of nitrophenyl substituent attached to furan ring and is *para* to –NH functionality containing phenylhydrazine group whereas **S3R3** is devoid of –NO₂ functionality on the furan ring. Binding of anion through strong hydrogen bond followed by a deprotonation event is expected to yield a well resolved colorimetric and electrochemical response through modulated internal charge transfer process.

5.2 EXPERIMENTAL SECTION

5.2.1 Materials and Methods

All chemicals and analytical grade reagents were used as bought without any further purification unless otherwise mentioned. Thin layer chromatography was performed using Merck TLC Silica Gel F₂₅₄ plates. Melting point was measured on Stuart SMP3 melting-point apparatus in open capillaries. Infrared spectra were recorded on Bruker alpha FTIR spectrometer. ¹H-NMR was performed using Bruker-400 AV-400

spectrometer. Chemical shift values are reported in ppm scale (in *DMSO-d*₆ with Tetramethylsilane as internal standard). UV-Vis experiments were carried out using Thermo Scientific Genysys 10S spectrometer in standard 3.0 mL quartz cell with 1 cm path length.

5.2.2 Preparation of agar plates containing receptor S3R1

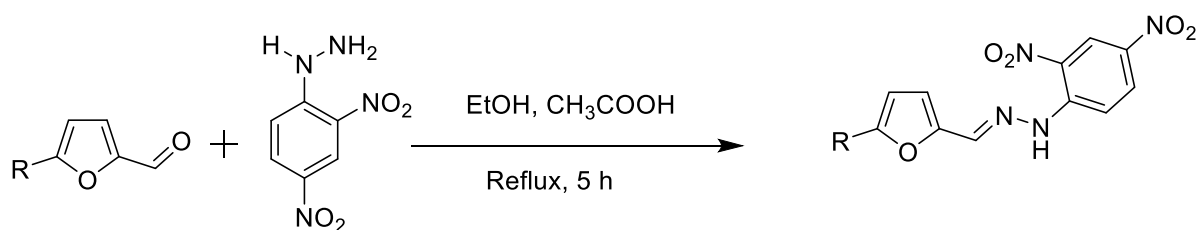
A 5% (w/V) receptor stock solution was prepared in 100% ethanol. To this solution, 1% (w/V) DMSO (Finar reagents) was added to dissolve receptor completely for use. The solution was prepared fresh for better results. The receptor solution (20 μ L) was spread on the Luria Bertani (LB) agar plates (20 mL) containing glucose (2 g/L). The solution was dried for 30 minutes in the laminar air flow chamber. Wells were made on agar plate to load *E. coli* BL21 culture.

5.2.3 Preparation of *E.coli* BL21 culture

The *E. coli* BL21 cells were grown in 50 mL liquid LB medium containing glucose (2 g/L) in orbital shaker for a period of 24 h at 37°C at 200 rpm. The samples were harvested at regular time intervals. Into each well, 100 μ L of the liquid of *E.coli* BL21 cells were inoculated. The plates were incubated at 37°C and observed for fluorescence at 365 nm after 24 h.

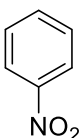
5.2.4 Synthesis of receptors S3R1, S3R2 and S3R3

Receptors **S3R1**, **S3R2** and **S3R3** were prepared by simple Schiff base condensation reaction between 2,4-dinitrophenylhydrazine and different substituted furaldehydes namely, 5-nitrofuraldehyde (0.70 mmol), 5-nitrophenylfuraldehyde (0.46 mmol) and furaldehyde (1.04 mmol) respectively. Ethanolic solution of resulting mixtures were refluxed at 70 °C for 5 h in the presence of catalytic amount of acetic acid. The formation of the product was confirmed through TLC by the generation of single spot indicative of the disappearance of starting materials. After cooling to room temperature, the reaction mixture was filtered through filter paper, washed with ethanol to obtain pure product. The general scheme of synthesis is shown in Scheme 5.1.



Where,

S3R1: R= NO₂

S3R2: R= 

S3R3: R= H

Scheme 5.1 General scheme for the synthesis of receptors **S3R1**, **S3R2** and **S3R3**

S3R1: (E)-1-(2,4-dinitrophenyl)-2-((5-nitrofuran-2-yl)methylene)hydrazine

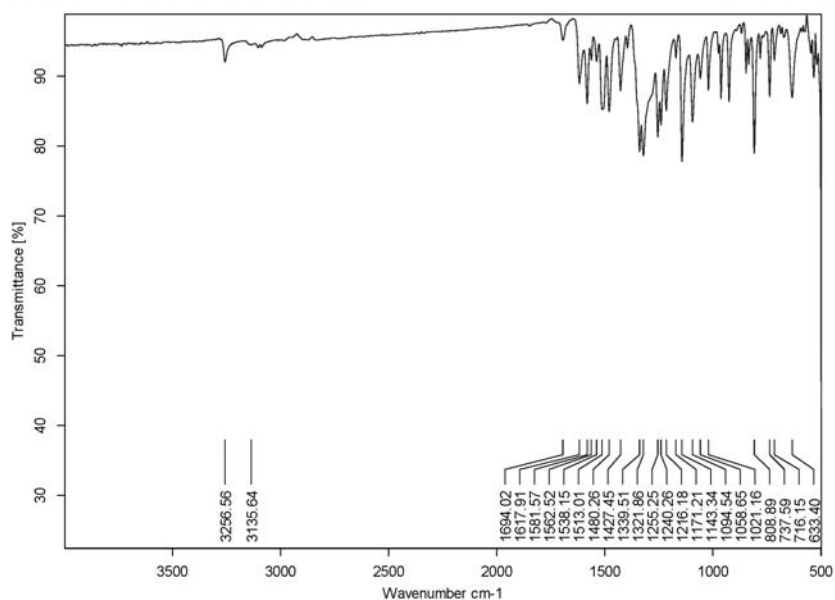
Yield: 87 %, melting point: 210 °C, ¹H NMR (DMSO- *d*₆, 400 MHz, ppm): δ 11.99 (m; NH), 8.73 (s; CH=N), 8.50 (dd; *J*= 9.5, 2.7; Ar-H), 8.25 (s; Ar-H), 8.03 (m; Ar-H), 7.86 (d; *J*=3.9; Ar-H), 7.38 (d; *J*=4.2; Ar-H). FTIR (KBr) (cm⁻¹): 3256 (NH), 3135 (Ar-CH), 1617 (CH=N), 1339 (NO₂).

S3R2: (E)-1-(2,4-dinitrophenyl)-2-((5-(4-nitrophenyl)furan-2-yl)methylene)hydrazine

Yield: 82 %, melting point: 242 °C, ¹H NMR (DMSO- *d*₆, 400 MHz, ppm): δ 11.83 (br. s; NH), 8.90 (d; *J*= 2.7; Ar-H), 8.72 (s; CH=N), 8.34 (m; 3Ar-H), 8.09 (m; 3Ar-H), 7.55 (d; *J*=3.7; Ar-H), 7.25 (d; *J*=3.7; Ar-H). FTIR (KBr) (cm⁻¹): 3266 (NH), 3084 (Ar-CH), 1614 (CH=N), 1329 (NO₂).

S3R3: (E)-1-(2,4-dinitrophenyl)-2-(furan-2-ylmethylene)hydrazine

Yield: 73 %, melting point: 206 °C, ¹H NMR (DMSO- *d*₆, 400 MHz, ppm): δ 11.7 (br. s; NH), 8.89 (m; Ar-H), 8.65 (s; CH=N), 8.41 (dd, *J*= 9.5, 2.7; Ar-H), 7.95 (m, 2Ar-H), 7.02 (d; *J*= 3.2); Ar-H), 6.70 (dd, *J*=3.4, 1.7; Ar-H). FTIR (KBr) (cm⁻¹): 3275 (NH), 3118 (Ar-CH), 1619 (CH=N), 1321 (NO₂).

5.2.5 CHARACTERIZATION DATA**Fig. 5.1** FT-IR spectrum of **S3R1**

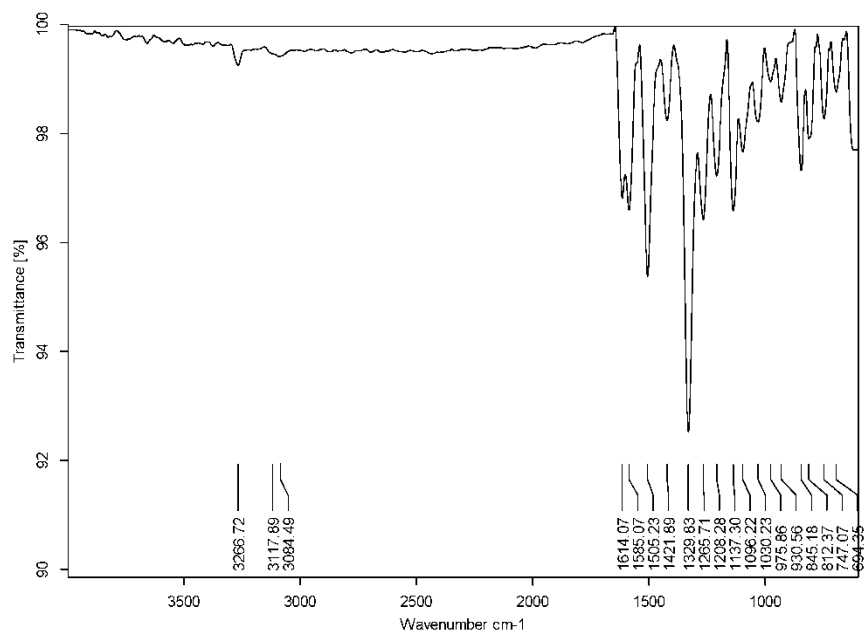


Fig. 5.2 FT-IR spectrum of S3R2

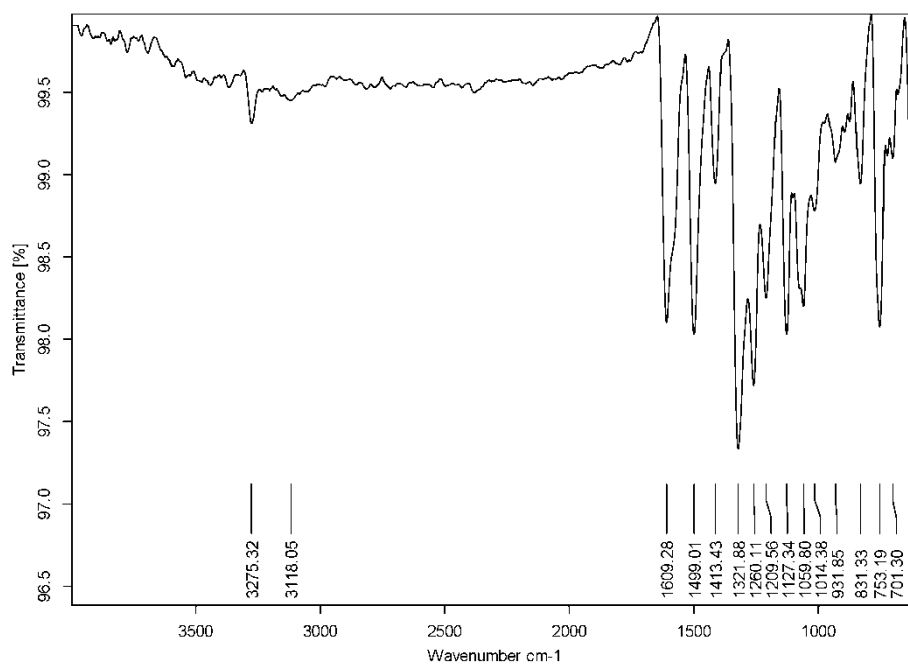


Fig. 5.3 FT-IR spectrum of S3R3

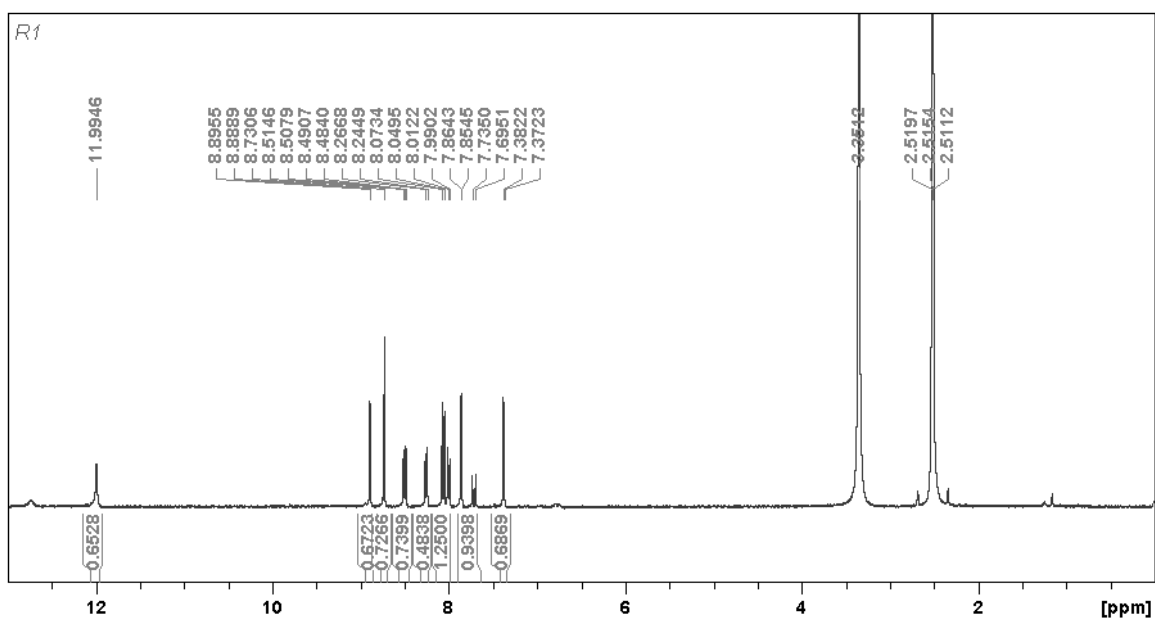


Fig. 5.4 ¹H NMR spectrum of S3R1

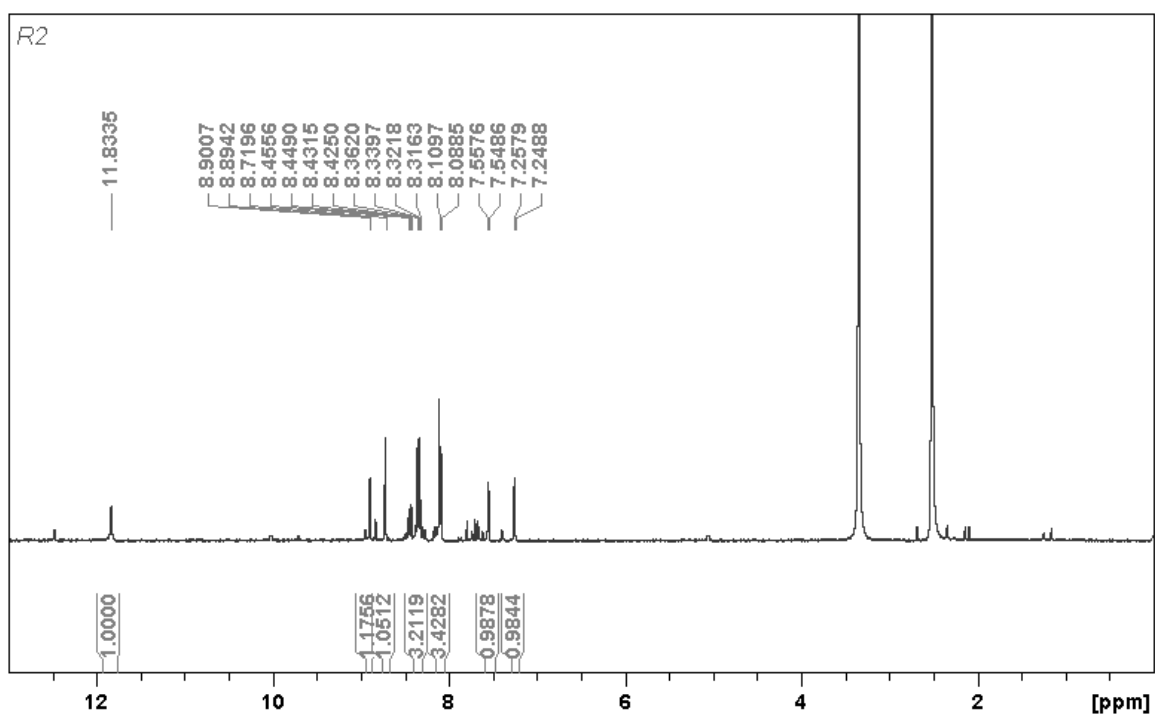


Fig. 5.5 ¹H NMR spectrum of S3R2

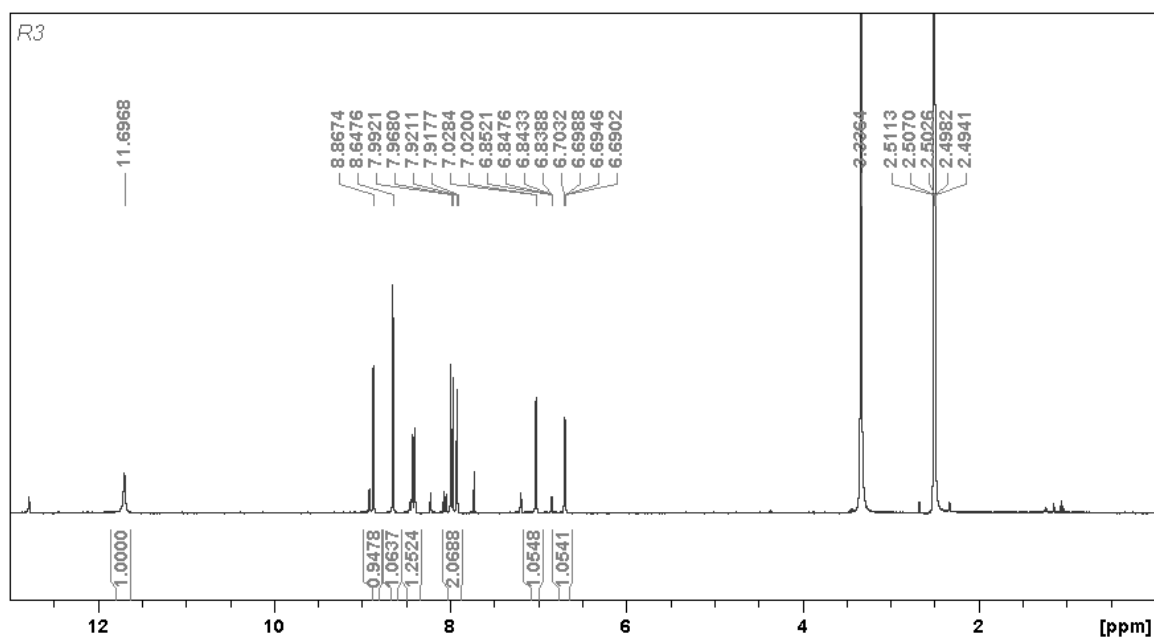


Fig. 5.6 ^1H NMR spectrum of **S3R3**

5.3 RESULTS AND DISCUSSION

5.3.1 Colorimetric detection of anions

With a view to evaluate the effect of structural modification on the optical properties of phenylhydrazones, positional substitution of $-\text{NO}_2$ and nitrophenyl functionality on the furyl moiety have been considered as part of the design strategy. The sensing ability of receptors **S3R1**, **S3R2** and **S3R3** ($1 \times 10^{-5} \text{ M}$ in DMSO) were analysed with the addition of series of tetrabutylammonium salts of anions ($[\text{Bu}_4\text{N}]^+\text{X}^-$, $\text{X} = \text{F}^-$, Cl^- , Br^- , I^- , NO_3^- , HSO_4^- , H_2PO_4^- and AcO^- ion). **S3R1**, **S3R2** and **S3R3** exhibited color change from pale yellow to blue, violet and pink respectively with the addition of 2 equiv. of F^- , H_2PO_4^- and AcO^- ions (Fig. 5.7).

UV-Vis spectroscopic study performed with $1 \times 10^{-5} \text{ M}$ DMSO solution of the receptors **S3R1**, **S3R2** and **S3R3** displayed strong absorption band at 432 nm, 442 nm and 405 nm respectively. The absorption maxima for **S3R1**, **S3R2** and **S3R3** could be assigned to the intramolecular charge transfer interactions in the presence of $\text{Ar}-\text{CH}=\text{N}-\text{NH}$ conjugation. The electron donor nature of $-\text{NH}$ and acceptor nature of $-\text{NO}_2$ functionality are known to impart pale yellow coloration to the receptor in

DMSO. Addition of F^- , $H_2PO_4^-$ and AcO^- ions to **S3R1**, resulted in the decrease in the band centered at 432 nm and growth of new band at 625 nm, 633 nm and 628 nm respectively (Fig. 5.8). With **S3R2**, addition of F^- , $H_2PO_4^-$ and AcO^- ions led to the decrease in the band centered at 442 nm with the emergence of new bands at 554 nm, 555 nm and 556 nm respectively (Fig. 5.9). Upon addition of F^- , $H_2PO_4^-$ and AcO^- ions to **S3R3**, the absorption band at 405 nm decreased at the expense of new bands centered at 500 nm, 486 nm and 501 nm respectively accounting for the observed color changes (Fig. 5.10).

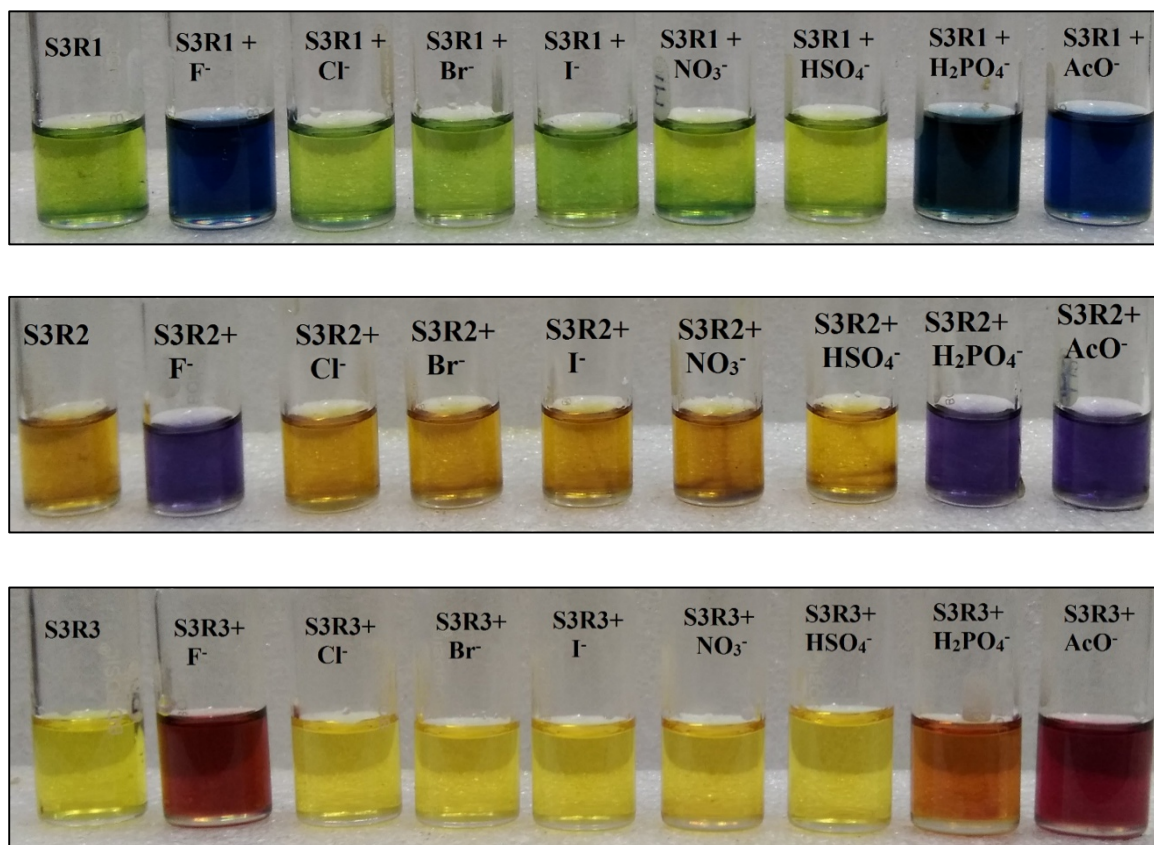


Fig. 5.7 Color change of the receptors **S3R1**, **S3R2** and **S3R3** (1×10^{-5} M in DMSO) with the addition of 1 equiv. of TBA salts of anions (1×10^{-2} M in DMSO)

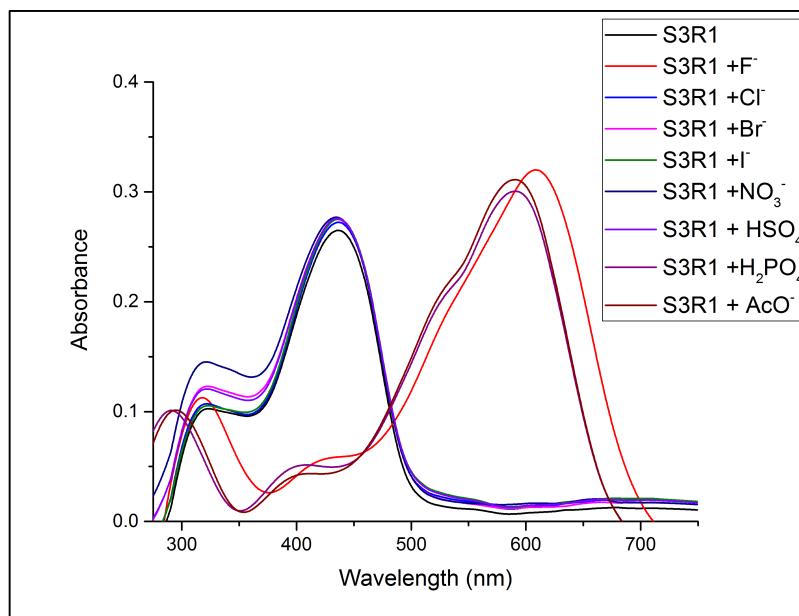


Fig. 5.8 UV-visible absorption spectra of **S3R1** (1×10^{-5} M in DMSO) upon addition of 1 equiv. of various anions as TBA salts

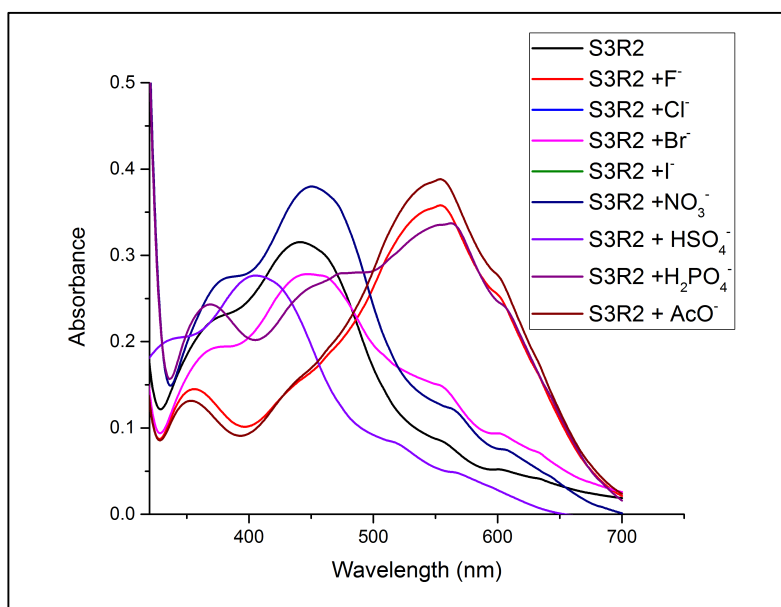


Fig. 5.9 UV-visible absorption spectra of **S3R2** (1×10^{-5} M in DMSO) upon addition of 1 equiv. of various anions as TBA salts

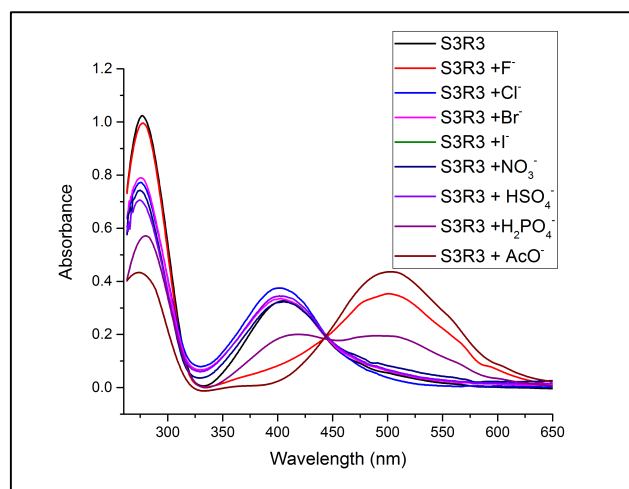


Fig. 5.10 UV-visible absorption spectra of **S3R3** ($1 \times 10^{-5} \text{M}$ in DMSO) upon addition of 1 equiv. of various anions as TBA salts

5.3.2 UV-Vis titration studies

For further investigation of the complex formation, UV-Vis titration experiments were performed with the incremental addition of anions to the receptor **S3R1**. With the gradual addition of F^- , H_2PO_4^- and AcO^- ions, the band at 328 nm and 432 nm decreased in its intensity signifying the hydrogen bond interactions of **S3R1** with -NH and the imine $-\text{CH}=\text{N}-$ moiety. The red shift observed at 625 nm, 633 nm and 628 nm respectively for F^- , H_2PO_4^- and AcO^- ions with a hyperchromic effect is indicative of the deprotonation of the -NH moiety with the higher equiv. of anion. The occurrence of unclear isobestic points at 435 nm, 471 nm, and 482 nm clearly represent a complex equilibrium process with the coexistence of more than one type of **S3R1**-anion complex. The new red shift band reached its limiting value with the addition of 1 equiv. of anions. The titration profiles are shown in Fig. 5.11, Fig. 5.12 and Fig. 5.13. The corresponding B-H plot yielded an appropriate binding ratio between **S3R1**-anion complex. (Fig. 5.14, Fig. 5.15 and Fig. 5.16).

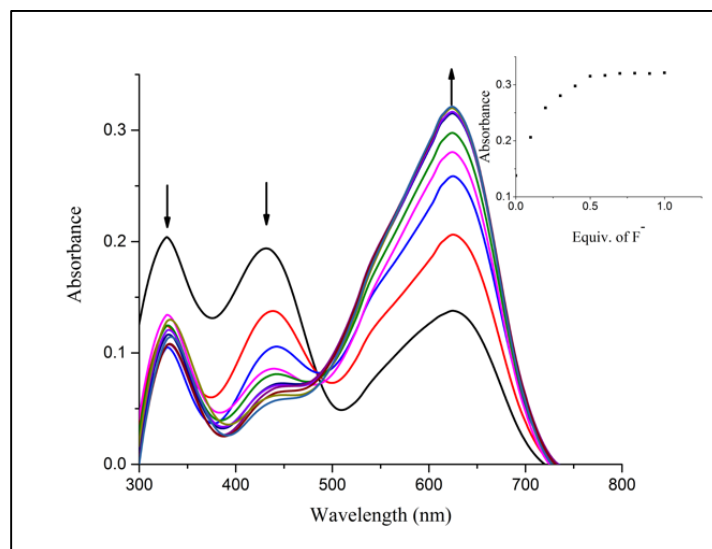


Fig. 5.11 UV-Vis titration spectra of receptor **S3R1** (10^{-5} M in DMSO) with the incremental addition of TBAF (10^{-2} M in DMSO); Inset plot representing the variation of absorbance with increasing concentration of TBAF

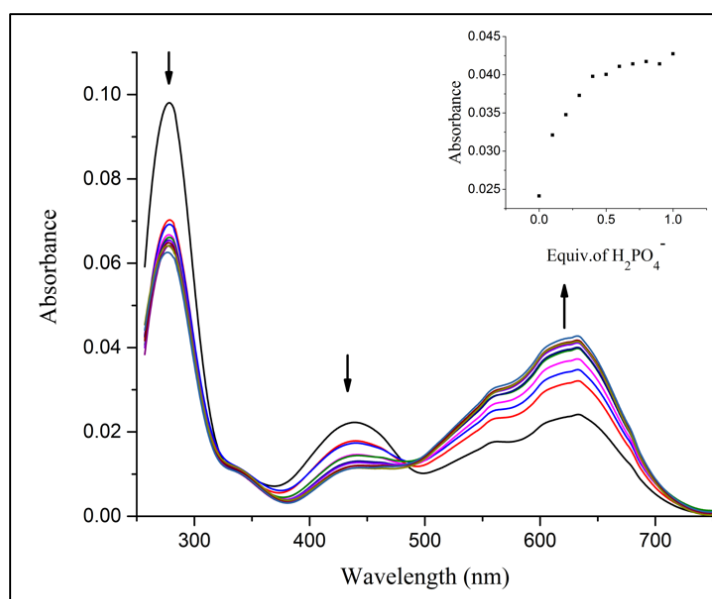


Fig. 5.12 UV-Vis titration spectra of receptor **S3R1** (10^{-5} M in DMSO) with the incremental addition of TBAH₂PO₄ (10^{-2} M in DMSO); Inset plot representing the variation of absorbance with increasing concentration of TBAH₂PO₄

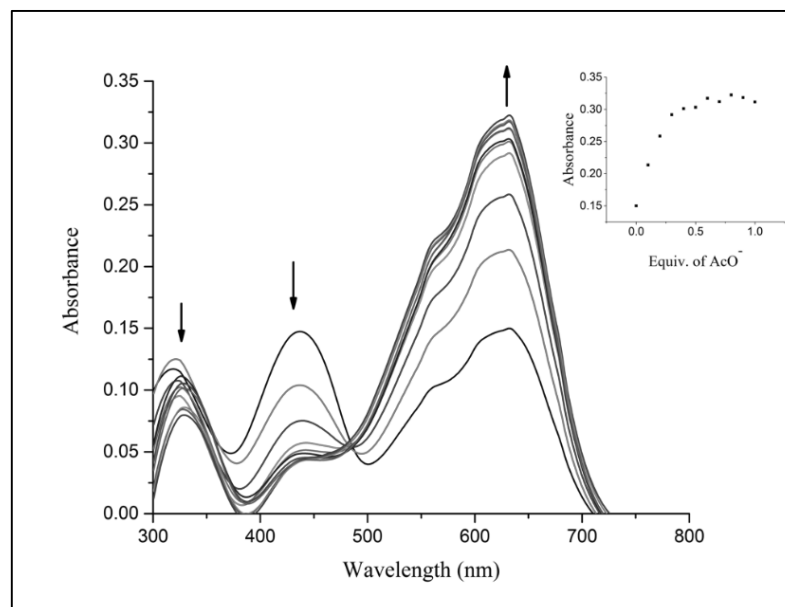


Fig. 5.13 UV-Vis titration spectra of receptor **S3R1** (10^{-5} M in DMSO) with the incremental addition of TBAAcO (10^{-2} M in DMSO); Inset plot representing the variation of absorbance with increasing concentration of TBAAcO

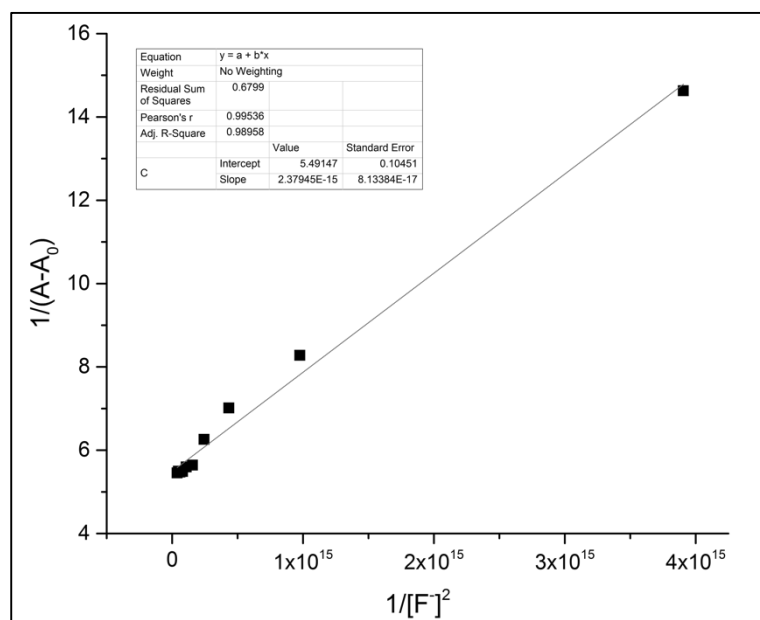


Fig. 5.14 B-H plot for **S3R1-TBAF** complex

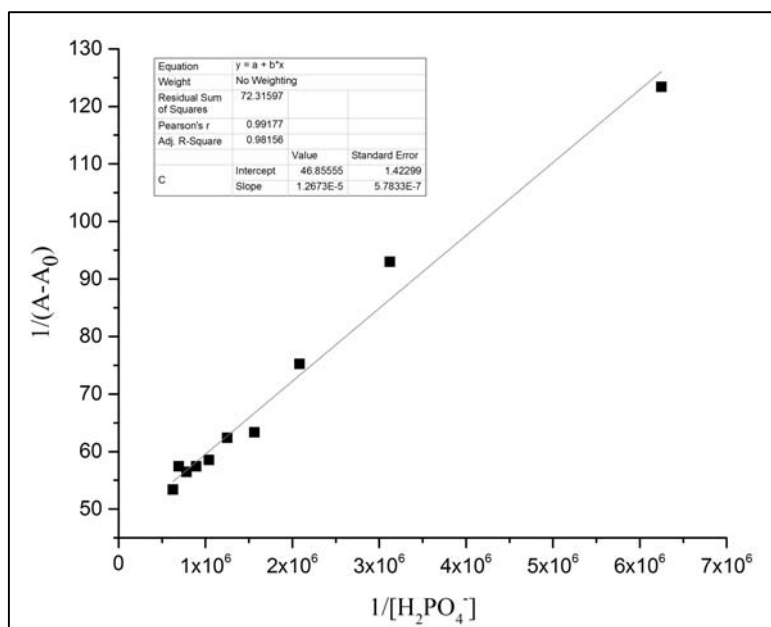


Fig. 5.15 B-H plot for **S3R1**-TBAH₂PO₄ complex

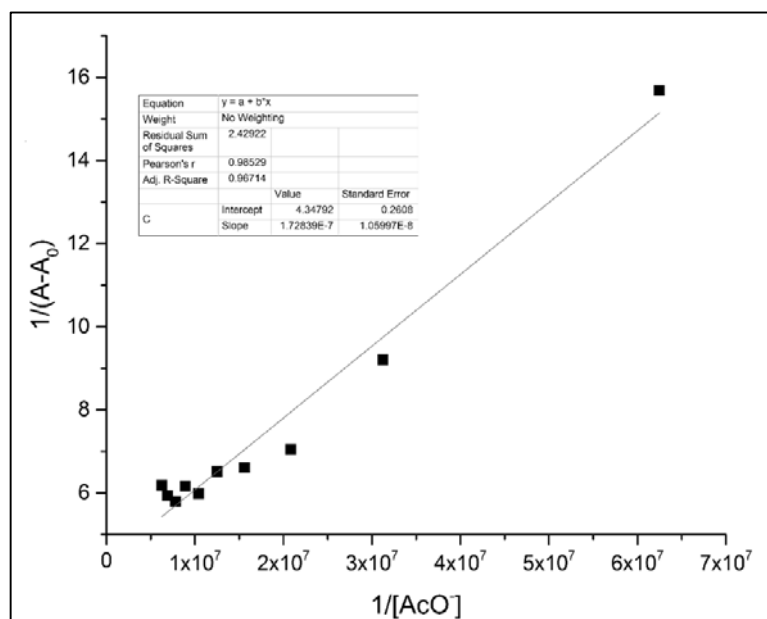


Fig. 5.16 B-H plot for **S3R1**-TBAAcO complex

Similarly, titration studies have been performed with the incremental addition of F⁻, H₂PO₄⁻ and AcO⁻ ions to **S3R2**, wherein the band centered at 442 nm decreased in its intensity with the gradual appearance of new red shift bands at 554 nm, 555 nm and 556 nm respectively. Isobestic points at 513 nm, 497 nm, 479 nm during the

incremental addition of 0.2 eq., 0.4 eq. and 0.5 eq. to 1.0 eq. of F^- and AcO^- ions respectively, represent complex equilibrium involved in the anion binding process (Sahu et al. 2016). Titration profile are represented in Fig. 5.16, Fig. 5.17 and Fig. 5.18. The corresponding B-H plot are shown in Fig. 5.19, Fig. 5.20 and Fig. 5.21.

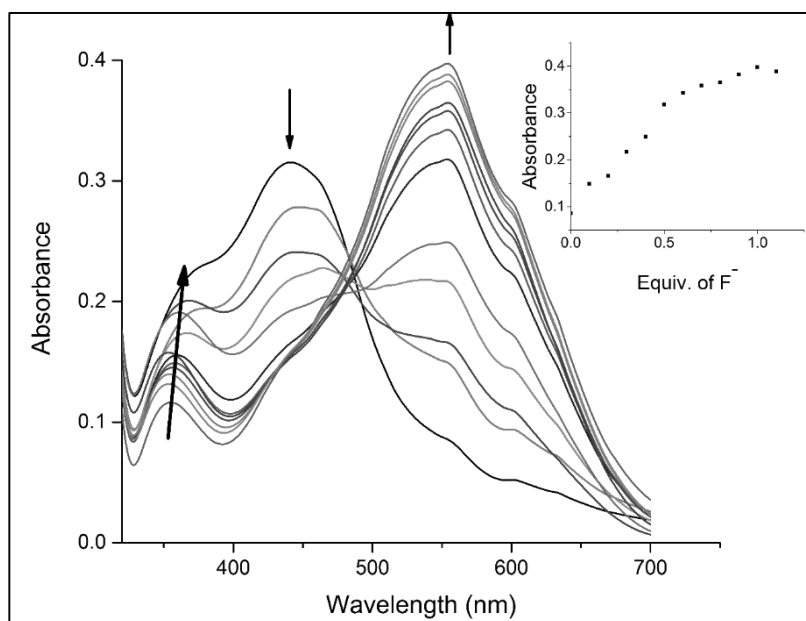


Fig. 5.17 UV-Vis titration spectra of receptor **S3R2** (10^{-5} M in DMSO) with the incremental addition of TBAF (10^{-2} M in DMSO); Inset plot representing the variation of absorbance with increasing concentration of TBAF

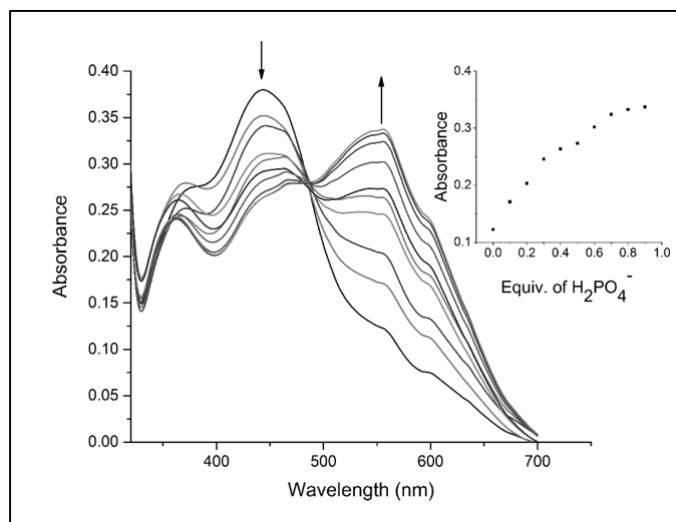


Fig. 5.18 UV-Vis titration spectra of receptor **S3R2** (10^{-5} M in DMSO) with the incremental addition of TBAH₂PO₄ (10^{-2} M in DMSO); Inset plot representing the variation of absorbance with increasing concentration of TBAH₂PO₄

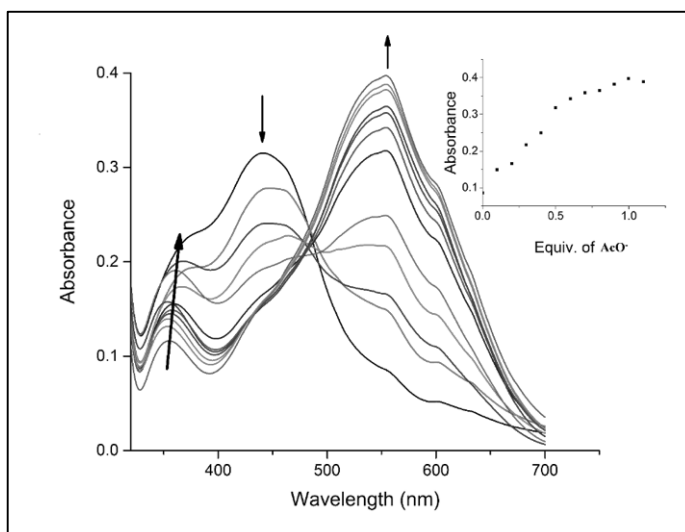


Fig. 5.19 UV-Vis titration spectra of receptor **S3R2** (10^{-5} M in DMSO) with the incremental addition of TBAAcO (10^{-2} M in DMSO); Inset plot representing the variation of absorbance with increasing concentration of TBAAcO

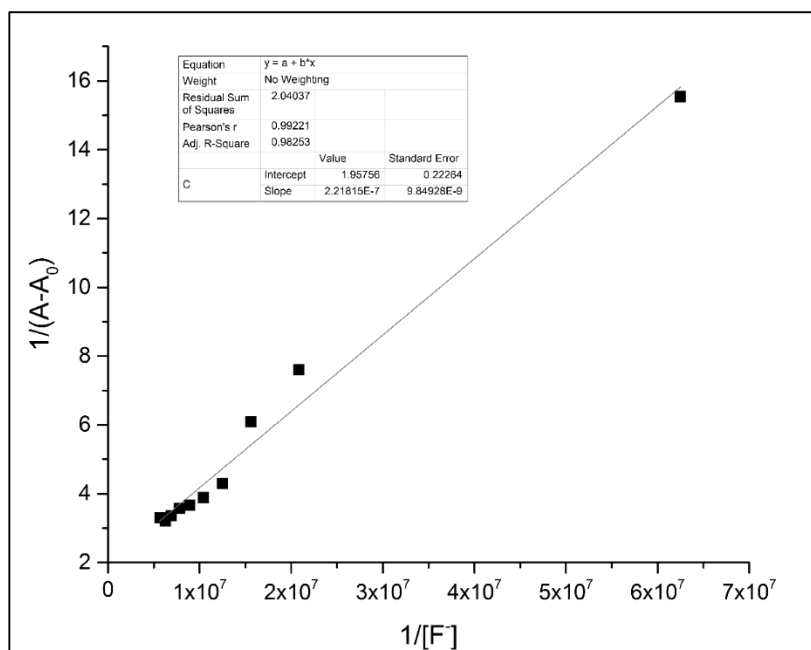


Fig. 5.20 B-H plot for S3R2-TBAF complex

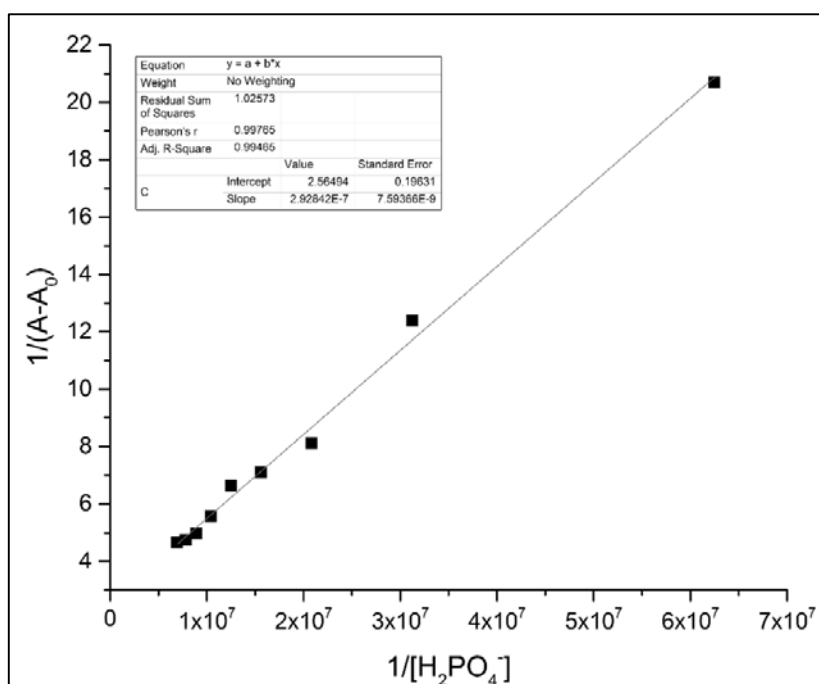


Fig. 5.21 B-H plot for S3R2-TBAH₂PO₄ complex

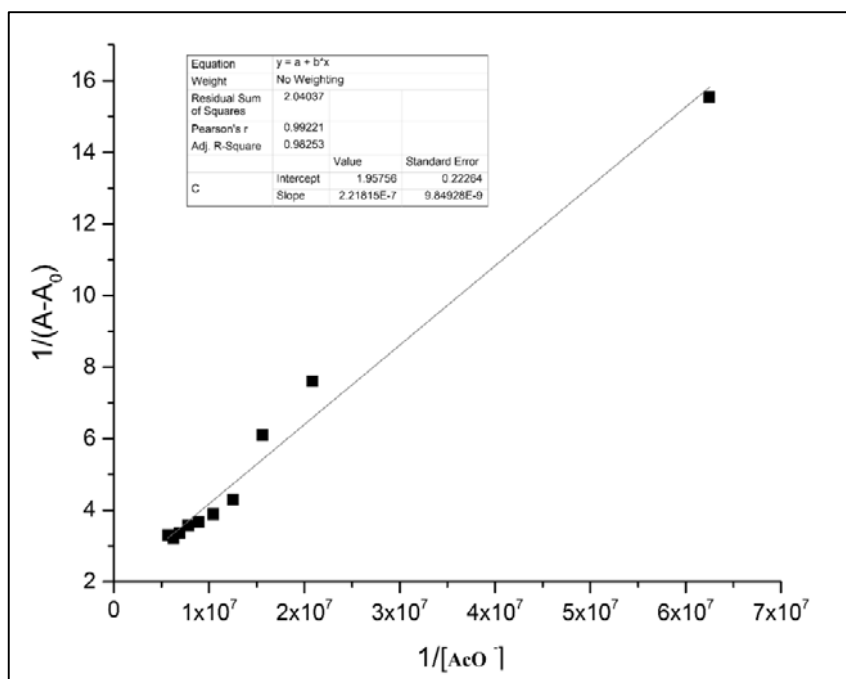


Fig. 5.22 B-H plot for **S3R2**-TBAcO complex

Similarly, titration studies have been performed with the incremental addition of F^- , $H_2PO_4^-$ and AcO^- ions to **S5R3**, wherein the band centered at 405 nm decreased in its intensity with the gradual appearance of new red shift band at 442 nm, 443 nm and 442 nm respectively. Isobestic points at 442 nm for F^- and AcO^- ions and 443 nm for $H_2PO_4^-$ ions represent complex formation in the anion binding process. Titration profile are represented in Fig. 5.23, Fig. 5.24 and Fig. 5.25. The corresponding B-H plot are shown in Fig. 5.26, Fig. 5.27 and Fig. 5.28.

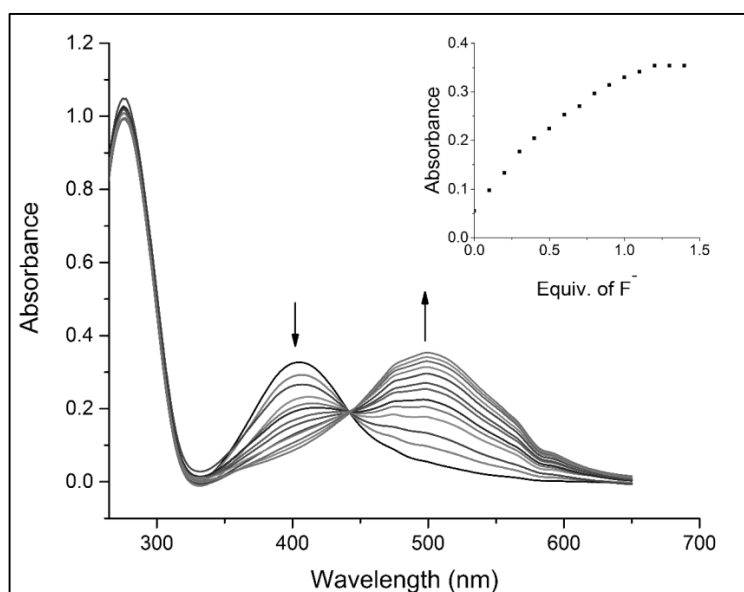


Fig. 5.23 UV-Vis titration spectra of receptor **S3R3** (10^{-5} M in DMSO) with the incremental addition of TBAF (10^{-2} M in DMSO); Inset plot representing the variation of absorbance with increasing concentration of TBAF

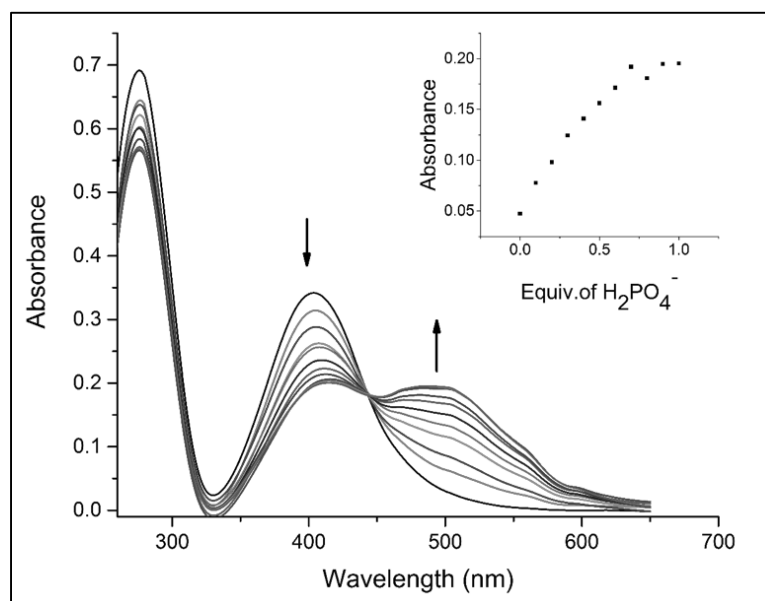


Fig. 5.24 UV-Vis titration spectra of receptor **S3R3** (10^{-5} M in DMSO) with the incremental addition of TBAH₂PO₄ (10^{-2} M in DMSO); Inset plot representing the variation of absorbance with increasing concentration of TBAH₂PO₄

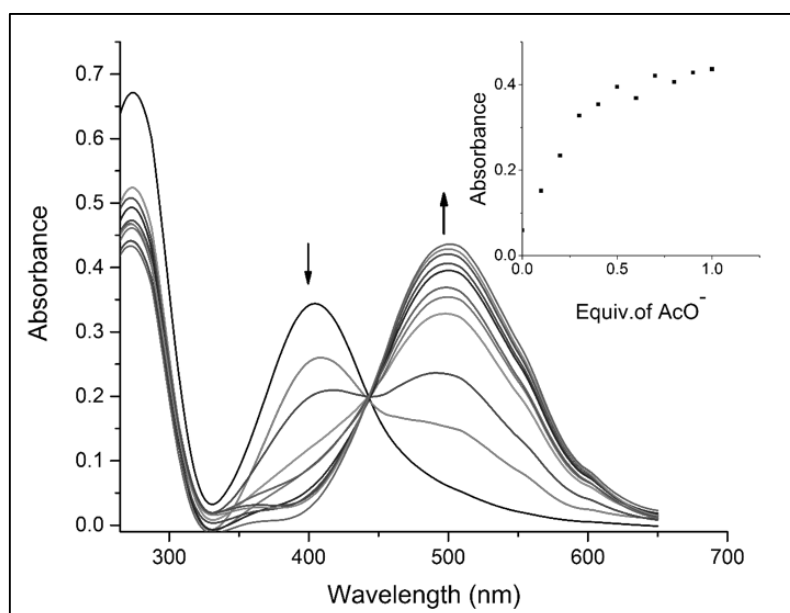


Fig. 5.25 UV-Vis titration spectra of receptor **S3R3** (10^{-5} M in DMSO) with the incremental addition of TBAAcO (10^{-2} M in DMSO); Inset plot representing the variation of absorbance with increasing concentration of TBAAcO

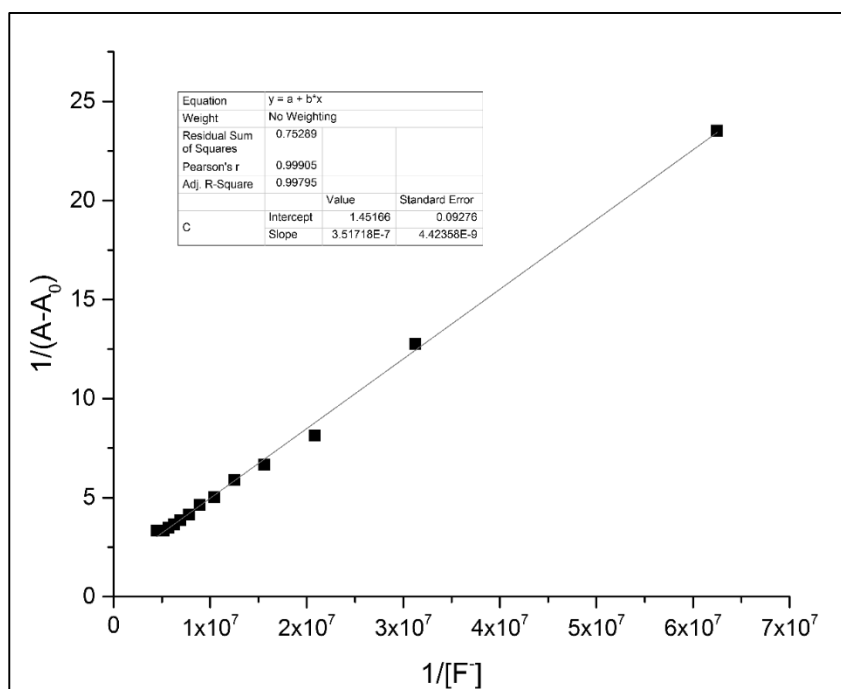


Fig. 5.26 B-H plot for **S3R3-TBAF** complex

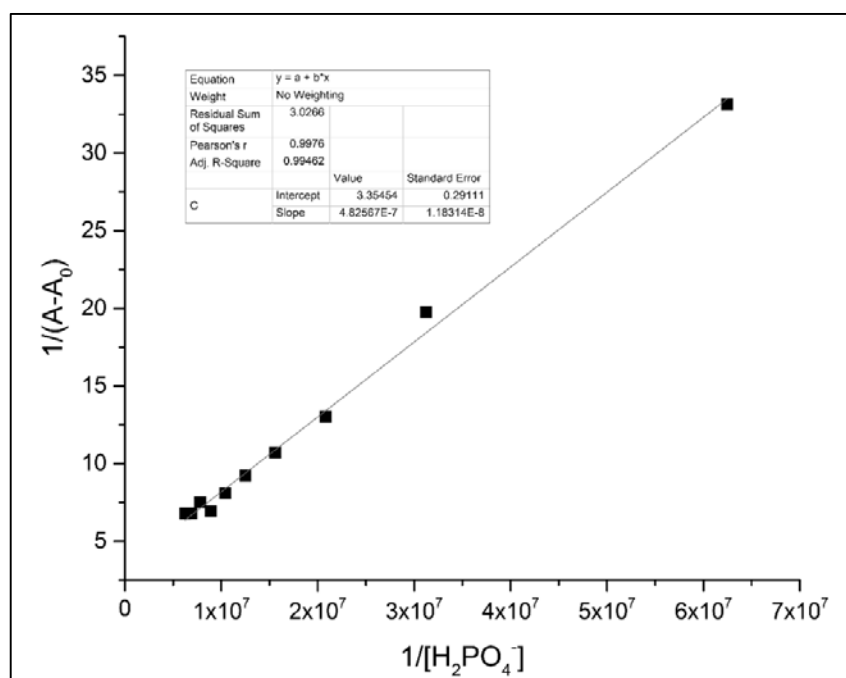


Fig. 5.27 B-H plot for S3R3-TBAH₂PO₄ complex

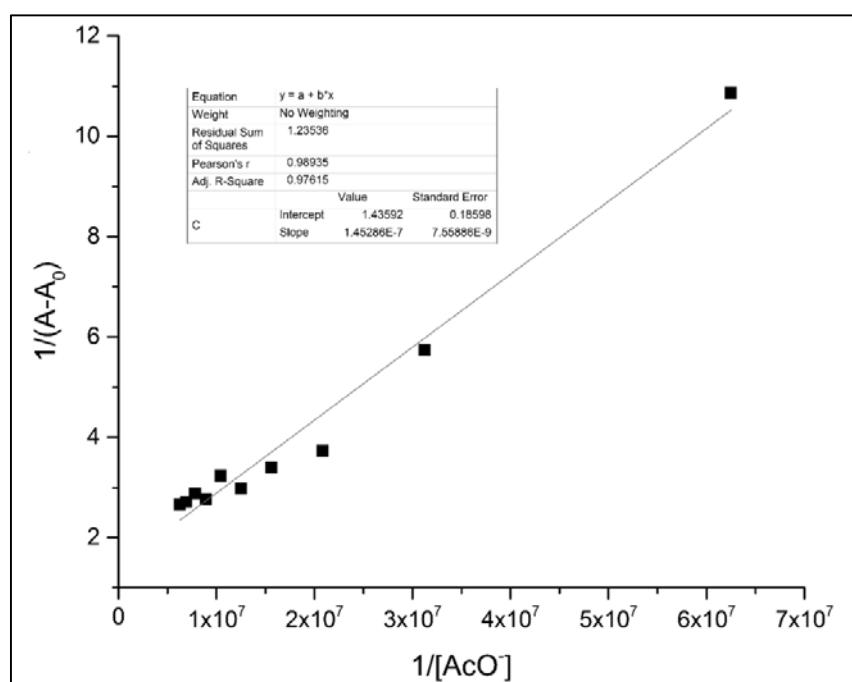


Fig. 5.28 B-H plot for S3R3-TBAAcO complex

Detection of sodium salt of anions by the receptors is highly necessary as it paves way for practical applications. Sodium fluoride is an essential ingredient of

toothpaste and mouthwash; sodium acetate is commonly found in vinegar. With this in view, UV-Vis studies have been performed with the addition of sodium salt of anions to receptors. With the incremental addition of F^- , $H_2PO_4^-$ and AcO^- ions to **S3R1**, **S3R2** and **S3R3**, the shift in absorption maxima reflected similarity with the titration profile obtained with the addition of TBA salts of anions. The titration profiles are represented in Fig. 5.29, Fig. 5.30, Fig. 5.31, Fig. 5.32, Fig. 5.33 and Fig. 5.34. The corresponding B-H plot are represented in Fig. 5.35, Fig. 5.36, Fig. 5.37, Fig. 5.38, Fig. 5.39 and Fig. 5.40.

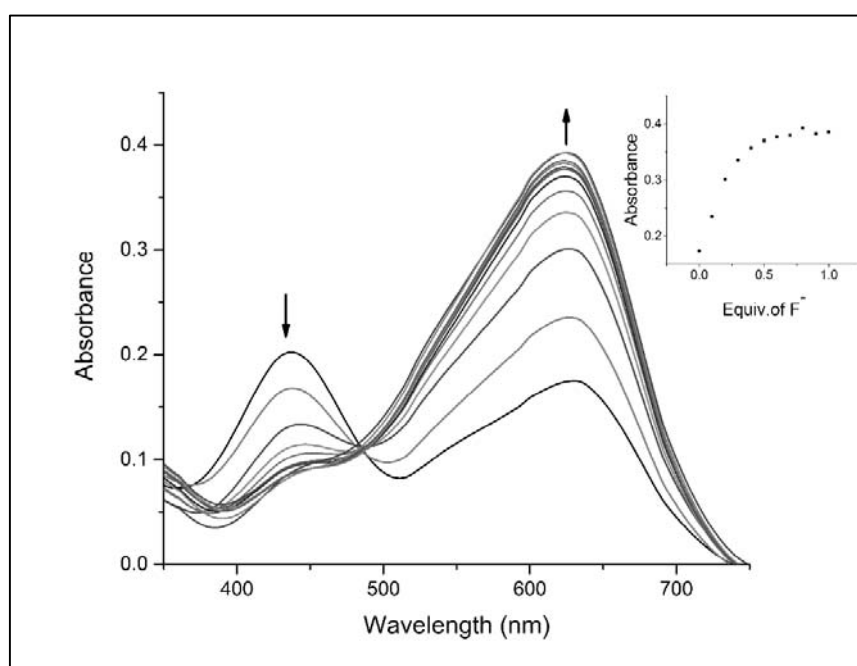


Fig. 5.29 UV-Vis titration spectra of receptor **S3R1** (10^{-5} M in DMSO) with the incremental addition of NaF (10^{-2} M in H_2O); Inset plot representing the variation of absorbance with increasing concentration of NaF

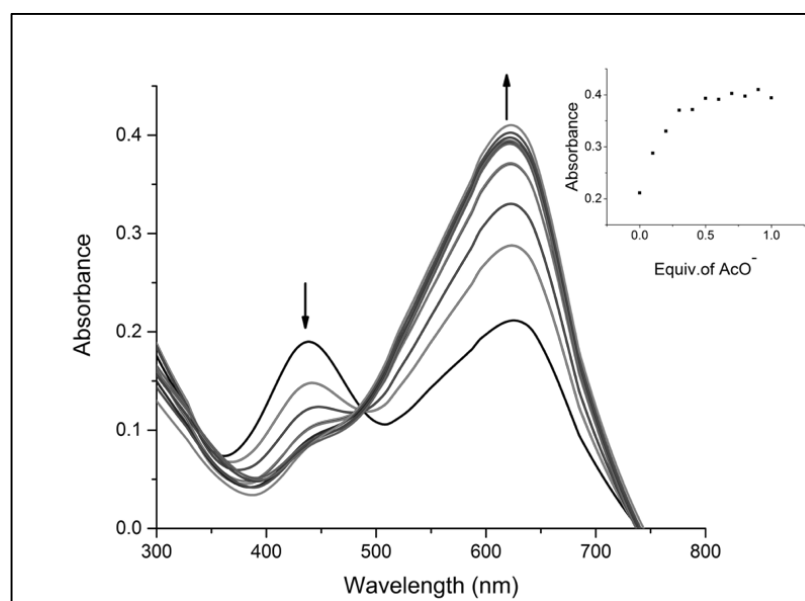


Fig. 5.30 UV-Vis titration spectra of receptor **S3R1** (10^{-5} M in DMSO) with the incremental addition of NaAcO (10^{-2} M in H₂O); Inset plot representing the variation of absorbance with increasing concentration of NaAcO

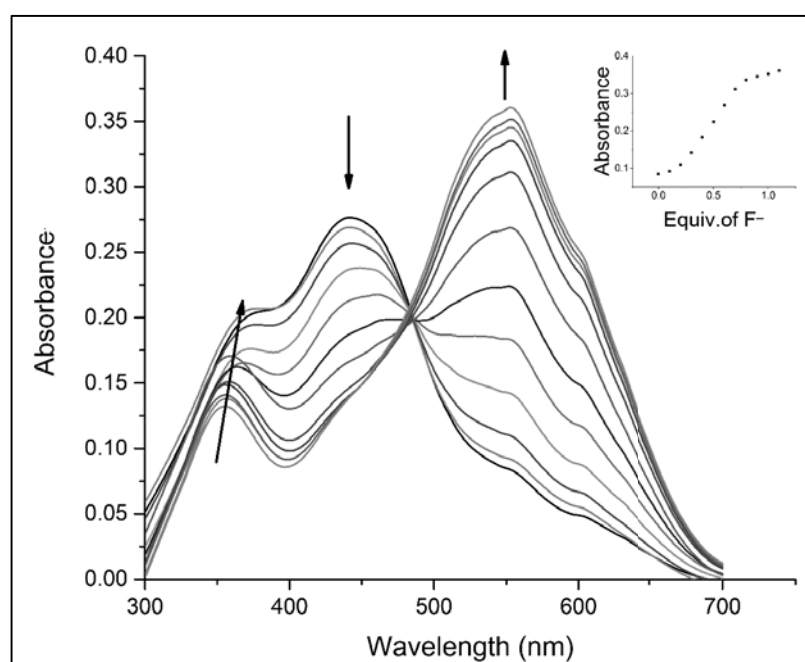


Fig. 5.31 UV-Vis titration spectra of receptor **S3R2** (10^{-5} M in DMSO) with the incremental addition of NaF (10^{-2} M in H₂O); Inset plot representing the variation of absorbance with increasing concentration of NaF

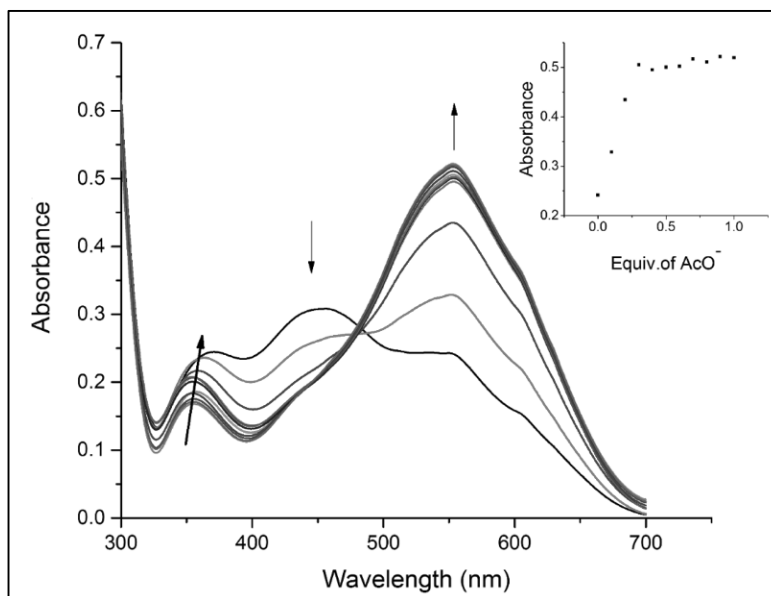


Fig. 5.32 UV-Vis titration spectra of receptor **S3R2** (10^{-5} M in DMSO) with the incremental addition of NaAcO (10^{-2} M in H₂O); Inset plot representing the variation of absorbance with increasing concentration of NaAcO

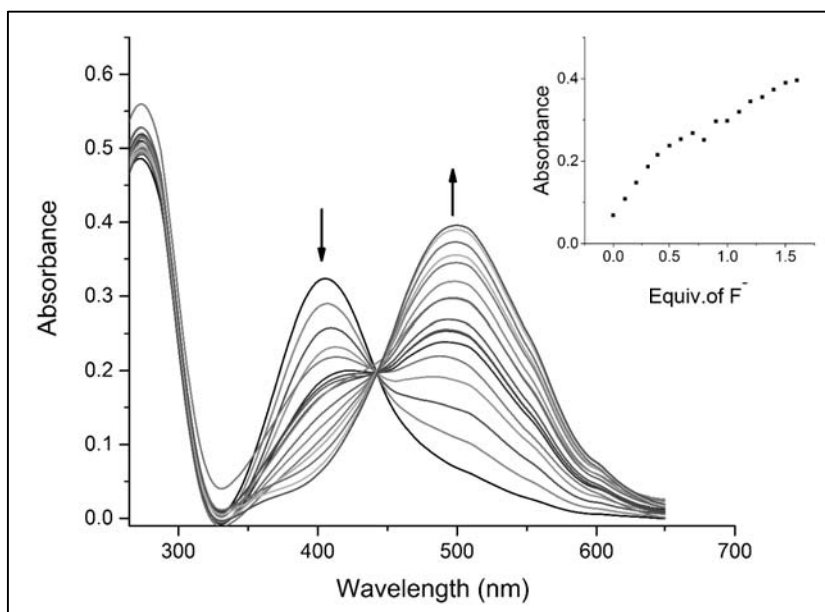


Fig. 5.33 UV-Vis titration spectra of receptor **S3R3** (10^{-5} M in DMSO) with the incremental addition of NaF (10^{-2} M in H₂O); Inset plot representing the variation of absorbance with increasing concentration of NaF

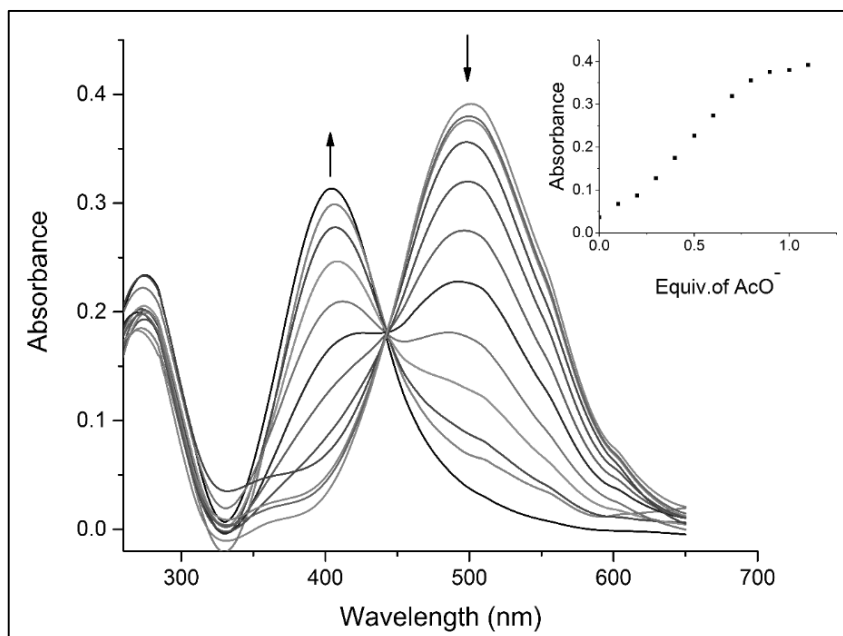


Fig. 5.34 UV-Vis titration spectra of receptor **S3R3** (10^{-5} M in DMSO) with the incremental addition of NaAcO (10^{-2} M in H_2O); Inset plot representing the variation of absorbance with increasing concentration of NaAcO

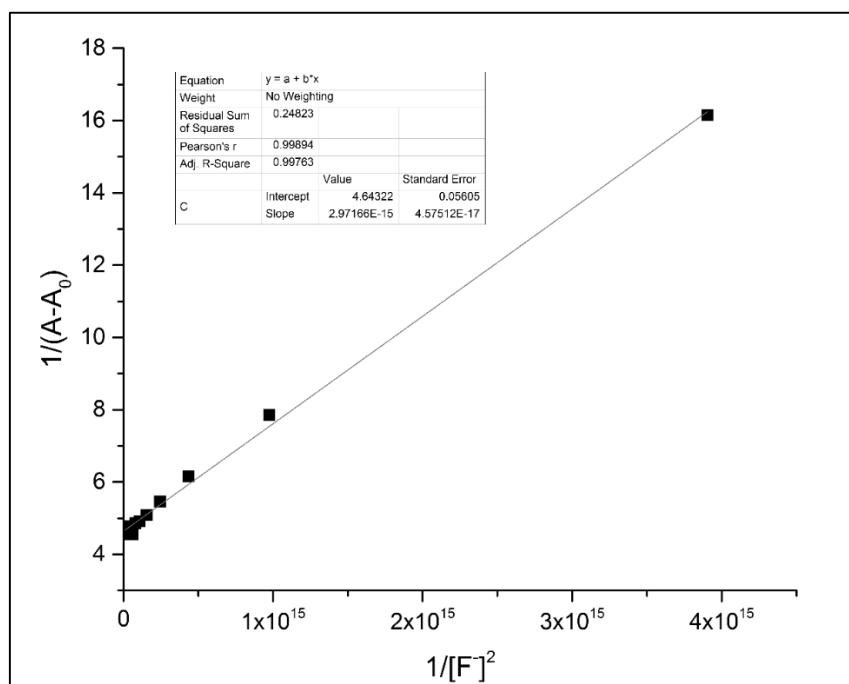


Fig. 5.35 B-H plot for **S3R1**-NaF complex

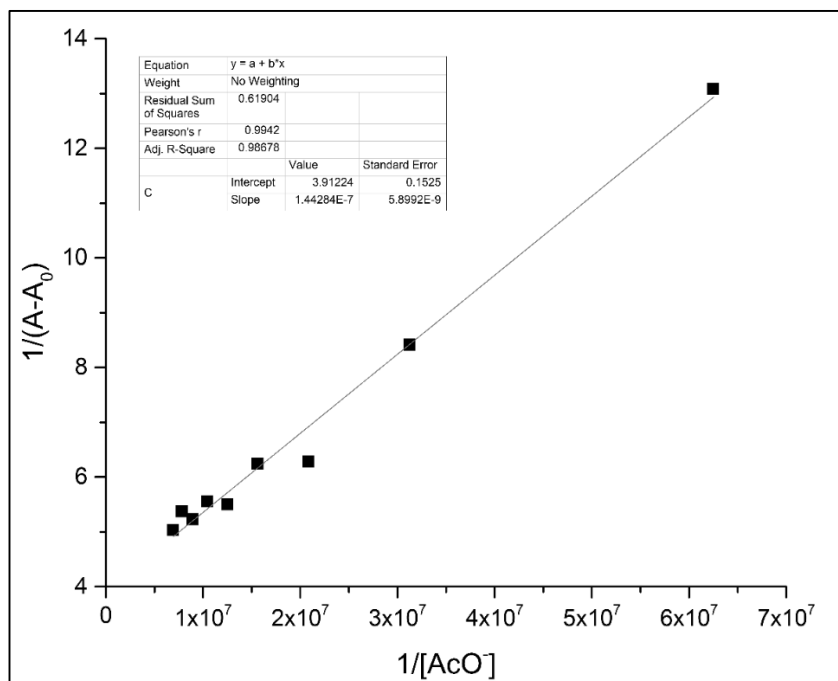


Fig. 5.36 B-H plot for S3R1-NaAcO complex

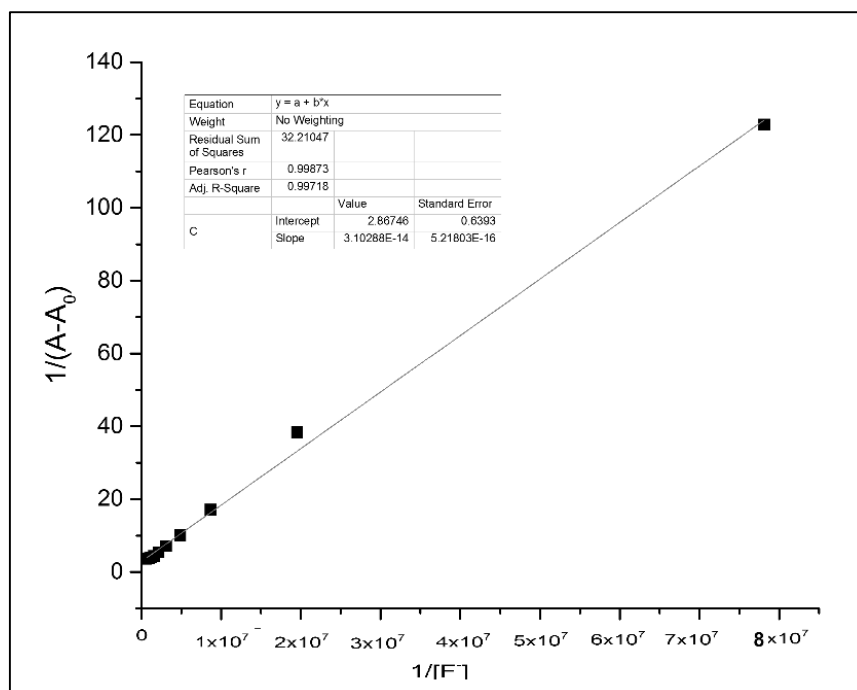


Fig. 5.37 B-H plot for S3R2-NaF complex

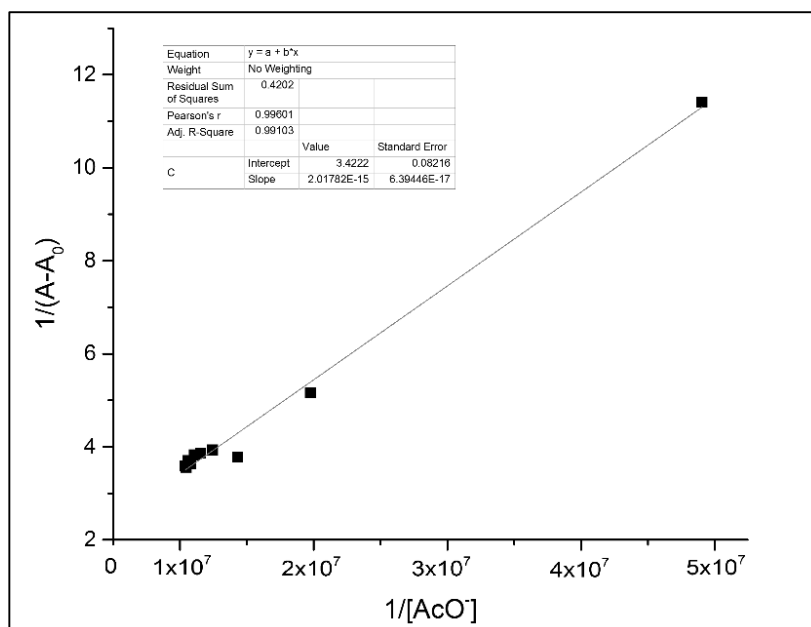


Fig. 5.38 B-H plot for S3R2-NaAcO complex

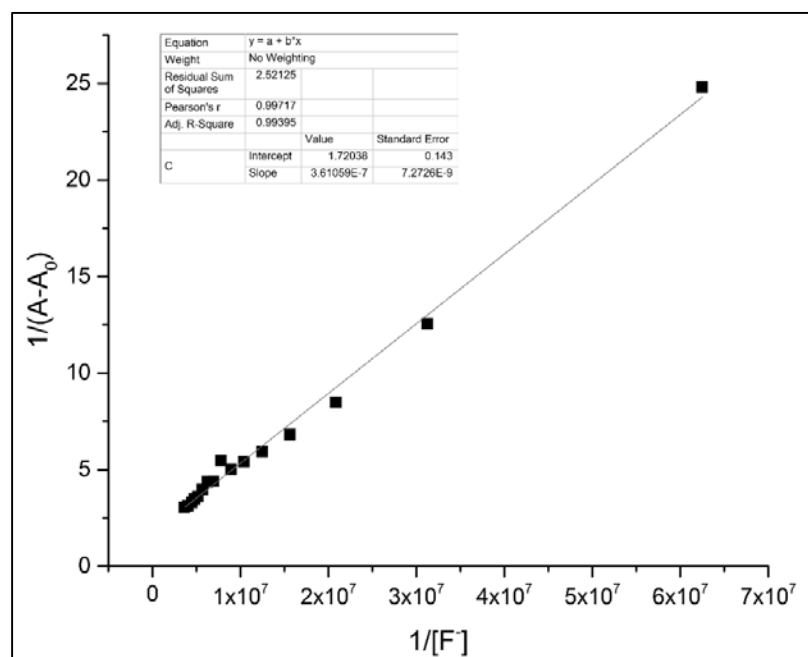


Fig. 5.39 B-H plot for S3R3-NaF complex

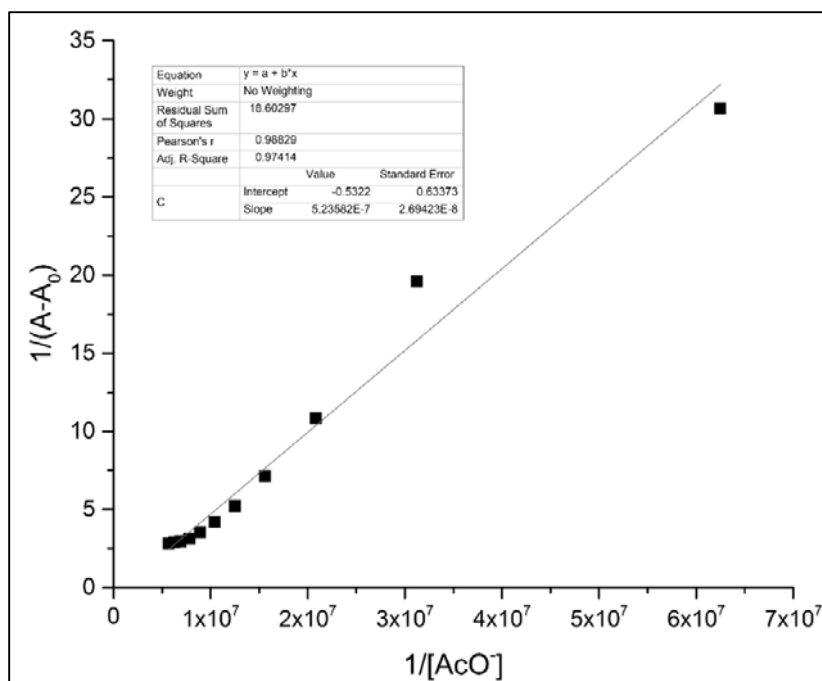


Fig. 5.40 B-H plot for **S3R3**-NaAcO complex

5.3.3 pH dependency studies

Further on, pH dependent studies were performed by introducing HEPES buffer into the receptor solution in DMSO. The receptors **S3R1**, **S3R2** and **S3R3** exhibited selective detection of AcO^- ions among all other anions used in the present study. The color change from pale green to dark green with the addition of AcO^- ion to **S3R1** could be explained based on the ability of $-\text{NH}$ functionality to withstand instant deprotonation in buffer media. The drastic color change observed with the addition of AcO^- ion to **S3R2** and **S3R3** could be attributed to the ease of deprotonation of $-\text{NH}$ functionality upon anion binding unlike **S3R1**. The color change of receptors with the addition of anions is represented in Fig. 5.41. The corresponding UV-Vis spectra are shown in Fig. 5.42, Fig. 5.43 and Fig. 5.44 respectively. Titration studies have been performed with the incremental addition of AcO^- ions to receptor **S3R1**, **S3R2** and **S3R3**, and the titration profile are represented in Fig. 5.45, 5.46 and 5.47 respectively. Binding constant has been calculated using B-H equation and is tabulated in Table 5.1. The occurrence of higher order of binding constant reveals the strength of hydrogen bond involved in binding the anion to the receptor

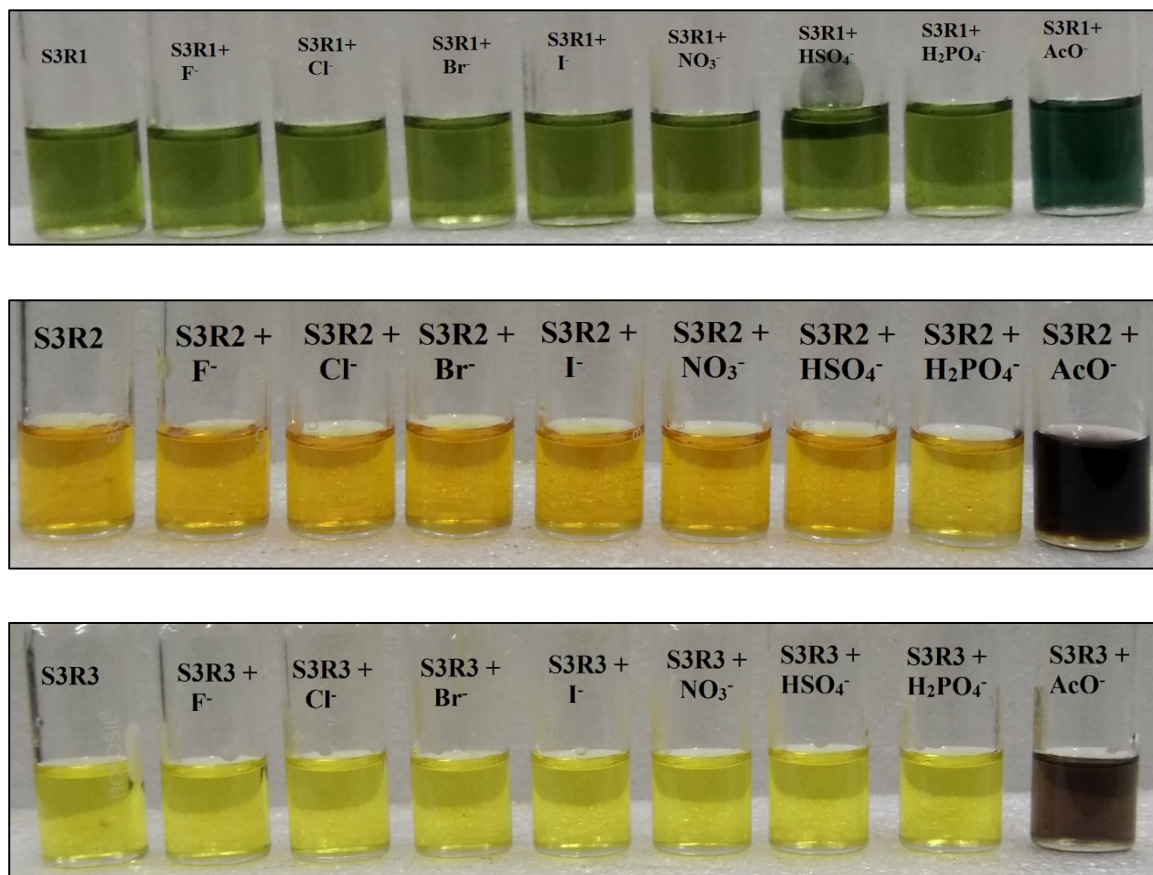


Fig. 5.41 Color change of receptors **S3R1**, **S3R2** and **S3R3** (1×10^{-5} M in HEPES: DMSO, 1:9, v/v) with the addition of TBA salt of anions (1×10^{-2} M in DMSO)

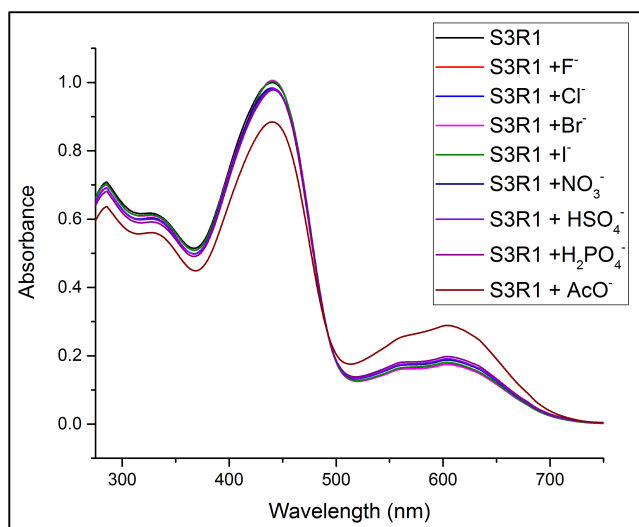


Fig. 5.42 UV-visible absorption spectra of **S3R1** (1×10^{-5} M in HEPES: DMSO, 1:9 v/v) upon addition of 1 equiv. of various anions as TBA salts (1×10^{-2} M in DMSO)

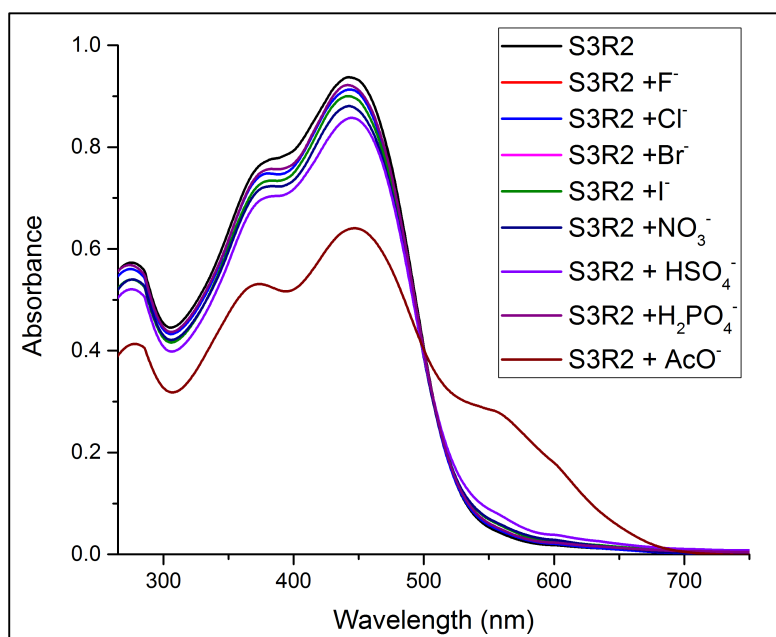


Fig. 5.43 UV-visible absorption spectra of **S3R2** (1×10^{-5} M in HEPES: DMSO, 1:9 v/v) upon addition of 1 equiv. of various anions as TBA salts (1×10^{-2} M in DMSO)

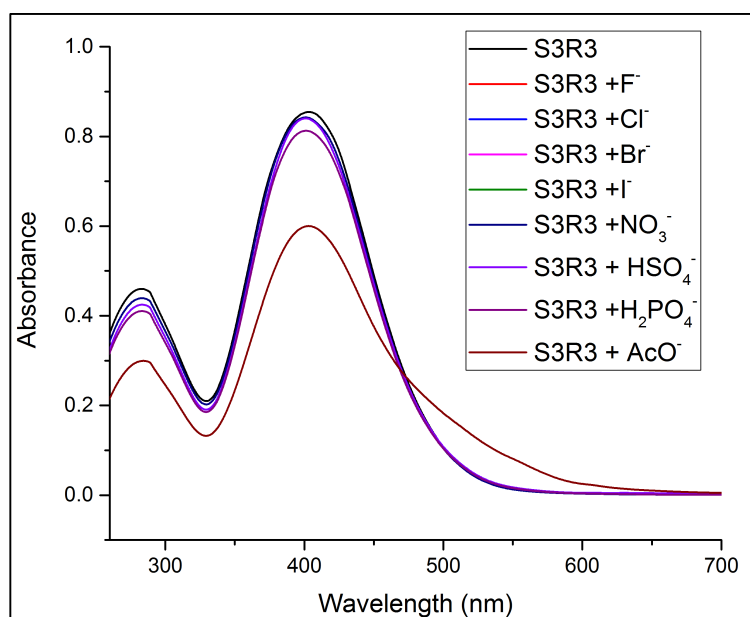


Fig. 5.44 UV-visible absorption spectra of **S3R3** (1×10^{-5} M in HEPES: DMSO, 1:9 v/v) upon addition of 1 equiv. of various anions as TBA salts (1×10^{-2} M in DMSO)

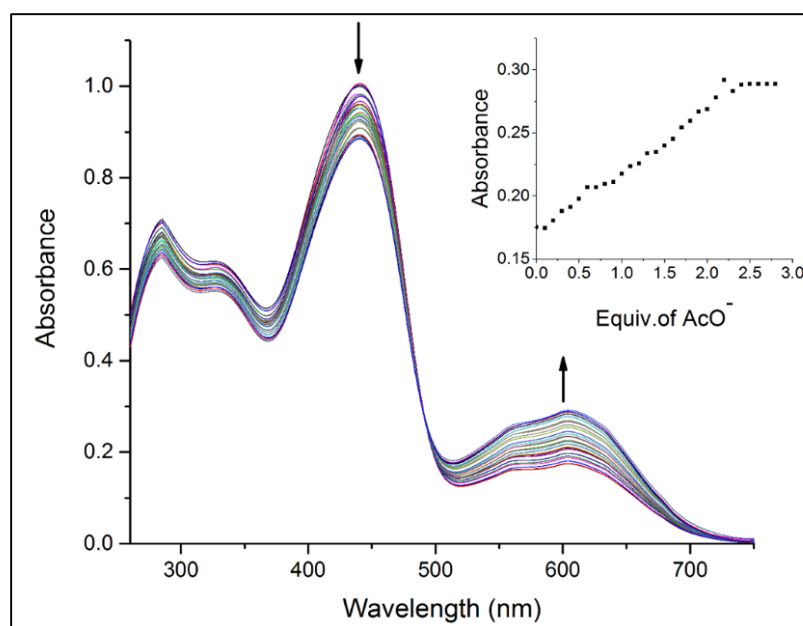


Fig. 5.45 UV-Vis titration spectra of receptor **S3R1** (1×10^{-5} M in HEPES: DMSO, 1:9 v/v) with the incremental addition of TBAAcO (10^{-2} M in DMSO); Inset plot representing the variation of absorbance with increasing concentration of TBAAcO

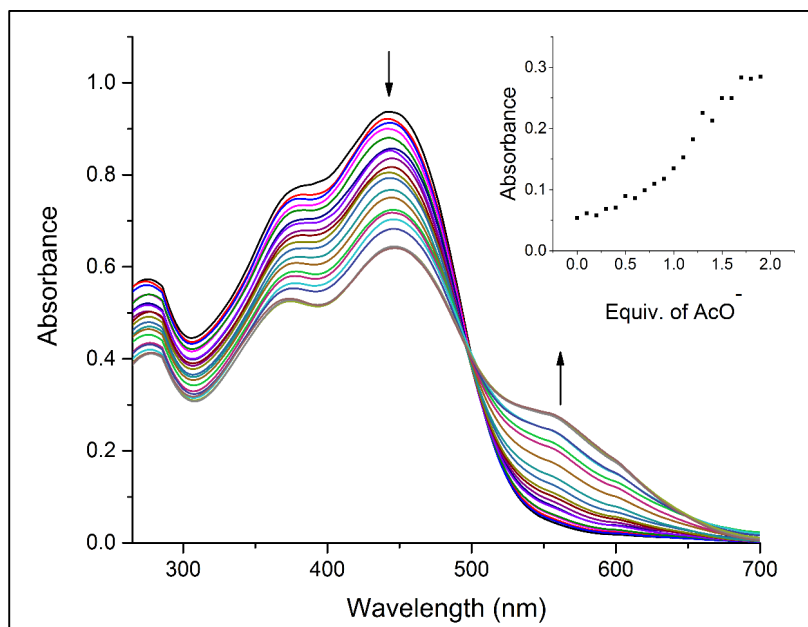


Fig. 5.46 UV-Vis titration spectra of receptor **S3R2** (1×10^{-5} M in HEPES: DMSO, 1:9 v/v) with the incremental addition of TBAAcO (10^{-2} M in DMSO); Inset plot representing the variation of absorbance with increasing concentration of TBAAcO

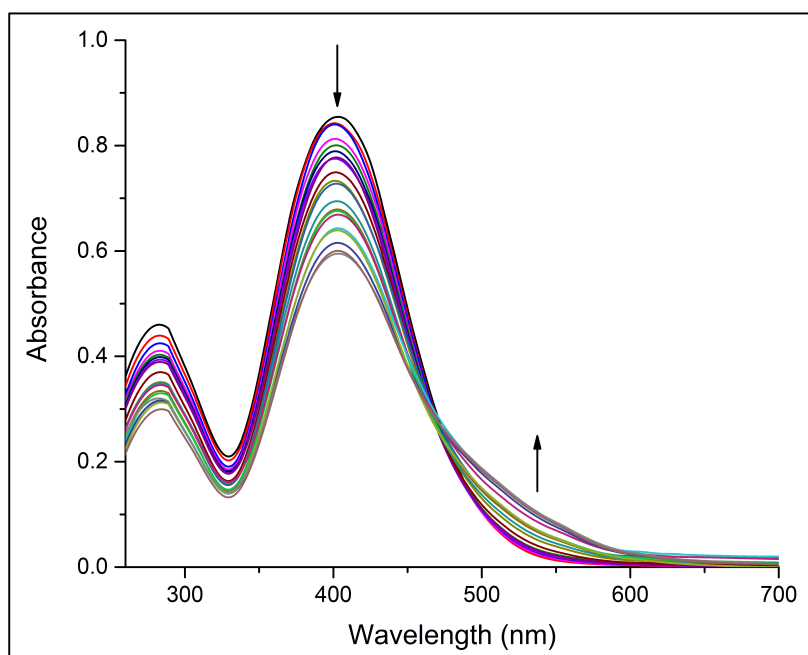


Fig. 5.47 UV-Vis titration spectra of receptor **S3R3** (1×10^{-5} M in HEPES: DMSO, 1:9 v/v) with the incremental addition of TBAAcO (10^{-2} M in DMSO)

5.3.4 Calculation of binding constant from UV-Vis studies

Binding constant has been calculated using Benesi-Hildebrand equation (Benesi and Hildebrand 1948) as given below;

$$1/(A-A_0) = 1/(A_{max} - A_0) + 1/K [X^-]^n (A_{max} - A_0)$$

where, A_0 , A , A_{max} are the absorption considered in the absence of anion, at an intermediate, and at a concentration of saturation. K is binding constant, $[X^-]$ is concentration of anion and n is the stoichiometric ratio.

Table 5.1 Binding constant and detection limit of receptors **S3R1**, **S3R2** and **S3R3** with active anions

Receptor	Ions	Binding constant	Detection limit (ppm)
S3R1	F ⁻ (TBAF)	2.3 x 10¹⁵ M⁻²	1.23
	H ₂ PO ₄ ⁻ (TBAH ₂ PO ₄)	3.8 x 10 ⁷ M ⁻¹	2.18
	AcO ⁻ (TBAAcO)	2.52 x 10 ⁷ M ⁻¹	1.98
	F ⁻ (NaF)	1.5 x 10 ¹⁵ M ⁻²	0.89
	AcO ⁻ (NaAcO)	2.7 x 10 ⁷ M ⁻¹	0.78
S3R2	F ⁻ (TBAF)	0.88 x 10 ¹⁴ M ⁻²	2.34
	H ₂ PO ₄ ⁻ (TBAH ₂ PO ₄)	0.87 x 10 ⁷ M ⁻¹	3.67
	AcO ⁻ (TBAAcO)	1.8 x 10 ⁷ M ⁻¹	2.31
	F ⁻ (NaF)	0.92 x 10¹⁴ M⁻²	0.62
	AcO ⁻ (NaAcO)	1.7 x 10 ⁷ M ⁻¹	0.58
S3R3	F ⁻ (TBAF)	0.412 x 10 ⁷ M ⁻¹	3.45
	H ₂ PO ₄ ⁻ (TBAH ₂ PO ₄)	0.69 x 10 ⁷ M ⁻¹	2.13
	AcO ⁻ (TBAAcO)	0.98 x 10⁷ M⁻¹	3.73
	F ⁻ (NaF)	0.47 x 10 ⁷ M ⁻¹	0.83
	AcO ⁻ (NaAcO)	0.102 x 10 ⁷ M ⁻¹	0.97

5.3.5 ^1H -NMR titration studies

^1H -NMR spectra were recorded to understand binding mechanism, with the addition of 1 eq. of AcO^- ions to receptor **S3R1**, **S3R2** and **S3R3**. The disappearance of proton signal corresponding to $-\text{NH}$ functionality is a clear indication of deprotonation involved in the anion binding mechanism. The ^1H -NMR spectra are represented in Fig. 5.48, Fig. 5.49 and Fig. 5.50 respectively.

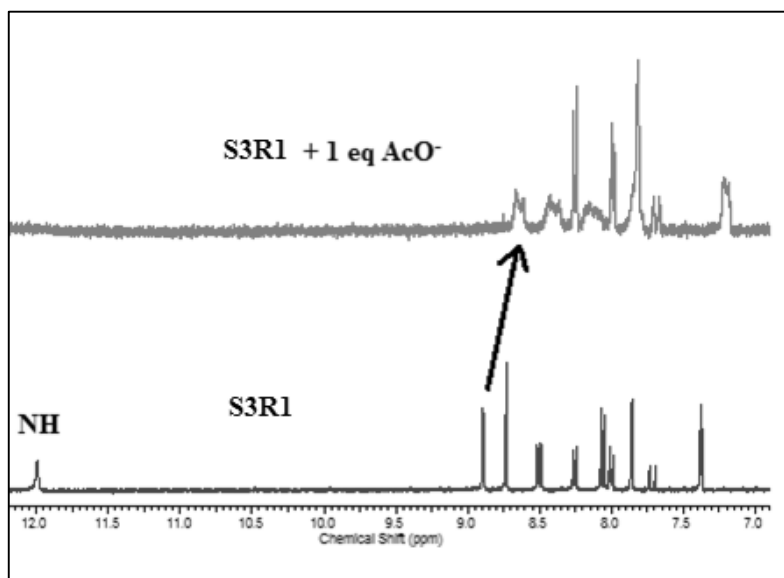


Fig. 5.48 ^1H NMR titration spectrum of receptor **S3R1** with the addition of TBAAcO

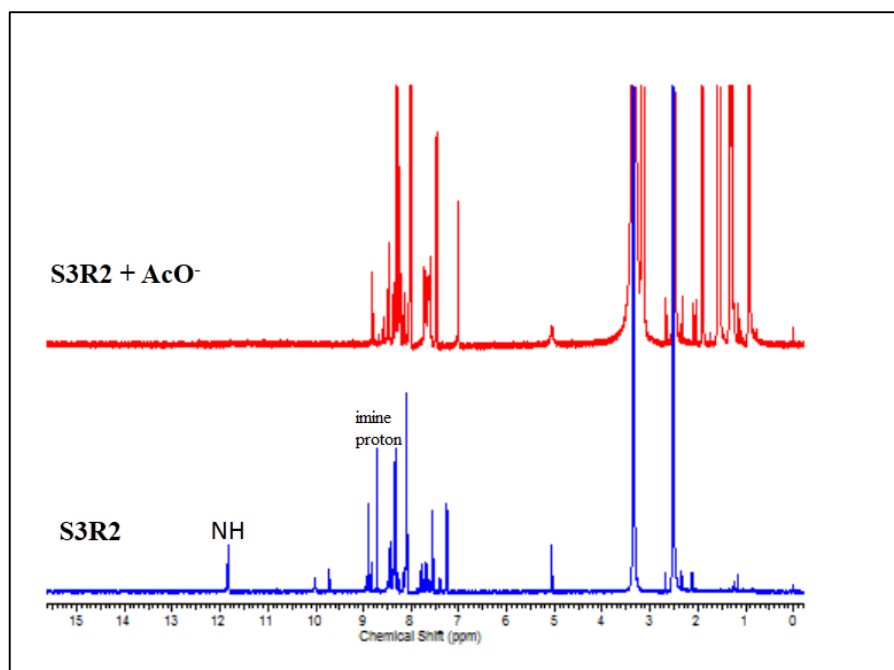


Fig. 5.49 ¹H NMR titration spectrum of receptor **S3R2** with the addition of TBAAcO

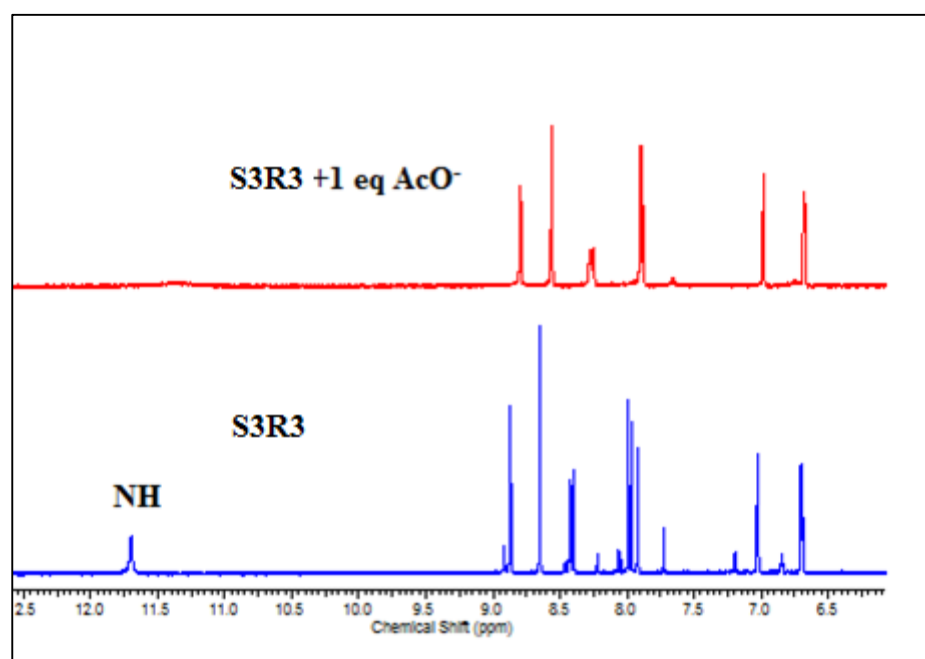
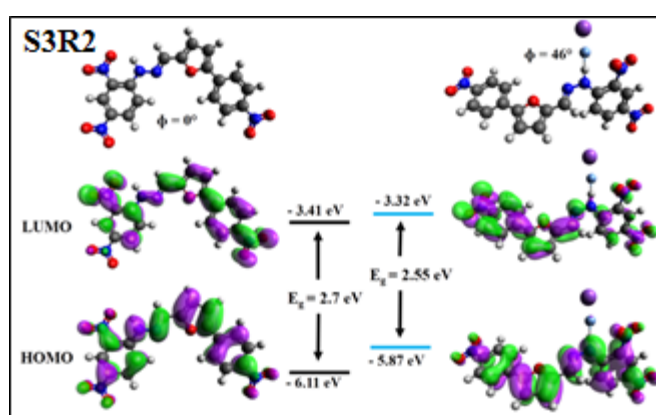
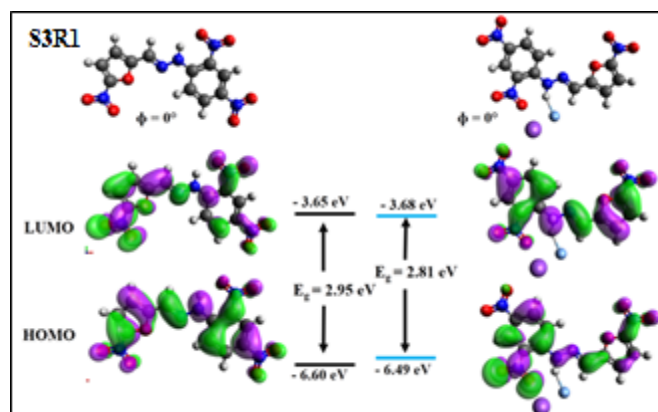


Fig. 5.50 ¹H NMR titration spectrum of receptor **S3R3** with the addition of TBAAcO

5.3.6 DFT Studies

The geometrical and electronic properties of the molecules were performed using Gaussian 09 package, in order to study the structure–property relationship. Singlet ground state optimization of the geometry was achieved by means of the B3LYP with the 6-311++G (d, p) basis set and electronic orbitals were visualized using Avogadro software. The effect of solvent on the energy parameters of the molecules was incorporated by self-consistent reaction field using conductor polarizable continuum model (SCRF-CPCM). Vertical transition energies up to first 10 singlet excited states and molar extinction coefficients of the entire series in solvent phase was estimated.



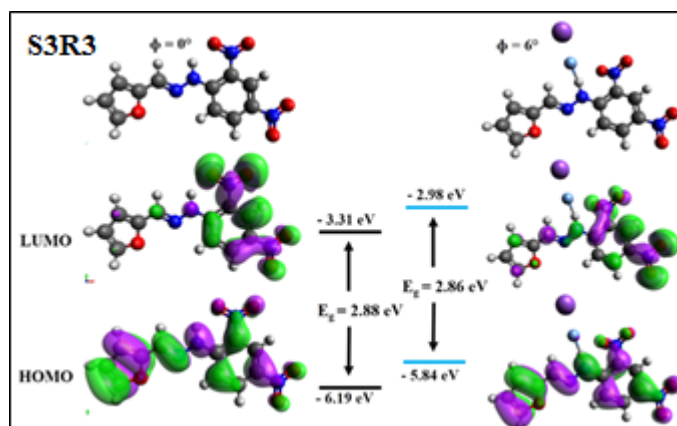


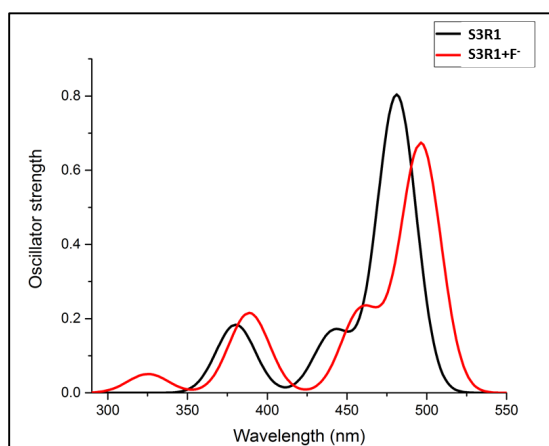
Fig. 5.51 Molecular orbitals of receptors **S3R1**, **S3R2** and **S3R3** and receptor-anion complex with their energy levels at 6-31+G (d,p)

Ground state optimized geometry of the series shows that the bare receptors of the series possess no dihedral angle. Receptor **S3R2** and **S3R3** upon binding with F^- ion lose their planarity and exhibits a steric hindrance in their structure with a dihedral angle of 46° and 6° respectively, while **S3R1** doesn't show any steric hindrance in their structure upon binding. Fig. 5.51 shows the spatial orbital distributions of the entire molecular series of bare receptors and ion bound receptors. Receptor **S3R1**, due to its structural planarity have their HOMO and LUMO spread across the entire molecular network and remains the same upon binding with the F^- ion. **S3R2**, prior to binding with ion exhibits a good structural planarity having their entire HOMO-LUMO distributed on the structure, and upon binding with F^- ion possess a dihedral angle which in turn delocalizes HOMO completely on the entire structure and LUMO localized. HOMO levels of receptor **S3R3** is delocalized on the entire network and LUMO localized only on the nitro phenyl moiety, the distribution of HOMO-LUMO of **S3R3** remains the same upon binding with the F^- ion. The energy value of HOMO and LUMO of the free receptors alter upon binding with the ion. Receptor **S3R1** possess a HOMO-LUMO value of -6.6 eV, - 3.65 eV with a bandgap value of 2.74 eV, upon binding with F^- ion, the bandgap is lowered to 2.55 eV, with HOMO being - 6.49 and LUMO being -3.68 eV. Receptor **S3R2** and **S3R3** show a change in bandgap with a value of 2.55 eV and 2.86 eV upon binding with F^- ion respectively and their corresponding HOMO and LUMO values are tabulated in Table 5.2.

Table 5.2. Energy distribution of receptor and receptor-anion complex

Receptor	HOMO (eV)	LUMO (eV)	E _g (eV)
S3R1	-6.60	-3.65	2.95
S3R1+F⁻	-6.49	-3.68	2.81
S3R2	-6.11	-3.41	2.70
S3R2+F⁻	-5.87	-3.32	2.55
S3R3	-6.19	-3.31	2.88
S3R3+F⁻	-5.84	-2.98	2.86

TD-DFT calculations were performed on the receptors to predict excited state transition and the nature of absorption bands in DMSO as a solvent. Receptors and receptor-anion complex were optimized in DMSO and then their excited state properties were computed. Singlet excited state transition of the receptors and the complex for entire series is as given in the Fig. 5.52, 5.53 and 5.54. The correlation between the experimental and theoretical results further confirm the anion binding event.

**Fig. 5.52** DFT derived UV-Vis spectra of the **S3R1** and **S3R1+F⁻** complex

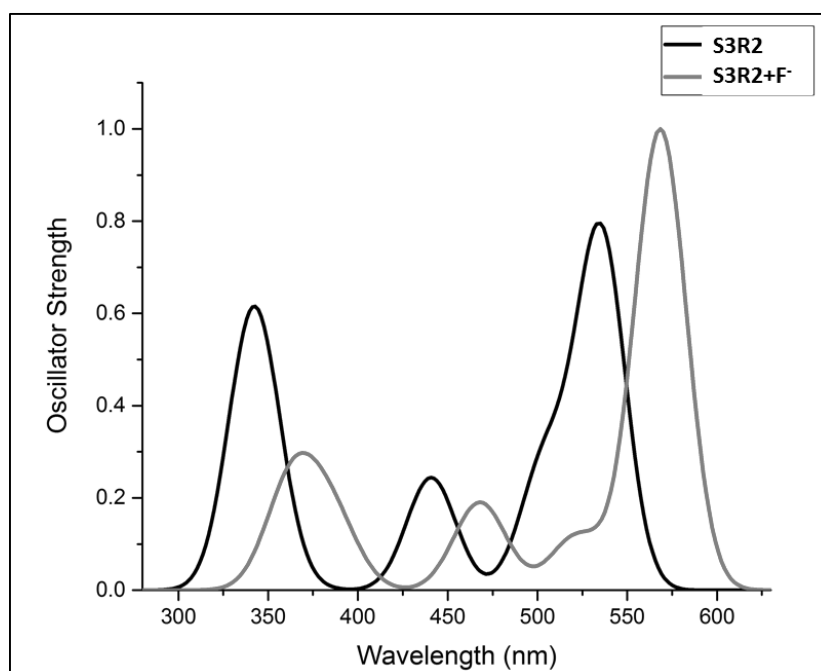


Fig. 5.53 DFT derived UV-Vis spectra of the **S3R2** and **S3R2+ F⁻** complex

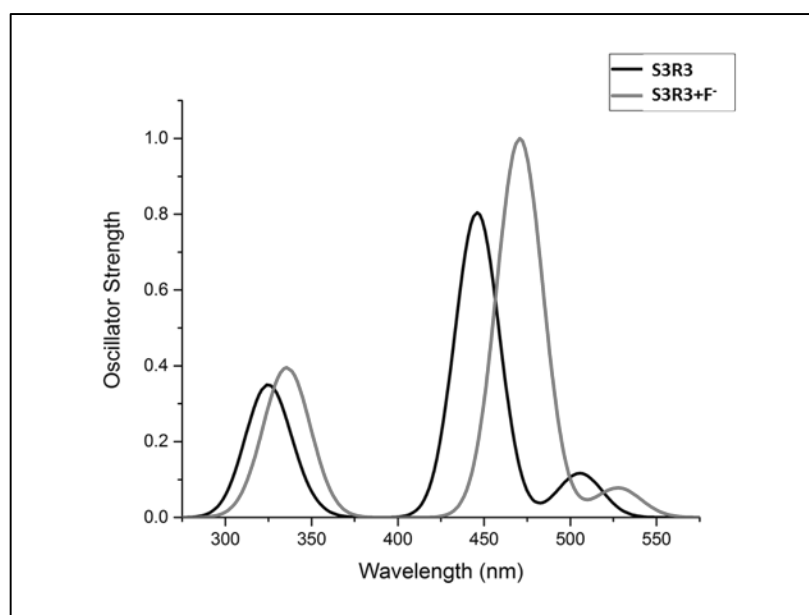
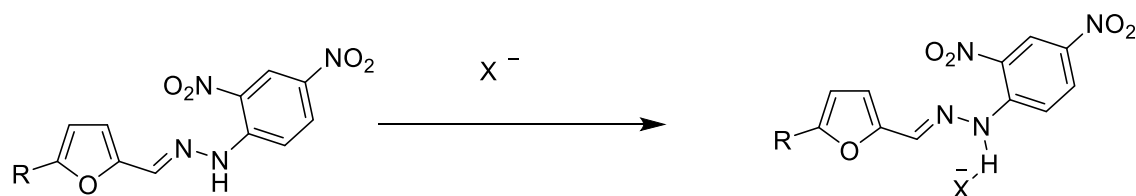


Fig. 5.54 DFT derived UV-Vis spectra of the **S3R3** and **S3R3+ F⁻** complex

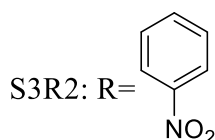
5.3.7 Binding mechanism

The proposed binding mechanism of receptors **S3R1**, **S3R2** and **S3R3** is shown in Scheme 5.2.



Where,

S3R1: R= NO₂



S3R3: R= H

X = F⁻, H₂PO₄⁻, AcO⁻

Scheme 5.2 Proposed binding mechanism of receptors **S3R1**, **S3R2** and **S3R3** with anions

5.3.8 Biological applications

Selective detection of acetate by the receptors drives in the need to investigate the application of receptor at physiological level. *E. coli* BL21 produces acetate by consuming glucose. The receptor-acetate complex produced fluorescence at excitation wavelength of 365 nm. Fig. 5.55 shows the fluorescence observed due to binding of acetate receptor with acetate produced in each well. The amount of acetate produced increased with *E. coli* BL21 growth, which is clearly visible under fluorescent light. Blank sample containing only LB medium did not show any fluorescence. High levels of acetate-receptor fluorescence have been observed on a glass plate. This shows excellent specificity to acetate ions.

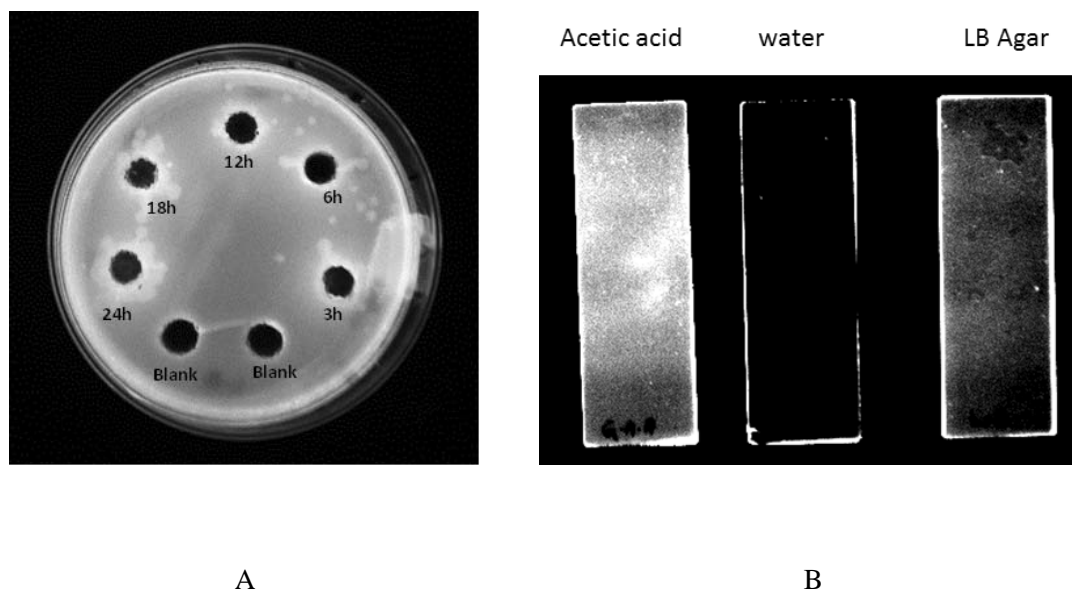


Fig. 5.55 (A) Fluorescence observed using *E.coli* BL21 at different time intervals of the growth in LB Agar plate, (B) fluorescence observed by acetic acid, water and LB agar, respectively, on a glass plate

5.4 CONCLUSIONS

Three new furan derivatives **S3R1**, **S3R2** and **S3R3** have been synthesized and their ion sensing abilities have been investigated by spectroscopic techniques. Visually observable color change of receptor **S3R1**, **S3R2** and **S3R3** towards AcO^- ions in buffer media reflects the selective sensing ability. ^1H NMR titration studies confirms the deprotonation process involved in the binding mechanism. Higher order of the binding constant reflects the strength of receptor-anion complex. Lower detection limit value of 0.78 ppm, 0.58 ppm and 0.97 ppm of receptor **S3R1**, **S3R2** and **S3R3** towards AcO^- ions has been achieved. Receptor **S3R1** could successfully detect the acetate ion produced in *E. coli* BL21 by exhibiting a visible fluorescence implying its utility in biological applications.

CHAPTER 6

RATIONALLY DESIGNED MULTI-ANION RESPONSIVE COLORIMETRIC RECEPTOR: AN INSIGHT ON THE EFFECTIVE INTERPLAY OF CHEMISTRY AND BIOLOGY IN REAL LIFE APPLICATIONS



Abstract

In this chapter, design, syntheses and characterization of three organic receptors have been described. The applicability of the receptors in the colorimetric detection of anions have been discussed in detail through UV-Vis spectrophotometric, spectrofluorometric, ¹H-NMR titration and electrochemical studies. The binding mechanism of the receptor towards active anion has been included. DNA binding studies, detection of cyanide ion in potato sprouts in support of the biological applications and detection of phosphate in detergents as an environmental application have been discussed.

6.1 INTRODUCTION

Biological process is primarily known to involve an effective interplay of chemical and biochemical mechanisms. Over recent decades, design of diverse receptors has been one of the most pressing challenges for researchers. The prime focus of researchers all over is on catering the needs of the society by monitoring the environmental pollution, ensuring food safety, improvising disease surveillance; eventually heading towards increasing care on human health (Carter et al. 2014; Grate et al. 2008; Khakh and North 2006; Nolan and Lippard 2008; Qiu 2013). Deoxyribonucleic acid (DNA), being a reservoir of genetic instructions have attracted great attention among molecular biologists and biochemists in a way towards development of DNA molecular probes and new therapeutic reagents (Maiti and Kumar 2007; Mrksich and Dervan 1993). Anticancer drugs, comprised of small organic molecules lead to significant changes in DNA, as a primary intracellular target leading to DNA damage in cancer cells, blocking the cell division and eventually leading to cell death (Cheng et al. 2006; Hecht 2000; Wang et al. 2013; Zuber et al. 1998). The unique properties of Schiff base derived receptors such as anti-carcinogenic, anti-bacterial and anti-fungal nature reflect them as potent DNA repair agents (Vijayalakshmi et al. 2006). The three most probable interactions of receptors include (a) non-covalent interactions such as intercalative

binding between DNA base pairs and ligand, (b) groove binding and (c) static electronic effects (Hurley 2002).

A monomeric unit of DNA is comprised of nucleobases, deoxyribose and a phosphate group. With this in view, the design strategy of Schiff base receptor is of paramount importance in order to dictate the binding of desired anionic species of interest. The intercalative binding of DNA with receptor would be tedious if there exists a higher binding affinity towards phosphate group present on the backbone of DNA in comparison with the nucleobases. Subsequently, the active nature of receptor towards phosphate reflects on the ability to detect arsenic ion owing to the similarity between arsenic and phosphorous in terms of similar atomic radii, the same number of valence electrons, and nearly identical electronegativity and orbital configurations. The resultant similarity is known to be translated to other molecules being formed such as phosphate and arsenate. Extensive study by researchers posits the fact that similarity between the two makes arsenic more dangerous; finding its implication in many homicides and deaths over past 2000 years (Hughes 2002; Moore et al. 1983; Wolfe-Simon et al. 2011).

Replication of DNA is an inherent phenomenon within each living cell. The presence of cyanide is known to inhibit the replication process by reducing the NAD/NADH ratio resulting in substantial number of single stranded interruptions. Higher concentration of cyanide results in depletion of intracellular pool of ATP via inhibition of cytochrome oxidase preventing regeneration of ATP (A Klein and Bonhoeffer 1972; Wickner and Kornberg 1973).

Prompted by the above facts, in quest of artificial receptors active for biologically important anions, a new series of thiadiazole based receptors **S4R1**, **S4R2** and **S4R3** possessing –SH functionality as an anion binding site have been synthesized. Further, the chromogenic signaling output in anion binding event could be fine-tuned by introducing substituent effect on the aromatic ring. Structurally, **S4R1** possesses –NO₂ functionality on the aromatic ring at position *para* to imine substituted thiadiazole group. **S4R2**

comprises of –SH (thiol) functionality and –NO₂ functionality at position *ortho* to the imine functionality. **S4R3** is devoid of any ancillary substituent on it. In the present study, we have reasoned the utility of receptor **S4R1** to be apt as a colorimetric sensor for fluoride (F⁻), acetate (AcO⁻), phosphate (H₂PO₄⁻), cyanide (CN⁻) and arsenite (AsO₂⁻) ions. The anion receptive nature of **S4R1** has been extended to DNA binding studies, cyanogenic glycoside detection in potato sprouts in support of the biological applications and detection of phosphate in detergents as an environmental application.

6.2 EXPERIMENTAL SECTION

6.2.1 Materials and Methods

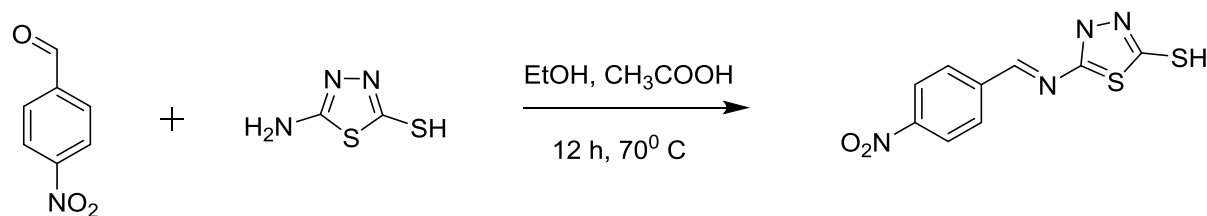
All chemicals and analytical grade reagents were used as bought without any further purification unless otherwise mentioned. Thin layer chromatography was performed using Merck TLC Silica Gel F₂₅₄ plates. Melting point was measured on Stuart SMP3 melting-point apparatus in open capillaries. Infrared spectra were recorded on Bruker alpha FTIR spectrometer. ¹H NMR was performed using Bruker-400 AV-400 spectrometer. Chemical shift values are reported in ppm scale (in *DMSO-d*₆ with Tetramethylsilane as internal standard). Mass spectra was recorded through DART-MS, JMS- T100LC, Accu TOF Mass Spectrometer. UV-Vis experiments were carried out using Jasco V-670 spectrophotometer in standard 3.0 mL quartz cuvette having 1 cm path length. Electrochemical studies were performed using Ivium (vertex) Electrochemical workstation using 50 mV scan rate, potential window –2.0 V to +2.0 V.

6.2.2 Synthesis of receptor **S4R1**

(E)-5-((4-nitrobenzylidene)amino)-1,3,4-thiadiazole-2-thiol

4-nitrobenzaldehyde (0.15 g, 0.99 mmol) and 5-amino-1,3,4-thiadiazole-2-thiol (0.132 g, 0.99 mmol) were refluxed in 5 ml ethanol at 70 °C for 12 h in the presence of drop of acetic acid as catalyst. The formation of the product was confirmed through TLC by the generation of single spot indicative of the disappearance of starting materials. The

reaction mixture was cooled to room temperature, filtered through filter paper and washed with ethanol to obtain pure product.



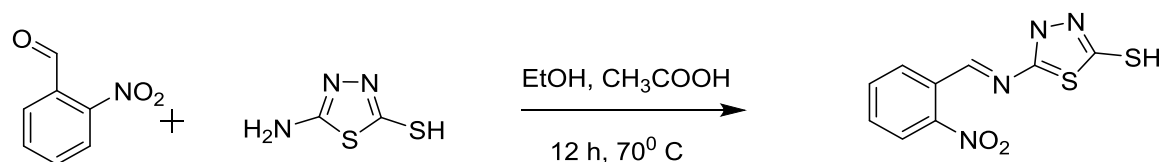
Scheme 6.1 Synthesis of receptor S4R1

Yield: 87 %, melting point: 230 °C, ¹H NMR (DMSO- *d*₆, 400 MHz, ppm): δ 8.18-8.16 (dd, 2H), 8.44-8.42 (dd, 2H), 8.77 (s, imine proton), 13.19 (s, SH). FTIR (KBr) (cm⁻¹): 3258 (SH), 3067 (Ar-CH), 1633 (CH=N), 1339 (NO₂). Mass (ESI): *m/z* Calculated: 265.99 Obtained: 265.35.

6.2.3 Synthesis of receptor S4R2

(E)-5-((2-nitrobenzylidene)amino)-1,3,4-thiadiazole-2-thiol (S4R2)

2-nitrobenzaldehyde (0.15 g, 0.99 mmol) and 5-amino-1,3,4-thiadiazole-2-thiol (0.132 g, 0.99 mmol) were refluxed in 5 ml ethanol at 70 °C for 12 h in the presence of acetic acid as catalyst. The formation of the product was confirmed through TLC by the generation of single spot indicative of the disappearance of starting materials. The reaction mixture was cooled to room temperature, filtered through filter paper and washed with ethanol to obtain pure product.



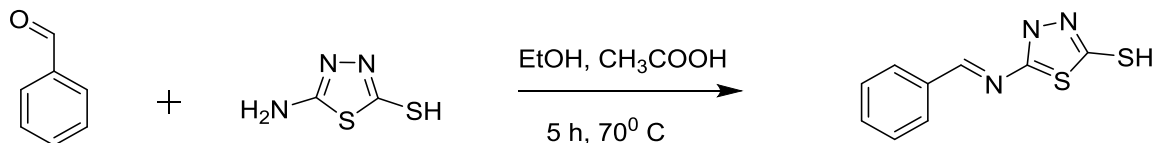
Scheme 6.2 Synthesis of receptor S4R2

Yield: 76%, melting point: 233 °C, ¹H NMR (DMSO- *d*₆, 400 MHz, ppm): δ 7.10 (dd, 2H), 7.78-7.90 (ddd, 2H), 8.15 (s, SH), 8.99 (s, imine proton), 13.18 (s, SH). FTIR (KBr) (cm⁻¹): 3234 (SH), 3083 (Ar-CH), 1603 (CH=N), 1348 (NO₂). Mass (ESI): m/z Calculated: 265.99 Obtained: 265.334.

6.2.4 Synthesis of receptor S4R3

(E)-5-(benzylideneamino)-1,3,4-thiadiazole-2-thiol (S4R3)

Benzaldehyde (0.15 g, 1.41 mmol) and 5-amino-1,3,4-thiadiazole-2-thiol (0.132 g, 1.41 mmol) were refluxed in 5 ml ethanol at 70 °C for 5 h in the presence of acetic acid as catalyst. The formation of the product was confirmed through TLC by the generation of single spot indicative of the disappearance of starting materials. The reaction mixture was cooled to room temperature, filtered through filter paper and washed with ethanol to obtain pure product.



Scheme 6.3 Synthesis of receptor S4R3

Yield: 74 %, melting point: 210 °C, ¹H NMR (DMSO- *d*₆, 400 MHz, ppm): δ 7.12 (dd, 2H), 7.46-7.52 (ddd, 2H), 7.97 (s, SH), 8.71 (s, imine proton), 13.20 (s, SH). FTIR (KBr) (cm⁻¹): 3240 (SH), 3031 (Ar-CH), 1603 (CH=N), 1322 (NO₂). Mass (ESI): m/z Calculated: 221.01 Obtained: 244.129 (M+Ag)⁺

6.2.5 Characterization data of receptors

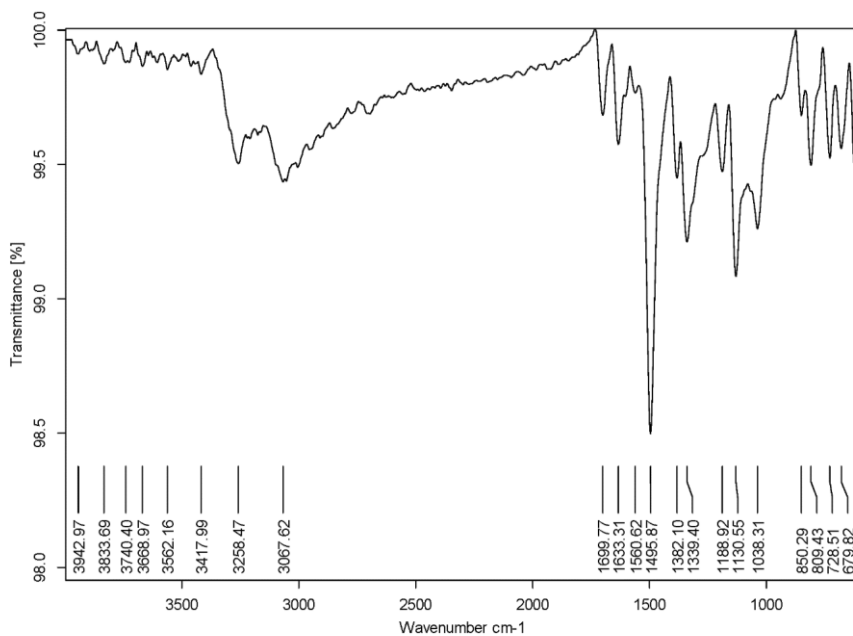


Fig. 6.1 FT-IR spectrum of receptor **S4R1**

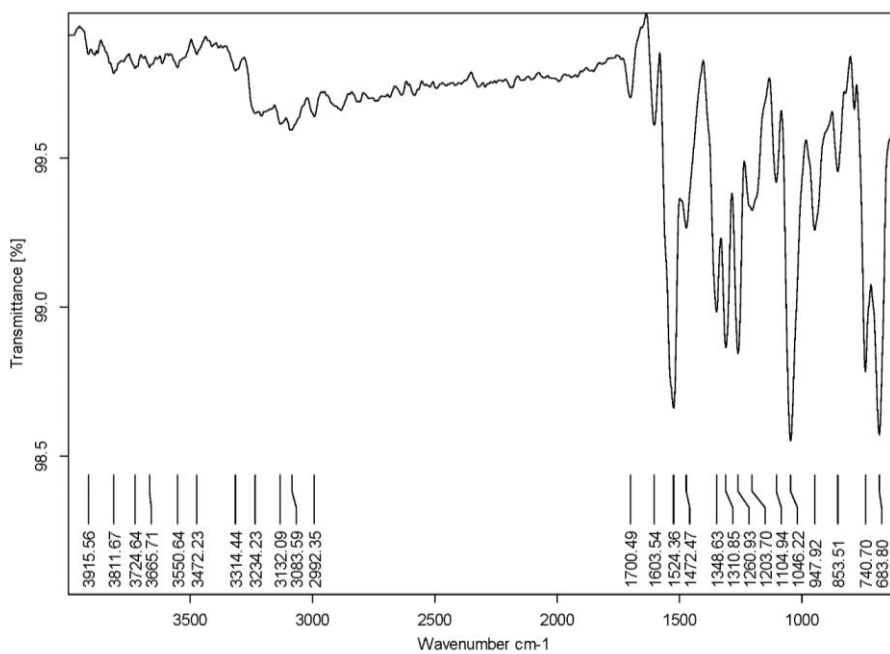


Fig. 6.2 FT-IR spectrum of receptor **S4R2**

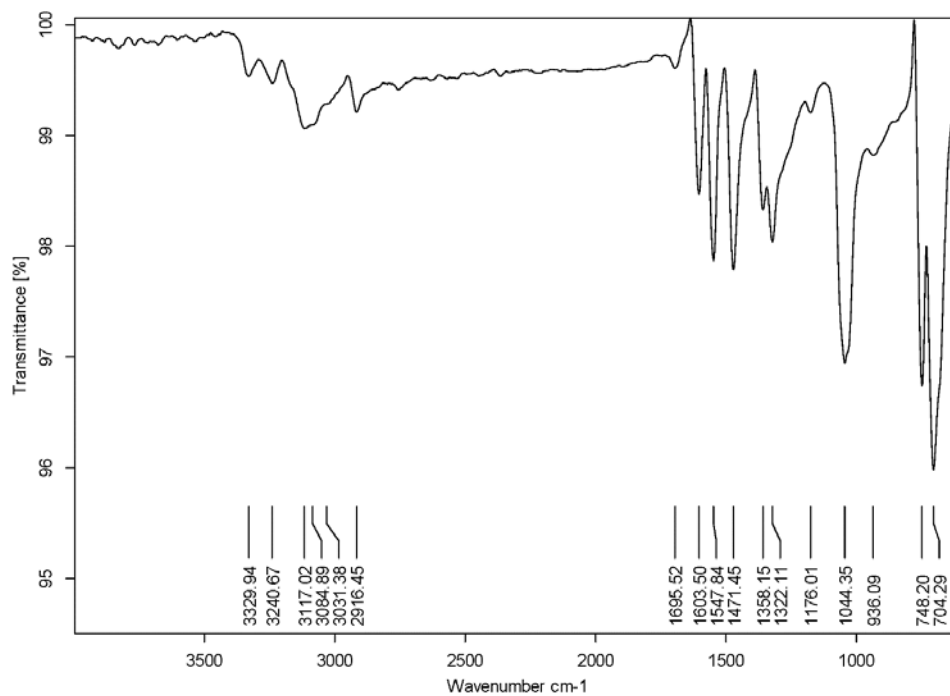


Fig. 6.3 FT-IR spectrum of receptor S4R3

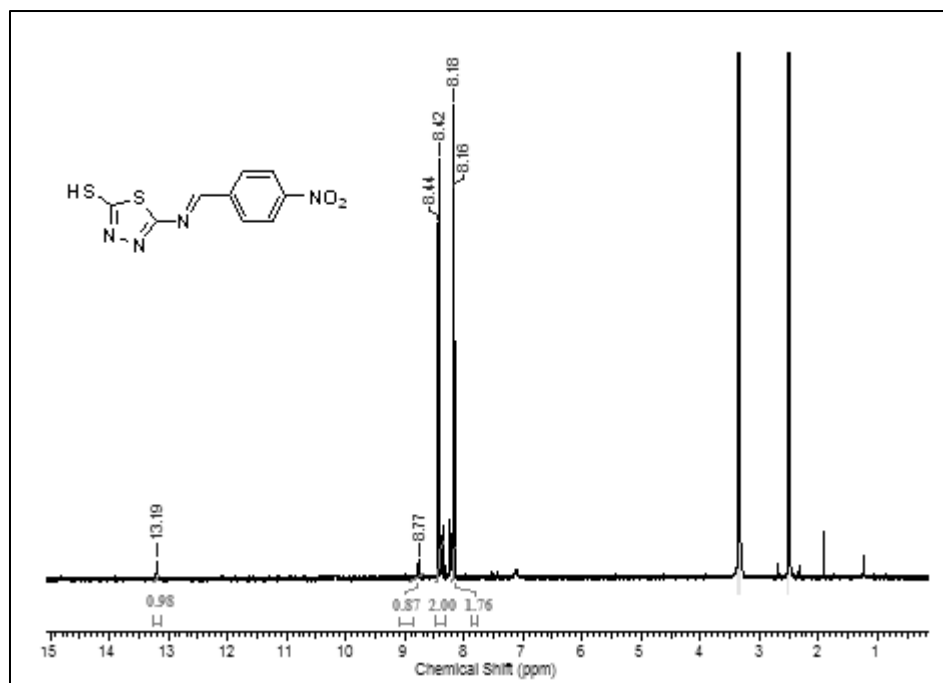


Fig. 6.4 ¹H NMR spectrum of receptor S4R1

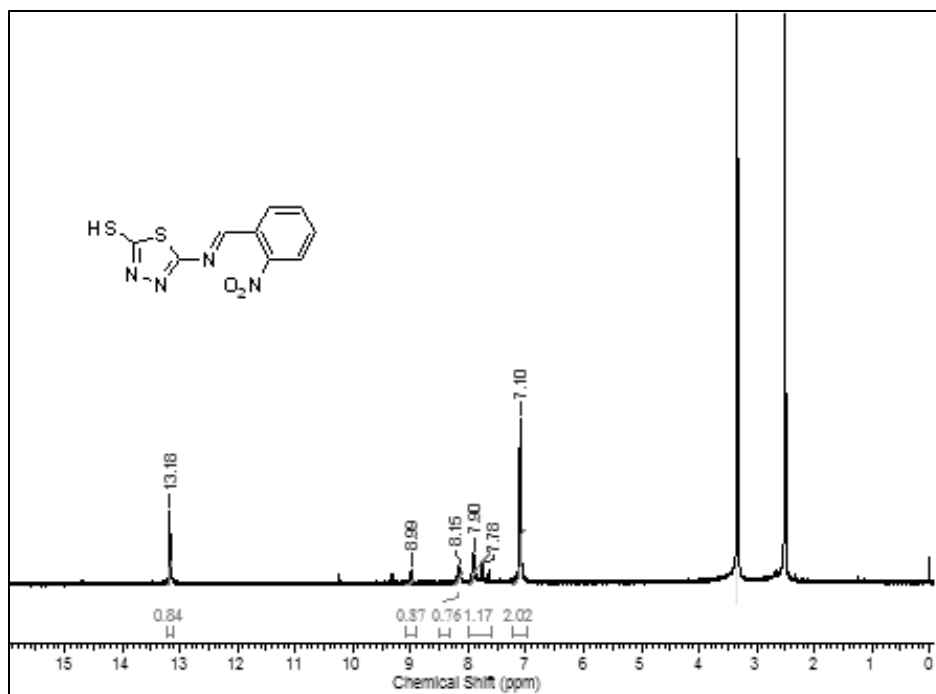


Fig. 6.5 ¹H NMR spectrum of receptor S4R2

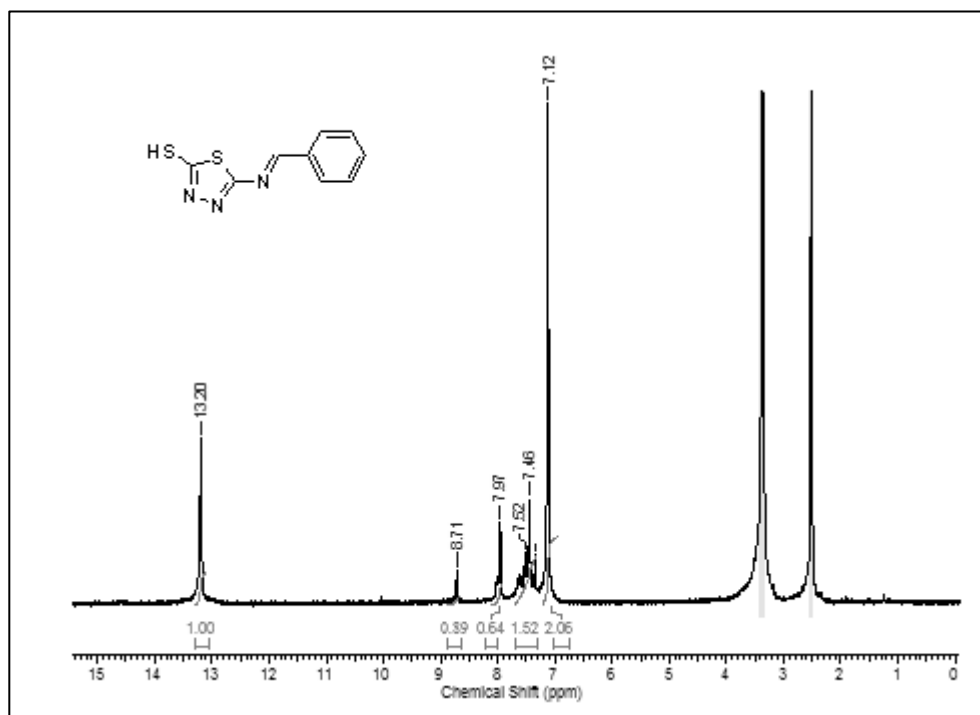


Fig. 6.6 ¹H NMR spectrum of receptor S4R3

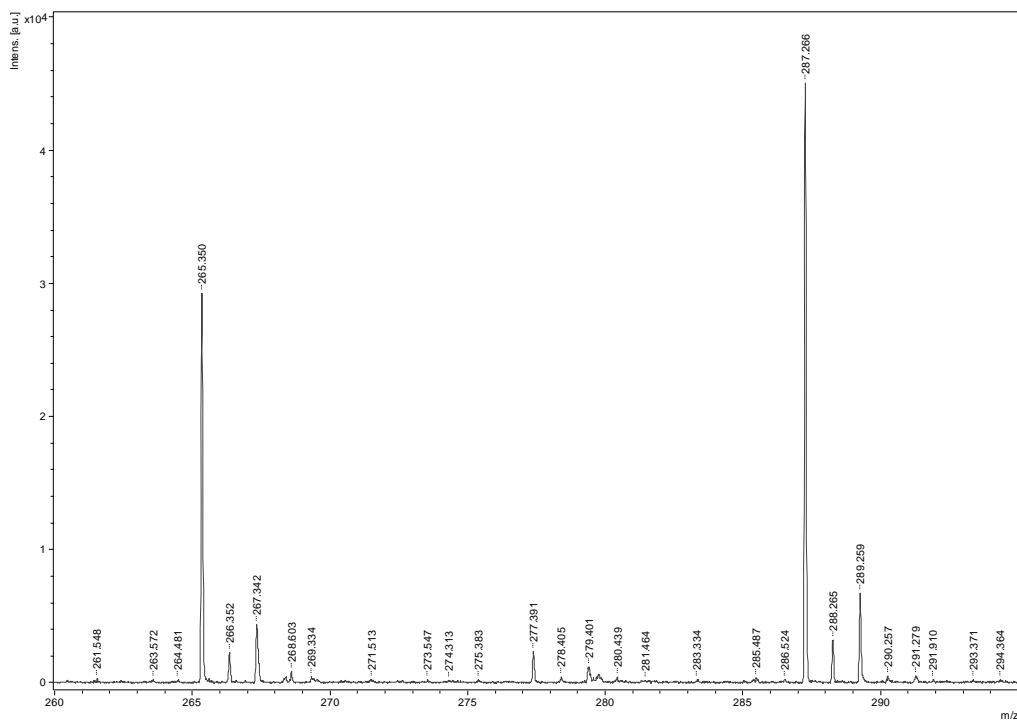


Fig. 6.7 ESI-MS spectrum of receptor S4R1

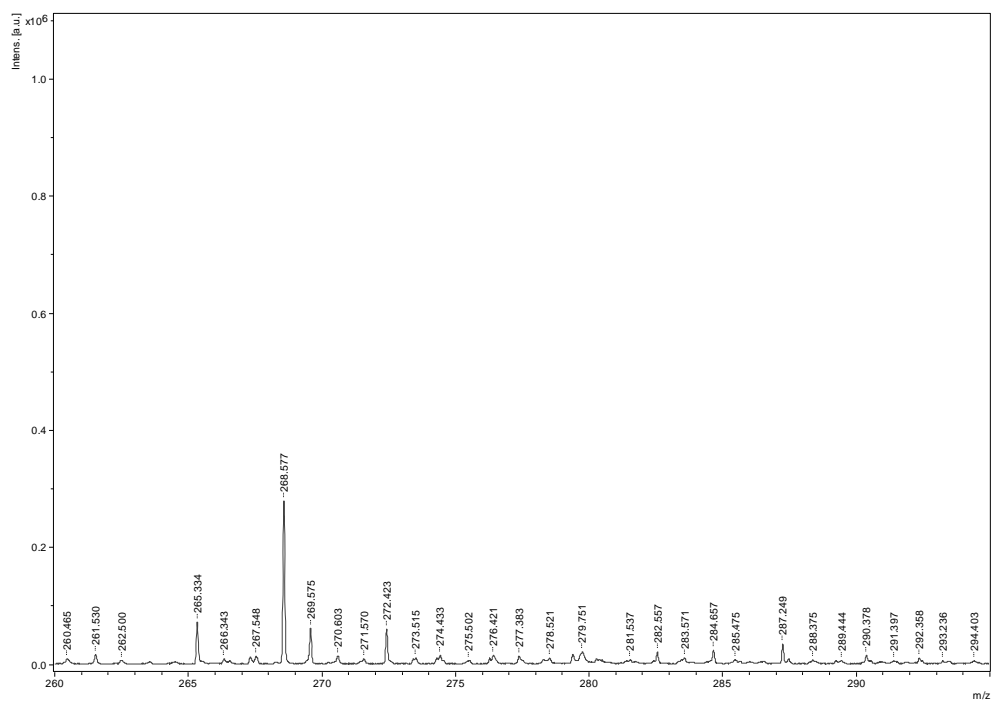


Fig. 6.8 ESI-MS spectrum of receptor S4R2

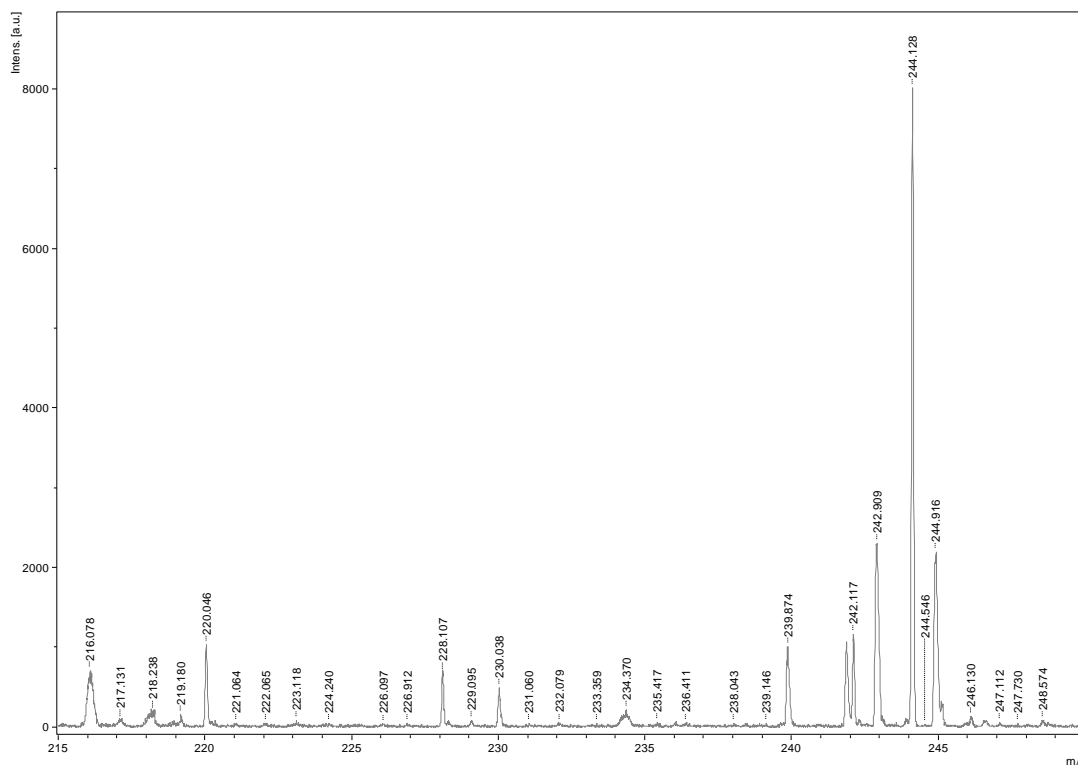


Fig. 6.9 ESI-MS spectrum of receptor **S4R3**

6.3 RESULTS AND DISCUSSION

6.3.1 Colorimetric detection of anions

Primarily, to 2 mL of test solution of **S4R1** in ACN of concentration 10^{-5} M, 1 eq. of tetrabutylammonium salts of anions such as F^- , Cl^- , Br^- , I^- , NO_3^- , HSO_4^- , $H_2PO_4^-$, AcO^- and CN^- ions (10^{-3} M in ACN) were added. **S4R1** exhibited visual colorimetric response from colorless to pink color towards F^- , $H_2PO_4^-$, AcO^- and CN^- ions (Fig. 6.10) and the corresponding UV-Vis spectra is shown in Fig. 6.11. Receptor **S4R2** exhibited mild color change towards AcO^- ion rendering other anions inactive, whereas **S4R3** was colorimetrically inactive towards test anions even with the addition of 10 eq. of anions UV-Vis spectra have been recorded in support of the observed color changes (Fig. 6.12 and Fig. 6.13).

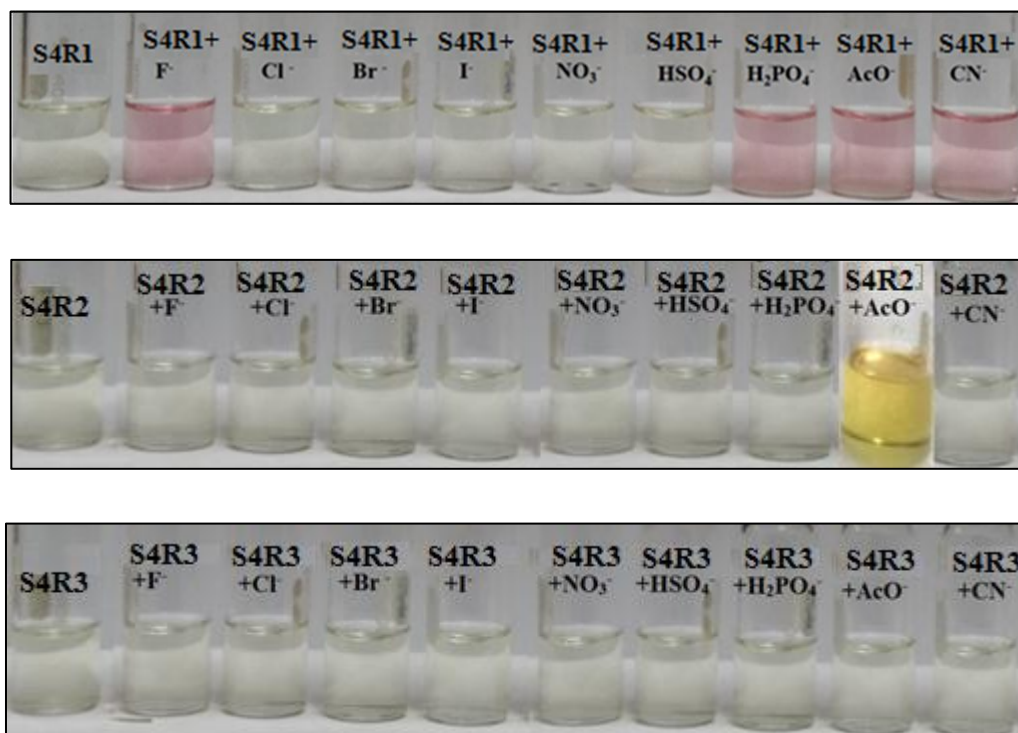


Fig. 6.10 Color change of the receptors **S4R1**, **S4R2** and **S4R3** (10^{-5} M in ACN) with the addition of 1 equiv. of TBA salts of anions (10^{-3} M in ACN)

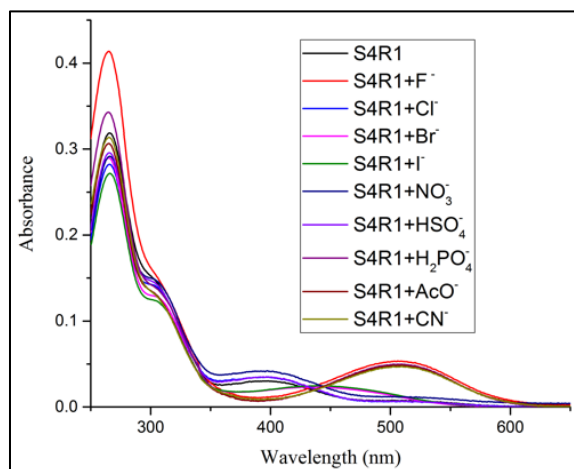


Fig. 6.11 UV-visible absorption spectra of **S4R1** (10^{-5} M in ACN) upon addition of 1 equiv. of various anions as TBA salts (10^{-3} M in ACN)

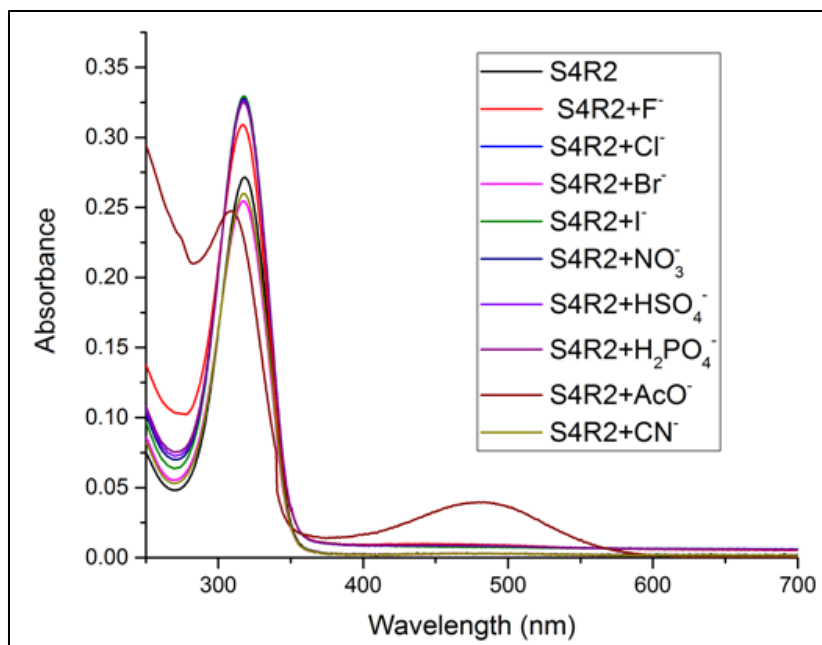


Fig. 6.12 UV-visible absorption spectra of **S4R2** (10⁻⁵ M in ACN)) upon addition of 10 equiv. of various anions as TBA salts (10⁻³ M in ACN)

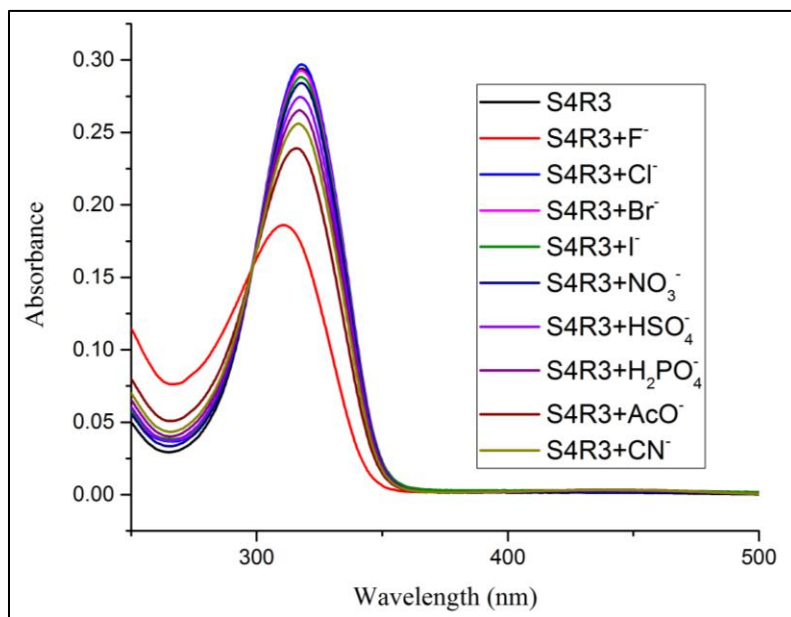


Fig. 6.13 UV-visible absorption spectra of **S4R3** (10⁻⁵ M in ACN) upon addition of 10 equiv. of various anions as TBA salts (10⁻³ M in ACN)

6.3.2 UV-Vis titration studies

Colorimetric response of receptors for anions was performed by UV-Vis titration experiments. Receptor concentration was set to 10^{-5} M to arrive at a lowest possible colorimetric detection limit. Titration experiments were performed with the incremental addition of 0.1 eq. of F^- , $H_2PO_4^-$, AcO^- and CN^- ions. Free receptor **S4R1** exhibited absorption bands at 396 nm and 506 nm, corresponding to the electronic transitions of the thiol functionality and localized transitions on the azomethine groups respectively. With the incremental addition of 0.1 eq. of F^- , AcO^- and CN^- ions, intensity of band centered at 506 nm increased with the concomitant appearance of unclear isobestic point at 430 nm (Fig. 6.14). The formation of higher order complexes could be attributed to the existence of unclear isobestic point in the titration studies (Sahu et al. 2016). B-H plot analysis revealed a 1:1 ratio for **S4R1**- F^- , **S4R1**- AcO^- and **S4R1**- CN^- and **S4R1**- $H_2PO_4^-$ complexes (Fig. 6.15). Titration of receptor **S4R2** with AcO^- ions did not exhibit significant red shift (Fig. 6.16). Table 6.1 represents binding constant for receptor **S4R1** with various active anions.

Table 6.1 Binding constant, binding ratio and detection limit values of receptor **S4R1**

Receptor	Anion	Binding constant (M^{-1})	Binding ratio	Detection limit (ppm)
S4R1	F^- (TBAF)	8.87×10^3	1:1	0.39
	AcO^- (TBAAcO)	0.086×10^3	1:1	0.15
	$H_2PO_4^-$ (TBAH ₂ PO ₄)	0.986×10^3	1:1	0.84
	CN^- (TBACN)	1.003×10^3	1:1	0.26
	F^- (NaF)	0.863×10^3	1:1	0.06
	AcO^- (NaAcO)	0.949×10^3	1:1	0.08
	AsO_2^- (NaAsO ₂)	7.20×10^4	1:1	0.03

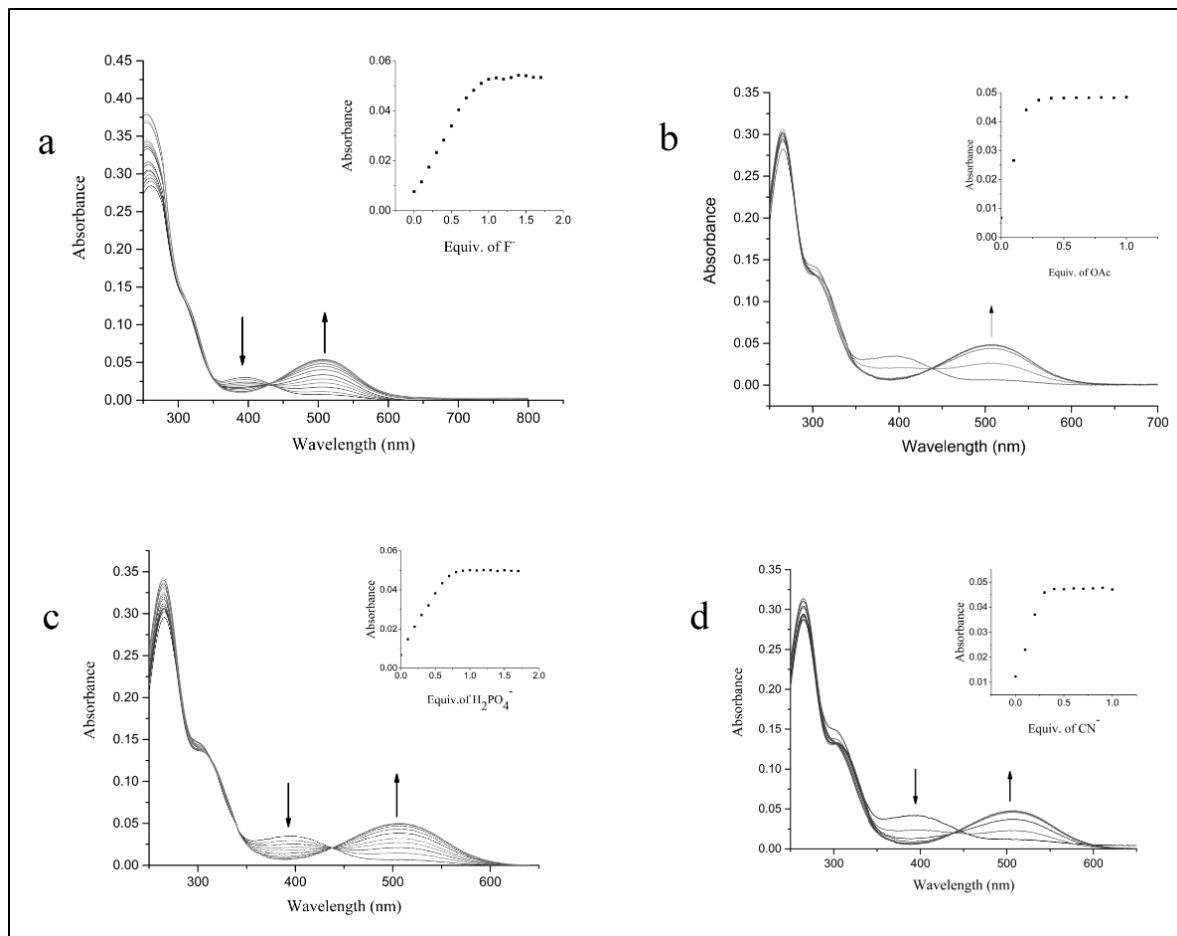


Fig. 6.14 UV-Vis titration spectra of receptor **S4R1** (10^{-5} M in ACN) with the incremental addition of TBA salts of anions (10^{-3} M in ACN); Inset plot representing the variation of absorbance with concentration of: (a) Receptor **S4R1**+ TBAF, (b) Receptor **S4R1** + TBAcO; (c) Receptor **S4R1** + TBAH₂PO₄; (d) Receptor **S4R1**+ TBACN

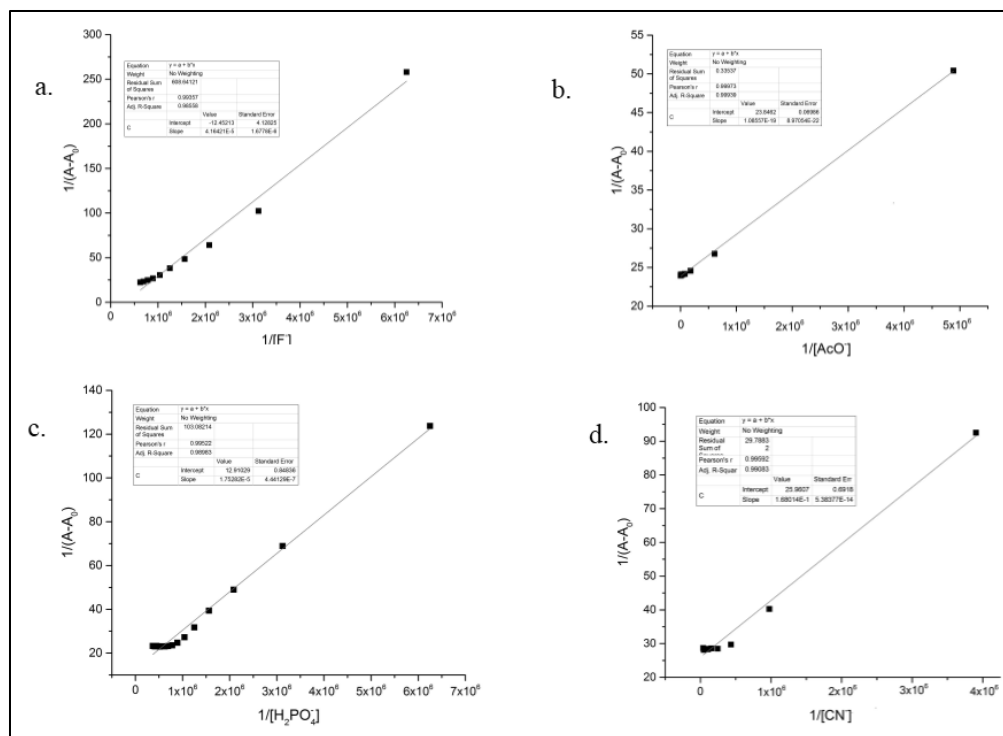


Fig. 6.15 B-H plot for 1:1 complex (a) Receptor **S4R1**: TBAF, (b) Receptor **S4R1**: TBAOAc; (c) Receptor **S4R1**: TBAH₂PO₄; (d) Receptor **S4R1**: TBACN

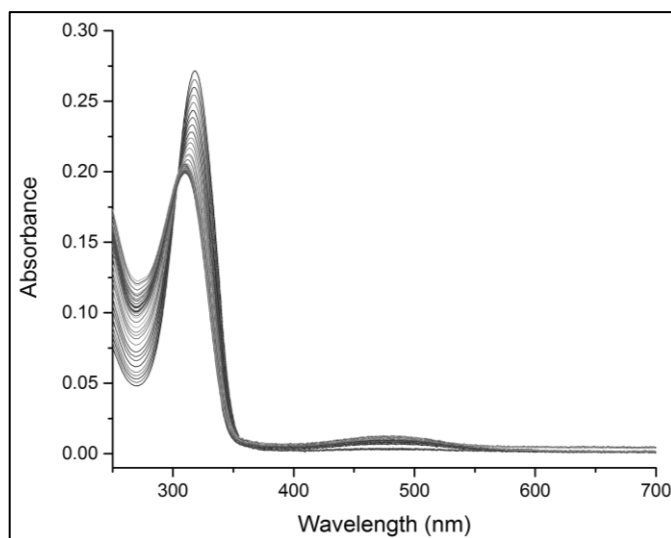


Fig. 6.16 UV-Vis titration spectra of receptor **S4R2** (10^{-5} M in ACN) with the incremental addition of TBAACO (10^{-3} M in ACN)

6.3.3 Fluorescence studies

Fluorescence behavior of receptors **S4R1**, **S4R2** and **S4R3** were analyzed and fluorescence spectra were recorded. **S4R1**, **S4R2** and **S4R3** exhibited similar fluorescence titration spectra in the region of 275-450 nm, although the λ_{\max} was at 397 for **S4R1**, 318 for **S4R2** and **S4R3** respectively. The fluorescence intensity of **R1** was ten times higher with the incremental addition of TBACN and TBAH₂PO₄ in comparison with the TBAF and TBAOAc. Receptors **S4R2** and **S4R3** exhibited higher emission intensity with TBAOAc in comparison with TBAF and did not exhibit fluorometric response in the presence of TBACN and TBAH₂PO₄. Fluorescence spectra are depicted in Fig. 6.17, 6.18, 6.19, 6.20, 6.21, 6.22, 6.23 and 6.24.

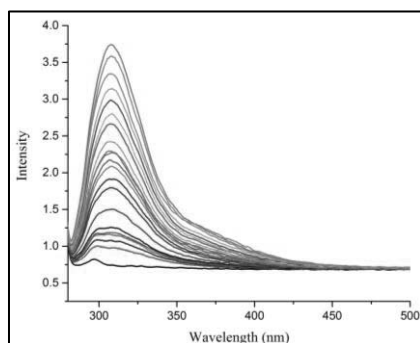


Fig. 6.17 Fluorescence spectra of receptor **S4R1** (10^{-5} M in ACN) with the incremental addition of TBAF (10^{-3} M in ACN)

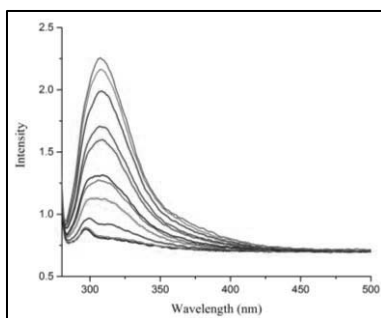


Fig. 6.18 Fluorescence spectra of receptor **S4R1** (10^{-5} M in ACN) with the incremental addition of TBAAcO (10^{-3} M in ACN)

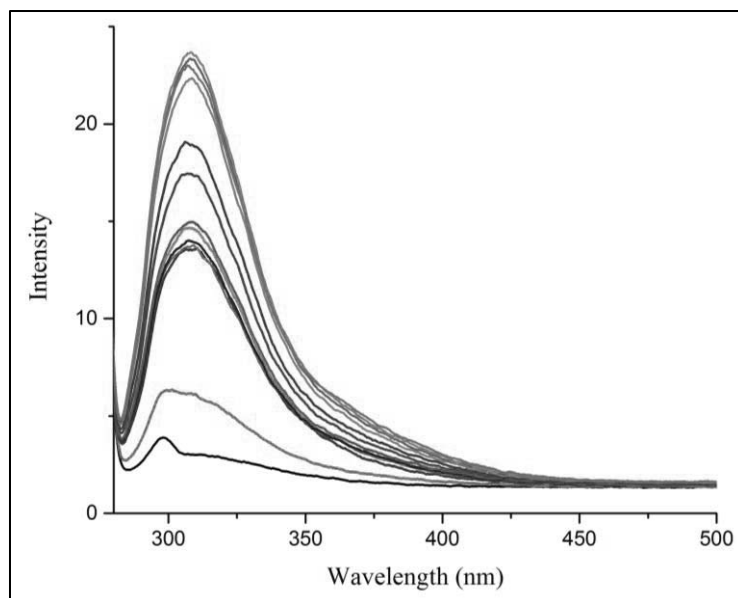


Fig. 6.19 Fluorescence spectra of receptor **S4R1** (10^{-5} M in ACN) with the incremental addition of TBACN (10^{-3} M in ACN)

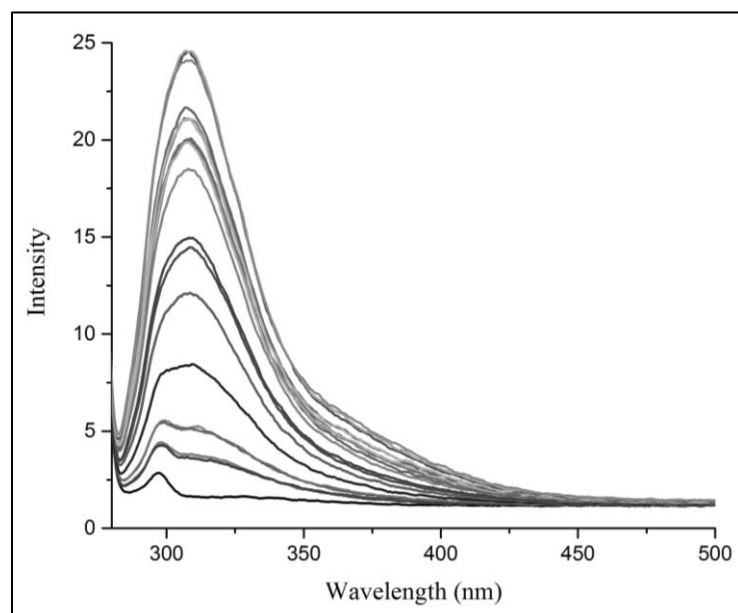


Fig. 6.20 Fluorescence spectra of receptor **S4R1** (10^{-5} M in ACN) with the incremental addition of TBAH₂PO₄ (10^{-3} M in ACN)

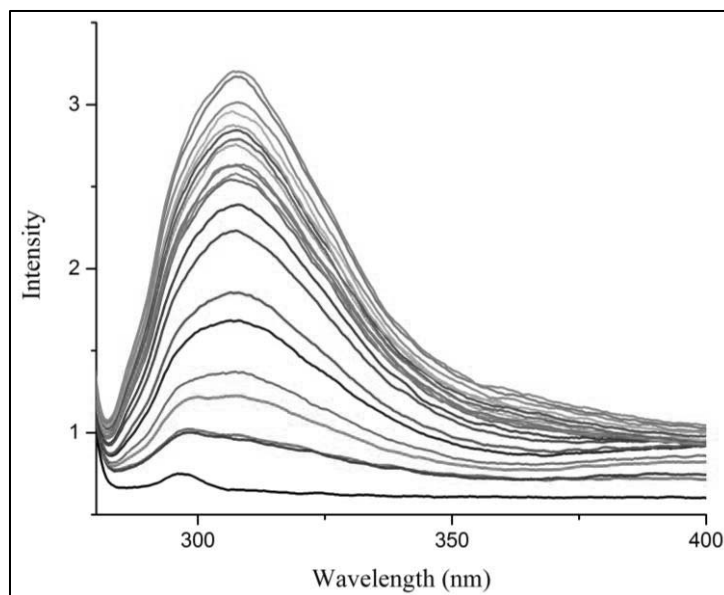


Fig. 6.21 Fluorescence spectra of receptor **S4R2** (10^{-5} M in ACN) with the incremental addition of TBAF (10^{-3} M in ACN)

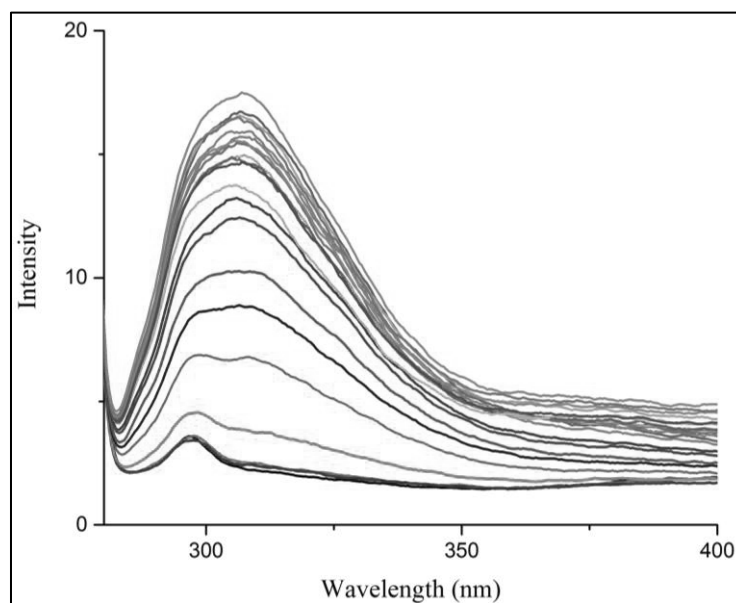


Fig. 6.22 Fluorescence spectra of receptor **S4R2** (10^{-5} M in ACN) with the incremental addition of TBAAcO (10^{-3} M in ACN)

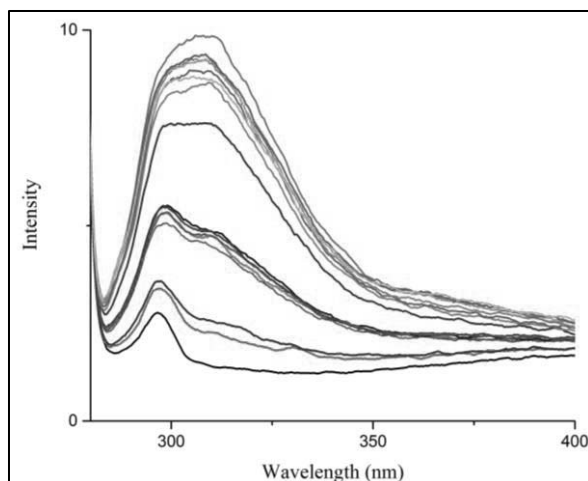


Fig. 6.23 Fluorescence spectra of receptor **S4R3** (10^{-5} M in ACN) with the incremental addition of TBAF (10^{-3} M in ACN)

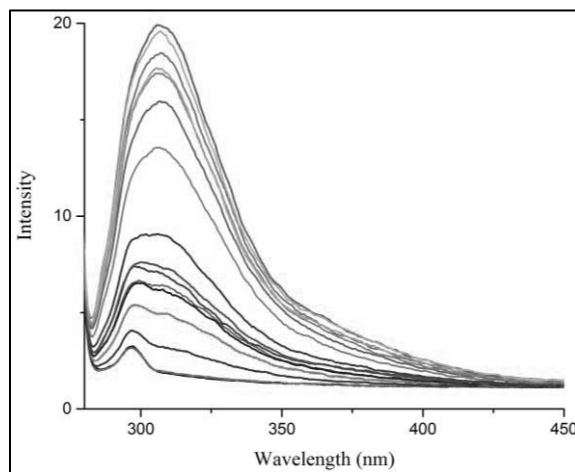


Fig. 6.24 Fluorescence spectra of receptor **S4R3** (10^{-5} M in ACN) with the incremental addition of TBAAcO (10^{-3} M in ACN)

6.3.4 pH dependency studies

Selectivity of receptor **S4R1** in Tris HCl buffer was investigated using UV-Visible spectrometry. 10^{-4} M ACN solution of receptor **S4R1**: Tris HCl (8:2, v/v) exhibited pale yellow color. Addition of 1 eq. of TBAF, TBAOAc, TBA H_2PO_4 and

TBACN to **S3R1**, color changed from pale yellow to pale orange with TBAAcO and TBAH₂PO₄ respectively (Fig. 6.25). TBAF and TBACN exhibited minute color change from pale yellow to dark yellow.

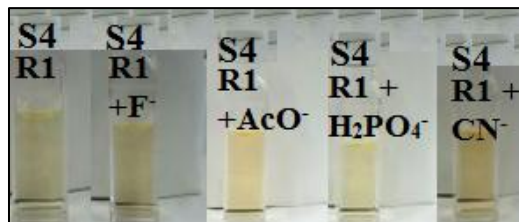


Fig. 6.25 Color change of receptor **S4R1** (ACN: Tris HCl, 8:2, v/v) with the addition of TBAF, TBAAcO, TBAH₂PO₄ and TBACN

6.3.5 Binding studies in organo-aqueous medium

Binding studies of **S4R1** as 10^{-5} M in ACN performed with sodium salt of anions such as F⁻ and AcO⁻ (10^{-3} M in distilled H₂O), revealed similar titration profile as observed with addition of TBA salts (Fig. 6.26 and 6.27). B-H plot for **S4R1**-NaF and **S4R1**-NaAcO complex revealed 1:1 binding ratio as shown in Fig. 6.28 and 6.29.

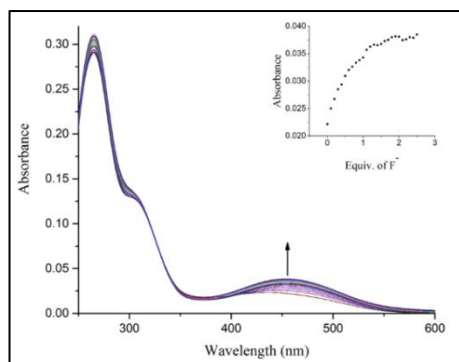


Fig. 6.26 UV-Vis titration spectra of receptor **S4R1** (10^{-5} M in ACN) with the incremental addition of NaF (10^{-3} M in distilled water); Inset plot representing the binding isotherm at 455 nm

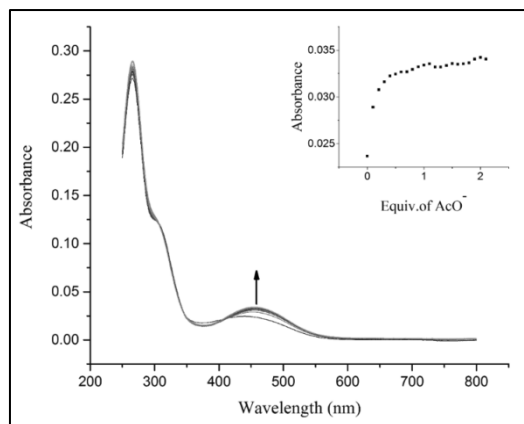


Fig. 6.27 UV-Vis titration spectra of receptor **S4R1** (10^{-5} M in ACN) with the incremental addition of NaAcO (10^{-3} M in distilled water); Inset plot representing the variation of absorbance with the increasing concentration of NaAcO at 457 nm

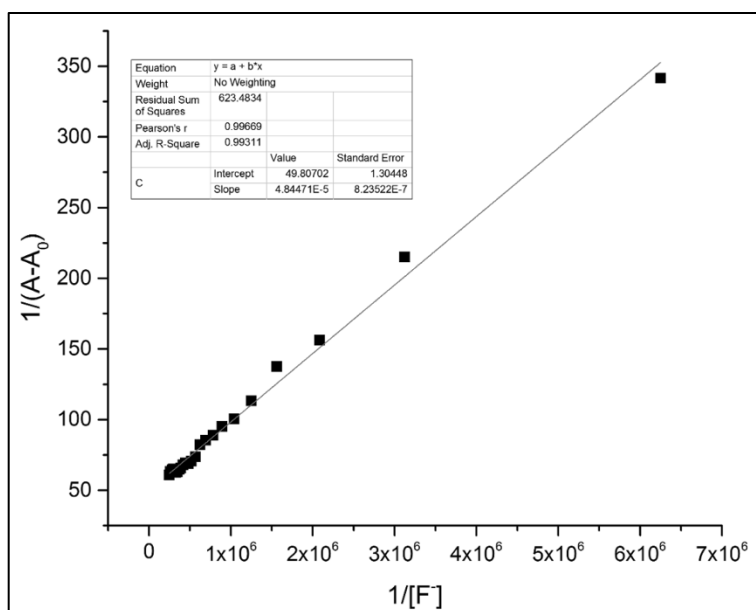


Fig. 6.28 B-H plot for 1:1 complex of **S4R1**-NaF

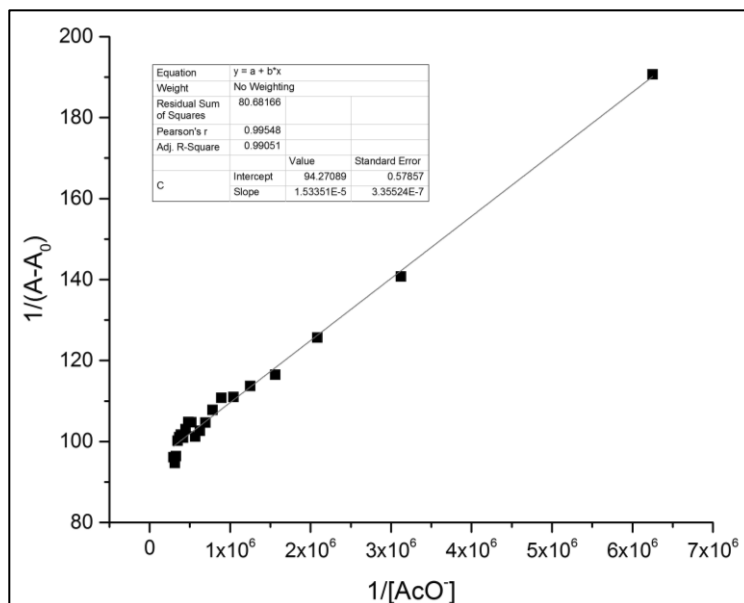


Fig. 6.29 B-H plot for 1:1 complex of **S4R1**-NaAcO

Receptor **S4R1**, by virtue of the colorimetric response towards H_2PO_4^- ions, is expected to exhibit activity towards arsenic ion. To the free receptor **S4R1** solution, 1.0 equiv. of NaAsO_2 was added. With the incremental addition of 0.1 eq. of NaAsO_2 , the color of the receptor **S4R1** changed from colorless to pink (Fig. 6.30 (a)). A gradual increment in the absorbance band centered at 500 nm with the incremental addition of NaAsO_2 solution was observed with a clear isobestic point at 435 nm (Fig. 6.30(b)). This is due to interaction of receptor and metal ion yielding a complex. Further, The B-H plot revealed 1:1 binding ratio of receptor and AsO_2^- complex (Fig. 6.31). Receptors **S4R2** and **S4R3** were inactive towards NaAsO_2 . The calibration curve of concentration of AsO_2^- (range from 0.0 M to 7.0×10^{-6} M) vs absorbance of **S4R1** + AsO_2^- complex at 500 nm is shown in Fig. 6.32.

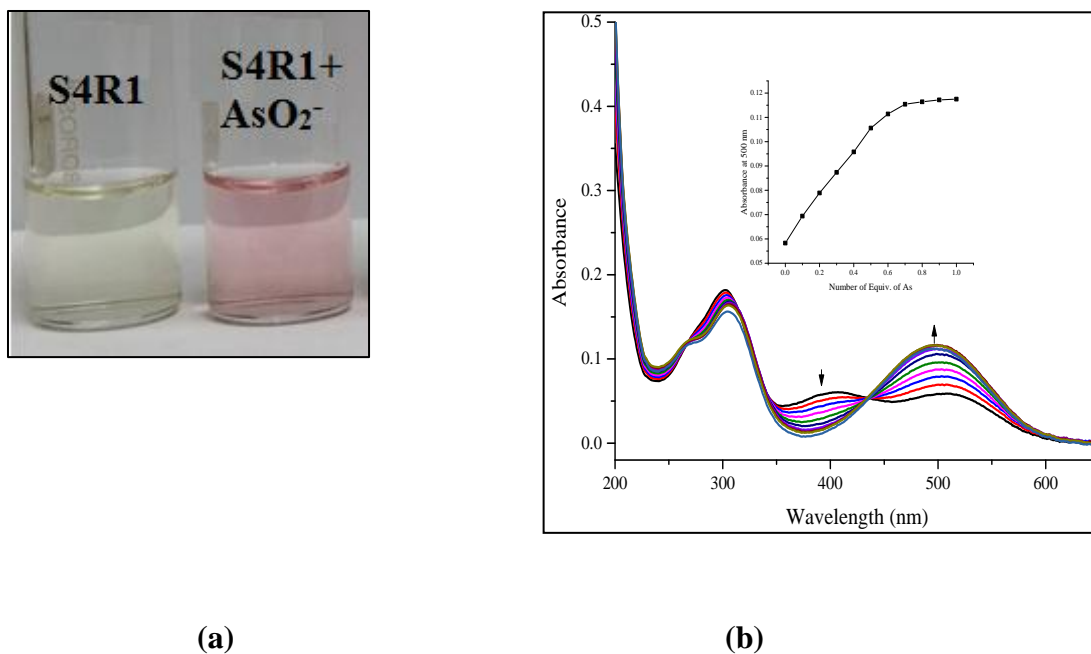


Fig. 6.30 (a) Color change of receptor **S4R1** with the addition of 1 eq. of NaAsO_2 ; (b) UV-Vis titration spectra of receptor **S4R1** (10^{-5} M in ACN) with the incremental addition of NaAsO_2 (10^{-3} M in distilled water); Inset plot representing the variation of absorbance with concentration of NaAsO_2 at 500 nm

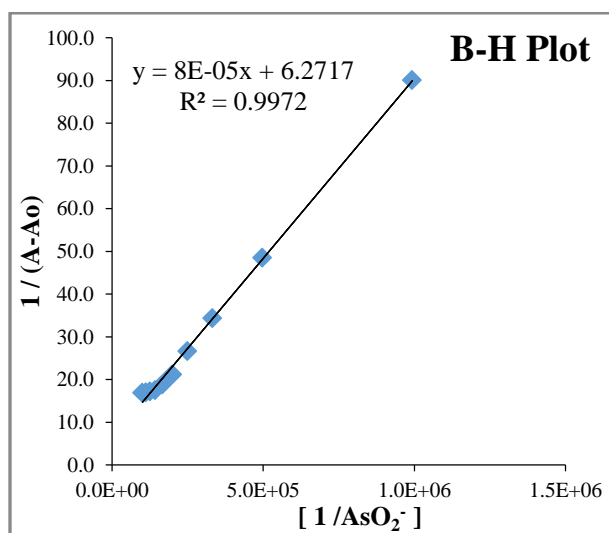


Fig. 6.31 B-H plot for 1:1 complex of **S4R1**- NaAsO_2

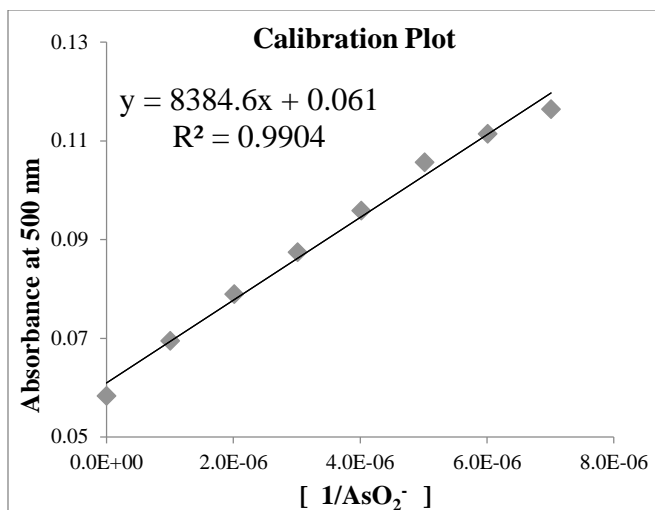


Fig. 6.32 Linear calibration curve between concentration of AsO_2^- (from 0.0 M to 7.0×10^{-6} M) and absorbance of receptor **S4R1** + AsO_2^- complex, monitored wavelength at 500 nm

6.3.6 ¹H NMR titration studies

¹H-NMR spectra have been recorded to understand binding mechanism with the addition of 1 eq. of F^- , H_2PO_4^- , AcO^- ions to receptor **S4R1**. The disappearance of proton signal corresponding to thiol functionality is a clear indication of deprotonation in the anion binding mechanism (Fig. 6.33). At higher equivalence of anion, deprotonation overrules hydrogen bond interaction resulting in the color change in the presence of active anions (Hong et al. 2001). The aforementioned fact is confirmed by the addition of 1 equiv. of TBAOH to solution of **S4R1**. In support of the ¹H NMR spectra, the UV-Vis spectra revealed the diminution of the peak corresponding to the thiol functionality affirming the deprotonation process.

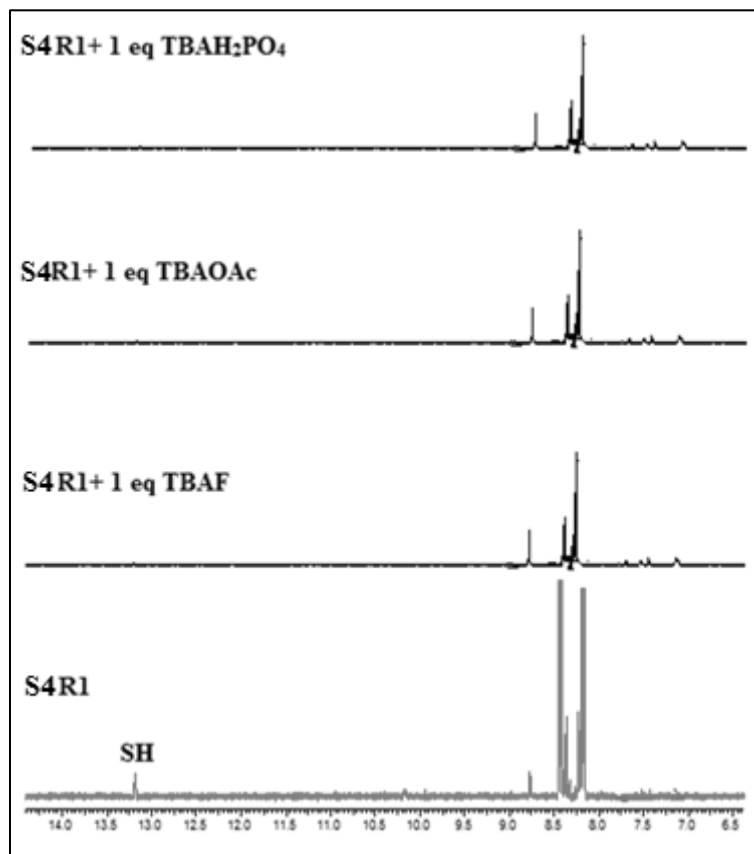


Fig. 6.33 ^1H -NMR spectra of receptor **S4R1** with the addition of 1 equiv. of TBAF, TBAAcO and TBAH_2PO_4

6.3.7 Electrochemical studies

Combined effect of the higher selectivity of optical techniques, and higher sensitivity in electrochemical analysis drives in the need to examine electrochemical properties of receptor **S4R1**. Cyclic voltammogram of free receptor **S4R1** exhibited an anodic peak at 0.225 V corresponding to the oxidation of thiol functionality. The addition of TBAF and TBAOAc did not induce any significant change in the oxidation peak. Yet with the addition of 0.5 eq. of TBAH_2PO_4 to **S4R1**, a cathodic peak appeared at -0.29 V corresponding to the reduction of NO_2 functionality (Chhibber et al. 2015). The subsequent shift of oxidation and reduction peak to 0.35 V and -0.67 V respectively is a

clear indicative of the complex electrochemical process occurring during the interaction. The cyclic voltammogram is represented in Fig. 6.34.

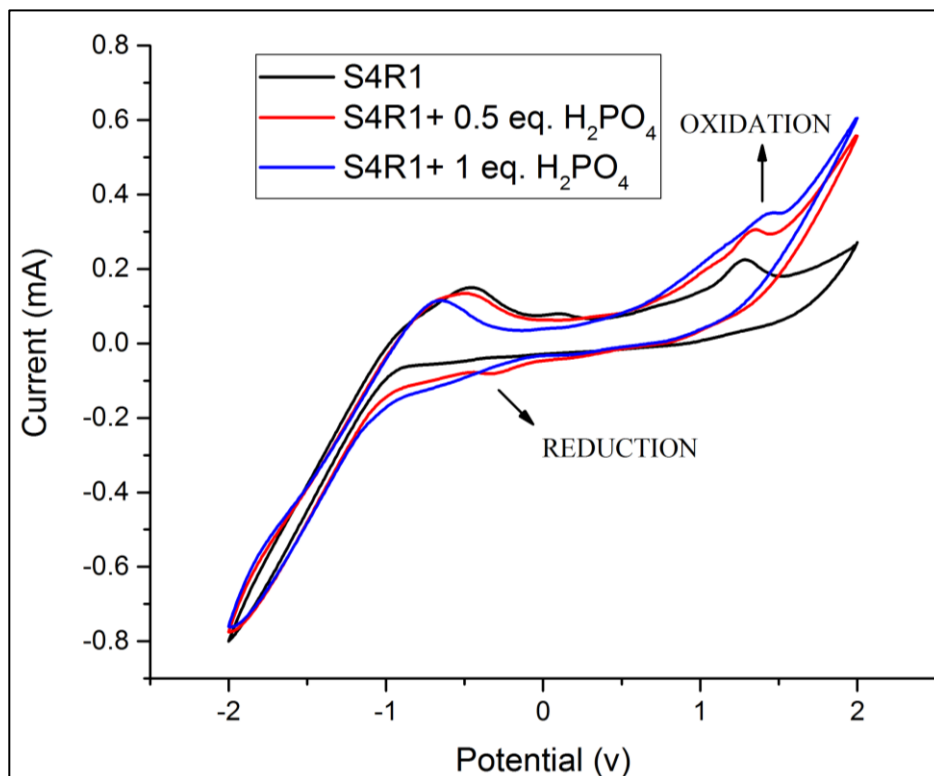


Fig. 6.34 Cyclic voltammogram of receptor **S4R1** with the incremental addition of TBAH₂PO₄

6.3.8 DNA binding studies

Enthused by the above results, we investigated the DNA binding ability of the receptor **S4R1**. The presence of hydrogen bond acceptor moieties (N) in thiadiazole group is expected to promote intercalative binding of receptor with DNA. UV-Vis absorption spectroscopy is a felicitous tool to analyze the DNA binding ability of the molecules. Bacterial DNA was isolated from *Serratia marcescens* strain ATCC 13880 and used in the present study. Solution were prepared with Tris-HCl/NaCl buffer (pH 7.2) in order to envisage the binding affinity between DNA and receptor **S4R1**. DNA purity was

confirmed with UV-Vis absorbance of DNA in buffer at 260 nm and 280 nm, which yielded a ratio of 1.8-1.9. To 2 mL Tris HCl/NaCl buffer and receptor **S4R1** (10^{-5} M in ACN: Tris HCl) taken in two individual cuvettes, one aliquot of DNA was added to each cuvettes in order to exclude the absorbance of DNA itself. Prior to recording the UV-Vis spectra, receptor-DNA solutions were incubated at room temperature for 5 min. The absorption peaks at 266 nm, 313 nm and ~ 400 nm could be assigned to the intraligand $\pi - \pi^*$ transitions. The absorption spectrum of **S4R1** in the presence of varying concentration of DNA is shown in Fig. 5.35. With the increasing concentration of DNA, hyperchromic shift of the band at 266 nm, hypochromic and blue shift of ~ 3 nm at 313 nm and a red shift band was observed at 455 nm. The occurrence of hyperchromic shift is suggestive of partial intercalative or electrostatic interactions between the DNA and chromophore. The red shift indicates the decrease in the energy band gap leading to the binding of DNA.

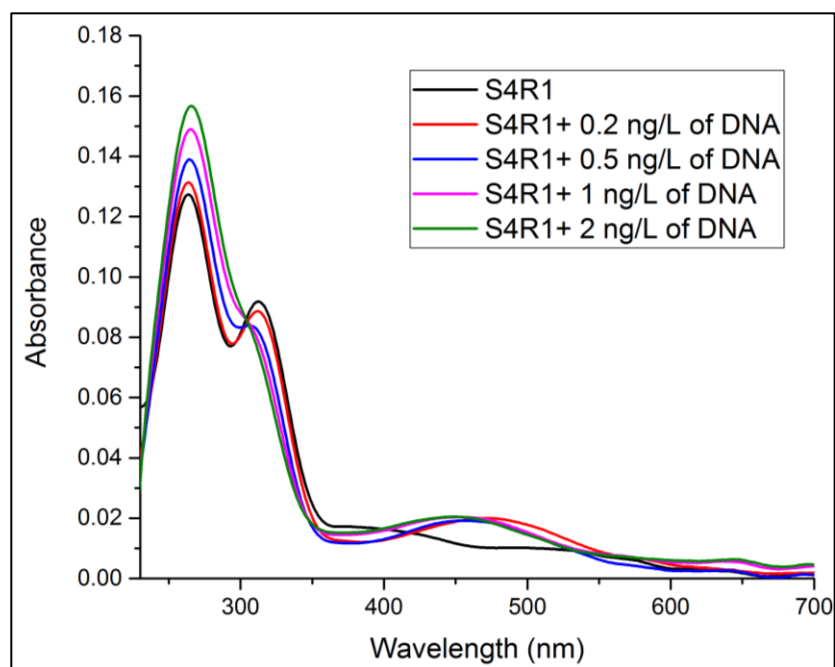


Fig. 6.35 UV-Vis spectra with the addition of increasing amounts of DNA at room temperature in Tris-HCl/NaCl buffer (pH 7.2) to receptor **S4R1**

6.3.9 Detection of CN^- ions in sprouting potatoes

The colorimetric response of receptor **S4R1** towards CN^- ions was extended further to explore the practical utility in day to day life. Inspired by the work of Wei and coworkers, we chose the sprouting potatoes as source of target anions (CN^-) owing to the presence of glycoalkaloids. The sprouting potato (150 g) was mashed initially and soaked in distilled water (200 mL) for 4 days. Upon appearance of muddy nature of the extract, the mixture was filtered, followed by elution with 100 mmol/L NaOH solution (100 mL) yielding the cyanide-containing solution. With the addition of cyanide-containing solution to **S4R1**, an instantaneous color change from colorless to pink was observed indicating the detection of CN^- ions by the receptor **S4R1**. The UV-Vis spectra were recorded which indicates the redshift of original band of receptor **S4R1** with the addition of cyanide-containing solution. (Fig. 6.36) This proves the practical utility of receptor **S4R1**.

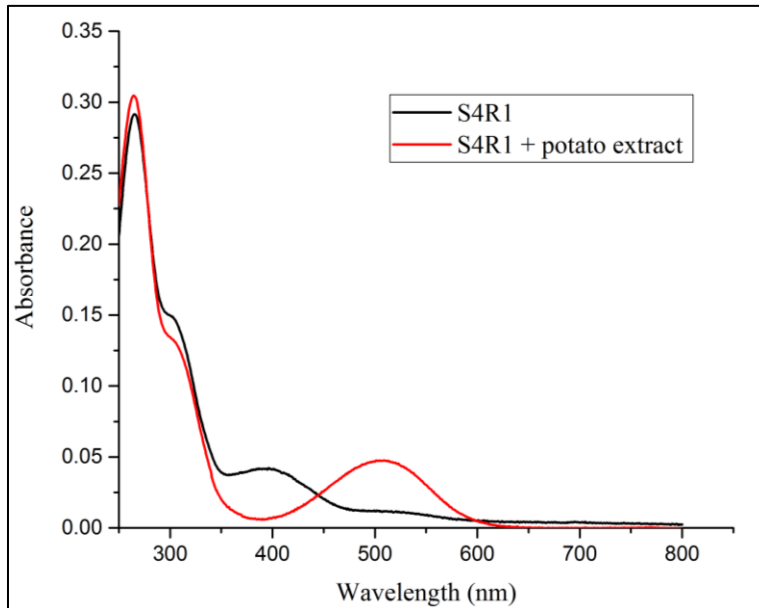


Fig. 6.36 UV-Vis spectra with the addition of sprouted potato extract to receptor **S4R1** (10^{-5} M in ACN)

6.3.10 Detection of H_2PO_4^- ions in detergent sample

Phosphates are commonly found in detergents and are known to enhance detergent's performance by softening hard water and suspend dirt in water. Detergent-loaded waste water are a threat to aquatic system as they reduce the surface tension of water, leading to damage of mucus layer on fish which usually protects them from bacteria and parasites. Owing to the colorimetric response of receptor **S4R1** towards H_2PO_4^- ions, we were keen to analyze the phosphate present in commercially available detergent sample. Calibration curve of absorbance vs concentration of H_2PO_4^- ions has been plotted to determine the amount of H_2PO_4^- in detergent sample. (Fig. 6.37) Prior to the analysis, detergent sample was diluted 50 times and the value obtained from the standard plot was multiplied by an appropriate dilution factor to arrive at the actual concentration of H_2PO_4^- in detergent sample.

In order to justify the colorimetric detection of H_2PO_4^- ions by receptor **S4R1**, a standard procedure was followed to detect H_2PO_4^- ions in detergent sample by using molybdenum blue method. With the addition of sample to 2 mL of ammonium molybdate solution and 2 mL of 1-amino-2-naphthol-4-sulfonic acid, the appearance of blue color indicated the detection of H_2PO_4^- ions. From the value of absorbance obtained at 690 nm, the concentration of H_2PO_4^- ions in detergent sample was determined from the calibration curve. The amount of phosphate present in detergent sample was estimated to be 1153.8 ppm by receptor **S4R1** and 1153.51 ppm by molybdenum blue method. The similar results obtained with receptor **S4R1** and molybdenum blue method indicated the successful application of receptor **S4R1** in the detection of H_2PO_4^- ions in detergent sample.

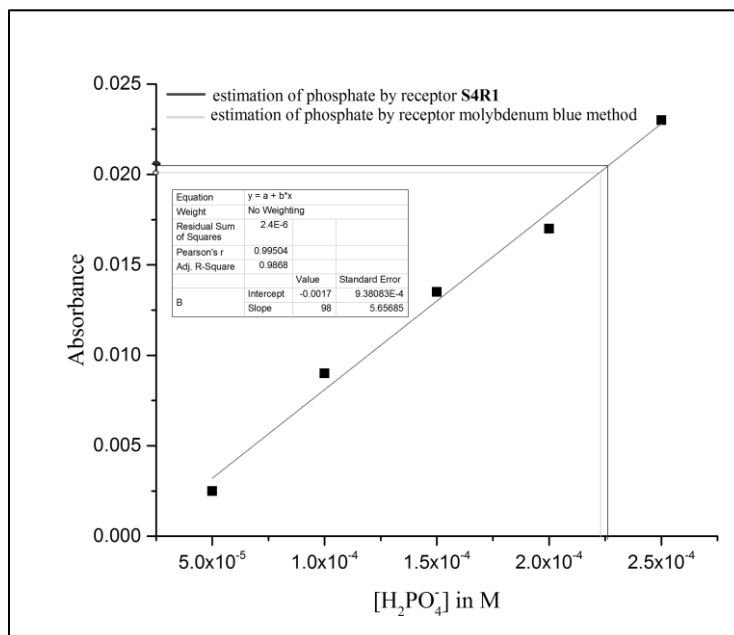


Fig. 6.37 Calibration plot for the quantitative estimation of phosphate in detergent sample

6.3.11 Calculation of binding constant from UV-Vis studies

Binding constant has been calculated using Benesi-Hildebrand equation (Benesi and Hildebrand 1948) as given below;

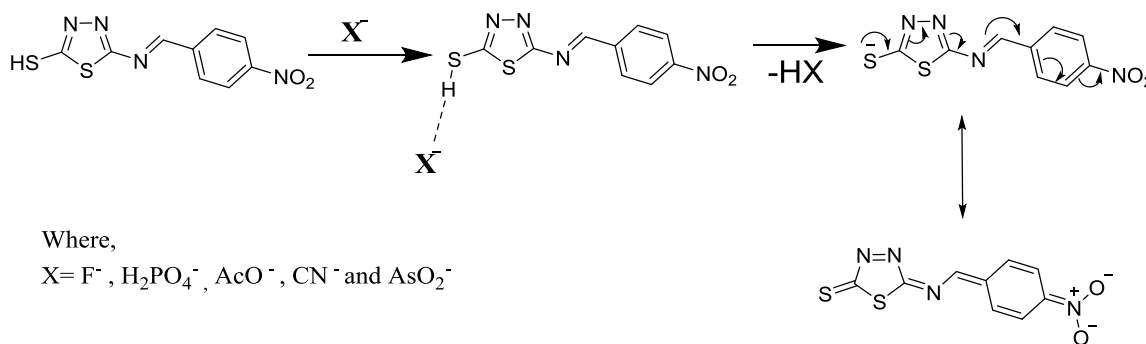
$$1/(A - A_0) = 1/(A_{\max} - A_0) + 1/K [X^-]^n (A_{\max} - A_0)$$

where, A_0 , A , A_{\max} are the absorption considered in the absence of anion, at an intermediate, and at a concentration of saturation. K is binding constant, $[X^-]$ is concentration of anion and n is the stoichiometric ratio.

6.3.12 Binding mechanism

The presence of nitro functionality at position *para* to the imine linked thiol functionality is known to promote strong hydrogen bond interactions in the presence of anions. $^1\text{H-NMR}$ studies of receptor **S4R1** in the presence of anions confirms the deprotonation of thiol functionality during the anion binding process. The occurrence of 1:1 binding ratio for **S4R1**-anion complex reveals the successful binding of anions to the

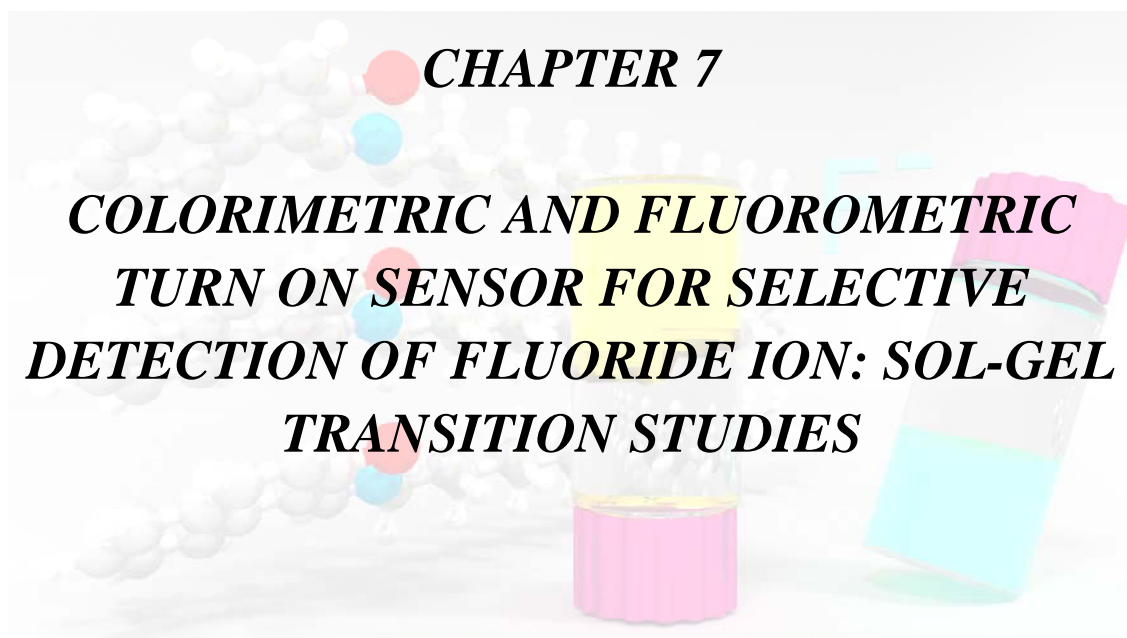
thiol functionality following a deprotonation event. The binding mechanism is shown in Scheme 6.4.



Scheme 6.4 Proposed binding mechanism of receptor **S4R1** with active anions

6.4 CONCLUSIONS

Detailed UV-Vis spectroscopic, fluorometric, 1H -NMR and cyclic voltammetric studies reveals the multi-anion binding behavior of receptor **S4R1**. The role of thiol functionality as a potent binding site and nitro functionality as signaling unit are highly significant in inducing the colorimetric response in the presence of anions such as F^- , $H_2PO_4^-$, AcO^- , CN^- and AsO_2^- ions of varying basicity. The detection of AsO_2^- ions by receptor **S4R1** confirms the analogous properties of phosphate and arsenite. The lower detection limit of 0.03 ppm and a higher binding constant value of $7.2 \times 10^4 M^{-1}$ for **S4R1**- AsO_2^- complex indicates the practical utility. The practical investigation of **S4R1** in DNA binding reveals partial intercalative or electrostatic interactions between the DNA and chromophore. Concurrently, analysis of sprouted potato sample reveals successful detection of CN^- ions with a visual colorimetric response. The receptor **S4R1** was successful in quantification of phosphate in detergent sample. Overall, the receptor **S4R1** serves as a multi anion chemosensor with its interesting real life practical applications.



Abstract

In this chapter, design, synthesis and characterization of a new organic receptors have been described. The applicability of the receptors in the colorimetric and fluorometric detection of anions have been discussed in detail through UV-Vis spectrophotometric, spectrofluorometric and ¹H-NMR titration studies. The binding mechanism of the receptor towards active anion has been included. The gelation property of the receptor and its response to anions has been evaluated.

7.1 INTRODUCTION

Multi-stimuli responsive supramolecular gels have emerged into a well-recognized class of “smart” materials (Ren et al. 2014; Steed 2011; Foster et al. 2010). Supramolecular gels have shown promising applications in tissue engineering, microfluidic devices, drug delivery, sensors, optoelectronic devices, smart films, bio-adhesion mediators and actuators etc. (Segarra-Maset et al. 2013; Kuksenok et al. 2013). Non-covalent interactions such as multiple hydrogen bonding, π - π^* interactions, metal–organic coordination, hydrophobic interactions, and Vander Waals forces are the driving force leading to gels assembled from low molecular weight supramolecular gelators (Noro et al. 2013; Wang et al. 2014; Datta and Bhattacharya 2011; Yan et al. 2012; Rajamalli et al. 2014). Stimuli responsive supramolecular gels which respond to external environmental stimuli, such as heat, (Rao and Sun 2013) cations/anions (Nebot et al. 2014) and oxidative/reductive reactions (Sun et al. 2014) have garnered more attention for the dynamic and reversible nature of non-covalent interactions.

The length of the alkyl chain is known to have great impact as it directly influences the vander Waals interaction in gel formation. The reports of organogels which exhibit selective response towards F⁻ ion is limited. Owing to the multiple interactions between gelators and different anions, the utilization of urea and amide group as recognition units have been a quest. Keeping this in view, a new naphthalene derivative, possessing –OH as anion binding site, covalently linked to a

long alkyl chain has been synthesized aiming towards the selective detection of anions.

7.2 EXPERIMENTAL SECTION

7.2.1 Materials and methods

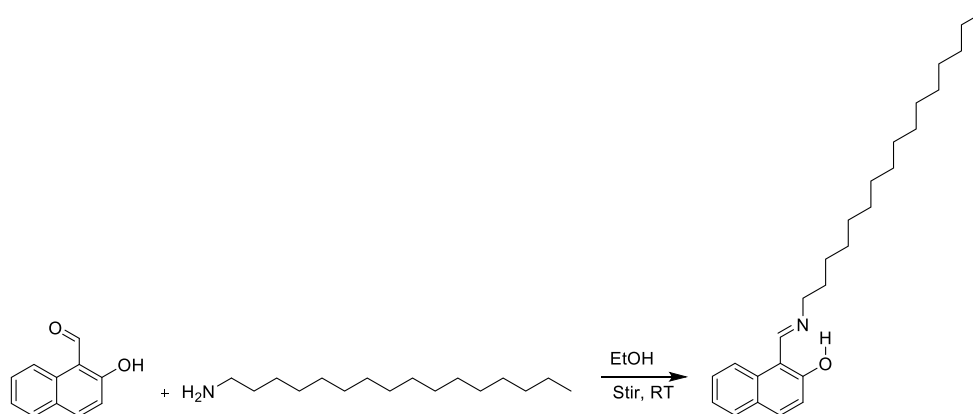
All the chemicals used in the present study were procured from Sigma-Aldrich, Alfa Aesar or Spectrochem and were used as received without further purification. All the solvents were purchased from SD Fine, India, were of HPLC grade and used without further distillation.

Melting point was measured on Stuart SMP3 melting-point apparatus in open capillaries. Infrared spectra were recorded on Bruker alpha FTIR spectrometer. UV/Vis spectroscopy was performed with analytik jena Specord S600 spectrometer in standard 3.0 mL quartz cell with 1cm path length. The $^1\text{H-NMR}$ spectra were recorded on Bruker Ascend (400 MHz) instrument using TMS as internal reference and $\text{DMSO-}d_6$ as solvent. $^{13}\text{C-NMR}$ spectra were recorded on Bruker Ascend(100MHz) instrument using TMS as internal reference and $\text{DMSO-}d_6$ as solvent. Resonance multiplicities are described as s (singlet), d (doublet), t (triplet) and m (multiplet). ESI-MS was recorded on Waters UPLC-TQD Mass spectrometer.

7.2.2 Synthesis of receptor S5R1

(E)-1-((hexadecylimino)methyl)naphthalen-2-ol

2-hydroxynaphthaldehyde (0.178 g, 0.414 mmol) and hexadecylamine (0.25 g, 0.412 mmol) were stirred in 10 ml ethanol at room temperature for 12 h in the presence of drop of acetic acid as catalyst. The reaction mixture filtered through filter paper and washed with ethanol to obtain pure product. The formation of the product was confirmed through TLC by the generation of single spot indicative of the disappearance of starting materials. (Scheme 7.1)

**Scheme 7.1** Synthesis of receptor **S5R1**

Yield: 76 %, melting point: 210 °C, ¹H NMR (DMSO- *d*₆, 400 MHz, ppm): δ 14.13 (td; J= 2.6 ×(2), 1.5; 1H), 9.1 (m; CH=N), 8.06 (d; J=8.6; 1H), 7.71 (d; J=9.3; 2H), 7.41 (m; 1H), 7.18 (d; J=7.8, 1H), 6.7 (d; J=9.3; 1H), 3.64 (m; 2H), 1.64 (m; 2H), 1.27 (m; 26H), 0.85 (m; 3H). ¹³CNMR (DMSO- *d*₆, 100 MHz, ppm): δ 178.07, 159.42, 137.46, 134.82, 129.30, 128.28, 126.14, 125.55, 122.49, 118.87, 105.99, 51.00, 40.62, 40.41, 40.21, 40.00, 39.79, 39.58, 39.37, 31.75, 30.61, 29.48, 29.38, 29.16, 28.99, 26.52. FTIR (KBr) (cm⁻¹): 3526 (OH), 2913 (Ar-CH), 1631 (CH=N). ESI-MS Calculated: 395.63, Obtained: 396.5 (M+H⁺).

7.2.3 Characterization data of receptor

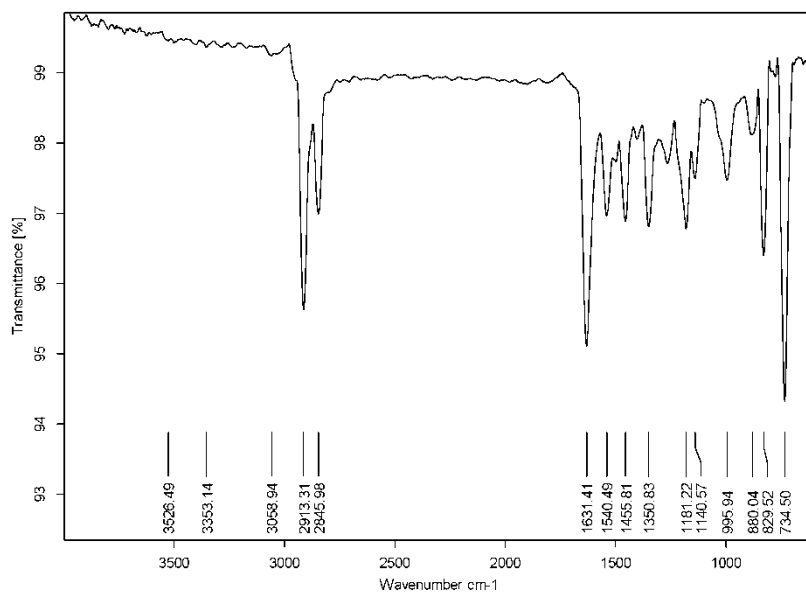
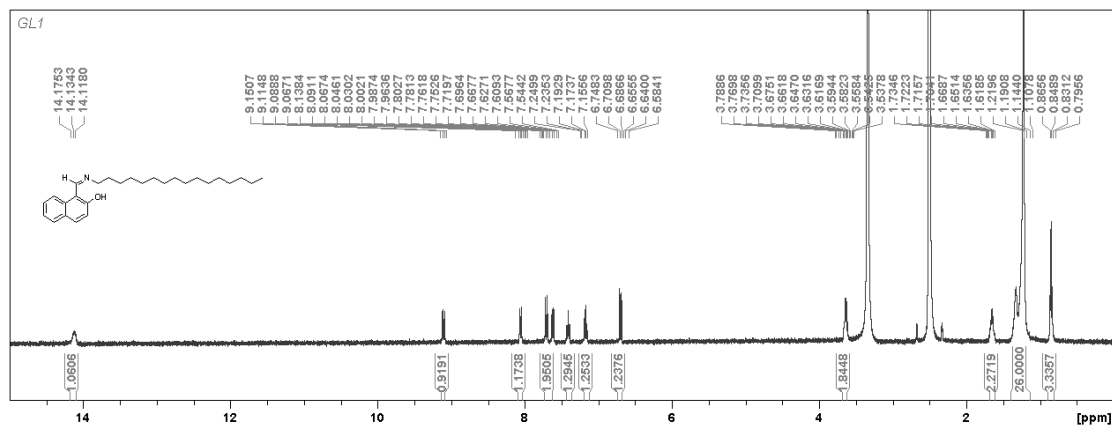


Fig. 7.1 FT-IR spectrum of receptor S5R1

Fig. 7.2 (a) ¹H-NMR spectrum of receptor S5R1

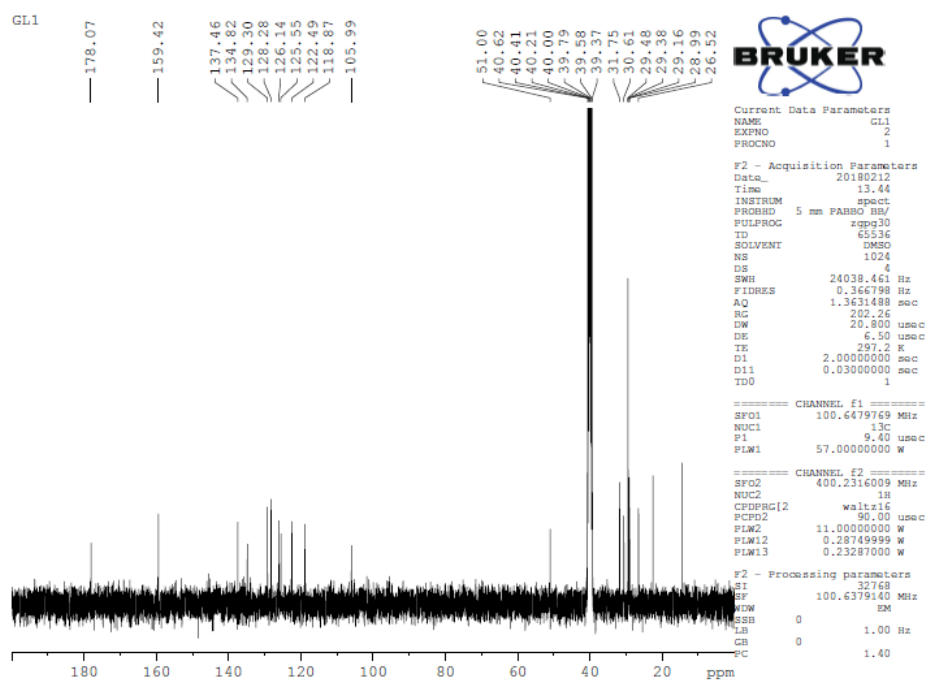


Fig. 7.2 (b) ^{13}C NMR spectrum of receptor S5R1

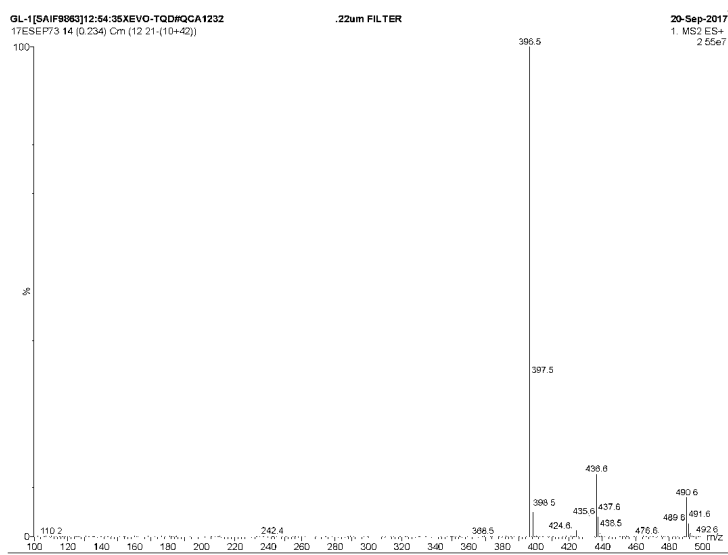


Fig. 7.3 ESI-MS spectrum of receptor S5R1

7.3 RESULTS AND DISCUSSION

7.3.1 Complexation studies

7.3.1.1 UV-Vis and Fluorescence studies

The anion binding ability of receptor **S5R1** was evaluated in DMSO (10^{-5} M) using the anions as their tetrabutylammonium salts (F^- , Cl^- , Br^- , I^- , NO_3^- , HSO_4^- , $H_2PO_4^-$ and AcO^- ions as 10^{-2} M in DMSO). Receptor **S5R1** exhibited a selective colorimetric response towards F^- ion exhibiting a color change from colorless to pale yellow (Fig. 7.4).

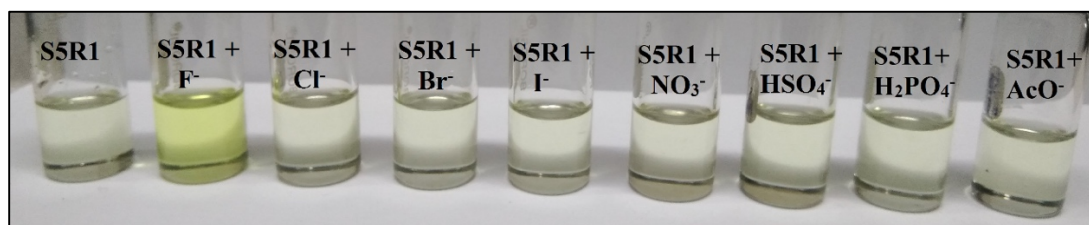


Fig. 7.4 Colour change of the receptors **S5R1** (10^{-4} M in DMSO) with the addition of 2 equiv. of TBA salts of anions (10^{-2} M in DMSO)

The UV-Vis spectra of receptor **S5R1** exhibited bands centered at 306 nm, 401 nm and 420 nm corresponding to the transitions between the π orbitals localized on the azomethine group ($C=N$) and aromatic π electron transitions corresponding to the naphthalene moiety (Fig. 7.5).

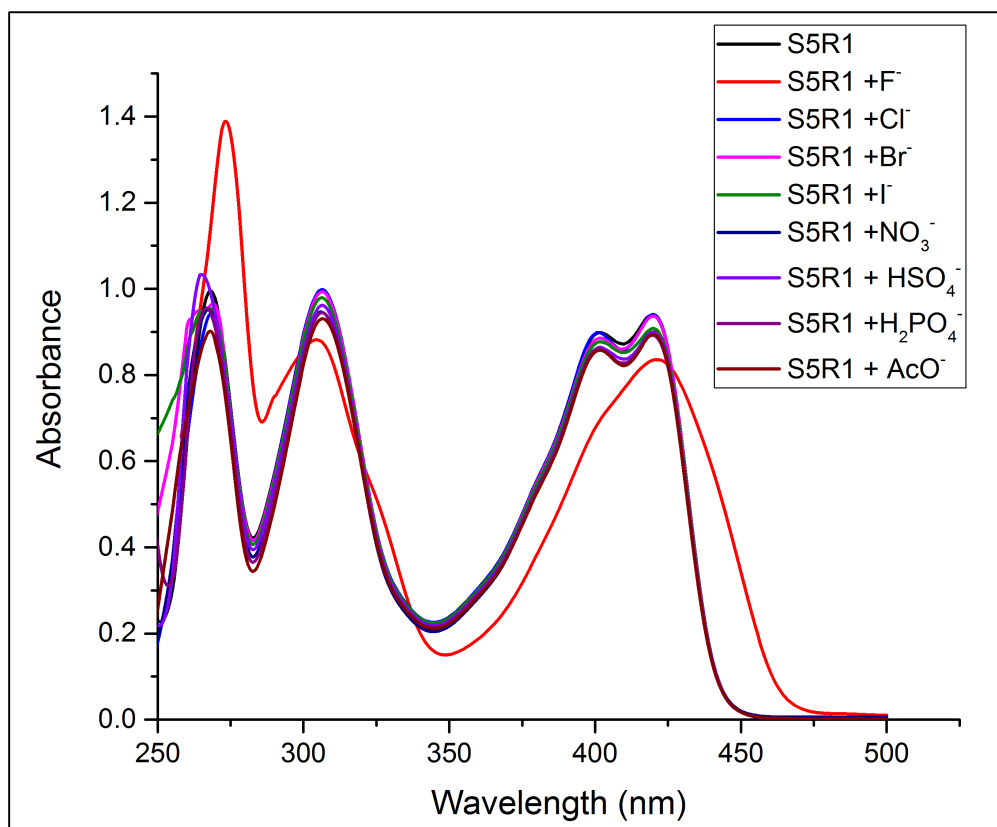


Fig. 7.5 UV-Vis absorption spectra of **S5R1** (1×10^{-5} M in DMSO) upon addition of 2 equiv. of various anions as TBA salts (10^{-2} M in DMSO)

When the DMSO solution of **S5R1** was investigated under fluorescent light, it was found to be non-fluorescent in the absence of F^- ion. With the addition of 2 equiv. of TBA salts of anions to **S5R1**, a strong blue fluorescence emission was observed in the presence of F^- ion. (Fig. 7.6). When DMSO solution of **S5R1** excited at 420 nm, it did not exhibit any emission proving its non-emissive nature. The addition of F^- ion resulted in an emission maximum at 475 nm whereas addition of other test anions could not induce similar response (Fig. 7.7). Receptor **S5R1** is non-emissive in DMSO owing to the photoelectron transfer (PET) process occurring between naphthalene and the hydroxyl moiety. In the presence of F^- ion, hydroxyl moiety partakes in hydrogen bonding with F^- ion and hinders the PET process. Consequently, strong fluorescent response of naphthalene is restored and receptor **S5R1** acts as turn on sensor for fluoride. (Tanaka et al. 2004)

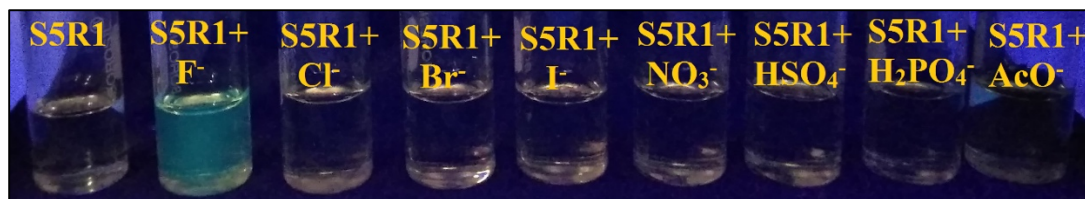


Fig. 7.6 Fluorometric response of the receptors **S5R1** (1×10^{-5} M in DMSO) with the addition of 2 equiv. of TBA salts of anions (10^{-2} M in DMSO)

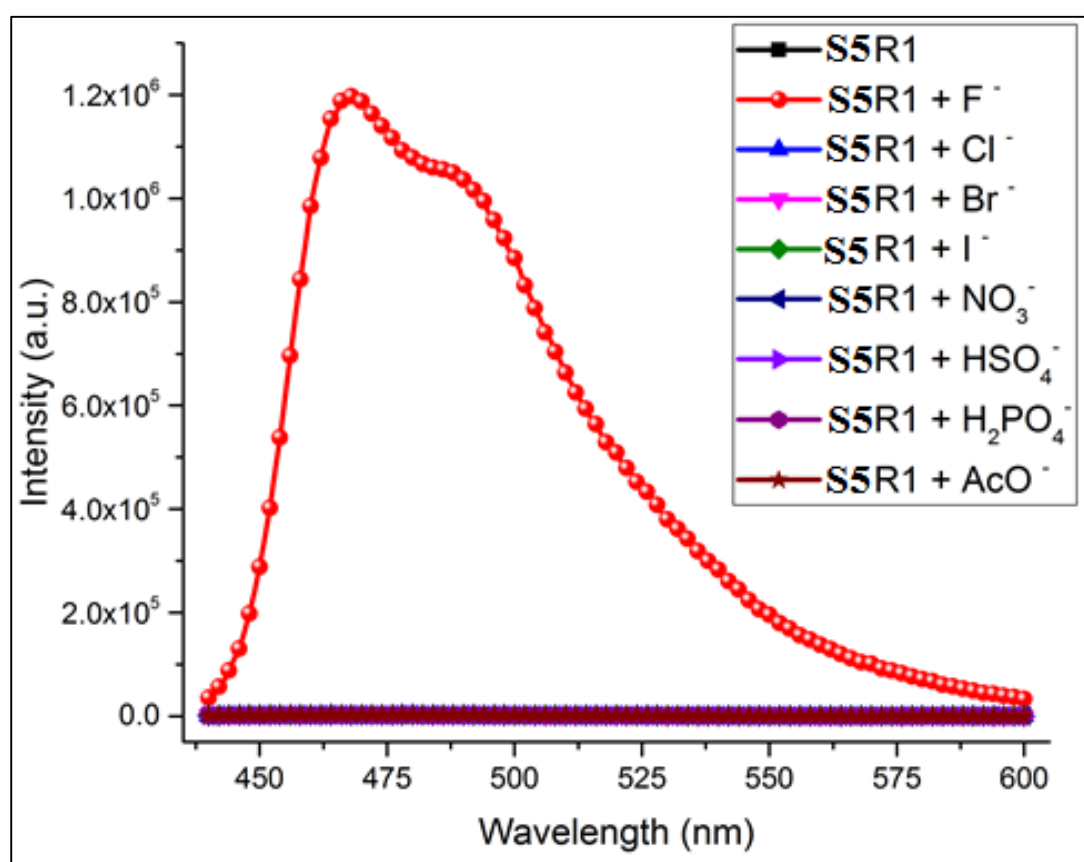


Fig. 7.7 Fluorescence spectra of **S5R1** (1×10^{-5} M in DMSO) upon addition of 2 equiv. of various anions as TBA salts (10^{-2} M in DMSO)

To confirm the anion binding event, UV-Vis and fluorescence titration studies have been performed with the incremental addition of F^- ions to receptor **S5R1**. The receptor solution was prepared in organic media, 1×10^{-5} M in DMSO and TBAF as

1×10^{-2} M in DMSO. In the UV-Vis titration studies, to a measured quantity of receptor, incremental amount of F^- (0.1 equiv.) was added each time until absorbance attained saturation. Mild bathochromic shift was observed with the emergence of new peak at 450 nm. The new peak at 450 nm could be assigned to the charge transfer interactions between the proton donor $-OH$ functionality and the acceptor viz., F^- ion. The concomitant decrease in the absorption maxima at 306 nm depicts subsiding O-H \cdots N intramolecular charge transfer within the receptor moiety upon binding of F^- ion. The band centered at 401 nm gradually diminished and band at 420 nm decreased in its intensity with the incremental addition of F^- ion. The presence of four well-defined isobestic points at 299 nm, 321 nm, 334 nm and 426 nm indicate the receptor – anion complex formation process and the co-existence of complex equilibrium between the free receptor and the anion-receptor complex. Upon addition of 1.5 equiv. of F^- , the absorption spectra reached a plateau, remaining steady till 2.0 equiv. indicating the saturation point of the receptor (Fig. 7.8). From the B-H plot, the binding stoichiometry was found to be 1:1 for **S5R1**: F^- complex and 1:2 for deprotonated form of the complex (Fig. 7.9(a)). Binding stoichiometry has been verified using Job's plot, which yielded 1:1 ratio for hydrogen bound R1: F^- complex and 1:2 ratio for deprotonated form (Fig. 7.9 (b)). The binding constant has been calculated using B-H equation considering 1:1 binding ratio and it was found to be of the order $5.9 \times 10^5 M^{-1}$. Detection limit has been calculated and found to 0.8 ppm.

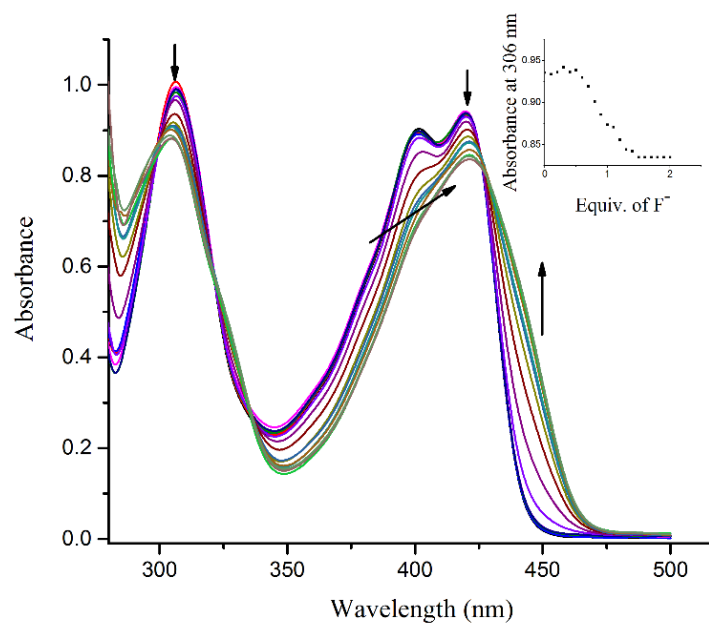


Fig. 7.8 UV-Vis titration spectra of receptor **S5R1** (10^{-5} M in DMSO) with the incremental addition of TBA salts of anions (10^{-2} M in DMSO); Inset plot representing the plot of absorbance at 306 nm vs concentration of TBAF

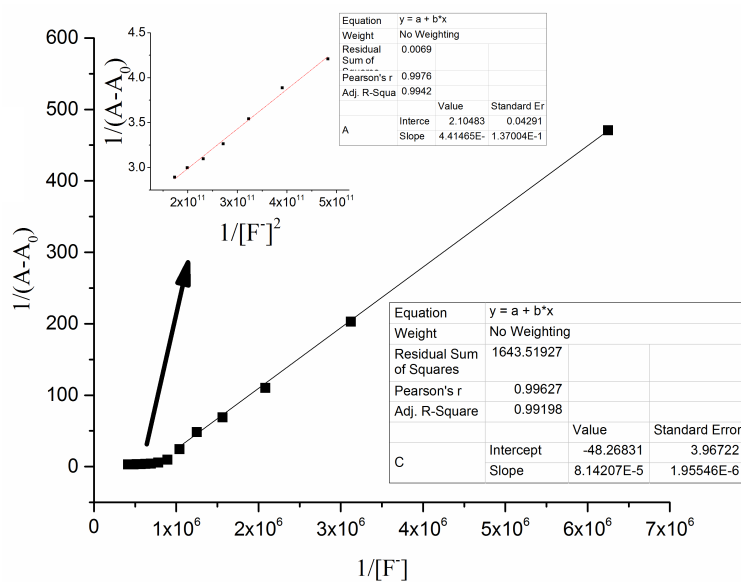


Fig. 7.9(a) B-H plot of $1/(A-A_0)$ at 450 nm indicating 1:1 binding between **S5R1** and F^- ion. Inset shows the B-H plot of $1/(A-A_0)$ at 450 nm vs. $1/[F^-]^2$ indicating 1:2 binding between **S5R1** and F^- ion.

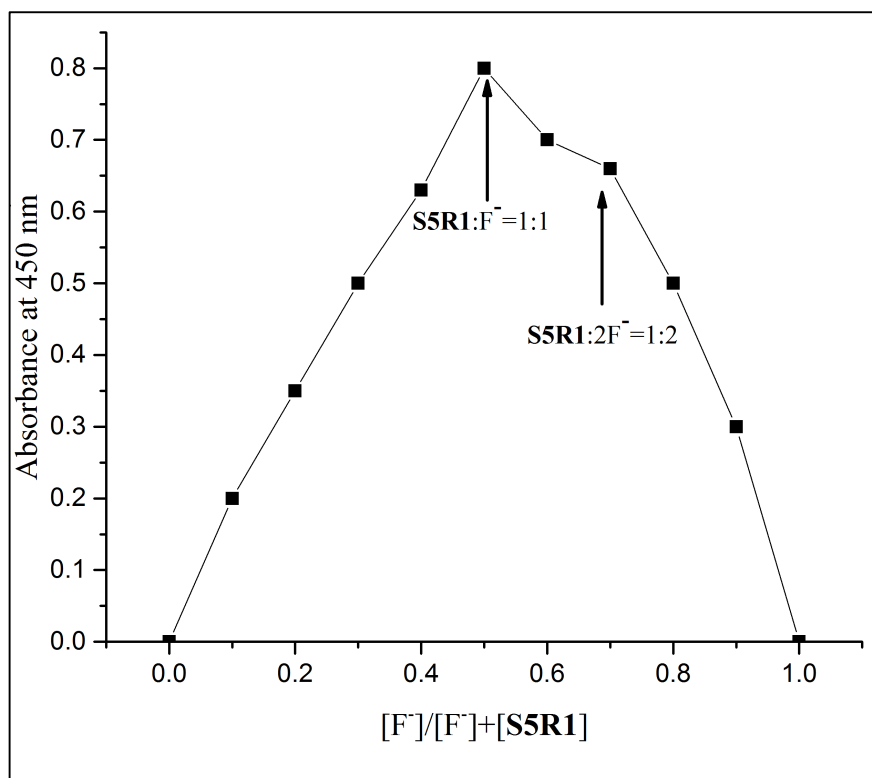


Fig. 7.9 (b) Job's plot for **S5R1**-TBAF complex

In the fluorescence titration studies, with the incremental addition of F^- ions to receptor **S5R1**, a strong emission band appeared at 475 nm which increased in its intensity until the addition of 1.5 equiv. of F^- ions, beyond which it exhibited saturation as shown in Fig. 7.10. Emission could be being attributed to the complexation-induced formation of excimer owing to the presence of naphthalene moiety (Ghosh et al. 2016).

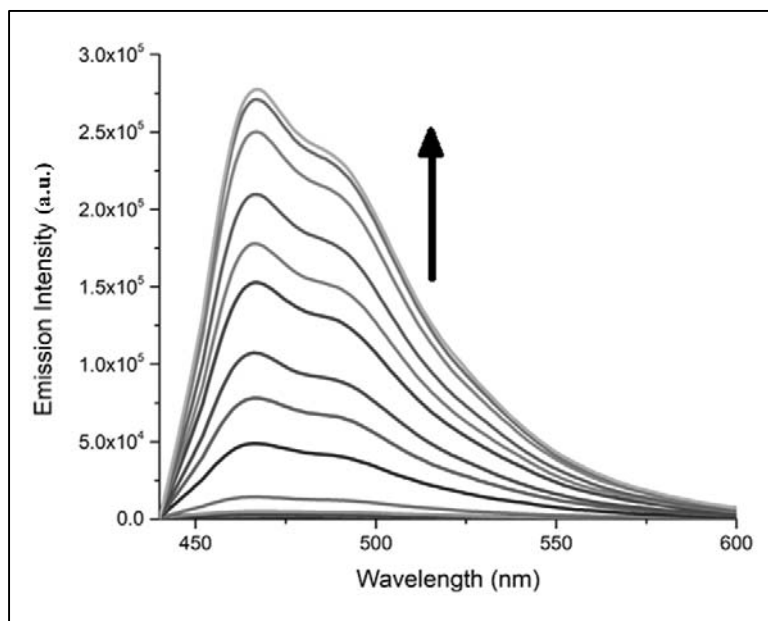


Fig. 7.10 Fluorescence spectra of receptor **S5R1** (10^{-5} M in DMSO) with the incremental addition of TBA salt of F^- ion (10^{-2} M in DMSO)

To confirm the deprotonation of hydroxyl functionality of the receptor **S5R1** in the anion binding process, studies has been performed with the addition 2 equiv. of base, TBAOH (10^{-2} M) to receptor **S5R1**. **S5R1** exhibited similar color changes as that was observed with the addition of TBAF which confirms the deprotonation mechanism. The color change observed with the addition of OH^- to **S5R1** are presented in Fig. 7.11 and Fig. 7.12. The corresponding spectral data are shown in Fig. 7.13 and Fig. 7.14. The large turn on increase with the addition of 2 equiv. of OH^- could be assigned to the formation of neutral species upon deprotonation of the fluoride bound $-OH$ group. The non-fluorescent nature of the complex formed by initial hydrogen bond interactions could be understood by fluorescence titration experiments. Until the addition of 0.5 equiv. of fluoride there was no much increase in the emission intensity, rather above 1 equiv. there has been substantial increase

indicative of deprotonation of the -OH group, confirming the fact that neutral form of the fluorophore is fluorescent in nature.

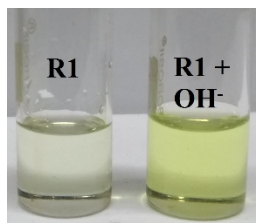


Fig. 7.11 Color change of **S5R1** with the addition of 2 equiv. of TBAOH

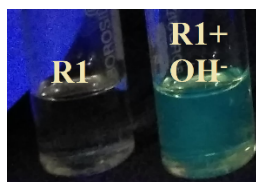


Fig. 7.12 Fluorometric response of **S5R1** with the addition of 2 equiv. of TBAOH

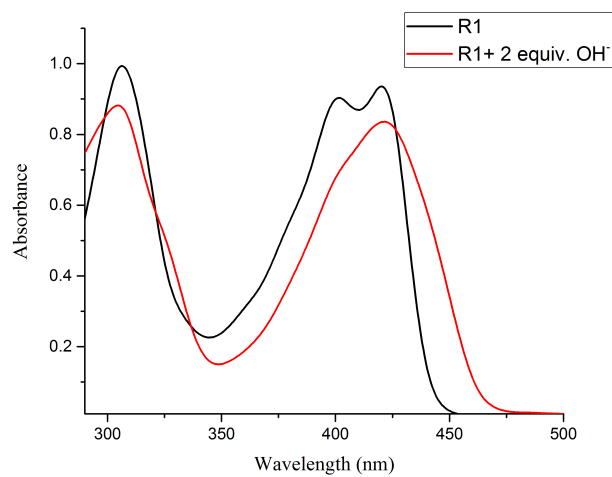


Fig. 7.13 UV-Vis spectra of **S5R1** with the addition of 2 equiv. of TBAOH

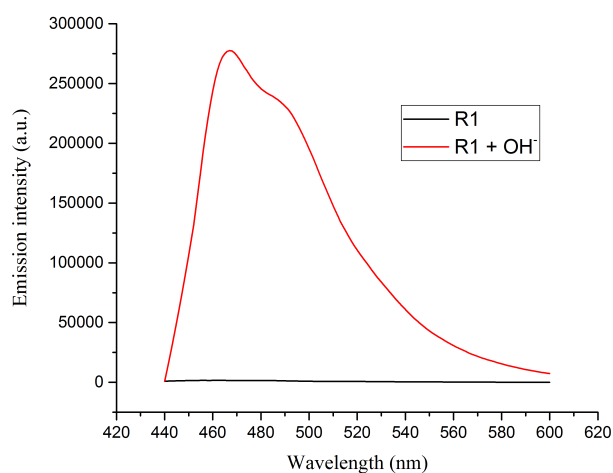


Fig. 7.14 PL spectra of **S5R1** with the addition of 2 equiv. of TBAOH

7.3.1.2 $^1\text{H-NMR}$ titration studies

The study has been further extended to monitor the binding of anions by the receptor through $^1\text{H-NMR}$ titration in $\text{DMSO-}d_6$ solvent. The $^1\text{H-NMR}$ spectrum of **R1** is characterized by the peaks for (a) $-\text{OH}$ proton around δ 14.13 ppm, (b) imine proton at 9.1 ppm and aromatic protons at 6.7 – 8.06 ppm. With the addition of F^- ions, there was initially a hydrogen bond interaction with OH proton, followed by disappearance of the peak at 14.13 ppm indicating the deprotonation process involved in the anion binding event (Fig. 7.15). The reduction in the splitting pattern in the aromatic region indicates the hydrogen bond interaction followed by deprotonation of the OH proton involved in the anion binding process. The appearance of new peak at δ 16.1 ppm (Fig. 7.15, inset) at higher equivalence of F^- ions correspond to the formation of HF_2^- (hydrogen difluoride), which confirmed the deprotonation of OH proton. (Boiocchi et al. 2004)

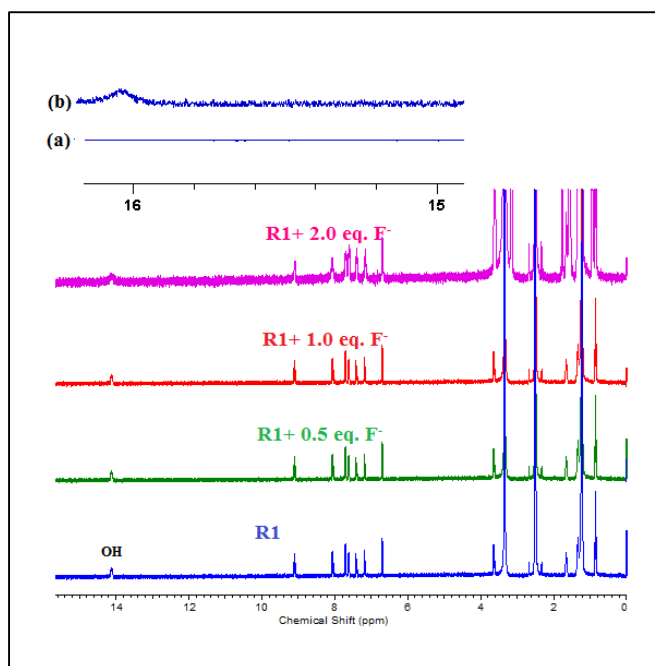


Fig. 7.15 ^1H -NMR spectra of **S5R1** with the incremental addition of TBAF. Inset: (a) absence of peak at 16.1 ppm in free receptor **S5R1** and (b) peak corresponding to HF_2 observed with the addition of 2.0 equiv. of F^- .

7.3.2 Gelation studies

Owing to the presence of long alkyl chain as a prerequisite for multiple self-assembly driving forces, such as π - π stacking, hydrogen bonds and Vander Waal forces, in the receptor, along with naphthalene moiety as a signaling scaffold, it was decided to explore the structure of **S5R1** in gel chemistry. The gelation ability of **S5R1** was scrutinized in fifteen different types of organic solvents through the standard heating-and-cooling method (Fig. 7.16) and the results are shown in Table 7.1. Among these solvents, **S5R1** formed stable and strong supramolecular organic gel in DMSO, DMF and ACN. Moreover, sol-gel transition was very rapid in DMSO wherein gelation occurred within a minute after the heating process. It could be assumed that formation of cross-linked network through hydrogen bonding between –OH functionality and imine nitrogen aiding the solvent trapping. The presence of π stacking interactions exerted by the naphthalene ring is expected to stabilize the hydrogen bonded network (Ghosh et al. 2016).

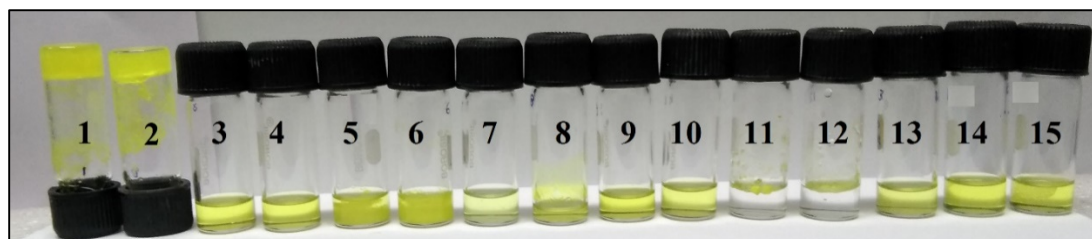


Fig. 7.16 Photographs showing the gelation behavior of **S5R1** in selected solvents (1) DMSO, (2) DMF, (3) Cyclohexane, (4) Chloroform, (5) Methanol, (6) ACN, (7) n-Hexane, (8) Diethyether, (9) DCM, (10) THF, (11) DMF: H₂O (1:2, v/v), (12) DMSO: H₂O (1:2, v/v), (13) Propyl alcohol, (14) Ethanol and (15) Dioxane

The UV-Vis spectrum revealed broad absorbance bands indicating the presence of intermolecular interactions through hydrogen bond in the gel state. (Fig. 7.17) Fluorescence emission was not observed in gel state as shown in Fig. 7.18 which could be probably associated with the aggregation-caused quenching (ACQ) phenomena that caused non-radiative decay of the fluorophore (Hong et al. 2011).

Table 7.1 Gelation properties of **S5R1**

Solvent	State
DMSO	G (26 mg/mL)
DMF	G (26 mg/mL)
Cyclohexane	S
Chloroform	S
Methanol	S
Acetonitrile	G (26 mg/mL)
n-Hexane	S
Diethyl ether	S
DCM	S
THF	S
DMF : H ₂ O (1:2 , v/v)	I
DMSO: H ₂ O (1:2 , v/v)	I
Propyl alcohol	S
Ethanol	S
Dioxane	S

S = solution; G = gel (minimum gelatination concentration); I = insoluble

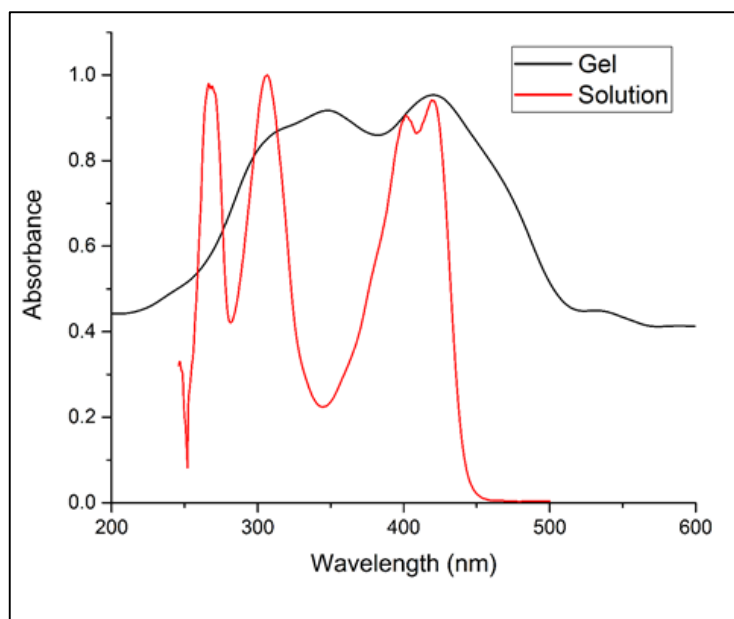


Fig. 7.17 Comparison of UV-Vis spectra of **S5R1** in the solution and gel state

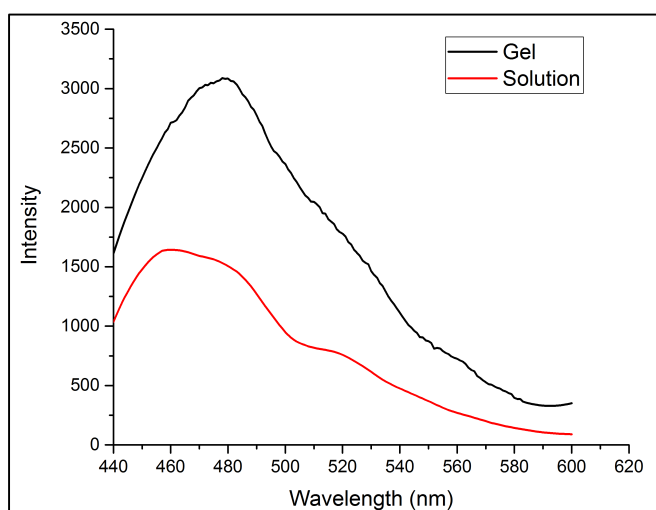


Fig. 7.18 Comparison of fluorescence spectra of **S5R1** in the solution and gel state

For the naked-eye sensing test of gelators **S5R1**, 2 equiv. of anions (tetrabutylammonium salts, 0.2 M) were dropped on the top of the organogel and the sample was inverted after 30 min to assess the gel-sol transition. The gel gradually turned into solution state in the presence of F^- ions. The disrupted gel resulted in sol

which exhibited fluorescence emission as observed in solution state studies. Under similar conditions, the gel state of **S5R1** remained unaffected in the presence of other anions studied. (Fig. 7.19) The gel–sol transition in the presence of F^- ions, is ascribed to the rupturing of hydrogen bonded network via intermolecular hydrogen bonding of **S5R1** with the anions and deprotonation with highly basic F^- ion. The deprotonation phenomenon has been confirmed in the sol state indicating the reason for disruption of gel. Fluorescence was observed upon gel to sol transformation as seen in Fig. 7.20.

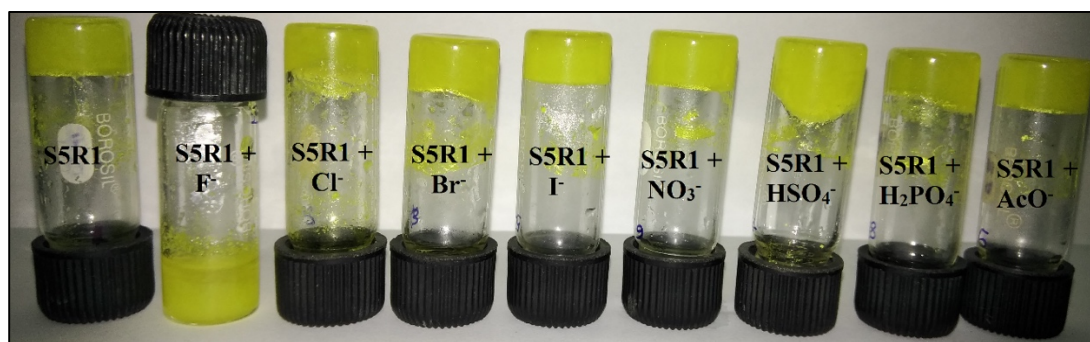


Fig. 7.19 Photographs showing the phase changes of gel (26 mg/mL) of **S5R1** (obtained from DMSO upon addition of 2 equiv. of TBA salts of anions)

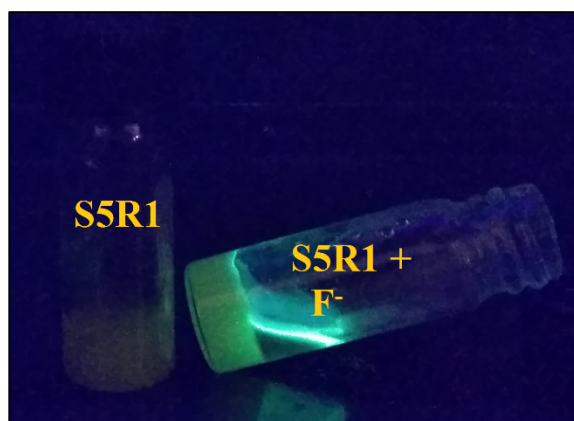


Fig. 7.20 Gel-sol transition and fluorescent response of **S5R1** with the addition of F^- ion

7.3.3 Calculation of binding constant from UV-Vis studies

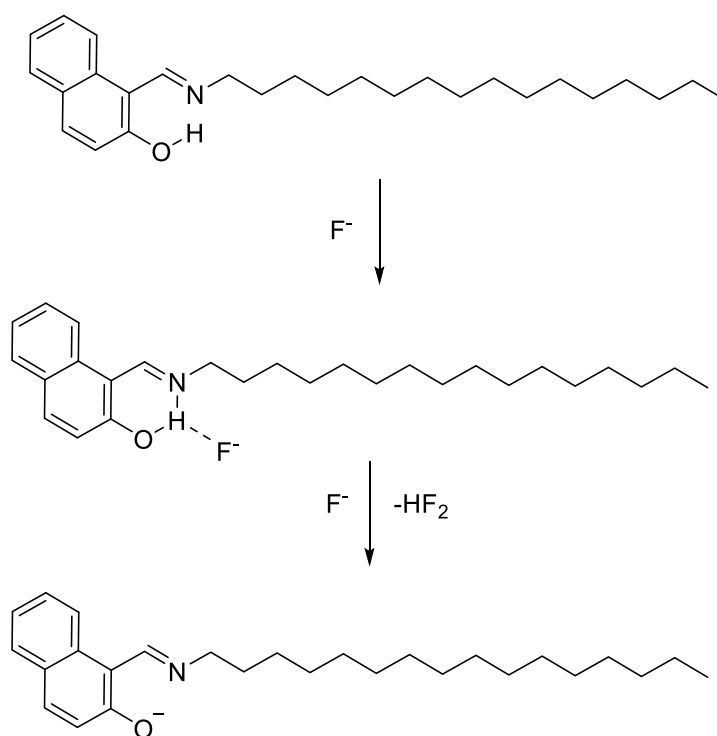
Binding constant has been calculated using Benesi-Hildebrand equation (Benesi and Hildebrand 1948) as given below;

$$1/(A-A_0) = 1/(A_{\max} - A_0) + 1/K [X^-]^n (A_{\max} - A_0)$$

where, A_0 , A , A_{\max} are the absorption considered in the absence of anion, at an intermediate, and at a concentration of saturation. K is binding constant, $[X^-]$ is concentration of anion and n is the stoichiometric ratio.

7.3.4 Binding mechanism

The presence of potent binding site viz., -OH functionality in the receptor **S5R1** aids selective binding of F^- ion. With the addition of F^- ion, initial hydrogen bond interaction with -OH functionality further diminishes with incremental addition indicating the deprotonation mechanism. Binding mechanism is shown in Fig. 6.13.



Scheme 7.2 Proposed binding mechanism of **S5R1** with F^- ion

7.4 CONCLUSIONS

A new organic receptor **R1** has been successfully utilized in the selective detection of F^- ion with a colorimetric and fluorometric turn on response. **R1** acts as good gelator in DMSO and the gel state is observed to yield a selective response to F^- ion with the disruption of gel. The efficacy of the naphthalene motif as signaling scaffold, long length alkyl chain aiding gelation and $-OH$ as F^- ion binding site has been recognized in sol-gel transition properties of **R1**. Higher order of binding constant of the order $5.9 \times 10^5 M^{-1}$ for hydrogen bound 1:1 **R1**: F^- complex in the solution phase indicates the strong recognition ability of the receptor **R1**. DFT studies provide full support of anion binding mechanism highlighting the energy minimized geometry of **R1**- F^- ion complex. Detection limit was found to 0.8 ppm and it indicates the utility of the receptor **R1** in practical applications.

CHAPTER 8
SUMMARY AND CONCLUSIONS

8.1 SUMMARY

- The main objective of the present work was to strategically design organic receptors for the colorimetric detection of anions.
- To this end, the application of designed receptors in the detection of anions in commercial, biological and environmental samples have been achieved.
- Six different series of receptors possessing signaling unit and anion binding site have been synthesized, characterized and applied in the colorimetric detection of anions.
- Binding of F^- , AcO^- , $H_2PO_4^-$, CN^- and AsO_2^- by different receptors in the series in organic and semi-aqueous media has been qualitatively and quantitatively assessed by UV-Vis spectroscopic, 1H -NMR, cyclic voltammetric and DFT studies.
- The evaluation of binding constants for the receptor-anion complexes by B-H equation revealed the dependence of hydrogen bond in fine tuning the binding strength.
- It was observed that there was significant increase in the binding constant of hydrogen bond with the decrease in the competition of solvent with the receptor.
- This implies the role of non-competitive and non-polar solvents towards the strong increase of binding constant.
- Of all, receptors **S4R1**, **S4R2** and **S4R3** displayed higher order of binding constant implying the strength of hydrogen bond interactions.
- The occurrence of lower order of binding constant of other receptors in the order of **S5** > **L** > **R** > **S4** > **S1** > **S2** could be attributed to the existence of shortest hydrogen bond distances between the receptor and anion.
- Binding constant values have been successfully utilized in analyzing the strength of hydrogen bond interaction in the receptor-anion complexation process.
- Lower detection limit of 0.25 ppm, 0.4 ppm and 0.8 ppm for F^- ions with receptors **S1R2**, **S2R4** and **S5R1** respectively; 0.92 ppm, 0.58 for AcO^- ions

with receptors **L** and **S3R2** and 0.03 ppm for AsO_2^- ions with receptor **S4R1** highlights the efficacy of the receptors in practical applications.

- Detection of F^- in mouthwash, seawater; AcO^- in *E. coli*; CN^- ions in sprouting potatoes; H_2PO_4^- in detergent sample; DNA binding studies elicit the practical applicability of the selected receptors in real life applications.

8.2 CONCLUSIONS

The present research work has merged in the field of anion receptor chemistry with the design strategy paving way for the detection of multitude of anions such as F^- , AcO^- , H_2PO_4^- , CN^- and AsO_2^- . The practical utility of the designed receptors in real life applications has enriched the early explorations in a way leading to successful physiological applications.

Six different series of organic receptors have been synthesized, characterized by standard spectroscopic techniques and evaluated for their anion sensing properties. Based on the evaluation of anion binding behavior by UV-Vis, ^1H NMR, cyclic voltammetric and DFT, following conclusions have been derived.

- Organic receptors **R** and **L** exhibited pink and blue coloration with the addition of F^- and AcO^- ions respectively and revealed sharp changes in the absorption maxima with the emergence of isobestic points. Quantification of F^- ions in mouthwash proves the utility of receptor **R** in practical applications. Rate constant values of receptor **L** with the addition of F^- and AcO^- ions confirmed the first order reaction kinetics. ^1H NMR titration studies and DFT studies confirmed the binding mechanism.
- Receptors **S1R1** and **S1R2** exhibited absorption ratiometric response in the UV-Vis spectra with the addition of F^- and AcO^- ions with a significant color change from yellow to bright pink. Anion binding studies of **S1R1** in DMSO: HEPES buffer (9:1, v/v) media exhibited selective detection of AcO^- ions with pale pink coloration. ^1H -NMR titration spectra of **S1R1** in the presence of

AcO⁻ ions confirmed the formation of azo-hydrazone tautomers in the anion binding process.

- The influence of positional substitution of nitro functionality in the series of phenylhydrazine based receptors **S2R1**, **S2R2**, **S2R3**, **S2R4** and **S2R5** has been confirmed. UV-Vis spectra of receptor **S2R4** revealed positive solvatochromism confirming the vivid color changes observed with the addition of AcO⁻ ions to receptor in solvents of varying polarity. Solid state sensing property and selective detection of AcO⁻ ions in solution phase highlights the efficacy of nitro group in fine tuning the colorimetric response of the receptor **S2R4**.
- The effect of suitable substitution of electron withdrawing moieties on furan based organic receptors **S3R1**, **S3R2** and **S3R3** proved for the colorimetric detection of F⁻, AcO⁻, H₂PO₄⁻ ions with sharp color changes in DMSO. Studies in DMSO: HEPES buffer (9:1, v/v) media confirmed the selective detection of AcO⁻ ions by receptors **S3R1**, **S3R2** and **S3R3**. Receptor **S3R1** has been successfully utilized in the detection of AcO⁻ ions in *E. coli* BL21 during its growth phase.
- In the series of thiadiazole based receptors **S4R1**, **S4R2** and **S4R3**, acetonitrile solution of receptor **S4R1** exhibited colorimetric response and a red shift band in the presence of F⁻, AcO⁻, H₂PO₄⁻, CN⁻ and AsO₂⁻ ions revealing multi-anion sensing property. Receptor **S4R1** was successfully applied in the detection of CN⁻ ions in sprouted potatoes, DNA binding and quantification of H₂PO₄⁻ ions in commercially available detergent sample.
- Naphthaldehyde based organic receptor **S5R1** exhibited selective colorimetric and fluorometric detection of F⁻ ions in DMSO. Gelation studies scrutinized in fifteen different organic solvents revealed the gelation properties of **S5R1** in DMSO. The gel was successfully utilized in the detection of F⁻ ions. Lower detection limit of 0.8 ppm implies the practical utility of the receptor **S5R1** in real life applications.

8.3 SCOPE FOR FUTURE WORK

The present research work has been successful in the detection of biologically and environmentally important anions paving way for practical applications. Yet, the selective and sensitive detection of anions have to be addressed in future as it could pave way for device applications. The reproducibility and reversibility of sensor have to be optimized by rational design of receptor with appropriate binding sites. If a receptor could be designed such that it exhibits vivid color change in the presence of different anions, it could certainly be utilized in the detection and extraction of anions from groundwater sources, industrial effluents. With the development of new receptors which could induce gelation upon anion binding, it would be a benchmark in the field of anion recognition chemistry heading towards more specific biological applications.

REFERENCES

-
- Adegoke, O. A. (2011). "Relative predominance of azo and hydrazone tautomers of 4-carboxyl-2,6-dinitrophenylazohydroxynaphthalenes in binary solvent mixtures." *Spectrochim. Acta. A. Mol. Biomol. Spectrosc.*, 83(1), 504–510.
- Agarwalla, H., Jana, K., Maity, A., Kesharwani, M. K., Ganguly, B., and Das, A. (2014). "Hydrogen Bonding Interaction between Active Methylene Hydrogen Atoms and an Anion as a Binding Motif for Anion Recognition: Experimental Studies and Theoretical Rationalization." *J. Phys. Chem. A*, 118(14), 2656–2666.
- Ali, H. D. P., Kruger, P. E., and Gunnlaugsson, T. (2008). "Colorimetric 'naked-eye' and fluorescent sensors for anions based on amidourea functionalised 1,8-naphthalimide structures: anion recognition via either deprotonation or hydrogen bonding in DMSO." *New J. Chem.*, 32(7), 1153–1161.
- Ajayakumar, M. R., Mukhopadhyay, P., Yadav, S., and Ghosh, S. (2010). "Single-Electron Transfer Driven Cyanide Sensing: A New Multimodal Approach." *Org. Lett.*, 12(11), 2646–2649.
- Amendola, V., Fabbrizzi, L., and Mosca, L. (2010). "Anion recognition by hydrogen bonding: urea-based receptors." *Chem. Soc. Rev.*, 39(10), 3889–3915.
- Amendola, V., Esteban-Gómez, D., Fabbrizzi, L., and Licchelli, M. (2006). "What Anions Do to N–H-Containing Receptors." *Acc. Chem. Res.*, 39(5), 343–353.
- Anderson, R. A., and Harland, W. A. (1982). "Fire Deaths in the Glasgow Area: III the Role of Hydrogen Cyanide." *Med. Sci. Law*, 22(1), 35–40.
- Anzenbacher, Pavel, Palacios, M. A., Jursíková, K., and Marquez, M. (2005). "Simple Electrooptical Sensors for Inorganic Anions." *Org. Lett.*, 7(22), 5027–5030.
- Arjmand, F., and Aziz, M. (2009). "Synthesis and characterization of dinuclear macrocyclic cobalt(II), copper(II) and zinc(II) complexes derived from 2,2,2',2'-S,S[bis(bis-N,N-2-thiobenzimidazoloxalato-1,2-ethane)]: DNA binding and cleavage studies." *Eur. J. Med. Chem.*, 44(2), 834–844.

-
- Atwood, J. L., Holman, K. T., and Steed, J. W. (1996). "Laying traps for elusive prey: recent advances in the non-covalent binding of anions." *Chem. Commun.*, 0(12), 1401–1407.
- Ball, P., and Nicholls, C. H. (1982). "Azo-hydrazone tautomerism of hydroxyazo compounds—a review." *Dyes Pigments*, 3(1), 5–26.
- Banerjee, S., K. Das, R., and Maitra, U. (2009). "Supramolecular gels 'in action.'" *J. Mater. Chem.*, 19(37), 6649–6687.
- Bao, X., Zheng, P., Liu, Y., Tan, Z., Zhou, Y., and Song, B. (2013). "Salicylaldehyde-indole-2-acylhydrazone: a simple, colorimetric and absorption ratiometric chemosensor for acetate ion." *Supramol. Chem.*, 25(4), 246–253.
- Basu, A., Dey, S. K., and Das, G. (2013). "Amidothiourea based colorimetric receptors for basic anions: evidence of anion induced deprotonation of amide –NH proton and hydroxide induced anion $\cdots\pi$ interaction with the deprotonated receptors." *RSC Adv.*, 3(18), 6596–6605.
- Bauer, V. J., Clive, D. L. J., Dolphin, D., Paine, J. B., Harris, F. L., King, M. M., Loder, J., Wang, S. W. C., and Woodward, R. B. (1983). "Sapphyrins: novel aromatic pentapyrrolic macrocycles." *J. Am. Chem. Soc.*, 105(21), 6429–6436.
- Becker, C. E. (1985). "The role of cyanide in fires." *Vet. Hum. Toxicol.*, 27(6), 487–490.
- Beer, P. D., and Hayes, E. J. (2003). "Transition metal and organometallic anion complexation agents." *Coord. Chem. Rev.*, 35 Years of Synthetic Anion Receptor Chemistry 1968-2003, 240(1), 167–189.
- Beer, P. D., and Gale, P. A. (2001). "Anion Recognition and Sensing: The State of the Art and Future Perspectives." *Angew. Chem. Int. Ed.*, 40(3), 486–516.
- Bencini, A., Coluccini, C., Garau, A., Giorgi, C., Lippolis, V., Messori, L., Pasini, D., and Puccioni, S. (2012). "A BINOL-based chiral polyammonium receptor for highly enantioselective recognition and fluorescence sensing of (S,S)-tartaric acid in aqueous solution." *Chem. Commun.*, 48(84), 10428–10430.

Benesi, H. and Hildebrand, H, (1949). "A spectrophotometric investigation of the interaction of iodine with aromatic hydrocarbons." *J. Am. Chem. Soc.* 71 (8), 2703-2707.

B. Berryman, O., and W. Johnson, D. (2009). "Experimental evidence for interactions between anions and electron-deficient aromatic rings." *Chem. Commun.*, 0(22), 3143–3153.

Berryman, O. B., Sather, A. C., Hay, B. P., Meisner, J. S., and Johnson, D. W. (2008). "Solution Phase Measurement of Both Weak σ and C–H \cdots X[–] Hydrogen Bonding Interactions in Synthetic Anion Receptors." *J. Am. Chem. Soc.*, 130(33), 10895–10897.

Best, M. D., Tobey, S. L., and Anslyn, E. V. (2003). "Abiotic guanidinium containing receptors for anionic species." *Coord. Chem. Rev.*, 35 Years of Synthetic Anion Receptor Chemistry 1968-2003, 240(1), 3–15.

Bhosale, S. V., Bhosale, S. V., Kalyankar, M. B., and Langford, S. J. (2009). "A Core-Substituted Naphthalene Diimide Fluoride Sensor." *Org. Lett.*, 11(23), 5418–5421.

Black, C. B., Andrioletti, B., Try, A. C., Ruiperez, C., and Sessler, J. L. (1999). "Dipyrrolylquinoxalines: Efficient Sensors for Fluoride Anion in Organic Solution." *J. Am. Chem. Soc.*, 121(44), 10438–10439.

Blondeau, P., Segura, M., Pérez-Fernández, R., and Mendoza, J. de. (2007). "Molecular recognition of oxoanions based on guanidinium receptors." *Chem. Soc. Rev.*, 36(2), 198–210.

Boiocchi, M., Del Boca, L., Gómez, D. E., Fabbrizzi, L., Licchelli, M., and Monzani, E. (2004). "Nature of Urea–Fluoride Interaction: Incipient and Definitive Proton Transfer." *J. Am. Chem. Soc.*, 126(50), 16507–16514.

Boiocchi, M., Del Boca, L., Esteban-Gómez, D., Fabbrizzi, L., Licchelli, M., and Monzani, E. (2005). "Anion-Induced Urea Deprotonation." *Chem. – Eur. J.*, 11(10), 3097–3104.

Bose, P., Ahamed, B. N., and Ghosh, P. (2011). "Functionalized guanidinium chloride based colourimetric sensors for fluoride and acetate: single crystal X-ray structural evidence of -NH deprotonation and complexation." *Org. Biomol. Chem.*, 9(6), 1972–1979.

Bratthall, D., Hänsel-Petersson, G., and Sundberg, H. (1996). "Reasons for the caries decline: what do the experts believe?" *Eur. J. Oral Sci.*, 104(4), 416–422.

Brooks, S. J., Gale, P. A., and Light, M. E. (2006). "Anion-binding modes in a macrocyclic amidourea." *Chem. Commun.*, 0(41), 4344–4346.

Caltagirone, C., and Gale, P. A. (2009). "Anion receptor chemistry: highlights from 2007." *Chem. Soc. Rev.*, 38(2), 520–563.

Caltagirone, C., A. Gale, P., R. Hiscock, J., J. Brooks, S., B. Hursthouse, M., and E. Light, M. (2008a). "1,3-Diindolylureas: high affinity dihydrogen phosphate receptors." *Chem. Commun.*, 0(26), 3007–3009.

Caltagirone, C., Hiscock, J. R., Hursthouse, M. B., Light, M. E., and Gale, P. A. (2008b). "1,3-Diindolylureas and 1,3-Diindolylthioureas: Anion Complexation Studies in Solution and the Solid State." *Chem. – Eur. J.*, 14(33), 10236–10243.

Camiolo, S., A. Gale, P., B. Hursthouse, M., and E. Light, M. (2003). "Nitrophenyl derivatives of pyrrole 2,5-diamides: structural behaviour, anion binding and colour change signalled deprotonation." *Org. Biomol. Chem.*, 1(4), 741–744.

Carter, K. P., Young, A. M., and Palmer, A. E. (2014). "Fluorescent Sensors for Measuring Metal Ions in Living Systems." *Chem. Rev.*, 114(8), 4564–4601.

Chang, K.-J., Kang, B.-N., Lee, M.-H., and Jeong, K.-S. (2005). "Oligoindole-Based Foldamers with a Helical Conformation Induced by Chloride." *J. Am. Chem. Soc.*, 127(35), 12214–12215.

Chen, X., Li, Z., Xiang, Y., and Tong, A. (2008). "Salicylaldehyde fluorescein hydrazone: a colorimetric logic chemosensor for pH and Cu(II)." *Tetrahedron Lett.*, 49(32), 4697–4700.

Cheng, H., Huq, F., Beale, P., and Fisher, K. (2006). "Synthesis, characterisation, activities, cell uptake and DNA binding of a trinuclear complex: $[\{\text{trans-PtCl}(\text{NH}_3)\}_2\mu\text{-}\{\text{trans-Pd}(\text{NH}_3)(2\text{-hydroxypyridine})\text{-}(\text{H}_2\text{N}(\text{CH}_2)_6\text{NH}_2)_2\}\text{Cl}_4]$." *Eur. J. Med. Chem.*, 41(7), 896–903.

Chifotides, H. T., Schottel, B. L., and Dunbar, K. R. (2010). "The π -Accepting Arene HAT(CN)₆ as a Halide Receptor through Charge Transfer: Multisite Anion Interactions and Self-Assembly in Solution and the Solid State." *Angew. Chem. Int. Ed.*, 49(40), 7202–7207.

Chmielewski, M. J., Charon, M., and Jurczak, J. (2004). "1,8-Diamino-3,6-dichlorocarbazole: A Promising Building Block for Anion Receptors." *Org. Lett.*, 6(20), 3501–3504.

Cho, E. J., Ryu, B. J., Lee, Y. J., and Nam, K. C. (2005). "Visible Colorimetric Fluoride Ion Sensors." *Org. Lett.*, 7(13), 2607–2609.

Choi, K., and Hamilton, A. D. (2003). "Macrocyclic anion receptors based on directed hydrogen bonding interactions." *Coord. Chem. Rev.*, 35 Years of Synthetic Anion Receptor Chemistry 1968-2003, 240(1), 101–110.

Chowdhury, A. R., Ghosh, P., Roy, B. G., Mukhopadhyay, S. K., Mitra, P., and Banerjee, P. (2015). "A simple and dual responsive efficient new Schiff base chemoreceptor for selective sensing of F⁻ and Hg²⁺: application to bioimaging in living cells and mimicking of molecular logic gates." *RSC Adv.*, 5(76), 62017–62023.

Christensen, D. (1984). "Determination of substrates oxidized by sulfate reduction in intact cores of marine sediments1." *Limnol. Oceanogr.*, 29(1), 189–191.

Czarnik, A. W. (1994). "Chemical Communication in Water Using Fluorescent Chemosensors." *Acc. Chem. Res.*, 27(10), 302–308.

Dalapati, S., Alam, M. A., Jana, S., and Guchhait, N. (2011). "Naked-eye detection of F⁻ and AcO⁻ ions by Schiff base receptor." *J. Fluor. Chem.*, 132(8), 536–540.

Datta, S., and Bhattacharya, S. (2011). "Evidence of aggregation induced emission enhancement and keto-enol-tautomerism in a gallic acid derived salicylideneaniline gel." *Chem. Commun.*, 48(6), 877–879.

Davis, A. P., and Joos, J.-B. (2003). "Steroids as organising elements in anion receptors." *Coord. Chem. Rev.*, 35 Years of Synthetic Anion Receptor Chemistry 1968-2003, 240(1), 143–156.

Dey, S. K., and Das, G. (2011). “A selective fluoride encapsulated neutral tripodal receptor capsule: solvatochromism and solvatomorphism.” *Chem. Commun.*, 47(17), 4983–4985.

Dickson, S. J., Paterson, M. J., Willans, C. E., Anderson, K. M., and Steed, J. W. (2008). “Anion Binding and Luminescent Sensing using Cationic Ruthenium(II) Aminopyridine Complexes.” *Chem. – Eur. J.*, 14(24), 7296–7305.

Dietrich, B., Fyles, T. M., Lehn, J.-M., Pease, L. G., and Fyles, D. L. (1978). “Anion receptor molecules. Synthesis and some anion binding properties of macrocyclic guanidinium salts.” *J. Chem. Soc. Chem. Commun.*, 0(21), 934–936.

Duke, R. M., and Gunnlaugsson, T. (2011). “3-Urea-1,8-naphthalimides are good chemosensors: a highly selective dual colorimetric and fluorescent ICT based anion sensor for fluoride.” *Tetrahedron Lett.*, 52(13), 1503–1505.

Duke, R. M., Veale, E. B., Pfeffer, F. M., Kruger, P. E., and Gunnlaugsson, T. (2010). “Colorimetric and fluorescent anion sensors: an overview of recent developments in the use of 1,8-naphthalimide-based chemosensors.” *Chem. Soc. Rev.*, 39(10), 3936–3953.

Esteban-Gómez, D., Fabbrizzi, L., and Licchelli, M. (2005). “Why, on Interaction of Urea-Based Receptors with Fluoride, Beautiful Colors Develop.” *J. Org. Chem.*, 70(14), 5717–5720.

Estroff, L. A., and Hamilton, A. D. (2004). “Water Gelation by Small Organic Molecules.” *Chem. Rev.*, 104(3), 1201–1218.

Evans, R. W., and Darvell, B. W. (1995). “Refining the Estimate of the Critical Period for Susceptibility to Enamel Fluorosis in Human Maxillary Central Incisors.” *J. Public Health Dent.*, 55(4), 238–249.

Evans, L. S., Gale, P. A., Light, M. E., and Quesada, R. (2006). “Anion binding vs. deprotonation in colorimetric pyrrolylamidothiourea based anion sensors.” *Chem. Commun.*, 0(9), 965–967.

-
- Farinha, A. S. F., Tomé, A. C., and Cavaleiro, J. A. S. (2010). "Synthesis of new calix[4]pyrrole derivatives via 1,3-dipolar cycloadditions." *Tetrahedron*, 66(38), 7595–7599.
- Fejerskov, O., Larsen, M. J., Richards, A., and Baelum, V. (1994). "Dental Tissue Effects of Fluoride." *Adv. Dent. Res.*, 8(1), 15–31.
- Fejerskov, O., Stephen, K. W., Richards, A., and Speirs, R. (1987). "Combined Effect of Systemic and Topical Fluoride Treatments on Human Deciduous Teeth – Case Studies." *Caries Res.*, 21(5), 452–459.
- Ferguson, J. F., and Gavis, J. (1972). "A review of the arsenic cycle in natural waters." *Water Res.*, 6(11), 1259–1274.
- Foster, J. A., Piepenbrock, M.-O. M., Lloyd, G. O., Clarke, N., Howard, J. A. K., and Steed, J. W. (2010). "Anion-switchable supramolecular gels for controlling pharmaceutical crystal growth." *Nat. Chem.*, 2(12), 1037–1043.
- Gale, P. A. (2001). "Anion receptor chemistry: highlights from 1999." *Coord. Chem. Rev.*, 213(1), 79–128.
- Gale, P. A., Sessler, J. L., Král, V., and Lynch, V. (1996). "Calix[4]pyrroles: Old Yet New Anion-Binding Agents." *J. Am. Chem. Soc.*, 118(21), 5140–5141.
- Gale, P. A. (2006). "Structural and Molecular Recognition Studies with Acyclic Anion Receptors." *Acc. Chem. Res.*, 39(7), 465–475.
- Gale, P. A. (2010). "Anion receptor chemistry: highlights from 2008 and 2009." *Chem. Soc. Rev.*, 39(10), 3746–3771.
- Gale, P. A. (2003). "Anion and ion-pair receptor chemistry: highlights from 2000 and 2001." *Coord. Chem. Rev.*, 35 Years of Synthetic Anion Receptor Chemistry 1968-2003, 240(1), 191–221.
- Gale, P. A., Busschaert, N., E. Haynes, C. J., E. Karagiannidis, L., and L. Kirby, I. (2014). "Anion receptor chemistry: highlights from 2011 and 2012." *Chem. Soc. Rev.*, 43(1), 205–241.

-
- Gale, P. A., E. García-Garrido, S., and Garric, J. (2008). “Anion receptors based on organic frameworks: highlights from 2005 and 2006.” *Chem. Soc. Rev.*, 37(1), 151–190.
- Gale, P. A., (2008). “Synthetic indole, carbazole, biindole and indolocarbazole-based receptors: applications in anion complexation and sensing.” *Chem. Commun.*, 0(38), 4525–4540.
- Gale, P. A., and Caltagirone, C. (2015). “Anion sensing by small molecules and molecular ensembles.” *Chem. Soc. Rev.*, 44(13), 4212–4227.
- Ghosh, P., Roy, B. G., Jana, S., Mukhopadhyay, S. K., and Banerjee, P. (2015). “Colorimetric and fluorimetric response of Schiff base molecules towards fluoride anion, solution test kit fabrication, logical interpretations and DFT-D3 study.” *Phys. Chem. Chem. Phys.*, 17(31), 20288–20295.
- Ghosh, S., Goswami, K., and Ghosh, K. (2017). “Pyrrole-based tetra-amide for hydrogen pyrophosphate ($\text{HP}_2\text{O}_7^{3-}$) and F⁻ ions in sol-gel medium.” *Supramol. Chem.*, 29(12), 946–952.
- Graf, E., and Lehn, J. M. (1976). “Anion cryptates: highly stable and selective macrotricyclic anion inclusion complexes.” *J. Am. Chem. Soc.*, 98(20), 6403–6405.
- Grate, J. W., Egorov, O. B., O’Hara, M. J., and DeVol, T. A. (2008). “Radionuclide Sensors for Environmental Monitoring: From Flow Injection Solid-Phase Absorptiometry to Equilibration-Based Preconcentrating Minicolumn Sensors with Radiometric Detection.” *Chem. Rev.*, 108(2), 543–562.
- Greenhalgh, S., and Selman, M. (2012). “Comparing water quality trading programs: what lessons are there to learn?” *J. Reg. Anal. Policy*, 42(2), 104.
- Gunnlaugsson, T., Ali, H. D. P., Glynn, M., Kruger, P. E., Hussey, G. M., Pfeffer, F. M., Santos, C. M. G. dos, and Tierney, J. (2005). “Fluorescent photoinduced electron transfer (PET) sensors for anions; from design to potential application.” *J. Fluoresc.*, 15(3), 287–299.

Gunnlaugsson, T., Glynn, M., Tocci (née Hussey), G. M., Kruger, P. E., and Pfeffer, F. M. (2006). "Anion recognition and sensing in organic and aqueous media using luminescent and colorimetric sensors." *Coord. Chem. Rev., Anion Coordination Chemistry II*, 250(23), 3094–3117.

Gunnlaugsson, T., Davis, A. P., Hussey, G. M., Tierney, J., and Glynn, M. (2004). "Design, synthesis and photophysical studies of simple fluorescent anion PET sensors using charge neutral thiourea receptors." *Org. Biomol. Chem.*, 2(13), 1856–1863.

Gunnlaugsson, T., Kruger, P. E., Jensen, P., Tierney, J., Ali, H. D. P., and Hussey, G. M. (2005). "Colorimetric 'Naked Eye' Sensing of Anions in Aqueous Solution." *J. Org. Chem.*, 70(26), 10875–10878.

Gunupuru, R., Kesharwani, M. K., Chakraborty, A., Ganguly, B., and Paul, P. (2014). "Dipicrylamine as a colorimetric sensor for anions: experimental and computational study." *RSC Adv.*, 4(95), 53273–53281.

Gupta, T., and van der Boom, M. E. (2008). "Redox-Active Monolayers as a Versatile Platform for Integrating Boolean Logic Gates." *Angew. Chem.*, 120(29), 5402–5406.

Hadjmohammadi, M. R., Chaichi, M. J., and Yousefpour, M. (2008). "Solvatochromism Effect of Different Solvents on UV-Vis Spectra of Flouresceine and its Derivatives." *Iran. J. Chem. Chem. Eng. IJCCE*, 27(4), 9–14.

Hay, B. P., Firman, T. K., and Moyer, B. A. (2005). "Structural Design Criteria for Anion Hosts: Strategies for Achieving Anion Shape Recognition through the Complementary Placement of Urea Donor Groups." *J. Am. Chem. Soc.*, 127(6), 1810–1819.

He, X., Hu, S., Liu, K., Guo, Y., Xu, J., and Shao, S. (2006). "Oxidized Bis(indolyl)methane: A Simple and Efficient Chromogenic-Sensing Molecule Based on the Proton Transfer Signaling Mode." *Org. Lett.*, 8(2), 333–336.

He, X., Zhang, J., Liu, X., Dong, L., Li, D., Qiu, H., and Yin, S. (2014). "A novel BODIPY-based colorimetric and fluorometric dual-mode chemosensor for Hg²⁺ and Cu²⁺." *Sens. Actuators B Chem.*, 192, 29–35.

Hecht, S. M. (2000). "Bleomycin: New Perspectives on the Mechanism of Action." *J. Nat. Prod.*, 63(1), 158–168.

Hiscock, J. R., Caltagirone, C., Light, M. E., Hursthouse, M. B., and Gale, P. A. (2009). "Fluorescent carbazolyurea anion receptors." *Org. Biomol. Chem.*, 7(9), 1781–1783.

HOFMEISTER, F. (1888). "About the science of the effects of salts: About the water withdrawing effect of the salts." *Arch Exp Pathol Pharmacol*, 24, 247–260.

Homocianu, M. (2011). "Solvent effects on the electronic absorption and fluorescence spectra." *J. Adv. Res. Phys.*, 2(1).

Hong, Y., Y. Lam, J. W., and Zhong Tang, B. (2011). "Aggregation-induced emission." *Chem. Soc. Rev.*, 40(11), 5361–5388.

Tanaka, F., Mase, N., and Barbas, C. F. (2004). "Design and Use of Fluorogenic Aldehydes for Monitoring the Progress of Aldehyde Transformations." *J. Am. Chem. Soc.*, 126(12), 3692–3693.

Hsieh, Y.-C., Chir, J.-L., Wu, H.-H., Chang, P.-S., and Wu, A.-T. (2009). "A sugar-aza-crown ether-based fluorescent sensor for Hg²⁺ and Cu²⁺." *Carbohydr. Res.*, 344(16), 2236–2239.

Huang, F., Cheng, C., and Feng, G. (2012). "Introducing Ligand-Based Hydrogen Bond Donors to a Receptor: Both Selectivity and Binding Affinity for Anion Recognition in Water Can Be Improved." *J. Org. Chem.*, 77(24), 11405–11408.

Huang, J., Ma, X., Liu, B., Cai, L., Li, Q., Zhang, Y., Jiang, K., and Yin, S. (2013). "A colorimetric and ratiometric turn-on BODIPY-based fluorescent probe for double-channel detection of Cu²⁺ and Hg²⁺." *J. Lumin.*, 141, 130–136.

Hughes, M. F. (2002). "Arsenic toxicity and potential mechanisms of action." *Toxicol. Lett.*, 133(1), 1–16.

Hurley, L. H. (2002). "DNA and its associated processes as targets for cancer therapy." *Nat. Rev. Cancer*, 2(3), 188–200.

Irie, M. (2000). "Diarylethenes for Memories and Switches." *Chem. Rev.*, 100(5), 1685–1716.

J. Chmielewski, M., Zhao, L., Brown, A., Curiel, D., R. Sambrook, M., L. Thompson, A., M. Santos, S., Felix, V., J. Davis, J., and D. Beer, P. (2008). "Sulfate anion templation of

a neutral pseudorotaxane assembly using an indolocarbazole threading component.” *Chem. Commun.*, 0(27), 3154–3156.

Jakusová, K., Donovalová, J., Cigáň, M., Gáplovský, M., Garaj, V., and Gáplovský, A. (2014). “Isatinphenylsemicarbazones as efficient colorimetric sensors for fluoride and acetate anions – Anions induce tautomerism.” *Spectrochim. Acta. A. Mol. Biomol. Spectrosc.*, 123(Supplement C), 421–429.

Jiménez, D., Martínez-Máñez, R., Sancenón, F., and Soto, J. (2002). “Selective fluoride sensing using colorimetric reagents containing anthraquinone and urea or thiourea binding sites.” *Tetrahedron Lett.*, 43(15), 2823–2825.

Jose, D. A., Kumar, D. K., Ganguly, B., and Das, A. (2004). “Efficient and Simple Colorimetric Fluoride Ion Sensor Based on Receptors Having Urea and Thiourea Binding Sites.” *Org. Lett.*, 6(20), 3445–3448.

Kaloo, M. A., and Sankar, J. (2013). “Exclusive fluoride ion recognition and fluorescence ‘turn-on’ response with a label-free DMN Schiff base.” *Analyst*, 138(17), 4760–4763.

Khakh, B. S., and North, R. A. (2006). “P2X receptors as cell-surface ATP sensors in health and disease.” *Nature*, 442(7102), 527–532.

Kim, E., Jung Kim, H., Ri Bae, D., Jin Lee, S., Jin Cho, E., Ryeong Seo, M., Seung Kim, J., and Hwa Jung, J. (2008a). “Selective fluoride sensing using organic–inorganic hybrid nanomaterials containing anthraquinone.” *New J. Chem.*, 32(6), 1003–1007.

Kim, U.-I., Suk, J., Naidu, V. R., and Jeong, K.-S. (2008b). “Folding and Anion-Binding Properties of Fluorescent Oligoindole Foldamers.” *Chem. – Eur. J.*, 14(36), 11406–11414.

Kirk, K. L. (1991). “Biochemistry of Inorganic Fluoride.” *Biochem. Elem. Halog. Inorg. Halides*, Biochemistry of the Elements, Springer, Boston, MA, 19–68.

Kleerekoper, M. (1998). “THE ROLE OF FLUORIDE IN THE PREVENTION OF OSTEOPOROSIS.” *Endocrinol. Metab. Clin.*, 27(2), 441–452.

Klein, A., and Bonhoeffer, F. (1972). “DNA Replication.” *Annu. Rev. Biochem.*, 41(1), 301–332.

Kubik, S. (2010). “Anion recognition in water.” *Chem. Soc. Rev.*, 39(10), 3648–3663.

Kuksenok, O., Dayal, P., Bhattacharya, A., Yashin, V. V., Deb, D., Chen, I. C., Vliet, K. J. V., and Balazs, A. C. (2013). "Chemo-responsive, self-oscillating gels that undergo biomimetic communication." *Chem. Soc. Rev.*, 42(17), 7257–7277.

Kumari, N., Jha, S., and Bhattacharya, S. (2011). "Colorimetric Probes Based on Anthraimidazolediones for Selective Sensing of Fluoride and Cyanide Ion via Intramolecular Charge Transfer." *J. Org. Chem.*, 76(20), 8215–8222.

Kwon, J. Y., Jang, Y. J., Kim, S. K., Lee, K.-H., Kim, J. S., and Yoon, J. (2004). "Unique Hydrogen Bonds between 9-Anthracenyl Hydrogen and Anions." *J. Org. Chem.*, 69(15), 5155–5157.

Lai, Y.-H., Sun, S.-C., and Chuang, M.-C. (2014). "Biosensors with Built-In Biomolecular Logic Gates for Practical Applications." *Biosensors*, 4(3), 273–300.

Lazarides, T., Miller, T. A., Jeffery, J. C., Ronson, T. K., Adams, H., and Ward, M. D. (2005). "Luminescent complexes of Re(I) and Ru(II) with appended macrocycle groups derived from 5,6-dihydroxyphenanthroline: cation and anion binding." *Dalton Trans.*, 0(3), 528–536.

Lee, D. H., Im, J. H., Son, S. U., Chung, Y. K., and Hong, J.-I. (2003). "An Azophenol-based Chromogenic Pyrophosphate Sensor in Water." *J. Am. Chem. Soc.*, 125(26), 7752–7753.

Lee, D. H., Lee, K. H., and Hong, J.-I. (2001). "An Azophenol-Based Chromogenic Anion Sensor." *Org. Lett.*, 3(1), 5–8.

Lee, J. Y., Cho, E. J., Mukamel, S., and Nam, K. C. (2004). "Efficient Fluoride-Selective Fluorescent Host: Experiment and Theory." *J. Org. Chem.*, 69(3), 943–950.

Lee, M. H., and Gabbai, F. P. (2007). "Synthesis and Properties of a Cationic Bidentate Lewis Acid." *Inorg. Chem.*, 46(20), 8132–8138.

Levin, B. C., Rechani, P. R., Gurman, J. L., Landron, F., Clark, H. M., Yoklavich, M. F., Rodriguez, J. R., Droz, L., Cabrera, F. de, and Kaye, S. (1990). "Analysis of Carboxyhemoglobin and Cyanide in Blood from Victims of the Dupont Plaza Hotel Fire in Puerto Rico." *J. Forensic Sci.*, 35(1), 151–168.

-
- Li, F., Carvalho, S., Delgado, R., Drew, M. G. B., and Félix, V. (2010). "Dimetallic complexes of macrocycles with two rigid dibenzofuran units as receptors for detection of anionic substrates." *Dalton Trans.*, 39(40), 9579–9587.
- Li, J.-Q., Wei, T.-B., Lin, Q., Li, P., and Zhang, Y.-M. (2011). "Mercapto thiadiazole-based sensor with colorimetric specific selectivity for AcO⁻ in aqueous solution." *Spectrochim. Acta. A. Mol. Biomol. Spectrosc.*, 83(1), 187–193.
- Lin, T.-P., Chen, C.-Y., Wen, Y.-S., and Sun, S.-S. (2007). "Synthesis, Photophysical, and Anion-Sensing Properties of Quinoxalinebis(sulfonamide) Functionalized Receptors and Their Metal Complexes." *Inorg. Chem.*, 46(22), 9201–9212.
- Lin, Y.-S., Tu, G.-M., Lin, C.-Y., Chang, Y.-T., and Yen, Y.-P. (2009). "Colorimetric anion chemosensors based on anthraquinone: naked-eye detection of isomeric dicarboxylate and tricarboxylate anions." *New J. Chem.*, 33(4), 860–867.
- Lin, Z., Ou, S., Duan, C., Zhang, B., and Bai, Z. (2006). "Naked-eye detection of fluoride ion in water: a remarkably selective easy-to-prepare test paper." *Chem. Commun.*, 0(6), 624–626.
- Lloyd, G. O., and Steed, J. W. (2009). "Anion-tuning of supramolecular gel properties." *Nat. Chem.*, 1(6), 437.
- Lou, X., Qin, J., and Li, Z. (2009). "Colorimetric cyanide detection using an azobenzene acid in aqueous solutions." *Analyst*, 134(10), 2071–2075.
- M.S, N. E. K., and Ph.D, Q. F. (1991). "A review of arsenic (III) in groundwater." *Crit. Rev. Environ. Control*, 21(1), 1–39.
- Maeda, H. (2008). "Anion-Responsive Supramolecular Gels." *Chem. – Eur. J.*, 14(36), 11274–11282.
- Mahapatra, A. K., Karmakar, P., Roy, J., Manna, S., Maiti, K., Sahoo, P., and Mandal, D. (2015). "Colorimetric and ratiometric fluorescent chemosensor for fluoride ions based on phenanthroimidazole (PI): spectroscopic, NMR and density functional studies." *RSC Adv.*, 5(47), 37935–37942.

Maiti, M., and Kumar, G. S. (2007). "Molecular aspects on the interaction of protoberberine, benzophenanthridine, and aristolochia group of alkaloids with nucleic acid structures and biological perspectives." *Med. Res. Rev.*, 27(5), 649–695.

March, J. (1992). *Advanced organic chemistry: reactions, mechanisms, and structure*. New York: Wiley.

Margolis, H. C., and Moreno, E. C. (1990). "Physicochemical Perspectives on the Cariostatic Mechanisms of Systemic and Topical Fluorides." *J. Dent. Res.*, 69(2_suppl), 606–613.

Marini, A., Muñoz-Losa, A., Biancardi, A., and Mennucci, B. (2010). "What is Solvatochromism?" *J. Phys. Chem. B*, 114(51), 17128–17135.

Marks, J., Debnam, E. S., and Unwin, R. J. (2010). "Phosphate homeostasis and the renal-gastrointestinal axis." *Am. J. Physiol. - Ren. Physiol.*, 299(2), F285–F296.

Martínez-Mañez, R., and Sancenón, F. (2003). "Fluorogenic and Chromogenic Chemosensors and Reagents for Anions." *Chem. Rev.*, 103(11), 4419–4476.

Masscheleyn, P. H., Delaune, R. D., and Patrick, W. H. (1991). "Arsenic and Selenium Chemistry as Affected by Sediment Redox Potential and pH." *J. Environ. Qual.*, 20(3), 522–527.

Matsubara, K., Akane, A., Maseda, C., and Shiono, H. (1990). "'First pass phenomenon' of inhaled gas in the fire victims." *Forensic Sci. Int.*, 46(3), 203–208.

Mayes, R. W. (1991). "The Toxicological Examination of the Victims of the British Air Tours Boeing 737 Accident at Manchester in 1985." *J. Forensic Sci.*, 36(1), 179–184.

Mendham. (2006). *Vogels Textbook Of Quantitative Chemical Analysis*. Pearson Education India.

Misra, A., Shahid, M., and Dwivedi, P. (2009). "An efficient thiourea-based colorimetric chemosensor for naked-eye recognition of fluoride and acetate anions: UV–vis and ¹HNMR studies." *Talanta*, 80(2), 532–538.

-
- Miyaji, H., Sato, W., and Sessler, J. L. (2000). "Naked-Eye Detection of Anions in Dichloromethane: Colorimetric Anion Sensors Based on Calix[4]pyrrole." *Angew. Chem.*, 112(10), 1847–1850.
- Miyaji, H., Sato, W., Sessler, J. L., and Lynch, V. M. (2000). "A 'building block' approach to functionalized calix[4]pyrroles." *Tetrahedron Lett.*, 41(9), 1369–1373.
- Miyaji, H., and Sessler, J. L. (2001). "Off-the-Shelf Colorimetric Anion Sensors." *Angew. Chem.*, 113(1), 158–161.
- Mizuno, T., Wei, W.-H., Eller, L. R., and Sessler, J. L. (2002). "Phenanthroline Complexes Bearing Fused Dipyrrolylquinoxaline Anion Recognition Sites: Efficient Fluoride Anion Receptors." *J. Am. Chem. Soc.*, 124(7), 1134–1135.
- Moore, S. A., Moennich, D. M., and Gresser, M. J. (1983). "Synthesis and hydrolysis of ADP-arsenate by beef heart submitochondrial particles." *J. Biol. Chem.*, 258(10), 6266–6271.
- Mrksich, M., and Dervan, P. B. (1993). "Enhanced sequence specific recognition in the minor groove of DNA by covalent peptide dimers: bis(pyridine-2-carboxamidonetropsin)(CH₂)₃₋₆." *J. Am. Chem. Soc.*, 115(22), 9892–9899.
- Murray, J. J. (1993). "Efficacy of Preventive Agents for Dental Caries." *Caries Res.*, 27(Suppl. 1), 2–8.
- M.S, N. E. K., and Ph.D, Q. F. (1991). "A review of arsenic (III) in groundwater." *Crit. Rev. Environ. Control*, 21(1), 1–39.
- N. Farrugia, K., Makuc, D., Podborska, A., Szaciłowski, K., Plavec, J., and C. Magri, D. (2015). "UV-visible and ¹H–¹⁵N NMR spectroscopic studies of colorimetric thiosemicarbazide anion sensors." *Org. Biomol. Chem.*, 13(6), 1662–1672.
- Naidu, V. R., Kim, M. C., Suk, J., Kim, H.-J., Lee, M., Sim, E., and Jeong, K.-S. (2008). "Biased Helical Folding of Chiral Oligoindole Foldamers." *Org. Lett.*, 10(23), 5373–5376.

-
- Narayan Sahu, S., Kumar Padhan, S., and Kumar Sahu, P. (2016). "Coumarin functionalized thiocarbonhydrazones as a new class of chromofluorescent receptors for selective detection of fluoride ion." *RSC Adv.*, 6(93), 90322–90330.
- Nebot, V. J., Ojeda-Flores, J. J., Smets, J., Fernández-Prieto, S., Escuder, B., and Miravet, J. F. (2014). "Rational Design of Heat-Set and Specific-Ion-Responsive Supramolecular Hydrogels Based on the Hofmeister Effect." *Chem. – Eur. J.*, 20(44), 14465–14472.
- Nguyen, B. T., and Anslyn, E. V. (2006). "Indicator–displacement assays." *Coord. Chem. Rev.*, Anion Coordination Chemistry II, 250(23), 3118–3127.
- Nie, L., Zhang, Q., Hu, L., Liu, Y., and Yan, Z. (2017). "Modified hydrazone derivatives for ratiometric and colorimetric F[–] recognition: Relationship between architectures and performances." *Sens. Actuators B Chem.*, 245(Supplement C), 314–320.
- Nishiyabu, R., and Anzenbacher, P. (2005). "Sensing of Antipyretic Carboxylates by Simple Chromogenic Calix[4]pyrroles." *J. Am. Chem. Soc.*, 127(23), 8270–8271.
- Nolan, E. M., and Lippard, S. J. (2008). "Tools and tactics for the optical detection of mercuric ion." *Chem. Rev.*, 108(9), 3443–3480.
- Noro, A., Matsushima, S., He, X., Hayashi, M., and Matsushita, Y. (2013). "Thermoreversible Supramolecular Polymer Gels via Metal–Ligand Coordination in an Ionic Liquid." *Macromolecules*, 46(20), 8304–8310.
- O. Yu, J., Browning, C. S., and H. Farrar, D. (2008). "Tris-2-(3-methylindolyl)phosphine as an anion receptor." *Chem. Commun.*, 0(8), 1020–1022.
- Pandurangan, K., Kitchen, J. A., and Gunnlaugsson, T. (2013). "Colorimetric 'naked eye' sensing of anions using a thiosemicarbazide receptor: a case study of recognition through hydrogen bonding versus deprotonation." *Tetrahedron Lett.*, 54(22), 2770–2775.
- Park, C. H., and Simmons, H. E. (1968). "Macrobicyclic amines. III. Encapsulation of halide ions by diazabicycloalkane ammonium ions." *J. Am. Chem. Soc.*, 90(9), 2431–2432.

-
- Pascal Jr., R. A., Spergel, J., and Van Engen, D. (1986). "Synthesis and X-ray crystallographic characterization of a (1,3,5)cyclophane with three amide N-H groups surrounding a central cavity. A neutral host for anion complexation." *Tetrahedron Lett.*, 27(35), 4099–4102.
- Petersson, G. A., and Al-Laham, M. A. (1991). "A complete basis set model chemistry. II. Open-shell systems and the total energies of the first-row atoms." *J. Chem. Phys.*, 94(9), 6081–6090.
- Petersson, G. A., Bennett, A., Tensfeldt, T. G., Al-Laham, M. A., Shirley, W. A., and Mantzaris, J. (1988). "A complete basis set model chemistry. I. The total energies of closed-shell atoms and hydrides of the first-row elements." *J. Chem. Phys.*, 89(4), 2193–2218.
- Pfeffer, F. M., Lim, K. F., and Sedgwick, K. J. (2007). "Indole as a scaffold for anion recognition." *Org. Biomol. Chem.*, 5(11), 1795–1799.
- Piątek, P., Lynch, V. M., and Sessler, J. L. (2004). "Calix[4]pyrrole[2]carbazole: A New Kind of Expanded Calixpyrrole." *J. Am. Chem. Soc.*, 126(49), 16073–16076.
- Pischel, U., and Heller, B. (2008). "Molecular logic devices (half-subtractor, comparator, complementary output circuit) by controlling photoinduced charge transfer processes." *New J. Chem.*, 32(3), 395–400.
- Preiss, J., and Handler, P. (1958). "Biosynthesis of diphosphopyridine nucleotide I. Identification of intermediates." *J. Biol. Chem.*, 233(2), 488–492.
- Qiu, J. (2013). "Tough talk over mercury treaty." *Nat. News*, 493(7431), 144.
- Quinlan, E., Matthews, S. E., and Gunnlaugsson, T. (2007). "Colorimetric Recognition of Anions Using Preorganized Tetra-Amidourea Derived Calix[4]arene Sensors." *J. Org. Chem.*, 72(20), 7497–7503.
- Rajamalli, P., Malakar, P., Atta, S., and Prasad, E. (2014). "Metal induced gelation from pyridine cored poly(aryl ether) dendrons with in situ synthesis and stabilization of hybrid hydrogel composites." *Chem. Commun.*, 50(75), 11023–11025.

Rao, M. R., and Sun, S.-S. (2013). "Supramolecular Assemblies of Amide-Derived Organogels Featuring Rigid π -Conjugated Phenylethynyl Frameworks." *Langmuir*, 29(49), 15146–15158.

Ren, C., Zhang, J., Chen, M., and Yang, Z. (2014). "Self-assembling small molecules for the detection of important analytes." *Chem. Soc. Rev.*, 43(21), 7257–7266.

Richards, A., Kragstrup, J., Josephsen, K., and Fejerskov, O. (1986). "Dental Fluorosis Developed in Post-secretory Enamel." *J. Dent. Res.*, 65(12), 1406–1409.

R. Ajayakumar, M., Hundal, G., and Mukhopadhyay, P. (2013). "A tetrastable naphthalenediimide: anion induced charge transfer, single and double electron transfer for combinational logic gates." *Chem. Commun.*, 49(70), 7684–7686.

Roy, A., Kand, D., Saha, T., and Talukdar, P. (2014). "A cascade reaction based fluorescent probe for rapid and selective fluoride ion detection." *Chem. Commun.*, 50(41), 5510–5513.

Sakai, R., Barasa, E. B., Sakai, N., Sato, S., Satoh, T., and Kakuchi, T. (2012). "Colorimetric Detection of Anions in Aqueous Solution Using Poly(phenylacetylene) with Sulfonamide Receptors Activated by Electron Withdrawing Group." *Macromolecules*, 45(20), 8221–8227.

Sancenón, F., Martínez-Máñez, R., and Soto, J. (2002). "A Selective Chromogenic Reagent for Nitrate." *Angew. Chem. Int. Ed.*, 41(8), 1416–1419.

Sancenón, F., Martínez-Máñez, R., Miranda, M. A., Seguí, M.-J., and Soto, J. (2003). "Towards the Development of Colorimetric Probes to Discriminate between Isomeric Dicarboxylates." *Angew. Chem.*, 115(6), 671–674.

Santos-Figueroa, L. E., Moragues, M. E., Raposo, M. M. M., Batista, R. M. F., Costa, S. P. G., Ferreira, R. C. M., Sancenón, F., Martínez-Máñez, R., Ros-Lis, J. V., and Soto, J. (2012). "Synthesis and evaluation of thiosemicarbazones functionalized with furyl moieties as new chemosensors for anion recognition." *Org. Biomol. Chem.*, 10(36), 7418–7428.

Saroj, M. K., Sharma, N., and Rastogi, R. C. (2011). "Solvent Effect Profiles of Absorbance and Fluorescence Spectra of Some Indole Based Chalcones." *J. Fluoresc.*, 21(6), 2213–2227.

Satheshkumar, A., El-Mossalamy, E. H., Manivannan, R., Parthiban, C., Al-Harbi, L. M., Kosa, S., and Elango, K. P. (2014). "Anion induced azo-hydrazone tautomerism for the selective colorimetric sensing of fluoride ion." *Spectrochim. Acta. A. Mol. Biomol. Spectrosc.*, 128(Supplement C), 798–805.

Schmidtchen, F. P. (1977). "Inclusion of Anions in Macrotricyclic Quaternary Ammonium Salts." *Angew. Chem. Int. Ed. Engl.*, 16(10), 720–721.

Schmidtchen, F. P., and Müller, G. (1984). "Anion inclusion without auxiliary hydrogen bonds: X-ray structure of the iodide cryptate of a macrotricyclic tetra-quaternary ammonium receptor." *J. Chem. Soc. Chem. Commun.*, 0(16), 1115–1116.

Schmuck, C., and Schwegmann, M. (2005). "A Molecular Flytrap for the Selective Binding of Citrate and Other Tricarboxylates in Water." *J. Am. Chem. Soc.*, 127(10), 3373–3379.

Segarra-Maset, M. D., Nebot, V. J., Miravet, J. F., and Escuder, B. (2013). "Control of molecular gelation by chemical stimuli." *Chem. Soc. Rev.*, 42(17), 7086–7098.

Sessler, J. L., Camiolo, S., and Gale, P. A. (2003). "Pyrrolic and polypyrrolic anion binding agents." *Coord. Chem. Rev.*, 35 Years of Synthetic Anion Receptor Chemistry 1968-2003, 240(1), 17–55.

Sessler, J. L., Gross, D. E., Cho, W.-S., Lynch, V. M., Schmidtchen, F. P., Bates, G. W., Light, M. E., and Gale, P. A. (2006). "Calix[4]pyrrole as a Chloride Anion Receptor: Solvent and Counteraction Effects." *J. Am. Chem. Soc.*, 128(37), 12281–12288.

Sessler, J. L., Maeda, H., Mizuno, T., Lynch, V. M., and Furuta, H. (2002). "Quinoxaline-oligopyrroles: Improved pyrrole-based anion receptors." *Chem. Commun.*, 0(8), 862–863.

Sessler, J. L., and Seidel, D. (2003). "Synthetic Expanded Porphyrin Chemistry." *Angew. Chem. Int. Ed.*, 42(42), 5134–5175.

Sessler, J. L., Gale, P. A., and Cho, W.-S. (2006). Anion receptor chemistry. Monographs in supramolecular chemistry, Cambridge, UK: Royal Society of Chemistry.

Shannon, R. D. (1976). "Revised effective ionic radii and systematic studies of interatomic distances in halides and chalcogenides." *Acta Crystallogr. A*, 32(5), 751–767.

Sharma, D., Sahoo, S. K., Chaudhary, S., Bera, R. K., and Callan, J. F. (2013). "Fluorescence 'turn-on' sensor for F⁻ derived from vitamin B6 cofactor." *Analyst*, 138(13), 3646–3650.

Sharma, R., Mittal, S. K., and Chhibber, M. (2015). "Voltammetric Sensor for Fluoride Ions Using Diphenylether Derivatives Supported by NMR and Theoretical Studies." *J. Electrochem. Soc.*, 162(9), B248–B255.

Shionoya, M., Furuta, H., Lynch, V., Harriman, A., and Sessler, J. L. (1992). "Diprotonated sapphyrin: a fluoride selective halide anion receptor." *J. Am. Chem. Soc.*, 114(14), 5714–5722.

Silva, A. P. de, and McClenaghan, N. D. (2004). "Molecular-Scale Logic Gates." *Chem. – Eur. J.*, 10(3), 574–586.

Sørensen, J., Christensen, D., and Jørgensen, B. B. (1981). "Volatile Fatty Acids and Hydrogen as Substrates for Sulfate-Reducing Bacteria in Anaerobic Marine Sediment." *Appl. Environ. Microbiol.*, 42(1), 5–11.

Steed, J.W., Atwood, J.L. (2009). *Supramolecular Chemistry*, 2nd edition, John Wiley & Sons, Ltd., United Kingdom.

Steed, J. W. (2011). "Supramolecular gel chemistry: developments over the last decade." *Chem. Commun.*, 47(5), 1379–1383.

Suganya, S., Velmathi, S., Venkatesan, P., Wu, S.-P., and Susai Boobalan, M. (2015). "A highly fluorescent zinc complex of a dipodal N -acyl hydrazone as a selective sensor for H₂PO₄⁻ ions and application in living cells." *Inorg. Chem. Front.*, 2(7), 649–656.

Suksai, C., and Tuntulani, T. (2003). "Chromogenic anion sensors." *Chem. Soc. Rev.*, 32(4), 192–202.

Suk, J., and Jeong, K.-S. (2008). "Indolocarbazole-Based Foldamers Capable of Binding Halides in Water." *J. Am. Chem. Soc.*, 130(36), 11868–11869.

Sun, Z., Huang, Q., He, T., Li, Z., Zhang, Y., and Yi, L. (2014). "Multistimuli-Responsive Supramolecular Gels: Design Rationale, Recent Advances, and Perspectives." *ChemPhysChem*, 15(12), 2421–2430

Szacilowski, K. (2008). "Digital Information Processing in Molecular Systems." *Chem. Rev.*, 108(9), 3481–3548.

Tanaka, F., Mase, N., and Barbas, C. F. (2004). "Design and Use of Fluorogenic Aldehydes for Monitoring the Progress of Aldehyde Transformations." *J. Am. Chem. Soc.*, 126(12), 3692–3693.

Terech, P., and Weiss, R. G. (1997). "Low Molecular Mass Gelators of Organic Liquids and the Properties of Their Gels." *Chem. Rev.*, 97(8), 3133–3160.

Tetilla, M. A., Aragoni, M. C., Arca, M., Caltagirone, C., Bazzicalupi, C., Bencini, A., Garau, A., Isaia, F., Laguna, A., Lippolis, V., and Meli, V. (2011). "Colorimetric response to anions by a 'robust' copper(II) complex of a [9]aneN3 pendant arm derivative: CN⁻ and I⁻ selective sensing." *Chem. Commun.*, 47(13), 3805–3807.

Thiampanya, P., Muangsin, N., and Pulpoka, B. (2012). "Azocalix[4]arene Strapped Calix[4]pyrrole: A Confirmable Fluoride Sensor." *Org. Lett.*, 14(16), 4050–4053.

Tsui, Y.-K., Devaraj, S., and Yen, Y.-P. (2012). "Azo dyes featuring with nitrobenzoxadiazole (NBD) unit: A new selective chromogenic and fluorogenic sensor for cyanide ion." *Sens. Actuators B Chem.*, 161(1), 510–519.

Tysoe, S. A., Morgan, R. J., Baker, A. D., and Streckas, T. C. (1993). "Spectroscopic investigation of differential binding modes of .DELTA.- and .LAMBDA.- Ru(bpy)₂(ppz)₂⁺ with calf thymus DNA." *J. Phys. Chem.*, 97(8), 1707–1711.

Valiyaveetil, S., Engbersen, J. F. J., Verboom, W., and Reinhoudt, D. N. (1993). "Synthesis and Complexation Studies of Neutral Anion Receptors." *Angew. Chem. Int. Ed. Engl.*, 32(6), 900–901.

Vijayalakshmi, R., Kanthimathi, M., Parthasarathi, R., and Nair, B. U. (2006). "Interaction of chromium(III) complex of chiral binaphthyl tetradentate ligand with DNA." *Bioorg. Med. Chem.*, 14(10), 3300–3306.

Vázquez, M., Fabbrizzi, L., Taglietti, A., Pedrido, R. M., González-Noya, A. M., and Bermejo, M. R. (2004). "A Colorimetric Approach to Anion Sensing: A Selective Chemosensor of Fluoride Ions, in which Color is Generated by Anion-Enhanced π Delocalization." *Angew. Chem.*, 116(15), 1996–1999.

Vella, F. (1990). "Biochemistry: By C K Mathews and K E van Holde. pp 1299. Benjamin/Cummings Publishing Co, Redwood City, CA, USA. 1990. £24.95 ISBN 0-8053-5015-2." *Biochem. Educ.*, 18(3), 154–154.

W. Steed, J. (2010). "Anion-tuned supramolecular gels: a natural evolution from urea supramolecular chemistry." *Chem. Soc. Rev.*, 39(10), 3686–3699.

Wan, L., Shu, Q., Zhu, J., Jin, S., Li, N., Chen, X., and Chen, S. (2016). "A new multifunctional Schiff-based chemosensor for mask-free fluorimetric and colorimetric sensing of F⁻ and CN⁻." *Talanta*, 152, 39–44.

Wang, L., He, X., Guo, Y., Xu, J., and Shao, S. (2011). "Tris(indolyl)methene molecule as an anion receptor and colorimetric chemosensor: tunable selectivity and sensitivity for anions." *Org. Biomol. Chem.*, 9(3), 752–757.

Wang, G., Wu, H., Wang, D., Yan, C., and Lu, Y. (2013). "Exploring the binding mechanism of phosphoramidate derivative with DNA: Spectroscopy, calorimetry and modeling." *Spectrochim. Acta. A. Mol. Biomol. Spectrosc.*, 104, 492–496.

Wang, X., Zhao, J., Guo, C., Pei, M., and Zhang, G. (2014). "Simple hydrazide-based fluorescent sensors for highly sensitive and selective optical signaling of Cu²⁺ and Hg²⁺ in aqueous solution." *Sens. Actuators B Chem.*, 193, 157–165.

-
- Wang, Y., Huang, Z., Kim, Y., He, Y., and Lee, M. (2014). "Guest-Driven Inflation of Self-Assembled Nanofibers through Hollow Channel Formation." *J. Am. Chem. Soc.*, 136(46), 16152–16155.
- Wenzel, M., R. Hiscock, J., and A. Gale, P. (2012). "Anion receptor chemistry: highlights from 2010." *Chem. Soc. Rev.*, 41(1), 480–520.
- Way, J. L. (1984). "Cyanide Intoxication and its Mechanism of Antagonism." *Annu. Rev. Pharmacol. Toxicol.*, 24(1), 451–481.
- Wei, T.-B., Li, W.-T., Li, Q., Su, J.-X., Qu, W.-J., Lin, Q., Yao, H., and Zhang, Y.-M. (2016). "A turn-on fluorescent chemosensor selectively detects cyanide in pure water and food sample." *Tetrahedron Lett.*, 57(25), 2767–2771.
- Whitford, G. M. (1996). "Overview of Fluoride Metabolism and Intake." 16, 1–9.
- Wickner, W., and Kornberg, A. (1973). "DNA Polymerase III Star Requires ATP to Start Synthesis on a Primed DNA." *Proc. Natl. Acad. Sci.*, 70(12), 3679–3683.
- Wiskur, S. L., Ait-Haddou, H., Lavigne, J. J., and Anslyn, E. V. (2001). "Teaching Old Indicators New Tricks." *Acc. Chem. Res.*, 34(12), 963–972.
- Wolfe-Simon, F., Blum, J. S., Kulp, T. R., Gordon, G. W., Hoefl, S. E., Pett-Ridge, J., Stolz, J. F., Webb, S. M., Weber, P. K., Davies, P. C. W., Anbar, A. D., and Oremland, R. S. (2011). "A Bacterium That Can Grow by Using Arsenic Instead of Phosphorus." *Science*, 332(6034), 1163–1166.
- Xu, Z., Chen, X., Kim, H. N., and Yoon, J. (2009). "Sensors for the optical detection of cyanide ion." *Chem. Soc. Rev.*, 39(1), 127–137.
- Yadav, U. N., Pant, P., Sahoo, S. K., and Shankarling, G. S. (2014). "A novel colorimetric and fluorogenic chemosensor for selective detection of Cu²⁺ ions in mixed aqueous media." *RSC Adv.*, 4(80), 42647–42653.
- Yan, X., Wang, F., Zheng, B., and Huang, F. (2012). "Stimuli-responsive supramolecular polymeric materials." *Chem. Soc. Rev.*, 41(18), 6042–6065.
- Yang, L., Song, Q., Damit-Og, K., and Cao, H. (2013). "Synthesis and spectral investigation of a Turn-On fluorescence sensor with high affinity to Cu²⁺." *Sens. Actuators B Chem.*, 176, 181–185.

-
- Ye, H., Ge, F., Chen, X.-C., Li, Y., Zhang, H., Zhao, B.-X., and Miao, J.-Y. (2013). "A new probe for fluorescent recognition of Hg²⁺ in living cells and colorimetric detection of Cu²⁺ in aqueous solution." *Sens. Actuators B Chem.*, 182, 273–279.
- Yin, S., Leen, V., Snick, S. V., Boens, N., and Dehaen, W. (2010). "A highly sensitive, selective, colorimetric and near-infrared fluorescent turn-on chemosensor for Cu²⁺ based on BODIPY." *Chem. Commun.*, 46(34), 6329–6331.
- Yoon, J., Kim, S. K., Singh, N. J., and Kim, K. S. (2006). "Imidazolium receptors for the recognition of anions." *Chem. Soc. Rev.*, 35(4), 355–360.
- You, G. R., Park, G. J., Lee, S. A., Choi, Y. W., Kim, Y. S., Lee, J. J., and Kim, C. (2014). "A single chemosensor for multiple target anions: The simultaneous detection of CN⁻ and OAc⁻ in aqueous media." *Sens. Actuators B Chem.*, 202(Supplement C), 645–655.
- Zen, J.-M., Jou, J.-J., and Senthil Kumar, A. (1999). "A sensitive voltammetric method for the determination of parathion insecticide." *Anal. Chim. Acta*, 396(1), 39–44.
- Zuber, G., Quada, J. C., and Hecht, S. M. (1998). "Sequence Selective Cleavage of a DNA Octanucleotide by Chlorinated Bithiazoles and Bleomycins." *J. Am. Chem. Soc.*, 120(36), 9368–9369.

LIST OF PUBLICATIONS

Papers published in international journals

1. Srikala, P., Kartick Tarafder, A. Nityananda Shetty and Darshak R. Trivedi (2016) "Insights into the electrooptical anion sensing properties of a new organic receptor: Solvent dependent chromogenic response and DFT studies." *RSC Adv.*, 6, 74649 – 74653.
2. Srikala, P., Kartick Tarafder and Darshak R. Trivedi (2017) "Design and synthesis of a new organic receptor and evaluation of colorimetric anion sensing ability in organo-aqueous medium." *Spectrochim. Acta Mol. Biomol. Spectrosc.*, 170, 29–38.
3. Srikala Pangannaya and Darshak R. Trivedi (2017) "Electrooptical characteristics and anion binding behaviour of organic receptors: Effect of substitution on colorimetric response" *Sensors and Actuators B*, 247, 673–680.
4. Srikala Pangannaya, Neethu Padinchare Purayil, Shweta Dabhi, Venu Mankad, Prafulla K. Jha, Satyam Shinde and Darshak R. Trivedi (2017) "Spectral and DFT studies of anion bound organic receptors: Time dependent studies and logic gate application" *Beilstein J. Org. Chem.*, 13, 222–238.
5. Srikala Pangannaya, Vikram Thimaradka and Darshak R. Trivedi (2018) "Design, synthesis and spectral investigation of organic receptors as colorimetric and absorption ratiometric anion chemosensor", *Supramolecular Chemistry*, 30:2, 103-114.
6. Srikala Pangannaya, Makesh Mohan and Darshak R. Trivedi (2018) "Colorimetric and fluorimetric turn on sensor for selective detection of fluoride ion: sol-gel transition studies" (*Accepted Manuscript, New J. Chem.*).

7. Srikala Pangannaya, Okabe Kun, Venkatadri Tekuri, Keyur Raval, Norifumi Fujita and Darshak R. Trivedi “Rationally Designed Multi-Anion Responsive Colorimetric Receptor: an Insight on the Effective Interplay of Chemistry and Biology in Real Life Applications” (**Communicated**).

8. Srikala Pangannaya, Goutam Pawaskar, Makesh Mohan, Keyur Raval, Ritu Raval and Darshak R. Trivedi “A New Method Development towards Microbial Screening for Chitin Deacetylase Activity: Combined Experimental-DFT Studies” (**Communicated**).

Papers presented in international conferences

1. Srikala, P. and Darshak R. Trivedi (2015). “Design, synthesis and characterization of simple naked-eye chemosensor for biologically important anions.” Paper presented in “International conference on Contemporary advances of Science and Technology and 6th Annual Conference of Indian JSPS Alumni Association” August 07-09, Banaras Hindu University, Varanasi.

2. Srikala, P., Vikram, T. and Darshak R. Trivedi (2016). “A New Colorimetric Receptor for Bioactive Anions: Anion Induced Azo-hydrazone Tautomeric Equilibrium” Paper presented in “International conference on Science and Technology: Future Challenges and Solutions and 7th Annual Conference of Indian JSPS Alumni Association” August 08-09, Mysore University, Mysore.

3. Srikala, P., Venkatadri, T. and Darshak R. Trivedi (2017). “Photophysical and electroanalytical response of organic receptors: anion and cation binding studies” Paper presented in “Crystal ball vision on science and engineering for societal upliftment” and 8th Annual Conference of Indian JSPS Alumni Association” August 07-08, CSIR-National Institute of Oceanography (NIO), Dona Paula, Goa.

4. Srikala Pangannaya, Goutam Pawaskar, Makesh Mohan, Keyur Raval, Ritu Raval, Darshak R. Trivedi, (2018). “Application of colorimetric receptor in biological screening: Experimental and theoretical studies”, Paper presented in “XXXII GUJARAT SCIENCE CONGRESS – 2018, Science and Technology for Capacity Building & Inclusive Growth: The Role of Academies and Academia” 4-5, February, CSIR-Central Salt and Marine Chemicals Research Institute, Bhavnagar, Gujarat.

CURRICULUM VITAE

SRIKALA P.

srikala_30@yahoo.in

+91-7259135627

Research interests

Design and synthesis of new organic receptors, their characterization and application as chemosensor for bioactive anions

Academic qualifications

- June 2014 – June 2018** Ph.D. in Chemistry under the guidance of Dr. Darshak R. Trivedi, Associate Professor, Department of Chemistry, National Institute of Technology Karnataka (NITK), Surathkal, Mangalore, Karnataka, India
- June 2010-May 2012** Masters in Chemistry (Specialization: Inorganic Chemistry), Vellore Institute of Technology, VIT, Vellore, Tamil Nadu, India, First class with distinction
- June 2007-May 2010** Bachelor in Biotechnology (Specialization) Ancillary subjects: Chemistry and Botany, St. Aloysius college (autonomous), Mangalore, Karnataka, India, First class with distinction
- June 2005-May 2007** Pre-University college education (PUC), Department of Pre-University Education, Government of Karnataka, First class
- April 2005** SSLC, Karnataka Secondary Education Examination Board, First class with distinction

Awards and scholarships

- Won 3rd place in Oral presentation in the 3rd International conference on Science, Engineering and technology organized by School of Mechanical and Building Sciences, VIT University, Vellore held from 17-18 November, 2011.
- Received merit scholarship for best academic performance for two consecutive academic years 2010-2011 and 2011-2012 from School of Advanced Sciences, VIT University, Vellore
- Silver medal for securing 2nd rank in B.Sc. (Biological sciences), 2010

Publications

- **Srikala, P.**, Tarafder, K., Shetty, A. N., Trivedi, D. R. (2016). "Insights into the electrooptical anion sensing properties of a new organic receptor: Solvent dependent chromogenic response and DFT studies." *RSC Adv.(Communication)*, **6**, 74649 – 74653.
- **Srikala, P.**, Tarafder, K., Trivedi, D. R. (2017). "Design and synthesis of a new organic receptor and evaluation of colorimetric anion sensing ability in organo-aqueous medium." *Spectrochim. Acta Mol. Biomol. Spectrosc.*, **170**, 29–38.
- **Srikala Pangannaya**, Arshiya Kaur, Makesh Mohan, Keyur Raval, Dillip Kumar Chand and Darshak R. Trivedi. (2017) "Synthesis and Spectral Investigation of Colorimetric Receptors for the Dual Detection of Copper and Acetate ions: Application in Molecular Logic Gates." *Supramolecular Chemistry*, **29:8**, 561-574.
- **Srikala Pangannaya**, Neethu Padinchare Purayil, Shweta Dabhi, Venu Mankad, Prafulla K. Jha, Satyam Shinde and Darshak R. Trivedi. (2017) "Spectral and DFT studies of anion bound organic receptors: Time dependent studies and logic gate application." *Beilstein J. Org. Chem.*, **13**, 222-238.
- **Srikala Pangannaya** and Darshak R. Trivedi, (2017) "Electrooptical characteristics and anion binding behaviour of organic receptors: Effect of

substitution on colorimetric response." *Sensors and Actuators B*, **247**, 673–680.

- **Srikala Pangannaya**, Vikram T. and Darshak R. Trivedi, (2018) “Design, synthesis and spectral investigation of organic receptors as colorimetric and absorption ratiometric anion chemosensor.” *Supramolecular Chemistry*, **30:2**, 103-114.
- Vikram Thimaradka, **Srikala Pangannaya**, Makesh Mohan, Darshak R. Trivedi, (2018) “Hydrazinylpyridine Based Highly Selective Optical Sensor for Aqueous Source of Carbonate Ions: Electrochemical and DFT studies” *Spectrochim. Acta Mol. Biomol. Spectrosc* , **193**, 330-337.
- Makesh Mohan, **Srikala Pangannaya**, Satyanarayan M. N., Darshak R. Trivedi (2018) “Photophysical and electrochemical properties of organic molecules: Solvatochromic effect and DFT studies” *Optical Materials*, **77**, 211-220.
- Makesh Mohan, **Srikala Pangannaya**, Satyanarayan M. N., Darshak R. Trivedi (2018) “Multicoloured Thiophene Based AIEgens: Single Crystal Structure Elucidation, Spectral Behaviour and DFT Studies” *Chemistry Select*, **3**, 3803-3813.
- **Srikala Pangannaya**, Makesh Mohan, Darshak R. Trivedi “Colorimetric and fluorimetric turn on sensor for selective detection of fluoride ion: sol-gel transition studies” (**Accepted Manuscript, New J. Chem.**).
- **Srikala Pangannaya**, Okabe, Venkatadri Tekuri, Keyur Raval, Norifumi Fujita, Darshak R. Trivedi “Rationally Designed Multi-Anion Responsive Colorimetric Receptor: an Insight on the Effective Interplay of Chemistry and Biology in Real Life Applications” (**Communicated**).
- **Srikala Pangannaya**, Goutam Pawaskar, Makesh Mohan, Keyur Raval, Ritu Raval, Darshak R. Trivedi “A New Method Development towards Microbial Screening for Chitin Deacetylase Activity: Combined Experimental-DFT Studies” (**Communicated**).

Papers presented in international conferences

Poster presentation

- Srikala, P., Trivedi, D. R. (2015). “Design, synthesis and characterization of simple naked-eye chemosensor for biologically important anions.”, Paper presented in “International conference on Contemporary advances of Science and Technology and 6th Annual Conference of Indian JSPS Alumni Association” August 07-09, Banaras Hindu University, Varanasi.
- Srikala, P., Vikram, T., Trivedi, D. R. (2016). “A New Colorimetric Receptor for Bioactive Anions: Anion Induced Azo-hydrazone Tautomeric Equilibrium”, Paper presented in “International conference on Science and Technology: Future Challenges and Solutions and 7th Annual Conference of Indian JSPS Alumni Association” August 08-09, Mysore University, Mysore.
- Srikala Pangannaya, Venkatadri Tekuri and Darshak R. Trivedi, (2017). “Photophysical and electroanalytical response of organic receptors: anion and cation binding studies”, Paper presented in “Crystal Ball Vision on Science and Engineering for Societal Upliftment and 8th Annual Conference of Indian JSPS Alumni Association” August 07-08, National Institute of Oceanography (CSIR-NIO), Dona Paula, Goa.
- Srikala Pangannaya, Goutam Pawaskar, Makesh Mohan, Keyur Raval, Ritu Raval, Darshak R. Trivedi, (2018). “Application of colorimetric receptor in biological screening: Experimental and theoretical studies”, Paper presented in “XXXII Gujarat Science Congress – 2018, Science and Technology for Capacity Building & Inclusive Growth: The Role of Academies and Academia” 4-5, February, CSIR-Central Salt and Marine Chemicals Research Institute, Bhavnagar, Gujarat.

Oral presentation

- Srikala P., Sudeshna Das and A. Sivakumar, “Studies on antimicrobial properties of nano TiO₂.” 2nd International conference on Science, Engineering and Technology organized by School of Biosciences and Technology, VIT University Vellore held from 20-21 April, 2011.

-
- Srikala P. and A. Sivakumar, “Studies on applications of Titania doped nanocomposites.”3rd International conference on Science, Engineering and Technology organized by School of Mechanical and Building Sciences, VIT University Vellore held from 17-18 November, 2011.

Specialized skills

- Mentored four post graduate project students and assisting practical laboratory for engineering graduates and post graduate science students
- Software skills : Microsoft, Origin
- Structural DATA collection using Bruker APEX II Single Crystal XRD and Structure solution (DATA reduction)

Instrumentation skills

Hands-on experience in handling and usage of UV-Vis spectrophotometer (analytik jena Specord S-600, Thermo scientific Genesys 10s), FT-IR (Bruker) spectrophotometer, Cyclic voltammetry-Ivium electrochemical workstation (Vertex) and Differential Scanning colorimeter (Shimadzu).

Personal Details

Date of birth : 9th September 1989
Nationality : Indian
Marital Status : Married
Languages known : English, Hindi, Kannada, Sanskrit, Tamil, Tulu
Permanent address : “Panchadurga” House
D. No. 7/207 ‘A’, Betkeri,
Moodbidri-574227, Mangalore
Karnataka, India

References:**Dr. Darshak R. Trivedi****(Research supervisor)**

Associate Professor
Department of Chemistry,
National Institute of Technology Karnataka
(NITK), Surathkal-575025,
Mangalore, Karnataka, India
Mob: +91-9481271272; Tel.: +91-824-2473205;
Fax: +91 824 2474033
E-mail: darshak_rtrivedi@yahoo.co.in

Prof. A. Nityananda Shetty

Professor,
Department of Chemistry,
National Institute of Technology
Karnataka (NITK), Surathkal-575025,
Mangalore, Karnataka, India
Mob: +91-9448779922;
Tel.:+91-824-24743200
E-mail: nityashreya@gmail.com;
nityanand@nitk.ac.in

Prof. Dillip Kumar Chand

Professor,
Department of Chemistry,
Indian Institute of Technology Madras,
Chennai-600036 (India)
Ph: +91 44 2257 4224
Fax: +91 44 2257 4202
E-mail: dillip@iitm.ac.in